Experimental Studies on Shear Connection Systems in Steel and Lightweight Concrete Composite Bridges

Estudo Experimental de Sistemas de Conexão para Pontes Mistas de Aço e Betão Leve

Tese apresentada à Universidade do Minho por

Maria Isabel Brito Valente

para a obtenção do grau de Doutor em Engenharia Civil

Civil Engineering Department - School of Engineering

University of Minho, Portugal

April 2007

Acknowledgments

The work here presented was enriched by the contact and share of experiences with various people. Therefore, I wish to address my thanks to all of those who in some way helped me fulfilling this job and especially:

- To Professor Paulo Cruz, my supervisor, for his guidance, scientific knowledge and trust during all this time;
- To Professor Josef Hegger, Claus Goralski and Sabine Rauscher from the Institute of Structural Concrete of RWTH, Aachen, Germany, for their interest in receiving me to perform experimental work and for creating the proper conditions to accomplish the job proposed. Their share of knowledge and support were indispensable during my stay in Aachen;
- To Heiko Trumpf from the Institute of Steel Construction of RWTH, Aachen, Germany, who was the first responsible for my stay in Germany, for his interest and support along time;
- To the technicians of the Laboratory of Civil Engineering of University of Minho for their valuable suggestions and particularly to Marco Jorge, António Matos and José Gonçalves for their technical expertise and interest on the production and testing of all the specimens;
- To Gustavo Veríssimo from the University of Viçosa, Brazil, for the long discussions, the share of knowledge and experiences that were constant since the first contact;
- To all my colleagues of the Structural Group of the Civil Engineering Department for the helpful suggestions;
- To Professor Aires Camões, for carefully reading and correcting part of the thesis;
- To my colleagues and friends, Dawid Wisniewski, Ismael Basílio and Rolando Estrada, for their support and help.

I would also like address my gratitude,

- To the University of Minho for giving me the conditions and the facilities to perform the work;
- To the Portuguese Foundation for Science and Technology, FCT, that financed the investigation project POCTI/ECM/33067/2000 - “Steel-concrete composite bridges: Use of lightweight high performance concrete”, that provided the major part of the financial resources needed and to the scholarship SFRH/BD/11399/2002 that financed my stay in Aachen, Germany;

- To Dr. Jan Cervenka, that kindly allowed the use of the software ATENA for this research;
- To the firms that gently provided materials and equipments that were indispensable to build the specimens and perform the experimental tests, namely: Maxit - Argilas Expandidas S.A., SECIL - Companhia Geral de Cal e Cimento, S.A., Degussa Construction Chemicals Portugal S.A., UTEC - União Técnicas de Soldadura, Lda., Sika Portugal S.A. and Balanças Marques, Lda..

and finally,

- To my family, especially my parents, Isabel and Fernando, and my sisters, Fernanda and Helena, whose care and support are always there;
- To João, Ana, Matilde and Eunice, who always show me the important things;
- To Renato for being always there with such care;
- and to Teresa, who makes every day a joy.

Abstract

The behaviour of composite structures accounts for the contribution of concrete and steel sections, provided that a composite action exists between these two materials. Composite action can be obtained by reducing or preventing the relative displacement of concrete and steel elements at their interface. Shear connectors are used to provide this composite action. The behaviour of the steel to concrete connection will have major importance on the global behaviour of the structural element.

Lightweight concrete is now a commonly used material that can successfully replace normal density concrete. There are some good examples of buildings and bridges where high strength lightweight concrete is used as the main material. The principal reason for using lightweight concrete is the advantage of reducing the concrete element self-weight. This weight saving permits larger spans or lower weight of the steel section and lowers the cost of the foundations. There is also a reduction in the cost of the formwork of elements constructed on site and in the cost of transportation and assembly of prefabricated elements.

It is possible to produce lightweight concrete that is comparable to normal weight concrete in terms of compressive strength. However, other mechanical properties, like modulus of elasticity, fracture energy or long-term properties show some differences that should be taken into account. Therefore, a part of this study is dedicated to the mechanical characterization of high strength lightweight concrete. Studies on its long term behaviour are also undertaken.

The use of lightweight concrete on composite structures requires testing of the connection between the steel and the concrete members. The connection behaviour influences the overall behaviour of the composite element in terms of strength and deformability. It is important to design connection systems adapted to lightweight concrete, that guarantee the ductile behaviour of the connection in order to maximize the connection strength and allow its plastic behaviour. Therefore, the characterization of different types of shear connection devices to be used in composite elements of steel and lightweight concrete is done. Headed studs, Perfobond connectors and T connectors are analysed for static loadings and compared. Failure modes, load capacity, deformation capacity, ductility and stiffness are the main parameters in analysis.

In bridges, live loads present important variation in value and in time. Some of these loads have also important repetition during the structure’s life time. When the composite beam is loaded, either statically or cyclically, the interface between steel and concrete

tends to present increasingly higher slip values. For cyclic loadings, the increase in slip depends on the number of load cycles applied and on the range of load imposed. The consequences of higher slip are a higher vertical deflection and the stress redistribution on the cross section. It is also verified that the repetition of load cycles can result in a diminution of the maximum load attained at the steel to concrete connection.

This work presents tests on steel and lightweight concrete composite beams submitted to static and cyclic loadings. During these tests, it is possible to measure the evolution of vertical deflection, slip and slip strain. All these parameters indicate if there is loss of interaction at the steel to concrete interface. For cyclic loadings, a relation between these parameters and the number of load cycles applied is established. It is also possible to check if there is loss of load capacity due to the repetition of the load cycles, by comparison with the results previously obtained for monotonic loadings. Push-out tests submitted to static and cyclic loadings are also performed, in order to collect useful information for the characterization of the steel and lightweight concrete connection and for the analysis of composite beams. Different types of shear connection dispositions are tested, in order to evaluate the effects of designing for total and for partial connection.

Concrete creep and shrinkage can influence the behaviour of a composite beam, because the concrete slab is restrained by the steel beam and therefore, they induce internal stresses on the composite section. The long term behaviour of lightweight concrete will have important influence on the long term behaviour of the composite beam, which is also analyzed with the experimental tests performed.

Resumo

A realização de estruturas mistas em aço e betão implica a necessidade de existir uma acção mista entre as secções de ambos os materiais. Esta acção mista pode ser obtida, reduzindo ou prevenindo o deslizamento relativo entre as secções de aço e de betão. Para tal, são utilizados conectores metálicos, que são soldados ao perfil metálico e ficam betonados no interior da laje de betão. O comportamento da conexão terá um papel fundamental no comportamento global do elemento misto.

O betão leve é já um material frequentemente utilizado e que pode substituir com sucesso o betão de massa volúmica normal. A principal vantagem do betão leve reside na redução do peso próprio da laje de betão. Esta redução no peso próprio permite aumentar o vão do elemento misto ou em alternativa, reduzir o peso da secção de aço. Permite ainda reduzir o custo das fundações. Verifica-se também uma redução do custo das cofragens para elementos betonados em obra e uma redução dos custos de transporte e montagem para elementos pré-fabricados.

Existem bons exemplos de edifícios e pontes construídos maioritariamente com este material. É possível produzir betão leve com resistência à compressão similar à de um betão de massa volúmica normal. Contudo, outras propriedades como o módulo de elasticidade, a energia de fractura ou aspectos relacionados com o comportamento diferido apresentam diferenças que devem ser tidas em conta. Deste modo, uma parte do estudo realizado é dedicado à caracterização mecânica de um betão leve de elevada resistência, complementada com um estudo do seu comportamento a longo prazo, nomeadamente com ensaios de caracterização da retracção e da fluência.

A utilização de betão leve em estruturas mistas requer uma avaliação do comportamento da conexão. A conexão aço-betão leve influencia o comportamento global do elemento misto em termos de capacidade resistente e deformabilidade. É importante conceber e dimensionar sistemas de conexão adaptados ao betão leve, de forma a garantir o comportamento dúctil da conexão, o qual permitirá mobilizar a máxima capacidade resistente do elemento estrutural e eventualmente permitirá o seu comportamento plástico. Deste modo, a caracterização da conexão aço-betão leve para diferentes tipos de elementos de conexão é um dos objectivos do trabalho. Pernos de cabeça, conector de tipo Perfobond e conector de tipo T são as tipologias testadas sob carregamentos monotónicos e posteriormente comparadas. Os principais parâmetros analisados são os modos de rotura, a capacidade resistente, a capacidade de deformação, a ductilidade e a rigidez. O objectivo final é fazer uma caracterização completa para que seja possível utilizar estes tipo de elementos de conexão em elementos mistos realizados em aço e betão leve.

Em pontes, as cargas variáveis apresentam importante variação em grandeza e ao longo do tempo. Algumas destas cargas repetem-se constantemente ao longo da vida destas estruturas. Numa viga mista, a interface entre as secções de aço e de betão tende a apresentar deslizamento progressivamente crescente quando submetida a carregamento. No caso dos carregamento cíclicos, este deslizamento depende do número de ciclos aplicado e do intervalo de carga correspondente a cada ciclo. As consequências principais do crescimento do deslizamento são o aumento da deformação vertical da viga e a redistribuição interna dos esforços. Verifica-se que a repetição de ciclos de carga e descarga pode resultar na diminuição da capacidade de carga da viga.

O presente trabalho apresenta ensaios experimentais em vigas mistas de aço e betão leve, submetidas a carregamentos monotónicos e cíclicos. Durante estes ensaios é possível medir a evolução da carga aplicada, da deformação vertical, do deslizamento na interface entre as secções de aço e de betão e das extensões em algumas secções transversais pré-definidas. Todos estes parâmetros permitem avaliar se há perda de interacção entre as secções de aço e de betão leve. No caso dos carregamento cíclicos, estabelecem-se relações entre estes parâmetros e o número de ciclos de carga e descarga aplicados. Também é possível avaliar se há perda de carga devido à repetição destes ciclos, comparando o valor de carga máximo atingido com o valor de carga máxima medida nos ensaios de carregamento monotónico. São ainda realizados ensaios de tipo push-out submetidos a carregamentos monotónicos e cíclicos, de forma a obter informação útil para a caracterização da conexão aço-betão leve e para a avaliação do comportamento de vigas mistas.

Os fenómenos de retracção e fluência do betão leve podem influenciar o comportamento das vigas mistas, uma vez que o perfil metálico restringe a variação de volume da laje de betão. Deste modo, o comportamento diferido do betão leve é analisado e testado através de ensaios experimentais, complementados por ensaios de vigas mistas realizadas em aço e betão leve e submetidas a carregamentos permanentes por um período de aproximadamente um ano.

Contents

Chapter 1

INTRODUCTION

1.1 Introduction and scope

Composite construction is gathering increasing interest in many European countries. The use of composite elements in the form of beams, columns and composite slabs is already a common practice in many countries. In multi-storey buildings, structural steelwork is typically used together with concrete. Steel beams with concrete floor slabs are a good example. The same applies to road bridges, where concrete decks are normally preferred. The extent to which the components or parts of a building structure should embody all steel construction, be constructed entirely in reinforced concrete, or be of composite construction depends on the circumstances. It is a fact, however, that engineers are increasingly designing composite and mixed building systems of structural steel and reinforced concrete to produce more efficient structures when compared to designs using either material alone, (ESDEP 1995).

Steel and concrete are materials with different nature and properties, but compatible and complementary to each other. When properly associated, it is possible, in a mechanical point of view, to take the best advantage of each one's capacities and of its association. In fact, they have almost the same thermal expansion and an ideal combination of strengths, because concrete is efficient in compression and steel is efficient in tension. Concrete also gives corrosion protection and thermal insulation to the steel at elevated temperatures and additionally can restrain slender steel sections from local or lateral-torsional buckling.

The use of composite structures accounts for the contribution of these two materials, provided that a composite action exists between the concrete and the steel sections. Composite action can be obtained by reducing or preventing the relative displacement of concrete and steel elements at their interface. Shear connectors are used to provide this composite action. The behaviour of the steel to concrete connection will have major importance on the global behaviour of the structural element.

The behaviour of the steel to concrete connection depends mainly on the behaviour of the shear connectors used. Shear connectors have different shapes and configurations that affect the transmission of forces between the concrete and the steel sections and condition the way they deform. In addition, the concrete mass that surrounds the connector plays an important part because the concrete elastic properties and the development of cracks contribute to the connection deformability. Resulting from this are the main

differences that are possible to find between different types of connectors, which are load capacity, deformation capacity and stiffness.

Lightweight aggregate concrete (LWAC) is now a commonly used material that can successfully replace normal density concrete. There are some good examples of bridges and buildings where high strength lightweight concrete was used as the main material, (BE96-3942/R22 2000). The principal reason for using lightweight concrete on composite structures is the advantage of reducing the concrete element self-weight, which usually constitutes an important parcel of the dead load. Therefore, a reduction in the steel section can be considered, resulting in a globally lighter solution. The combination of steel and lightweight concrete opens new possibilities regarding the weight reduction of high-rise buildings, projects with a difficult foundation situation or in the case of heightening old buildings. On the other hand, the smaller density of LWAC allows greater spans without any supports during the construction, which benefits the construction progress, (Faust et al. 2000).

It is possible to produce structural lightweight concrete that is comparable to normal weight concrete in terms of compressive strength. Other mechanical properties, like tensile strength, modulus of elasticity or long-term properties show some differences that should be taken into account, when the same grade of compressive strength for normal density concrete and lightweight concrete is in comparison. The use of high strength lightweight concrete in composite buildings or bridges should consider both the short-term and the long-term properties of lightweight concrete and the behaviour of the connection between steel and lightweight concrete. In bridges, the effects of repeated loadings should also be accounted, because they cause slip damage to accumulate in the shear connection with a consequent loss of stiffness and an increase in the deflection, (Taplin 1999). In a structural point of view, these are important aspects that can be altered by substituting normal density concrete (NDC) with lightweight concrete (LWC).

1.2 Motivation

The use of lightweight concrete in composite structures should consider the connection between steel and lightweight concrete, which influences the transfer of stresses between the steel beam and the concrete slab and the overall behaviour of the composite element in terms of strength and deformability. It is important to design connection systems adapted to lightweight concrete, that present high load capacity and guarantee the ductile behaviour of the connection, which is important to maximize the connection strength and allow its plastic behaviour. This is the main motivation for this work, as lightweight concrete and normal density concrete are materials with similar characteristics but with some particular differences that can influence the global behaviour of the connection.

A large number of experimental tests have been done in order to explore the structural behaviour of different types of steel connectors. Beside the commonly used headed studs, some investigators showed that the use of Perfobond connectors and T connectors is adequate when using high strength concrete. Recent experimental work, carried out by Oguejiofor and Hosain (1994), Ferreira (2000), Machacek and Studnicka (2002), Medberry and Shahrooz (2002), Galjaard and Walraven (2001) and Poot (2001) with Perfobond and rib connectors, and studies developed by Faust et al. (2000), Hegger et al. (2000/2001) and Galjaard and Walraven (2001) with headed studs and T connectors, made it possible to describe and analyse the steel to concrete connection properties. These studies that primarily focus normal density concrete (NWC) with normal and high strength compressive strength, are a reference to the work developed. An overall characterization of the connection between steel and lightweight concrete is intended with this work. Some authors, like Galjaard and Walraven (2000) or Faust et al. (2000) developed experimental work to study the behaviour of the connection between steel and lightweight concrete. The first performed static push-out tests with various types of shear connectors and the second performed static and cyclic push-out tests with headed studs.

The investigation performed within this thesis intends to go further. First, by testing the connection between steel and lightweight concrete with Perfobond connectors and T connectors. In normal weight concrete, these connectors usually present higher load capacity than the common headed studs and therefore, a smaller number of Perfobond or T connectors can substitute a large number of headed studs in the composite beam. These types of connectors also present some particular characteristics that can influence the overall behaviour of the connection and of the composite beam. Second, by testing steel and lightweight concrete composite beams under static and cyclic loadings. The test of a composite beam gives information about the beam failure modes or its deformability that is not possible to obtain with the push-out test. Push-out tests under static and cyclic loadings are also performed, in order to collect useful data for the analysis of composite beams. Cyclic loadings are important to study, simulate and evaluate the behaviour of the steel and lightweight concrete connection in bridges.

1.3 Objectives

An objective of this work is to define a mixture for high strength lightweight concrete that will be used in composite elements. For that, it is also necessary to define a good procedure to produce this concrete in the laboratory environment. The intention is to evaluate the principal properties of high strength lightweight concrete that are important for the structural behaviour of a composite element in which this material is used. These include

density, compressive strength, modulus of elasticity, tensile strength, fracture energy and shear strength. With that knowledge, it is possible to anticipate the main differences of using normal density concrete or lightweight concrete in composite structures. The experimental evaluation of these properties is also important for the good quality of analytical or numerical analysis made on composite elements that use this material.

Experimental testing on the connection between steel and lightweight concrete members is also intended. The push-out test, defined in EN1994-1-1 (CEN 2004c), is the standard test to analyse and characterize the behaviour of the connection between steel and concrete. This test type is used in this work because it is appropriate for the study of the phenomena in analysis and because the work performed can afterwards be compared with the work of other authors. The types of shear connectors chosen for analysis reflect the intention of defining a steel to concrete connection that presents high load capacity associated with a ductile behaviour. Different types of shear connectors are tested in order to characterize each one's behaviour. In reality, each type has different characteristics that are possible to evaluate with push-out tests.

Therefore, the connectors' load capacity, deformation capacity and load-slip relation are determined, before and after the maximum load is attained. The values of maximum load and maximum slip at the connection between steel and lightweight concrete are important to the design of a composite beam, because they condition one of the possible failure modes. The connection deformability is also analyzed for service loads in order to evaluate the loss of composite action associated. The loss of composite action results on the increase of vertical deflection, on the redistribution of shear stresses along the beams and on a redistribution of normal stresses on each cross section. All the parameters mentioned are compared with the ones obtained for normal weight concrete in experimental tests performed by other authors.

The push-out test simulates the behaviour of a steel and concrete composite beam. However, the distribution of load along the composite beam is not quite the same as it occurs on the push-out specimen, where the load is evenly distributed between studs. On a composite beam, the shear flow at the steel to concrete interface varies along the beam and depends on the load distribution. In addition, on a composite beam, the deformation of the studs alters the shear forces flow, by diminishing the maximum shear force and redistributing it. Therefore, it is important to check if the results obtained in push-out tests are adequate to be used on the analysis of composite beams. Other types of failure and aspects of behaviour that are not possible to observe and evaluate with the push-out tests can also be studied with the beams' tests.

In bridges, repeated loadings are an important part of the live loads. When submitted to repeated loading, the interface between steel and concrete tends to present increasingly

higher slip values. The value of slip tends to increase with the number of load cycles applied and with the range of load imposed. The consequences of higher slip are a higher vertical deflection and the stress redistribution on the cross section. It is also verified that the repetition of load cycles can result in a diminution on the maximum load attained at the steel to concrete connection. Failure can occur during the application of the load cycles, even if the maximum load applied is far from the connection load capacity. It is possible to relate the rate of slip growth with the number of load cycles applied by performing push-out tests where a large number of load cycles is applied. If different load ranges are applied, then it is also possible to relate the rate of slip growth with the load range imposed. In the end, it should be possible to identify the number of load cycles of a certain load range that would be necessary to apply in order to achieve failure that is conditioned by a maximum slip value.

Again, the slip growth may not be the same for push-out specimens and for composite beams, which is the reason for testing push-out specimens and composite beams made of the same steel and lightweight concrete and submitted to repeated loadings.

The long-term behaviour of lightweight concrete is mainly dependent on concrete creep and shrinkage effects and also on the variation of temperature. The long-term behaviour of lightweight concrete can alter the behaviour of a composite structural element, because creep and shrinkage will induce internal stresses. Shrinkage and creep are usually studied with experimental tests performed on small specimens, which in the present case are cylinders. The intention is to use this data, collected during approximately one year, on the analysis of composite beams under long-term loadings and then compare these results with the ones directly measured on the beams.

1.4 Outline of the thesis

This thesis begins with the present chapter, where the scope of the work, its motivation and the main objectives are established. A resume of the thesis is also presented, with a brief description on the contents of each chapter.

The first part of this study, presented in Chapter 2, is dedicated to the mechanical characterization of high strength lightweight concrete. Several mixtures of lightweight concrete were previously studied and one of them is chosen for complete characterization. Concrete properties like compressive strength, elasticity modulus, splitting tensile strength, flexural tensile strength, fracture energy and shear strength are fully characterized. The results obtained with the tests described are compared and evaluated for possible strong correlations between the various parameters studied. The long term behaviour of this

material is also studied with shrinkage and creep tests, performed during a period of around 400 days. The study also includes a description on the procedures needed to fabricate high strength lightweight concrete.

An extensive experimental study on the connection between steel and lightweight concrete is developed within Chapter 3. The standard push-out test defined in EN1994-1-1 (CEN 2004c) is chosen for this analysis. Three types of shear connectors are studied in the experimental campaign. These are headed studs with 19 mm, 22 mm and 25 mm of shank diameter, Perfobond with three circular openings and T connectors made of half IPE200.

All the tests are performed with displacement control. The values of applied load and slip between the concrete slab and the steel beam are continuously measured. The connection behaviour is analysed in terms of its load-slip relation and with identification of the failure modes. Also, the load capacity, maximum slip, elastic slip and plastic slip are quantified. The various elements that constitute the steel to concrete connection contribute to its load capacity. Some of the push-out tests performed try to isolate these components of the connection in order to evaluate each one's contribution.

The value of stiffness is evaluated for a level of loading that is suitable for serviceability analysis. The results obtained are adequate to define load-slip curves that can be used in the analysis of steel and lightweight concrete composite elements.

A special series of push-out tests was performed on the laboratory of the Structural Concrete Institute from RWTH University, at Aachen, in Germany. This series consist of a single push-out test that was developed at this university. The specimens are smaller and therefore less material in needed for the experimental test. They are also lighter, which facilitates the work with the test set up. The results obtained are object of analysis and comparison with the standard push-out tests performed at University of Minho.

All the results, that allow the characterization of the connection between steel and lightweight concrete are compared with the results obtained by other authors with similar specimens made of normal density concrete.

Chapter 4 describes the experimental campaign of push-out tests with headed studs of 13 mm diameter in high strength lightweight concrete solid slabs. The tests follow the description and procedure presented in Chapter 3. Static and cyclic loadings are considered for comparison.

The specimens tested for static loadings are analysed in terms of failure mode, maximum load, maximum slip and stiffness, as was previously done in Chapter 3 for studs

with larger diameters. The specimens tested for cyclic loadings are analysed for the same parameters and are compared to the specimens statically loaded to identify if there is a loss of load capacity associated with the load repetition.

The specimens failure is mainly achieved when a maximum value of slip is attained. Therefore, emphasis is put on the slip evolution in order to identify the trends of slip growth and to define equations that can properly relate the slip growth with the number of load cycles applied and the load range associated with each cycle. The trends identified are then compared to the results obtained by other authors with normal density concrete.

The work done for Chapter 5 consists on the testing and analysis of composite beams with 4.5 m span. The cross section, geometrical configuration and supports are common to all the beams and the number and distribution of connectors is varied between them.

The beams are composed by a steel profile of type IPE120 and a lightweight concrete slab with $350\ \text{mm} \times 60\ \text{mm}$. The properties of steel and lightweight concrete are experimentally characterized. The steel to concrete connection is accomplished with headed studs of 13 mm diameter, equally spaced along the beams. Three types of stud distribution is considered, one with total connection design and single stud distribution, other with total connection design and double stud distribution and the last one with partial connection design and single stud distribution.

Three beams are tested with six points of loading and other three are tested with four points of loading. The first loading distribution is close to a uniformly distributed loading and the second one is similar to a concentrated loading on the beams' mid span. All tests are conducted until failure is reached. The behaviour of the composite beams during testing is described, the failure modes are identified and the beams load and deformation capacity are quantified. The different distributions of shear connectors and the two loading configurations permit an analysis on the shear load distribution along the steel to concrete interface. Total connection design and partial connection design are also analysed in terms of failure modes, load capacity, deflection and slip at the steel to concrete interface.

Simple numerical models are also drawn to evaluate if the behaviour observed and quantified with the tests is possible to obtain without performing experimental testing.

Chapter 6 repeats the work presented in Chapter 5, but now the composite beams are subjected to cyclic loadings. The cross section, geometrical configuration and supports are common to all the beams and to the beams tested within Chapter 5. All the composite beams tested with cyclic loadings present 4.5 m span. Again, the number and distribution of the connection devices is varied between beams.

Four beams are tested with six points of loading. The tests are conducted with load control in the phase of cyclic loading, for a predetermined number of load cycles. If failure is attained during the phase of cyclic loading, the test ends at this moment. If the total number of load cycles is completed without the failure of the beam, then the test proceeds with displacement control at a constant growing rate, until failure is attained. The load cycles range is constant for two of the tested beams. The other two are submitted to one thousand load cycles for each load range. Applied load, vertical deflection, end-slip and strain at predefined cross sections are measured during all the test.

During the procedure described, it is possible to measure the evolution of vertical deflection, slip and slip strain. All these parameters indicate if there is loss of interaction at the steel to concrete interface. A relation is established between these parameters and the number of load cycles applied. As the applied load is measured during the loading process, it is also possible to check if there is loss of load capacity due to the repetition of the load cycles, when the values measured are compared to the results previously obtained for monotonic loadings.

Chapter 7 describes the experimental tests performed on long term loadings applied to composite beams. The beams that are submitted to long term loadings have the same geometry, supports, free span and materials that were used for the composite beams tested for short term loadings (Chapter 5). These beams are simply supported and submitted to a constant loading during a total period of one year, and are maintained under similar conditions of temperature and relative humidity. In order to characterize the behaviour of the lightweight concrete used, tests on creep and shrinkage are also performed during the same period as the beams tests, under the same thermo-hygrometric conditions. The values of vertical deflection, end-slip and strain at particular cross-sections, measured during testing, are compared to the results obtained with numerical methods applied on the measurements of shrinkage, creep and variation of temperature. Partial interaction at the steel to concrete interface is considered. The connection stiffness is evaluated with the results previously obtained in Chapter 4 and is adjusted with the results obtained on the loading phase.

Chapter 8 concludes this thesis by resuming the principal results obtained and the main conclusions achieved with the work done. During the development of the present work, some questions raised that could not be addressed, due to lack of time or because they drift away from the main issues here discussed. These questions and some other ideas that result directly from the work done are now suggested for future work.

Chapter 2

EXPERIMENTAL STUDIES ON HIGH STRENGTH LIGHTWEIGHT CONCRETE

2.1 Introduction

This chapter summarizes the investigation performed at the Structural Engineering Laboratory, located at University of Minho, LEST-UM, to characterize a high strength lightweight concrete. LEST-UM has already considerable experience on the production and characterization of lightweight concrete.

The aim is to define an adequate mixture that can be applied on composite structures to be studied later.

The following tasks are established:

- choosing the most adequate and available raw materials;
- defining an adequate mixture and the proper mixing procedures;
- producing specimens to evaluate the material properties.

The principal reason for using lightweight concrete on composite structures is the advantage of reducing the concrete element self-weight. Other advantages have already been identified, like an enhanced durability or the improvement of some physical properties. Some examples of these advantages are related to bridge structures: the lower modulus of elasticity, that leads to a decreased loss of pre-stressing, thus reducing the adverse effects of support sinking, or the lower thermal dilation coefficient, that leads to less movements of thermal origin, making it possible to reduce the number of joints on long bridges.

Several lightweight concrete mixtures are studied. All of them use expanded clay aggregates available in Portugal during the period while the study took place. The expanded clay aggregates substitute the normal density aggregates commonly used. In order to obtain high strength concrete, no lightweight sand is used.

Several mixtures were studied, as referred, but only one is presented. The chosen mixture is designed to be applied in steel and concrete composite elements and presents the following properties: high strength, reduced density and good workability.

A large number of mixtures were produced based on the lightweight aggregate concrete (LWAC) composition chosen. Those mixes were produced for the specimens studied in Chapter 3, 4, 5, 6 and 7. Other mixes were produced to study and evaluate relevant properties of this lightweight concrete, as will be presented. All the properties studied in this chapter are chosen with the purpose of complementing and justifying the results obtained in the referred chapters.

Several tests are performed to characterize the LWAC mechanical properties: compressive strength on 100mm cubes and 150mm diameter standard cylinders, modulus of elasticity, splitting tensile strength, flexural tensile strength, shear, creep and shrinkage. This group of tests allows the definition of the short and long term behaviour of the chosen mixture. Compressive strength and modulus of elasticity are important in all the following chapters of the thesis, tensile strength and fracture energy are useful for the calibration of numerical models presented in Chapter 5, shear strength is used in the analysis of the Perfobond shear connector made in Chapter 3, creep and shrinkage are needed for the analysis of the long term loadings presented in Chapter 7.

The chosen mixture uses the following components:

- Lightweight aggregate - expanded clay with bulk density equal to 750±50 kg/m^3;
- Natural sand - grade from 0 to 4.76 mm;
- Cement CEM I 52.5 R;
- Water;
- High range water reducing agent (superplasticizer).

All the tests are performed for different concrete ages in order to establish evolution curves along time for the different properties.

2.2 Lightweight concrete definition

Lightweight concrete is usually defined considering its density. One proposed classification, (Asgeirsson 1994), is presented in Figure 2.1, where the complete range, from low density to structural concretes, is represented in a graphical way.

In many countries, concrete is considered to be lightweight if its dry density is equal or inferior to 2000 kg/m³ (BE96-3942/R14 2000). However, this parameter can present values that go from 300 to 2000 kg/m³, corresponding to compressive strength values that vary from 1 to more than 60 MPa and thermal conductivity values that vary between 0.2 and 1.0 W/mK (Newman 1993).

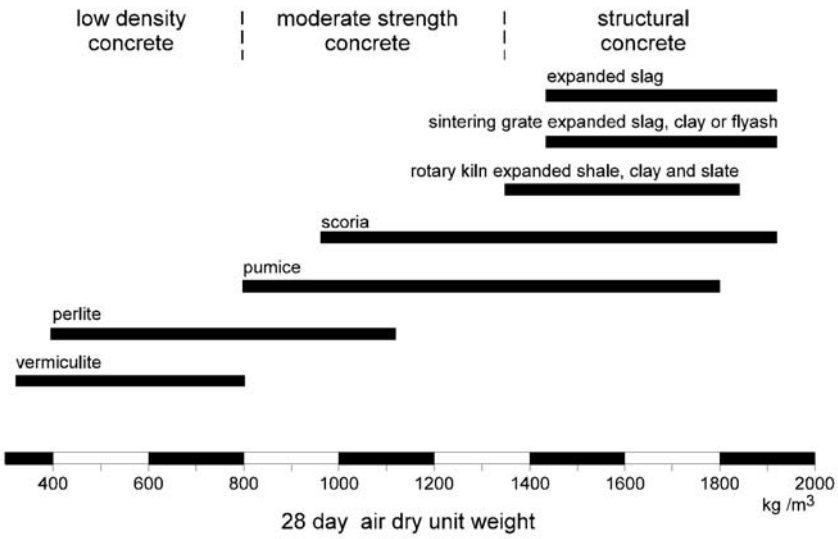

Figure 2.1 - Lightweight concrete classification, according to its density, (Asgeirsson 1994)

In Norway, only structural lightweight concrete is considered in the national rules. The national rule NS 3473 (NS 1992) considers lightweight concrete for densities between 1200 and 2200 kg/m³. This rule was updated in 1998, (NS 1998), and the superior limit was eliminated. Therefore, the difference between normal density and lightweight concrete is less clear now. For concretes where normal density aggregates were only partially substituted by lightweight ones, a modified normal density concrete is now considered. This type of concrete, with concrete strengths starting at 75 MPa was used in the offshore petroleum and gas platforms placed on the Northern Sea. The methodologies for normal density concrete are applicable to these modified concretes, (BE96-3942/R2 1998).

In Australia, structural lightweight concrete present density values superior to 1800 kg/m³, and in Japan no limit values for lightweight concrete density are defined.

The European Union uses EN 1992-1-1 (CEN 2004a), where lightweight concrete is defined as concrete with closed structure and density values not superior to 2000 kg/m³, consisting or containing a proportion of natural or artificial lightweight aggregates with particles density inferior to 2000 kg/m³. Also, NP EN 206-1 (2005) defines LWC with an oven-dry density equal or superior to 800 kg/m³ and inferior to 2000 kg/m³, for concrete totally or partially produced with lightweight aggregate. This norm considers strength classes that go from LC8/9 to LC80/88, where the characteristic compressive strength measured in cylinders varies between 8 MPa and 80 MPa. Also, the density classes vary from D1.0 to D2.0, where density varies between a minimum of 800 kg/m³ for D1.0 and a maximum of 800 kg/m³ for D2.0.

2.3 Historical background

Pumice and scoria are volcanic natural lightweight aggregates. Greeks and Romans used pumice, even before the Christian era. Magnificent structures, like the Sofia Cathedral in Istambul, dated from the 2nd Century A.C. prove the material “competence”. The Pantheon vault in Rome was built with lightweight mortar, made with pumice. More than a thousand of years were passed before Miguel Angelo surpassed the benchmark of 44 m of span, with the St. Peter's Basilica in the Vatican.

Until the 20th century, LWC was not systematically used. It was only in that century that the industrial production of lightweight aggregates began. Because of its uniformity, it became possible to produce concretes with a higher strength. By 1917, S. J. Hayde developed, in the United States, an industrial process to expand clay, using a tubular kiln. The aggregates obtained through this production method were applied on the construction of ship hulls during World War I.

The Hotel Park Plaza in St. Louis, the Bell Telephone building in Kansas City and the Oakland bridge superior deck, in San Francisco, are examples of structural lightweight aggregate concrete (LWAC) early applications, in the United States, during the 20’s and the 30’s.

A rapid development on the production of LWAC took place during World War II. Various buildings were total or partially built with LWAC during the 50’s and the 60’s. Some examples are the Prudential Life building in Chicago, the New York TWA airport terminal and the Dulles Airport in Washington, these two last of the architect Eero Saarinen.

Other well-known structures are the Tromsø Polar Sea Cathedral, in Norway, the Dyckerhoff Bridge at Wiesbaden, Germany, or the Harmsen viaduct in Rotterdam, The Netherlands.

In Germany, the industrial use of lightweight aggregates was initiated in 1945, with the production of masonry blocks made of pumice and burnt lime as a binder. In Island, pumice has been used in the building industry since 1928. Nowadays, most of the pumice is extracted and exported to Germany to be used in building construction. A total amount of 300000 tons was used in 1995.

In general, Denmark can be considered as the first european country where expanded clay was produced, with the construction of the first processing plant. Many more were built throughout Europe during the 60’s. Nowadays, Norway and Denmark are among the countries that consume more lightweight aggregates.

2.4 Economy of LWAC

The cost per cubic meter of LWAC is usually higher than a comparable unit of conventional concrete. Therefore, it is important to estimate the project total cost when the use of lightweight concrete is considered. The following economies and functionality improvements can easily annul the cost increase that results from replacing normal density concrete with lightweight concrete, (ACI 2003):

- The reduction in foundation loads may result in smaller footings, fewer piles, smaller pile caps, and less reinforcement;
- Reduced dead loads may result in smaller supporting members (decks, beams, girder, and piers), resulting in a major reduction in cost;
- Reduced dead load will mean reduced inertial seismic forces;
- In bridge rehabilitation, the new deck may be wider or an additional traffic lane may be added without structural or foundation modification;
- On bridge deck replacements or overlays, the deck may be thicker to allow more cover over reinforcing or to provide better drainage without adding additional dead load to the structure;
- With precast presstress technology, longer or larger elements can be manufactured without increasing overall mass. This may result in fewer columns or pier elements in a system that is easier to lift or erect, and fewer joints or more elements per load when transporting. There are several documented cases where the savings in shipping costs far exceeded the increased cost of using lightweight concrete. At some precast plants, each element's shipping cost is evaluated by computer to determine the optimum concrete density;
- In marine applications, increased allowable topside loads and the reduced draft resulting from the use of lightweight concrete may permit easier movement out of dry docks and through shallow shipping channels; and
- Due to the greater fire resistance of lightweight concrete, as reported in ACI 216.1, the thickness of slabs may be reduced, resulting in significantly less concrete volumes.

The architectural expression and construction efficiency of a structure are often enhanced with the use of lightweight concrete. In building construction, this usually applies to cantilevered floors, expressive roof design, taller buildings, or additional floors added to existing structures. With bridges, this may allow a wider bridge deck (additional lanes) being placed on existing structural supports. Improved constructive procedures may result, for example, in cantilever bridge construction, where lightweight concrete is used

on one side of a pier and normal weight concrete used on the other to provide weight balance while accommodating a longer span on the lightweight side of the pier, (BE96-3942/R22 2000). The use of lightweight concrete may also be necessary for better insulating.

Significant economies can also result from the use of lightweight concrete in situations where transportation costs are directly related to the weight of concrete products. The range of products includes large structural members (girders, beams, walls, hollow-core panels, double tees) to smaller consumer products (precast stair steps, fireplace logs, wall board). Two trucking studies conducted at a U.S. precast plant demonstrated that the transportation cost savings were seven times more than the additional cost of lightweight aggregate, (ACI 2003). Savings vary with the size and mass of the product and are most significant for the smaller consumer-type products.

More than 500 bridges have incorporated lightweight concrete into decks, beams, girders, or piers, according to ACI (2003). Transportation engineers generally specify higher concrete strengths primarily to ensure high-quality mortar fractions (high compressive strength combined with high air content) that will minimize maintenance. The following are the principal advantages of using lightweight concrete in new bridges and in the rehabilitation of existing bridges, (ACI 2003): increased width or number of traffic lanes, increased load capacity, balanced cantilever construction, reduction in seismic inertial forces, increase cover with equal weight, thicker slabs, improve deck geometry with thicker slabs and longer spans save pier costs.

The good behaviour of this concrete and new technological advances have encouraged its use in large buildings and offshore platforms. The application of lightweight concrete in bridge construction is a field that is starting to emerge and is associated with certain advantages such as, (Daly 2000):

Weight reduction — It is particularly in pedestrian footbridges or in large span bridges where a significant reduction in the weight of the materials used is achieved. This weight saving permits larger spans and also lowers the cost of the foundations. There is also a reduction in the cost of the formwork, in the elements constructed on site and in the cost of transportation and assembly of prefabricated elements.

Improvement of some physical properties — Some of the differences between the properties of lightweight concrete compared with conventional concrete, translate into a clear advantage of the former over the latter. As the modulus of elasticity is lower, loss of pre-stressing also decreases, thus reducing the adverse effects of support sinking. As the thermal dilation coefficient is lower, movements of thermal origin also decrease and thus it is possible to reduce the number of joints on long bridges.

Durability — With the use of lightweight concrete, structures usually last longer and their maintenance is less costly.

Experimental tests performed by (Magalhães et al 2002) showed that LWC presents a better behaviour than NDC regarding durability aspects.

In Germany, Holland and Norway, lightweight concrete has been used intensely in the construction of large bridges of all kinds (fluctuating, cable-stayed, by successive advances, etc.), (Daly 2000). From 1960 to 1973, 15 large-span bridges were built in Holland using expanded clay aggregate. After 1970, several bridges were constructed with fly-ash lightweight aggregate.

2.5 Lightweight concrete properties

Concrete is a heterogeneous material whose properties depend upon the individual properties of the mixture components and their compatibility. Different lightweight aggregates can significantly differ from each other. Their properties depend mainly on the material natural condition and sequent transformation process. This transformation process can influence the properties of natural aggregates that need posterior processing. Lightweight aggregates that result from industrial by-products are only altered within certain limits. Lightweight aggregates that consist of natural products have properties that depend mainly on its origin, (BE96-3942/R2 1998).

The main influence of lightweight aggregates on the concrete properties is due to the fact that they occupy more than 50% of the lightweight concrete total volume. The aggregate properties influence some of the concrete ruling properties like: workability, compressive strength, modulus of elasticity, density and durability. The knowledge on the aggregate properties is very important to predict the resulting concrete properties, (BE96-3942/R1 1998).

Lightweight concrete is usually produced for structural or insulating purposes. Compressive strength and modulus of elasticity are the most influencing properties when it is used as a structural material. The most recommendable aggregates for structural concrete, are expanded clay, shale and slate, but other natural aggregates can also be used. Volcanic ashes can be added to obtain high values of compressive strength. The disadvantage is the tendency to attain higher density values.

If the intention is an insulating material, then the thermal conductivity is of most interest. The value of thermal conductivity grows with decreasing concrete density. Low-density aggregates should be used to produce a lightweight concrete with proper insulating properties. Perlite, vermiculite and expanded plastic particles are the recommended aggregates to produce a lower than 800 kg/m³ density concrete. The

respective compressive strength is however very small. With a combination of expanded clay and glass aggregates, a structural concrete with less than 800 kg/m³ density can be obtained, (BE96-3942/R2 1998).

2.5.1 Aggregates shape and texture

The shape and texture of aggregate particles of diverse origin and production methods can differ considerably. The aggregate shape can vary from highly angular to almost perfectly spherical and its surface can vary from rough and porous, to smooth and dense. The cylindrical rotational kiln produces the most rounded particles, especially when clay, shale or slate, are previously prepared.

The choices on raw materials and production methods have a determinant influence on the particles surface. The differences on porosity and particle surface, verified on the large variety of existing aggregates, will particularly influence the behaviour of the aggregate with respect to water absorption on fresh concrete. This aspect will influence mixing, transporting, pumping and casting procedures for fresh concrete.

Good workability is important for concrete pouring and vibration. A certain amount of water should be added to lightweight aggregates before mixing other components, in order to saturate the particles porous surface and prevent their high water absorption during transport, pouring and vibration procedures. Workability is also improved with the addition of a superplasticizer to the mixture.

There is an efficiency loss on the vibration of lightweight concrete when compared to normal density concretes. This process is improved by enlarging the vibration period, reducing the concrete layers size, using higher vibration frequencies or even using a higher number of vibrating devices, (BE96-3942/R1 1998).

2.5.2 Coefficient of thermal expansion

Generally, lightweight aggregates (LWA) suffer lower thermal expansion than normal density aggregates (NDA), which is reflected in the thermal expansion of concrete. A range of typical values is given in Table 2.1. As presented here, the thermal expansion coefficient of LWA varies from one type to another. The thermal expansion coefficient of LWC is probably dominated by the coefficient of the paste, due to its greater stiffness thus a major difference between the various LWAC is not to be expected.

The coefficient of thermal expansion of lightweight expanded clay, shale or slate has been reported to be 50 to 70% lower than that of gravel, (CEB-FIP 1977). The coefficients of thermal expansion of hardened LWAC’s made with these aggregates can vary between

7×10^{-6} and 11×10^{-6}/ºC. The coefficient of thermal expansion is substantially affected by the moisture content. Smeplass (referred in BE96-3942/R2 (1998)) has determined the coefficient of thermal expansion for high strength LWAC and high strength NWC. The values varied between 8×10^{-6} and 10×10^{-6}/ºC. It was concluded that there is no significant influence of the LWA type. As presented in Table 2.1, a different opinion is expressed by Neville et al. (1987), for whom the linear coefficient of thermal expansion of LWAC made with different aggregates varies between 3.8×10^{-6} and 14.2×10^{-6}/ºC.

Table 2.1 - Coefficient of thermal expansion of LWAC (Neville et al. 1987)

Type of aggregate	Linear coefficient of thermal expansion (temperature range: -22 to +52 ºC) (10^{-6}/ºC)
Pumice	9.4 to 10.8
Perlite	7.6 to 11.0
Vermiculite	8.3 to 14.2
Cinders	about 3.8
Expanded shale	6.5 to 8.1
Expanded slag	7.0 to 11.2
NWC limestone (Newman, 1993)	8 to 9

2.5.3 Compressive strength

A high number of factors influence LWAC compressive strength. The excellent bond between the aggregate particles and the cement matrix and the similarity between mortar and aggregates modulus of elasticity guarantee the good behaviour of the composite. In general, concrete failure does not happen with separation or relative displacement between phases. Instead, failure occurs with the collapse of the structure formed by the cement paste over the aggregate particles, and the failure line crosses the particles, opposite to what happens on conventional concretes.

For normal density concrete, with compressive strength up to 80 MPa, cracking develops at the paste and at the interface between aggregate and paste, which is typical of a composite material. Between 80 MPa and 100 MPa of concrete strength, cracking begins to penetrate the aggregates. In this case, concrete behaves as a homogeneous material in which the load capacity of paste and aggregates is similar. When compressive strength is higher than 100 MPa, aggregates are the weaker element and concrete behaves again in a heterogeneous way, (Almeida 2005). These observations made for high strength normal density concrete have in common with LWAC the fact that the aggregates properties are more important to the concrete behaviour than in conventional normal density concretes. LWAC behaviour could be described as the one observed for normal density concretes with 80 MPa to 100 MPa of concrete strength.

As the aggregate compressive strength is relatively low, the cement paste strength and its arch effect over the aggregate particles conditions the lightweight concrete compressive strength. Various authors established that the maximum compressive strength value attained for lightweight concrete with silica fume addition is around 100 MPa.

To produce high strength lightweight concrete, it is necessary to use lightweight aggregates with higher compressive strength. Compressive strength and modulus of elasticity for the aggregate and the paste are closer than verified for NWC, resulting in a more homogeneous material, with an improved behaviour.

According to Thorenfeldt (1995), lightweight concrete is not so influenced by the specimens' type or speed of load application, as it happens for NWC. According to this author, the relation between compressive strength obtained with cubes and with cylinders is more dependent on the type and quantity of lightweight aggregate used. This is an aspect to consider, as there are standards, like NP EN 206-1 (2005) that define lightweight concrete compressive strength based on tests with cylinders and then establish a fixed relation between cubes and cylinders values results. This can lead to the incorrect estimation of this value.

2.5.4 Modulus of elasticity

LWAC modulus of elasticity depends on the aggregates used, their mixture proportion and bond achieved between aggregates and mortar. Modulus of elasticity for LWA is lower than for aggregates normally used to produce NWC. Due to the high percentage of lightweight aggregates present in the mixture, a decrease on the modulus of elasticity value is expected when compared to NWC.

According to Smeplass (1992), modulus of elasticity is around 20 to 30% inferior to NWC for high strength concretes with 60 to 90 MPa compressive strength and water/binder ratio between 0.32 and 0.43. A reduction on the water/binder relation has no effect on this parameter. According to Hammer et al. (1995) and Curcio et al. (1998), there is a good correlation between modulus of elasticity and compressive strength for LWC.

A lower modulus of elasticity value for a structural element made of lightweight concrete means that this element is more flexible, considering that stiffness is defined as the product of modulus of elasticity and second moment of area, *EI*. Reduced stiffness can be beneficial for specific situations, and the use of lightweight concrete should be considered in these cases instead of normal weight concrete. In cases requiring improved impact or dynamic response, where differential foundation settlement may occur, and in certain types or configurations of shell roofs, the property of reduced stiffness may be desirable, (ACI 2003).

The lower stiffness of LWA particles and the often higher cement content result in larger deformations, (Newman 1993). These larger deformations, however, are somewhat offset in LWA reinforced concrete by the lower self weight and the higher modular ratio ($E_{steel}/E_{concrete}$), which increases the equivalent moment of area of the cracked section. In prestressed concrete, however, there are no such relieving circumstances. The lower stiffness leads to a higher camber and less relief can be expected as the dead load is generally less, (Bardhan-Roy et al. 1995).

2.5.5 Stress-strain relationship

When compared to NWC, the LWAC stress-strain curve presents in general a more linear ascending branch, a more limited plastic strain and a steeper descending branch. As compressive strength rises, linear brittle behaviour frequently occurs. This will appear in concrete with moderate strength too, when moderate density LWA is combined with a high strength cementitious matrix, (Thorenfeldt 1995).

The more brittle stress-strain relationship for LWAC, which has also been found by Curcio et al. (1998), is probably attributable to a greater compatibility between the LWA particles and the surrounding cementitious matrix. In the case of NWC, the formation and propagation of small micro-cracks, 2 to 5 μm, have long been recognized as the cause for concrete failure and the stress-strain curves non-linearity, particularly clear near the ultimate stress level, (BE96-3942/R2 1998).

2.5.6 Tensile strength

Concrete tensile strength is an important property, considering cracking. Regarding this property, the main differences between NWC and LWAC are:

- The failure surface crosses the aggregates instead of going around them;
- The total water quantity is higher, which can lead to a tensile strength reduction;

According to Zhang (1992), LWAC presents smaller values for splitting tensile strength than NWC. For Curcio et al. (1998), the relation between flexural tensile strength and splitting tensile strength for LWAC varies between 1.5 and 1.6.

For Weigler et al (1972), LWAC compressive strength grows faster than tensile strength. The relation between tensile and compressive strength varies between 5 and 15% for concretes whose compressive strength is higher than 20 MPa. Smeplass (1992) verified that LWAC with natural or lightweight sand present tensile strength values similar to the ones obtained for NWC of the same strength class. According to Curcio et al (1998),

splitting tensile strength corresponds to 6-6.5% of compressive strength measured in cylinders while flexural tensile strength corresponds to 9.8-10.5% of the same value.

Lightweight concrete splitting tensile strengths vary from approximately between 75 to 100% of normal density concrete with similar compressive strength. Replacing lightweight fine aggregate with normal weight fine aggregate will normally increase tensile strength. Further, natural drying will increase tensile-splitting strength, (ACI 2003).

2.5.7 Fracture energy

Fracture energy is defined as the necessary energy to create the opening of a unitary area crack. Curcio et al. (1998), and Hoff et al. (1995) verified that the values for LWAC fracture energy are only a bit lower than the ones for NWC. Smeplass (1992) obtained fracture energy values for LWAC corresponding to 50% of the ones obtained for NWC with the same cylinder compressive strength. Both results indicate that fracture energy for LWAC is smaller than fracture energy for NDC.

2.5.8 Shrinkage

Internal transformations caused by chemical reactions and changes on concrete relative internal humidity may result on its change of volume. A volume diminution caused by this phenomenon, which does not result from external applied stresses, is called shrinkage. Shrinkage can be defined as the dimensional variation suffered by concrete elements under constant or variable thermal-hygrometric conditions and in the absence of external applied stresses.

The shrinkage phenomenon is caused by:

- evaporation of free water used for mixing that was not used on cement hydration;
- the volume of hydrated cement constituents being inferior to the sum of water and cement dry constituents;
- the concrete cure temperature causing its initial dilatation and later contraction, when the temperature equilibrium with the exterior is re-established.

The total shrinkage deformation considers the contribution of shrinkage caused by different effects. However, only two types of shrinkage will be analysed within this work, as they will have importance on structural behaviour:

- *Autogenous shrinkage*, that is associated with the chemical reactions and sequent reduction on concrete internal relative humidity; it does not depend on the external relative humidity conditions;

- *Drying shrinkage*, that is associated with the volume reduction caused by the loss of internal humidity resulting from transfer with the external environment.

The porous structure of lightweight aggregates may contribute to higher concrete permeability. In the same way, the aggregates can work as small water "containers" that will influence the water presence and transport in concrete. The water transport through concrete is the most important cause for shrinkage or swelling. The aggregate properties will therefore have major influence on the way shrinkage develops.

A higher paste quantity is necessary to produce LWAC with the same compressive strength as NWC. As the paste content influences the shrinkage evolution, higher values of shrinkage are expected for LWAC when compared to NWC, when both present the same compressive strength.

Shrinkage tests performed in a dry room resulted in drying shrinkage of structural LWAC of 0.4 to 1.0‰. This is about 1 to 1.5 times the final shrinkage strain of NWC of equal strength, (Cembureau 1974). A final shrinkage of 0.5 to 0.6‰ has been found, (CEB-FIP 1977), for LWAC made with expanded shale and expanded clay, with compressive strength of 30 to 50 MPa, stored at 20 ºC and 65% RH. These shrinkage values are only indicative, as they depend on the particular way of curing and size of the specimen used in the tests.

Hofmann et al. (1983) performed shrinkage tests with different concretes. A difference in shrinkage strains of about 30% was found.

According to Theissing et al. (referred in BE96-3942/R2 (1998)), shrinkage in LWAC is usually higher if compared to NWC, particularly for low compressive strength values. For concrete with cylinder strength of 21 MPa at 28 days, the shrinkage after 1 year was 35% higher than that of NWC.

If the aggregate particles are partially or totally saturated and then used in mixtures with a low value for the water/binder relation, the aggregates existing water can compensate the diminution of the water present on the cement paste. This water, supplied by the aggregates, will compensate relative humidity diminution on the paste and therefore will reduce autogenous shrinkage. This phenomenon is known as "internal cure".

Moisture movement from the paste to the environment is at first partly compensated by the water stored in the porous aggregates. This causes a time lag of LWAC shrinkage when compared to NWC, (Cembureau 1974). Theissing et al. reported the same phenomenon. At first, shrinkage is lower than for NWC because of the aggregate in the moisture. This is a positive aspect in view of early-age shrinkage effects: there is low shrinkage in the period when tensile strength is still low.

During concrete production, the porous LWA influences water absorption, affecting both workability and water/binder ratio. Later, during concrete hardening, the relatively low specific heat value and the high insulating capacity will induce higher hydration temperatures. At this phase, the water that is initially contained in the porous aggregate particles can affect the mixture, resulting in volume variations.

2.5.9 Creep

Creep is characterized by the progressive increase of deformation on concrete elements submitted to constant stress values and constant or variable thermal and hygrometric conditions. Crystalline slip, non-absorbed water movements, viscous slip or even solubility increase of cement constituents due to applied stresses, can explain this phenomenon.

Creep depends on concrete type, hygrometric conditions, concrete element characteristics, age of concrete when the first load is applied and load magnitude. Creep is variable along time.

A concrete element submitted to compressive stress suffers deformation that can be divided in two parcels: one is the instantaneous deformation that occurs right after the stress application and the other is a deformation that develops in time. The deformation parcel that develops in time is caused by two phenomena: creep and shrinkage. Creep is usually evaluated with the creep coefficient, $\phi(t,\sigma)$, defined in (2.1),

$$\phi(t,\sigma) = \frac{\varepsilon_{cr}(t)}{\varepsilon_{el}(t)} \tag{2.1}$$

where,

$\varepsilon_{cr}(t)$ – total deformation measured between initial moment, t_0 , and final moment, t_{final};

$\varepsilon_{el}(t)$ – elastic deformation measured right after the stress application.

A tendency observed during creep tests on LWAC is that it tends to maintain a higher growth rate for later ages. As the concrete mortar is responsible for creep deformation, there is a stress transfer form mortar to aggregates along time. If the aggregate gets stiffer, more stress is transferred to it and less goes to the mortar. On the contrary, a decrease on the aggregate stresses leads to higher stresses on the cimenticious paste and therefore, to higher concrete creep. The majority of lightweight aggregates present smaller elasticity values than normal density aggregates, which will certainly result in increased stresses on the paste and therefore higher concrete creep. A difference of 20 to 60 % on the creep values of LWC and NWC is to be expected, (BE96-3942/R30 1998). The ultimate value of creep coefficient gets higher with lower concrete compressive strengths.

The CEB Manual for lightweight concrete, (CEB-FIP 1997), refers that creep coefficient is 10 to 20% higher for LWAC than for NWC with similar composition. This document proposes equation (2.2) to establish a relation between creep coefficient for NWC and LWAC,

$$\phi_{LWC} = 1.2 \frac{E_{NDC}}{E_{LWC}} \cdot \phi_{NDC} \tag{2.2}$$

where,

E_{NWC} – modulus of elasticity of NWC

E_{LWC} – modulus of elasticity of LWC

Experimental results collected, (CEB-FIP 1977), reveal that for the same applied stress, LWAC specific creep is of the same magnitude than NWC specific creep. The same report presents typical values for specific creep, varying between 65 e 90 μm/m/MPa. Similar results were presented by other authors, (Cembureau 1974) and (Neville et al. 1987).

Based on the comparison of creep tests performed on LWAC and NWC specimens, Reichard (1964), concluded that after one year, creep measured in LWAC is 20% higher than creep measured in NWC.

The relation between the stress value applied on the creep test and the compressive strength value of the concrete specimen is very important. The same author, (Reichard 1964), evaluated this parameter and confirmed that LWAC creep is proportional to the value of applied stress until around 60% of the concrete compressive strength is reached, similarly to what happens for NWC.

2.6 Other LWAC characteristics

Beside lower self-weight and high insulating capacity, there are other characteristics that turn lightweight concrete into a unique material.

During mixing and pouring, lightweight aggregates influence water absorption, affecting both concrete workability and water/binder ratio. Later, during concrete hardening, the relatively low specific heat and the high isolating capacity will cause high hydration temperatures. The water that is initially present on the porous aggregate particles can affect the mixture hardening process inducing a volume variation that is related to the water variation.

The use of lightweight aggregates can significantly change the concrete behaviour due to the way in which the interaction between the concrete paste and the aggregates takes

place during concrete's life. For hardened concrete, the differences are related with compressive strength and modulus of elasticity. At microscopic level, the differences are located on the contact surface between paste and aggregates. These differences determinate concrete heterogeneity/homogeneity, (BE96-3942/R2 1998). For lightweight concrete, stresses show a more uniform distribution due to the similarity between paste and aggregates stiffness. For this type of concrete, the interface paste-aggregate is of better quality, due to their surface characteristics, cellular structure and relative humidity. There are less micro-cracks in this interface, and the crack pattern is localized.

Under long-term loadings, LWAC compressive strength is approximately 75 to 80% of NWC compressive strength, when low to medium density aggregates are used, and 80 to 85% when high-density aggregates are used, (BE96-3942/R2 1998).

An important aspect to mention is the high temperature attained during concrete curing that can reach 10 to 20ºC more than NWC curing temperature. The risk of premature cracking due to high temperature is however reduced, as a result of the lightweight aggregates deformation capacity.

2.7 Lightweight concrete components

In order to produce LWAC, it is necessary to choose the most adequate raw materials. In such a work, it is important to choose materials that are readily available when needed and that can maintain very similar properties during the period of analysis. So, the choices made were conditioned not only by the materials own characteristics, but also by the national suppliers guarantees on the materials uniformity during work development. A good balance was achieved in this particular aspect and therefore special thanks are addressed to the firms mentioned as suppliers within this item.

2.7.1 Binder

Binders are materials that have the ability to adhere to other materials. They are used in construction to fix or agglomerate other materials (generally inert ones), to cover them with a particular layer or to form more or less plastic pastes that can be initially moulded and later attain the solid state after hardening.

Portland cement was used as a binder material, during this work execution. It was supplied by the portuguese cement producer "SECIL, Companhia Geral de Cal e Cimento, S. A". Cement of type CEM I 52.5 R was chosen to produce a high strength lightweight concrete, (NP EN 197-1 2001).

In general, LWAC needs a higher quantity of cement to attain the same compressive strength of a NWC. This difference is even larger for concretes with compressive strength superior then 40 MPa. According to Newman (1993), a 10% rise on cement quantity results in 5% growth of the respective compressive strength. The water/binder ratio is also a very important parameter, even more influencing than the cement quantity.

2.7.2 Sand

Aggregate materials can be classified as natural or artificial. Gravel and sand are natural aggregates usually dug or dredged from a pit, river, lake, seabed or sedimentary deposits. Crushed stone is an artificial aggregate produced by crushing quarry rock, boulders, cobbles, large-size gravel or scoria granulation.

Sand is one of the raw materials used to produce concrete and is included in the aggregates group. An aggregate material is defined as sand if its maximum dimension is less than 5 mm.

The river sand used was chosen because of its grading and also because it was always available in the local supplier. An important quantity of cement is to be used in order to achieve a high strength concrete. Therefore, the sand did not need to have many fine parts. The respective grading analysis is presented in Table 2.2 and Figure 2.2. The sand maximum size is equal to 4.76 mm and the fineness modulus is equal to 3.09. Current values for the fineness modulus usually vary between 2.7 and 3.0 for high strength concrete, (Aïtcin 1998).

LWAC can incorporate natural sand and also lightweight sand. The use of lightweight sand usually leads to concrete with less workability, (BE96-3942/R2 1998).

Table 2.2 – Grading analysis for the used natural sand

Sieves		Retained weight	% passed
(inches)	(mm)	(g)	
3/8"	9.52	-	100.00
4	4.76	6.77	99.31
8	2.38	104.52	88.69
16	1.19	284.56	59.76
30	0.595	287.61	30.53
50	0.297	202.51	9.95
100	0.149	72.36	2.59
200	0.074	15.49	1.02
Rest		10.02	
Total		983.84	

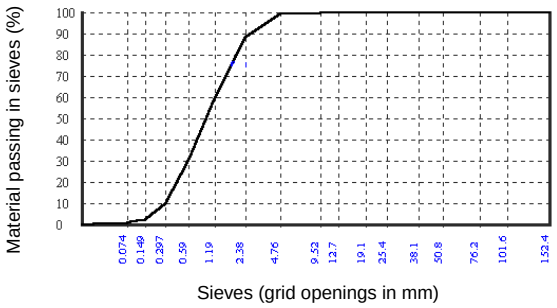

Figure 2.2 - Grading diagram for the natural sand used

2.7.3 Lightweight aggregate

Expanded clay is a coarse clay aggregate with a cellular internal structure and a resistant external surface that is obtained when submitted to a 1200ºC of temperature. These aggregates are the result of clay sintering on a drying and expansion rotational kiln. With this process, clay transforms itself into granular and spherical particles with an alveolar internal structure covered by a high strength external surface of brown colour.

Different types of lightweight aggregate are used throughout the world, covering a high range of materials with different strength capacities. Figure 2.3 presents the relation between crushing strength and particle density of different types of lightweight aggregate.

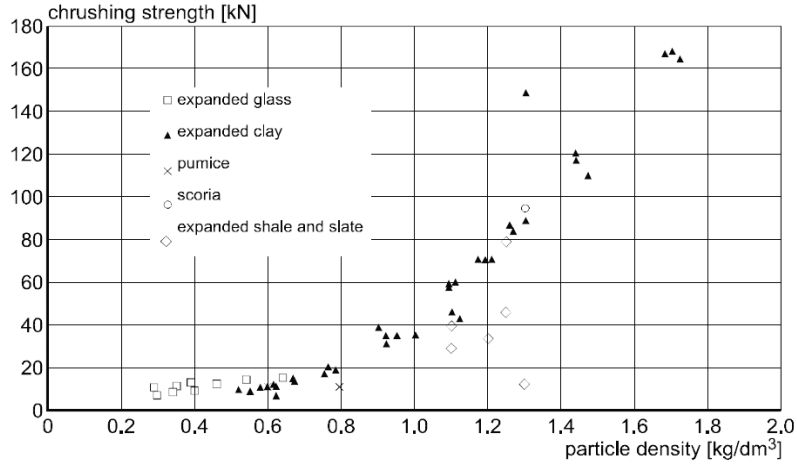

Figure 2.3 – Relation between crushing strength and density of some lightweight aggregate of different origins, (BE96-3942/R2 1998)

Lightweight aggregate properties can differ significantly for different source materials. They mainly depend on the source material natural state and sequent processing method. Their influence on concrete properties is important because approximately 50% of concrete total volume is occupied with lightweight aggregates.

The following characteristics of expanded clay turn this material into an interesting alternative: natural product; durable; light (25% of sand or gravel weight); inorganic thermal insulator; acoustic absorber; fire resistant; inert; resistant to compressive stresses; dimensionally stable.

Expanded clay is used to produce the high strength lightweight concrete proposed in this work. Lightweight aggregates are supplied by the portuguese firm “Maxit - Argilas Expandidas, S. A.” and the special grade Arlita®F7 is chosen, as it is the denser aggregate at disposal. This lightweight aggregate comes from a spanish production unit belonging to the same group, because the portuguese production units and commercial market are still more interested in producing low density aggregates destined for insulating purposes.

A visual aspect of expanded clay Arlita®F7 is presented in Figure 2.4. According to technical specification presented by the supplier, (Maxit 2004), Arlita®F7 aggregate presents a spherical form, light brown colour and particle size between 3 and 10 mm, bulk density varying between 750±50 kg/m^3 and resistance to fragmentation varying between 13.6±3 MPa. Volume stability is smaller than 0.1% of the lost mass and water absorption is less than 15% of its dry mass. Durability to thaw-freeze action is less than 0.18% of the lost mass, durability for alcali-silica reactivity is total and thermal conductivity is less than 0.147 W/mK.

Figure 2.4 – Expanded clay Arlita®F7

The grading analysis for expanded clay Arlita®F7 is presented in Table 2.3 and Figure 2.5. The tests done on the grading of this aggregate show that its maximum dimension is equal to 9.52 mm.

Table 2.3 – Grading analysis of expanded clay type Arlita® F7

Sieves		Retained weight	% passed
(inches)	(mm)	(g)	
1/2"	12.7		100.00
3/8"	9.52	0.31	99.98
4	4.76	1103.64	34.34
8	2.38	565.98	0.68
16	1.19	4.01	0.44
30	0.595	0.10	0.44
50	0.297		0.44
100	0.149		0.44
200	0.074		0.44
Rest		7.34	
Total		1681.38	

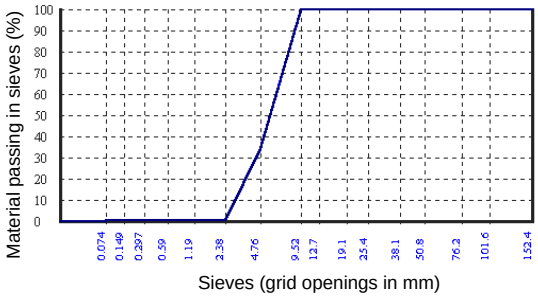

Figure 2.5 - Grading diagram of expanded clay type Arlita®F7

2.7.4 High Range Water Reducing Agent

A high range water reducing agent (HRWRA) is an admixture that allows either an increase on concrete workability or a decrease on the total water quantity used for mixing. Both effects can also be achieved in simultaneous. The HRWRA effects are essentially achieved with its capacity to induce cement molecular dispersion and deflocculation.

The HRWRA used is Glenium52®, which is a new generation superplasticizer, supplied by the portuguese firm "Degussa Construction Chemicals Portugal, S. A." (initially the same product was supplied by was Bettor-MBT).

This product is based on a policarboxilic modified eter chain that allows the possibility of using low water/binder ratios. A good concrete quality associated with high initial compressive strengths and a good aesthetic looks are also achieved.

The principal advantages of using Glenium52® are, (Bettor-MBT 2000):

- its fluidity capacity;
- the diminution on concrete holes formation;
- the increase on initial and final compressive strength, when used as water reducing agent;
- the lower concrete permeability and higher durability, when porosity decreases;
- the capacity to maintain a fluid concrete, with a low water/binder ratio and without segregation or swelling;
- the reduction on cure cycles (in time and temperature), caused by the reduction on the water/binder ratio;
- a better visual look and a better concrete superficial texture;
- improved compactatibility trough vibration.

The recommended dosage is approximately 0.7 to 2.6 kg per 100 kg of cement. It can be reduced or augmented depending on the need for fluidity, water reduction or initial strength. It should be added to the mixture as an individual component. Its best fluidity effect is obtained after the total concrete water is already added. Therefore, it should not be added on dry sand or aggregates.

2.7.5 Water

In concrete mixing, the water function is to give workability properties to concrete and to enhance the adequate development of cement hydration. The low water/binder ratio needed

to achieve a high strength lightweight concrete and the necessary workability are only possible if a high range water reducing agent is added.

The quality of mixing water is defined in (EN 1008 2002). The use of potable water, distributed by public services, is in general considered adequate for concrete mixing. Local water, supplied by Guimarães public water services was used during all the work.

2.8 Studies on concrete mixture

The mixture quantities are evaluated with Faury method, although other methods are available. The water quantity is predefined. It is difficult to determine exactly how much water is absorbed by the lightweight aggregates. Because of this water absorption, the effective W/B ratio will decrease and inside the LWA a “water tank” will be found. This water absorption makes it possible that hydration continues relatively long, namely when at later ages initially absorbed water is transported to the hydrating paste. It is not clear how much water in the mixture will be absorbed by the LWA. Water absorption in a completely water environment or in a concrete mixture is totally different, (BE96-3942/R23 2000). The cement quantity was also predefined, but adjusted with the aggregates grading.

2.9 Concrete production

All lightweight concrete produced within this work is manufactured in laboratory conditions, which makes it easier to maintain the concrete properties and to control the aggregates humidity along time. Before each mixing, the aggregate humidity is measured and proper corrections are made on the concrete total water quantity.

The equipments needed for the mixing procedure are the laboratory mixer (with 120 litters of capacity, vertical axis and rotational mixing blades), a precision balance, containers for each concrete component, vibrator, water supplier and several smaller devices to help dealing with fresh concrete like shovels, spoons and gloves (Figure 2.6).

The mixer equipment walls are always wetted before any component is added. It avoids that concrete water is wasted, conditioning the mixture quantities.

The first task is to join sand together with lightweight coarse aggregate. These two elements should be joined until a homogeneous mix is obtained. As the lightweight aggregate tends to rise up, some water should be added in order to achieve this. This water addition has also the advantage of allowing the aggregate to absorb some water, as this is a highly porous material.

The energy used to mix concrete depends on the equipment in use. Some equipment possess excessive mixing energy for lightweight aggregate and have a tendency to crush it. Reducing the dry mixing period or even substituting the equipment if necessary can avoid the material properties disruption.

The next task is to add cement. The majority of the total water is also added at this phase, resulting in the total cement wetting. The water addition is done little by little, in order to achieve a good dispersion in the mixture. After approximately 2 minutes, the high range water reducing agent is added with the objective of reducing the concrete total water quantity and enhancing the concrete workability. Around 20% of the total water quantity is reserved for this last phase and added together with the high range water reducing agent.

Lightweight concrete production requires some knowledge and care. After mixing, it is necessary to fill all the specimens' moulds. To achieve a proper compaction state, this concrete requires strong vibration, particularly if the consistency is dry. It is to be noticed that an excessive vibration can cause some expanded clay segregation, (Vieira 1999).

First, concrete is introduced into the moulds until half of its capacity. The first vibration is applied, after positioning the moulds on the vibrating table, (Figure 2.7). The vibration duration and energy is defined automatically for a first period of 15 seconds. The moulds total capacity is then fulfilled and they are submitted to a second vibration period. Some fails or irregularities on the concrete exposed surface can be corrected with the aid of a spoon.

Figure 2.6 – Concrete production

Unless the lightweight aggregates are satisfactorily pre-wetted, they may absorb mixing water and subsequently cause difficulty in pumping the concrete. For this reason, it is important to adequately condition the aggregate by fully pre-wetting before batching, (ACI 2003). Pre-wetting minimizes the mixing water being absorbed by the aggregate, therefore minimizing the slump loss. In practice, LWAC is normally loosing its workability faster than NWC.

Figure 2.7 – Concrete vibration

In the present work, the aggregates were not pre-wetted. It was considered that sand and lightweight aggregate could have maximum moisture contents of 1.5% and 5.3%, respectively. The aggregates moisture content was always measured before each casting in order to compensate the total water quantity.

Finally, the moulds are placed on the humidity chamber, if it is the case (Figure 2.8). Concrete specimens, like cubes or cylinders are kept in the humidity chamber until the day of testing. The specimens are not immersed. For larger specimens, as the ones that will be presented in the following chapters, this is not possible due to space limitation. In this case, the concrete surface exposed to the atmosphere is covered with wet textiles, to minimize the concrete water losses. 24 hours after casting, all the specimens are demoulded.

Humidity chamber conditions

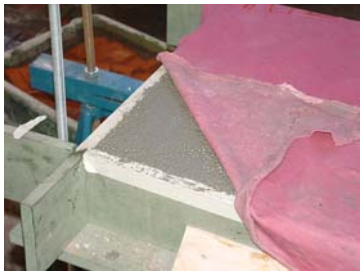

Moulds covered with wet textiles

Figure 2.8 – Test specimens during curing

2.10 Experimental tests

2.10.1 Compressive strength test

The concrete mechanical characterization includes tests for compressive strength. The specimens used to evaluate this parameter are cubes with 100 mm dimension and cylinders with 150 mm diameter and 300mm high (Figure 2.9).

Figure 2.9 – Compressive strength tests on cubes and cylinders

The recommendations referred in document EN 12390-3 (2001) are considered to establish the test procedures. The compressive load is applied with a stress rate that is between 0.2 and 1.0 MPa/s. Compressive strength is calculated establishing a relation between the maximum load and the cross-sectional area of the specimen, (2.3),

$$f_c = \frac{P_{max}}{A} \tag{2.3}$$

where,

P_{max} - maximum load applied to the tested specimen;

A - area of load application.

Three specimens are cast for each different mixing. The compressive strength value of each mixture, f_{cm}, corresponds to the average value calculated from these three results.

2.10.2 Test on modulus of elasticity

The test to determine modulus of elasticity is performed in accordance with document E-397 from LNEC (1993). The test specimen is a cylinder with the same dimensions as the one used for the compressive strength test.

The specimens are loaded incrementally. The load values are calculated to obtain stress values between 0.5 MPa and $0.3 \times f_{cm}$ at the test date. These limits guarantee the concrete elastic behaviour.

Figure 2.10 presents the load application law that was defined for the modulus of elasticity test. The load is established according to rates of stress increase or decrease that can fit between 0.5 and 1.0 MPa/s. When the maximum value is attained, the load is maintained during 60 s. The modulus of elasticity value is determined for each cycle of load/unload, by adjusting a linear trend to the ascending branch of the σ–ε diagram.

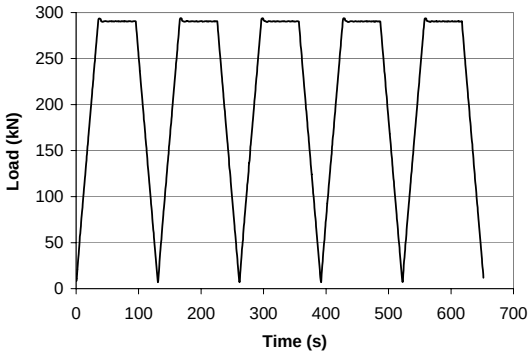

Figure 2.10 – Load application law, defined for the modulus of elasticity test

Five load and unload cycles are repeated for each tested specimen. This number of cycles is considered enough to obtain differences in strain values that are smaller than 10% from one cycle to another. The final value of the tested specimen modulus of elasticity is the mean value taken from the last four cycles. It is considered that the first cycle value is less precise, due to adjustments on the testing machine and setup.

Three specimens are cast for each particular mixture. These three specimens should be tested in a specific date and the concrete modulus of elasticity is the mean value calculated from these three specimens.

To accomplish the necessary measurements, two circular rings are fixed at 1/3 and 2/3 of the concrete specimen high. The rings are concentric with the specimen and fixed to it in 3 points with equal radial spacing. Displacement transducers are positioned at the superior ring in proper support devices localized between the fixing points (Figure 2.11).

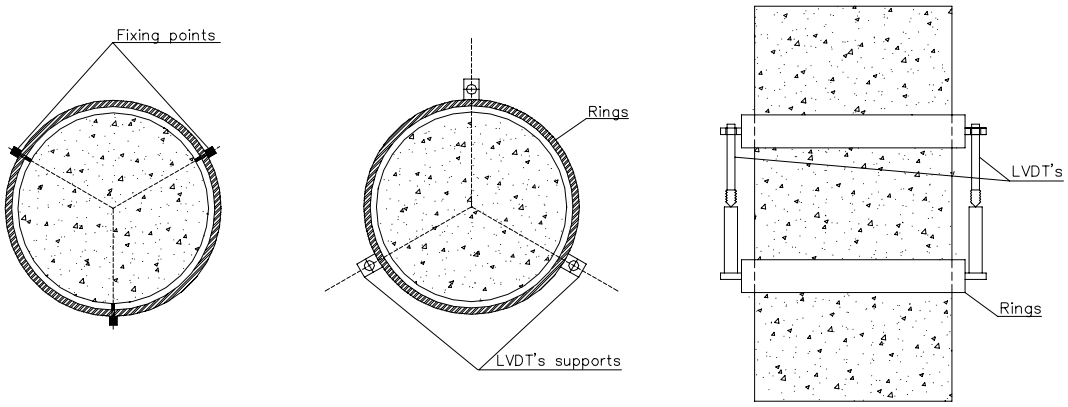

Figure 2.11 – Test setup for the modulus of elasticity test

2.10.3 Splitting tensile strength test

The splitting tensile strength test, represented in Figure 2.12, is done to determine the concrete tensile strength in an indirect way.

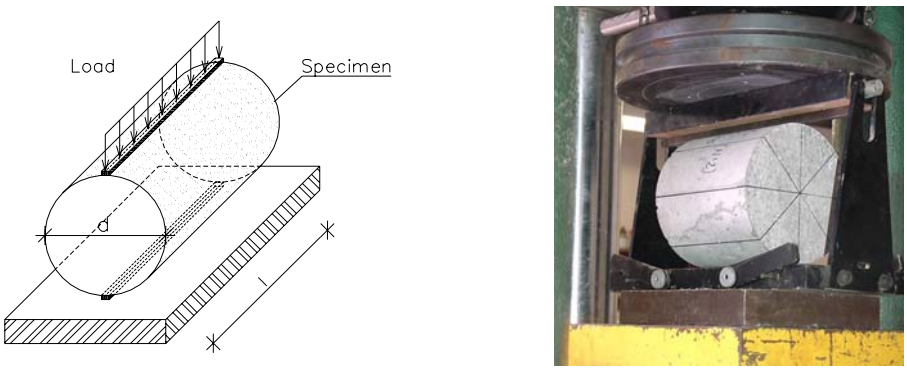

Figure 2.12 – Splitting tensile strength test

The test procedure is defined in EN 12390-6 (2000). The test specimen is a cylinder. In the present case, the cylinders have 150 mm diameter and are similar to the ones used for compressive strength test and for modulus of elasticity test. The cylinder total length is 150 mm in order to keep the specimen within the limits of the testing machine actuator plate during loading.

The test consists on applying a distributed load along two opposite generating lines of the cylinder. To guarantee this, the specimen has to be centred in the testing machine according to the setup presented in Figure 2.12, by using a centring jig.

For the test to be valid, the specimen failure should to be similar to the scheme presented in Figure 2.13. A total separation between two cylinder halves is expected.

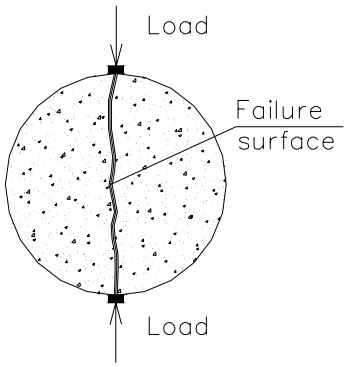

Figure 2.13 – Failure pattern expected on the splitting tensile strength test

The maximum splitting tensile stress applied to specimen is calculated with equation (2.4),

$$f_{ct,sp} = \frac{2P}{\pi D L} \tag{2.4}$$

where,

P – maximum applied load (kN);

L – cylinder length (m);

D – cylinder diameter (m);

2.10.4 Flexural tensile strength and fracture energy test

The flexural test is performed according to standard CPC5 from RILEM (1985). This test allows the evaluation of two important parameters related to the concrete behaviour: flexure tensile strength and fracture energy.

The test specimen is represented in Figure 2.14 and consists on a beam with quadrangular cross section and the following dimensions: b=100 mm, d=100 mm and L=850 mm.

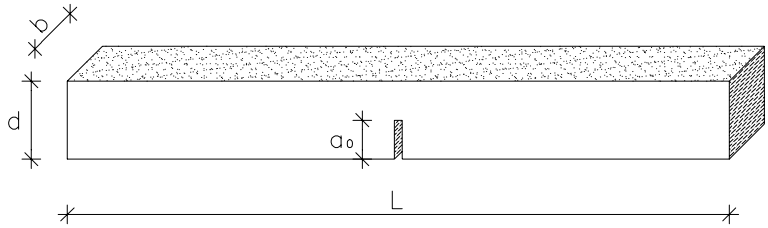

Figure 2.14 – Specimen for flexural tensile strength test

Figure 2.15 presents the test conditions. The beam specimen is simply supported and the load is locally applied on its mid span. The test is valid only when the failure surface is positioned on the beam mid span. A small precise cut is done in the lower fibbers of the beam midspan cross section to guarantee the failure surface position. This cut is represented in Figure 2.14 and Figure 2.15 with the depth a_0.

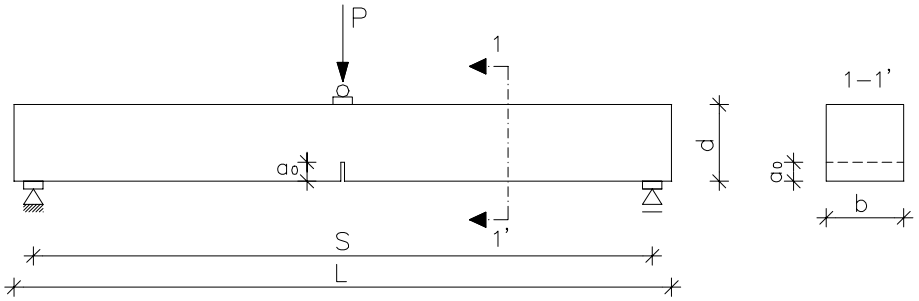

Figure 2.15 – Load and support dispositions for flexural tensile strength test

The hydraulic jack used for these tests has 25 kN maximum load capacity. The supports allow for the beam extremity rotation. One of the supports has the ability to rotate on the bending perpendicular direction in order to reduce the effect of imperfections.

This test is controlled with the beam deformation. The control measure is done at the beam midspan with a high precision displacement transducer, of 5 mm linear measuring length (Figure 2.16). The imposed displacement rate is 3 μm/s and the applied load is such that this required displacement rate is verified. The value of the midspan deformation rate is also calculated according to document CPC5 from RILEM.

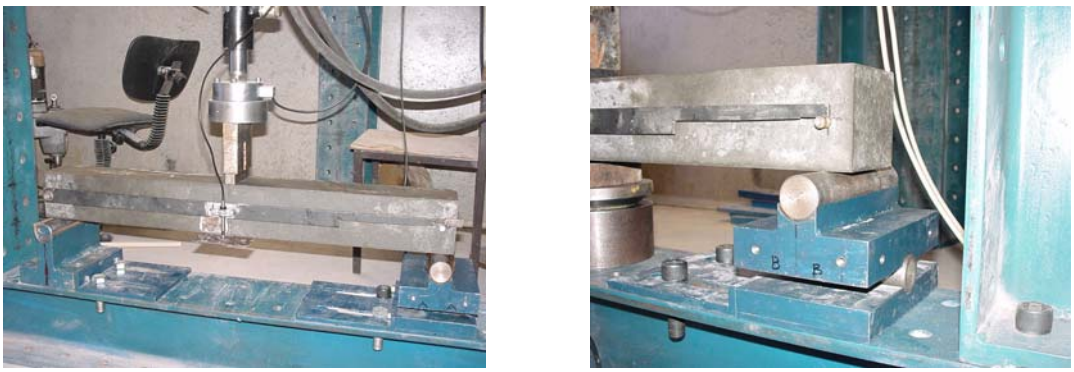

Figure 2.16 – Flexure tensile strength test setup

The measurement and control of loading and displacement is done, taking into account the following conditions:

- the test is performed with deformation control in order to allow the measuring of the beam behaviour after the maximum load is reached;
- the reaction structure stiffness should be sufficiently high in order to guarantee the test stability and the correct measurement readings;
- the load cell should be able to measure forces with 0.1 kN precision;
- the test should be disregarded if the failure surface is not localized on the cross section with cut a_0.

The flexure tensile strength is a result from this test and is calculated, (Barros 1995), with (2.5).

$$f_{ct,fl} = 1.5\frac{\left[P + 0.5\,m_1\,g\left(1-\alpha^2\right) + m_2\,g\right]\cdot S}{b\left(d-a_0\right)^2} \tag{2.5}$$

The fracture energy value is calculated with equation (2.6),

$$G_F = \frac{W_0 + \left[m_1\left(1-\alpha^2\right) + 2\,m_2\right]g\delta_0}{b\left(d-a_0\right)} \tag{2.6}$$

where α is defined with equation (2.7),

$$\alpha = L/S - 1 \tag{2.7}$$

and,

$f_{ct,fl}$ – flexural tensile strength (kPa);

P – maximum applied load (kN);

b – beam cross section depth (m);

d – beam cross section height (m);

a_0 – indent height (m);

L – total length of the specimen (m);

S – distance between supports (m);

W_0 – area calculated from the diagram Load vs. Mid span deformation (Nm);

m_1 – beam mass between supports (kg);

m_2 – mass of devices acting on the beam, whose weight is not registered by the load cell (kg);

g – gravity acceleration = 9.81 m/s^2;

δ_0 – beam deflection at failure, measured at midspan (m).

2.10.5 Shear test

Experimental testing was conducted to evaluate the high strength lightweight concrete shear strength. The testing machine used, allows the simultaneous application of load in two perpendicular directions, one corresponding to an axial loading and the other corresponding to a shear loading. The testing machine allows the test to be controlled either by displacement or load application.

The test characteristics require the use of fixing plates attached to the test specimen to avoid its dislodgment during load application (Figure 2.17). Each plate is fixed to one half of the specimen, creating a pure shear zone. A small gap is left between the two fixing plates, so that they do not touch each other and the failure surface is positioned within the gap.

The shear load is applied through the displacement of the machine inferior plate. To avoid or at least minimize bending effects, small steel pieces are positioned between the fixing plates and the specimen, adjacent to the gap (Figure 2.17). The load is now transferred from the machine to the specimen through these elements in order to minimize its eccentricity.

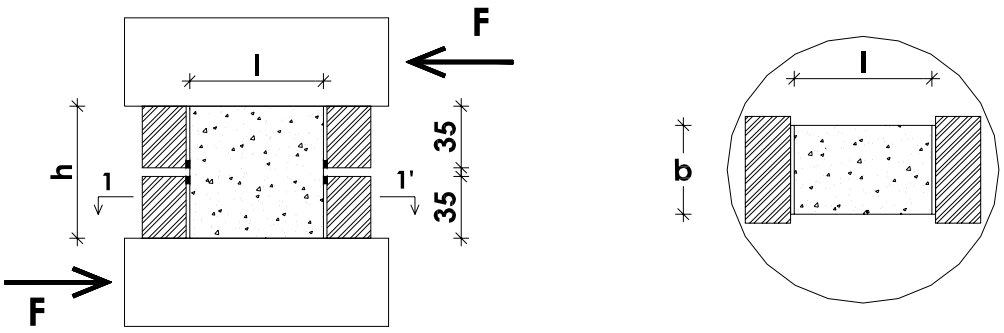

Front view Plan view 1-1’

Figure 2.17 – Shear test setup

The test objective is to induce pure shear stress to the specimen. A small and constant axial load is applied to the specimen before initiating the shear load application, which avoids the specimen rotation during testing. This axial load results in a very small compressive stress value.

As this is not a standard test, some preliminary tests are performed to define the specimen dimensions. The machine load limits and fixing plates size condition these dimensions. The final choice is a parallelepiped with approximately l = 75 mm, b = 50 mm and h = 75 to 80 mm, as represented in Figure 2.17.

The shear strength is calculated by relating the maximum applied force and the resulting shear failure area, (2.8),

$$\tau = \frac{F}{A_{shear}} \tag{2.8}$$

where,

P – maximum applied load (kN);

A_{shear} – shear failure area (m^2).

2.10.6 Shrinkage test

The shrinkage phenomenon can be studied by measuring autogenous and drying shrinkage. Two cylinders of 150 mm diameter and 300 mm high are used to measure shrinkage strains, (Figure 2.18). One of them is covered with aluminium adherent sheets that prevent humidity changes between the specimen and the environment. This cylinder is used to measure autogenous shrinkage. The other cylinder has no protection and is used to measure total shrinkage. Drying shrinkage results from the difference between total and autogenous shrinkage, and is calculated considering the measurements done with both cylinders.

Not isolated specimen Isolated specimen

Figure 2.18 – Shrinkage test setup

Strain gauges are glued to the cylinders in order to measure shrinkage strains. They are aligned with two specimen longitudinal axes (Figure 2.18) and positioned in radial opposite positions. The strain gauges are supplied by TML®, type PL-60-11, (TML 2001). The gauge length is 60 mm and its resistance is 120 Ω. Measurements are recorded along time with the acquisition system MGCPlus®, from HBM, (HBM 2000).

In the absence of a test chamber with temperature and humidity controlled conditions, the specimens are kept in a room where temperature and relative humidity are less variable than the exterior ones. These parameters values are also registered along time.

The strain gauges measurements are corrected because of temperature variation. The thermal dilatation coefficient for lightweight concrete is not experimentally measured. Therefore, a mean value of $6 \times 10^{-6}/^{o}C$ is used for calculations.

The absence of a chamber with temperature and humidity controlled conditions is not important as could be thought, because the idea is to compare the obtained results in these specimens with the ones obtained in other structural elements kept in the same room.

2.10.7 Creep test

The creep test uses similar specimens to the ones chosen for the shrinkage test: two cylinders of 150 mm diameter and 300 mm high (Figure 2.19). An initial load is applied to the cylinders and maintained for a pre-determined period that should be at least equal to six months. In the present case, the concrete creep test is maintained for around 410 days.

By testing two specimens, one isolated and the other not isolated, it is possible to evaluate the importance of the humidity interaction with the environment. The specimens' preparation is similar to what was done for the shrinkage test specimens (item 2.10.6).

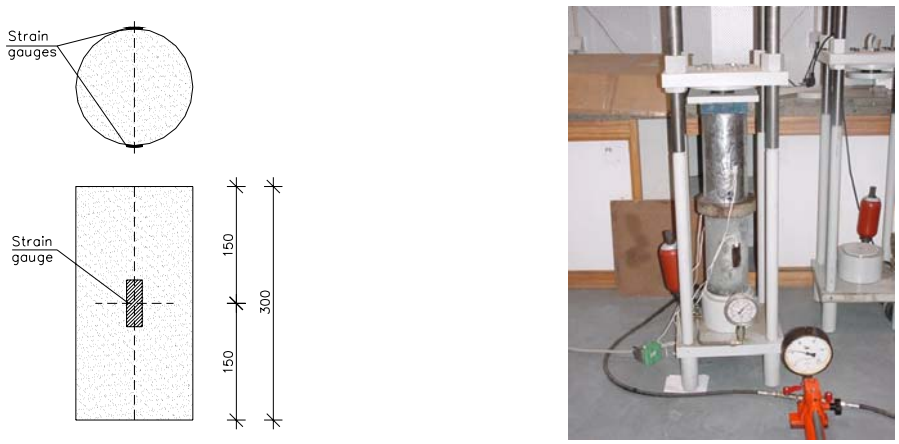

Figure 2.19 – Creep test setup

The testing equipment is hydraulic and allows the application of a constant axial load. The testing frame is specifically designed to compensate the specimen volume changes, so that the axial load maintains its value along time. The two cylinders are vertically disposed, so that the same axial stress is applied to both (Figure 2.19).

As for the shrinkage test, the measurements done along time are corrected because of temperature variation. The thermal dilatation of $6x10^{-6}/^{o}C$ is considered.

2.11 Experimental results obtained

2.11.1 Composition

The aim of this work phase is to evaluate the mechanical characteristics of a high strength lightweight concrete (HSLWC). This concrete was initially planned to be LC 45/55 or LC50/60. As mentioned before, the Faury method is used to choose the proper mixture. Water and high range water reducing agent (HRWRA) quantities are defined in order to obtain a good concrete workability and a low water/binder ratio. Expanded clay and natural sand are used as aggregate materials.

The aggregates have always the same source, although they were renewed in time because of the large quantities needed. The grading curves are always determined each time the materials were renewed and the mixture quantities are adjusted to the aggregates grading curves. As the sources are kept, the differences found can be considered irrelevant, as they lead to very small changes.

Table 2.1 – LWAC composition

		Quantity
Arlita® F7 (expanded clay)	(kg/m^3)	525
Natural sand	(kg/m^3)	482
Cement CEM I 52.5 R	(kg/m^3)	475
Water	(l/m^3)	155
HRWRA – Glenium 52®	(l/m^3)	8.0
Void volume	(l/m^3)	40
W/B ratio		0.325

Concrete composition and workability are maintained through the work. The *Slump Test* is used to assess workability. An average *Slump Test* result of 18 cm is verified. The quantities for concrete components are presented in Table 2.1. The void volume is predefined, according to Magalhães (2002).

A large number of mixtures were produced based on the LWAC composition defined in Table 2.1. These mixtures are all referenced as BL followed by a serial number. The

majority of the mixtures produced were done to build the specimens for the studies presented in Chapter 3, 4, 5, 6 and 7. Other mixtures were produced to study and evaluate relevant properties of this lightweight concrete, as will be presented in the following.

2.11.2 Concrete density

The evolution of density and compressive strength with concrete age is evaluated with the reference mix BL15. Three specimens from BL15 are used to determine LWAC oven-dry density. These specimens have different shapes and weights. Table 2.2 shows the values measured. An average value of 1811.5 kg/m^3 is found.

Table 2.2 – BL15 oven-dry density

Mixing ref.	Specimen Ref.	Age (days)	Initial weight (g)	Inside water weight (g)	Outside water weight (g)	Oven-dry weight (g)	Volume (dm^3)	Oven-dry density (kg/m^3)
BL15	S1	3	3097.4	1501.5	3132.6	2968.8	1631.1	1820.1
BL15	S2	3	1336.1	655.3	1349.0	1260.2	693.7	1816.6
BL15	S3	3	1752.7	849.0	1771.3	1658.1	922.3	1797.8
Average value								1811.5

All the tested cylinders of reference mixing BL15 are also weighted and measured right after leaving the humidity chamber. They are presumably saturated, although they are not immersed in water. The corresponding values for this apparent density are presented in Table 2.3. An average difference between oven-dry and apparent density of 82 kg/m^3 is verified, when comparing the results presented in Table 2.2 and Table 2.3.

Table 2.3 – BL15 apparent density

	Age (days)	Weight (g)	Volume (dm^3)	Density (kg/m^3)
BL15-Cylinder 1	3	10026	1910.3	1910.3
BL15-Cylinder 2	3	9996	1914.2	1914.2
BL15-Cylinder 3	3	10079	1920.4	1920.4
BL15-Cylinder 4	7	10023	1916.2	1916.2
BL15-Cylinder 5	7	9757	1862.2	1862.2
BL15-Cylinder 6	7	9814	1866.7	1866.7
BL15-Cylinder 7	28	9880	1873.0	1873.0
BL15-Cylinder 8	28	9920	1883.7	1883.7
BL15-Cylinder 9	28	9980	1914.4	1914.4
BL15-Cylinder 10	90	9925	1878.4	1878.4
BL15-Cylinder 11	90	9881	1879.5	1879.5
BL15-Cylinder 12	90	10016	1898.8	1898.8
Mean value				1893.2

2.11.3 Compressive strength

As referred in 2.11.1, a large number of concrete mixes have been done, based on the composition presented in Table 2.1. In 18 of those mixes, cubic specimens were cast for compressive strength evaluation, at 7 and 28 days of age. These specimens use a smaller quantity of concrete than cylinders (1 litre for cubes instead of 5.3 litres for cylinders) and are suitable for evaluating both the compressive strength and the results variability.

Table 2.4 presents the results of compressive strength determined in 100 mm edge cubic specimens. The analysis of Table 2.4 results shows that the compressive strength evolution in time is not significant. An average increase of 3 MPa is measured between 7 and 28 days of concrete age. The results on variation coefficient are small, which means that a good homogeneity on compressive strength results is obtained.

Table 2.4 – Compressive strength determined in cubes at age of 7 and 28 days

	Age	$f_{lc,\ Cube1}$	$f_{lc,\ Cube2}$	*Average (C1,C2)*	$(f_{lci}-f_{lcm})^2$		Age	$f_{lc,\ Cube1}$	$f_{lc,\ Cube2}$	*Average (C1,C2)*	$(f_{lci}-f_{lcm})^2$
	(days)	(MPa)	(MPa)	(MPa)			(days)	(MPa)	(MPa)	(MPa)	
BL3.1	7	61.13	59.51	60.32	2.63	BL3.1	28	61.13	60.93	61.03	16.31
BL3.2	7	58.86	57.83	58.35	12.94	BL3.2	28	63.33	-	63.33	3.02
BL4.1	7	59.16	58.81	58.99	8.74	BL4.1	28	58.06	59.11	58.59	42.04
BL4.2	7	63.37	-	63.37	2.04	BL4.2	28	69.70	56.31	63.01	4.26
BL5.1	7	64.39	60.97	62.68	0.54	BL5.1	28	68.86	71.71	70.29	27.21
BL5.2	7	64.22	63.75	63.99	4.17	BL5.2	28	67.86	-	67.86	7.79
BL8.1	7	65.79	63.98	64.88	8.66	BL8.1	28	66.21	65.49	65.85	0.61
BL8.2	7	64.73	63.62	64.17	4.98	BL8.2	28	65.46	-	65.46	0.15
BL9.1	7	64.97	-	64.97	9.17	BL9.1	28	65.09	63.91	64.50	0.32
BL9.2	7	65.19	65.81	65.50	12.67	BL9.2	28	63.96	68.53	66.24	1.38
BL10.1	7	61.39	60.70	61.05	0.80	BL10.1	28	62.74	65.59	64.16	0.82
BL10.2	7	52.52	59.10	55.81	37.60	BL10.2	28	64.83	64.07	64.07	1.00
BL11.1	7	65.79	63.72	64.75	7.91	BL11.1	33	61.58	66.76	64.17	0.81
BL11.2	7	65.68	59.29	62.48	0.29	BL11.2	33	64.61	60.60	62.60	6.07
BL12.1	7	61.19	60.77	60.98	0.92	BL12.1	28	68.68	-	68.68	13.04
BL12.2	7	62.40	66.08	64.24	5.29	BL12.2	28	67.81	68.71	68.26	10.19
BL13.1	7	59.72	-	59.72	4.95	BL13.1	28	68.37	68.60	68.49	11.68
BL13.2	7	58.37	59.04	58.71	10.47	BL13.2	28	66.12	-	66.12	1.11
f_{cm}	61.94					f_{cm}	65.07				
Δ	3.74					Δ	5.08				
δ	6.0%					δ	7.8%				

where Δ is the standard deviation and δ is the variation coefficient.

Cylinders are also used to evaluate the concrete compressive strength evolution along time. These specimens are tested at 3, 7, 28 and 90 days for the reference mixes BL15 and BL16. The corresponding results are presented in Table 2.5.

Figure 2.20 presents the obtained results for BL15. This concrete achieves a high compressive strength of 48.4 MPa, early at 3 days of age. At 7 days, the compressive strength value is 53.6 MPa and from this moment until the 28 days of age, it increases to 54.3 MPa. At 90 days of age, a value of 55.3 MPa is measured, which means that from 7 to 90 days, the compressive strength shows hardly any evolution. Two reasons can be appointed to this fact: one is the use of cement CEM I 52.5 R, which confers high initial strength to concrete and the other is a lightweight concrete characteristic, referred by many authors, (BE96-3942/R2 1998).

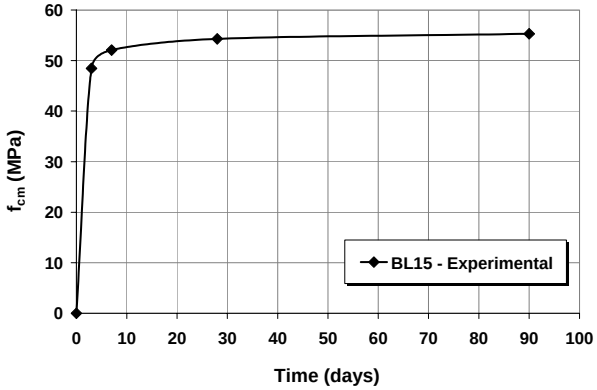

Figure 2.20 – Concrete compressive strength evolution with age

Smeplass (1992) verified that the compressive strength growth between 28 and 90 days is usually low and decreases for higher LWAC compressive strength. This author assumed this to be a consequence of the compressive strength limits imposed by the lightweight aggregate.

EN 1992-1-1, (CEN 2004a), proposes an equation to estimate the value of compressive strength for normal density concrete, in different ages. Coefficient $\beta_{cc}(t)$, from equations (2.9) and (2.10) establishes the relation between the concrete compressive strength measured at 28 days of age and the concrete compressive strength measured at another concrete age,

$$f_{cm}(t) = \beta_{cc}(t) \cdot f_{cm} \tag{2.9}$$

$$\beta_{cc}(t) = \exp\left\{ s\left[1 - \left(\frac{28}{t/t_1} \right)^{1/2} \right] \right\} \tag{2.10}$$

where,

t_1 = 1 day;

t – concrete age at the considered moment;

s – coefficient that accounts for the cement type (in this case, s = 0.20).

Table 2.5 – Compressive strength values for reference mixings BL15 and BL16

	Casting date	Concrete age at testing date (days)	f_{lcm} (MPa)	f_{lcm} Equation (2.9) (MPa)
BL15	05-02-03	3	48.45	36.00
BL15	05-02-03	7	52.09	44.45
BL15	05-02-03	28	54.29	54.29
BL15	05-02-03	90	55.31	59.32
BL16	11-02-03	3	48.30	34.54
BL16	11-02-03	7	-	-
BL16	11-02-03	28	52.10	52.10
BL16	11-02-03	90	54.67	56.91

The hardening coefficient, $\beta_{cc}(t)$, can be estimated for any concrete age. An average value of 0.95 is verified for cubic specimens (Table 2.4), at 7 days of age. The value found for cylinders is even higher: as presented in Table 2.5, a hardening coefficient of 0.98 is found for BL15, for the same age. According to EN 1992-1-1, a value of β_{cc} (t = 7 days) = 0.82 is obtained, which is significantly inferior to what is obtained for LWAC. If the age t = 90 days is considered, than we have a hardening coefficient of 1.02 for BL15 and 1.05 for BL16, while equation (2.9) presents a value of 1.09. These values show that after the 28 days age, the EN 1992-1-1 equations can better predict lightweight concrete compressive strength evolution, although the tendency is to continue having higher growth rates than verified experimentally, as presented in Figure 2.21.

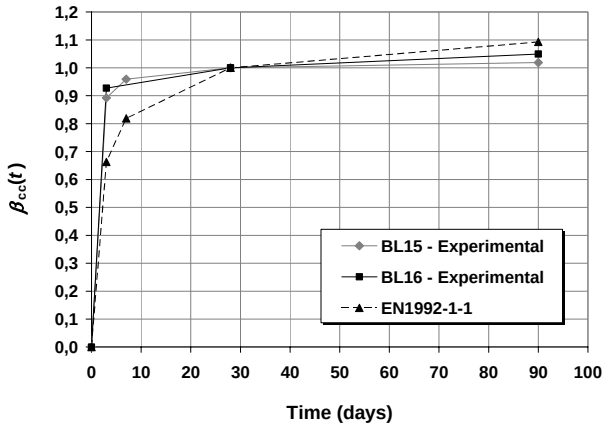

Figure 2.21 – Hardening coefficient for LWAC

Another comparison is established between the compressive strength measured on cubes with 100 mm and cylinders with 150 mm diameter and 300mm high. Both specimens type are tested at the same concrete age, for each different mix. The compressive strength values presented in Table 2.6 are the mean value of three identical specimens.

Table 2.6 – Comparison between compressive strength measured in cubes and cylinders

	Concrete age (days)	$f_{lcm,cubes}$ (MPa)	$f_{lcm,cylinders}$ (MPa)	$f_{lcm,\ cylinders} / f_{lcm,cubes}$
BL2.2	77	71.07	60.30	0.85
BL3.1	70	67.36	61.74	0.92
BL3.2	70	69.03	58.80	0.85
BL4.1	62	68.58	60.13	0.88
BL4.2	62	73.58	60.80	0.83
BL5.1	56	70.04	65.67	0.94
BL5.2	56	66.88	60.58	0.91
Average				0.88

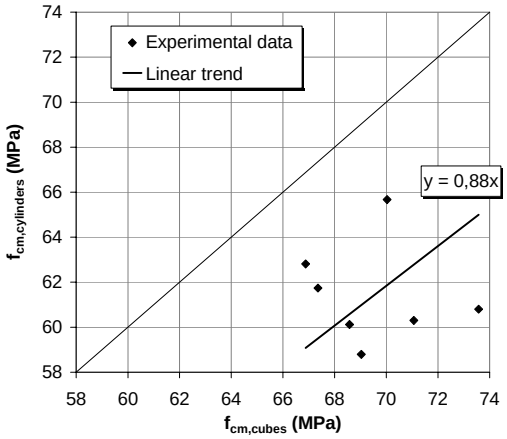

Figure 2.22 - Compressive strength - cubes vs. cylinders

According to NP EN 206-1 (2005), the relation between compressive strength measured for cylinders and cubes is around 0.909 for lightweight concrete and 0.836 for normal density concrete. As presented in Table 2.6 and Figure 2.22, the compressive strength values measured are always higher for cubes than for cylinders. An average value of 0.88 is determined for the relation between cylinders and cubes compressive strength, which is close to the value defined by NP EN 206-1 (2005).

2.11.4 Modulus of elasticity

EN 1992-1-1, (CEN 2004a), proposes equation (2.11) to calculate the modulus of elasticity. This parameter is defined as a function of compressive strength. Equation (2.11) is established for normal density concretes.

$$E_{cm}(t) = 22 \cdot \left(\frac{f_{cm}}{10} \right)^{0.3} \tag{2.11}$$

In case of lightweight concrete, the modulus of elasticity value can be calculated by affecting equation (2.11) with a reducing factor, (2.12). This factor, η_E, accounts for the concrete density, where ρ is the lightweight concrete oven-dry density.

$$E_{lcm}(t) = \eta_E \cdot E_{cm}(t) \tag{2.12}$$

$$\eta_E = (\rho/2200)^2 \tag{2.13}$$

ACI (2003) recommends expression (2.14) to calculate the value of modulus of elasticity, where C = 0.038.

$$E_c = \rho \cdot C \cdot \sqrt{f_c'} \tag{2.14}$$

According to Zhang et al (1990), equation (2.15) establishes the relation between compressive strength and modulus of elasticity for lightweight concrete.

$$E_c = 1.19 \cdot \sqrt[3]{f_{ck}^2} \tag{2.15}$$

The norwegian standard, (NS 1998), proposes equation (2.16) to determine modulus of elasticity value. Again, this parameter is defined as a function of concrete compressive strength and density.

$$E_c = 9500\, f_c^{0.3} \cdot (\rho/2200)^2 \tag{2.16}$$

The modulus of elasticity test is carried out for mix BL16 at the ages of 3, 7, 28 and 90 days. The test is also repeated at 7 and 28 days for mix BL42. Three specimens are tested at each concrete age and the respective average value is considered. Table 2.7 presents the corresponding results.

Table 2.7 also presents the results of using equations (2.11) to (2.16) on the experimental results for compressive strength. An average oven-dry density value of 1820 kg/m^3 is considered, based on the results obtained in 2.11.2.

Table 2.7 – Compressive strength and modulus of elasticity for BL16 and BL42

	Concreting date	Concrete age at testing date	f_{lcm}	E_{lcm}	E_{cm} Equation (2.12)	E_{cm} Equation (2.14)	E_{cm} Equation (2.15)	E_{cm} Equation (2.16)
		(days)	(MPa)	(GPa)	(GPa)	(GPa)	(GPa)	(GPa)
BL16	11-02-03	3	48.30	20.27	24.15	20.51	15.78	20.81
BL16	11-02-03	7	-	22.10	-	-	-	-
BL16	11-02-03	28	52.10	23.07	24.70	21.30	16.60	21.28
BL16	11-02-03	90	54.67	23.32	25.06	21.81	17.14	21.59
BL42	24-03-04	7	56.43	21.63	25.30	22.16	17.51	21.80
BL42	24-03-04	28	59.54	23.17	25.71	22.77	18.14	22.15

Figure 2.23 presents the evolution with concrete age of the experimental results on modulus of elasticity for mix BL16. The same figure presents the modulus of elasticity values that result from applying equations (2.11) to (2.16) on the compressive strength experimental values. The curves are established for comparison purposes.

The use of EN 1992-1-1 equations (2.11) to (2.13), results in higher values for modulus of elasticity than the experimentally measured. On the opposite, both Zhang and NS 3473 equations, (2.15) and (2.16) respectively, underestimate the modulus of elasticity values, although equation (2.14) from ACI and equation (2.16) from NS 3473 give better approximations. The results are very similar between these two equations.

There is some discrepancy on the absolute results given by the proposed equations. For the first days of concrete age, 3 and 7 days, the modulus of elasticity experimental values tend to grow faster and the growing rate does not meet any of the proposed equations. However, it is important to notice that, after the 28 days of concrete age, the modulus of elasticity growing rate is similar for all curves.

Equations (2.11) to (2.16) are defined for any type of lightweight concrete. It is possible that the use of another type of lightweight aggregate in the same concrete mixture can conduce to different modulus of elasticity values, which can justify the variability observed in Figure 2.23.

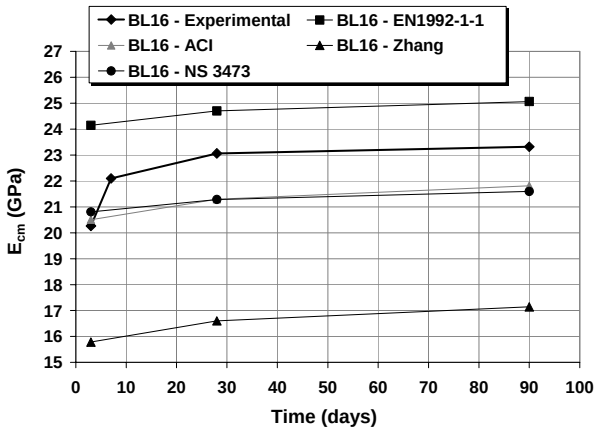

Figure 2.23 – Modulus of elasticity evolution with concrete age

It is evident from the obtained results that the modulus of elasticity of lightweight concrete is smaller than the modulus of elasticity of normal density concrete. The coefficient η_E shows that lightweight concrete modulus of elasticity is around 30% inferior to the expected values for normal density concrete.

2.11.5 Splitting tensile strength

The splitting tensile strength test, represented in Figure 2.12, is suited to determine the concrete tensile strength. The test is performed on cylindrical specimens with 150 mm diameter and 150 mm high. The tested specimens should present a constant failure pattern that is defined by a failure surface that crosses the specimen, unifying the opposite lines of load application (see Figure 2.13). Figure 2.24 presents some of the tested specimens, confirming the expected type of failure and validating the tests.


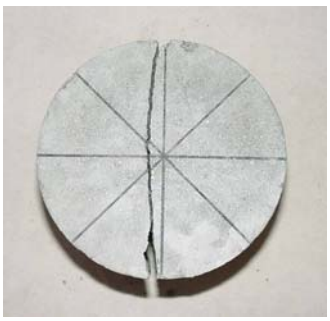


P3 P5 P7

Figure 2.24 – Observed failures during the splitting tensile strength test

The maximum tensile stress applied to the specimen is calculated with equation (2.17),

$$\sigma_c = \frac{2P}{\pi D L} \tag{2.17}$$

where,

P – applied load (kN);

L – specimen length (m);

D – specimen diameter (m).

According to EN 1992-1-1, (CEN 2004a), the tensile strength of a normal density concrete can be estimated with the splitting tensile strength test, taking into account equation (2.18),

$$f_{ct} = 0.9 \cdot f_{ct,sp} \tag{2.18}$$

where,

f_{ct} - concrete tensile strength;

$f_{ct.sp}$ - concrete splitting tensile strength.

EN 1992-1-1 establishes a relation between tensile strength of normal density concrete and respective compressive strength with equation (2.19),

$$f_{ct} = 0.3\, f_{ck}^{2/3} \tag{2.19}$$

in which, f_{ck} is the characteristic concrete compressive strength.

According also with EN 1992-1-1, it is possible to calculate lightweight concrete tensile strength from the tensile strength of normal density concrete with equation (2.20).

$$f_{ct,LWC} = f_{ct,NWC}\left(0.4 + 0.6\frac{\rho}{2200}\right) \tag{2.20}$$

The relation (2.18) will also be used for lightweight concrete.

According to Zhang et al (1990), it is possible to establish a relation between the compressive strength value and the tensile strength value of lightweight concrete, as defined by equation (2.21),

$$f_{ct,sp} = 0.23 \cdot \sqrt[3]{f_{ck}^2} \tag{2.21}$$

The test is repeated for 3, 7, 28 and 90 days of concrete age. Figure 2.25 shows the obtained results.

The tested specimens are cast with mix BL15. The results presented for each age are the average value determined from three identical specimens. The use of equations (2.18) to (2.21) takes into account the compressive strength values of mixing BL15 presented in Table 2.5.

Concrete age	$f_{lct,sp}$ (Experimental)	$f_{lct,sp}$ Equation (2.20)	$f_{lct,sp}$ Equation (2.21)
(days)	(MPa)	(MPa)	(MPa)
3	2.77	3.97	3.06
7	3.12	4.17	3.21
28	3.25	4.28	3.30
90	3.47	4.34	3.34

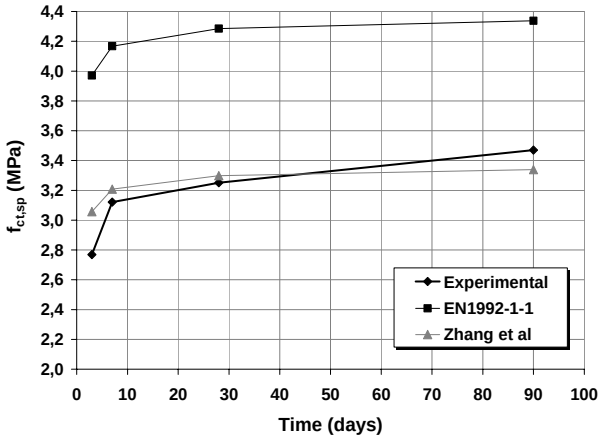

Figure 2.25 – Evolution of lightweight concrete splitting tensile strength along time

The values for splitting tensile strength experimentally determined are very close to the values that result from applying equation (2.21). EN 1992-1-1 equations result in significantly higher values for this property. The experimental testing for splitting tensile strength shows that this property tends to grow faster, in time, than predicted by the standard equations.

2.11.6 Flexural tensile strength and fracture energy

The flexural tensile strength test is done on prismatic specimens, as defined in 2.10.4. The experimental study is done with specimens from mixes BL42 and BL43, at the concrete ages of 7 and 28 days. Three specimens are tested at each concrete age and the final result considers the average value calculated from the three results.

Table 2.8 presents the specimens' dimensions on failure zone, the maximum load applied during the tests and the corresponding maximum tensile stress.

Table 2.8 – Flexural tensile stress

Concrete Ref.	Specimen Ref.	Concrete age (days)	$d - a_0$ (cm)	b (cm)	P_{max} (kN)	$f_{lct,fl}$ (MPa)	$f_{lctm,fl}$ (MPa)
BL42	V1	7	7.41	10.17	1.81	4.17	
BL42	V2	7	7.44	10.10	1.91	4.35	4.26
BL42	V3	7	7.41	10.15	1.85	4.25	
BL42	V5	28	7.41	10.11	1.81	4.16	4.16
BL42	V6	28	7.41	10.05	1.81	4.17	
BL43	V7	28	7.57	10.09	1.73	3.84	
BL43	V8	28	7.57	10.10	1.74	3.87	3.84
BL43	V9	28	7.56	10.15	1.72	3.81	

The results presented in Table 2.8 for lightweight concrete tensile strength present a reduced variability. Maximum applied force and tensile strength tend to maintain a constant value between 7 and 28 days for mixing BL42. An average value of 4.26 MPa at 7 days and 4.16 MPa at 28 days confirm this observation. The comparison of values measured at 28 days for BL42 and BL43, shows that tensile strength has small variation from one mixing to another, although a small decrease is verified for BL43.

At 7 days, tensile strength results for BL42 present a standard deviation of 0.09 MPa and a variation coefficient of 2.1%. At 28 days, tensile strength results present a standard deviation of 0.03 MPa and a variation coefficient of 0.6% for BL42 and a standard deviation of 0.04 MPa and a variation coefficient of 1.0% for BL43.

Using parameters measured in the same test, it is possible to calculate the value of fracture energy. Table 2.9 resumes the obtained results on fracture energy. Average values of 68.02 N/m at 7 days of age (BL42) and 78.42 N/m at 28 days of age (BL43) are found. The value of fracture energy measured at 7 days is around 87% of the value determined at 28 days of concrete age (although the comparison is between two different mixings). This means that lightweight concrete fracture energy has also a reduced evolution in time. At 7 days fracture energy results present a standard deviation of 2.58 N/m and a variation coefficient of 3.8%. At 28 days fracture energy results present a standard deviation of 2.24 N/m and a variation coefficient of 2.9%. The variability on fracture energy results is very similar for both concrete ages.

It is verified that the values of fracture energy obtained for lightweight concrete are smaller than the values obtained for normal density concretes produced with the same quantity of cement and similar compressive strength, (Camões 2002).

Table 2.9 –Fracture energy

Concreting Ref.	Specimen Ref.	Age of testing (days)	m_1 (kg)	m (kg)	δ_0 (mm)	A_{lig} (m^2)	W_0 (Nm)	$G_{F,i}$ (N/m)	$G_{F,m}$ (N/m)
BL42	V1	7	15.15	19.77	0.747	0.00754	0.3895	70.82	
BL42	V2	7	14.87	19.49	0.637	0.00752	0.3731	65.75	68.02
BL42	V3	7	14.76	19.37	0.695	0.00752	0.3761	67.48	
BL42	V5	28	15.02	19.64	-	0.00749	-	-	-
BL42	V6	28	14.93	19.54	-	0.00744	-	-	-
BL43	V7	28	14.70	20.98	0.834	0.00764	0.4440	80.51	
BL43	V8	28	15.02	21.30	0.858	0.00764	0.4228	78.70	78.42
BL43	V9	28	14.78	19.39	0.841	0.00767	0.4239	76.08	

2.11.7 Shear strength

Lightweight concrete shear behaviour is a parameter that needs further study, as there is little information on the subject. As for other concrete properties, experimental testing is defined in order to better evaluate this property.

The test and specimens characteristics, as described in 2.10.5, require the use of fixing plates to avoid the specimen displacement during the application of load. The shear load is applied with a minimum eccentricity to minimize bending moments. The axial load is applied with a very small value, just to avoid the specimen's rotation. The test objective is to induce pure shear stress on the specimens and therefore the resulting compressive stress needs to be very small.

Some preliminary tests were performed in order to assess the proper test procedures. During these tests, it was verified that the specimens' behaviour is not ductile. The reduced deformability makes deformation control very difficult, even with high precision transducers as the ones used, with 1 mm of linear measuring length. Failure is rapidly attained even when a low deformation rate is imposed. As a result, it was decided to perform the tests with load control. A load rate of 0.1 kN/s is defined. This load rate value allows a suitable test control and is within the load cell control limits. The maximum load allowable for this equipment is 20 kN.

The specimens' failure follows a common pattern that is in accordance with the expected failure type. Figure 2.26 presents some of the specimens, after testing.

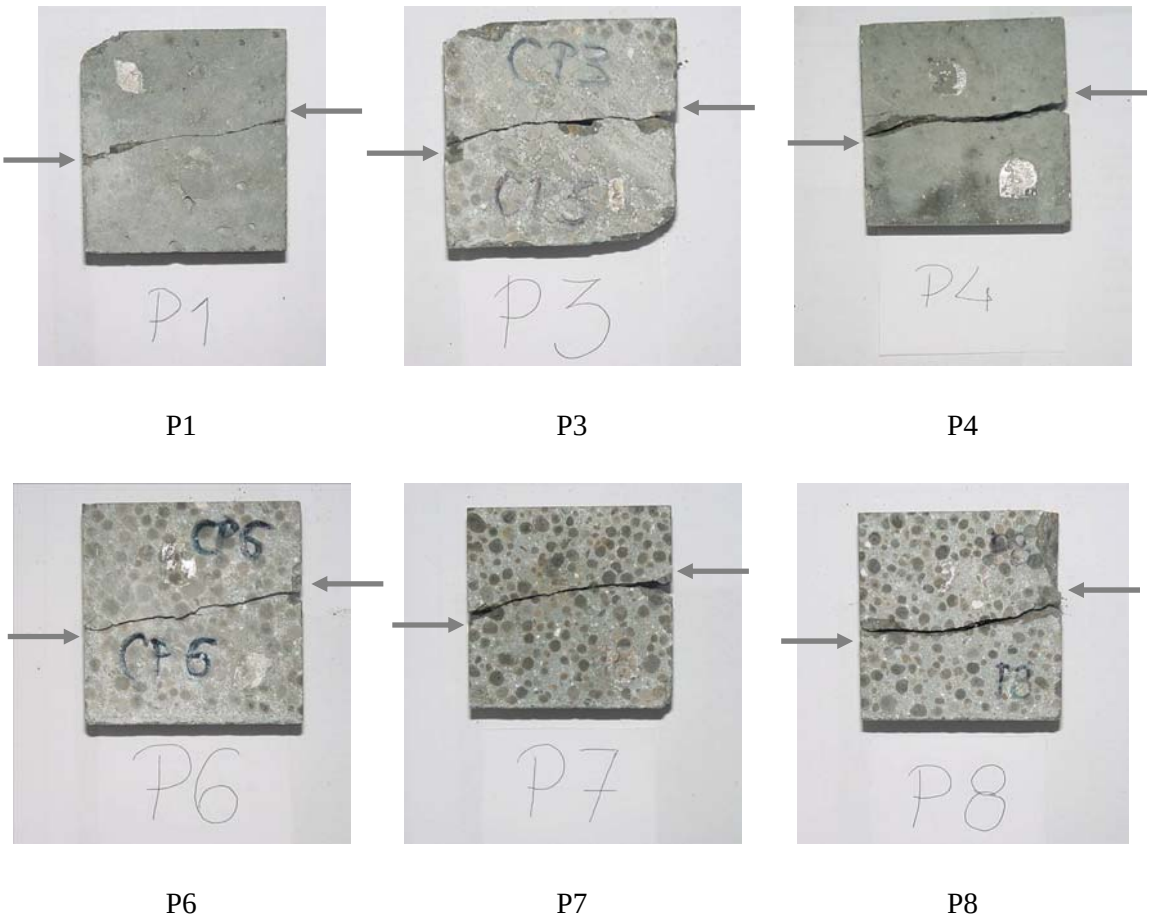

Figure 2.26 – Failures observed on shear test

The maximum shear stress applied to each specimen is calculated according to equation (2.22),

$$\tau_{lc} = \frac{P}{bl} \tag{2.22}$$

where, P is the maximum applied load; b is the cross section minor dimension and l is the cross section maximum dimension.

Table 2.10 presents the dimensions of the specimens used in the shear test, the failure load values and the maximum corresponding shear stress. A_{shear} is the cross section area ($= b \times l$), $N_{average}$ is the average axial applied during the test procedure and $\sigma_{average}$ is the average axial load divided by the shear area.

Although the axial load value is not the same for every test, all the specimens tested at 28 days of concrete age are considered in the following calculations. It is considered that the value of compressive stress is sufficiently small to have little influence on the shear stress strength. A shear strength average value of 3.71 MPa is found at 28 days of concrete age. At this age, shear strength results present a standard deviation of 0.50 MPa and

variation coefficient of 13.4%. Comparing to the test results already presented for other concrete properties, it is clear that shear strength results present higher variability. This has probably to do with the test procedure itself and the difficulties on maintaining the proper conditions for the test to be performed.

Table 2.10 – Specimens dimension for shear test, failure load and maximum shear stress

Specimen Ref.	Age of testing	b	l	h	A_{shear}	P	τ_{lc}	$N_{average}$	$\sigma_{average}$
	(days)	(m)	(m)	(m)	(m^2)	(kN)	(kPa)	(kN)	(MPa)
BL43_CP_1	28	0.0464	0.0705	0.0812	0.0035	12.678	3643.1	170.5	0.049
BL43_CP_2	28	0.0465	0.0778	0.0760	0.0036	13.862	3831.8	213.5	0.059
BL43_CP_3	28	0.0473	0.0790	0.0761	0.0037	16.413	4392.4	510.5	0.137
BL43_CP_4	28	0.0477	0.0774	0.0760	0.0037	15.880	4301.3	510.0	0.138
BL43_CP_6	28	0.0480	0.0776	0.0782	0.0037	11.254	3021.5	410.4	0.110
BL43_CP_7	28	0.0484	0.0795	0.0772	0.0038	13.676	3554.2	203.5	0.053
BL43_CP_8	28	0.0506	0.0763	0.0787	0.0039	15.832	4100.8	2015.6	0.522
BL43_CP_9	28	0.0500	0.0790	0.0771	0.0040	14.473	3664.0	232.9	0.059
BL43_CP_10	28	0.0493	0.0794	0.0774	0.0039	11.378	2908.4	244.0	0.062
BL43_CP_11	28	0.0507	0.0780	0.0766	0.0040	14.667	3708.8	215.8	0.055
BL43_CP_12	28	0.0484	0.0777	0.0771	0.0038	13.036	3466.3	218.2	0.058
BL43_CP_13	28	0.0495	0.0776	0.0774	0.0038	10.967	2855.0	238.1	0.062
BL43_CP_16	28	0.0498	0.0811	0.0753	0.0040	15.701	3887.6	213.1	0.053
BL43_CP_17	28	0.0472	0.0761	0.0778	0.0036	14.116	3934.1	518.8	0.145
BL43_CP_18	28	0.0497	0.0770	0.076	0.0038	16.812	4393.1	203.0	0.053
Average value							3710.8		

Further testing is needed on this concrete property in order to have a larger number of results. This would allow a better assessment on the results variability.

One possibility for other studies is to change the test configuration. In the present case, the equipment available put some geometrical restraints when the specimens were defined. A second step is to consider various levels of axial stress in order to find a relation between normal stress and shear stress. This aspect is important when lightweight concrete under shear stress is also confined, which is thought to be the case on the specimens with Perfobond connectors to be analysed in Chapter 3 where shear strength is important.

2.11.8 Relation between compressive strength and density

Table 2.11 presents the results on density, compressive strength and modulus of elasticity for several concrete mixings. These results are all obtained on specimens with more than 120 days of age. Each value presented in Table 2.11 is the average result of three specimens tested at the corresponding age. It was observed in 2.11.3 that both compressive strength and modulus of elasticity tend to grow slower for older concrete ages. A

comparison between the properties presented in Table 2.11 can be established for all the mixings presented, considering that the influence of concrete age is now diminished.

Table 2.11- Density, compressive strength and modulus of elasticity, tested after 120 days of age

Ref.	Age (days)	Density (kg/m^3)	$f_{lcm,i}$ (MPa)	$E_{lcm,I}$ (GPa)	Ref.	Age (days)	Density (kg/m^3)	$f_{lcm,i}$ (MPa)	$E_{lcm,i}$ (GPa)
BL8.1	332	1976.8	62.57	27.72	BL8.2	332	1987.1	64.19	28.14
BL9.1	330	1966.5	65.79	29.30	BL9.2	330	1935.0	64.14	27.78
BL10.1	324	1835.4	56.20	25.47	BL10.2	324	1854.2	56.96	24.79
BL11.1	316	1853.7	58.36	26.31	BL11.2	316	1860.0	57.38	25.80
BL12.1	307	1916.7	57.36	26.98	BL12.2	307	1925.8	55.93	28.90
BL13.1	297	1886.2	52.43	26.39	BL13.2	297	1851.1	55.07	26.36
BL14.1	272	1924.6	61.98	28.05	BL14.2	272	1906.5	57.08	26.95
BL17.1	195	1892.4	52.73	24.44	BL17.2	195	1905.4	54.71	25.01
BL18.1	187	1868.0	52.01	24.06	BL18.2	187	1873.7	59.96	24.91
BL19.1	181	1914.7	53.61	24.27	BL19.2	181	1913.0	57.25	25.08
BL20.1	142	1936.8	62.40	25.27	BL20.2	142	1890.6	55.03	24.51
BL21.1	139	1946.6	55.58	26.45	BL21.2	139	1932.9	54.76	25.01
BL22.1	152	1783.6	53.29	22.48	BL22.2	152	1787.6	54.84	22.28
BL23.1	179	1771.2	55.17	22.32	BL23.2	179	1795.2	54.10	22.80
BL24.1	179	1881.0	65.83	28.13	BL24.2	179	1834.3	56.64	27.91
BL25.1	171	1825.0	59.38	26.33	BL25.2	171	1807.8	56.78	25.62
BL26.1	135	1830.6	55.61	24.07	BL26.2	135	1821.6	55.05	24.39
BL27.1	133	1826.3	56.64	24.43	BL27.2	133	1811.4	52.62	24.51
BL28.1	126	1812.3	54.09	22.45	BL28.2	126	1812.5	52.69	22.46
BL29.1	130	1821.9	57.18	24.37	BL29.2	130	1817.7	56.77	24.58

The values presented in Table 2.11 result in a mean compressive strength value of 56.9 MPa, associated with a standard deviation of 3.80 MPa and a variation coefficient of 6.7%. This last value is reduced validating the values previously presented in 2.11.3 and the homogeneity of results.

As for density, the values presented in Table 2.11 result in a mean density value of 1870 kg/m^3, associated with a standard deviation of 57.5 kg/m^3 and a variation coefficient of 3.1%.

Figure 2.27 is focused primarily on the relation between density and compressive strength. There is an observable relation between these two variables: compressive strength tends to grow with increasing density. The correlation coefficient is equal to 0.53, which means that the correlation between density and compressive strength is not as strong as could be expected. It is possible that this result is influenced by the fact that the same LWAC composition is used and therefore the range of density and compressive strength values obtained is not sufficiently wide.

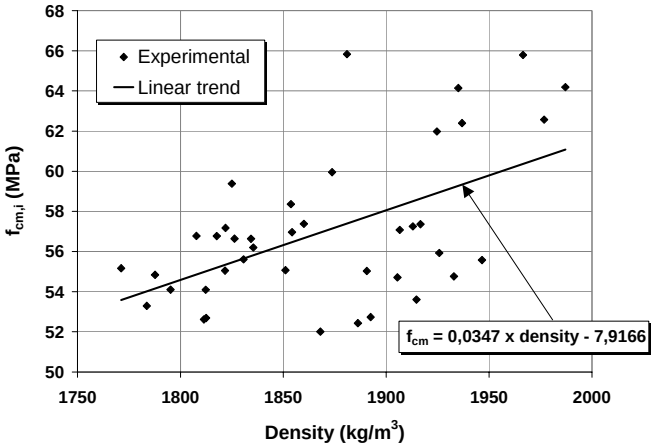

Figure 2.27 – Relation between compressive strength and density

2.11.9 Relation between modulus of elasticity and density

Table 2.11 presents the results on compressive strength and modulus of elasticity for several concrete mixings. The analysis on the values presented in Table 2.11 result in an average value of 25.4 GPa for the modulus of elasticity, associated with a standard deviation of 1.88 GPa and a variation coefficient of 7.4%. The variation coefficient for modulus of elasticity is a bit higher than for compressive strength, but is still a small value. This means that there is also a small variability associated with this parameter.

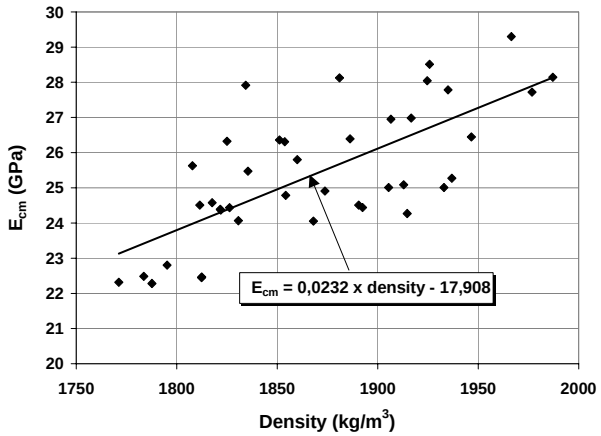

Figure 2.28 – Relation between modulus of elasticity and density

According to Figure 2.28, there is a close relation between modulus of elasticity and concrete density. The correlation coefficient is equal to 0.71, which means that there is a stronger relation between modulus of elasticity and density than between compressive strength and density.

2.11.10 Relation between modulus of elasticity and compressive strength

A relation can also be established between modulus of elasticity and compressive strength measured in cylinders, as presented in Figure 2.29. According to this figure, there is a close relation between modulus of elasticity and concrete compressive strength. The correlation coefficient is equal to 0.69, which means that there is also a strong dependence between these two variables.

The curves that result from equations (2.12) and (2.16) are also plotted in the same figure. The value considered for the oven-dry density is 1820 kg/m^3. Both of these curves, (EN 1992-1-1 and NS 3473), show the same growing rate. The variation on the experimental compressive strength values results in a higher variation on the modulus of elasticity values than reflected by EN 1992-1-1 or NS 3473 standard curves.

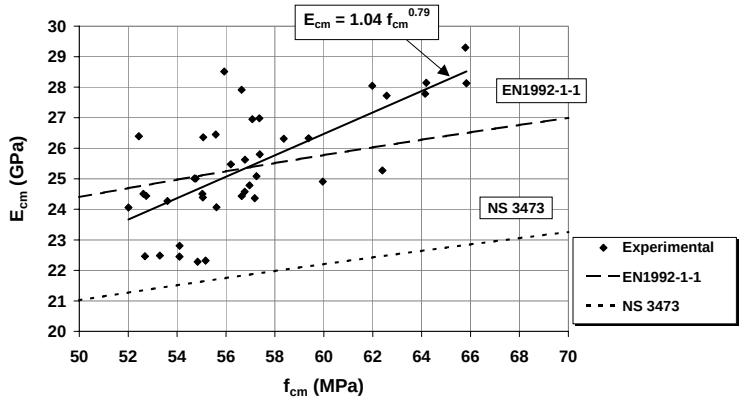

Figure 2.29 – Relation between modulus of elasticity and compressive strength

2.11.11 Ratio between flexure tensile strength and compressive strength

Table 2.12 presents the results for tensile strength previously discussed in 2.11.6 and the corresponding results for compressive strength determined in cylinders. The specimens used in both tests come from mixing BL43 and are tested at the same concrete age. A comparison between these two parameters is then established.

According to Curcio et al (1998), flexure tensile strength corresponds to 9.8-10.5% of compressive strength measured in cylinders. The ratio between tensile strength and compressive strength experimentally measured and presented in Table 2.13 is only a bit smaller than found by Curcio.

For Weigler et al (1972), the relation between tensile and compressive strength varies between 5 and 15% for lightweight concretes whose compressive strength is higher than 20 MPa. This range of values is in agreement with the values experimentally determined.

Table 2.12 – Ratio between flexure tensile strength and compressive strength

Concrete Ref.	Specimen Ref.	Concrete age (days)	f_{lc} (MPa)	$f_{ct,fl}$ (MPa)	$f_{ct,fl\ ,average}$ (MPa)	$f_{ct,fl}$ / f_c (%)
BL42	V1	7	56.43	4.17	4.26	7.6
BL42	V2	7		4.35		
BL42	V3	7		4.25		
BL42	V5	28	59.54	4.16	4.16	7.0
BL42	V6	28		4.17		
BL43	V7	28	59.07	3.84	3.84	6.5
BL43	V8	28		3.87		
BL43	V9	28		3.81		

2.11.12 Ratio between splitting tensile strength and compressive strength

Table 2.13 presents the results for tensile strength previously discussed in 2.11.6 and the corresponding results for compressive strength determined in cylinders. The specimens used in both tests come from mix BL15 and are tested at the same concrete age.

According to Curcio et al (1998), splitting tensile strength corresponds to 6-6.5% of compressive strength measured in cylinders. The experimental results obtained confirm this observation.

According to Zhang (1992), LWAC presents smaller values for splitting tensile strength than NWC. According to EN1992-1-1 equations (2.18) and (2.19), this observation is confirmed. In the case of a NWC with compressive strength values identical to the ones presented in Table 2.13, values of 4.43 to 4.84 MPa are expected for splitting tensile strength. These values are significantly higher than the ones determined experimentally.

Table 2.13 – Ratio between splitting tensile strength and compressive strength

Concrete Ref.	Concrete age (days)	f_{lcm} (MPa)	$f_{lctm,sp}$ (MPa)	$f_{lctm,sp}$ / f_{lcm} (%)
BL15	3	48.45	2.77	5.7
BL15	7	52.09	3.12	6.0
BL15	28	54.29	3.25	6.0
BL15	90	55.31	3.47	6.3

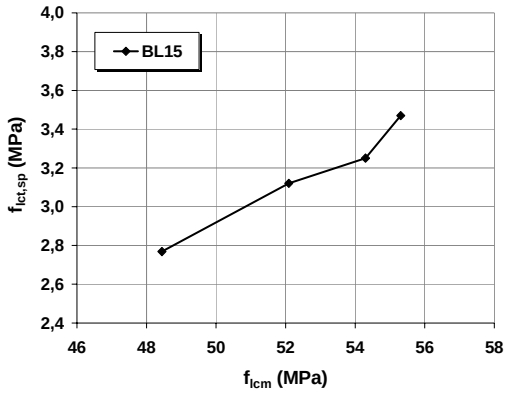

2.11.13 Ratio between flexure tensile strength and splitting tensile strength

The comparison between Table 2.12 and Table 2.13 results shows a higher ratio between flexure tensile strength and compressive strength than between splitting tensile strength and compressive strength.

Table 2.14 – Ratio between splitting tensile strength and compressive strength

Concrete Ref.	Concrete age	f_{lcm}	$f_{lctm,sp}$ (Experimental)	$f_{lctm,fl}$ (Experimental)	$f_{lctm,fl}$ / $f_{lctm,sp}$
	(days)	(MPa)	(MPa)	(MPa)	
BL15	7	52.09	3.12		1.37
BL42	7	56.43		4.26	
BL15	28	54.29	3.25	-	
BL42	28	59.54	-	4.16	1.28
BL43	28	59.07	-	3.84	1.18

According to Curcio et al (1998), the relation between flexure tensile strength and splitting tensile strength varies between 1.5 and 1.6. In the present case, there is a good proximity between these two parameters, although flexure tensile strength tends to be higher than splitting tensile strength.

2.11.14 Shrinkage

Concrete shrinkage is influenced by environmental conditions like temperature variation or relative humidity. If the test is done on a special chamber, with constant temperature and relative humidity values, then it is only necessary to consider the initial and the final strain values in order to calculate the total shrinkage strain value within a certain period of time, as expressed by equation (2.23).

$$\varepsilon_L = \varepsilon_f - \varepsilon_i \tag{2.23}$$

Equation (2.23) expresses,

ε_L - longitudinal strain;

ε_i - initial strain value;

ε_f - final strain value.

When the test is performed under environmental conditions, it is necessary to consider the strain that results from temperature variation, (2.24).

$$\varepsilon_{LT} = \varepsilon_L - \gamma \times \Delta T \tag{2.24}$$

Equation (2.24) expresses,

ε_{LT} - longitudinal strain, considering temperature variation;

ΔT - temperature variation;

γ - concrete coefficient of thermal expansion.

Autogenous shrinkage is measured in a sealed specimen. The sealing disables the water movements between the specimen and the atmosphere. The specimen used to measure total shrinkage is totally in contact with the surrounding environment. Drying shrinkage results from subtracting autogenous shrinkage value to the total shrinkage value.

The tests performed within this work are carried out in environmental conditions. It is important to point out that the objective is to evaluate the long-term behaviour of some structural elements later presented and therefore it is necessary that the shrinkage test conditions are the same as the structural elements have during their testing period. Therefore, all the measured values are corrected in order to account for the temperature variation.

Temperature varied during the period in which the tests were done. The tests were initiated during January and finalized during February of the following year. Figure 2.30 presents the measured values of temperature for the period in which shrinkage and creep tests took place. As the period of measuring took approximately 400 days, the initial values of temperature are close to the final values measured.

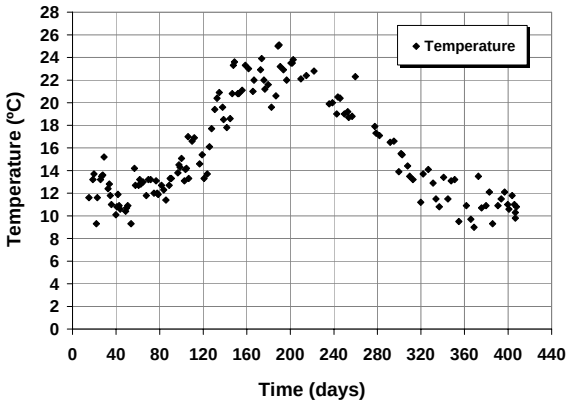

Figure 2.30 – Temperature variation during shrinkage and creep testing period

Relative humidity conditions are recorded along time. It is not possible to correct the measured values in order to consider the effect of relative humidity variation, but it is important to know this parameter evolution in time and evaluate its variation effect on the obtained results.

2.11.14.1 Shrinkage - experimental measurements

Figure 2.31 presents the final shrinkage test diagrams, performed on specimens from mixtures BL35 and BL36. Three curves are plotted: autogenous shrinkage, drying shrinkage and total shrinkage. Autogenous shrinkage is measured with the sealed specimens, total shrinkage is measured with the unsealed specimen and drying shrinkage is calculated from the difference between the values measured in the sealed and in the unsealed specimens.

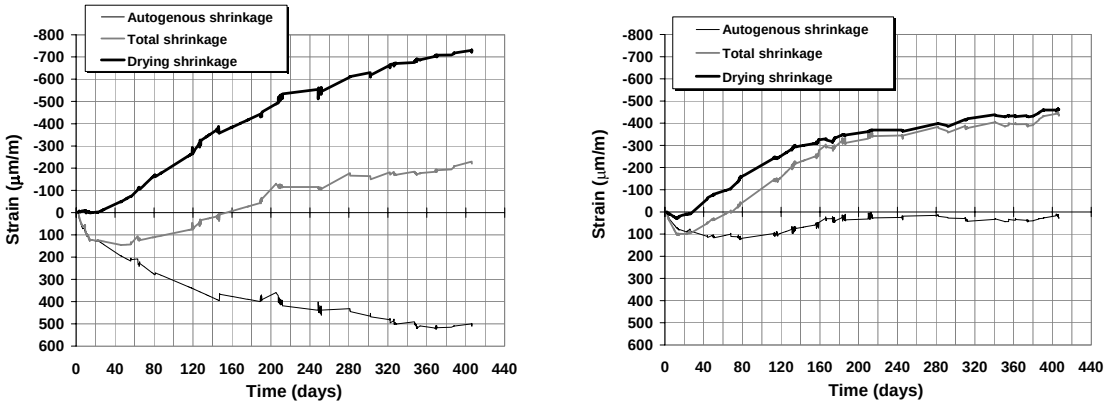

a) BL35 b) BL36

Figure 2.31 – Shrinkage test: autogenous shrinkage, drying shrinkage and total shrinkage experimentally measured

Although the composition used to fabricate BL35 and BL36 is the same, the specimens behaved rather differently. The lightweight concrete in study suffers some initial expansion, until around 160 days of concrete age for BL35 and 80 days of concrete age for BL36. This initial expansion can be explained by the transfer of water between lightweight aggregate particles to the cement matrix, (BE96-3942/R31 2001). From this moment on, the tendency is altered for BL36 and concrete begins to have some autogenous shrinkage. However, the autogenous shrinkage value is not sufficient to compensate the initial expansion, for the period in analysis. From the age of 240 days on, autogenous shrinkage tends to maintain an almost constant value. For BL35, the values of autogenous expansion keep growing until the final measurements.

According to Lourenço et al (2004), the differences observed in the curves of autogenous shrinkage for BL35 and BL36 can result from deficiencies on the protection used to seal the specimen of BL36. However, both specimens of BL35 and BL36 were sealed in the same manner and it is hard to believe that the differences measured can result from this.

In the same way, the values of total shrinkage are higher for BL36 than for BL35, which can result from the autogenous expansion that is compensating some of the drying shrinkage in both specimens, and particularly in the specimen of BL35.

Total shrinkage is higher for concrete BL36 than for concrete BL35. However, as the difference between total shrinkage and autogenous shrinkage is higher for concrete BL35, drying shrinkage is higher for concrete BL35.

For both mixtures, drying shrinkage presents an almost constant growing rate until around the 200 days of concrete age. From this moment on, the growing rate tends to be softer and maintains a similar trend until 400 days of concrete age.

The test was initially predicted for a total period of one year, but the measurements are done until around 400 days of concrete age. At the end of this period, for t = 406 days, the value of autogenous shrinkage is equal to +511 μm/m for BL35 and +12 μm/m for BL36, the value for drying shrinkage is equal to –732 μm/m for BL35 and –464 μm/m for BL36 and the value for total shrinkage is equal to –220 μm/m for BL35 and –452 μm/m for BL36.

Relative humidity was measured during the time while the shrinkage test was performed. The corresponding values are presented in Figure 2.32. Relative humidity suffered a large variation because the test took more than one year to be completed. An average value equal to 64.3% was determined considering all the measurements done in time. This value is associated with a standard deviation of 9.76 % HR and a variation coefficient of 15.2%.

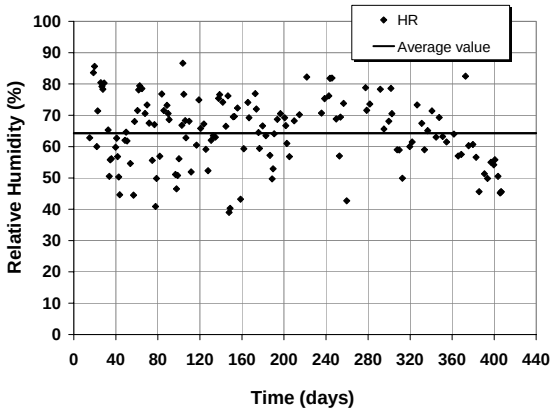

Figure 2.32 – Evolution of relative humidity, in time

2.11.14.2 Shrinkage according to EN 1992-1-1

According to EN 1992-1-1, (CEN 2004a), autogenous shrinkage strain takes place during hardening of concrete and therefore its major part develops in the early days after casting.

The value for NWC autogenous shrinkage can be estimated with equation (2.25), considering an infinite period of time.

$$\varepsilon_{ca,\infty} = -2.5 \cdot \left(f_{ck} - 10 \right) \cdot 10^{-6} \tag{2.25}$$

EN 1992-1-1 considers autogenous shrinkage as a linear function of the concrete strength. The evolution of autogenous shrinkage strain in time is defined by equation (2.26) and equation (2.27) is used to calculate coefficient $\beta_{as}(t)$.

$$\varepsilon_{ca}(t) = \beta_{as}(t) \cdot \varepsilon_{ca,\infty} \tag{2.26}$$

$$\beta_{as}(t) = 1 - exp\left(-0.2t^{0.5}\right) \tag{2.27}$$

In the present case, equation (2.25) gives the following value for autogenous shrinkage at $t = \infty$, $\varepsilon_{ca,\infty}$ = -120 μm/m, considering that the measured compressive strength at 28 days of age is equal to 58 MPa.

According also to EN 1992-1-1, the value of drying shrinkage for NWC can be predicted with equations (2.28) to (2.31),

$$\varepsilon_{cd,0} = \left[\left(220 + 110\alpha_{ds1}\right) \cdot exp\left(-\alpha_{ds2} \cdot \frac{f_{cm}}{f_{cm0}} \right) \right] \cdot 10^{-6} \cdot \beta_{RH} \tag{2.28}$$

$$\beta_{RH} = -1.55 \cdot \left[1 - \left(\frac{RH}{RH_0} \right)^3 \right] \quad \text{, if } RH < 99\% \cdot \beta_{sl} \tag{2.29}$$

$$\beta_{RH} = 0.25 \quad \text{, if } RH \geq 99\% \cdot \beta_{sl} \tag{2.30}$$

$$\beta_{sl} = \left(\frac{3.5 \cdot f_{cm}}{f_{cm0}} \right)^{0.1} \tag{2.31}$$

where, α_{ds1} = 6 and α_{ds2} = 0.11 for rapidly hardening high-strength cement.

Drying shrinkage for NWC, at an infinite period of time, is calculated with expressions (2.28) to (2.31), corresponding to the result of $\varepsilon_{cd,\infty}$ = -499 μm/m. In the case of lightweight concrete, the value of drying shrinkage calculated for NWC should be multiplied by the coefficient η_3 = 1.2. The calculation takes into consideration an average relative humidity value of 64.3% (see 2.11.14.1). The sum of autogenous and drying shrinkage gives the value for total shrinkage, $\varepsilon_{cs,\infty}$ = -719 μm/m.

Considering equation (2.32), it is possible to calculate the value of drying shrinkage strain for a particular moment in time, t, where $\beta_{ds}(t,t_s)$ is a function of moment t and of the cross section dimensions of the tested specimen and k_h depends on the value of h.

$$\varepsilon_{cd}(t) = \beta_{ds}(t,t_s) \cdot k_h \cdot \varepsilon_{cd,0} \tag{2.32}$$

The function $\beta_{ds}(t,t_s)$ is defined by equation (2.33), where $h = \frac{2A_c}{\mu}$ and h_1 = 100 mm.

$$\beta_{ds}(t,t_s) = \frac{(t-t_s)}{(t-t_s)+0.04\sqrt{h_0^3}} \tag{2.33}$$

For the present case, the use of equations (2.32) and (2.33) results in ε_{cd} (t = 400) = 1.2 × -468.7 = -562.5 μm/m. The total shrinkage strain value is obtained by summing the values of autogenous and drying shrinkage. The result is approximately equal to ε_{cs} (t = 400) = -680 μm/m. This value is higher than the value experimentally determined for BL36 and much higher than the value obtained for BL35.

Also, the evolution of autogenous and drying shrinkage of lightweight concrete tends to be very different than predicted by EN 1992-1-1, as can be observed in the following. Figure 2.33 presents evolution curves correspondent to autogenous, drying and total shrinkage strain, according to EN 1992-1-1, considering the specimens and test conditions defined in 2.10.6. These curves are the result of applying equations (2.25) to (2.33) to the present test conditions.

According to (2.33), the value for drying shrinkage at t = 400 days corresponds to 82% of the total value of drying shrinkage measured until t = ∞ and therefore it is considered that the period of approximately 1 year defined for this test is representative of the shrinkage phenomena.

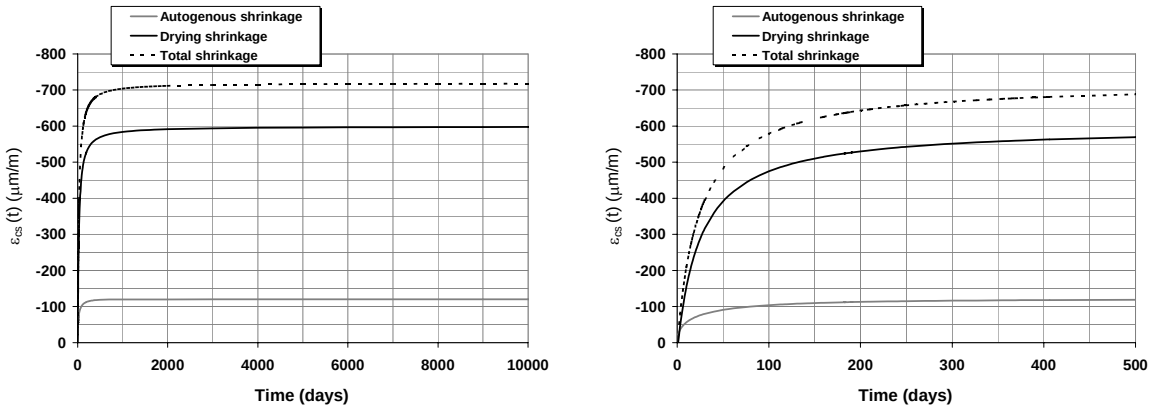

a) Values for t = 10000 days

b) Values for t = 400 days

Figure 2.33 – Evolution of autogenous, drying and total shrinkage values, according to EN 1992-1-1

Figure 2.34 presents a comparison between autogenous shrinkage strain values, experimentally measured and calculated according to EN 1992-1-1, (CEN 2004a). The experimental curve shows an initial trend opposite to defined by EN 1992-1-1. The experimental values show that concrete BL36 suffers expansion until around 80 days of age, with an absolute value that is very close to the value of contraction predicted by EN 1992-1-1. From this moment on, there is some contraction of the specimen, but it never annuls the initial value of expansion, at least until the last registered measurement. For the specimen of BL35, the expansion is verified until the last registered measurements.

According to EN 1992-1-1, autogenous shrinkage at the age of $t = 80$ days corresponds to 83% of the total value of autogenous shrinkage. As observed for the specimens tested, these reference equations cannot be used for the lightweight concrete tested.

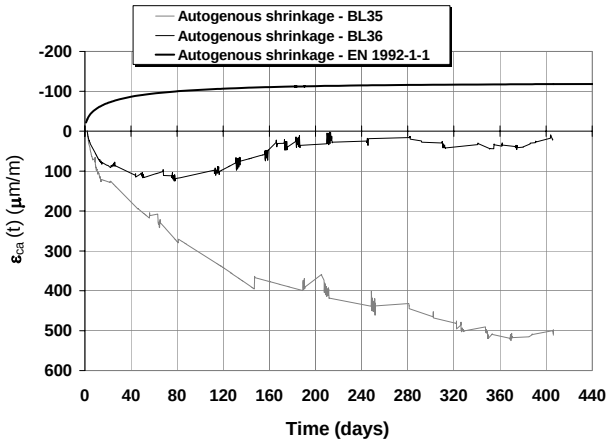

Figure 2.34 – Autogenous shrinkage: comparison between experimental results and EN 1992-1-1 prediction

Figure 2.35 presents a comparison between drying shrinkage strain values, experimentally measured and calculated according to EN 1992-1-1, (CEN 2004a). The experimental curves show that this concrete experiences an initial period when the drying shrinkage values are null. This happens because concrete suffers initial autogenous expansion. When drying shrinkage overcomes autogenous shrinkage values, the growing rate on drying shrinkage is higher than predicted by EN 1992-1-1. From $t = 200$ days on, the evolution trend is more similar for both curves, although the experimental values grow faster. At the final period of $t = 400$ days, the value of drying shrinkage is higher than the value predicted by EN 1992-1-1, for BL35, but smaller than predicted for BL36.

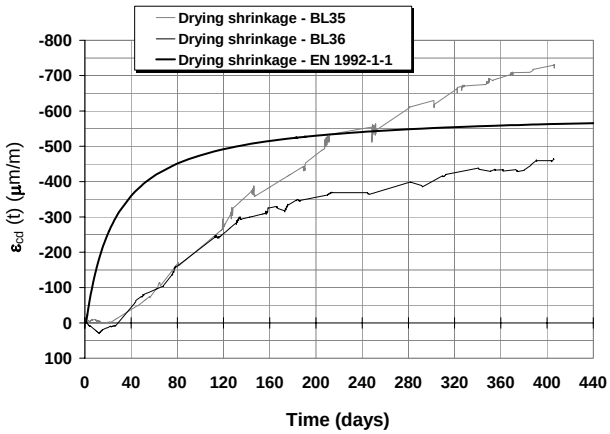

Figure 2.35 – Drying shrinkage: comparison between experimental results and EN 1992-1-1 prediction

It is important to state that EN 1992-1-1 should consider the effect of initial swelling verified for lightweight concrete, as the main differences found in the shrinkage values concern this aspect. This phenomenon has been recognized by some authors and is confirmed within this work. There are also some differences between experimental results and EN 1992-1-1 as far as drying shrinkage concerns, especially on the growing rate until the 200 days of concrete age.

2.11.15 Creep

As mentioned for the shrinkage test, the measurements done for creep should take into account temperature and relative humidity variation. In this case, the alteration introduced by equation (2.24) is also valid. The measurements done for creep should only consider the strain variation after loading, which means that the strain variation resultant from the load application should be discounted.

Equation (2.34) resumes the calculations for creep strain: the value of shrinkage strain and the values of instantaneous strain are discounted from the total strain measured at the creep specimen, in a particular moment *t*,

$$\varepsilon_c(t) = \varepsilon_t(t) - \varepsilon_s(t) - \varepsilon_i \tag{2.34}$$

where,

$\varepsilon_t(t)$ - total strain measured in a moment *t* that is counted from the initial measurement;

$\varepsilon_s(t)$ - average strain measured on shrinkage specimens at the same moment;

ε_i - instantaneous strain measured during load application, right after the maximum load is applied.

As referred in 2.10.7, two cylinders are overlaid during the creep test. One of them is completely isolated from the exterior and the other is in plain contact with the involving atmosphere. The creep test is carried out in environmental conditions, for the same reasons that were mentioned for the shrinkage test (see 2.11.14).

2.11.15.1 Creep - experimental measurements

Figure 2.36 presents the strain diagrams that result from the measurements done on the unsealed specimens, during the testing period. Two curve types are plotted in Figure 2.36: one considers the total strain variation measured in the unsealed specimens and the other considers only the creep strain, because the strain measured in the shrinkage specimens is discounted.

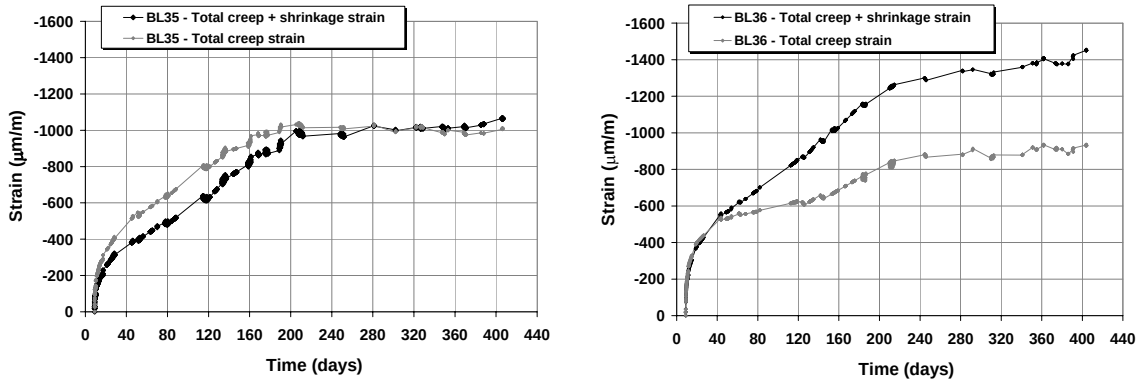

a) BL35 b) BL36

Figure 2.36 – Creep strain curves measured in unsealed specimens of BL35 and BL36

Figure 2.36.a) presents two curves concerning the sealed specimen, one for total strain and the other for creep strain. Because of the autogenous shrinkage reduced values, the two curves for the sealed specimen are closer than the curves for unsealed specimens.

The results presented in Figure 2.36.b) show that shrinkage corresponds to an important percentage of the total strain measured during the creep test. Creep strain shows an initial fast evolution that tends to soften after the 60 days of concrete age, and has a very slow growing rate after the 240 days. This last growing rate is maintained until the final measurements.

The curves for creep strain are similar in both diagrams. The final value for creep strain is equal to –825 μm/m for the unsealed specimen, while the final value for creep strain is equal to –780 μm/m for the sealed specimen.

2.11.15.2 Creep coefficient

Creep test procedure and creep coefficient are both defined in recommendation E399 from LNEC (1993). Equation (2.35) is considered to calculate this parameter.

$$\phi(t,t_0) = \frac{\varepsilon_c(t) \cdot E'_{c,28}}{\sigma_c} \tag{2.35}$$

Specimens from mixtures BL35 and BL36 are used for the creep test. An average modulus of elasticity, E_{cm}=22.9 MPa, is determined at the age of 28 days for BL35 and an average modulus of elasticity, E_{cm}=22.2 MPa, is determined at the same age for BL36. The load applied during the creep test corresponds to a uniform compressive stress of 16.5 MPa. This value is calculated considering that the applied stress is around 30% of the concrete compressive strength at the age of loading. The specimens are loaded at the age of 9 days, but the compressive strength tests are done later. Therefore, the stress value was estimated considering that compressive strength at loading age is around 55 MPa, which is a valid hypothesis considering the compressive strength evolution studied for mixing BL15 and presented in 2.11.3.

The values for creep coefficient determined until t = 406 days are presented in Figure 2.37.

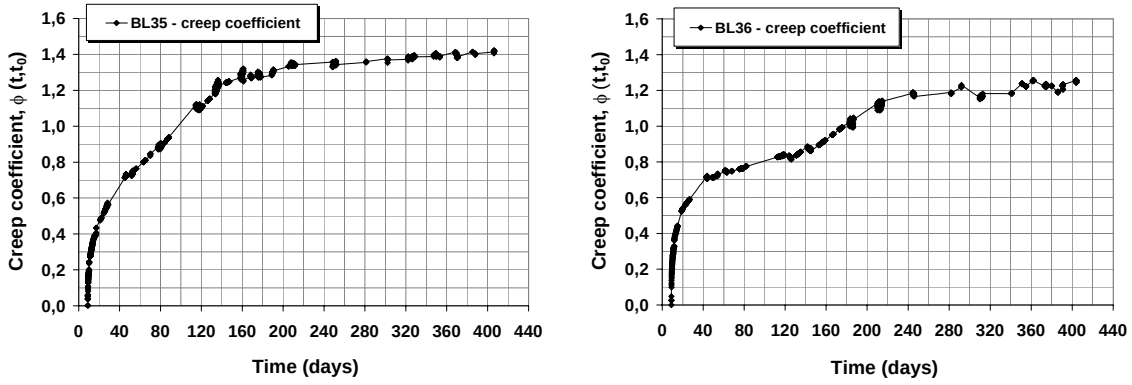

a) BL35 b) BL36

Figure 2.37 – Creep coefficient for BL35 and BL36, measured until t = 406 days

The creep coefficient evolution is similar to the strain evolution presented in Figure 2.36, as it results from the multiplication of the total creep strain values by the two constants, E_c and σ_c. According to Figure 2.37, concrete BL35 presents a higher creep coefficient than concrete BL36 for the final phase of loading. In both cases, the creep coefficient grows very fast during the initial phase of loading and after around 200 days of age, the values tend to stabilize, presenting a very slow growing rate from this moment on.

2.11.15.3 Creep according to EN 1992-1-1

EN 1992-1-1 proposes equations (2.36) to (2.42) for calculating creep coefficient, where RH = 64.3%, RH_0 = 100%, h = 0.075 m and h_0 = 0.10 m.

$$\phi_{RH} = 1 + \frac{1 - \frac{RH}{100}}{0.1 \cdot \sqrt[3]{h}}, \text{ if } f_{cm} \leq 35 \text{ MPa} \tag{2.36}$$

$$\phi_{RH} = \left[1 + \frac{1 - \frac{RH}{100}}{0.1 \cdot \sqrt[3]{h}} \cdot \alpha_1 \right] \cdot \alpha_2 \text{ if } f_{cm} > 35 \text{ MPa} \tag{2.37}$$

$$\beta_c(f_{cm}) = \frac{16.8}{\sqrt{f_{cm,28}}} \tag{2.38}$$

$$\beta(t_0) = \frac{1}{0.1 + t_0^{0.2}} \tag{2.39}$$

$$\phi_0 = \phi_{RH} \ \beta_c(f_{cm}) \beta(t_0) \tag{2.40}$$

$$\beta_c(t, t_0) = \left[\frac{(t - t_0)}{(\beta_H + t - t_0)} \right]^{0.3} \tag{2.41}$$

$$\phi(t, t_0) = \phi_0 \ \beta_c(t - t_0) \tag{2.42}$$

Figure 2.38 represents the creep coefficient curves for the test conditions referred in 2.10.7. At t = 400 days, the calculated value for creep coefficient corresponds to 84% of the value estimated for an infinite period of time.

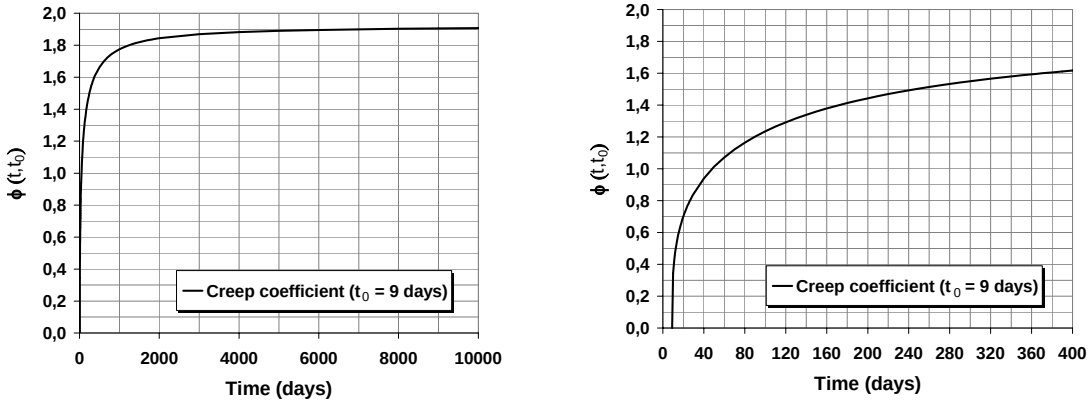

a) Values for $t = \infty$ b) Values for t = 400 days

Figure 2.38 – Creep coefficient evolution, according to EN 1992-1-1

The values for creep coefficient are calculated for the test conditions referred in 2.10.7, considering the presented equations. Table 2.15 shows the value of creep coefficient calculated for an infinite period of time and for t = 400 days. These values are then compared to the ones measured for BL35 and BL36. In both cases, the creep coefficient measured in the experimental tests is smaller than the creep coefficient predicted with the equations proposed in EN1992-1-1. At t = 400 days, the experimental value of BL35 for creep coefficient corresponds to 88% of the EN 1992-1-1 value and the experimental value of BL36 for creep coefficient corresponds to 77% of the EN 1992-1-1.

Table 2.15 – Creep coefficient values at $t = \infty$ and t = 400 days

Concrete ref.	t_0 (days)	t = 400 days	$t = \infty$
EN 1992-1-1	9	1.62	1.92
BL35	9	1.42	-
BL36	9	1.24	-

The same conclusion is obtained with Figure 2.39 that present the total curves of creep coefficient experimentally measured and calculated according to EN 1992-1-1 equations.

A general observation, taken from the results obtained from shrinkage and creep tests, is that both phenomena tend to have a rapid growth for early ages. This growth is softened after the age of 180 to 200 days, and this rate is kept until the final measurements, taking place around t = 400 days.

The results on shrinkage and creep tests of HSLWC show that the two phenomena have similar expression in terms of total values, as the values magnitude is similar. The values of creep and shrinkage measured in the tests performed present some agreement to the values measured by Lopez et al. (2004) in specimens with similar quantity of cement.

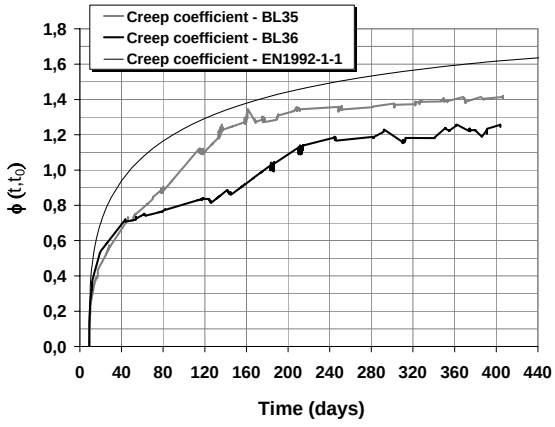

Figure 2.39 – Creep coefficient: comparison between experimental values and EN 1992-1-1

2.12 Conclusions

High strength lightweight concrete was experimentally tested and characterized within this chapter. In general, this concrete presents similar characteristics in terms of behaviour to the ones expected for a normal density concrete with the same compressive strength. However, there are some important differences: density, modulus of elasticity, tensile strength and fracture energy are all lower than could be expected for a normal density concrete with the same compressive strength. The value of density determined for the HSLWC analysed is around 75% of the density of a NDC. The modulus of elasticity value is around 65-70% of the corresponding value of a NDC and tensile strength value is similar to the corresponding value of a NDC. Fracture energy is around half the corresponding value of a NDC.

The relation between some of these parameters was also analysed. The strongest correlation verified in the experimental tests performed is between modulus of elasticity and density, followed by the correlation between modulus of elasticity and compressive strength.

The long-term behaviour of HSLWC was analysed by means of creep and shrinkage tests. Two mixes were used to perform this analysis and each one gave different results. Both concretes suffered swelling, particularly during the initial phase of loading. The total shrinkage suffered by the specimens of BL36 is higher than the total shrinkage suffered by the specimens of BL35, while the creep coefficient for BL35 is higher than the creep coefficient for BL36. Both creep and shrinkage strains show different growing rates before and after the 200 days of age. During an initial phase, these values grow faster and in the last phase, they tend to grow slower. In general, the experimental values obtained on creep and shrinkage are not close to the corresponding values obtained with EN1992-1-1.

Chapter 3

EXPERIMENTAL STUDIES ON SHEAR CONNECTION BETWEEN STEEL AND HIGH STRENGTH LIGHTWEIGHT CONCRETE

3.1 Introduction

The use of composite steel structures accounts for the contribution of the two materials, provided that a composite action exists between concrete and steel members. A composite action can be obtained by reducing or preventing the relative displacement of concrete and steel elements at their interface. Shear connectors are used to provide the composite action. The behaviour of the steel to concrete connection will have major importance on the global behaviour of the structural element. This is the main subject for the analysis performed within this chapter.

A large number of experimental testing has been done in order to explore the structural behaviour of different types of steel connectors. Beside the commonly used headed studs, some investigators showed that the use of Perfobond connectors and T connectors is adequate when dealing with high strength concrete. Recent experimental work, carried out by Oguejiofor and Hosain (1994), Ferreira (2000), Machacek and Studnicka (2002), Medberry and Shahrooz (2002), Galjaard and Walraven (2001) and Poot (2001) with Perfobond and rib connectors, and studies developed by Hegger et al. (2000/2001) and Galjaard and Walraven (2001) with headed studs and T connectors, made it possible to describe and analyse the steel to concrete connection properties. These studies that primarily focus normal density concrete (NWC) with normal and high strength compressive strength, are a reference to the work here presented.

Recent investigation proved that the use of studs is adequate when using high strength concrete, (An and Cederwall 1996), (Hegger et al 2001). Headed studs covered with ultra-high strength concrete were also tested by Hegger et al (2005), with some improvement on the load capacity and a ductile behaviour. Good results were obtained with lightweight concrete in push-out tests recently performed, (Galjaard and Walraven 2000).

As referred, the behaviour of headed studs, Perfobond rib and T connector was studied by various authors for normal weight concrete with average compressive strength. Within this chapter, the study is centred on the use of high strength lightweight concrete.

This is now a commonly used material that can successfully replace NWC on a concrete structure as there are some good examples of bridges and other construction where high strength lightweight concrete (HSLWC) was used as the main material. However, the use of this material in composite structures requires testing of the composite connection between the steel and the concrete members.

The studies here presented are essentially of experimental type. The first of the experimental studies carried out include monotonic tests on headed studs with diameters of 19, 22 and 25 mm and on studs of 19 mm diameter, now grouped in pairs. The second part of the study is related with monotonic tests on Perfobond connectors and T connectors.

The aim of the experiments conducted is to determine the load-bearing capacity as well as the deformation capacity of different shear connectors when using high strength lightweight concrete. The comparison of these tests with results of similar tests performed with NWC is done in order to evaluate the adequacy and effectiveness of this material applied in composite structures.

3.2 Shear connectors

Shear connectors are welded to the steel beam and later cast inside the concrete slab. They are made of steel, are easily welded to the steel beam and establish a mechanical bond with the concrete slab. The aim of an optimal performance led investigators to study different typologies and geometries in order to define connectors with good behaviour and minimum cost. The minimum cost has to do with the total amount of material necessary to produce the connector, with the connectors production conditions, with welding conditions (at site or at an industrial unit) and with man ship time needed for the welding task.

The types of shear connectors studied within this work are presented in Figure 3.1, where the connectors are already welded to the steel beam flange. The study here presented analyses headed studs, Perfobond connectors and T connectors.

a) Headed stud b) Perfobond c) T

Figure 3.1– Connector types

3.2.1 Headed stud connector

Headed studs shear connectors are well-known and largely used, in spite of the various types of connection between steel and concrete already studied and commercialised. These connectors are industrially produced and are available in various diameters, usually varying from 6 to 25 mm, and various heights, that can go from 30 to 500 mm.

Studs are welded to the steel beam, by means of an electric arch, causing a total continuity between the two elements. The welding material has a very good quality and the welding zone becomes even more resistant than the rest of the connector. Studs and ceramic ferrules for arc stud welding, and the arc stud welding of metallic materials are defined in EN ISO 13918 (2000) and EN ISO 14555 (2000).

The success of the stud connector has to do with the characteristics of site work: the stud welding is fast, they anchor well in concrete and it is easy to dispose the reinforcement through the slab, between the studs. Other advantages of this device are the facility of massive production, the standard dimensioned head that resists to the slab uplift without extra care and the possibility of being used in steel deck slabs, a constructive system that does not require temporary support and provides extra resistance for positive bending moments (see Figure 3.2).

Some disadvantages can also be pointed out: this shear connection solution demands for equipment that needs high energetic resources to work, the equipment is initially expensive to buy and the welding conditions can be affected by climate conditions at work site. Besides, when embedded in high strength concrete, this connector behaviour is not optimal as there is the possibility of an earlier failure in the composite element. This early failure can occur by fatigue, caused by cyclic loadings that are usual, for example, in bridge decks. Fatigue problems can also occur for service load level.

Figure 3.2 – Welding of shear studs

One of the first studies on shear studs structural behaviour was done in Japan, in the early 60's, (Yamamoto and Nakamura 1962), and has continued along time until today. The evolution on structural materials enhanced the search for new applications. Examples of this are high strength and lightweight concretes.

A description of the load-bearing and deformation behaviour of headed stud shear connectors in standard-strength concrete is given in the following, (Lungershausen 1988). According this author, four load-bearing portions are considered: concrete compression strut force behind the weld collar, bending and shearing load-bearing capacity in the lower area of the connector shaft, tensile force in the connector shaft as well as friction forces in the composite interface. These four components are detailed in the following paragraphs.

Stud connectors in a solid concrete slab are subjected to shear forces *P*, applied essentially on the stud basis and directly transmitted to the surrounding concrete zone. The compression forces concentrate mostly near the welding collar and are transmitted to the concrete slab in a reduced angle β. This force will provoke a great part of the slip deformation, corresponding to part *A* of the load-deformation diagram of Figure 3.3.

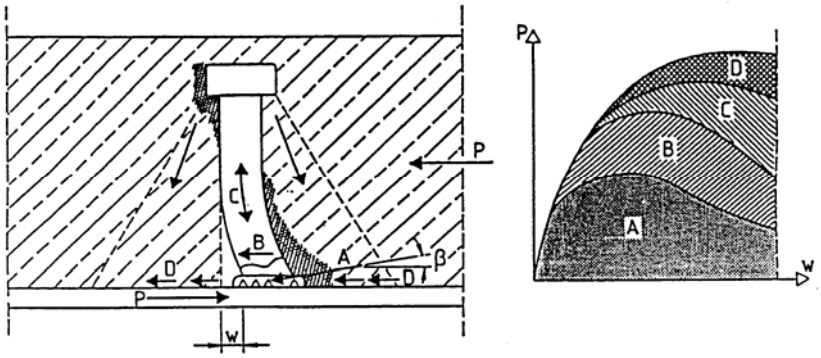

Figure 3.3 – Shear stud connector failure mechanism, in normal weight concrete, (Roik et al 1988)

As the *P* load rises, the compression stresses around the stud basis are higher and lead to the concrete crushing. The loss of concrete resistance enhances a transfer of stress to an upper part of the stud connector making it progressively more submitted to bending. Thus, the stud bears higher loadings and its shear resistance becomes more important. The connector shear strength corresponds to the force component *B*, as represented in Figure 3.3.

As the connector vertical deformation is restrained, compression forces are installed on the shank and a higher concrete compressive strength is attained between the connector's head and the upper layer of the steel beam. This force is represented as *C* in Figure 3.3 and its horizontal component also contributes to the connection load capacity.

As there is slip at the interface between steel and concrete, friction forces are mobilized between these two elements. These forces are represented as *D* in Figure 3.3.

In resume, the behaviour of a stud connector inside a NWC solid slab is conditioned by the following parcels:

– the force component *A* that is related to the concrete compression strut force before the weld collar; when there is slip between the concrete slab and the steel profile, the

larger deformations take place on the stud basis and concrete can be crushed near the welded collar;

- the force component *B* that results from the connector bending and shear strength in the lower area of the connector shaft and is dependent on the stud material tensile strength;
- the force component *C* that results form the tensile force installed on the stud shaft, needed to guarantee the equilibrium of the concrete struts that go from the stud basis to the slab mid height;
- the force component *D* that results from the friction forces mobilized between the concrete slab and the steel profile.

The materials used to produce shear connectors differ between countries. Mechanical properties like tensile ultimate strength, tensile yielding strength and ultimate strain can vary, which results in an additional difficulty for comparing experimental tests results. In this case, the connector's steel tensile strength is taken as the basic parameter and the changes on this or other properties caused by the welding process are not considered as an influent parameter.

The headed stud steel connectors produced in Germany and used in this work are specified by the norm DIN 32500 and are fabricated with steel of type St-37-3 K, cold formed, according to regulation DIN 17100 Roik et al (1988), which corresponds to S235J2G3 according to EN 10025 (2004).

Studies that took place at the University of Bochum, (Roik et al 1988), led to a variation coefficient of 5% on the value of the tensile strength of tested steel, used in the fabrication of connectors. In the same way, measurements done on the variation of the diameter of headed studs, led to a variation coefficient of 3% on the value of this parameter.

3.2.2 Perfobond connector

Moved by the unsatisfactory behaviour of shear studs that result from fatigue problems caused by live loads on composite bridges, the German office *Leonhardt, Andrå and Partners* developed, in the late 1980's, a new type of connector, the Perfobond rib shear connector. This new type of connector was designed to be used in the third bridge over the Caroni River, in Venezuela, (Leonhardt et al 1987).

The Perfobond rib shear connector consists on a metallic plate, with a limited number of holes, welded to the steel beam and concreted inside the slab (Figure 3.1b). During casting, the plate openings are filled with concrete, forming dowels that provide

resistance to horizontal shear and prevent vertical separation between the steel beam and the concrete slab.

The load capacity of a Perfobond connector results from the following parcels, (Oguejiofor and Hosain 1994/1996): the tensile strength on the concrete slab, along the Perfobond alignment; the tensile strength of the transversal reinforcement bars; the shear resistance of the confined concrete that lies inside the connector's openings and the bearing of compressed concrete positioned in front of the Perfobond rib. The connector itself usually presents high shear resistance, as the steel plate has sufficient width and length. Thus, the connector shear failure is unusual, contrary to what happens for headed studs.

In consequence, failure usually occurs in concrete. After the concrete dowels failure, the connector still holds considerable shear strength, due the concrete friction at the cracked concrete surfaces that are pressed against each other by the transversal reinforcement, (Zellner 1987).

When compared to headed stud connectors, some advantages can be pointed out for Perfobond connectors: they can be produced in large scale with different shapes and sizes, they can easily be welded without need for special equipment, the welding task can be performed both at site or at an industrial unit, and in terms of load capacity, a significant number of studs can be replaced by a smaller number of Perfobond ribs, as this connector shows a very high load bearing capacity.

In terms of fatigue resistance, Perfobond connectors proved to have better behaviour than headed stud connectors, as the values of slip required to mobilize this connector maximum load capacity are much smaller. If the live load is an important part of the total working load, then slip will occur with every cycle of live load, creating fatigue problems, (Zellner 1987). Other advantage related to fatigue behaviour is that the connection behaviour until maximum load is essentially elastic, contrary to what happens for headed studs, where an important parcel of plastic slip has already developed when the connection attains the maximum load. In addition, the small longitudinal fillet welds cause smaller residual welding stresses and fatigue problems than the welds of shear studs, (Zellner 1987). For serviceability loadings, the Perfobond connector usually shows good behaviour, with a much smaller deformation than obtained for stud connectors. This deformation is essentially elastic, (Zellner 1987).

According to Kraus and Wurzer (1997b), the shear force is transmitted from the steel strip to the concrete slab by extreme local compression acting at the contact surfaces of the connector openings. In Figure 3.4, the dashed lines mark the area where the load spread takes place in the concrete dowel. This area may be separated into two main parts, named zone A and zone B. In the load transmission zone A, concrete is confined causing tri-axial compression. Here, the bearing and deformation behaviour of concrete depends mainly on

the pore structure of the paste. Above a critical load step, crushing of the pore sides occurs, caused by the tri-axial compression. Afterwards, damaged concrete material fills up the pores. In load distribution zone B, compression acts longitudinally and tension transversely to the direction of the load spread. Cracking parallel to the composite force occurs when the transverse stresses exceed the tensile strength of the concrete. After cracking, the splitting reinforcement of the concrete dowel receives the transverse tensile forces. Other reinforcement close to the concrete dowel participates in this process as well.

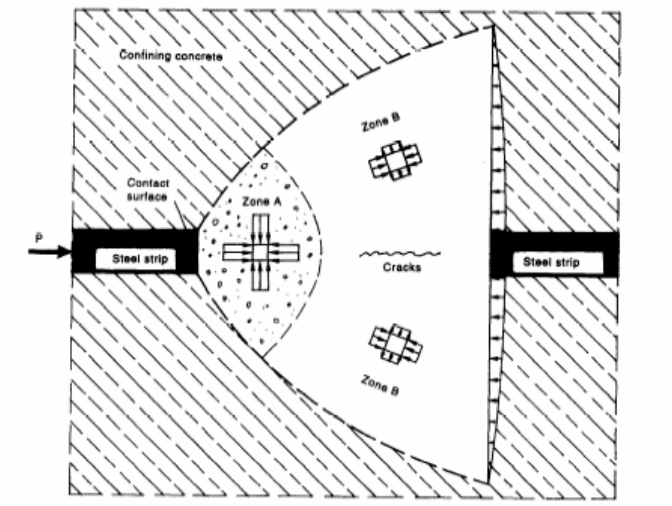

Figure 3.4 – Loading of concrete dowel (Kraus and Wurzer 1997b)

According to Nishido et al. (2000), the shear strength increases with the number of holes on the Perfobond rib, but this increase is not proportional to the number of holes. The authors observed that the cracking in one opening can influence the other openings if the distance between them is not enough.

The principal disadvantage of perforated plates with closed openings is the difficulty of placing the transversal bottom slab reinforcement. To avoid this disadvantage, some new geometries have been studied, considering open apertures on the plates. A first type is the perforated plate with undercut open apertures, as represented in Figure 3.5b. The apertures can have diameters of 70, 100 or even 150 mm, which improves the deformational behaviour of the concrete dowels. Another type is the new S-shape cut, where the symmetry of the cut assures that no material is wasted in manufacturing (Figure 3.5c). The resistance to uplift is achieved with an undercut. Perforated plates with open apertures facilitate the reinforcement placing. Machacek and Studnicka (2002) and Marecek et al. (2005) describe the tests performed with rib connectors that combine O-form and C-form apertures. Veríssimo et al (2006a/b) describe the advantages and the behaviour of the S- form perforated connector and quantifies the principal parameters related to its load and deformation capacity.

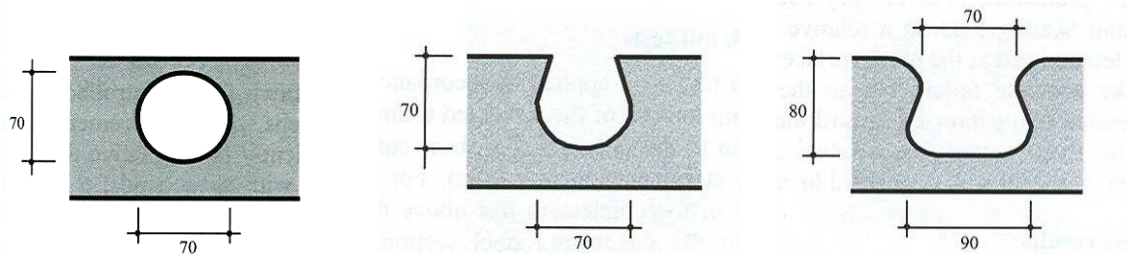

O-form perforated plate C-form perforated plate S-form perforated plate

Figure 3.5 – Perforated plate with closed and open apertures (Hauke 2005)

3.2.3 T connector

The T connector can be produced with different shapes, but usually is made from a commercial profiled steel section. The web width and the web length form the connector shear area, which is normally higher than the stud connector shear area. For this connector however, the stresses transmission zone is always more concentrated in an upper part of the connector as the T cross section area is concentrated on the flange. Oguejiofor and Hosain (1994) observed that a large part of the bearing capacity of a Perfobond strip results from the direct bearing of the concrete at its front end. Unlike headed studs, the T connector should contribute to the transfer of forces by its whole component high, (Hegger et al. 2001). The T shape has a larger contact area than a single strip and therefore it may be a good alternative. In addition, the shape of the T connector is appropriate to prevent vertical separation between the steel beam and the concrete slab.

The load capacity resistance for this type of connector depends on the shear strength of the T web and on the concrete compressive strength in front of the connector. The presence of reinforcement on the concrete slab is important to distribute the tensile forces on the concrete slab (perpendicular to the steel profile) and to prevent early failure caused by cracking.

In terms of fatigue, T connectors show the same problems as studs, as they present important deformation for service loadings, and they need to develop high deformation to mobilize the maximum load, (Hegger et al. 2001), (Galjaard and Walraven 2001).

The possibility of producing T connectors that are cut from profiled sections is an advantage, as there is no need for producing a new element. The welding task has the same characteristics as referred for Perfobond, with the possibility of doing it at site or at an industrial unit. When compared to stud connectors some disadvantages can be pointed out, like the use of more material to produce one single connector and the higher difficulties in disposing the reinforcement along the beam. However, the T connector usually presents higher load capacity than the headed stud connector, which may overcome the first

disadvantage. Therefore, the issue of material quantity used to produce one connector will be further discussed.

Some alterations on the T connectors have been tested, in order to increase their load capacity. Hegger et al. (2001) tested T-profiles of different degrees of inclinations, like HEB and IPE with 30° and 45°. In the limiting region, the end face of the profile intersects with the concrete such that a high degree of ductility is reached. The load that is carried is not however satisfactory for the amount of material in service. The projected area is increased by inclining the profile such that better use is made of the cross-section. These authors observed that he flange did not change its position in the concrete bed during the experiment and neither did any cracks occur. This is because the forces are well-distributed over the flange's projected surface. The displacements were taken up exclusively by the shear deformation of the web and the failure initiated by having exceeded the ductile yield on the reverse side.

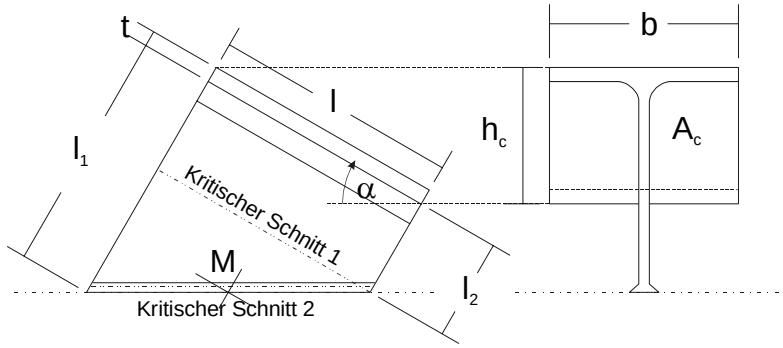

Figure 3.6 - Arrangement of the inclined T connector (Hegger et al. 2000)

3.3 Failure mechanisms

3.3.1 Headed stud connector

As referred in Chapter 6 of EN1994-1-1, (CEN 2004b), the failure mode of stud connectors inside a solid slab of normal density concrete can be described as one of the modes presented in Figure 3.7 or a combination of more than one.

Figure 3.8 shows in detail the deformation stages of a stud shear connector in high-strength concrete solid slab. Compression forces in concrete develop directly in front of the weld collar as represented in Figure 3.8a. Increasing the load causes this force to concentrate within a compressive wedge (Figure 3.8b). Deformation of the connector only takes place in the area of the bolt weld. The high-strength concrete ensures that the connector is rigidly held above this deformation zone. If the load is increased further, then the compression wedge begins to crush and the remainder of the concrete body moves away over this wedge (Figure 3.8c). The force from the connector is still transferred over

the concrete wedge and base of the connector since there are high friction forces acting in the joint between the wedge and the concrete body. These deformations lead to yielding of the connector in the region of the base (Figure 3.8d). Friction does not occur in the joint between concrete and steel, (Hegger et al. 2001).

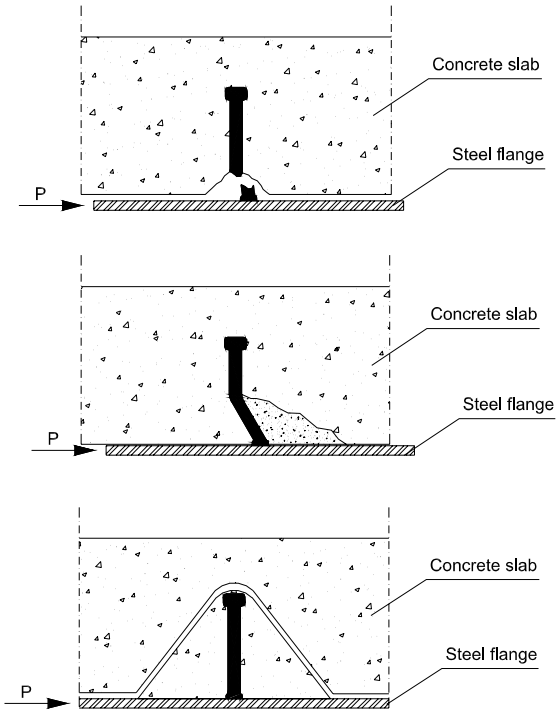

a) Shear failure of the connector, right above the welded collar

b) Local concrete crushing around the foot of the shear stud

Plastic hinges on the shaft basis and mid height

c) Pull-out of a concrete cone

Figure 3.7 – Stud connectors' failure modes

There is almost no load-bearing portion resulting from the tensile force, for connectors in high-strength concrete. This happens because the bending deformation of the connector shaft is low due to the fixing effect of the high-strength concrete (Figure 3.8).

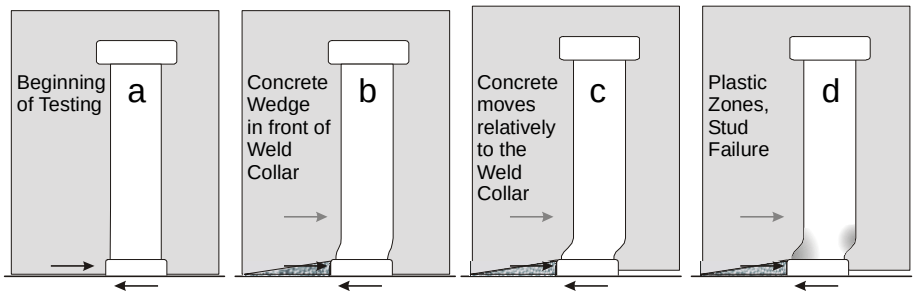

Figure 3.8 - Failure mechanism for a stud shear connector in high-strength concrete (Hegger et al. 2001)

The external forces acting on the connector are shown with greater detail in Figure 3.9, in order to illustrate the deformation behaviour. The deformation of the stud is mainly concentrated on the basis of the shank. The upper part of the stud remains practically undeformed.

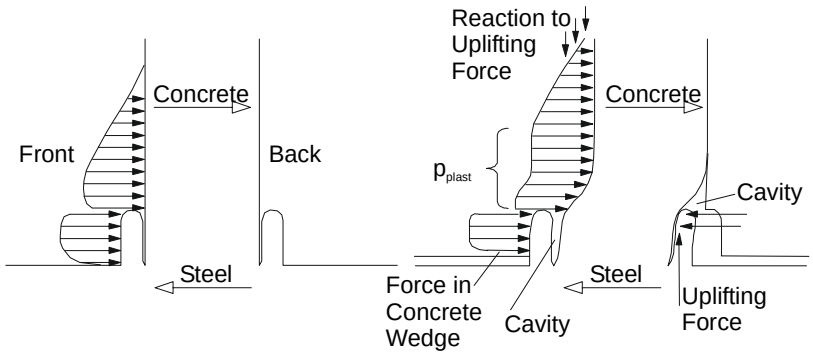

a) Load distribution at non-deformed stud b) Load distribution at deformed stud

Figure 3.9 - Load distribution and deformation of the connector shaft (Hegger et al. 2001)

3.3.2 Perfobond connector

Failure on composite structural elements that use the originally proposed Perfobond connectors is not usually conditioned by the connector, as it shows a very high shear resistance. It is mainly caused by the concrete behaviour with major focus on the concrete strength, which was recognized since the early studies. Figure 3.10 puts in evidence the results obtained by Leonhardt (1987), where the connection load capacity increases with higher concrete compressive strength.

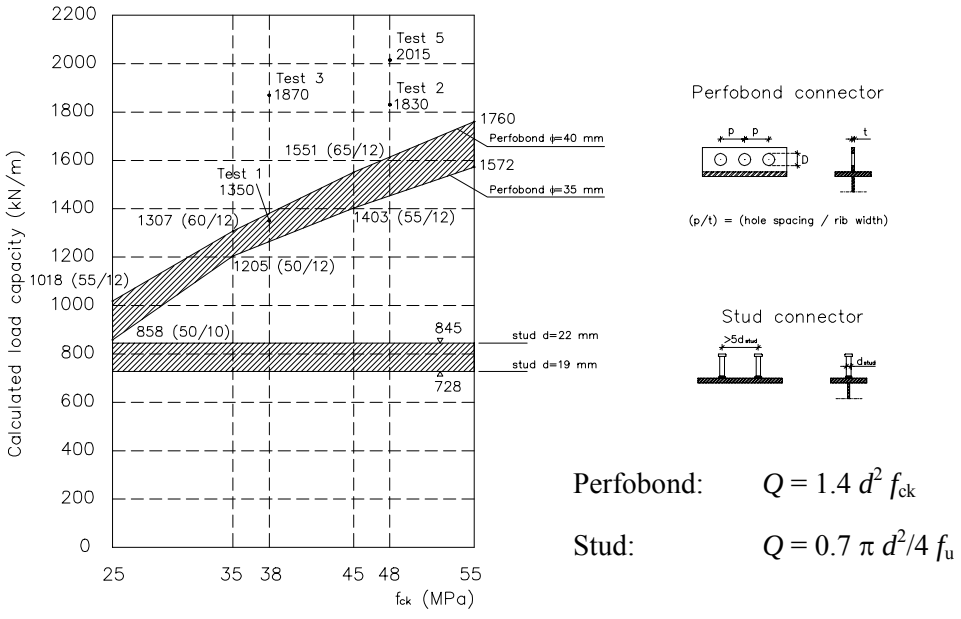

Figure 3.10 – Comparison between Perfobond and headed stud load capacity, depending on the concrete strength, (Leonhardt 1987)

For perforated plates, four principal failure modes are known, as represented in (Figure 3.11): a) shear failure of concrete dowels; b) local concrete pressure failure; c) concrete pry-out failure and d) steel failure due to yielding of the connector plate. For the

originally proposed Perfobond rib, shear failure of concrete dowels is found governing, due the relatively reduced size of the circular openings. New configurations for Perfobond connectors choose to open and enlarge the connector's openings, enhancing new types of failure: concrete pry-out failure and steel failure due to yielding of the connector plate (Figure 3.11c and Figure 3.11d).

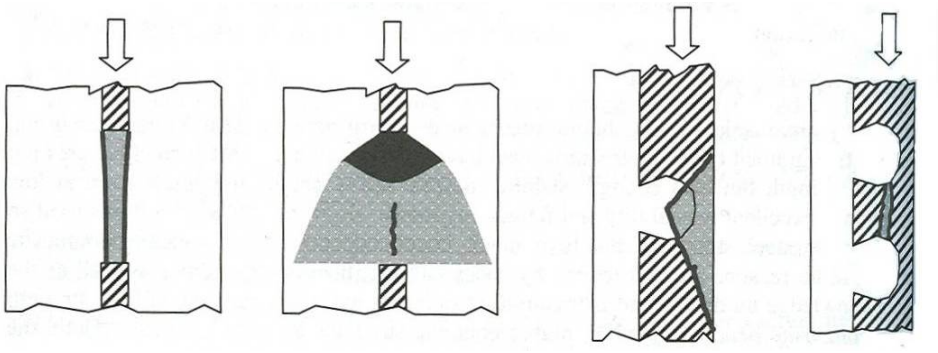

a) concrete shearing b) concrete contact pressure c) concrete pry-out d) steel yielding

Figure 3.11 – Failure modes for perforated plates (Hauke 2005)

Ushijima et al (2001) tested Perfobond connectors with variable rib width. The connectors widths varied from 8 mm to 22 mm and the specimens had no transversal reinforcement passing through the rib holes. During testing, concrete was crushed and disappeared inside the rib holes for specimens with 8 mm width. On the other side, for specimens with larger widths, concrete failure occurred with double shear on both sides of the Perfobond rib. The differences found in failure are explained in Figure 3.12.

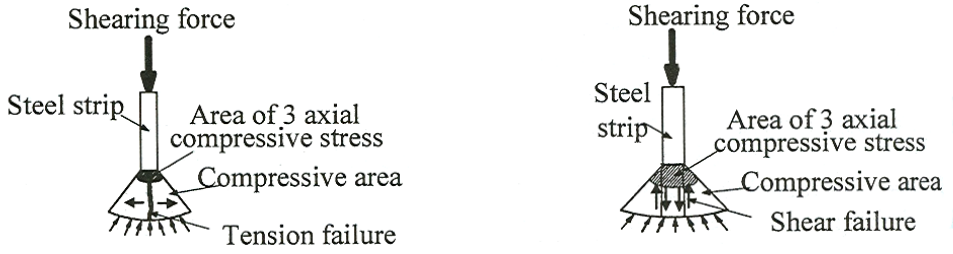

a) Specimen with thin strip b) Specimen with thick strip

Figure 3.12– Failure of Perfobond shear connection: the influence of the rib width (Ushijima et al. 2001)

Thinner plates of around 8 mm width, create a very small concrete compression area. The load is concentrated in a small area of concrete, rising very high transversal tensile stresses. This author suggests that the high stress concentration create a crack on the connector's opening plane that leads to concrete tensile failure. When the rib width is higher, the region under compression is larger, allowing a better distribution of forces in concrete. Concrete attains its shear strength in two planes aligned with the rib lateral faces, as represented in Figure 3.12b, resulting in shear failure. The concrete placed near the

openings' borders is compressed against the openings, developing a tri-axial state of stress (see Figure 3.4). In this case, no tensile forces are developed.

For openings with insufficient concrete cover, pry-out of a concrete cone has been observed in push-out tests. With concrete pry-out, the hydrostatic state of stress in the concrete dowel within the opening is diminished and hence the ultimate load level is lower. Although pry-out failure is basically caused by concrete cracking, the behaviour is not brittle. This is because the pry-out cracks that develop on the concrete surface may limit a further strength gain through confinement of the concrete dowels, but they do not cause an immediate failure of the concrete dowel itself, (Hauke 2005).

Other influencing parameter is the amount of transversal reinforcement, specially the part that passes through the connectors' openings. In the tests performed by Oguejiofor and Hosain (1994), there were specimens with no transversal reinforcement. A sudden failure due to longitudinal splitting is mentioned, occurring instantaneously in the entire length of the concrete slab. When this happened, the specimens lost all ability to sustain the load. For specimens with transversal reinforcement, the longitudinal crack begins in the bottom of the concrete slab and the longitudinal crack growth can be observed. The presence of this transversal reinforcement delays the cracking process and enhances some stress redistribution.

With the longitudinal crack formation, there is also concrete crushing in front of the Perfobond rib. The concrete crushing enhances the development of cracks that are visible on the concrete slab surface positioned right under the Perfobond rib. Studies developed by Medberry and Sharooz (2002) reveal that the tensile stresses developed in front of the Perfobond rib tend to separate the slab in two halves. The transversal reinforcement located under the Perfobond rib plays an important role in resisting and redistributing the tensile stresses and controlling the cracking progress.

3.3.3 T connector

The possible failures modes for T connector are similar to the ones presented for stud connectors. Failure may occur by shear on the connector web, above the welding zone, by concrete crushing around the foot of the T section and by Pull-out of a concrete cone.

Figure 3.13 – Failure of an inclined T connector (Hegger et al 2000)

Usually, the T connector is made of half a profiled section. In this case, shear failure often occurs on the connector basis, even for inclined connectors, as represented in Figure 3.13.

3.4 Transmission of shear force on a composite beam with headed stud connectors

The flux of forces on a steel and concrete composite beam, subjected to bending, is represented in Figure 3.14. Forces D_b (resulting from principal stresses) are slightly inclined in relation to the medium plan of the concrete slab. These forces, together with Z forces acting on the reinforcement and P_d shear forces introduced on the connector basis, are in equilibrium. There are still two other forces, perpendicular to the slab: P_D which is a compression force acting on the headed stud and P_B acting on the concrete slab, that result from the inclination of force D_b. The two forces, P_D and P_B, generate bending in the slab transversal direction.

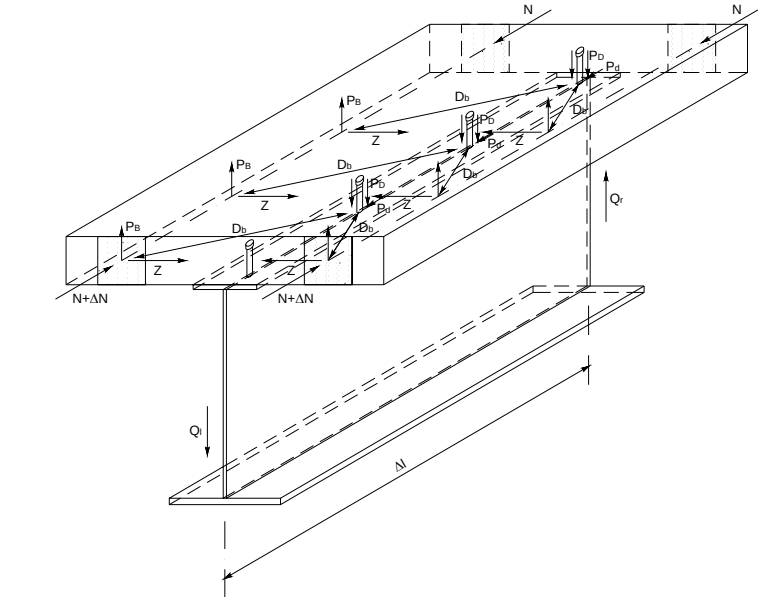

a) 3-D view

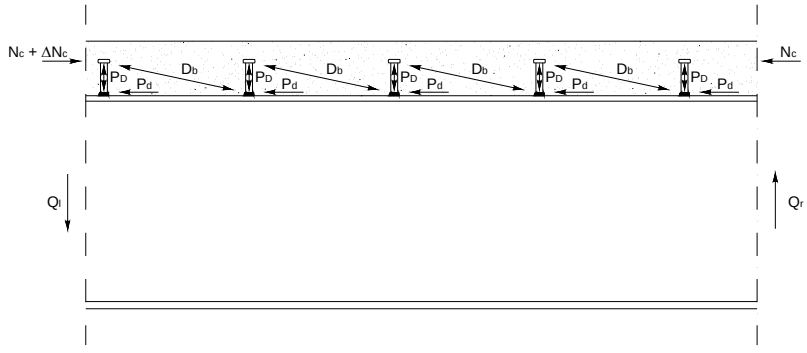

b) Longitudinal view

Figure 3.14 – Flux of forces on a steel and concrete composite beam, (Roik et al 1988)

If shear stresses are constant on the beam longitudinal direction ($Q_l = Q_r$), the forces P_D and P_B, are in equilibrium, remaining active the horizontal shear forces P_d at the steel to concrete interface.

This equilibrium is modified when external forces acting perpendicularly to the slab, like a uniformly distributed loading, q, are applied. The equilibrium state is now ruled by equation (3.1).

$$\Delta Q = Q_l - Q_r = q \cdot \Delta l \tag{3.1}$$

If the loading q is applied over the concrete slab, additional forces of value $q \cdot \Delta l$ act on the steel to concrete interface.

The results of a test on a beam subjected to bending may raise some problems of analysis:

- the stresses on the shear connectors must be calculated through an indirect way, because of the variability of the modulus of elasticity of concrete and because of the possible slip at the steel to concrete interface that can falsify the results;
- in hogging bending moment zones, the concrete is subjected to tensile stresses that induce cracking. In this case, the tension-stiffening effect can only be estimated;
- the value of shear stress installed on the connector can be calculated by measuring the difference of strain between the concrete slab and the steel profile. This may not be an accurate way of measuring the shear flow because of the lack of exactitude on these measurements.

3.5 The Push-Out test

In order to avoid these disadvantages, the push-out test was developed to simulate the transmission of forces on a composite beam. The forces flow on a push-out test model is represented in Figure 3.15. The push-out specimen consists on a steel beam section held in the vertical position by two identical concrete slabs. The link between the concrete slab and the steel profile is accomplished with steel connectors. Chemical or adherence bond between the concrete slab and the steel profile is avoided.

The steel profile is subjected to a vertical load, which produces shear load along the interface between the concrete slab and the beam flange on both sides. The shear forces P_d, applied to the connectors' basis, are transmitted to the concrete slab with inclined compression forces, as happens in composite beams. The bending moment $(P \cdot e)$ results from introducing the load eccentrically and is mobilized by the forces D and Z. The compression component of forces D are perpendicular to the steel to concrete interface and

therefore mobilize some friction forces in the upper zone of the specimen. Forces *D* concentrate in a narrow zone, over the welded collar of the connector.

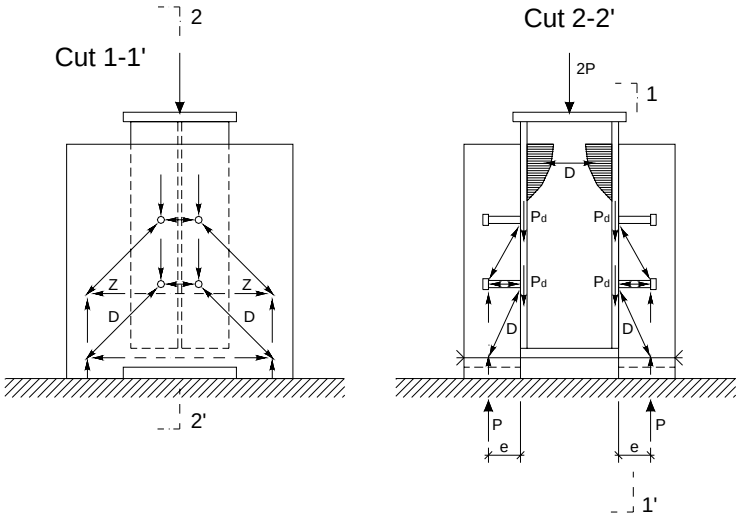

Figure 3.15 – Flux of forces on the standard push-out test

The choice for the push-put test configuration is adequate as the relations established between forces become simpler than those obtained with a bending test. The most important advantage of this test is that the shear stresses applied on the connector basis result directly from the forces *P* introduced by the test load cell and it is possible to measure the relative displacement between the steel profile and the concrete slabs during the load application. Results are therefore obtained in a direct way.

The push-out test allows for a rigorous analysis on the shear connection behaviour, by assessing the load-slip relation until failure and the failure mechanisms. This test can adequately simulate the forces flow through the concrete slab of a composite beam and is especially adequate to analyse the shear connectors load capacity. If a complete simulation of the composite beam behaviour is intended, taking into account the slip between steel and concrete, concrete cracking and the beam deformation, it is more adequate to perform a complete beam bending test.

3.5.1 The Standard Push-Out Test (POST)

The standard push-out test (POST) is described in EN 1994-1-1, (CEN 2004b). This test tries to simulate the transfer of shearing forces in the composite joint of composite girders.

Some alternative dispositions for the push-out test can be chosen, as represented in Figure 3.16. One possibility is to indent the concrete slab base in order to fully guarantee the forces flow established in Figure 3.15. Another possibility is to limit the lateral separation between the concrete slabs, by disposing transversal bars that can equilibrate the tensile forces resultant from the vertical component of forces *D*.

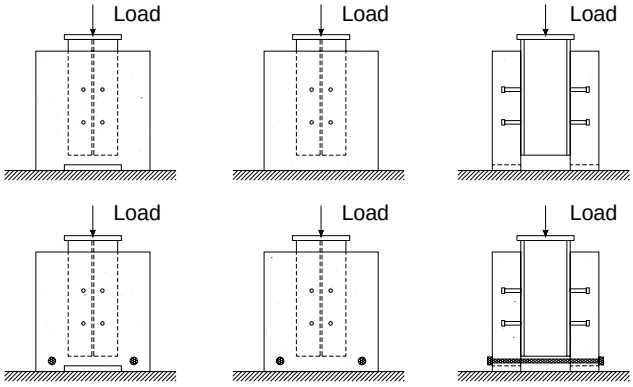

Figure 3.16 – Alternative dispositions for the push-out test

The push-out test configuration suffered some changes in time, related with the specimens' geometry and the materials used. Various authors tested push-out specimens with different slab, reinforcement and stud dispositions, as represented in Figure 3.17.

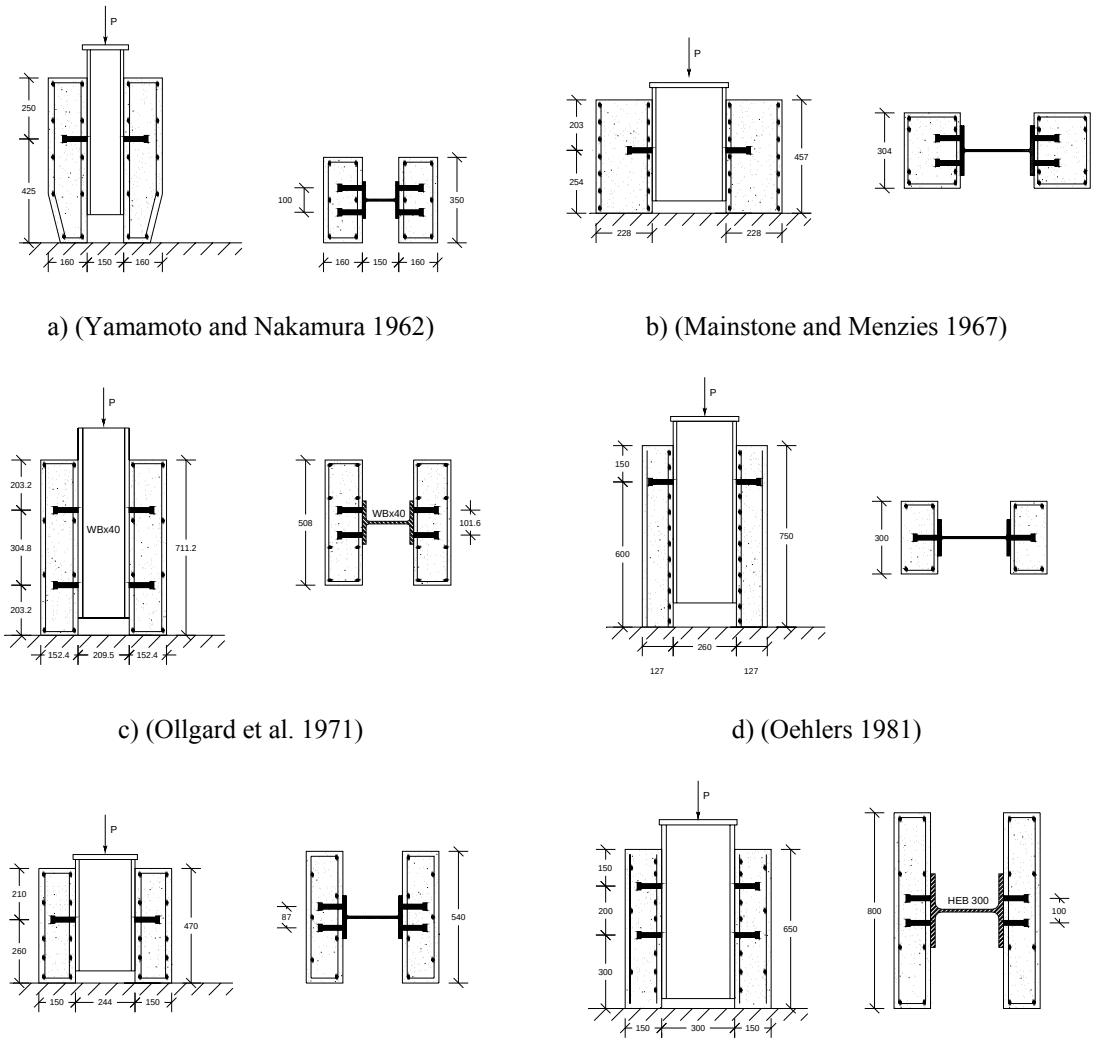

a) (Yamamoto and Nakamura 1962)

b) (Mainstone and Menzies 1967)

c) (Ollgard et al. 1971)

d) (Oehlers 1981)

e) (Hiragi et al. 1981)

f) (Roik and Hanswille 1983)

Figure 3.17 – Push-out test specimens tested by various authors

The test set up defined for this work follows the EN 1994-1-1 dispositions for shear connection between steel and concrete tests, (CEN 2004b). For each type of connector, the geometry of the test set-up is similar, with variation on the connector type and disposition. The slab dimensions are 650 mm × 600 mm × 150 mm. Connectors are welded to the steel profile and later embedded on the concrete slab after concreting, (Figure 3.18).

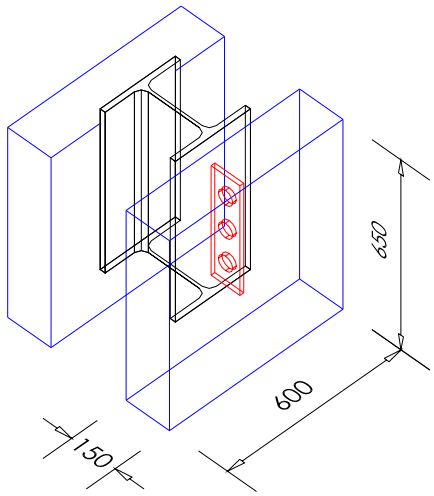

Figure 3.18 - Specimens configuration (with Perfobond connector)

The dimensioning of these test specimens is matched to standard-strength concrete. By using the higher concrete-quality grades and the thereby associated reduction of the load propagation zone, the magnitude of this test specimen is no longer necessary to prevent premature failing of the concrete. Yet, for reasons of comparability, the push-out standard test is also used where high-strength concrete is concerned.

The statics of this system are not optimal. During the experiments, the steel girder shall be displaced relatively to both of the reinforced-concrete belts such that the shear connectors undergo stress of the purely shearing type. However, horizontal forces cannot be avoided between the three construction members in the practical execution of the experiment. Thus, not the ultimate shear carrying capacity of one headed stud can be determined, but an average load-bearing capacity, (Hegger et al. 2004).

3.5.2 The Single Push-Out Test (SPOT)

In order to obtain the characteristic curve for a single shear connector, a new shear test was developed at the Institute of Structural Concrete, at RWTH. In the Single Push-Out Test (SPOT) a single shear connector can be tested individually. Here, the structural stability does not result from the symmetrical construction but from the nearly identical straining lines of the acting forces. Since the resulting lateral force during shearing does not remain at a constant level, the experimental set-up should be capable of tracking such changes without loosing its stable state of equilibrium.

A shoe enveloping the reinforced concrete was chosen as the solution (Figure 3.19). Two additionally attached stirrups created a moment opposing the resulting moment ($M = 0.055 \times F$, where 0.055 m is the distance between the straining lines). This neutralising moment adapts to every load level. Even a parallel shift in the resulting shear force (perpendicular to the shaft of the connector) is accepted by the system without any kinematic reaction. A slight twist of the steel relative to the reinforced concrete is to be expected during the experiment, but the upper stirrup of the shoe does constitute a horizontal restriction. As soon as twisting has set in, the steel nuts impact on the stirrup and form a vertical sliding bearing. As the detachment process progresses, the plate turns back to a parallel position. A falsifying influence on the load-bearing behaviour could not be seen in the series of experiments conducted, (Döinghaus 2001).

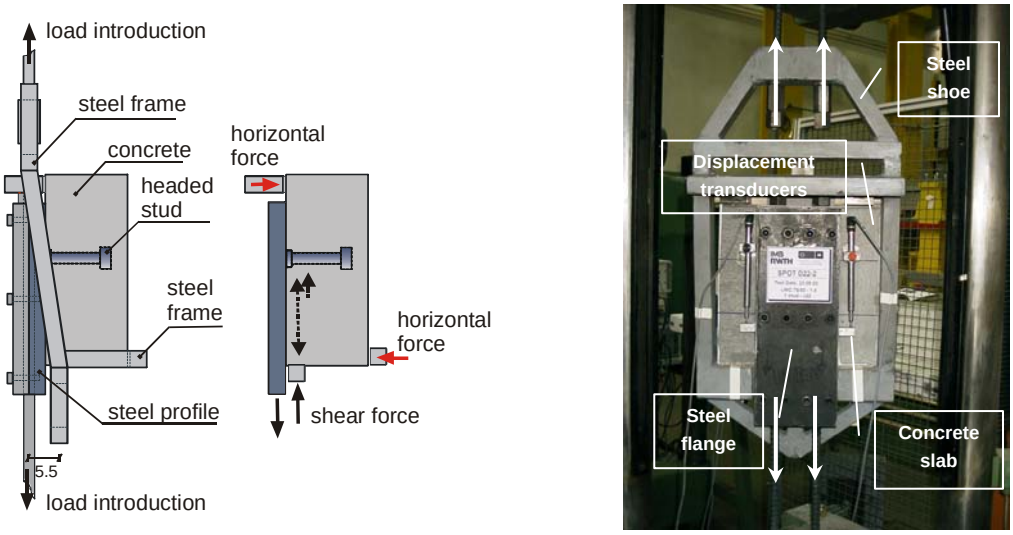

Figure 3.19 - Single Push-Out test: acting forces and setup, (Hegger et al. 2004)

This test specimen is straightforward to fabricate, can be inserted in the testing frame by a single person and lower hydraulic loads are required compared to the push-out standard test (POST). It is particularly suitable for high-strength concrete due to the limited volume of concrete. The SPOT specimens were fabricated according to Figure 3.63.

3.5.3 Test procedures

The equipment used for the POST and the SPOT tests allow the tests to be controlled either by load or by displacement.

The procedures for the push-out test are defined in the EN 1994-1-1, (CEN 2004b). According to this standard, the following steps should be taken, considering that P_{pred} corresponds to the predicted failure load value, calculated before testing begins:

- initially, the loadings is incrementally applied until 40% of the predicted failure load value (P_{pred}) is attained;
- when 40% P_{pred} is reached, 25 cycles of loading/unloading, between 5% and 40% P_{pred} are performed;
- after the load cycles, the test is controlled by deformation; the measurement control is the slip between the steel profile and the concrete slab;
- the imposed deformation rate is such that failure does not take place before 15 minutes;
- slip between the steel profile and the concrete slab is continuously measured during the test;
- the slip measuring takes place until the load value drops at least 20% of the maximum applied load;
- lateral separation between the concrete slabs is also measured during the test.

Figure 3.20 shows a graphical representation of the load-time curve imposed to the tested specimens.

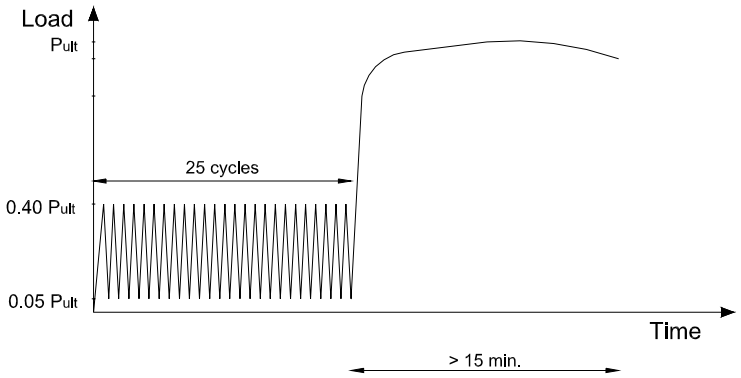

Figure 3.20 – Push-out test procedure

The test procedures are the same for POST and for SPOT setup, with the same sequence of load and displacement control. The objective is to establish a direct comparison between the two tests.

3.5.4 Fabrication and setup of the push-out test specimens

EN1994-1-1, (CEN 2004b), presents some considerations on the fabrication of push-out test specimens that were considered on the fabrication of the push-out specimens tested in this work:

- each concrete slab should be concreted in the horizontal position, as normally composite slabs are concreted;

- discontinuity between the steel profile flange and the concrete slab is assured by oiling the steel flange with a mould release agent before concreting;
- specimens should be cured in uncontrolled environmental conditions, similar to the specimens curing conditions and not in protected temperature and humidity conditions;
- some concrete quantity should be reserved for cylindrical or cubic specimens, in order to test the concrete for compressive strength;
- the value for compressive strength, f_{cm}, at the test date should be between 60 and 80% of the compressive strength characteristic value defined for the composite element that is in analysis;
- the connector material should be tested for yielding strength, maximum tensile strength and maximum deformation.

In terms of compressive strength, the performed tests do not take into account the need for the 60 to 80% value limitation, as the intention is not to reproduce an existing structure or a future existing structure, but instead to produce several specimens with similar concrete properties, suitable for comparison. Therefore, all the cylinders are tested for compressive strength and modulus of elasticity on the same day of the respective push-out test.

All the specimens' slabs are cast in the horizontal position to simulate the casting conditions in a real structure. For POST specimens, both slabs are concreted simultaneously, which implies the cut of the steel beam in two halves, as presented in Figure 3.21. For laboratory capacity reasons, each specimen is concreted at a time.

Figure 3.21 – Casting conditions for POST specimens

After the concrete hardening it is possible to put both slabs in vertical position and then weld the two HEB260 half webs (Figure 3.22). The concrete strength is intended to be approximately the same. This could not be completely accomplished, because each specimen is cast in a different day, but the concrete main properties were determined for all castings at the same day of the respective specimen push-out test.

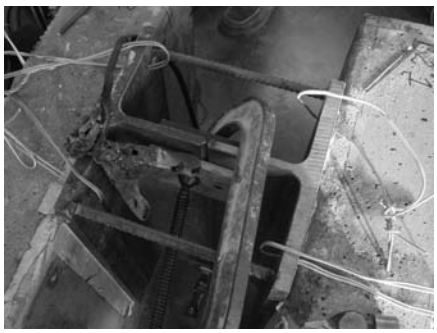
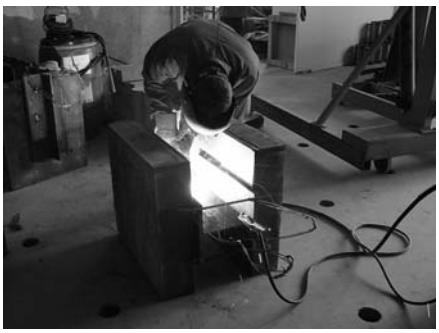

Figure 3.22 – Welding of the two half webs

SPOT specimens use much less concrete than POST specimens. With the available resources of the laboratory, it was possible to concrete six specimens simultaneously (Figure 3.23). If possible, this is always a preferable option as the variability of the concrete properties is not an extra parameter to take into account.


Figure 3.23 – Casting conditions for SPOT specimens

The test set up for POST tests is shown in Figure 3.24. The testing frame consists on a pair of rigid steel plates with 200 mm width, separated by four circular hollow section columns of 275 mm diameter, 40 mm width and 1150 mm high. Four pre-stressed Macalloy bars are positioned inside the hollow columns, guarantying that the steel plates and the steel cylinders are working together. This setup provides the needed reaction.

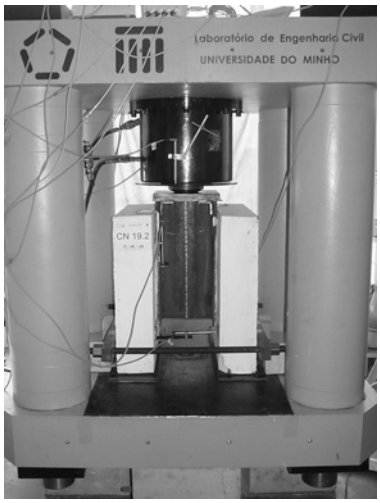

Figure 3.24 – Testing frame for POST tests

The vertical load is applied to the specimens using a hydraulic test machine with 5000 kN capacity. The load is applied in increments, according to an imposed load or deformation rate. This load cell can only apply compression forces, which is appropriate for this test.

A spherical seat is positioned between the actuator and the POST specimen. This spherical seat is laid over a steel plate with spherical concavity. The steel plate is placed over the steel profile and is designed to insure that the load is centred. The contact zone between the spherical seat and the steel plate is greased, so that these two elements permit adjustments between the actuator and the specimen, guarantying a hinge at this position. This aspect seems important as all the elements of the test are very stiff and there is the possibility of existing small imperfections in the specimens that can cause deficiencies in the load application.

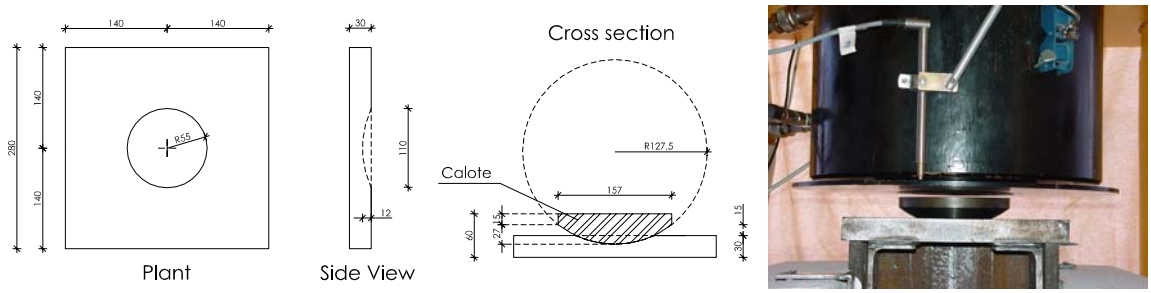

Figure 3.25 – Spherical seat between the actuator and the specimen

The vertical slip at the steel to concrete interface is measured in two points at a regular period of time. The lateral displacement of the slabs is also regularly measured. The horizontal force is annulled by using steel bars across the two concrete slabs, as presented in Figure 3.24.

To reduce de effect of some imperfections, neoprene sheeting is placed in the base of the concrete slabs. Two steel plates with two greased Teflon sheets between them are used, under the neoprene, to eliminate the lateral confinement produced by the friction between the slab and the testing machine (Figure 3.26).

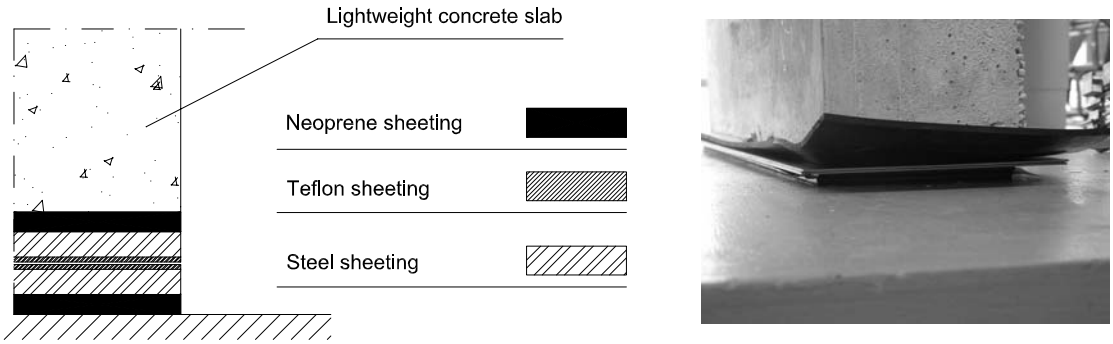

Figure 3.26 – Sheeting under the test specimen

On the lower part of the specimens, two Macalloy bars are attached to the concrete slabs avoiding a large separation between them (Figure 3.27). The bars are not tensioned, but just adjusted to the slabs. As later checked using the measurements done with the displacement transducer positioned near the bars level, there were always some lateral separation between the two slabs, as desirable.

Figure 3.27 – Steel bars to limit horizontal separation

For SPOT tests the machine applies tensile forces. Two steel bars are attached to the specimen steel plate and to the lower part of the testing machine. The steel plate that is welded to the headed stud connector has two holes that combined with a second steel plate, makes the proper device to fix the steel bars of the testing machine. The other two bars are attached to the steel frame that involves the concrete slab and to the upper part of the testing machine (Figure 3.28).

a) Back view

b) Front view

c) Transducer to measure slip

Figure 3.28 – Testing frame for SPOT tests

The steel frame that involves the concrete slab applies a horizontal force to the specimen, as presented in Figure 3.19. The area to make the force transmission is rather narrow and because of that some textile ribs were disposed between the concrete slab and the steel frame, in both sides of the specimen, whenever there was contact between them, to avoid some possible concrete crushing in this zone.

3.5.5 Measuring devices

For POST tests, the measuring devices are positioned as represented in Figure 3.29. The first part of the test is controlled by load. The second phase of the test is controlled by the specimen deformation. The **transducer 1** is positioned over a steel plate attached to the actuator. This measurement is directly related to the slip measured between the steel profile and the concrete slabs and therefore can be used as a control parameter. The slip between the steel profile and the concrete slab is measured with **transducer 2** and **transducer 3**, attached to the concrete slab and measuring in the steel profile. Two of these devices are similarly positioned, in each concrete slab. The test slip values are an average value resultant from these two measures. **Transducer 4** measures de horizontal separation between the two concrete slabs.

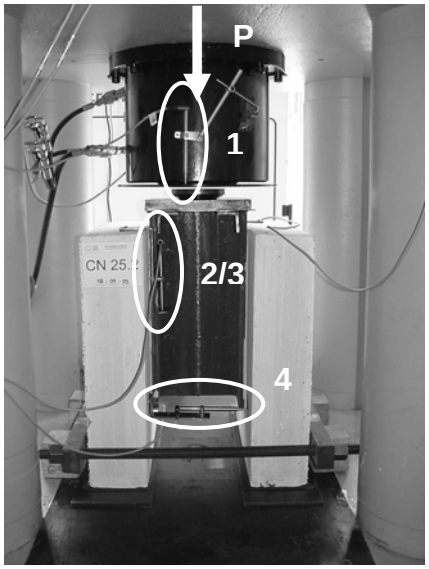

P – load

1 – test displacement control

2 and **3** – measurement of slip

4 – measurement of horizontal separation

Figure 3.29 – Testing frame setup and test dispositions (POST tests)

Some of the tested specimens with Perfobond connectors and T connectors were instrumented with strain gauges positioned at the concrete slab transversal reinforcement (Figure 3.30).

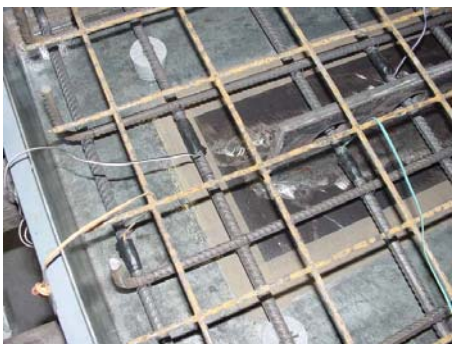

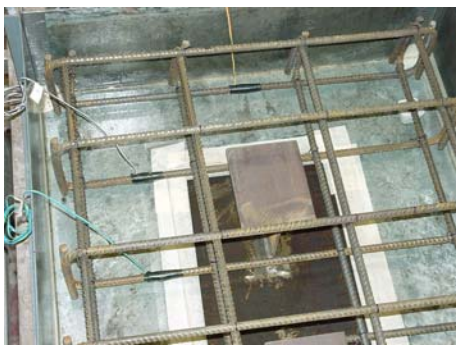

Figure 3.30 – Details of strain gauges dispositions (POST tests)

The intention of using strain gauges is to evaluate how this reinforcement is carrying the loads and its contribution to the connection load and deformation capacity. Strain gauges from TML, type FLA-3-11, were attached to the reinforcement bars. These strain gauges read in ¼ bridge, with a 120Ω resistance and an error margin of 0.3Ω.

For SPOT tests, the measuring devices are positioned as represented in Figure 3.31. The first part of the test is controlled by load. The second phase of the test is controlled by the specimen deformation. In this case, the machine internal transducer was used to impose the deformation rate, because this measurement is directly related to slip between the concrete slab and the steel plates.

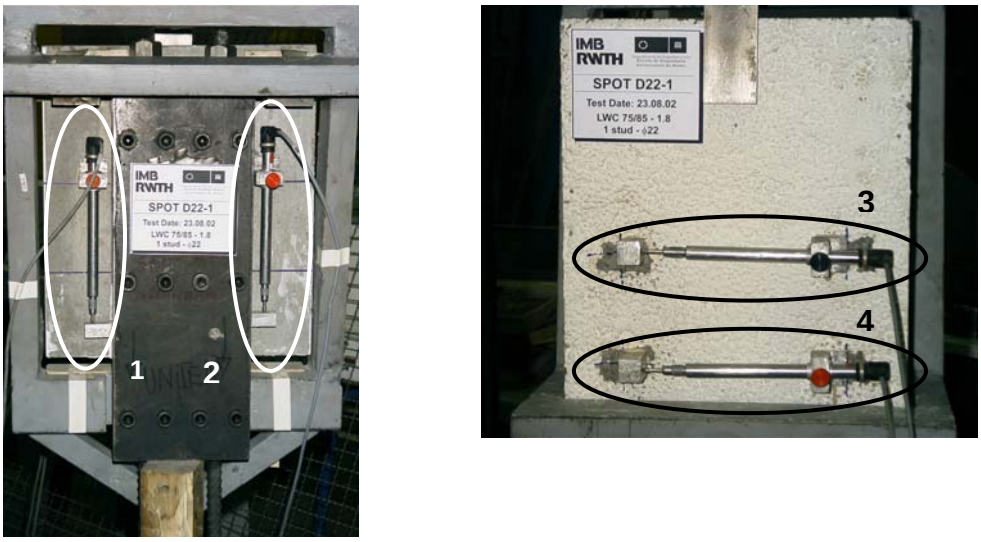

a) Back view – two displacement transducers to measure slip

b) Displacement transducers in the front

Figure 3.31 – Testing frame setup and test dispositions (SPOT tests)

Transducer 1 is attached to the concrete slab and has its measuring base on the specimen steel plate. The same happens with **transducer 2** and therefore, the slip between the steel plate and the concrete slab is an average value from these two measuring devices. **Transducer 3** and **transducer 4** are horizontally positioned on the specimen opposite side. These devices try to identify crack openings and measure crack width.

3.6 Tests with stud connectors

3.6.1 Objectives

A large number of standard push-out tests have already been performed with normal weight concrete and stud connectors. The experimental campaign here presented is the result of performing push-out tests that follow the description and procedure presented in 3.5, but now using high strength lightweight concrete.

The objectives of this research are:

- to analyse the adequacy of using lightweight concrete in composite structures, focusing on the shear connection behaviour with stud connectors;
- to determine the stud connector connection load bearing capacity;
- to evaluate the connection ductility;
- to evaluate the connection deformation capacity and the load-slip relation, before and after the maximum load is attained;
- to analyse the connection stiffness for service loads;
- to compare all the mentioned parameters with the ones obtained for normal weight concrete in experimental tests performed by other authors;
- to assess if the equations proposed in the standards to evaluate the maximum load are appropriate for high strength lightweight concrete.

3.6.2 Materials properties

The HSLWC mixtures were defined in UM and RWTH with the available materials at each country. The POST tests used a lightweight concrete studied at the Structural Laboratory of University of Minho (LEST-UM) and for the SPOT a lightweight concrete developed at the Institute of Structural Concrete (IMB-RWTH) was used. Concrete properties are not exactly the same for both mixtures, but the values for compressive strength and modulus of elasticity presented in Table 3.1 were determined for all castings at the same day of the respective test.

Concrete specimens were cast simultaneously with the push-out tests. At LEST-UM, cylinders of 150mm diameter and 300mm high were used, while at IMB-RWTH both cylinders and cubes of 150mm^3 were chosen (Figure 3.32).

a) Concrete specimens at UM

b) Concrete specimens at RWTH

Figure 3.32 – Specimens for the determination of concrete properties

Table 3.1 – Concrete properties for push-out test specimens with stud connectors

Specimens	Concrete Ref.	Test	Connectors disposition	Concrete density (kg/m^3)	$f_{c,cylinder}$ (MPa)	$f_{c,cube}$ (MPa)	E_c (GPa)
CN 19.1	B17	POST	Single	1899	53.72	-	24.72
CN 19.2	B18	POST	Single	1871	55.98	-	24.48
CN 19.3	B19	POST	Single	1914	55.43	-	24.68
CN 22.1	B20	POST	Single	1914	58.72	-	24.89
CN 22.2	B21	POST	Single	1940	55.17	-	25.73
CN 22.3	B22	POST	Single	1786	54.07	-	22.38
CN 25.1	B26	POST	Single	1826	55.33	-	24.23
CN 25.2	B27	POST	Single	1819	54.63	-	24.47
CN 25.3	B28	POST	Single	1812	53.39	-	22.46
CDN 19.1	B23	POST	Double	1783	54.63	-	22.27
CDN 19.2	B24	POST	Double	1854	61.23	-	28.02
CDN 19.3	B25	POST	Double	1816	58.08	-	25.98
KBD19/P1 KBD19/P2	Ba	SPOT	Single	1800	-	94.0	23.5
KBD19/1 KBD19/2 KBD19/3	Bb	SPOT	Single	1800	-	84.6	26.6
KBD22/1 KBD22/2 KBD22/3	Bc	SPOT	Single	1800	-	78.5	25.7
KBD25/1 KBD25/2 KBD25/3	Bc	SPOT	Single	1800	-	78.5	25.7
KBDD19/1 KBDD19/2 KBDD19/3	Bb	SPOT	Double	1800	-	84.6	26.6

Steel specimens were sampled from the same reinforcement and stud group used in the push-out tests and later tested. The test specimens and the tensile test procedure follow the dispositions defined in EN 10002-1 (2001) for studs and ENV 10080 (1995) for reinforcement bars. Table 3.2 presents the corresponding results and Figure 3.33 presents the test setup,

Table 3.2 – Steel properties

Type of specimen	diameter	POST tests		SPOT tests	
	d (mm)	f_y (MPa)	f_u (MPa)	f_y (MPa)	f_u (MPa)
Stud	19	501	596	502	534
	22	458	559	532	548
	25	466	557	566	584
Reinforcement	10	576	675	-	-

where, f_y is steel yielding tensile strength and f_u is the steel maximum tensile strength.

a) Stud specimen | b) Test on stud specimen | c) Stud specimen after failure | d) Reinforcement specimen

Figure 3.33 – Specimens for the determination of steel properties

3.6.3 Standard Push-Out Test

3.6.3.1 POST test specimens

The specimens prepared for the standard push-out test were produced according to Figure 3.35. The geometry of the test specimens is always the same, with variation on the stud diameter and disposition. Three stud diameters were used: 19 mm, 22 mm and 25 mm. These diameters were chosen as they present high load capacity and are suitable to be used in bridge decks.

The specimen represented in Figure 3.35a corresponds to the isolated stud series. The slab dimensions and the stud spacing is always the same for each chosen diameter. The double stud disposition is tested only for 19 mm diameter studs (Figure 3.35b).

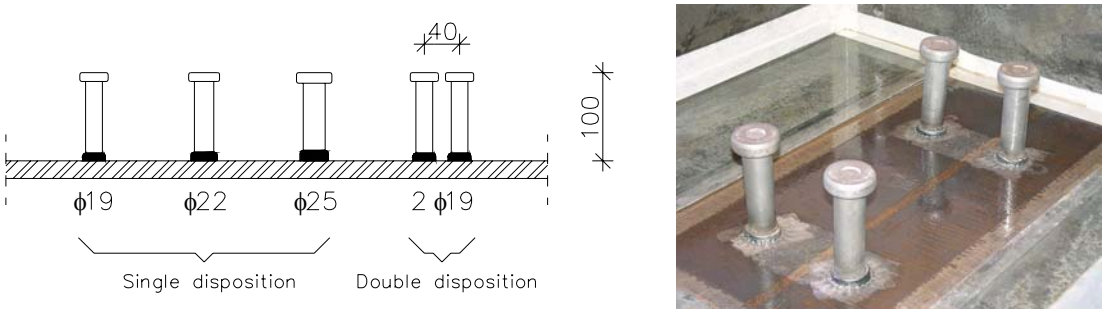

Figure 3.34 – Headed studs configuration and dimensions

The specimens consist of two lightweight concrete slabs held in the vertical position, and steel HEB260 profile positioned between them, with welded studs concreted inside the slabs. The slab dimensions are 600 mm × 650 mm × 150 mm. All the slab reinforcement represented in Figure 3.35 corresponds to 10 mm diameter bars.

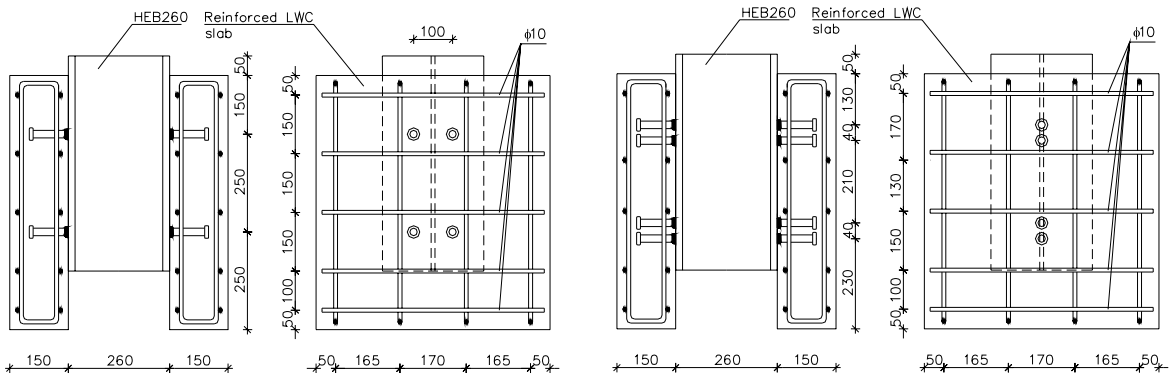

a) Isolated stud: diameters of 19, 22 and 25 mm (CN series)

b) Double stud of 19 mm diameter (CDN series)

Figure 3.35 – Specimens geometry for experimental POST tests

3.6.3.2 POST test results

The load carrying capacity of one headed stud in normal weight concrete essentially results from four components:

– concrete compressive strength around the welded collar;

– shear and bending of the stud shank;

– tensile forces in the stud's shank;

– and friction forces between steel and concrete on the composite joint.

The load carrying capacity due to friction is not considered in the tests performed because the steel surface was greased before concreting. In high strength concrete there are almost no tensile forces acting in the shank, (Döinghaus 2001). In addition, the deformation concentrates on a small area directly above the welded collar. In case of lightweight concrete this behaviour is not well known, making experimental testing necessary.

In all the specimens tested with 19 mm and 22 mm diameter studs, shear failure is identified on studs. Failure always occurs first on one side of the specimen, even though the specimens are symmetric. Usually, there is one or two studs that suffer failure before the rest, after what the specimen still holds some load capacity for a while and then total failure occurs in one slab of the specimen, with the failure of those four studs.

Figure 3.36 presents the shank failure and the cracked slab near the stud position for specimens with 19 mm diameter, both with single and double disposition. In the double stud disposition, the two studs are closely welded creating a more concentrated stressed zone and thus provoking a larger crushed concrete zone. The stud positioned above suffers

higher deformation, as visible in Figure 3.36 for specimens CDN19. This happens because the higher stresses are concentrated between the two studs, causing the total crushing of concrete in this zone.

a) CN 19.2 b) CDN 19.3 c) CDN 19.3

Figure 3.36 – Stud failure for single and double stud disposition (POST tests with 19 mm diameter)

As the stud diameter gets larger, the load bearing capacity of the shear connection increases. The concrete slab is subjected to higher stresses and thus more cracks are developing as can be seen in Figure 3.37. This was observed during testing, for different specimens, (Valente and Cruz 2003).

a) CN 19.2 b) CN25.2

Figure 3.37 - Concrete crack patterns (POST tests)

The stud failure always happens right above the welded collar, as presented in Figure 3.38a. There is a zone of crushed concrete under the stud welded collar. This zone is very localized, as can be observed in the same picture, but it gets more developed for larger stud diameters (Figure 3.38b and Figure 3.38c).

a) CN25.1 b) CN19.1 c) CN25.1

Figure 3.38 – Stud failure for experimental POST tests

After the tests were performed, some slabs were destroyed in order to observe the deformed connectors. Some of these deformed studs are presented in Figure 3.39. The stud deformation is particularly localized on the stud basis and its magnitude is always directly related to the total slip developed during the load application. The stud shear failure is a common failure mode for studs in high strength concrete. In this perspective, the use of high strength lightweight concrete introduces no changes on the connection behaviour when compared to high strength normal weight concrete. When relating the stud deformed shape with the generalized failure types presented in Figure 3.7, a combination of failure types a) and b) is identified, with a predominance of type a) failure. For the double stud disposition (Figure 3.39d) the stud positioned on top suffers a more pronounced bending at its mid height, which means that there is loss of compressive strength on the concrete positioned between the two studs, leading to a behaviour that is similar to the one verified for headed studs in normal weight concrete. Therefore, more deformed studs should be expected if normal strength lightweight concrete was used. In this case, the deformation should be more localized at the stud mid height.

a) CN19.3 b) CN22.2 c) CN25.1 d) CDN19.1

Figure 3.39 – Stud redrawn from the lightweight concrete slabs of POST test specimens

Figure 3.40 to Figure 3.42 present the load-slip curves for tested specimens with 19 mm diameter studs. Three identical specimens were tested and the three correspondent load-slip curves show very similar evolution, proving the good quality of the test procedure. The values for the maximum load obtained in the three tested specimens are very similar, with a maximum difference of 1.6 kN. This corresponds to a standard deviation of 0.8 kN and a variation coefficient of 0.57%.

The load-slip curves for 19 mm diameter studs show an initial almost linear progression, until about 65% of the maximum load value is attained. Then, the curve develops a new branch with a softer slope, while the load is still increasing. This branch of the curve has high importance on the connection behaviour, as significant values of slip are mobilized at this phase. After the maximum load is reached, the load tends to decrease in a faster rate than it did while increasing.

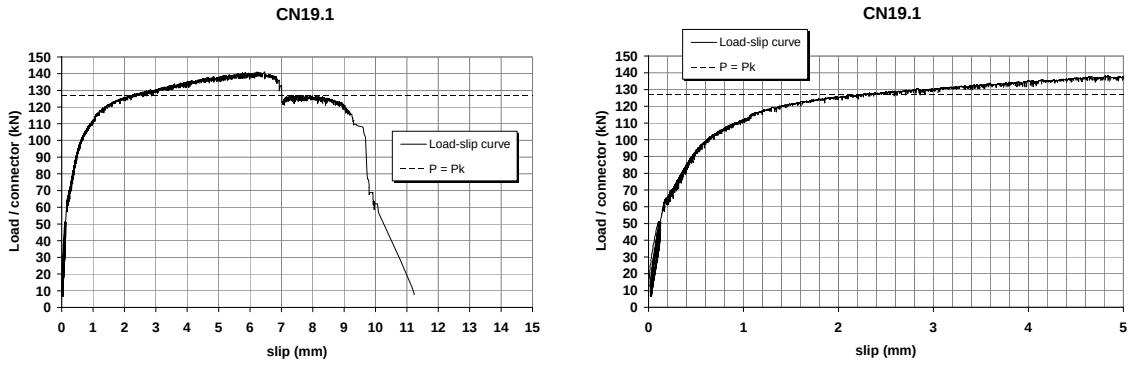

a) Complete load-slip curve b) Initial part of the load-slip curve

Figure 3.40 – Load-slip curves for specimen CN19.1 (POST test)

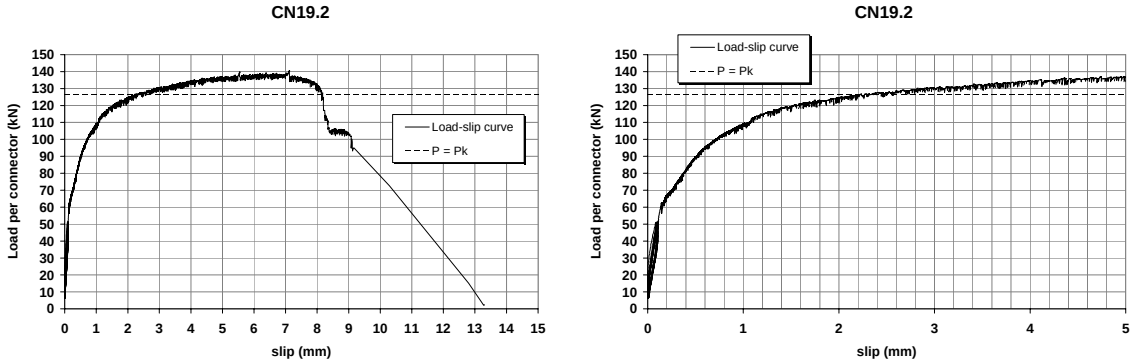

a) Complete load-slip curve b) Initial part of the load-slip curve

Figure 3.41 – Load-slip curves for specimen CN19.2 (POST test)

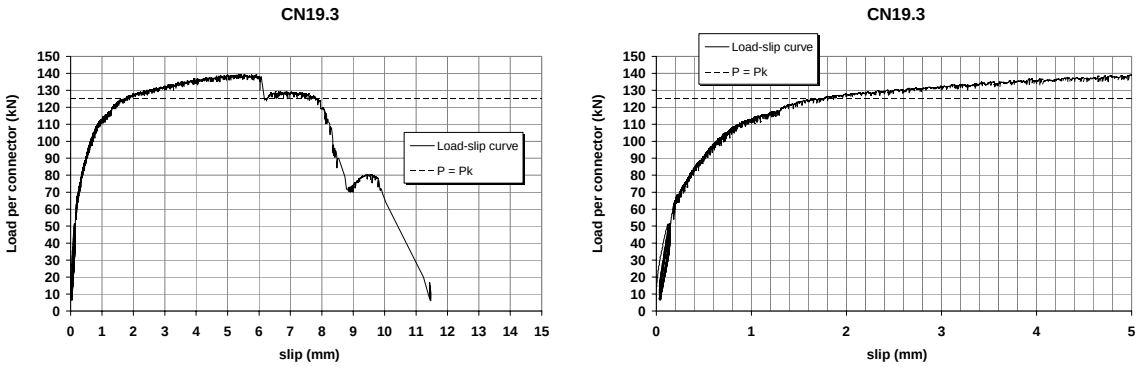

a) Complete load-slip curve b) Initial part of the load-slip curve

Figure 3.42 – Load-slip curves for specimen CN19.3 (POST test)

Figure 3.43 presents the three curves for CN19 specimens. In terms maximum load, the three specimens with 19 mm diameter stud present very similar results. The principal difference observable between the three tests relates to the slip value when failure is approaching. In fact, some of the specimens show higher deformation capacity than others. The measured slip difference is of about 2 to 2.5 mm.

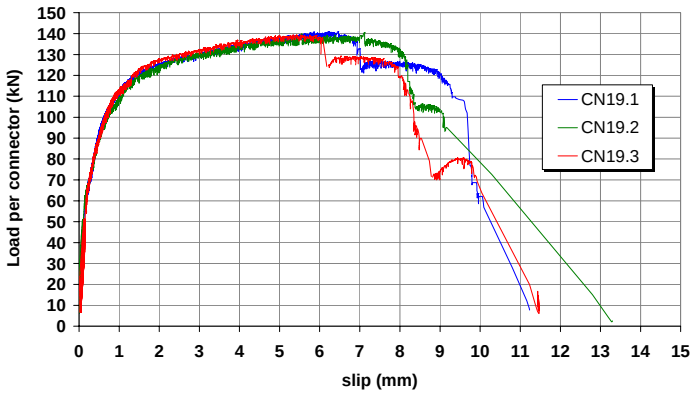

Figure 3.43 – Load-slip curves for studs with 19 mm diameter (POST tests)

One possibility for this difference is that in some specimens, there may be a more efficient redistribution of load between the several studs that constitute the connection, allowing the load to be sustained for a while longer. Other possibility is that the studs' characteristics can differ. However, specimens were cut from studs, were tested in a tensile strength test, as presented in Table 3.2, and the results obtained show that tensile strength has small variation. In this case, the welded collar dimensions may justify the differences, as the steel and the stud production follow predetermined procedures and are subjected to quality control. In fact, some differences regarding the welded collar dimensions were measured, which may affect the connection behaviour during the failure process. However, this influence is very difficult to evaluate because for one side it is almost impossible to test specimens without the welding collar and on the other side, there are four studs in each slab, so the variability on the welded collar dimensions is present in every specimen.

As presented in Figure 3.44 and Figure 3.45, the specimens tested with studs of 22 mm diameter show very similar behaviour to what was observed for the specimens with 19 mm diameter. The types of failure observed are also related to shearing, occurring first in on side of the specimen as it did with the smaller stud diameter tests. The values for the maximum load obtained in the three tested specimens are again very similar, with a maximum difference of 1.5 kN. These results present a standard deviation of 0.7 kN and a variation coefficient of 0.48%.

The load-slip curves for 22 mm diameter studs show an initial almost linear progression, until about 65% of the maximum load value is reached. Then, the curve develops a new branch with a softer slope, while the load is still increasing. When comparing this branch with the correspondent branch of the load-slip curve of CN19 series, it is observable that the load increase at this phase is much smaller. For the 22 mm diameter studs, this branch of the load-slip curve is almost horizontal, meaning that slip develops for an almost constant load value. This branch of the curve has a high importance on the connection behaviour, as significant values of slip are mobilized at this phase. The values of plastic slip are a bit higher for this diameter than for the 19 mm diameter, which was expected. After the maximum load is reached, the load tends to decrease in a faster rate than it did while increasing, leading to a similar load loss and failure as was observed for the previous tests.

The load-slip curve for specimen CN22.1 is not presented, as there were some problems with the test control, during experimental work.

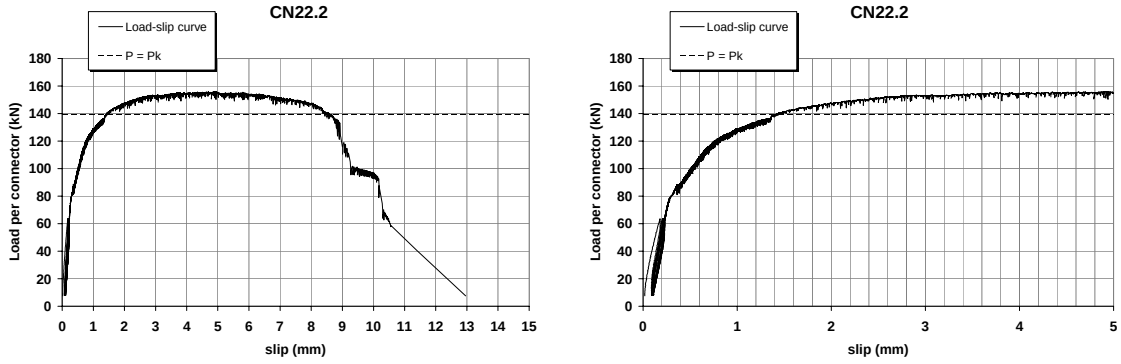

a) Complete load-slip curve b) Initial part of the load-slip curve

Figure 3.44 – Load-slip curves for specimen CN22.2 (POST test)

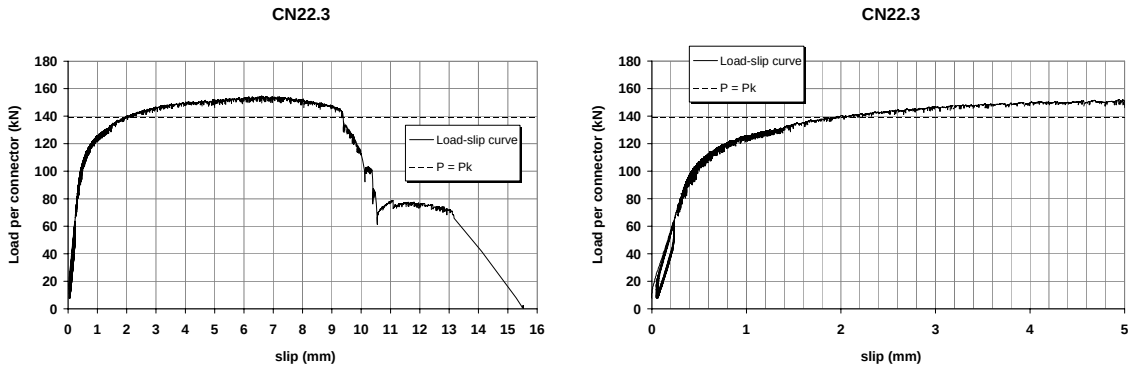

a) Complete load-slip curve b) Initial part of the load-slip curve

Figure 3.45 – Load-slip curves for specimen CN22.3 (POST test)

Figure 3.46 shows the load-slip curves for tested specimens with 22 mm diameter studs. Again, the maximum load is similar for both specimens and the main differences have to do with maximum slip capacity.

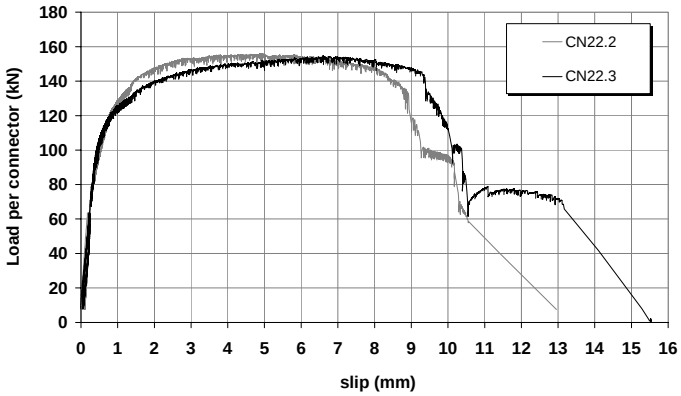

Figure 3.46 – Load-slip curves for studs with 22 mm diameter (POST tests)

Unlike the other tested stud diameters, for 25 mm diameter stud, shear failure on the T web occurred for specimen CN25.1 and concrete failure occurred for specimens CN25.2 and CN25.3. The load-slip diagrams for specimens with 25 mm diameter are represented in Figure 3.47 to Figure 3.49.

The high loads imposed during these tests lead to significant concrete slab cracking and concrete crushing near the studs. Initially, the relation between load and slip is almost linear, until around 70% of the maximum load is reached. After this, the curve takes a new rate of growth with a softer slope, but the maximum load is rapidly attained. After the maximum load, the connection is slowly loosing load capacity, as the concrete slabs are progressively cracked. From this point on, the slip growth results mainly from the concrete cracking and not from the stud deformation. As a consequence, the descending branch is softer on 25 mm diameter specimens, as failure happens with progressive cracking and crushing of the concrete slabs, without shear failure on studs.

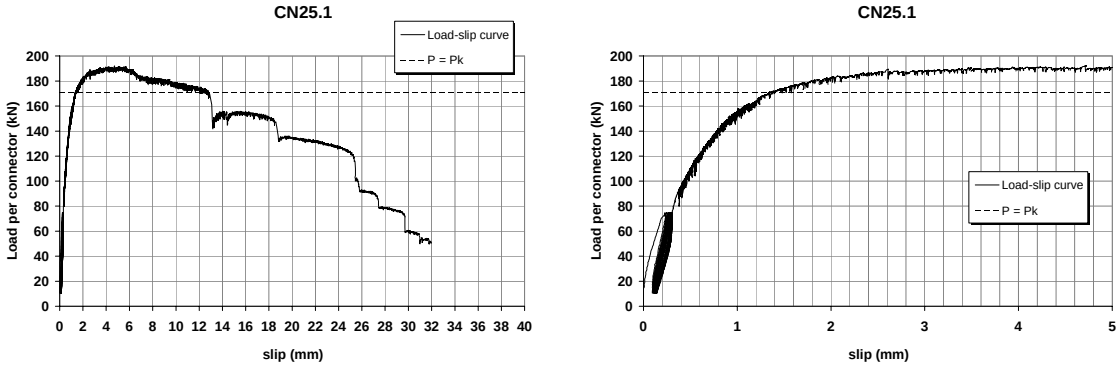

a) Complete load-slip curve b) Initial part of the load-slip curve

Figure 3.47 – Load-slip curves for specimen CN25.1 (POST test)

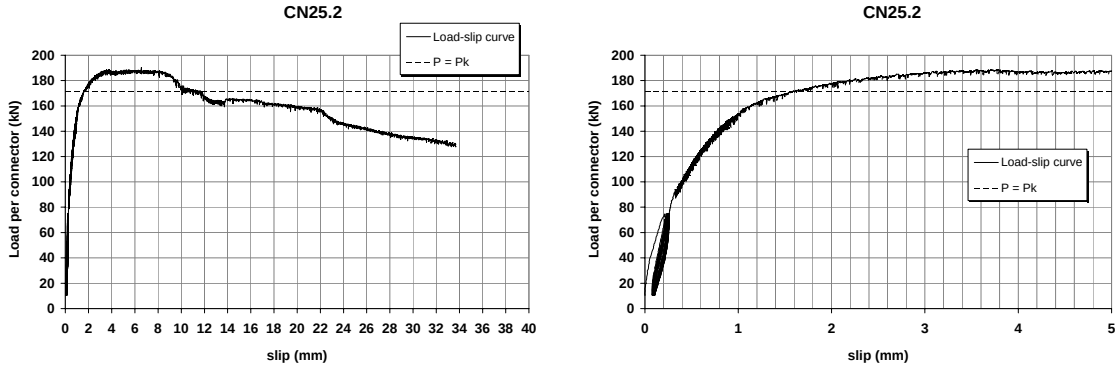

a) Complete load-slip curve b) Initial part of the load-slip curve

Figure 3.48 – Load-slip curves for specimen CN25.2 (POST test)

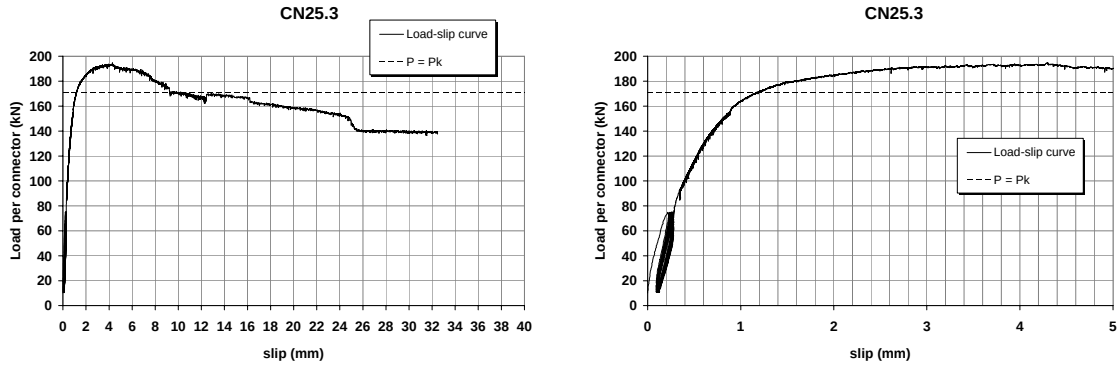

a) Complete load-slip curve b) Initial part of the load-slip curve

Figure 3.49 – Load-slip curves for specimen CN25.3 (POST test)

Only for specimen CN25.1, the load-slip curve is similar to the curves determined for smaller diameters because the failure of the different studs can be identified by the singular load losses of the diagram presented in Figure 3.50.

Thus, the curve for CN25.1 specimen differentiates from the curves of CN25.2 and CN25.3 when the first stud suffers failure. Apart from this aspect, the three curves, correspondent to the three 25 mm diameter specimens are very similar, with the same magnitude of load and slip values. The values for the maximum load obtained in the three tested specimens have a maximum difference of 4.5 kN. The obtained results correspond to a standard deviation of 2.2 kN and a variation coefficient of 1.17%.

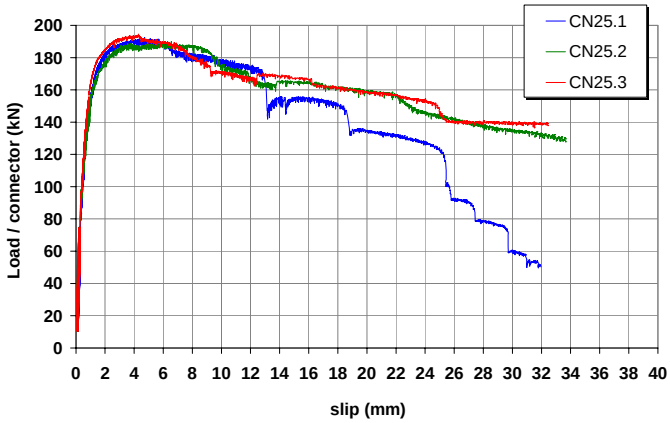

Figure 3.50– Load-slip curves for studs with 25 mm diameter (POST tests)

In the last series of POST tests with headed stud connectors, a new disposition for the studs is chosen. Two studs of 19 mm diameter are closely welded, so that the spacing between them is only the necessary for allowing proper welding and concrete pouring. This disposition is represented in Figure 3.35. The intention is to compare the obtained results in terms of load capacity and slip, with the ones obtained for the single stud disposition, used in series CN19. The load-slip curves for the three tested specimens are presented in Figure 3.51, Figure 3.52 and Figure 3.53.

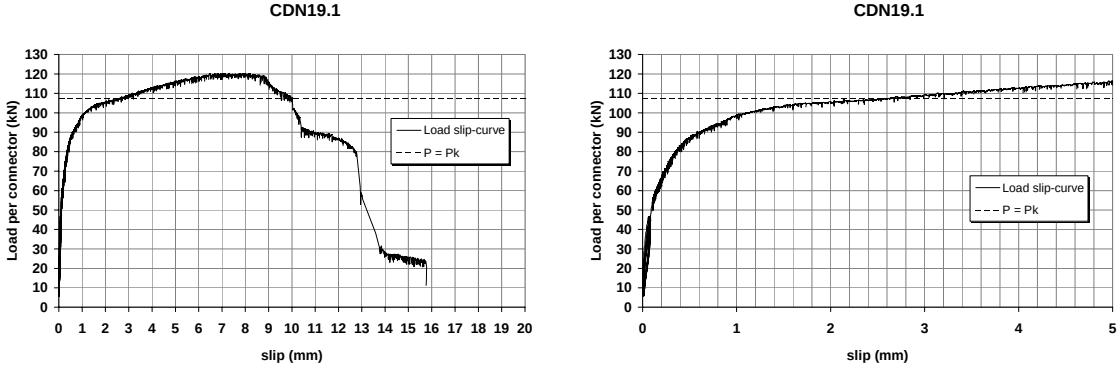

a) Complete load-slip curve

b) Initial part of the load-slip curve

Figure 3.51 – Load-slip curves for specimen CDN19.1 (POST test)

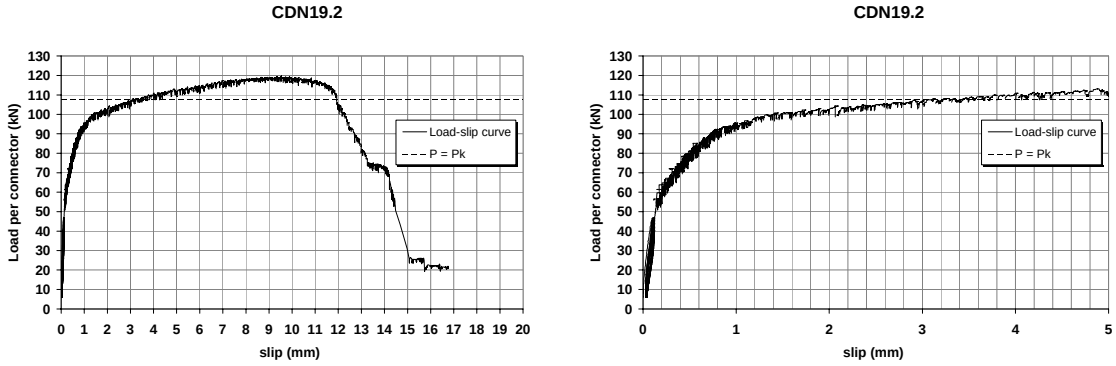

a) Complete load-slip curve b) Initial part of the load-slip curve

Figure 3.52 – Load-slip curves for specimen CDN19.2 (POST test)

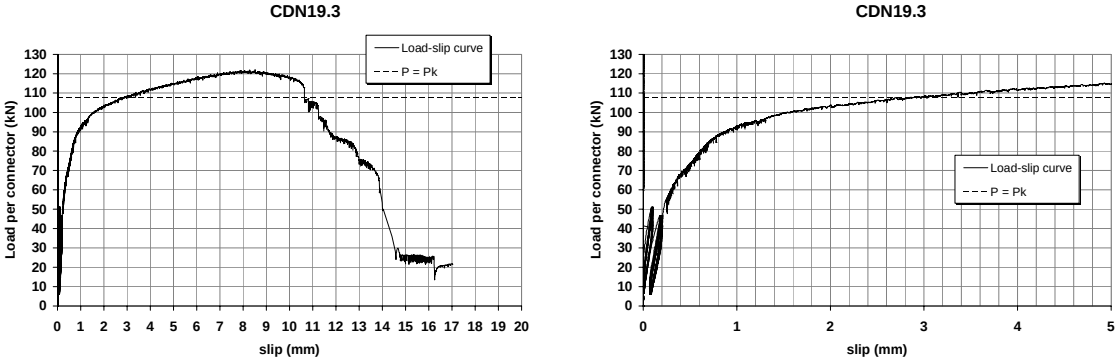

a) Complete load-slip curve b) Initial part of the load-slip curve

Figure 3.53 – Load-slip curves for specimen CDN19.3 (POST test)

The load-slip curves for the three tested specimens are presented in Figure 3.54.

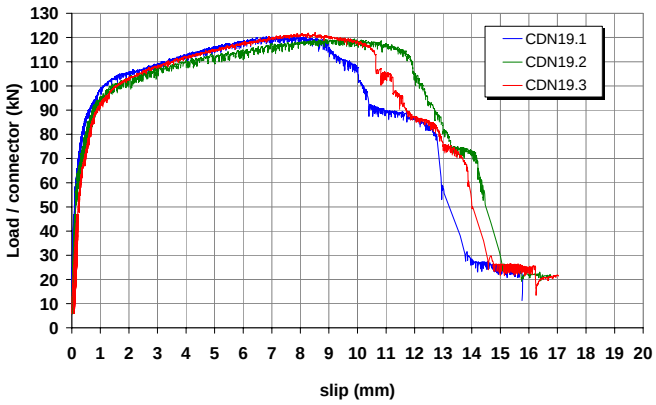

Figure 3.54 – Load-slip curves for double stud disposition, with 19 mm diameter (POST tests)

The curves that result from the three tested specimens are very similar. As it happened for the single stud disposition, the main difference between them is the final slip value before failure, where maximum differences of around 2 mm are found. The obtained

results correspond to a standard deviation of 1.2 kN and a variation coefficient of 1.0%. In terms of global behaviour, the curves obtained for single and double stud disposition are very similar, with a first branch of almost linear relation between load and corresponding slip, and a second branch where important slip deformation takes place, while the load grows at a softer rate.

Figure 3.55 presents two load-slip curves, one corresponding to a specimen of the single stud disposition series and the other corresponding to a specimen of the double stud disposition series. The superposition of the two curves shows that in general the two curves are very similar, denoting the same type of behaviour. It is to notice that the load–slip relation for the second branch of the load–slip curves presents similar growth trend for CN19 and CDN19 specimens, which is rather surprising, because the concentration of stresses on concrete and the studs' deformation are not the same for both configurations.

The main difference regards a loss of load bearing capacity for the double stud disposition. This loss of load capacity is however accompanied by an increase on the connection deformation capacity. Comparing the obtained results, it is verified that the double stud disposition results in a reduction of 14% on the average maximum load value, for the tested specimens. However, this result comes together with a deformation capacity increase of 22.3% of the characteristic slip value (see Table 3.3).

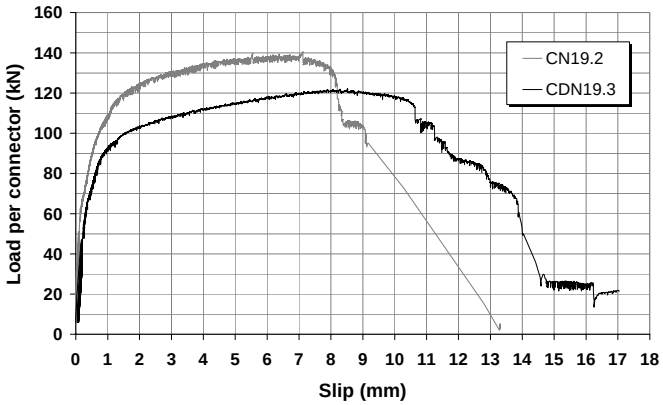

Figure 3.55 – Load-slip curves for single and double stud disposition, with 19 mm diameter (POST tests) – Specimens CN19.2 and CDN19.3

Figure 3.56 presents the load-slip curves that result from the testing of one specimen of each chosen stud diameter. Comparing all the different tested diameters, it becomes clear that load capacity increases with stud diameter. This is obviously an expected result, as the same result was measured in tests performed by other authors with normal weight concrete. The other significant result is that there is also an increase of the maximum measured slip, as the stud diameter gets larger.

As visible in all the load-slip curves presented, headed studs are characterized by an initially stiffer behaviour, followed by a plastic behaviour, with a constant or slow increasing load capacity in the plastic range.

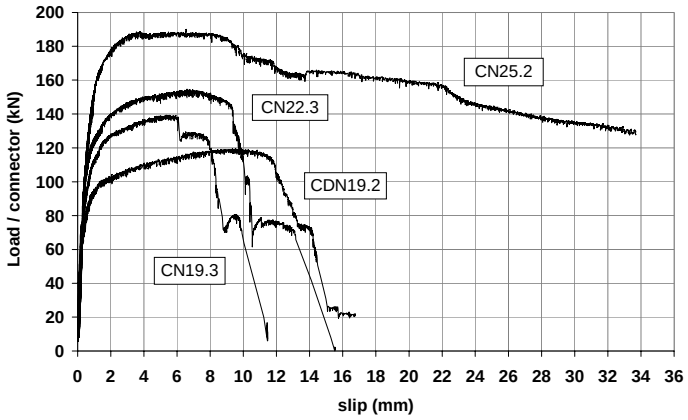

Figure 3.56 - Load vs. slip (POST tests)

The first important result, measured in a push-out test, is the maximum applied load. This value, divided by the number of similar loaded connectors in the specimen, corresponds to the connection ultimate load capacity. According to EN1994-1-1, (CEN 2004b), at least three identical specimens are needed to determine the connection characteristic load capacity value. The maximum load value is measured for of each of the three specimens used for the push-out test and the connection characteristic load capacity value, P_k , is calculated considering 90% of the minimum value taken from this group.

In agreement with this, Table 3.3 presents the maximum load value determined for each tested specimen, $P_{max,i}$, and the corresponding characteristic load value determined for three identical specimens, P_k.

In each of the diagrams presented (from Figure 3.40 to Figure 3.53), the characteristic load value is a defined with the curve $P = P_k$. This load limit is also used to define the elastic slip value and the plastic slip value. The elastic slip values correspond to the value of slip when $P < P_k$. From this point forward, all of the slip is considered as plastic. The slip characteristic value is determined as the plastic slip value correspondent to the characteristic load value. Graphically, it can be defined as the slip portion measured between the two intersections of the line $P = P_k$. with the load-slip curve.

Paragraph 6.6.1.1(5) of EN 1994-1-1, (CEN 2004b), recommends a characteristic plastic deformation value, δ_k of 6 mm for stud connectors, if a ductile behaviour is intended. This limit is verified for most of the tested specimens, guarantying ductility, (Cruz et al. 2005). Results of tests performed in Germany at RWTH, (Hegger et al. 2000), with HSNWC reveal that this minimum deformation value of 6 mm is not always achieved. However, it is important to refer that this aspect is only relevant when the connection elastic-plastic behaviour is assumed.

The determination of the characteristic slip value with the process described results in considerably high values of elastic slip, especially for the smaller diameters, as was verified during calculations. In this case, elastic slip may be overestimated, while plastic slip is underestimated. The difficulty here is to establish a limit for which the slip value is no longer elastic. For that purpose, this criterion needed to be imposed.

Table 3.3 - Experimental results for POST tests

Specimen Ref.	$P_{max,i}$ (kN)	$s_{Pmax,i}$ (mm)	P_{medium} (kN)	P_k (kN)	$s(P_{max})$ (mm)	$s_{elast,90\%}$ (mm)	$s_{plast,90\%}$ (mm)	$s_{total,90\%}$ (mm)	s_k (mm)
CN 19.1	141.0	6.45			6.45	1.85	6.74	8.59	
CN 19.2	140.4	7.11	140.2	125.4	7.11	2.11	6.09	8.19	5.42
CN 19.3	139.4	5.33			5.33	1.77	6.02	7.79	
CN 22.1	155.1	*			*	*	*	*	
CN 22.2	156.0	4.90	155.2	139.1	4.90	1.40	7.26	8.65	6.53
CN 22.3	154.5	6.60			6.60	1.94	7.44	9.39	
CN 25.1	192.1	4.71			4.71	1.35	11.45	12.80	
CN 25.2	190.0	6.55	192.2	171.0	6.55	1.54	10.25	11.79	9.23
CN 25.3	194.5	4.29			4.29	1.17	11.84	13.01	
CDN 19.1	120.3	7.31			7.31	2.63	7.37	10.00	
CDN 19.2	119.6	9.52	120.6	107.7	9.52	3.08	8.83	11.91	6.63
CDN 19.3	122.0	8.51			8.51	2.69	8.12	10.81	

* Deformation control on CN22.1 was not properly accomplished; therefore, this result is not considered.

$P_{max,i}$ maximum load (for each specimen)

$P_k = 0.9\ P_{max}$, where P_{max} is the minimum value for a group of three similar specimens

$s_{elast,90\%}$ elastic slip for load P_k

$s_{plast,90\%}$ plastic slip for load P_k

$s_{total,90\%}$ elastic slip + plastic slip for load P_k

s_k 0.9 × minimum plastic slip for a group of three similar specimens

There is a close linear relation between maximum load and corresponding characteristic slip value for specimens with single stud disposition, as presented in Figure 3.57. The results on double stud distribution don't follow the tendency presented.

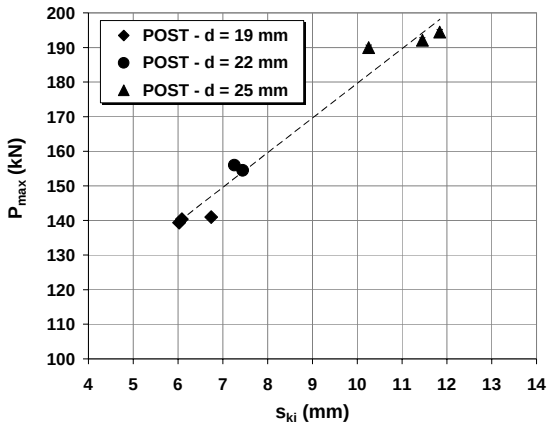

Figure 3.57 - Maximum load and corresponding characteristic slip (POST tests)

Transforming now the load-slip curves obtained into shear stress-slip curves, where the value of shear stress is calculated dividing the applied load by the stud shear area, new aspects are put in evidence (Figure 3.58). The first is that the shear stress attained for 19 mm diameter studs is significantly higher than the values attained for higher diameters and the second is that the values attained for 22 mm and 25 mm diameter are of similar value, even though different types of failure were observed for these two diameters.

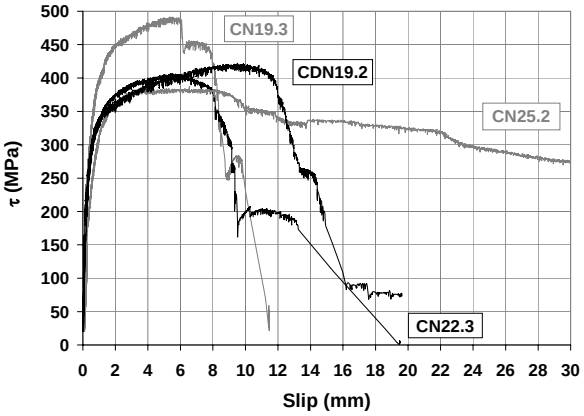

Figure 3.58 - Maximum shear stress and corresponding slip (POST tests)

According to the studies developed at the University of Leipzig, in Germany, (Faust et al. 2000), the expression (3.2), proposed to evaluate the load bearing capacity of headed stud connectors, is also valid for lightweight concrete and can be expressed in terms of stress, (3.2).

$$\tau_u = 0.5 \cdot \sqrt{f_{ck} \cdot E_c} \tag{3.2}$$

This study gathered results from a group of experimental tests performed with normal weight and lightweight concretes of different compressive strengths. The transition between concrete failure and steel failure was measured for a value of parameter $\sqrt{f_{ck} \cdot E_c}$ equal to 1100 MPa. For higher values, a ceiling was identified, and failure was always caused by the connector shear failure.

Figure 3.59 results from plotting the experimental results obtained within this work with the curve defined by equation (3.2). Concrete failure was observed for two of the 25 mm diameter specimens, which is confirmed with the diagram, as their result is in the frontier between the two types of failure.

In global terms, the results obtained are below curve (3.2), which means that the tests performed with the present work seem to result in smaller ultimate loads than the ones obtained by Faust et al. (2000). Equation (3.2) is replaced by equation (3.3), used in EN1994-1-1 (CEN 2004b), that is closer to the experimental results obtained.

$$\tau_u = 0.36 \cdot \sqrt{f_{cm} \cdot E_{cm}} \tag{3.3}$$

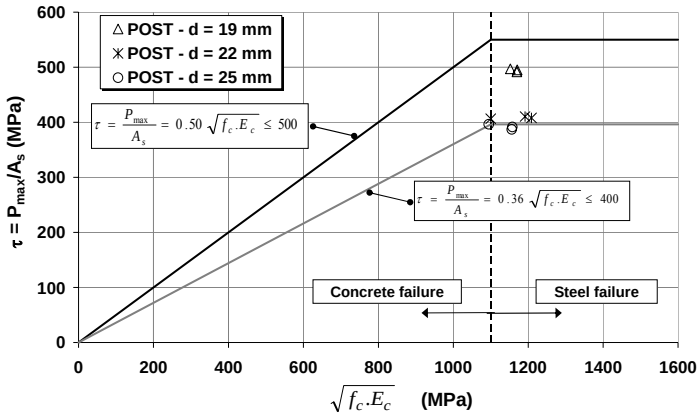

Figure 3.59 – Shear stress for maximum load vs. $\sqrt{f_c \cdot E_c}$

The values of slip correspondent to the test maximum load are presented in Figure 3.60 (symbols with no background). These values are all of similar magnitude, with exception to the CDN19 series (double stud disposition), whose values are higher. Even so, slip for maximum load shows a tendency to decrease as the stud diameter increases, which means that in order to mobilize the maximum shear force, the studs with smaller diameters have to deform more than the studs with larger diameters. This should not be the case if the maximum load depended only on the shear stud. One possibility is that the larger studs make a more effective transmission of load between the stud and the concrete slab, because the contact area is larger.

The values of characteristic slip measured (see Table 3.3 and Figure 3.60) are much higher than the values of slip measured when $P = P_{max}$ and seem higher than the deformation measured in studs after they are collected from the concrete slab after testing. As referred, there is concrete crushing under the stud, in front of the welded collar. It is thought that an important part of the plastic slip is obtained with the deformation of concrete.

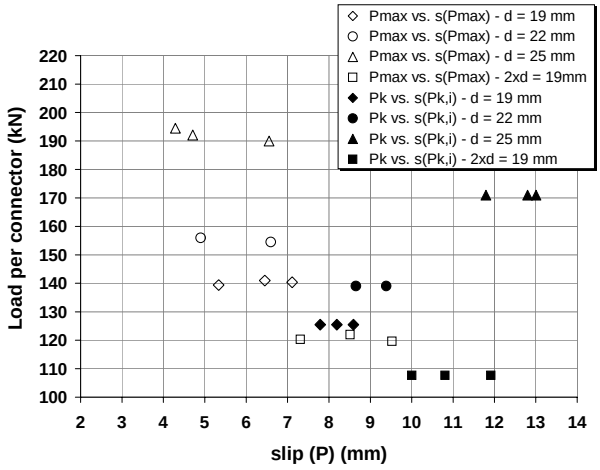

Figure 3.60 – Load vs. correspondent slip (POST tests)

3.6.4 Stiffness measured for POST tests with headed stud connectors

In order to evaluate the connection stiffness, k, it is usual to define a relation between a defined percentage of the maximum applied load and the correspondent value of slip.

Table 3.4 and Table 3.5 establish direct relations between applied load (per connector) and corresponding slip value, for each tested specimen. The values of stiffness, k, are determined assuming an elastic behaviour of the connection, until a particular percentage of the test maximum load per connector is reached, as defined in (3.4) (X is variable).

$$k\left(X\%P_{max}\right)=\frac{P_{X\%P_{max}}}{s_{X\%P_{max}}} \tag{3.4}$$

Table 3.4, Table 3.5 and Figure 3.61 present the evolution of the value of stiffness, k, in respect to the level of shear load applied to the connector, P/P_{max}.

Table 3.4 - Connection stiffness values (for 40%, 45% and 50% of P_{max})

	P_{max} / 8	0.40 P	s (0.40P)	k	0.45 P	s (0.45P)	k	0.50 P	s (0.5P)	k
		(kN)	(mm)	(kN/mm)	(kN)	(mm)	(kN/mm)	(kN)	(mm)	(kN/mm)
CN19.1	140.96	56.39	0.141	**399.90**	63.43	0.178	**357.37**	70.48	0.258	**273.18**
CN19.2	140.39	56.16	0.122	**460.29**	63.17	0.173	**366.23**	70.19	0.255	**275.81**
CN19.3	139.39	55.76	0.161	**346.31**	62.72	0.187	**336.33**	69.69	0.248	**281.03**
CN22.2	155.99	62.39	0.231	**270.69**	70.19	0.251	**280.21**	77.99	0.282	**276.57**
CN22.3	154.52	61.81	0.228	**271.08**	69.53	0.256	**271.61**	77.26	0.293	**263.68**
CN25.1	192.12	76.85	0.314	**245.13**	86.45	0.341	**253.90**	96.06	0.403	**238.66**
CN25.2	189.99	75.99	0.264	**288.40**	85.49	0.289	**296.34**	94.99	0.352	**270.25**
CN25.3	194.48	77.79	0.285	**273.44**	87.52	0.322	**271.79**	97.24	0.379	**256.57**
CDN19.1	120.31	48.12	0.091	**531.75**	54.14	0.105	**518.08**	60.15	0.140	**431.22**
CDN19.2	119.61	47.85	0.129	**370.90**	53.83	0.142	**380.40**	59.81	0.200	**299.04**
CDN19.3	121.96	48.79	0.212	**230.67**	54.88	0.225	**244.47**	60.98	0.318	**192.07**

Table 3.5 – Connection stiffness values (for 55%, 60% and 65% of P_{max})

	P_{max} / 8	0.55 P	s (0.55P)	k	0.60 P	s (0.60P)	k	0.65 P	s (0.65P)	k
		(kN)	(mm)	(kN/mm)	(kN)	(mm)	(kN/mm)	(kN)	(mm)	(kN/mm)
CN19.1	140.96	77.53	0.325	**238.92**	84.58	0.397	**213.04**	91.63	0.477	**192.09**
CN19.2	140.39	77.21	0.341	**226.43**	84.23	0.429	**196.58**	91.25	0.528	**172.83**
CN19.3	139.39	76.66	0.320	**239.95**	83.63	0.392	**213.62**	90.60	0.492	**184.15**
CN22.2	155.99	85.79	0.349	**245.82**	93.59	0.444	**210.79**	101.39	0.520	**195.17**
CN22.3	154.52	84.98	0.328	**259.10**	92.71	0.370	**250.57**	100.44	0.424	**237.16**
CN25.1	192.12	105.67	0.470	**225.06**	115.27	0.564	**204.38**	124.88	0.630	**198.22**
CN25.2	189.99	104.49	0.424	**246.74**	113.99	0.503	**226.85**	123.49	0.583	**211.82**
CN25.3	194.48	106.97	0.437	**244.77**	116.69	0.504	**231.53**	126.41	0.571	**221.39**
CDN19.1	120.31	66.17	0.200	**330.85**	72.19	0.258	**280.33**	78.20	0.327	**239.15**
CDN19.2	119.61	65.79	0.266	**247.32**	71.77	0.349	**205.94**	77.75	0.441	**176.50**
CDN19.3	121.96	67.08	0.385	**174.23**	73.18	0.496	**147.54**	79.28	0.612	**129.54**

The stiffness value, k, tends to decrease as higher values of load are considered. The more significant variation is verified in specimens with 19 mm diameter, as a relation of around 2 to 1 is measured when the values of stiffness calculated for $0.40P_{max}$ and $0.65P_{max}$ are compared. In the case of studs with 22 mm diameter and 25 mm diameter, the stiffness value, k, is almost constant until the load reaches 50% of the maximum load, and then a soft decrease of this parameter is verified as the load increases.

As presented in Figure 3.61d, the evolution of the average curves k-P/P_{max} is very similar for all diameters, with exception to diameter 19 mm, when $P/P_{max} \leq 0.45$. The difference between these two curves and the average curve for studs with 19 mm diameter should be explained by the interaction between the stud and the concrete slab. It is possible that slip deformation is more dependable on the connector deformation for studs with 19 mm diameter and more dependable on the concrete cracking for studs with 22 and 25 mm, because the loads applied are higher and therefore impose more cracking on the slabs. However, for values of load over $0.5P_{max}$, the value of stiffness k tends to be similar for all diameters.

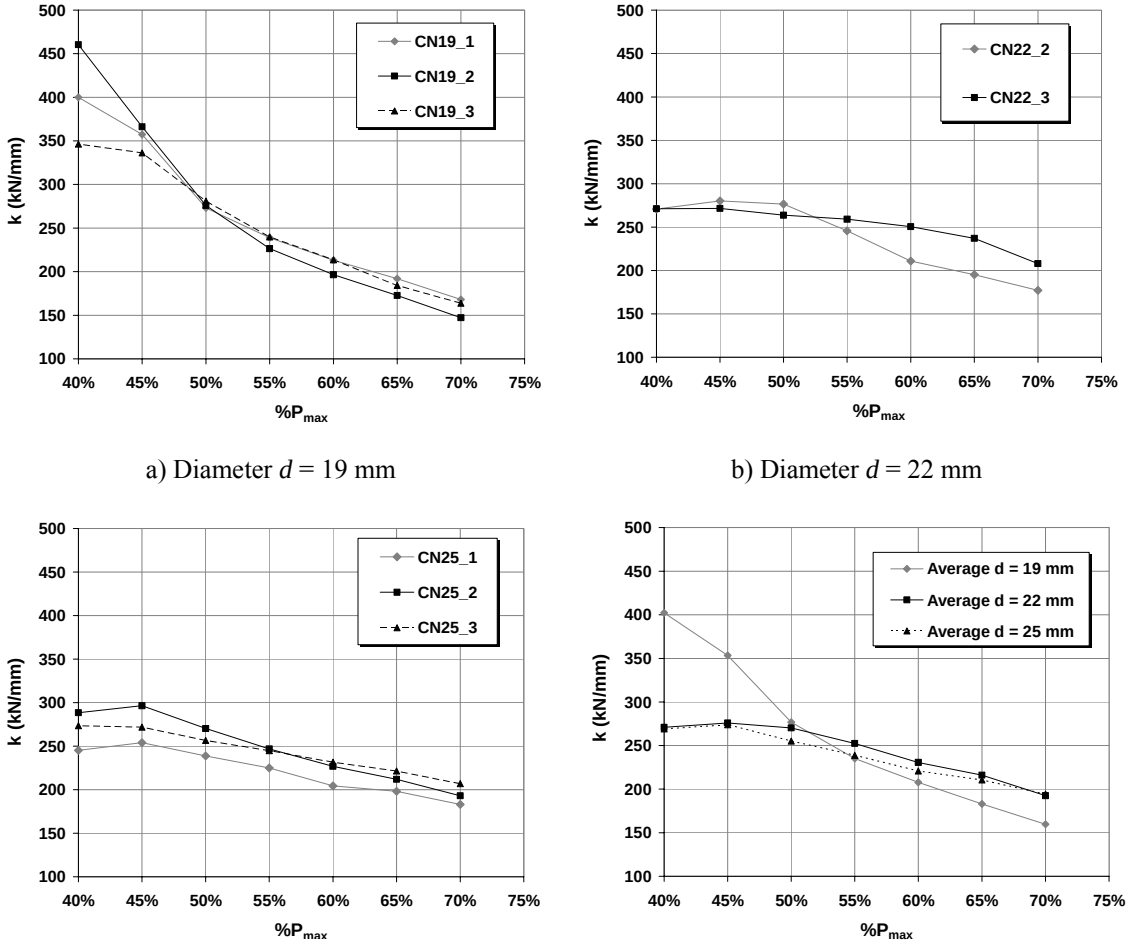

a) Diameter d = 19 mm

b) Diameter d = 22 mm

c) Diameter d = 25 mm

d) Average d = 19, 22 and 25 mm

Figure 3.61 - k-%P_{max} for isolated stud disposition (d = 19, 22 and 25 mm)

If the value of stiffness is established for around 0.50 P_{max}, then it can be considered that the value of stiffness is approximately equal to 270 kN/mm, for all the specimens. If it is established for around 0.6 P_{max}, then the value of stiffness is approximately equal to 220 kN/mm, for all the specimens. This variation of stiffness is not significant.

The first objective of this analysis is to assess the variation of stiffness k with the level of the load applied. The second objective is to find out if this is the better way of defining this parameter. In other words, if the degradation of the concrete slab is an important factor, it may be better to define parameter k in relation to the load level, and not to a percentage of the maximum load, because of the high load level attained for specimens with larger stud diameters.

The main interest of this analysis concerns the evaluation of k values for service loadings. The idea is to define a region of the load-slip curve where the slip deformation is mainly elastic and recoverable after unloading. During the analysis presented in 3.6.3.2, it was observed that the elastic behaviour can be considered for all specimens at least until around 0.60 P_{max}. Therefore, a stiffness value that is between 220 and 270 kN/mm should be appropriate.

It is important to focus that the value of stiffness determined is valid for all the tested diameters, which means that the connection behaviour is more dependent on the concrete properties than on the stud itself.

The values of k obtained for the double connector disposition show higher variation than previously obtained for the single stud disposition. However, the average curve k-P/P_{max} shows an evolution that is very similar to the curve obtained for isolated studs with diameter equal to 19 mm. Again, it seems that the concrete behaviour determines the deformability of the connection and the studs diameter or disposition.

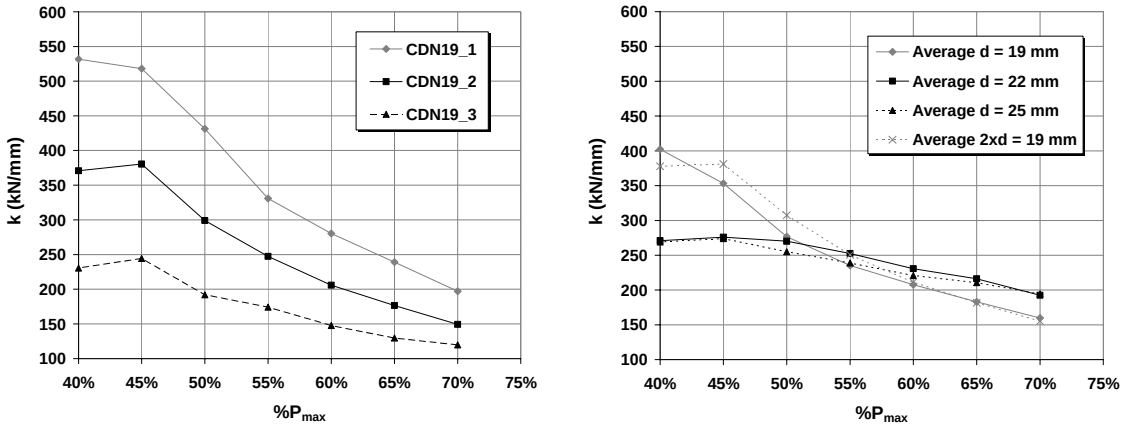

Figure 3.62 – k-$\%P_{max}$ for double stud disposition (d = 19mm)

3.6.5 Single Push-Out Test

3.6.5.1 SPOT test specimens

The specimens prepared for the single push-out test are produced according to Figure 3.63. The geometry of the test specimens is always the same, with variation on the stud diameter and disposition. Three stud diameters are used: 19 mm, 22 mm and 25 mm. These diameters are chosen in agreement to the choices considered for the standard push-out tests, as the intention is to obtain comparative values of load and deformation capacity of the shear connection from the two test types. For each diameter, a series of three specimens are tested.

The specimens consist simply of one lightweight concrete slab held in the vertical position, and a steel plate positioned behind the slab, with one or two welded studs cast inside the slab, depending on the chosen stud disposition. The slab dimensions are 300 mm × 350 mm × 150 mm. The slab reinforcement represented in Figure 3.35 corresponds to 10 mm diameter bars.

One of the great advantages of the SPOT test is the economy of material. The concrete slab and consequently the specimen is much smaller than the specimen used for POST tests. The total volume of concrete used to fabricate one SPOT specimen is 0.01575 m^3, while a total quantity of 0.117 m^3 is needed for a POST specimen. Therefore, the total quantity of concrete used for a SPOT specimen is around 13.5% of the total quantity of concrete used for a POST specimen. Another advantage is that the specimens are lighter and therefore easier to transport and set up for testing. In addition, less studs and less reinforcement are needed for each SPOT specimen, when compared to POST specimens.

The SPOT specimen with double stud disposition has one less bar of transversal reinforcement because its position should be between the two studs. However, it was verified that disposing a reinforcement bar right in front of the welded collar is disadvantageous, (Hegger et al 2000).

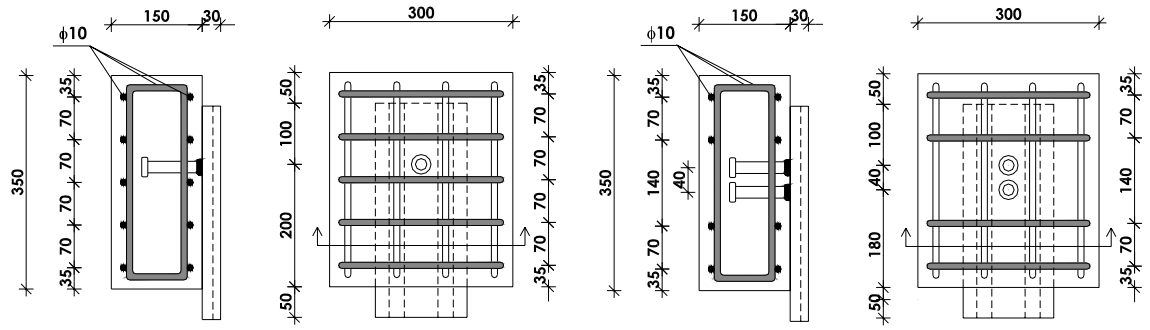

a) Side view for **single stud** b) Front view for **single stud** c) Side view for **double stud** d) Front view for **double stud**

Figure 3.63 - Single Push-Out Test specimens

3.6.5.2 SPOT test results

Headed studs with a diameter of 19, 22 and 25 mm were tested. In all the series of SPOT tests performed, shear failure occurred. In all the tested specimens a concrete wedge developed in front of the welded collar.

a) SPOT KBD 22 b) SPOT KBD 25 c) SPOT KBDD 19

Figure 3.64 – Shear failure of studs (SPOT tests)

As the stud diameter increases, higher loads are applied to the specimens during the tests. As visible in Figure 3.65, this load increase leads to a more and more cracked slab. For SPOT KBD 19 series, the cracks are almost invisible. They become more accentuated with higher loads applied, particularly for SPOT KBD 25 and SPOT KBDD 19.

The majority of the visible cracks appear in the last phase of loading, when high slip is developing. The cracks are mainly visible on the internal surface of the slabs and its diffusion is not so significant as was verified during POST tests. On the external surface of the slab, only very small cracks are visible, and only for the specimens with larger studs. One possible reason for less cracking is the higher concrete compressive strength of SPOT specimens.

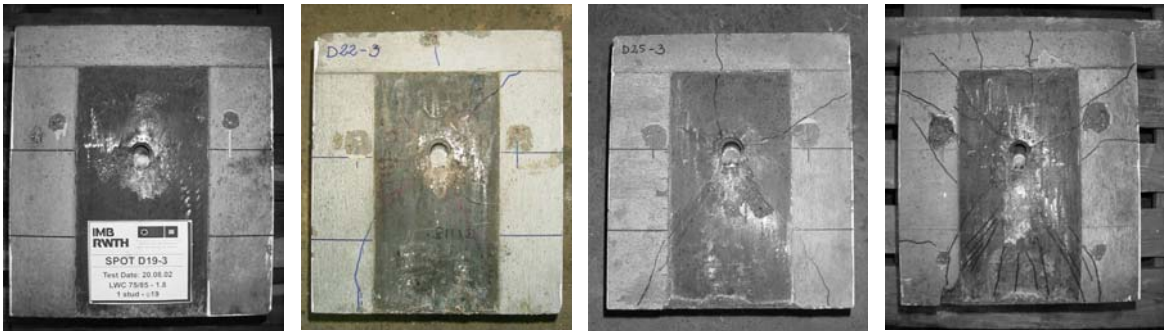

SPOT KBD 19 SPOT KBD 22 SPOT KBD 25 SPOT KBDD 19

Figure 3.65 - Concrete crack patterns (SPOT tests)

As was done for POST tests, some studs were redrawn from the slabs after testing in order to check on its deformed shape after load and unload. Figure 3.66 shows the stud form prior to testing and after testing. It is observed that the stud deformation is mainly

concentrated on the basis of the shank. The upper part of the shank is almost straight. This deformed shape corresponds to the deformed shape observed for the studs redrawn from POST specimens and is also in agreement with the deformed shape expected for high strength concrete, as described in 3.3.1.

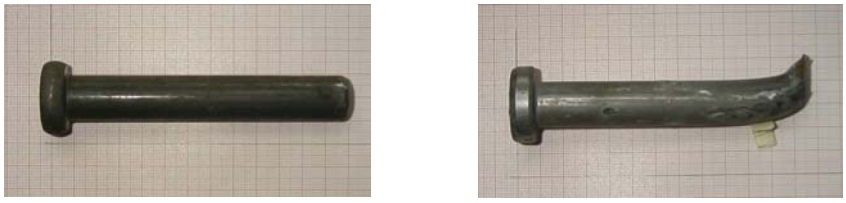

a) Undeformed stud b) Deformed stud, after push-out test

Figure 3.66 - Deformed stud, after push-out test (SPOT tests)

Figure 3.67 to Figure 3.69 present the load-slip curves for each of the tested specimens with 19 mm diameter studs. Figure 3.70 presents the load-slip curves for the three tested specimens. Three identical specimens were tested and the correspondent load-slip curves show very similar configuration, especially during the initial phase of loading, until the characteristic load value is attained. The values for the maximum load obtained in the three tested specimens are similar. The obtained results correspond to a standard deviation of 3.0 kN and a variation coefficient of 1.9%. A good agreement between results is obtained. The variation coefficient is only a bit higher than the one verified for POST tests.

The load-slip curves for 19 mm diameter studs show an initial almost linear progression, until about 70% of the maximum load value is attained. Then, the curve develops a new branch with a very soft slope. The load is almost constant while the slip deformation is still increasing. After the maximum load is reached, the load decreases more rapidly than in POST tests, ending up with failure because there is only one stud in the connection and therefore no possibility for load redistribution.

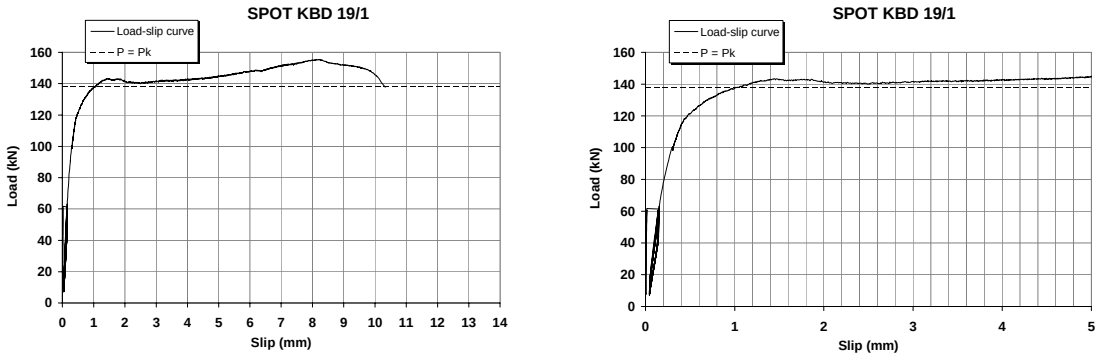

a) Complete load-slip curve b) Initial part of the load-slip curve

Figure 3.67 – Load-slip curve for specimen KBD 19/1 (SPOT test)

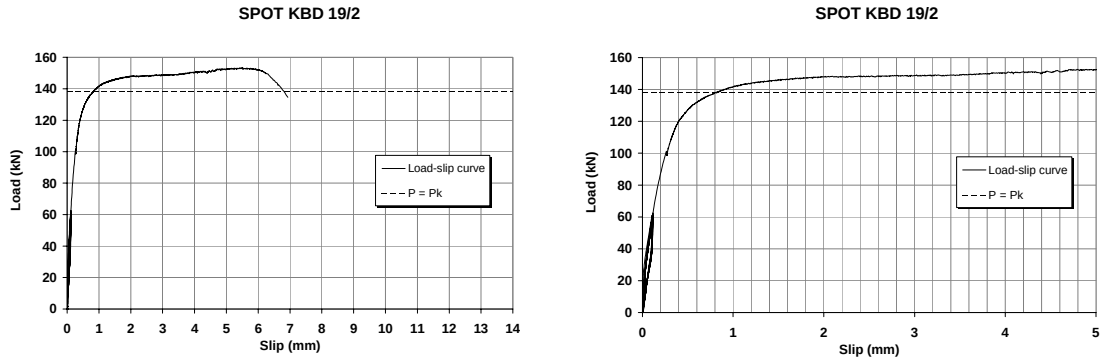

a) Complete load-slip curve b) Initial part of the load-slip curve

Figure 3.68 – Load-slip curve for specimen KBD 19/2 (SPOT test)

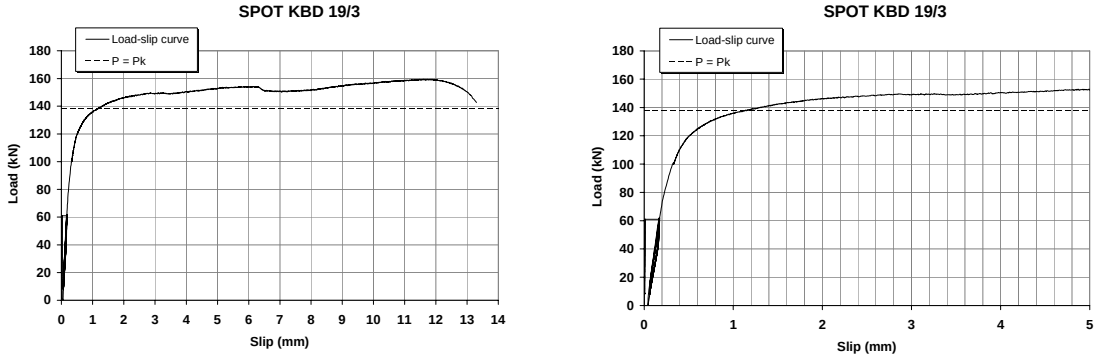

a) Complete load-slip curve b) Initial part of the load-slip curve

Figure 3.69 – Load-slip curve for specimen KBD 19/3 (SPOT test)

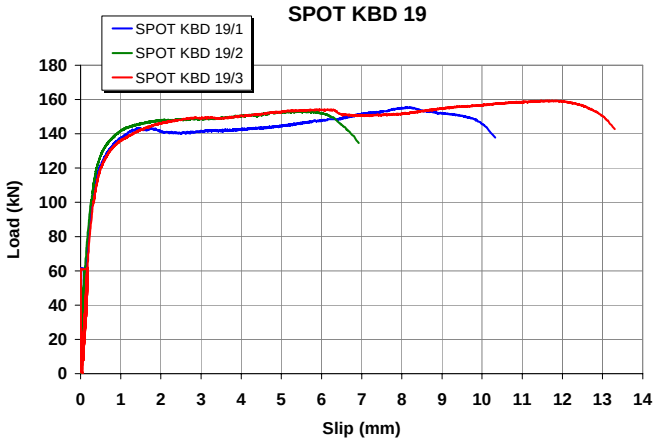

Figure 3.70 - Load-slip curves for studs with 19 mm diameter (SPOT tests)

The principal difference observable between the three tests with 19 mm diameter stud relates to the slip value when failure is approaching. In fact, some of the specimens

show higher deformation capacity than others and this difference can be significant as observable in Figure 3.70. The measured maximum slip difference is of about 6 mm if the maximum slip is measured before the specimen begins to lose load capacity. These differences in the maximum deformation attained for each specimen make the evaluation on deformability more difficult.

For POST tests, the difference in measured total slip was explained with the possibility of a more efficient load distribution between all the studs that compose the steel to concrete connection. Surprisingly, the variability associated with slip deformation is higher for SPOT specimens than it was verified for POST specimens. In the case of the SPOT tests, this is no longer a valid reason as there is only one stud in each specimen. It is quite interesting to observe Figure 3.71 that shows specimens KBD19/1 and KBD19/3 after failure. These specimens use the same stud diameter, disposition and were cast at once. It is distinctly shown a more deformed stud for specimen KBD19/3.

Other possibility is that the characteristics of the studs can differ. In this case, the differences should mainly focus on the welded collar dimensions, as the stud production is normalized and subjected to quality control. In fact, some differences were measured in the welded collar dimensions, but it is difficult to accept that that their influence on deformation can be highly significant.

As presented in Table 3.2, steel specimens were cut from studs and were tested in a tensile test. Several specimens from each stud diameter were tested and no big differences were found in terms of the steel characteristics between them.

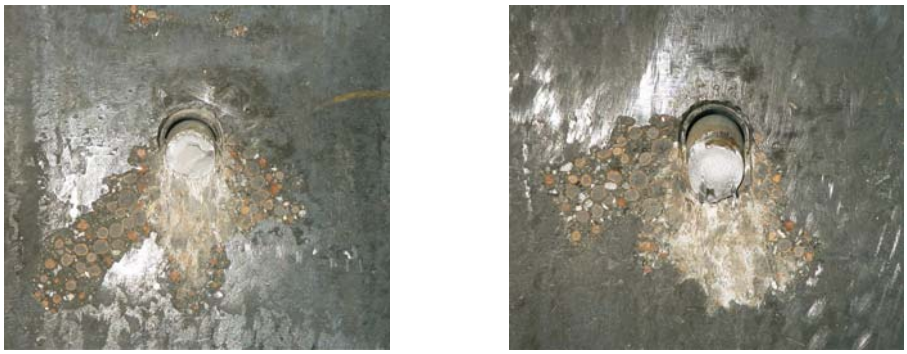

a) SPOT KBD 19/1 b) SPOT KBD 19/3

Figure 3.71 – Failure of 19 mm diameter stud (SPOT tests)

The specimens tested with studs of 22 mm diameter, show a very similar behaviour to what was observed for the specimens with 19 mm diameter. The type of failures observed are also of the shearing type. The values for the maximum load obtained in the three tested specimens are similar. The obtained results correspond to a standard deviation of 7.6 kN and a variation coefficient of 4.2%, which is larger than the variation coefficient obtained for POST tests and for SPOT test with studs of 19 mm diameter.

The load-slip curves for 22 mm diameter studs show an initial almost linear progression, until about 75% of the maximum load value is reached. Then, the curve develops a new branch where the load presents an almost constant or a slow growing value.

The principal difference observable between the three tests with 22 mm diameter stud relates to the slip value when failure is approaching. In fact, some of the specimens show higher deformation capacity than others. In average, the values of plastic slip are a not higher for this diameter than for the 19 mm diameter, which is a surprise. There is a maximum difference of 2.45 mm for the slip value correspondent to the characteristic load value.

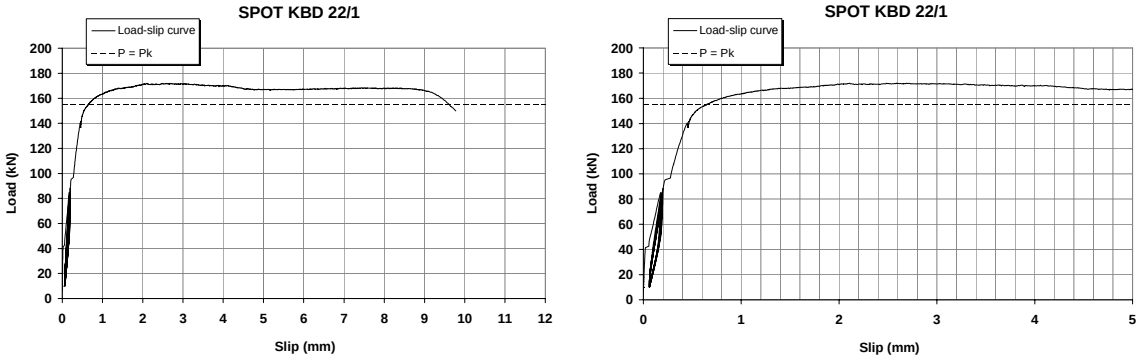

a) Complete load-slip curve b) Initial part of the load-slip curve

Figure 3.72 – Load-slip curve for specimen KBD 22/1 (SPOT test)

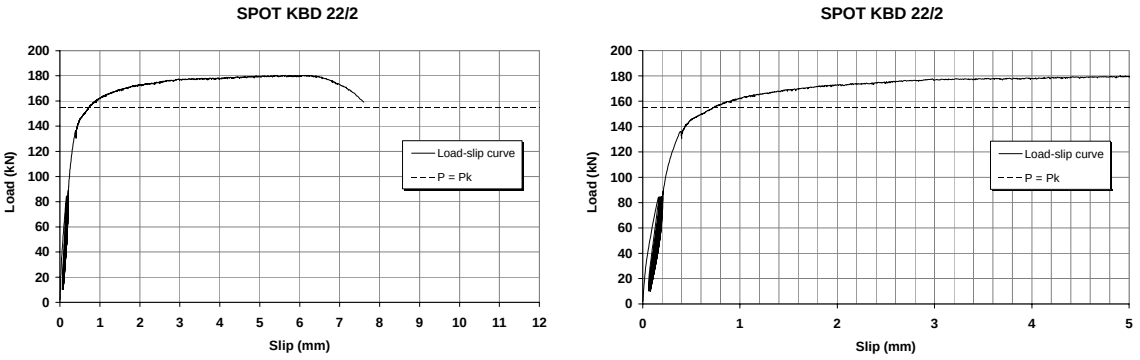

a) Complete load-slip curve b) Initial part of the load-slip curve

Figure 3.73 – Load-slip curve for specimen KBD 22/2 (SPOT test)

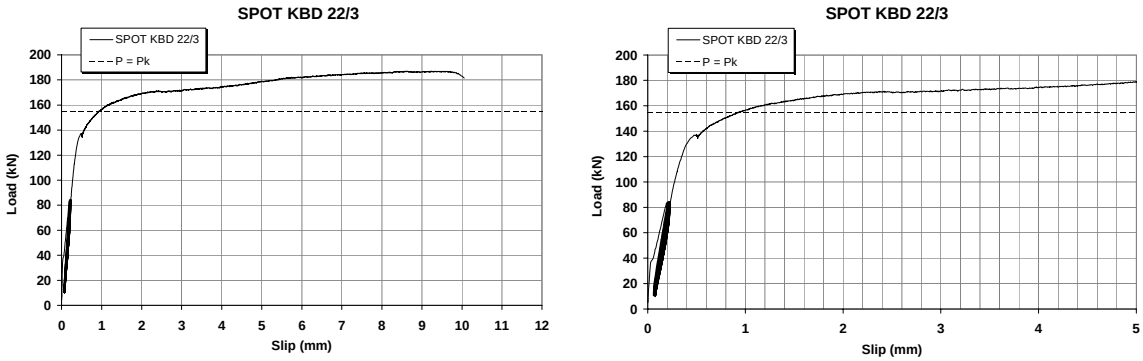

a) Complete load-slip curve b) Initial part of the load-slip curve

Figure 3.74 – Load-slip curve for specimen KBD 22/3 (SPOT test)

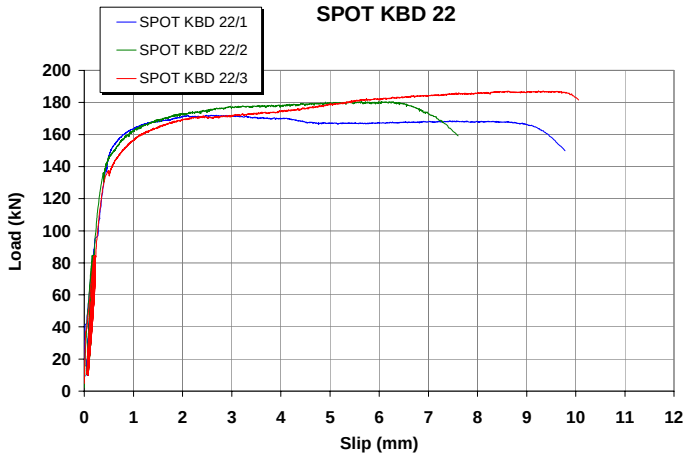

Figure 3.75 - Load-slip curves for studs with 22 mm diameter (SPOT tests)

No particular differences are observed on the broken specimens of series SPOT KBD 22 (Figure 3.76). Specimen SPOT KBD 22/2 suffered smaller deformation, but this is not visible in this figure.

a) SPOT KBD 22/1 b) SPOT KBD 22/2 c) SPOT KBD 22/3

Figure 3.76 – Failure of 22 mm diameter stud (SPOT tests)

The higher loads imposed during these tests lead to some visible concrete slab cracking and concrete crushing near the studs. Initially, the relation between load and slip is almost linear, until around 70% of the maximum load is reached. After this, the curve takes a new rate of growth with a softer slope, developing high deformation before the stud attains failure. After the maximum load, the connection loses load capacity and the concrete slabs become progressively cracked.

The three curves, correspondent to the three specimens 25 mm diameter studs are represented in Figure 3.77, Figure 3.78 and Figure 3.79. The load-slip curves obtained are very similar, with the same magnitude of load and slip values. The obtained results on maximum load correspond to a standard deviation of 2.4 kN and a variation coefficient of 1.0%. This result is comparable in terms of variability to the results obtained in POST tests with the same diameter of 25 mm.

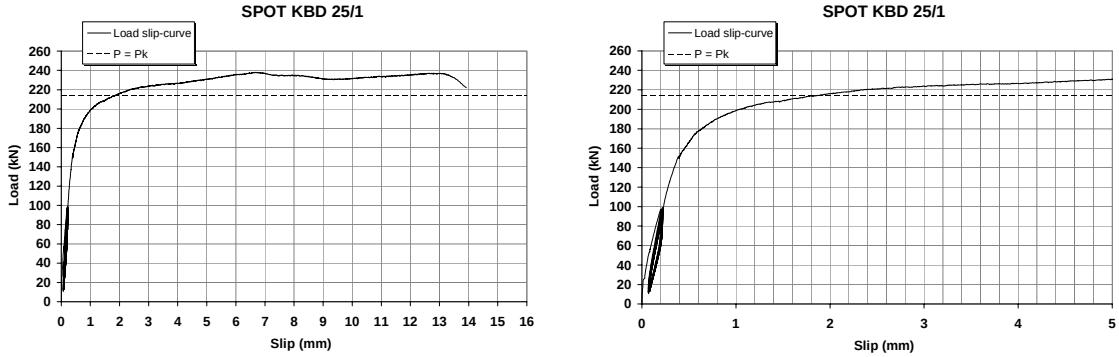

a) Complete load-slip curve b) Initial part of the load-slip curve

Figure 3.77 – Load-slip curve for specimen KBD 25/1 (SPOT test)

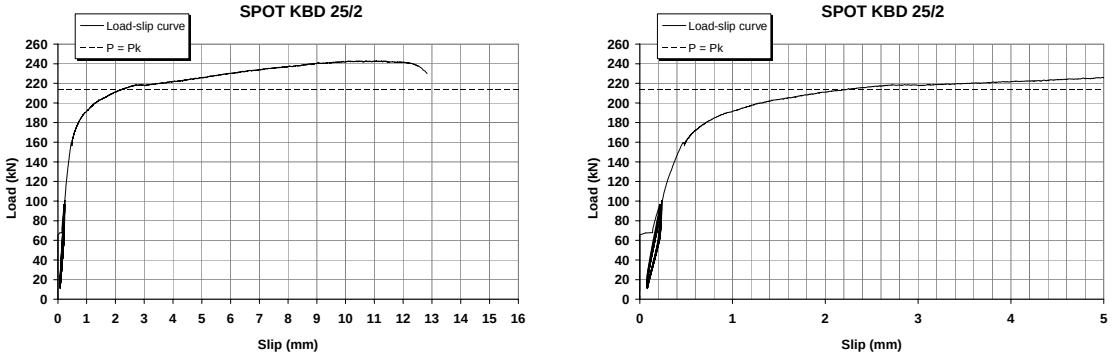

a) Complete load-slip curve b) Initial part of the load-slip curve

Figure 3.78 – Load-slip curve for specimen KBD 25/2 (SPOT test)

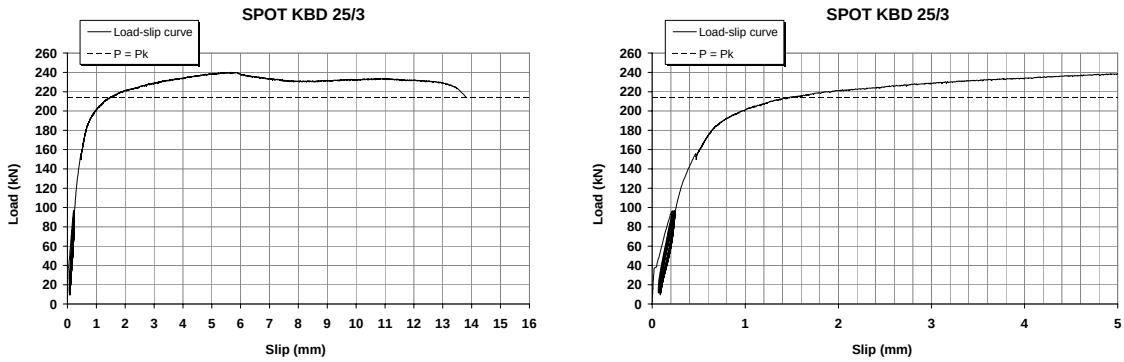

a) Complete load-slip curve b) Initial part of the load-slip curve

Figure 3.79 – Load-slip curve for specimen KBD 25/3 (SPOT test)

There is a maximum difference of 1.09 mm for the slip values correspondent to the characteristic load value, which is rather smaller than the variation obtained for specimens with 19 mm and 22 mm studs. As presented in Figure 3.80, the evolution of the load slip curves for the specimens with 25 mm studs tested with SPOT are very close.

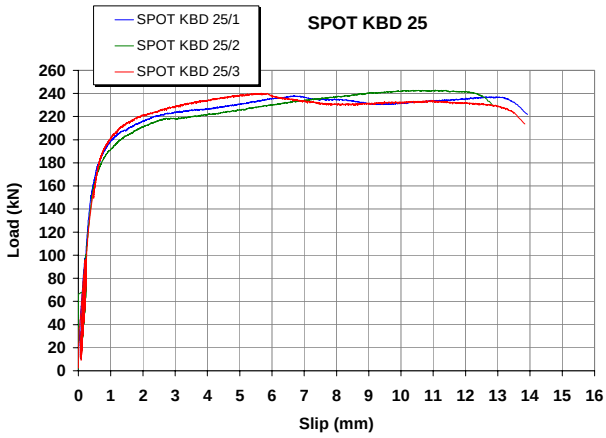

Figure 3.80 - Load-slip curves for studs with 25 mm diameter (SPOT tests)

No particular differences are observed on the broken specimens of series SPOT KBD 25 (Figure 3.81), which is in agreement with the results obtained.

a) SPOT KBD 25/1 b) SPOT KBD 25/2 c) SPOT KBD 25/3

Figure 3.81 – Failure of 25 mm diameter stud (SPOT tests)

The double stud disposition was again chosen for the last series of single push-out tests with headed stud connectors. Two studs of 19 mm diameter are closely welded, so that the spacing between them is only the necessary for allowing the proper welding and the concrete pouring. This disposition is presented in Figure 3.63c and Figure 3.63d. The intention is to compare the obtained results in terms of load bearing capacity and slip, with the ones obtained for the single stud disposition. The load-slip curves for the three tested specimens are presented in Figure 3.82, Figure 3.83 and Figure 3.84.

In terms of global behaviour, the curves obtained for single and double stud disposition are very similar, with a first branch of almost linear relation between load and corresponding slip, and a second branch where important slip deformation takes place, while the load grows at a slow rate.

The load-slip curves obtained are very similar, with the same magnitude of load and slip values. The obtained results on maximum load correspond to a standard deviation of 4.5 kN and a variation coefficient of 3.3%. This result presents higher variability than the results obtained in POST tests with the double stud disposition and diameter of 19 mm.

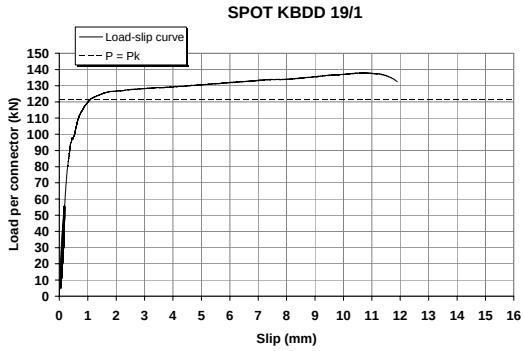

a) Complete load-slip curve

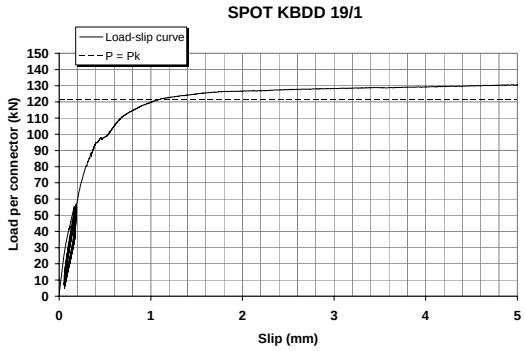

b) Initial part of the load-slip curve

Figure 3.82 – Load-slip curve for specimen KBDD 19/1 (SPOT test)

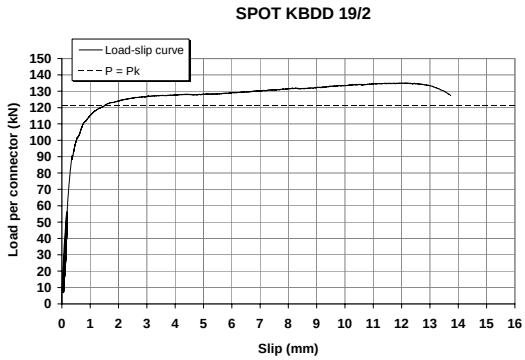

a) Complete load-slip curve

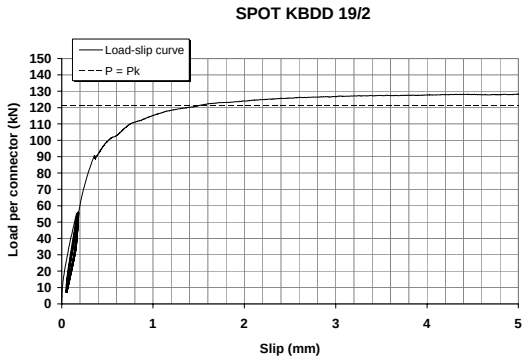

b) Initial part of the load-slip curve

Figure 3.83 – Load-slip curve for specimen KBDD 19/2 (SPOT test)

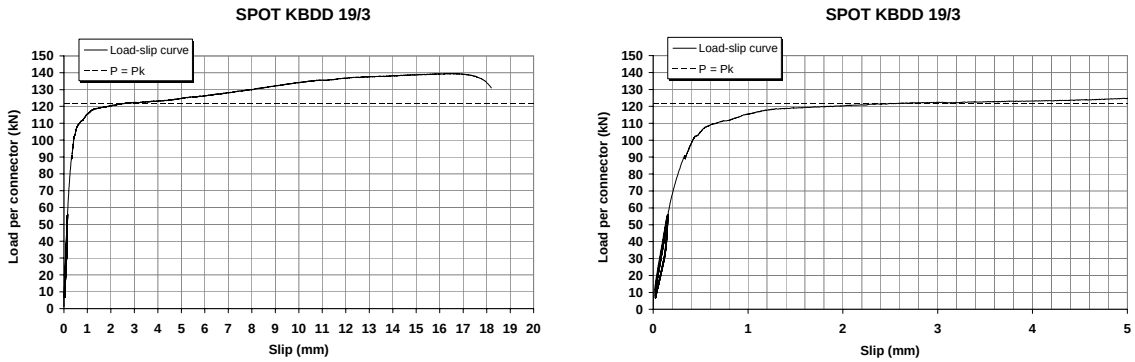

a) Complete load-slip curve b) Initial part of the load-slip curve

Figure 3.84 – Load-slip curve for specimen KBDD 19/3 (SPOT test)

The load-slip curves that result from the three tested specimens are very similar, with exception to the slip value at failure. Again, there is a high variation on the values of maximum slip that the specimens can attain.

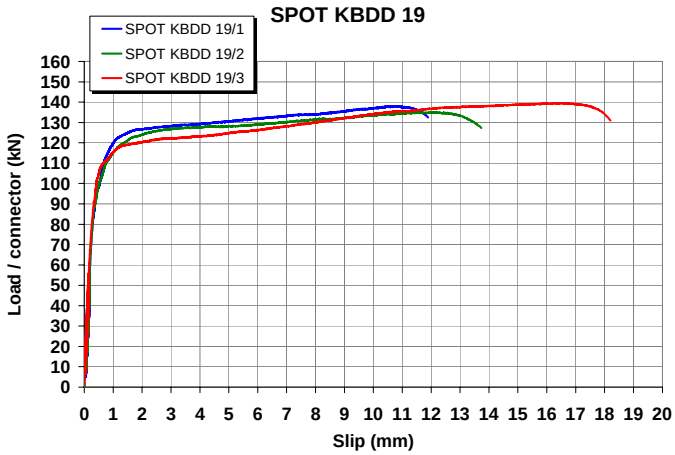

Figure 3.85- Load-slip curves for double stud disposition with 19 mm diameter (SPOT tests)

Despite, the different maximum slip values measured, no particular differences are observed on the broken specimens of series SPOT KBDD 19 (Figure 3.86).

a) SPOT KBDD 19/1 b) SPOT KBDD 19/2 c) SPOT KBDD 19/3

Figure 3.86 – Failure of double stud with 19 mm diameter stud (SPOT tests)

Figure 3.87 presents two load-slip curves, one correspondent to one specimen with single stud disposition (SPOT KBD 19/1) and the other correspondent to one specimen with double stud disposition (SPOT KBDD 19/2). The superposition of the two curves shows that in general they are very similar, denoting the same type of behaviour: an initial elastic behaviour that is followed by a second phase where the load increase is very slow and large deformation develops. As for differences, there is first the confirmation that the double stud disposition results in a loss of load capacity. This loss of load capacity is however accompanied by an increase on the connection slip deformation capacity.

The double stud disposition results in a reduction of 12% of the average maximum load value, on the tested specimens, which is very similar to the decrease measured for POST tests. At the same time this results in a deformation capacity increase that is equal to 80% of the characteristic slip value, which is much more than verified in POST tests (see Table 3.6).

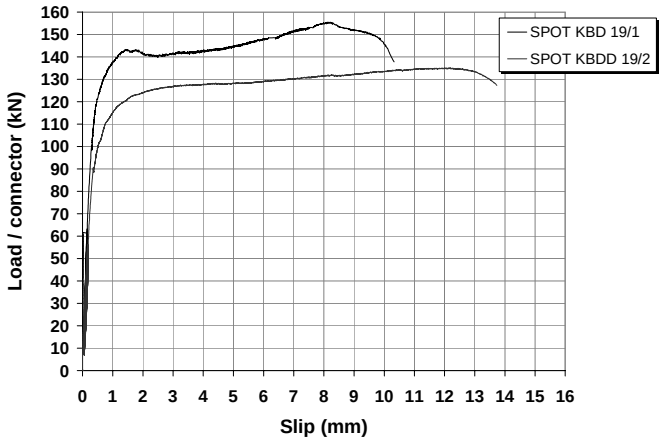

Figure 3.87 – Load-slip curves for single and double stud disposition, with 19 mm diameter (SPOT tests) – Specimens SPOT KBD 19/1 and SPOT KBDD 19/2

Figure 3.88 presents the load slip curves that result from the testing of one specimen of each chosen stud diameter.

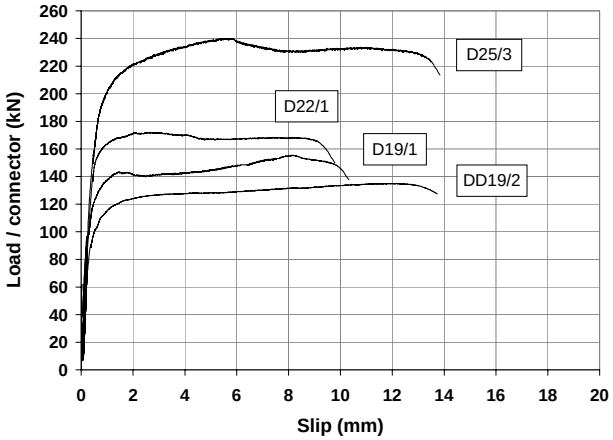

Figure 3.88 - Load vs. slip (SPOT tests)

Comparing all the different tested diameters, it becomes clear that load capacity increases with stud diameter. This is obviously an expected result, as the same result was measured in POST tests and in push-out tests performed by other authors with normal weight concrete. The other significant result is that there is also an increase of the maximum measured slip, as the stud diameter gets larger, as occurred with POST tests.

However this increase of slip deformation is not significant between studs of 19 and 22 mm. The increase of load capacity between these two diameters seems small when compared to the increase of load and slip capacity that is measured between studs of 22 and 25 mm diameter (see Table 3.6). It is more difficult in this type of test to identify a clear tendency on the relation between the value of maximum load applied and the characteristic slip value. A good relation as was obtained for the POST tests (see Figure 3.56), but not for the SPOT tests, as there is some variability in the specimens deformation capacity (see Figure 3.88).

The final phase of loading is characterized by the increase in slip for an approximately constant load. The loss in stiffness at this phase is more noticeable in the SPOT tests than in POST tests. This is an expectable result, since some extra load capacity can be obtained in POST tests due to the redistribution of shear load between all the studs of the specimen. Of course, this redistribution can not occur if there is only one stud loaded.

Since the stud failure occurred for all the tested specimens, it can be assumed that the load capacity does not depend mainly on the concrete strength, although it is an important parameter for the connection's load capacity. Table 3.6 and Figure 3.89 resume the principal results obtained in the SPOT tests performed.

Table 3.6 - Experimental results for SPOT tests

Specimen Ref.	$P_{max,i}$ (kN)	$s_{Pmax,I}$ (mm)	P_{medium} (kN)	P_k (kN)	$s(P_{max})$ (mm)	$s_{elast,90\%}$ (mm)	$s_{plast,90\%}$ (mm)	$s_{total,90\%}$ (mm)	s_k (mm)
KBPD19-1	155.9	7.21	158.4	140.3	7.21	1.00	6.75	7.75	6.08
KBPD19-2	160.9	10.5			10.5	0.69	10.15	10.84	
KBD19-1	155.4	8.14	156.2	138.2	8.14	1.06	9.15	10.20	5.39
KBD19-2	153.6	5.50			5.50	0.82	5.99	6.81	
KBD19-3	159.5	11.63			11.63	1.15	12.15	13.30	
KBD22-1	172.1	2.69	179.9	154.8	2.69	0.64	8.98	9.62	6.19
KBD22-2	180.5	5.65			5.65	0.73	6.88	7.61	
KBD22-3	187.1	9.24			9.24	0.93	9.13	10.06	
KBD25-1	238.2	6.69	240.4	214.4	6.69	1.89	12.03	13.92	9.52
KBD25-2	243.0	11.06			11.06	2.25	10.58	12.83	
KBD25-3	240.2	5.66			5.66	1.48	12.28	13.76	
KBDD19-1	138.1	10.68	137.6	121.6	10.68	1.08	10.81	11.89	9.72
KBDD19-2	135.1	12.19			12.19	1.54	12.20	13.74	
KBDD19-3	139.5	16.42			16.42	2.43	15.77	18.20	

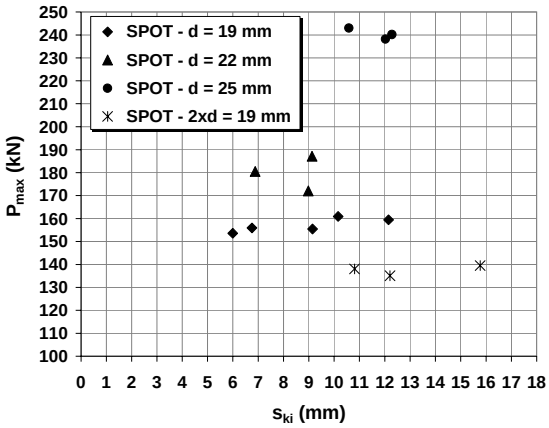

Figure 3.89 - Maximum load and correspondent slip (SPOT tests)

3.6.6 Comparison between POST and SPOT results

The choice of using two types of push-out test, the standard push-out test and the single push-out test, was done to better analyse the behaviour of the connection between steel and lightweight concrete. In addition, this duplication makes it possible to explore the differences, advantages and disadvantages of each type of test. It is though important to present a comparison of the results obtained in each test.

In terms of the specimens' behaviour during testing, it is observed for both test types, POST and SPOT, that the quantity and width of cracks is higher as high diameter studs are used. However, when POST is compared to SPOT for the same stud diameter, it is verified that the cracking is higher for the first test type. One possible reason is the higher compressive strength of the concrete used for SPOT specimens. Another reason is that the distribution of stress on the POST specimen is different from the one obtained in SPOT tests, inducing higher tensile stresses on the concrete slabs. Higher shear loads are also applied to the specimens with larger stud diameters for both test types.

In general, a comparison of the test results obtained with POST and SPOT tests on headed studs of diameters 19, 22 and 25 mm, respectively, shows an increase of the shear connection load capacity when the SPOT test is used. As registered on Table 3.7, 10 to 20% higher loads are achieved with the SPOT test. The differences on characteristic load capacity are of about 10%, except for tests with stud diameter of 25 mm. This difference is similar to the one previously obtained for POST and SPOT performed with NWC (see Table 3.8).

The higher load capacity can result first from the higher concrete strength used in the SPOT specimen. However this is not the principal cause, as similar differences on the load capacity were found for POST and SPOT tests performed on normal weight concrete at RWTH, (Hegger et al 2000). It is verified that the relation between maximum load

obtained with POST and SPOT using LWC is the same as the relation of maximum load obtained with POST and SPOT using NWC, which shows that both test types are adequate to study the use of lightweight concrete. Therefore, it is valid to choose SPOT tests for the study of the shear connection between steel and LWC, confirming that this type of experimental test is an alternative to the POST test.

As referred before, two POST specimens with 25 mm studs failed with severe cracking and crushing of the concrete slabs. This explains the lower value for the relation $P_{k,POST}$ / $P_{k,SPOT}$, presented in Table 3.7, when compared to the same relation obtained for studs with 19 and 22 mm diameter. This type of failure probably induced a reduction on the connection load capacity.

In terms of slip deformation, there is a good similarity between all the specimens, with exception for the double stud disposition that has better performance in the SPOT tests, as the slip values obtained with this type of test are higher than the slip values obtained with the POST test. The general tendency is to have higher deformation values in SPOT tests. However, there is higher variability in the SPOT test results than with POST results, and as the characteristic values result from the smaller slip from a group of three tests, the resulting characteristic slip is similar for both test types.

Table 3.7 - Comparison between POST and SPOT tests, for lightweight concrete

stud diameter	P_k (POST-LWC) / P_k (SPOT-LWC)	s_k (POST-LWC) / s_k (SPOT-LWC)
d = 19 mm	0.908	1.005
d = 22 mm	0.898	1.054
d = 25 mm	0.798	0.969
Double d = 19 mm	0.886	0.682

Figure 3.90 establishes a comparison between stud shear area and the characteristic load value or the characteristic slip value, for the tested specimens.

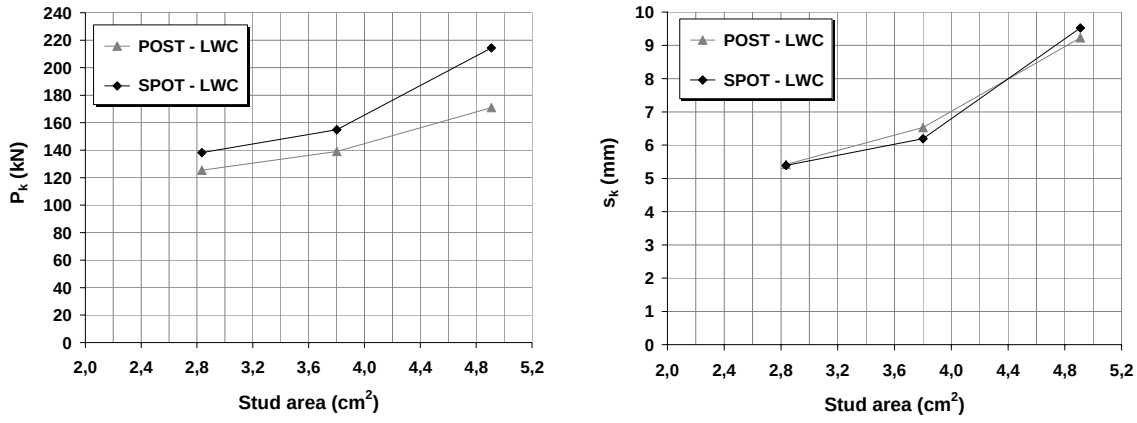

a) Stud shear area and characteristic load b) Stud shear area and characteristic slip

Figure 3.90 – Stud shear area vs. characteristic load value and characteristic slip value

Figure 3.90 shows that both the characteristic load value and the characteristic value of slip vary approximately linearly with the stud shear area.

Looking now to the available data presented in the bibliography for comparing POST test and SPOT test when normal density concrete is used, (Hegger et al. 2000/2001) and (Döinghaus 2001), it is verified that the relation between the results obtained with POST and SPOT tests is around 90%. This result is very similar to the relation obtained with push-out tests performed with LWC.

In terms of slip, POST tests with 19 mm diameter studs have larger characteristic slip than the corresponding SPOT tests. For studs with 22 mm diameter, the results present the opposite tendency. However, it can be considered that the relation between the results obtained in both tests is proximate.

Table 3.8 - Comparison between POST and SPOT tests, for normal weight concrete

stud diameter	P_k (POST-NWC) / P_k (SPOT-NWC)	s_k (POST-NWC) / s_k (SPOT-NWC)
d = 19 mm	0.923	1.354
d = 22 mm	0.896	0.919
d = 25 mm	-	-
Double d = 19 mm	-	-

The linear tendency observed on the relation between stud shear area and characteristic load value is not confirmed with the results for normal weight concrete, because the tests performed with 25 mm diameter studs attain a lower load than expected (Figure 3.91).

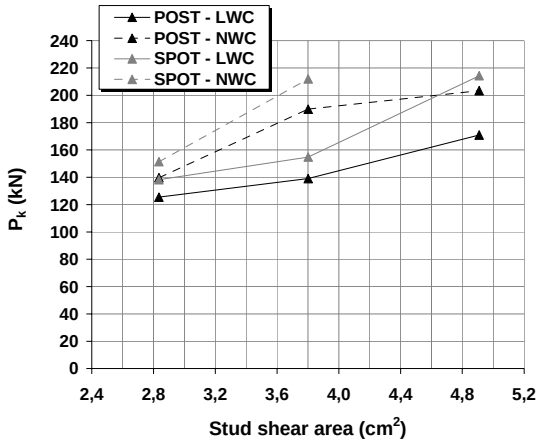

Figure 3.91 – Stud shear area vs. characteristic load value – comparison of POST and SPOT tests

Figure 3.92 presents the comparison of characteristic load values and corresponding characteristic slip values, done for each stud diameter tested. Table 3.7 shows a constant difference of about 10% between the characteristic load values and similar characteristic slip values obtained for POST and SPOT tests. This new diagram puts in evidence a very closely linear relation between these two parameters, characteristic load capacity and

characteristic slip, for the tested diameters. This is an interesting result, because it was verified in the two test types. The possibility of predicting the characteristic slip value using a simple function that only depends on the characteristic load capacity value is promising.

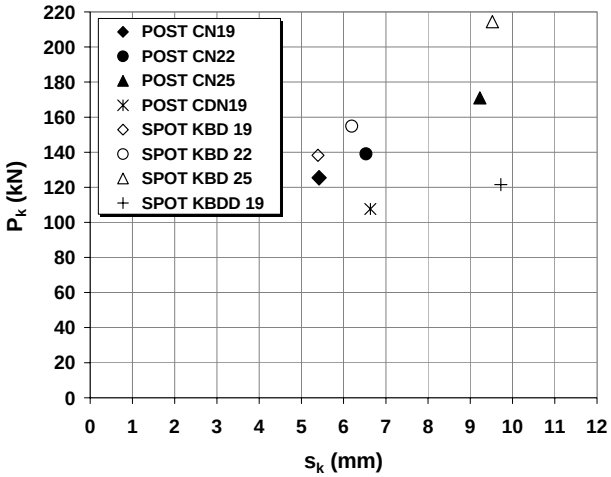

Figure 3.92 – Characteristic load vs. characteristic slip for POST and SPOT series

This relation can be established for the tested diameters. Equation (3.5) presents the relation between the characteristic values of load capacity and slip, obtained for POST specimens. The correlation coefficient determined is equal to 0.827.

$$s_k = 0.0492 P_k \tag{3.5}$$

3.6.7 Comparison between POST tests performed with normal weight concrete and lightweight concrete

This comparison is based on the results obtained within this chapter and the results obtained by Doinghäus (2001) with high strength normal density concrete. This experimental work is chosen for comparison, because there are similarities between both works in the way the tests are performed and in the stud diameters chosen for analysis. The concrete used to fabricate the POST specimens has the compressive strength presented in Table 3.9. The same table presents the corresponding results on characteristic load and characteristic slip.

The values for characteristic load and characteristic slip presented in Table 3.9 are also represented in Figure 3.93. An average ratio of $P_{k,POST\text{-}LWC}$ / $P_{k,POST\text{-}NWC}$ equal to 0.82 is found. Figure 3.93b shows that the use of LWC induces a loss of load capacity that is accompanied by an increase on the connection deformation capacity.

Table 3.9 – Concrete properties, characteristic load and characteristic slip for (Doinghäus 2001) POST tests

Specimens	Stud diameter (mm)	Test	Connectors disposition	$f_{c,cube}$ (MPa)	P_k (GPa)	s_k (mm)
POST KBD19/4						
POST KBD19/5	19	POST	Single	83.6	139.7	5.68
POST KBD19/6						
POST KBD22/4						
POST KBD22/5	22	POST	Single	83.6	189.9	6.71
POST KBD22/6						
POST KBD25/4						
POST KBD25/5	25	POST	Single	88.1	203.4	7.62
POST KBD25/6						

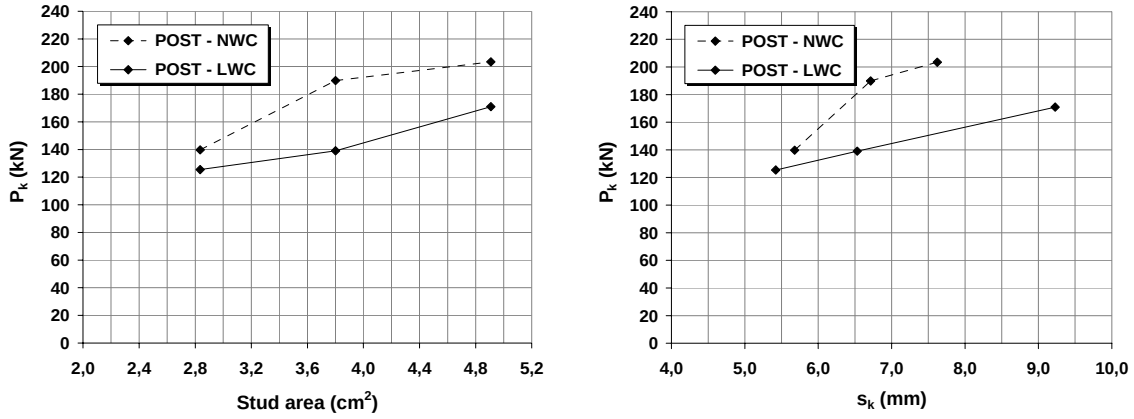

a) Characteristic load

b) Characteristic slip

Figure 3.93 – Characteristic load and characteristic slip for POST tests with NWC and LWC

Comparing the HSNWC and the HSLWC results, it is verified that HSLWC specimens show higher deformation values. On the other hand, maximum load values are smaller. It is possible that the observed differences result principally from the differences between concrete modulus of elasticity and tensile strength of the two materials. If the modulus of elasticity is higher, then the connection behaviour is less ductile and shear failure will occur in the connector. On the other hand, if the modulus of elasticity is lower, the behaviour is more ductile and the tensile component tends to increase.

3.6.8 Comparison between SPOT tests performed with normal weight concrete and lightweight concrete

Like for the previous item, this comparison is also based on the results obtained by Doinghäus (2001) with high strength normal density concrete. Regarding the SPOT tests,

this author only made tests with 19 mm and 22 mm diameter studs. The concrete used to fabricate the SPOT specimens has the characteristics presented in Table 3.9. The same table presents the corresponding results on characteristic load and characteristic slip.

Table 3.10 – Concrete properties, characteristic load and characteristic slip for (Doinghäus 2001) SPOT tests

Specimens	Stud diameter (mm)	Test	Connectors disposition	$f_{c,cube}$ (MPa)	P_k (GPa)	s_k (mm)
SPOT KBD19/4						
SPOT KBD19/5	19	SPOT	Single	115.4	151.4	4.19
SPOT KBD19/6						
SPOT KBD22/4						
SPOT KBD22/5	22	SPOT	Single	115.8	212.0	7.31
SPOT KBD22/6						

The values for characteristic load presented in Table 3.10 are represented in Figure 3.94. An average ratio of $P_{k,SPOT\text{-}LWC}$ / $P_{k,SPOT\text{-}NWC}$ equal to 0.82 is found, which is coherent with the result already obtained for POST tests. Although the LWC and NWC concrete strength is not the same, all the specimens suffered stud failure and the relation between the characteristic loads is consistent between POST and SPOT tests performed. As occurred for POST tests, using LWC induces a loss of load capacity that occurs with an increase on the connection deformation capacity (Figure 3.94.b).

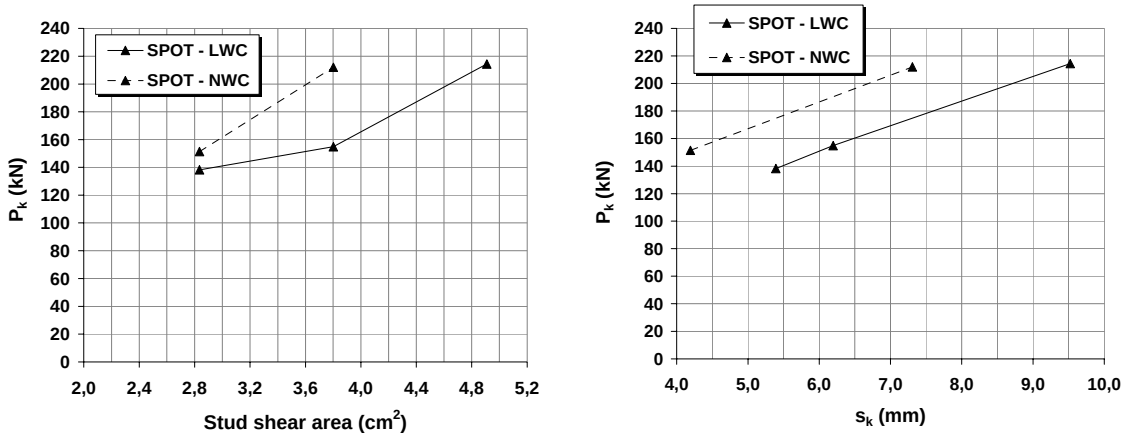

Figure 3.94 – Characteristic load and characteristic slip for SPOT tests with NWC and LWC

3.6.9 Standard equations to predict the ultimate load capacity of headed studs

A good prediction of the characteristic load capacity is important. In order to do so, a check on the expressions currently recommended in the actual codes is presented. The idea

is to evaluate the adequacy of using these expressions to evaluate the load bearing capacity of stud shear connectors in high strength lightweight concrete, because these expressions were mainly developed to analyse normal weight concrete shear connection capacity.

Based on the results of experimental tests performed with the standard push-out test, EN 1994-1-1, (CEN 2004b), proposes equations (3.6) and (3.7) to calculate the characteristic load capacity value for one single stud. These equations correspond to two possible failure modes: equation (3.6) has to do with the shank shear failure and equation (3.7) has to do with concrete crushing failure.

$$P_{Rk} = k \cdot f_u \cdot \frac{\pi d^2}{4} \tag{3.6}$$

$$P_{Rk} = 0.29 \alpha \, d^2 \sqrt{f_{ck} E_{cm}} \tag{3.7}$$

where,

k = 0.8

d - stud shank diameter

f_u - steel tensile ultimate strength for the used studs

f_{ck} - characteristic value of concrete compressive strength, measured in cylinders

Figure 3.95a presents the ultimate loads obtained in push-out tests performed by several authors. These results are compared with the characteristic load obtained by using equations (3.6) and (3.7) and considering the characteristics of concrete and steel described by these authors. The tendency is that the characteristic load obtained is smaller than the experimental load and there is a strong linear relation between these parameters. In average, the characteristic loads determined correspond to 80% of the experimental load. This value is in accordance with the dispositions of EN1994-1-1 that calculates the characteristic load from the push-out tests, by considering 90% of the experimental ultimate load (see 3.6.3.2).

Figure 3.95b presents the same comparison between experimental and characteristic load, but now considering tests performed with lightweight concrete. In fact, the diagrams indicate that the characteristic and the experimental loads are similar, which leads to the following conclusions:

– when lightweight concrete substitutes normal density concrete there is a tendency to obtain smaller loads;

– the equations proposed by EN1994-1-1 should consider a reduction factor for lightweight concrete. If this reduction factor is equal to 0.9, the procedure described to calculate the characteristic loads from experimental push-out tests results is reasonable.

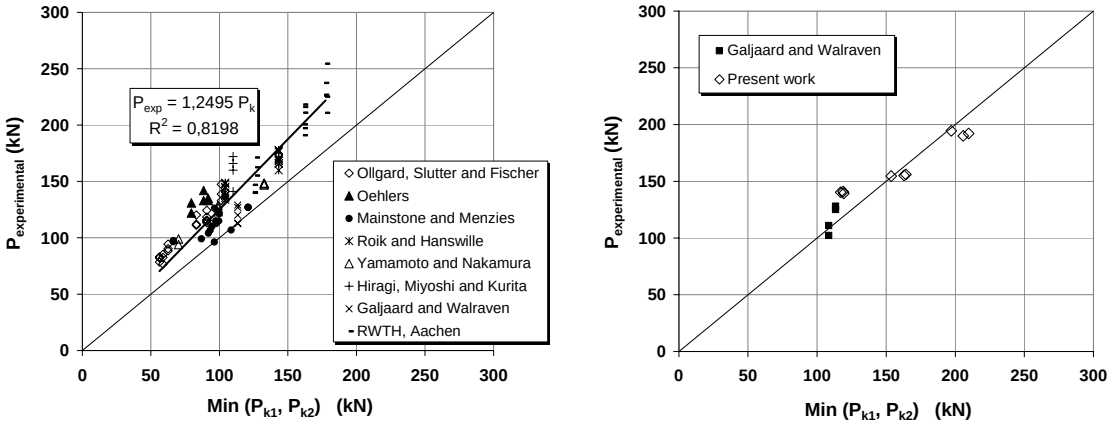

a) NWC b) LWC

Figure 3.95 – Characteristic load and characteristic slip for POST tests with NWC and LWC

In AASHTO (2004), the shear strength of one headed stud shear connector embedded in a concrete slab is defined by equation (3.8),

$$P_R = \phi\, 0.5 A_{sc} \sqrt{f_{ck} E_{cm}} \leq \phi\, A_{sc}\, f_u \tag{3.8}$$

where, ϕ is a resistance factor equal to 0.85 and A_{sc} is the cross section of the stud connector shank (in mm^2).

Another expression was proposed by Oehlers and Jonhson (1987) to calculate the shear load capacity for headed studs. Equation (3.9) was established in an empirical way, but includes the main essential parameters that influence the shear connector load capacity, where, $k = 4.16$ and E_s is the Young's modulus for steel.

$$P_R = k \cdot \frac{\pi d^2}{4} \cdot f_c^{0.35} \cdot \left(\frac{E_{cm}}{E_s} \right)^{0.4} \cdot f_u^{0.65} \tag{3.9}$$

A large experimental campaign of push-out tests was performed in the RWTH Structural Concrete Laboratory for specimens done with high strength normal weight concrete, (Hegger et al 2000). For the RWTH model, (Hegger et al. 2001), it is assumed that both the connector as well as the weld collar contribute to the overall load-bearing capacity of the connector. Since the connector in high-strength concrete is subjected to an almost purely shearing type of stress, the shear-stress bearing capacity of this is calculated using the full stress to failure. The concrete forces that are activated in front of the collar depend on the area projected by the weld bead as well as on the strength of the concrete (greater than 70 N/mm²).

The assumed shearing force of the shaft, acting directly above the weld collar is defined by equation (3.10), where, f_u is the tensile strength of the connector material used and A_s is the cross-sectional area of the shaft.

$$F_s = f_u \cdot A_s \tag{3.10}$$

The concrete compression force activated by the weld collar in the concrete wedge in front of the connector is defined by (3.11),

$$F_{sw} = A_p \cdot \eta_{concrete} \cdot f_{ck,cube,average} \tag{3.11}$$

where,

A_P - - projected area of the bead

$\eta_{concrete}$ - empirical correction value to determine the multi-axial load-bearing action of the concrete in front of a shear connector (= 1.5)

$f_{ck,cube,average}$ - average cube compressive strength on the 150 mm cube

The assumed connector shearing force, (3.12), corresponds to the sum of forces (3.10) and (3.11).

$$F_{connector} = F_s + F_{sw} \tag{3.12}$$

Table 3.11 presents the evaluation of load capacity on POST specimens with studs experimentally tested with equations proposed by EN 1994-1-1 (CEN 2004b), Oehlers and Jonhson (1987) and AASHTO (2004).

The steel tensile ultimate strength for studs is determined experimentally and the corresponding results are presented in Table 3.11. As defined in EN1994-1-1, it is necessary to limit f_u value to 500 MPa to apply equation (3.6).

Table 3.11 – Characteristic load capacity of headed stud connectors (POST specimens)

Specimens	Conc. Ref.	Connectors disposition	Conc. density (kg/m^3)	f_{lcm} (MPa)	E_{lcm} (GPa)	f_u (MPa)	P_k *Exp.* (kN)	*P* (3.6) (kN)	*P* (3.7) (kN)	*P* (3.8) (kN)	*P* (3.9) (kN)
CN 19.1	BL17	Single	1899	52.73	24.44				118.8	136.8	125.4
CN 19.2	BL18	Single	1871	52.01	24.06	596	125.4	113.4	117.1	134.8	124.0
CN 19.3	BL19	Single	1914	53.61	24.27				119.4	137.4	125.8
CN 22.1	BL20	Single	1914	55.03	24.51				163.0	180.6	163.9
CN 22.2	BL21	Single	1940	54.76	25.01	559	139.1	152.1	164.3	180.6	164.9
CN 22.3	BL22	Single	1786	53.29	22.48				153.6	176.8	156.6
CN 25.1	BL26	Single	1826	55.61	24.07				209.7	232.4	210.4
CN 25.2	BL27	Single	1819	52.62	24.51	557	171.0	196.3	205.8	232.4	207.9
CN 25.3	BL28	Single	1812	52.69	22.46				197.2	229.9	200.8
CDN 19.1	BL23	Double	1783	54.10	22.80				116.2	133.7	122.9
CDN 19.2	BL24	Double	1854	56.64	27.91	596	107.7	113.4	131.6	143.6	135.6
CDN 19.3	BL25	Double	1816	56.78	25.62				126.3	143.6	131.2

f_{lcm} - mean value of concrete compressive strength, measured in cylinders (minimum value from the two concrete slabs concrete, BLXX.1 and BLXX.2)

E_{lcm} - mean value of modulus of elasticity, measured in cylinders (minimum value from the two concrete slabs concrete, BLXX.1 and BLXX.2)

The results presented in Table 3.11 and Figure 3.96 show that all the standard equations give high values for the characteristic load capacity, with exception to diameter 19 mm. Very significant is that this load capacity value tends to diverge from the experimental values as the stud diameter increases.

Equation (3.7) gives load capacity values that are close to the results obtained with equation (3.6), showing that for this type of concrete, there is a good balance between connector strength and concrete strength. The tendency verified for equation (3.6) is repeated, as equation (3.7) results diverge from the experimental results when the stud diameter gets larger. The results of applying equation (3.9) follow the same trend as equations (3.6) and (3.7). There is no accuracy increase in using this equation.

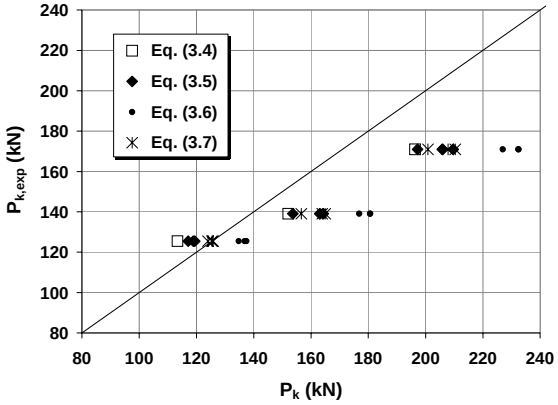

Figure 3.96 – Comparison between experimental results and standard equation for headed studs load capacity (POST specimens)

Table 3.12 presents the evaluation of characteristic load capacity on headed stud SPOT specimens experimentally tested, as was done in Table 3.12.

Table 3.12 – Characteristic load capacity of headed stud connectors (SPOT specimens)

Specimens	Conc Ref.	Connectors disposition	Conc. density (kg/m^3)	$f_{lc,cube}$ (MPa)	E_{cm} (GPa)	f_u (MPa)	P_k *Exp.* (kN)	*P* (3.6) (kN)	*P* (3.7) (kN)	*P* (3.8) (kN)	*P* (3.9) (kN)
KBD19/P1 KBD19/P2	BL.a	Single	1800	94.0	23.5	534	140.3	113.4	155.6	132.5	143.5
KBD19/1 KBD19/2 KBD19/3	BL.b	Single	1800	84.6	26.6	534	138.2	113.4	157.1	128.7	137.0
KBD22/1 KBD22/2 KBD22/3	BL.c	Single	1800	78.5	25.7	548	154.8	152.1	199.6	177.1	183.3
KBD25/1 KBD25/2 KBD25/3	BL.d	Single	1800	78.5	25.7	584	214.4	196.3	257.7	243.7	246.4
KBDD19/1 KBDD19/2 KBDD19/3	BL.e	Double	1800	84.6	26.6	534	121.6	113.4	157.1	128.7	137.0

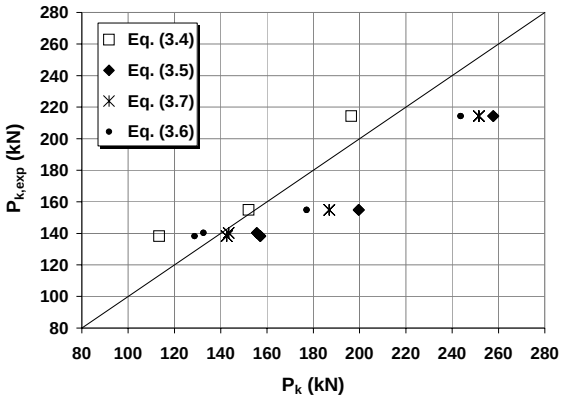

Figure 3.97 – Comparison between experimental results and standard equation for headed studs load capacity (SPOT specimens)

The results presented in Table 3.12 and Figure 3.97 show that the results on load capacity obtained experimentally are always higher than the values obtained with equation (3.6). On the contrary, both equations (3.7) and (3.9) result in strength values higher than obtained during experimental testing, confirming the tendency observed for the POST specimens.

3.7 Tests with Perfobond connector

3.7.1 Objectives

Standard push-out tests with normal weight concrete and Perfobond connectors have already been performed by different authors, since the late 80's. The experimental campaign here presented is the result of performing push-out tests that follow the description and procedure presented in 5.3, but now using high strength lightweight concrete and Perfobond connectors. The objectives of this research are:

- to analyse the adequacy of using lightweight concrete in composite structures, focusing on the shear connection behaviour with Perfobond connectors;
- to determine the Perfobond connector connection load bearing capacity;
- to evaluate the connection ductility;
- to evaluate the connection deformation capacity and the load-slip relation, before and after the maximum load is attained;
- to analyse the connection stiffness for service loads;
- to compare all the mentioned parameters with the ones obtained for normal weight concrete in experimental tests performed by other authors;
- to compare the test results with the ones obtained for stud connectors.

3.7.2 Materials properties

Concrete properties are not the same for all the tested specimens with Perfobond connector, but are very similar. The values for compressive strength and elasticity modulus presented in Table 3.13 were determined for all castings at the same day of the respective test. Between Series CP X.1 and Series CP X.2, the lightweight concrete mixture was slightly modified, in order to lower the concrete density. In average, the compressive strength value suffered a very small diminution, but the values are very close.

Table 3.13 - Concrete properties for push-out test specimens with Perfobond connectors

Specimens	Concrete Ref.	Test	Connectors disposition	Concrete density (kg/m^3)	$f_{lcm,\ Slab1}$ (MPa)	$f_{lcm,\ Slab2}$ (MPa)	$E_{lcm,\ Slab1}$ (GPa)	$E_{lcm,\ Slab2}$ (GPa)
CP 1.1	BL2	POST	Single	1934	60.30	60.30	*	*
CP 2.1	BL3	POST	Single	1919	61.74	58.80	*	*
CP 3.1	BL4	POST	Single	1918	60.13	60.80	*	*
CP 4.1	BL5	POST	Single	1986	65.67	62.81	*	*
CP 1.2	BL10	POST	Single	1845	56.20	56.96	25.47	24.79
CP 2.2	BL13	POST	Single	1869	52.43	55.07	26.39	26.36
CP 4.2	BL11	POST	Single	1857	58.36	57.38	26.31	25.80
CP 5.2	BL12	POST	Single	1921	57.36	55.93	26.98	28.90
CP 6.2	BL14	POST	Single	1916	61.98	57.08	28.05	26.95

* - Modulus of elasticity for Series CP X.1 was not determined

Steel specimens were collected from the same reinforcement and stud group used in the push-out tests and later tested. Table 3.2 presents the corresponding results,

Table 3.14 - Steel properties for POST tests with Perfobond connector

Type of specimen	d (mm)	f_y (MPa)	f_u (MPa)
Reinforcement – Bars	10	576	675
	12	523	697
Reinforcement – Welded wire mesh	5	583	606

where f_y is the steel yielding tensile strength and f_u is the steel maximum tensile strength.

3.7.3 Test specimens

The Perfobond connector consists on a steel rib, welded to the upper flange of the steel section, in the longitudinal direction of the beam. This steel rib has several openings, which are usually circular but can assume other shapes. The number and size of these openings, the connector length, the rib width and the openings spacing are all variable parameters that can be changed according to the purpose of the structural element and the available knowledge on the connector characteristics.

The Perfobond rib used in this work is represented in Figure 3.98. The dimensions, width, number of openings and openings spacing are defined considering other authors works, like Oguejiofor and Hosain (1994/1996), Ferreira (2000) and Galjaard and Walraven (1999). The idea of producing a similar connector reflects one of the objectives of this work, that is to evaluate the adequacy of substituting NWC with LWC in composite structural elements, where the connection is accomplished with Perfobond ribs. Therefore, it is important to obtain results using LWC that can be compared to the ones obtained with NWC.

The specimens prepared for the standard push-out test with Perfobond connector were produced with the geometries represented in Figure 3.99 and Figure 3.100. This geometry of the test specimens is always the same, with variation on the reinforcement disposition and diameter. Besides the connector geometry, all other elements (steel profile, concrete slabs, etc) have similar dimensions to the ones chosen for the POST tests performed with headed stud connectors. The various dispositions chosen for the reinforcement are also presented in Figure 3.99 and Figure 3.100.

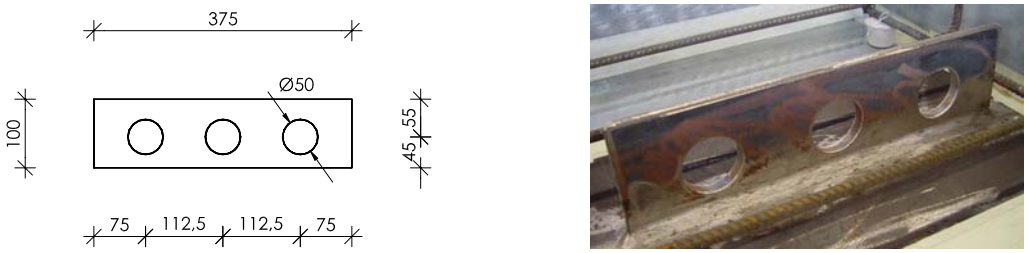

Figure 3.98 – Perfobond rib: configuration and dimensions (in mm)

As described in 3.5.1, the specimens consist of two lightweight concrete slabs held in the vertical position, and a steel HEB260 profile positioned between them, with welded studs concreted inside the slabs. The slab dimensions are 600 mm × 650 mm × 150 mm.

The Perfobond rib connector is itself a very strong element, with high load capacity, whose failure is not expected. Therefore, the principal parameters in evaluation are the use of lightweight concrete and the reinforcement quantity and distribution.

Push-out tests with Perfobond connector are divided in two series. The specimens geometry is common between the two series, with exception to the welded wire mesh positioned on the top layer of the lightweight concrete slab that only exists in the second series of tests (Series CP X.2). Other main difference between the two series is the testing procedure. The first series of Perfobond tests was totally performed with load control, while the second series was performed first with load control and then with deformation control, as described in 3.5.3. The reason why the first series of tests was performed just with load control is that by the time these tests were made, the testing control system was not yet available.

Figure 3.99 presents the specimens geometry for Series CP X.1. All the reinforcement bars are represented, as well as the positions for strain gauges.

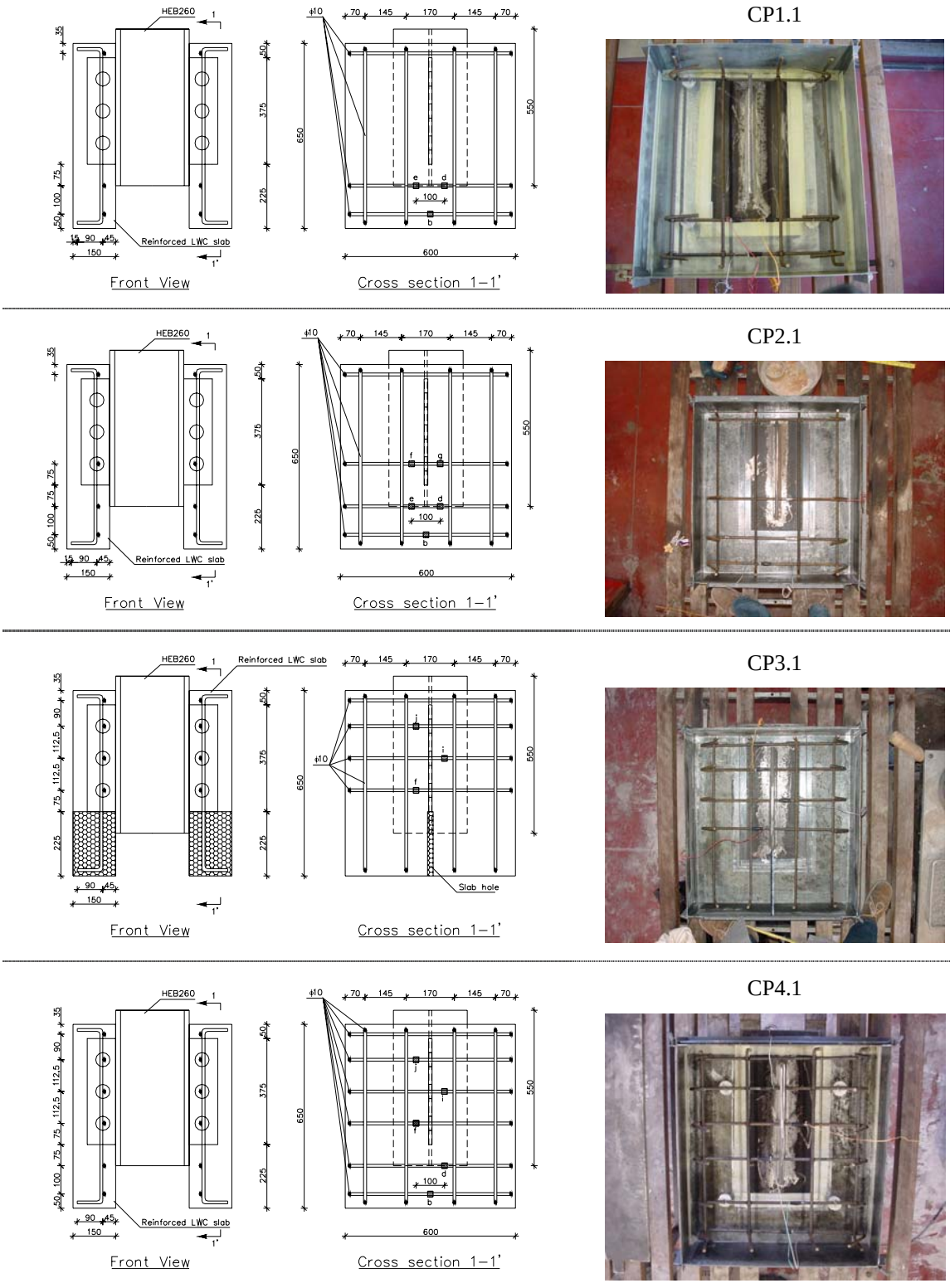

Figure 3.99 – Specimens geometry for experimental POST tests with Perfobond connector (Series CP X.1)

Figure 3.100 and Figure 3.101 present the specimens geometry for Series CP X.2. All the reinforcement bars and welded wire mesh are represented, and also the positions for strain gauges.

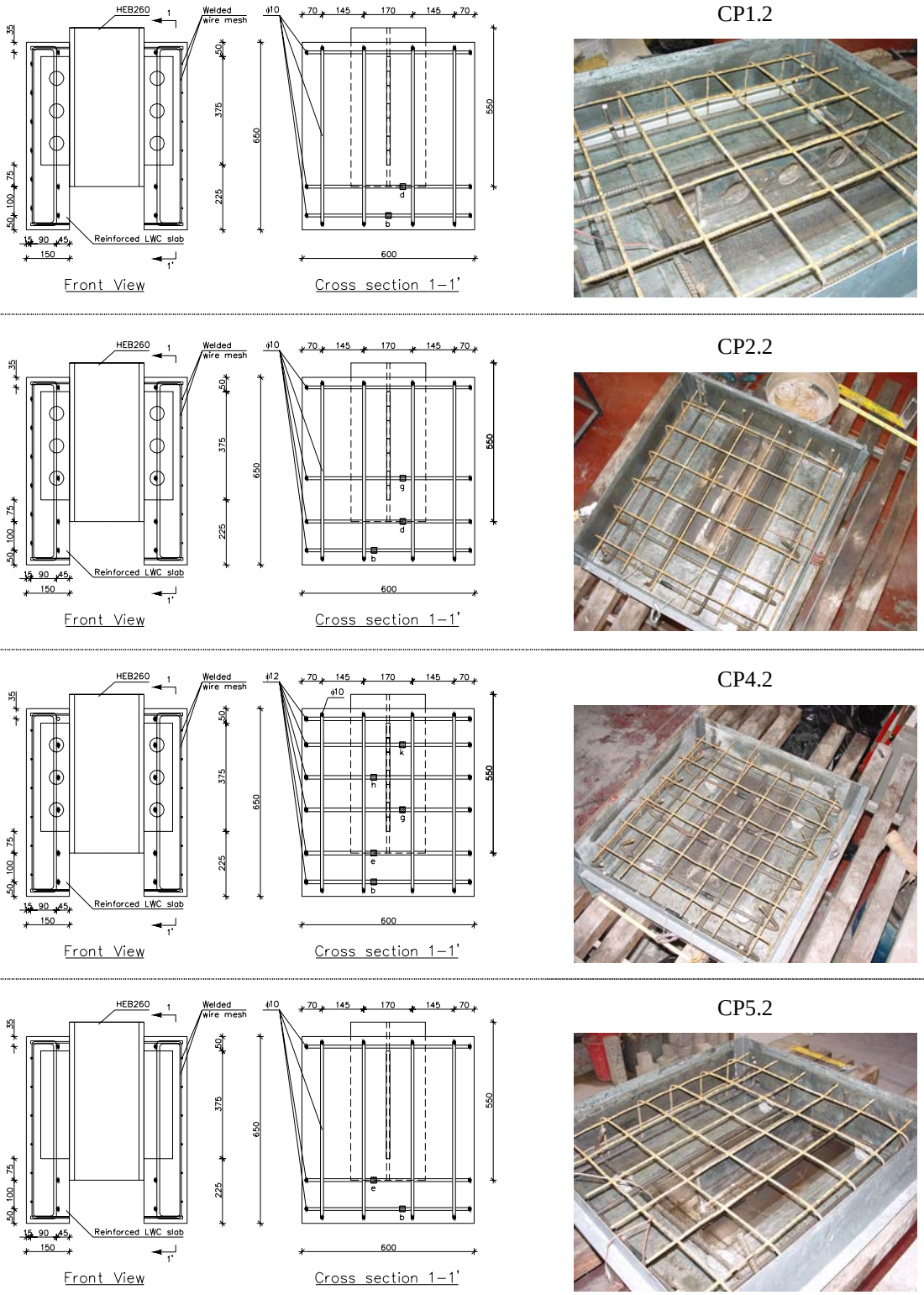

Figure 3.100 – Specimens geometry for experimental POST tests with Perfobond connector (Series CP X.2)

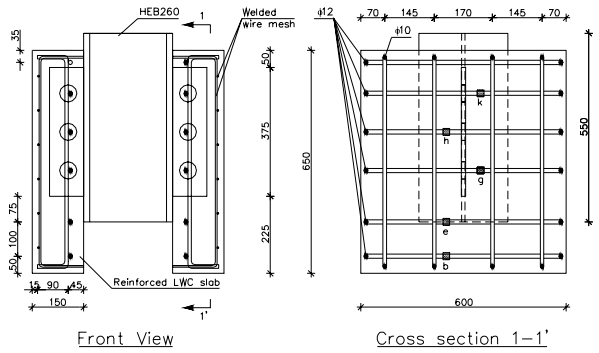

CP6.2

Figure 3.101 – Specimens geometry for experimental POST tests with Perfobond connector (Series CP X.2) – continuation

The dispositions schematically presented in Figure 3.99, Figure 3.100 and Figure 3.101 are resumed in Table 3.15,

Table 3.15 - Perfobond specimens geometry and reinforcement disposition

Specimen Ref.	Concrete slab		Perfobond Rib				Welded wire mesh*				
	H (mm)	*L* (mm)	*h* (mm)	*l* (mm)	*e* (mm)	*D* (mm)		n_1	n_2	n_3	ϕ_{tr}
CP 1.1	150	650	100	375	13	50	No	3	3	0	10
CP 2.1	150	650	100	375	13	50	No	3	3	1	10
CP 3.1	150	650	100	375	13	50	No	3	1	3	10
CP 4.1	150	650	100	375	13	50	No	3	3	3	10
CP 1.2	150	650	100	375	13	50	Yes	3	3	0	10
CP 2.2	150	650	100	375	13	50	Yes	3	3	1	10
CP 4.2	150	650	100	375	13	50	Yes	3	3	3	10
CP5.2	150	650	100	375	13	50	Yes	0	3	0	10
CP6.2	150	650	100	375	13	50	Yes	3	3	3	12

where,

H – slab height;

L – slab width;

h – Perfobond rib height;

l – Perfobond rib length;

e – Perfobond rib width;

D – Perfobond opening diameter;

n_1 – number of openings in each connector;

n_2 – number of transversal reinforcement bars passing outside the connectors' openings;

n_3 – number of transversal reinforcement bars passing inside the connectors' openings;

ϕ_{tr} – diameter of transversal reinforcement bars;

* – the welded wire mesh consists of six bars with 5 mm diameter, equally spaced (see Figure 3.100 and Figure 3.101).

3.7.4 Test setup for Perfobond specimens

The test setup includes the hydraulic machine used to apply the load, the measuring instruments, the control system, the electronic data acquisition unit and all the devices that are needed to effectuate the test. The test setup for the push-out test with Perfobond connector follows all the dispositions described in 3.5.3, 3.5.4 and 3.5.5.

3.7.5 Test results

Load capacity in Perfobond connection results from concrete slab shear strength, both through connector openings and outside the connector and from transversal reinforcement crossing the concrete shear area. Another resistant component appointed by Oguejiofor and Hosain (1996) is the effect of the localized concrete compression under the Perfobond rib.

The concrete positioned inside the connector's openings is considered to be confined and therefore, a higher shear strength is expected in this area, when compared to the slab portion that is outside the rib submitted to shear stresses. An evaluation on the contribution of the concrete dowels formed inside these openings is intended.

Horizontal tensile stresses occur on the concrete slab when the specimen is loaded. These tensile stresses are easily identified with the longitudinal cracking that takes place close to the Perfobond position, in all tested specimens. As reported by Oguejiofor and Hosain (1994), a sudden failure is identified for specimens with no transversal reinforcement, with complete lost of load capacity after the maximum load is attained. Transversal reinforcement avoids or at least delays the crack opening in this particular zone and allows the connection to maintain high load capacity after the maximum load. The transversal reinforcement area is varied between specimens, and therefore, it is possible to evaluate this reinforcement contribution in terms of load and deformation capacity.

The transversal reinforcement bars that pass through the connectors' openings are used to limit cracking, but they are not positioned in the slab centre, which results in larger cracks on the slab upper face. To avoid or diminish this effect, a layer of welded wire mesh is disposed on the slabs' upper face. This reinforcement layer is only used in the second series of push-out tests (Series CP X.2), as represented in Figure 3.100. Therefore, a comparison between Series CP X.1 and CP X.2 can be established, in terms of this reinforcement contribution on the slab behaviour and in terms of load capacity.

The effect of concrete bearing under the Perfobond rib is also evaluated, by testing one specimen with no concrete under the Perfobond rib (see Figure 3.102). In this case, the crack evolution is similar to the crack evolution observed for the other tested specimens.

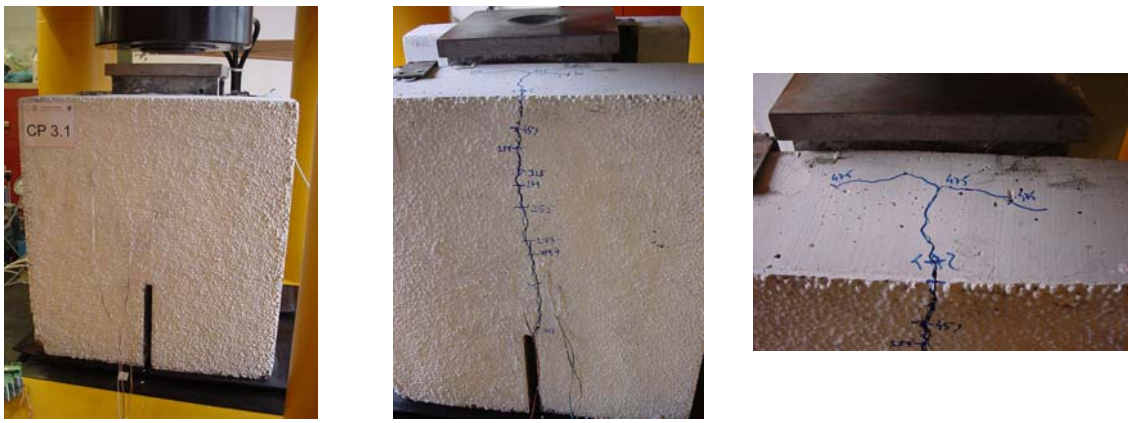

Figure 3.102 – Testing of specimens CP3.1

The crack opening is particularly visible in Figure 3.103, for the specimens of Series CP X.1, where the lack of reinforcement on the slab top layer enhances a principal crack positioned in front of the Perfobond connector, with larger width close to the exterior surface. As the applied load increases, this principal crack grows from the lower part of the concrete slab, until its upper face, (Valente and Cruz 2004a). When the crack is close to the slab upper face, the maximum load is attained.

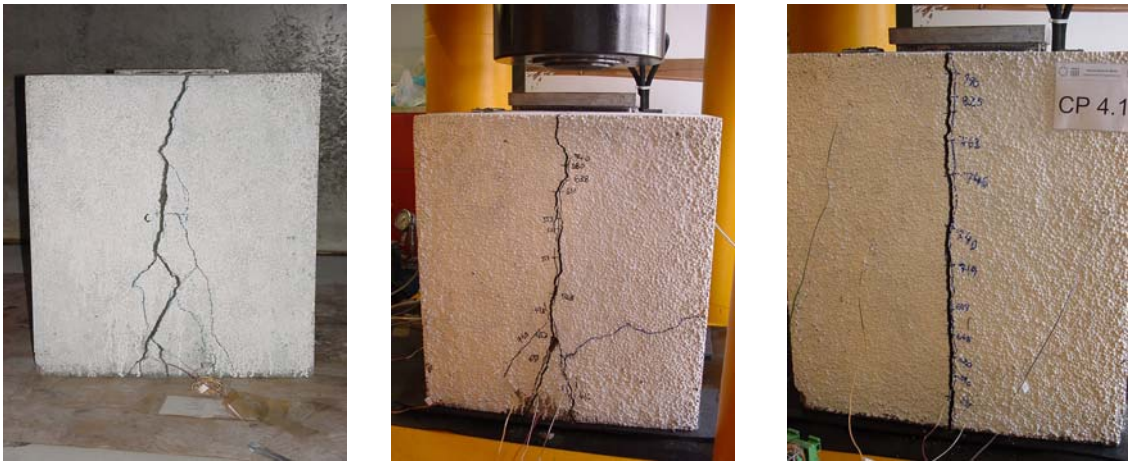

a) CP1.1 – front view b) CP2.1 – front view c) CP4.1 – front view

d) CP1.1 – top view e) CP2.1 – top view f) CP4.1 – top view

Figure 3.103 – Crack opening on the lightweight concrete slab (Series CP X.1)

In the case of Series CP X.2 specimens, the presence of the welded wire mesh, enhances the appearance of more distributed cracking and limits the width of the principal crack (Figure 3.104).

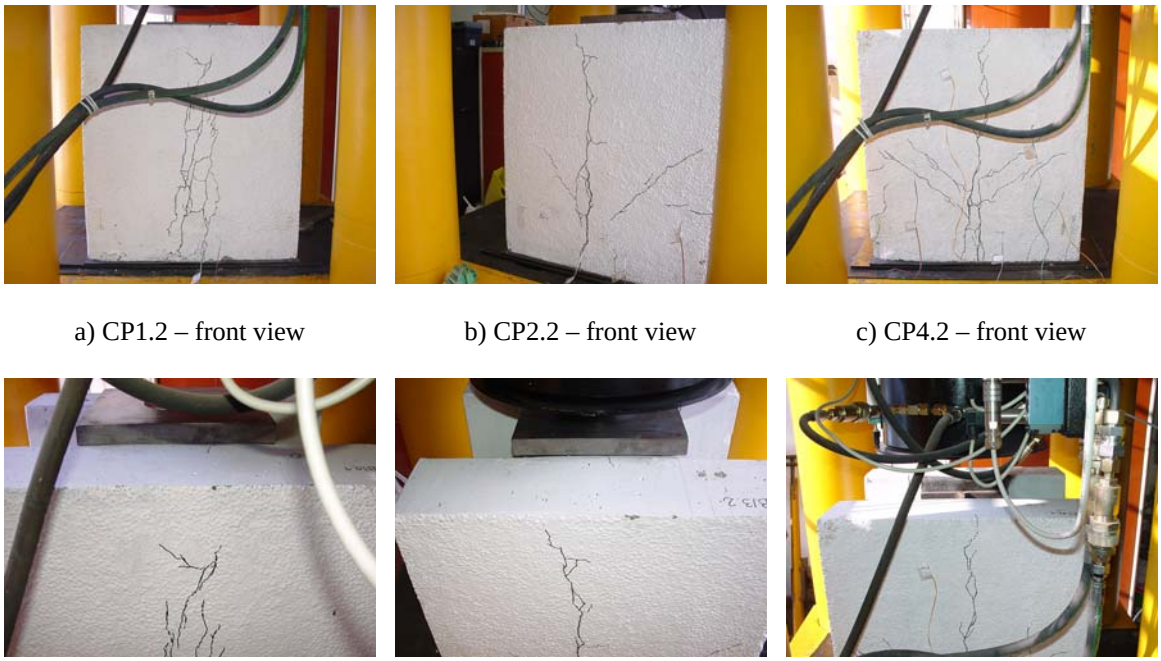

a) CP1.2 – front view b) CP2.2 – front view c) CP4.2 – front view

d) CP2.1 – top view e) CP2.2 – top view f) CP4.2 – top view

Figure 3.104 – Crack opening on the lightweight concrete slab (Series CP X.2)

In all the performed tests, it was observed that the longitudinal principal crack grows from the bottom of the slab and presents an increasingly larger width as the load is higher. The presence of the welded wire mesh limits the crack opening and helps generating other smaller cracks. This aspect is particularly clear when comparing Figure 3.103 and Figure 3.104.

After the testing, some specimens are destroyed in order to observe the effect of loading on the concrete slab, Perfobond rib and reinforcement. In general, the Perfobond rib is intact, with the exception of its lowest part, where some lateral distortion can be observed (Figure 3.105). In all the tested specimens, the connector itself never fails and tends to maintain its initial shape.

It can also be noticed that the reinforcement positioned under the Perfobond rib suffered some bending, although the rib was never in direct contact with the reinforcement bar positioned right bellow (the reinforcement bar is positioned in the center of the Perfobond opening), (Figure 3.105a). This bending is not pronounced and probably takes place only when large deformation is allowed during the test procedure, because the maximum load is achieved for relatively low values of slip.

a) CP1.1 b) CP3.1

Figure 3.105 – Small distortion on the front of the Perfobond rib

In the longitudinal splitting zone, the concrete surface shows two different aspects: close to the Perfobond rib, the concrete surface is very smooth, showing little or no adherence to the rib. On the other hand, outside the rib zone, the concrete surface is rough, showing that splitting occurred with the expanded clay failure (Figure 3.106a).

As visible in Figure 3.106, there is some concrete inside the connectors holes after the separation between the Perfobond rib and the concrete slab. This concrete is not crushed, which means that concrete shear failure occurs in both sides of the Perfobond rib, in agreement with the failure type of Figure 3.11a.

The existence of concrete inside the connectors' openings after failure may also confirm Zellner (1987) hypothesis, in which the author states that the connector may hold considerable shear strength after the concrete dowels failure due concrete friction at the cracked concrete surfaces.

Figure 3.106 - Concrete failure

The concrete zone localized under the Perfobond rib always shows distributed cracking. This cracking develops mainly at the inside face of the concrete slab and initiate under the Perfobond rib. Some of the cracks are develop vertically and others tend to spread and change their inclination until around 45 degrees. The pattern of cracking shows that there is a high stress concentration at this location, indicating that part of the concrete slab beneath the Perfobond rib contributes to the connection load capacity (Figure 3.107).

a) CP2.1 b) CP2.2

Figure 3.107 – Localized cracking under the Perfobond rib

The results of the push-out tests are first analysed with the load-slip curves (Figure 3.108 to Figure 3.113). As in previous push-out tests, the slip value corresponds to an average of the slip values, measured in each slab, during the load application.

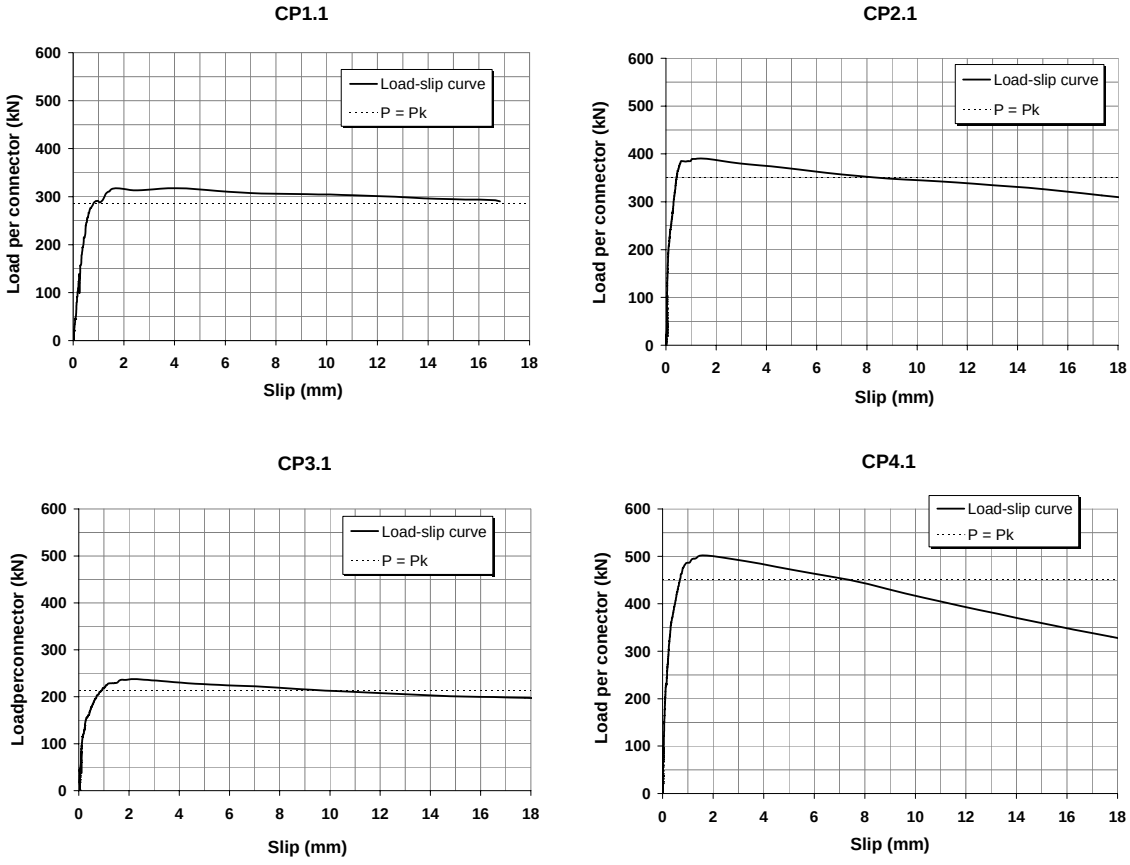

Figure 3.108 – Complete load –slip curves for specimens CP1.1, CP2.1, CP3.1 and CP4.1

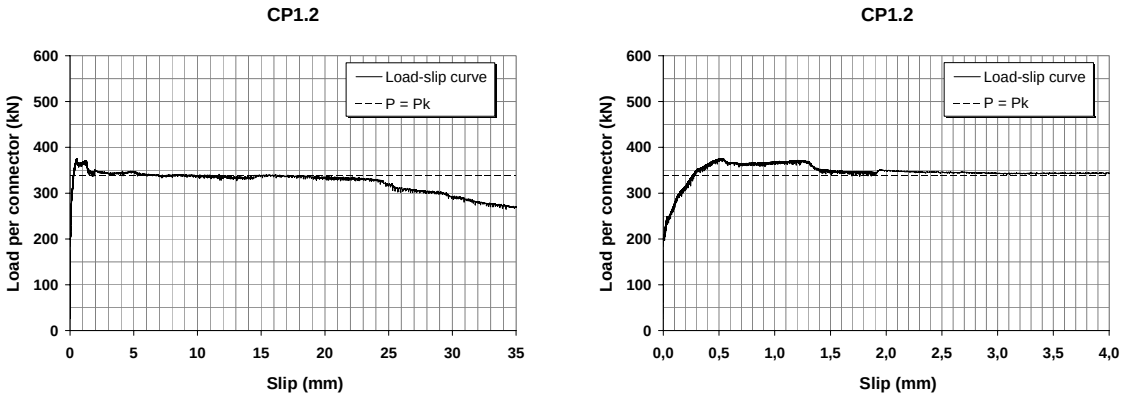

a) Complete load-slip curve b) Initial part of the load-slip curve

Figure 3.109 – Load–slip curve for specimen CP1.2

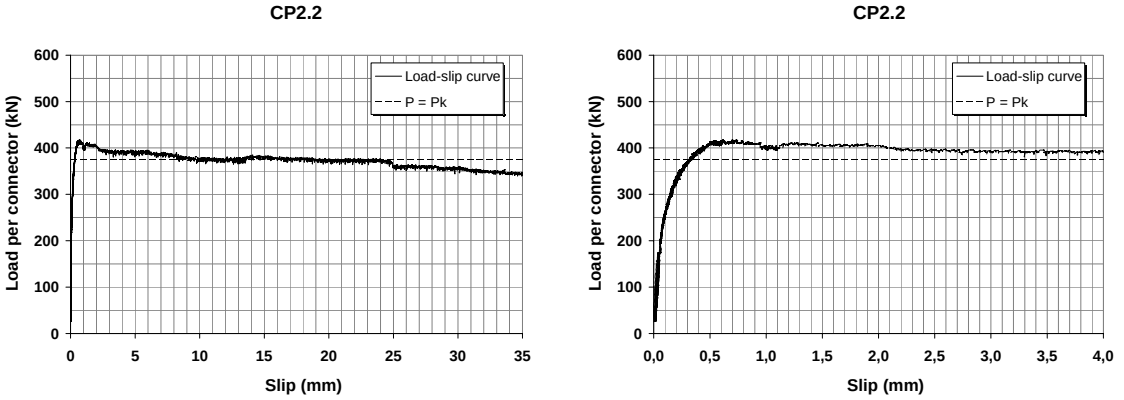

a) Complete load-slip curve b) Initial part of the load-slip curve

Figure 3.110 – Load–slip curve for specimen CP2.2

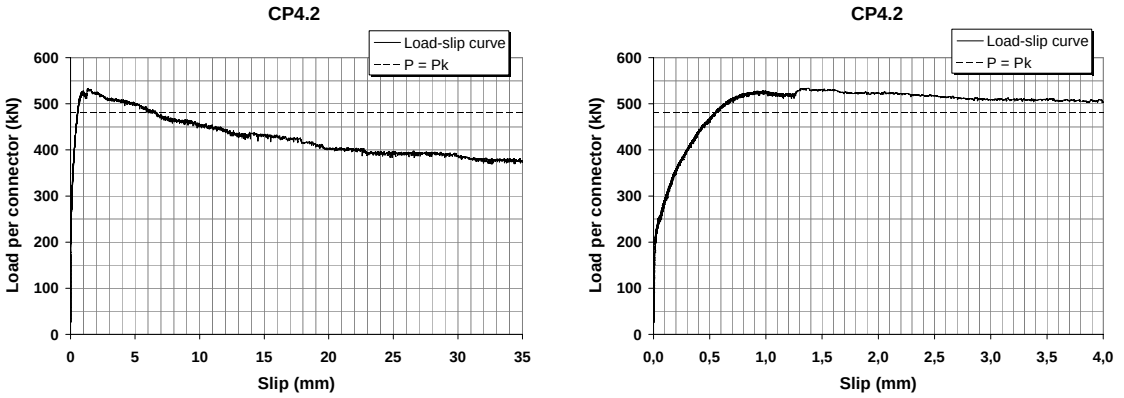

a) Complete load-slip curve b) Initial part of the load-slip curve

Figure 3.111 – Load–slip curve for specimen CP4.2

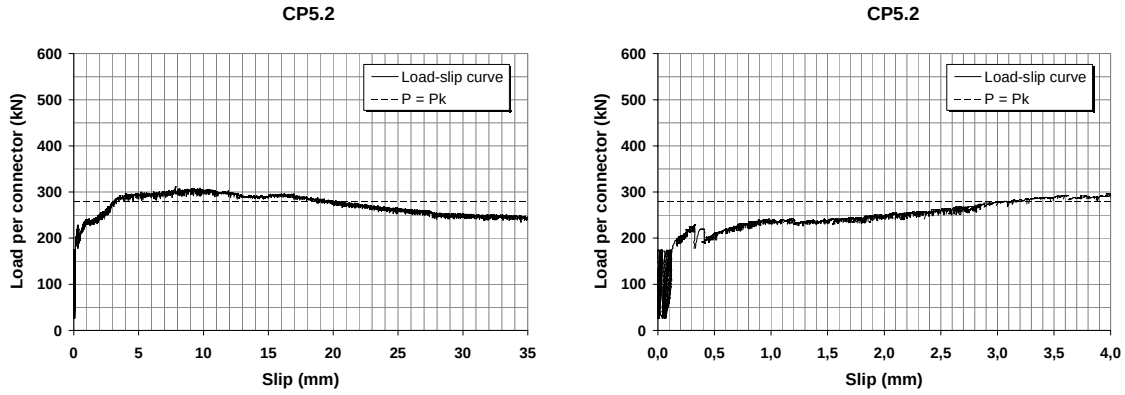

a) Complete load-slip curve b) Initial part of the load-slip curve

Figure 3.112 – Load–slip curve for specimen CP5.2

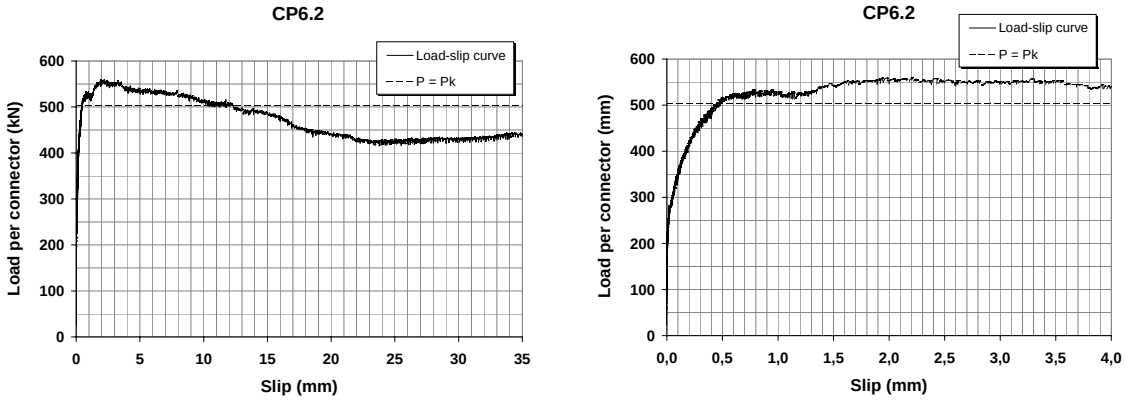

a) Complete load-slip curve b) Initial part of the load-slip curve

Figure 3.113 – Load–slip curve for specimen CP6.2

Perfobond connection has a very stiff behaviour during the initial part of the test. This high stiffness is maintained until the maximum load is reached. As presented in Table 3.16 and Table 3.17, the correspondent values of slip are small.

The maximum loads measured are attained for reduced values of slip and following this, the decrease of load capacity is slow and very large deformation values are measured. For very high deformation values, the connection still holds important load capacity and never gets to a complete failure. Failure is always conditioned by the concrete slab as it gets progressively cracked and is never conditioned by the connector failure.

According to EN1994-1-1, (CEN 2004b), three identical specimens are needed to determine the connection characteristic load capacity value. In the Perfobond test series, this recommendation was not followed because experimental push-out tests are expensive and time consuming, and therefore the option of testing just one specimen of a kind was

taken. This choice is justified by the good results that had been previously obtained with headed studs, as these tests results showed very small variability.

The maximum applied load value, divided by the number of similar connectors existent, corresponds to the connection maximum load capacity. The maximum load value is measured for each push-out test specimen and the connection characteristic load capacity value is calculated considering 90% of this value.

In all of the load-slip diagrams, from Figure 3.109 to Figure 3.113, the characteristic load value is represented. The slip $s_{elast,90\%}$ value is calculated considering the first intersection of the load-slip curve with the curve $P=P_k$. The slip value measured between the first and the second intersection of the load-slip curve with the curve $P=P_k$ corresponds to the plastic slip, $s_{plast,90\%}$. The connection characteristic slip value is considered equal to 90% of the plastic slip. The slip $s_{total,90\%}$ corresponds to the sum of $s_{elast,90\%}$ and $s_{plast,90\%}$.

Table 3.16 presents the results obtained for the first series of tests with Perfobond connector, Series CP X.1, where A_s is the transversal reinforcement area passing through the connectors' openings and A_d is the transversal welded wire mesh disposed on the slab's upper face (see Figure 3.100 and Figure 3.101).

Table 3.16 - Experimental results for Perfobond connector (Series CP X.1)

Specimen Reference	P_{max} (kN)	P_k (kN)	s (P_{max}) (mm)	$s_{elast,90\%}$ (mm)	$s_{plast,90\%}$ (mm)	$s_{total,90\%}$ (mm)	s_{ki} (mm)	A_s (cm^2)	A_d (cm^2)
CP1.1	317.7	285.9	1.676	0.792	16.041	16.833	14.437	0.000	0.000
CP2.1	390.6	351.5	1.390	0.426	7.833	8.259	7.050	0.785	0.000
CP3.1	237.7	213.9	2.197	0.907	8.399	9.306	7.559	2.356	0.000
CP4.1	502.1	451.9	1.575	0.684	6.706	7.391	6.036	2.356	0.000

In the same way, Table 3.17 presents the results obtained for the second series of tests with Perfobond connector, CP X.2.

Table 3.17 - Experimental results for Perfobond connector (Series CP X.2)

Specimen Reference	P_{max} (kN)	P_k (kN)	s (P_{max}) (mm)	$s_{elast,90\%}$ (mm)	$s_{plast,90\%}$ (mm)	$s_{total,90\%}$ (mm)	s_{ki} (mm)	A_s (cm^2)	A_d (cm^2)
CP1.2	375.1	337.6	0.532	0.264	18.133	18.396	16.319	0.000	1.178
CP2.2	416.8	375.1	0.615	0.315	23.619	23.934	21.257	0.785	1.178
CP4.2	533.6	480.3	1.364	0.543	6.126	6.669	5.513	2.356	1.178
CP5.2	311.0	277.0	7.874	3.131	17.035	20.166	15.332	0.000	1.178
CP6.2	559.4	503.5	2.207	0.458	11.827	12.284	10.644	3.393	1.178

Despite the difference in the test procedure (specimens of Series CP X.1 were tested with load control and specimens of Series CP X.2 were tested with displacement control), a comparison of connection load capacity can be established between Series CP X.1 and

Series CP X.2. In terms of deformation values, only the slip values obtained with Series CP X.2 will be considered as reliable for the analysis, although some comparisons are established between Series CP X.1 and Series CP X.2 results.

Figure 3.114 presents the load-slip curves for specimens from series CP X.1 and CP X.2, for specimens where only the transversal reinforcement is varied. Although the first series were not tested with deformation control, the general behaviour is similar for all specimens. Some principal aspects, common to both series can be pointed out from the analysis of Table 3.16, Table 3.17 and Figure 3.114:

- the initial phase of loading is very stiff for all the tested specimens;
- the load-slip behaviour can be considered as elastic almost until the maximum load;
- maximum load is attained for very small deformation values, with exception to specimen CP5.2, in which the connector openings are suppressed;
- after the maximum load value is attained, the load decreases very slowly;
- all the specimens maintain high load capacity for large deformation values, well beyond the slip measured for maximum load;
- after the maximum load value is attained, the load decrease is more pronounced for specimens with higher transversal reinforcement area;
- elastic slip is considered for 90% of the maximum load value and is similar for both series, with exception to specimen CP5.2;
- the specimens with no transversal reinforcement tend to loose load capacity slower than other specimens, although the maximum load value is smaller.

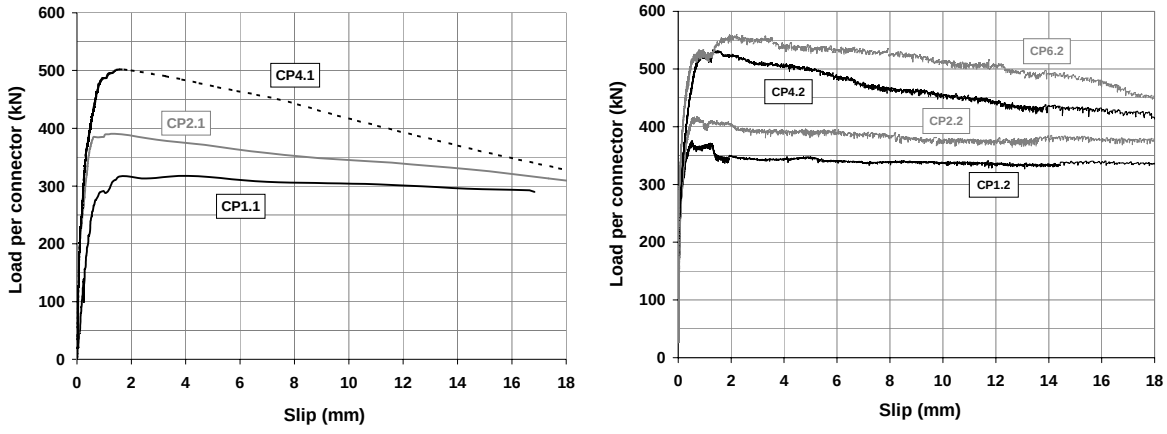

a) Series CP X.1 b) Series CP X.2

Figure 3.114 – Comparison of load-slip curves for Series CP X.1 and CP X.2

Some differences can also be appointed when comparing both series results:

- the values of slip correspondent to maximum load are a little higher for specimens of Series CP X.1 which probably results from the test being load controlled instead of displacement controlled;
- the values of total slip measured for 90% of the maximum load are higher for series CP X.2 specimens, with exception for specimen CP4.2;
- The resulting characteristic slip value is considered equal to 90% of the difference between the total slip measured at 90% of maximum load and elastic slip correspondent to the same load level; this values are higher for Series CP X.2 specimens, with exception to CP4.2.

It is possible to identify a close relation between maximum load per connector and slip for maximum load, for specimens with increasing transversal reinforcement area, as presented in Figure 3.115a. This relation does not show a linear trend, although the slip value increases with increasing maximum load and increasing transversal reinforcement area. On the contrary, for the relation between maximum load per connector and characteristic slip, it is not possible to identify a clear relation (see Figure 3.115b).

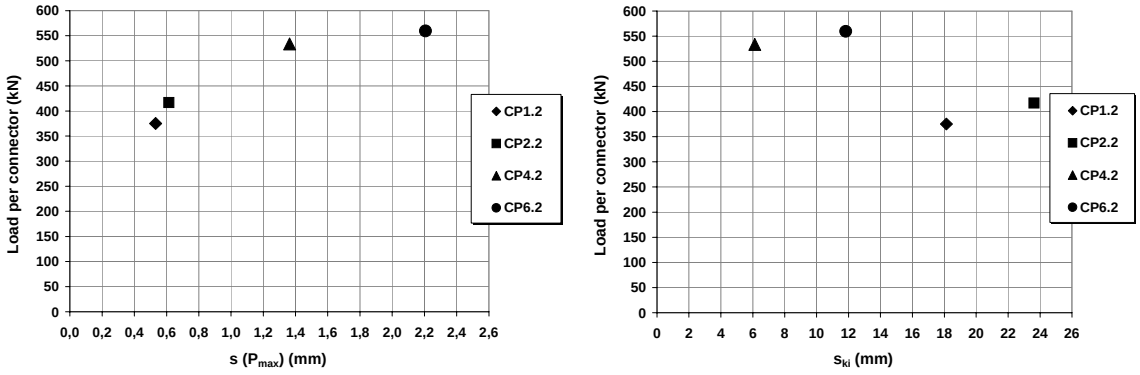

a) Maximum load and slip for maximum load b) Maximum load and characteristic slip

Figure 3.115 - Maximum load vs. slip for maximum load

3.7.6 Comparison with tests performed on normal density concrete

Based on a regression analysis made on the results of normal weight concrete specimens, with Perfobond connectors of various geometries and reinforcement distribution, (Oguejiofor and Hosain 1994/1996) established equation (3.14) that quantifies the shear connection load capacity.

This expression accounts for the contribution of four essential components. The first parcel considers the concrete slab compressed in front of the rib connector, the second parcel accounts the concrete dowels formed on the connectors' openings, the third parcel evaluates the concrete slab subjected to tensile stresses and the fourth parcel measures the contribution of the transversal reinforcement disposed on the concrete slab,

$$P = B_1\, h\, t\, f_c + \left(B_2\, A_{cd} + B_3\, A_{cc}\right)\sqrt{f_c} + B_4\, A_{tr}\, f_y \tag{3.14}$$

where,

f_c – concrete compressive strength;

f_y – steel yielding strength;

A_{cd} – concrete shear area (inside the connectors' openings, $A_{cd} = n \cdot \pi \cdot d^2 / 4$));

A_{cc} – concrete shear area (outside the connectors' openings);

t – Perfobond rib width;

h – Perfobond rib high;

d – diameter of the Perfobond rib openings;

n – number of Perfobond rib openings;

A_{tr} – area of transversal reinforcement.

Initially, the adjusted equation presented the following factors: $B_1 = 0$, $B_2 = 3.655$, $B_3 = 0.59$ and $B_4 = 1.233$. After performing more experimental tests and using numerical models, a new equation was proposed by the same authors to calculate the connection load capacity, with the following factors: $B_1 = 4.47$, $B_2 = 4.20$, $B_3 = 0.01$ and $B_4 = 0.91$. This new equation is based on the results of a regression analysis performed on a large number of results obtained from a numerical model calibrated from experimental results and is confirmed with more experimental tests. The equation maintains the contribution of the concrete dowels, the contribution of the transversal reinforcement, the contribution of the slab tensile strength and adds the effect of localized compression in front of the Perfobond rib (1st parcel).

$$P = 4.47\, h\, t\, f_c + \left(3.30\, n\, d^2 + 0.01\, A_{cc}\right)\sqrt{f_c} + 0.91\, A_{tr}\, f_y \tag{3.15}$$

Later, (Veríssimo et al. 2007) tested a large number of push-out specimens with a new type of shear connector, the CRESTBOND connector, that is an indented connector formed by a rib that is similar to the Perfobond rib, but with open apertures. The experimental results obtained with the Crestbond connector showed that:

- to consider the ratio between the transversal reinforcement and the concrete slab transversal area gives better results than to consider only the transversal reinforcement area;

- the connector eccentricity in relation to the concrete slab height should be considered in the analytical model; this is done by multiplying the force developed in front of the rib connector by the ratio between the connector height and the concrete slab height (h_{sc}/t_c).

Considering the similarities observed between Perfobond and Crestbond specimens in terms of failure mechanisms, the authors made a new study in order to define an equation that could properly quantify the connection load capacity for both connection types. The new adjusted equation has the form presented in equation (3.16).

$$P = B_1 \frac{h_{sc}}{t_c} h_{sc}\, t_{sc}\, f_c + B_2\, n\, D^2 \sqrt{f_c} + B_3\, A_{cc} \sqrt{f_c} + B_4 \left(\frac{A_{tr}}{A_{cc}} \right) \qquad (3.16)$$

Then, they performed a new multiple regression analysis on the results presented by Oguejiofor and Hosain (1994/1996) with the equation proposed. The multiple regression analysis performed gave the following coefficients: $B_1 = 4.044$, $B_2 = 2.369$, $B_3 = 0.157$ and $B_4 = 31.85 \times 10^6$. (3.17) is the resulting equation, (Verissimo 2007). The adjusted correlation coefficient is equal to 0.995.

$$P = 4.04 \frac{h_{sc}}{t_c} h_{sc} t_{sc}\, f_c + 2.37\, n\, D^2 \sqrt{f_c} + 0.16\, A_{cc} \sqrt{f_c} + 31.85 \times 10^6 \left(\frac{A_{tr}}{A_{cc}} \right) \qquad (3.17)$$

The results of this equation applied on the results of (Oguejiofor and Hosain 1994/1996) proved to give results that are closer to the experimental ones than the results obtained with equation (3.15) that was proposed by the same authors.

3.7.6.1 Influence of concrete bearing in front of the connector edge

In order to evaluate the influence of concrete bearing in front of the connector edge, experimental results obtained within this work are compared with the results obtained by Ferreira (2000). The tested specimens are similar for both experimental studies, with small differences regarding the connector height and the concrete slab dimensions and a more important difference that has to do with concrete compressive strength (Table 3.18). For comparison purposes, two types of specimens are tested: one with a plain slab and other with a longitudinal opening that goes from the bottom of the slab until the Perfobond rib basis (see Figure 3.99).

The values presented in Table 3.18 show that, for NWC, the results of quantifying the influence of localized concrete compression in front of the connector edge with equation (3.14) are proximate to the experimental results obtained. In this case, the experimental result is slightly higher than results obtained with equation (3.14).

The opposite happens for LWC: the experimental load result corresponds to approximately 80% of the load predicted with the first parcel of equation (3.16), which means that this equation should be modified in order to better account the effect of localized compression on LWC.

Table 3.18 - Experimental results for Perfobond connector – difference between CP4.1 and CP3.1

Specimen Ref.	Specimen Type	Concrete Type	$f_{lcm,Slab1}$	$f_{lcm,Slab2}$	P_{max}	ΔP	Concrete slab		Perfobond rib		1st parcel from (3.16)
							L	H	h	t	
			(MPa)	(MPa)	(kN)	(kN)	(mm)	(mm)	(mm)	(mm)	(kN)
CP4.1	Plain slab	LWC	65.67	62.81	502.1	264.4	650	150	100	13	317.5
CP3.1	Slab with opening**	LWC	60.13	60.80	237.7		650	150	100	13	337.4
PB06 (*)	Plain slab	NWC	9.65		278.0	62.5	720	100	80	12.7	44.1
PB07 (*)	Plain slab	NWC	10.00		274.4		720	100	80	12.7	45.7
PB05 (*)	Slab with opening**	NWC	12.80		220.1		720	100	80	12.7	58.5
PB08 (*)	Slab with opening**	NWC	11.73		207.4		720	100	80	12.7	53.6

* – specimens tested by (Ferreira 2000)

** – the slab opening is in front of the rib connector (see Figure 3.100 and Figure 3.102)

3.7.6.2 Influence of concrete dowels passing inside the connectors' openings

As presented in Figure 3.100 and Table 3.15, the difference between specimens CP5.2 and CP1.2 are the openings on the Perfobond rib. The Perfobond connector used has three circular openings with 50 mm diameter, as represented in Figure 3.98. The difference between these two specimens is the contribution of the concrete dowels in terms of load bearing capacity and deformation. Table 3.19 expresses the results obtained for specimens CP5.2 and CP1.2.

Table 3.19 - Experimental results for Perfobond connector – difference between specimens CP5.2 and CP1.2

Specimen Reference	$A_{c,openings}$	P_{max}	CP1.2 – CP5.2	s_{Pmax}	$s_{total,90\%}$
	(cm^2)	(kN)	(kN)	(mm)	(mm)
CP1.2	58.905	375.1	64.2	0.532	18.396
CP5.2	0.0	311.0		7.874	20.166

The first main result obtained from this comparison is that the load bearing capacity of the specimen with openings is higher. The difference in load bearing capacity between the two specimens is equal to 64.2 kN.

In item 2.11.7 from Chapter 2, the average shear strength experimentally determined for LWC is equal to 3.71 MPa. For specimen CP1.2, a total concrete shear area of 117.8 cm^2 corresponds to the connectors' holes, considering that concrete shear failure

occurs in both sides of the connector rib. A prediction on the concrete dowels load capacity contribution is obtained by multiplying these two values. The result is equal to 43.7 kN.

The predicted value corresponds to 68% of the experimental result, which probably means that there is a higher concrete confinement on the push-out specimen, provided by the layer of welded wire mesh and the transversal reinforcement positioned outside the Perfobond rib. However, there is a good proximity between these two results.

Figure 3.116 plots the experimental values presented in Table 3.19 and Table 3.20, based on calculations made with the second parcels of equations (3.15) and (3.17).

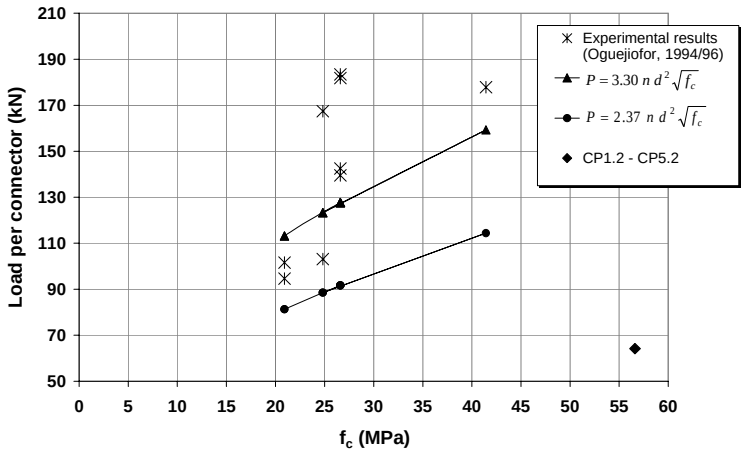

Figure 3.116 – Evaluation on the concrete dowels load capacity, for NWC and LWC

Other comparable experimental results considering Perfobond connectors with very similar geometry, but now using NWC, were obtained by Oguejiofor and Hosain (1994/96). These results are collected in Table 3.20. As done for specimens CP5.2 and CP1.2, two similar specimens, one with Perfobond rib with three openings and the other with steel rib without openings are compared and the respective maximum loads are subtracted.

There is a great variability associated with the results obtained by Oguejiofor and Hosain (1994/96). To define equation (3.14), they performed more experimental tests, varying also the number of the connector openings and studied a numerical model calibrated with the experimental results, in order to produce more results for analysis.

The result obtained with specimens CP1.2 and CP5.2 is much smaller than the results experimentally obtained by predicted by Oguejiofor and Hosain (1994/96) and also the results obtained with equation (3.14). One possible reason is that LWC shear strength is lower than NWC shear strength, which should be considered.

Table 3.20 - Experimental results for Perfobond connector obtained by Oguejiofor and Hosain (1994/96)

Specimen Reference	Description	f_{cm} (MPa)	t (mm)	P_{max} (kN)	$A_{c,openings}$ (cm^2)	$P_{max,\ no}$ - $P_{max,\ 3o}$
EB-1	No openings	20.91	13	179.4	0.0	94.6
EB-3	Three openings	20.91	13	274.0	58.91	
EB-5	No openings	20.91	13	292.0	0.0	101.6
EB-7	Three openings	20.91	13	393.6	58.91	
ED-1	No openings	24.82	13	240.7	0.0	103.1
ED-3	Three openings	24.82	13	343.8	58.91	
EC-5	No openings	41.43	13	431.0	0.0	160.4
EC-3	Three openings	41.43	13	597.8	58.91	
EC-7	Three openings	41.43	13	584.9	58.91	
ED-5	No openings	24.82	13	413.5	0.0	167.4
ED-7	Three openings	24.82	13	580.9	58.91	
A-1	No openings	26.60	13	384.6	0.0	183.4
A-2	Three openings	26.60	13	568.0	58.91	
C-1	No openings	26.60	13	338.8	0.0	181.8
C-2	Three openings	26.60	13	520.6	58.91	

3.7.6.3 Influence of the transversal reinforcement passing inside the connectors' openings

Figure 3.117 displays the connection maximum applied load, in relation to the transversal reinforcement area passing through the connectors' openings, for Series CP X.1 and Series CP X.2. The linear relation that better fits the obtained results is plotted for each series. Both series show that there is a strong linear relation between the connection load capacity and the transversal reinforcement area.

Results on series CP X.1 show a slightly higher increase on load capacity growth with area of transversal reinforcement, when compared to series CP X.2.

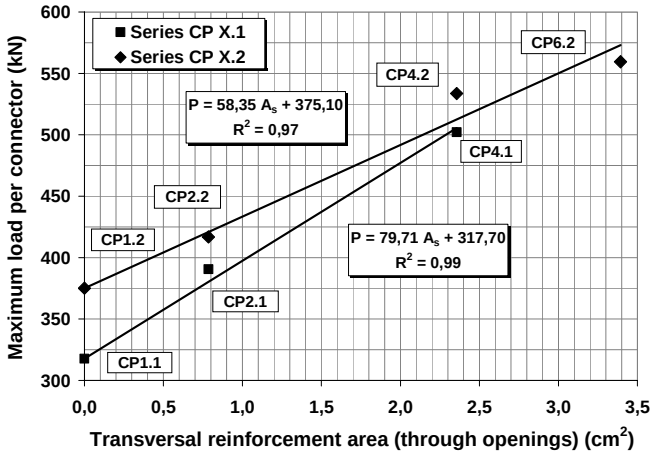

Figure 3.117 - Maximum load vs. reinforcement area for Series CP X.1 and Series CP X.2

The inclination of the trend line associated with each series, gives the reinforcement contribution on the connection load capacity, corresponding to $P(A_s) = 797137\ A_s$ for series CP X.1 and $P(A_s) = 583514\ A_s$ for series CP X.2, expressed in kN. This contribution can be related to the reinforcement yielding strength, as presented in Table 3.21.

Table 3.21 – Load capacity contribution obtained with reinforcement bars passing through the connectors' openings

Type of specimen	Concrete type	Reinforcement diameter - d (mm)	POST tests	
			f_y (MPa)	P (kN)
Series CP X.1	LWC	10	576	$P(A_s) = 1.38 \cdot f_y \cdot A_s$
Series CP X.2	LWC	10	576	$P(A_s) = 1.01 \cdot f_y \cdot A_s$
	LWC	12	523	$P(A_s) = 1.12 \cdot f_y \cdot A_s$
C2 , C2-R	NDC	10	478	$P(A_s) = 1.71 \cdot f_y \cdot A_s$
C3 , C3-R	NDC	10	478	$P(A_s) = 1.30 \cdot f_y \cdot A_s$

where,

f_y – steel yielding tensile strength;

A_s – transversal reinforcement through openings (m^2).

The same approach is followed for some of the results obtained by Oguejiofor and Hosain (1996), regarding four specimens with the same concrete compressive strength and geometric disposition, where the area of transversal reinforcement passing through the connectors' openings is the only parameter varied (Figure 3.118). The Perfobond connector used by these authors is very similar to the Perfobond connector used within this work. The results obtained are in agreement with the ones here obtained, which means that the contribution of transversal reinforcement on the connection load capacity is not altered by substituting normal density concrete with lightweight concrete.

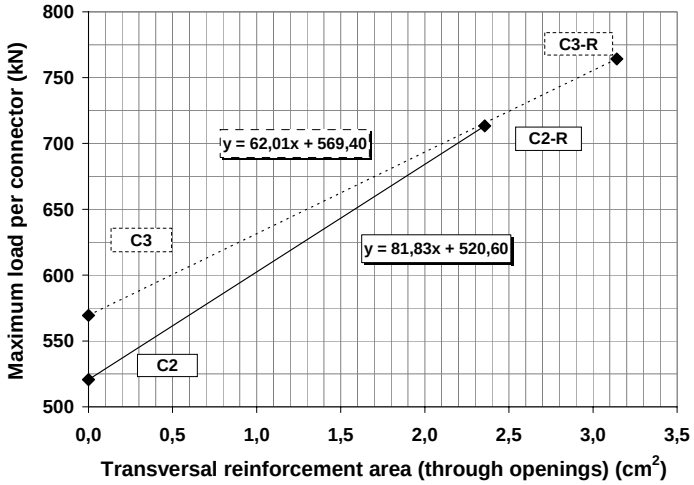

Figure 3.118 - Maximum load vs. reinforcement area (results from Oguejiofor and Hosain 1996)

3.7.6.4 Influence of the layer of welded wire mesh

Between Series CP X.1 and Series CP X.2, the main difference is the layer of welded wire mesh positioned on the upper face of the concrete slabs, as represented in Figure 3.99 and Figure 3.100. As plotted in Figure 3.119, there is an almost linear relation between the transversal reinforcement area that passes through the connector's openings and the connection maximum load capacity. The difference in load capacity between series CP X.1 and series CP X.2 is almost constant.

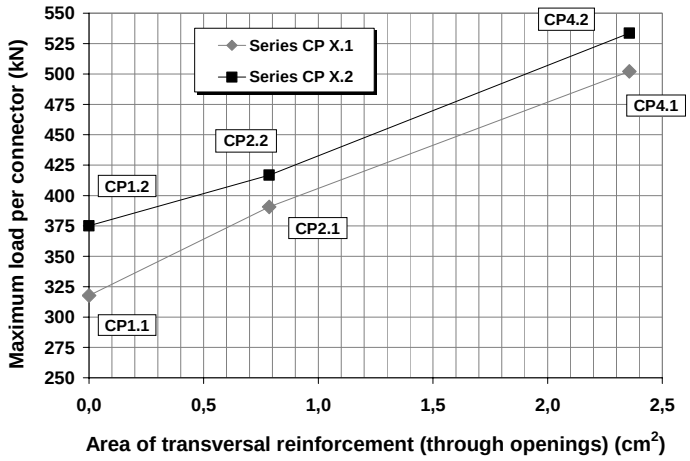

Figure 3.119 - Maximum load vs. reinforcement area – Comparison for Series CP X.1 and Series CP X.2

As referred, the difference between the two curves is also almost constant, with a minor deviation for the specimens that have no reinforcement passing through the connector's holes (CP X.1). Table 3.22 shows that a medium value of 38.4 kN is obtained for the maximum load difference. In order to establish the contribution of the welded wire mesh reinforcement, the minimum difference between similar tested specimens is considered. This value is equal to 26.2 kN and the following relation is obtained to quantify this parameter, $P(A_s) = 0.38 \cdot f_y \cdot A_s$. It is to be noticed that the welded wire mesh contribution to the connection load capacity is smaller than the contribution of reinforcement bars positioned inside the connectors´ openings.

Table 3.22 - Experimental results for Perfobond connector – difference between Series CP X.1 and Series CP X.2

Specimen Reference	P_{max} (kN)	$P_{series\ CP\ X.2} - P_{series\ CP\ X.1}$ (kN)	A_s (cm^2)	$A_{s,d}$ (cm^2)	$f_y(A_{s,d})$ (MPa)
CP1.1	317.7	57.4	0.0	0.0	583
CP1.2	375.1			1.178	
CP2.1	390.6	26.2	0.785	0.0	583
CP2.2	416.8			1.178	
CP4.1	502.1	31.5	2.356	0.0	583
CP4.2	533.6			1.178	
Average		38.4			

Table 3.23 collects some experimental results obtained by Oguejiofor and Hosain (1994) for specimens without the layer of welded wire mesh (Series EB) and specimens with one layer of welded wire mesh (Series ED). The specimens in comparison are identical with exception to the referred reinforcement.

It was not possible to identify the welded wire mesh used by the authors referred, but it is clear from Table 3.23 that its contribution to the shear connection load capacity is similar to the one obtained in the results performed with lightweight concrete.

Table 3.23 - Experimental results for Perfobond connector – difference between Series CP X.1 and Series CP X.2

Specimen Reference	P_{max} (kN)	$P_{series\ ED} - P_{series\ EB}$ (kN)	A_s (cm^2)	$A_{s,d}$	$f_y(A_{s,d})$ (MPa)
EB-1	179.4	61.3	0.0	no	660.2
ED-1	240.7			yes	
EB-2	249.1	55.8	0.0	no	660.2
ED-2	304.9			yes	
EB-3	274.0	69.8	0.0	no	660.2
ED-3	343.8			yes	
EB-4	276.5	88.2	0.0	no	660.2
ED-4	364.7			yes	
Average		68.8			

3.7.6.5 Regression analysis

A new regression analysis build on the results obtained with lightweight concrete and presented within this chapter is made, considering the general equation (3.16) defined by Veríssimo et al. (2007).

The multiple regression analysis performed gave the following coefficients: $B_1 = 1.58$, $B_2 = 1.10$ and $B_4 = 36\times10^6$. The coefficient B_3 was imposed equal to zero, because the concrete slab shear area was constant in all the tested specimens. Therefore, the multiple regression analysis could not properly evaluate the value of B_3. The connector eccentricity in relation to the concrete slab height is not considered in this analysis. The resulting equation corresponds to equation (3.18) and the adjusted correlation coefficient is equal to 0.998.

$$P = 1.58\, h_{sc} t_{sc} f_c + 1.10\, n D^2 \sqrt{f_c} + 36\times10^6 \left(\frac{A_{tr}}{A_{cc}} \right) \tag{3.18}$$

Figure 3.120 presents a comparison between the maximum load measured in the experimental push-out tests performed with Perfobond connector and the analytical results obtained by using the adjusted equation (3.18).

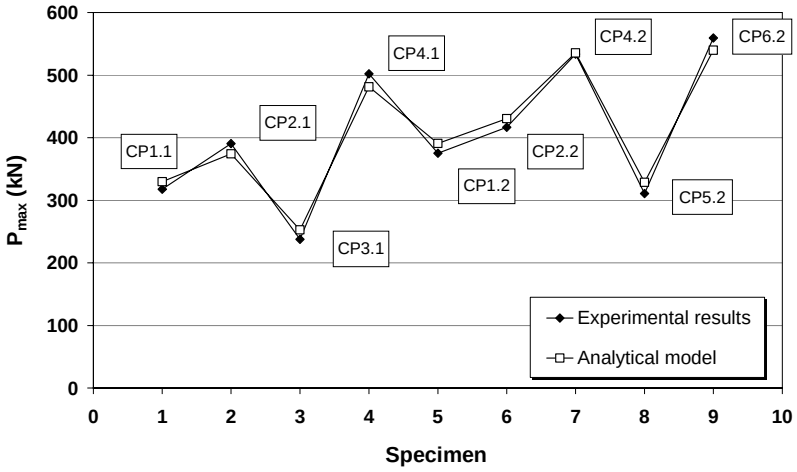

Figure 3.120 – Comparison between experimental results and analytical results obtained with equation (3.18)

The equation proposed shows some important aspects regarding the use of lightweight concrete:

- the contribution of the compressed concrete positioned in front of the connector rib is around 39.2% of the corresponding contribution verified for normal weight concrete, showing that lightweight concrete is much more sensible to concentrated loadings than normal density concrete;
- the contribution of the concrete dowels formed on the connector openings is around 46.4% of the corresponding contribution verified for normal weight concrete, which should result from the lower shear strength of LWC;
- the contribution of the transversal reinforcement disposed on the concrete slab is around 13% higher than the corresponding contribution for normal weight concrete. This confirms the observations previously made, in which was identified that the contribution of the transversal reinforcement to the connection load capacity is similar for NDC and LWC. The fact that the value of B_4 for LWC is higher than the value of B_4 for NDC may result from a better bond between the reinforcement bars and the lightweight concrete used. The LWC used presents a compressive strength that is always higher than 52 MPa, while the compressive strength of the normal density concrete used by Oguejiofor and Hosain (1994/1996) is never higher than 41.5 MPa.

Table 3.24 presents an evaluation on each component of the connection load capacity given by equation (3.18). It also presents the relative importance of each component on the total load capacity. The results presented show that the transversal reinforcement is always the component with higher contribution to the connection load capacity, even in specimens where there is no reinforcement passing inside the connectors' openings.

The second parcel of equation (3.18) is the one that considers the contribution of the concrete dowels formed inside the connectors' openings. It is verified in Table 3.24 that the contribution of the concrete positioned in front of the Perfonbond rib is always higher than the contribution of the concrete dowels, when lightweight concrete is used.

Table 3.24 – Relative importance of each component of the connection load capacity given by equation (3.18)

Specimens	P_{exp}	P Eq. (3.18)	1st parcel of eq. (3.18)	2nd parcel of eq. (3.18)	3rd parcel of eq. (3.18)	1st parcel of eq. (3.18)	2nd parcel of eq. (3.18)	3rd parcel of eq. (3.18)
	(kN)	(kN)	(kN)	(kN)	(kN)	(%)	(%)	(%)
CP 1.1	317.7	329.7	124.2	64.1	141.4	37.7	19.4	42.9
CP 2.1	390.6	374.3	122.2	63.5	188.6	32.6	17.0	50.4
CP 3.1	237.7	252.7	0.0	64.2	188.6	0.0	25.4	74.6
CP 4.1	502.1	481.3	132.3	66.1	282.9	27.5	13.7	58.8
CP 1.2	375.1	390.7	116.5	62.1	212.2	29.8	15.9	54.3
CP 2.2	416.8	430.5	110.7	60.5	259.3	25.7	14.1	60.2
CP 4.2	533.6	535.5	119.2	62.8	353.6	22.3	11.7	66.0
CP 5.2	311.0	328.8	116.7	0.0	212.2	35.5	0.0	64.5
CP 6.2	559.4	539.9	122.6	63.7	353.6	22.7	11.8	65.5

3.7.7 Other proposed equations

Medberry and Sharooz (2002) compared their own results obtained from push-out tests performed at Cincinnati University, with the ones reported by Oguejiofor and Hosain (1994) and realized that equation (3.14) overestimates a large number of experimental results. Therefore, they proposed an equation to estimate the Perfobond connector load capacity, that better fits the experimental results. Equation (3.19) is the result of this analysis,

$$P = 9bh\sqrt{f_c} + 60b_f L_c + 20n\pi\left(\frac{D}{2}\right)^2\sqrt{f_c} + 0.9A_{vf}\,f_y \qquad (3.19)$$

where,

P – Perfobond connector load capacity (lbs.);
b – slab width (in.);
h – slab height bellow the connector (in.);
f_c – concrete compressive strength determined in cylindrical specimens (psi);
b_f – steel flange width (in.);
L_c – contact length between the concrete slab and the steel profile (in.);
n – number of connector openings;
D – diameter of connector openings (in.);
A_{vf} – total area of transversal reinforcement (in^2);
f_y – steel yielding strength of reinforcement (psi).

The second parcel of equation (3.19) reflects the chemical adherence between the concrete slab and the steel beam.

From the analysis of experimental results, Ushijima et al. (2001) proposed two equations to predict the load bearing capacity of Perfobond connectors. The first equation, (3.20), considers that there is no reinforcement passing through the connector's openings.

$$Q_u = 3.38\, D^2 \sqrt{\frac{t}{D}}\, f_c - 39.0 \tag{3.20}$$

Its application is limited by condition (3.21),

$$22.0 < D^2 \sqrt{\frac{t}{D}}\, f_c < 194.0 \tag{3.21}$$

where,

f_c – concrete compressive strength measured in cylinders;

t – Perfobond rib thickness;

D – diameter of the Perfobond openings.

The second equation, (3.22), considers the existence of reinforcement passing through the connectors' openings.

$$Q_u = 1.45\left[\left(D^2 - D_{st}^2\right) f_c + D_{st}^2\, f_{st}\right] - 26.1 \tag{3.22}$$

Its application is limited by condition (3.23),

$$51.0 < \left(D^2 - D_{st}^2\right) f_c + D_{st}^2\, f_{st} < 488.0 \tag{3.23}$$

where,

D_{st} – diameter of the reinforcement bars that pass through the connectors' openings;

f_{st} – steel tensile strength of reinforcement bars that pass through the connectors' openings.

3.7.8 Strains measured in the reinforcement bars

Figure 3.121 shows the load-strain diagrams, measured during the test of specimen CP1.2. The diagrams present all the registered values until the maximum test load is reached.

With exception to device SG 2.b, all strain gauges measure similar values of strain for this specimen. The maximum registered value is equal to 321.7 μm/m for SG 1.b, 240.7 μm/m for SG 1.d and 150.6 μm/m for SG 2.d. This level of strain indicates that in those positions, concrete should be cracked. However, there are probably cracks in close positions, so that the values show the proximity effect.

SG 2.b is positioned on Slab 2 of specimen CP1.2. The high values measured by SG 2.b show that this device is in the position of a concrete crack. The strain values

attained indicate that for the test maximum load, there is already some yielding of the reinforcement.

Although this was not visible during the test, it seems that this crack was already initiated during the 25 cycles of loading and unloading. SG 2.d is not coincident with the crack location and therefore, the measured strains are much smaller, but similar to the strain measured in Slab 1.

As visible in Figure 3.121, the crack formation is a bit different between the two slabs. Cracking is more dispersed in Slab 1 and concentrated in a principal crack in Slab 2, which can justify the larger strain verified in SG 2.b.

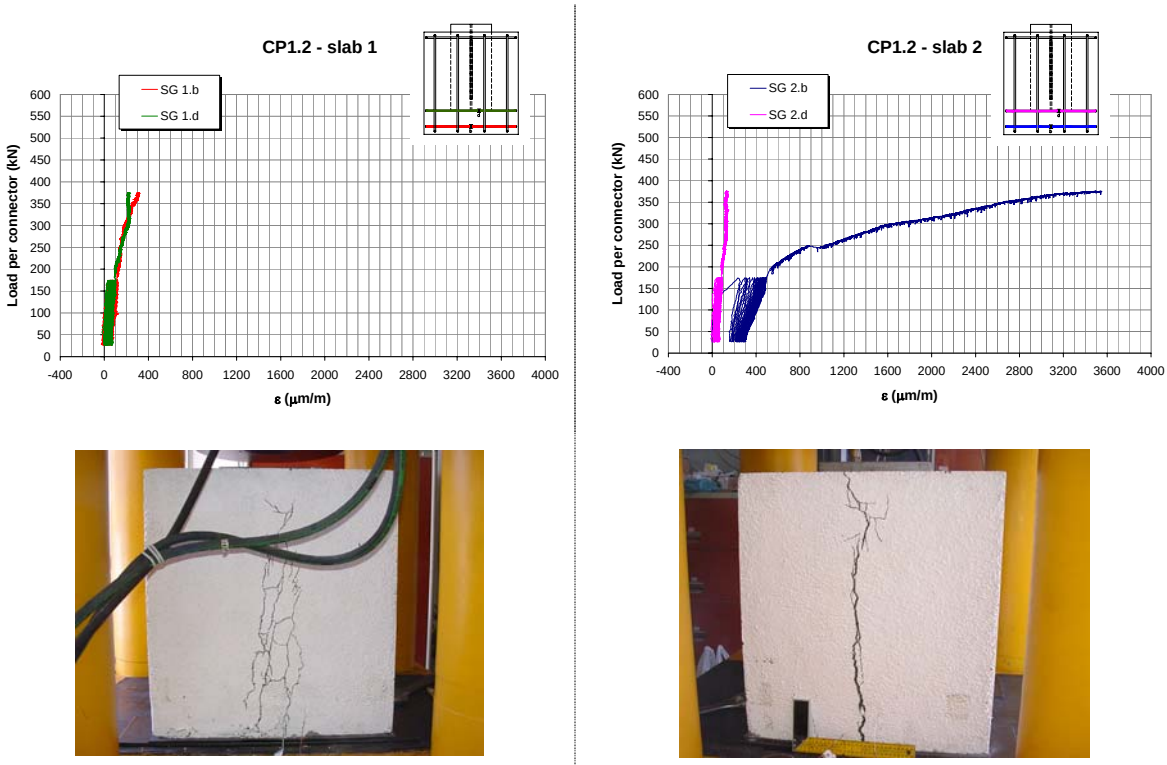

a) b)

Figure 3.121 – Strain measurements in specimen CP1.2: a) Slab 1; b) Slab 2

For specimen CP2.2, the strain gauges are only disposed in Slab 2, with one strain gauge in each transversal reinforcement bar (Figure 3.122). Maximum measured strains are equal to 118.6 μm/m for SG 2.b, 1105.4 μm/m for SG 2.d and 1724.9 μm/m for SG 2.g. These values show that all the reinforcement bars are still in the elastic range and the superior reinforcement bars suffer higher tensile stresses.

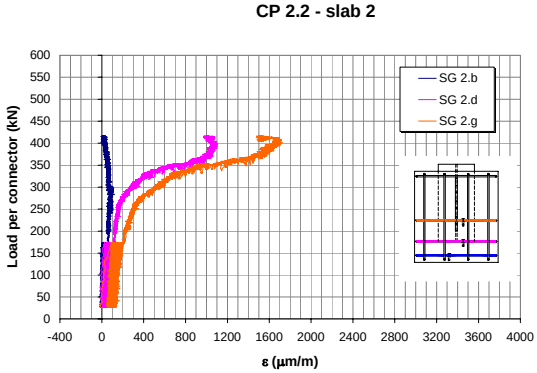

a) b)

Figure 3.122 – Strain measurements in specimen CP2.2: a) Slab 2; b) Crack pattern

Figure 3.123 presents the strain gauges disposed in specimens CP4.2 and the corresponding load-strain curves, until maximum load.

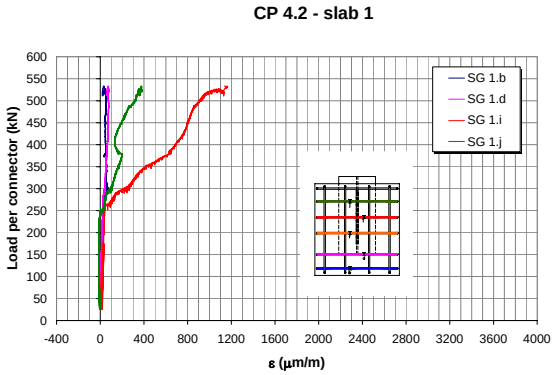

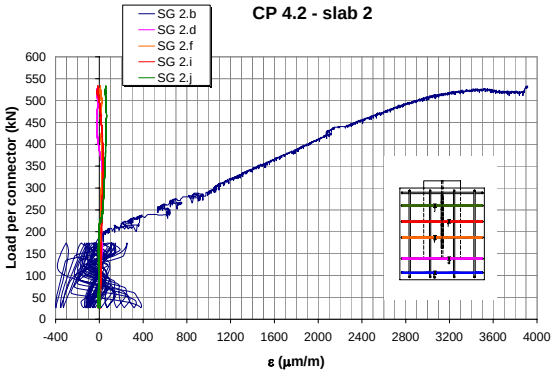

a) b)

Figure 3.123 – Strain measurements in specimen CP4.2: a) Slab 1; b) Slab 2

Maximum measured strains are equal to 71.9 μm/m for SG 1.b and 77.6 μm/m for SG 1.d, which shows that there is no principal crack near the strain gauges positions. Strains are higher in the reinforcement bars that pass through the connectors' holes, with 382.3 μm/m for SG 1.j and 1166.6 μm/m for SG 1.j. This means that higher tensile stresses

are mobilized in the Perfobond rib area, for Slab 1, although all the measured strains are within the steel elastic range when maximum load is attained.

For Slab 2 of specimen CP4.2, high strain values are concentrated on the lower reinforcement bar, where strain is equal to 3915.2 μm/m for SG 2.b. This value corresponds to the yielding of the bar cross section. Other strain gauges measure very small strain values: 28.7 μm/m for SG 2.d, 33.3 μm/m for SG 2.f, 33.7 μm/m for SG 2.i and 67.1 μm/m for SG 2.j.

The presented strain results, measured during push-out tests performed on Perfobond specimens put in evidence some important aspects:

- the measured strain values depend on the position of longitudinal cracks, although all the measured cross sections are close to the Perfobond rib position;
- when failure occurs with a principal longitudinal crack, that grows from the bottom to the top of the concrete slab, high tensile stresses are mobilized on the inferior zone of the concrete slab;
- in this case, after the longitudinal crack appears, high tensile strain are transmitted to the reinforcement bar that crosses the main crack;
- when failure occurs with a more dispersed cracking along the slab's height, the upper positioned reinforcement tends to be more effective and tensile stresses are higher in this zone.

3.7.9 Stiffness measured for POST tests with Perfobond connectors

The connection stiffness, *k*, is calculated considering the relation between load and slip deformation defined with equation (3.4). This parameter is established for the ascending branch of the load-slip curve and is expressed in percentage of the maximum load.

Figure 3.124 shows the values of *k* determined for Series CP.2. The results presented show high variability, specially for the initial phase of loading. The values of *k* presented in Figure 3.124 are all calculated after the 25 cycles of load and unload, which should diminish the importance of initial adjustments. However, the connection is very stiff, which makes the specimen more sensible to any adjustments, and the variability found results from the fact that a small variation on the slip value induces high variation on the value of stiffness *k*.

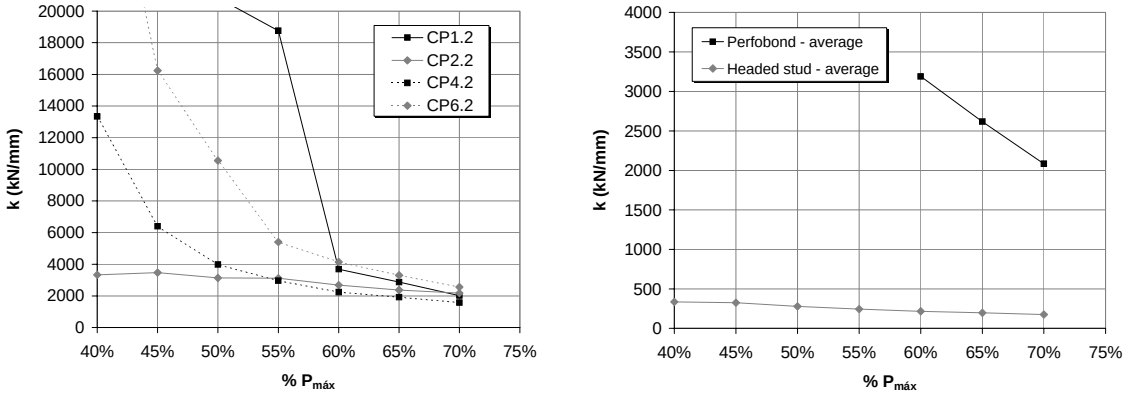

a) Series CP X.2

b) Comparison between average CP X.2 and average headed stud connectors

Figure 3.124 - Stiffness measured in Perfobond connectors specimens

For load values higher than 60% of the maximum load P_{max}, the results tend to be more consistent. For $0.60P_{max}$, the average value is equal to 3190 kN/mm/connector. As the value of P raises, a loss of stiffness is verified. When the average Perfobond values are compared to the average values determined for headed stud connectors, a relation between approximately 12 and 15 is verified for the load range in analysis.

It is clear that one Perfobond connector is much stiffer than one headed stud. Due to their high load capacity, a small number of Perfobond connectors can substitute a higher number of studs, when used in composite beams. If we consider that, in average, one Perfobond connector replaces around 4 headed studs with 19 mm diameter (both in LWC), it is concluded that the connection with Perfobond is still stiffer and therefore a higher interaction between the concrete slab and the steel beam is guaranteed.

3.8 Tests with T connector

3.8.1 Objectives

Some standard push-out tests have already been performed with normal weight concrete and T connectors. The experimental campaign here presented is the result of performing push-out tests that follow the description and procedure presented in 5.3, but now using high strength lightweight concrete and T connectors. The objectives of this research are:

- to analyse the adequacy of using lightweight concrete in composite structures, focusing on the shear connection behaviour with T connectors;
- to determine the T connector connection load bearing capacity;
- to evaluate the connection ductility;

- to evaluate the connection deformation capacity and the load-slip relation, before and after the maximum load is attained;
- to analyse the connection stiffness for service loads;
- to compare all the mentioned parameters with the ones obtained for normal weight concrete in experimental tests performed by other authors;
- to compare the test results with the ones obtained for headed studs and Perfobond.

3.8.2 Materials properties

Concrete properties are not the same for all the tested specimens with T connector, but are very similar. The values for compressive strength and elasticity modulus presented in Table 3.25 were determined for all castings at the same day of the respective test.

Table 3.25 - Concrete properties for Push-Out test specimens with T connectors

Specimen Ref.	Concrete Ref.	Test	Concrete density (kg/m^3)	$f_{lcm,Slab1}$ (MPa)	$f_{lcm,Slab2}$ (MPa)	$E_{lcm,Slab1}$ (GPa)	$E_{lcm,Slab2}$ (GPa)
T.1	BL8	POST	1982	62.57	64.19	27.72	28.14
T.2	BL9	POST	1946	65.79	64.14	29.30	27.78
T.3	BL29	POST	1820	57.18	56.77	24.37	24.58

3.8.3 Tests specimens

The T connector can be created by joining together steel plates in a T shape or, as happens with the chosen T connector, can be cut from a laminated profile. The present T connector was produced by cutting an IPE200 profile in two halves. The T connector consists on half of an IPE section, with respective web welded to the upper flange of the steel section, in the longitudinal direction of the beam (Figure 3.125). The size of the connector can be varied, as it implies only to use more or less profile length or choosing another class of laminated I Profile.

Figure 3.125 – T connector configuration and dimensions

The first advantage of using this type of connector, is that the steel profiles are already available in the market and the second one is that by cutting them in two symmetrical halves, both parts can be used, avoiding the loss of material.

The specimens prepared for the standard push-out test with Perfobond connector were produced according to Figure 3.126. The geometry of the test specimens is always the same. Besides the connector geometry, all other elements (steel profile, concrete slabs, etc) have dimensions similar to the ones chosen for the POST tests performed with headed stud connectors and with Perfobond connectors. The reinforcement bars represented in Figure 3.126 correspond to bars with 10 mm diameter.

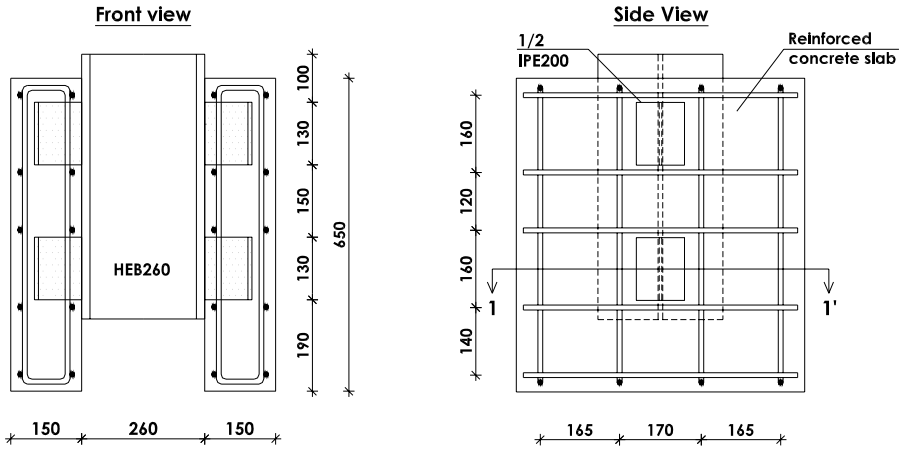

Figure 3.126 – Specimens geometry for experimental POST tests with T connectors

3.8.4 Test setup for T connector specimens

The test setup includes the hydraulic machine used to apply the load, the measuring instruments, the control system, the electronic data acquisition unit and all the devices that are needed to effectuate the test. The test setup for the push-out test with T connector follows all the dispositions described in 3.5.3, 3.5.4 and 3.5.5.

3.8.5 Test results

The T connector load capacity in normal weight concrete results essentially from three components: concrete compression under the T transversal section, shear on the half T web and tension on the T web. In the same way as happened for studs, tension stresses on the T web are reduced because of high strength material.

Figure 3.127.a shows the steel profile zone where the T connectors were welded. Every tested specimen suffered shear failure, localized near the web basis, right above the

welded fillet, (Valente and Cruz 2004b). The area of failure is visible, showing important deformation on the T web.

Figure 3.127.b shows the concrete slab zone that was in contact with the steel profile before the connection failure. A significant deformation of the T web inserted in the concrete slab is visible, proving that the slip measured between the steel profile and the concrete slabs is mostly resultant from the T web deformation.

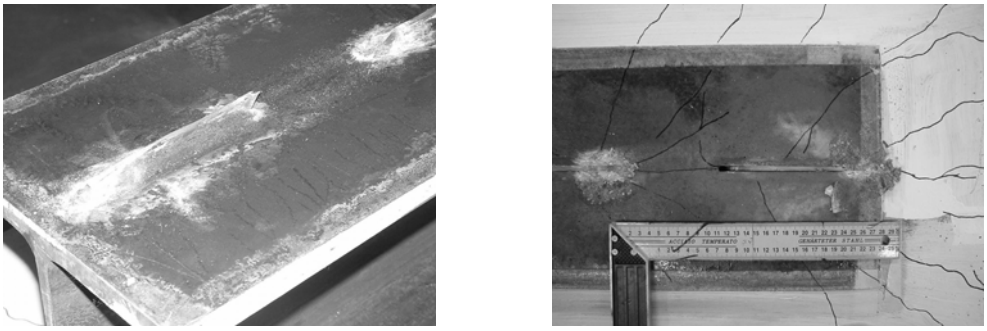

a) b)

Figure 3.127 - Failure in T connector specimen

In the lower part of the connector there is a concentrated zone of crushed concrete and several inclined cracks are rising from there. Concrete deformation should also provide important contribution to the slip between the steel profile and the concrete slab.

After the tests were performed, some slabs were destructed in order to observe the deformed connectors. Figure 3.128 shows that the T connector deformation is concentrated on the connector basis. The type of deformation observed is very similar to the deformation suffered by the stud connectors presented in Figure 3.39.

Figure 3.128 – T connectors redrawn from the lightweight concrete slabs of POST test specimens

The slabs cracking on the upper face of the concrete slab is presented in Figure 3.129 for all the tested specimens. The cracking pattern is very similar to every specimen slab.

The cracking is distributed over the slab and the more cracked zone is situated between the two connectors. All the visible cracks begin at this position and grow towards the slabs' top and bottom. Horizontal cracks are visible under both connectors position.

In the lower part of the slab, all the cracks are vertical, which means that possibly, the reinforcement is more stressed in this zone. This aspect can be analysed through the results measurements obtained with strain gauges.

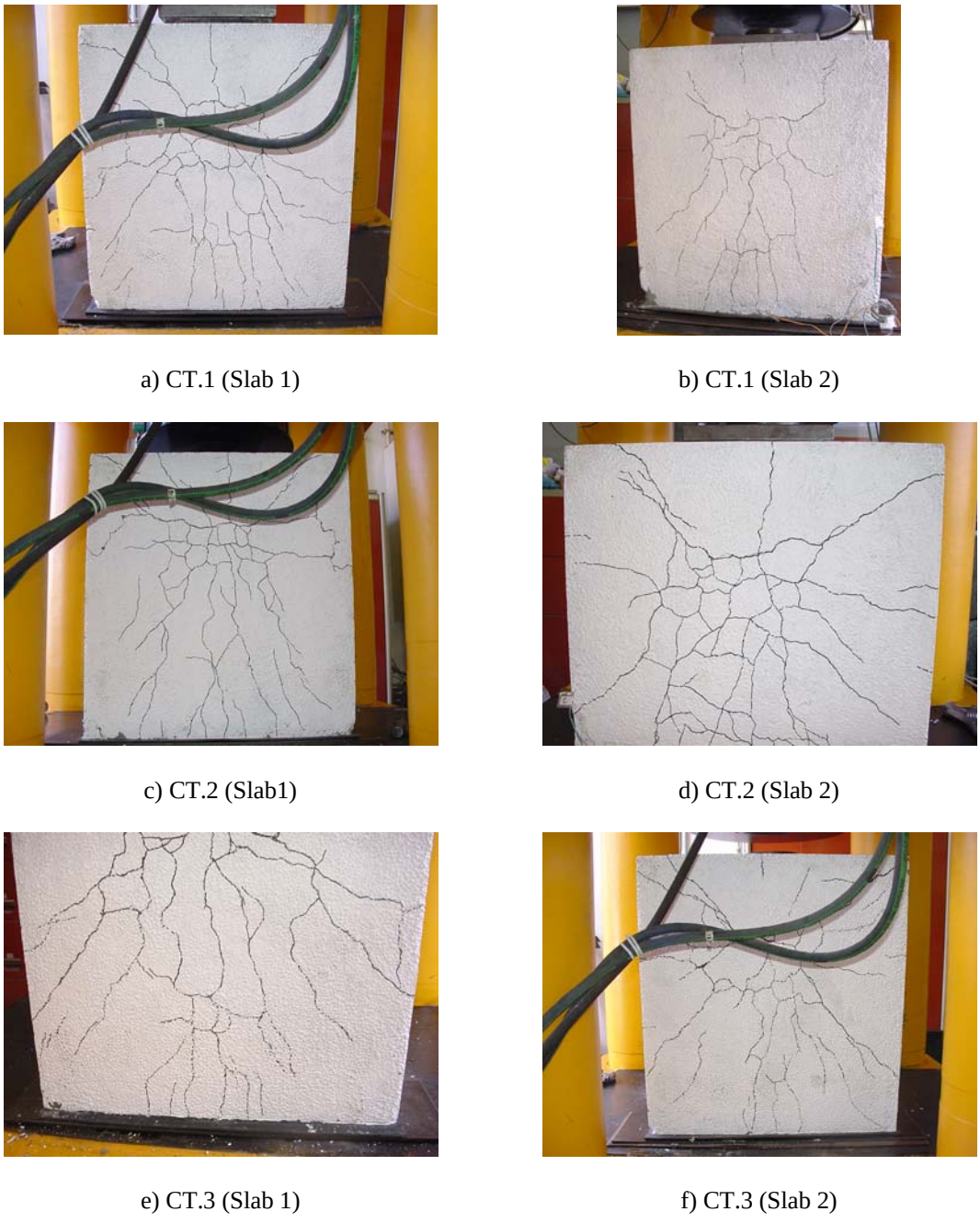

a) CT.1 (Slab 1)

b) CT.1 (Slab 2)

c) CT.2 (Slab1)

d) CT.2 (Slab 2)

e) CT.3 (Slab 1)

f) CT.3 (Slab 2)

Figure 3.129 – Cracking on specimens with T connector

In all the specimens tested with T connectors, shear failure is identified on the T web. Failure always occurs first on one side of the specimen, even though the specimens are symmetric. Usually, both connectors locate in one of the slabs suffer simultaneous failure.

Figure 3.130 and Figure 3.131 present the load-slip curves for tested specimens with T connectors. Three identical specimens were tested. Specimen CT.3 load-slip curve is not

presented because the deformation control of the tests was not well accomplished. The slip results of this specimen are not considered, but the load capacity values are, as they are independent of the testing procedure.

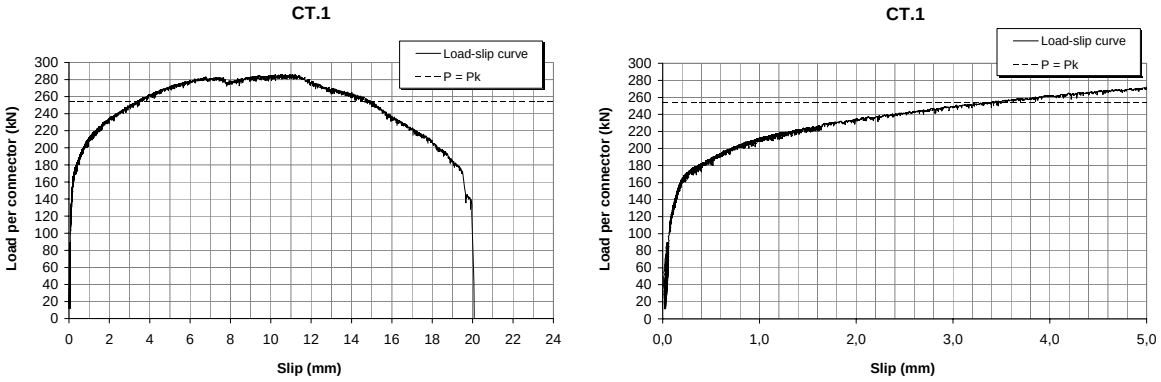

a) Complete load-slip curve b) Initial part of the load-slip curve

Figure 3.130 - Load-slip curves for T connector specimen CT.1 (POST test)

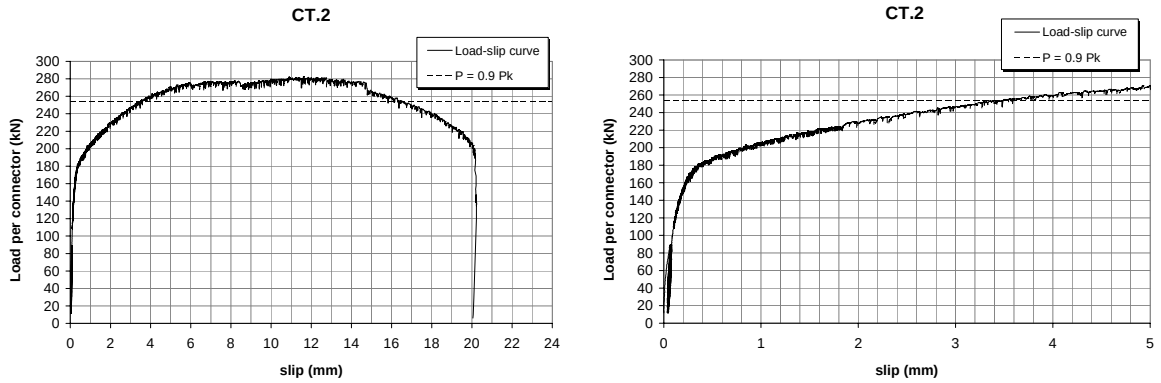

a) Complete load-slip curve b) Initial part of the load-slip curve

Figure 3.131 - Load-slip curves for T connector specimen CT.2 (POST test)

The two presented load-slip curves show very similar development. The values for the maximum load obtained in the three tested specimens are very similar. The obtained results correspond to a standard deviation of 3.3 kN and a variation coefficient of 1.2%. There is a good agreement between results.

The load-slip curves for T connector tests show an initial almost linear progression. For this part of the load-slip diagram, the cycles of loading and unloading of the specimens do not cause any change on the connection stiffness. Then, the curve develops a new branch with a softer slope, while the load is still increasing. The change between the first and second branch of the curves is particularly visible in Figure 3.130.b and Figure 3.131.b, for a load level that varies between 160 and 180 kN. This value corresponds to

56-63 % of the maximum average load measured in these tests. The second branch assumes a lower rate on the load increase, until a total slip of around 6 to 7 mm is reached.

After this value, a new branch can be identified, characterized by an almost constant load level and increasing deformation, until a total slip of around 11 to 13 mm is attained. Then the load slowly starts to decrease, at a similar rate to the increase correspondent to the second branch. Important slip values are measured in this last part of the load-slip curve, making this part of the curve important to the connection global behaviour.

When compared to the results obtained for headed studs, it is clear that this descending branch of the load slip-curve is only important for the T connector tests, as it has no expression in the stud tests.

As for the majority of headed stud specimens, this connection suffered shear failure. T connectors show high load and high deformation capacity (Table 3.26).

Table 3.26 – Experimental results for T connector

Specimen Reference	$f_{lcm,Slab1}$ (MPa)	$f_{lcm,Slab2}$ (MPa)	P_{max} (kN)	$s_{Pmax,i}$ (mm)	P_{medium} (kN)	P_k (kN)	$s_{elast,90\%}$ (mm)	$s_{plast,90\%}$ (mm)	$s_{total,90\%}$ (mm)	s_k (mm)
CT.1	62.57	64.19	285.8	11.06			3.40	11.53	14.94	
CT.2	65.79	64.14	282.7	11.61	285.9	254.4	3.49	12.99	16.49	10.38
CT.3	57.18	56.77	289.3	*			*	*	*	

* – deformation control on CT.3 was not properly accomplished; therefore, this result is not considered.

The values for the maximum load obtained in the three tested specimens are very similar. The results obtained present a standard deviation of 3.3 kN and a variation coefficient of 1.16%.

The steel used in the T connectors was not tested for tensile strength. For calculation purposes, it is considered that the steel ultimate strength, f_u, should be around 450 MPa. As the T connector suffers shear failure, it is thought that equation (3.6) may be applied to this type of connection as it was for headed studs. The results are presented in Table 3.27.

It is observed that using equation (3.6) gives similar results to the experimental ones obtained of maximum load. Equation (3.6) gives the characteristic value of the connection load capacity. As the characteristic load, P_k, is defined as $0.9 \times P_{max}$, (see Table 3.26), it is considered that equation (3.6) is also adequate for T connectors. Figure 3.132 puts in evidence this aspect.

If the concrete area positioned in front of the T connector is crushed, the value of P_{max} divided by the T connector area ($A_{connector}$) would be close to the value of f_{lcm}. In this case, this quotient is equal to 200.8 MPa, which is much higher than f_{lcm}. This means that concrete is probably crushed in an area that is larger than the cross section of the T

connector. This connector is capable of distributing the load on the concrete slab in a more effective way than the headed stud connector.

Table 3.27 – Calculation of the T connector load capacity with equation (3.6)

Specimen Reference	$f_{lcm,Slab1}$ (MPa)	$f_{lcm,Slab2}$ (MPa)	L (mm)	t_w (mm)	$A_{connector}$ (cm^2)	P_{max} (kN)	P_k Eq. (3.6) (kN)
CT.1	62.57	64.19	130	5.6	14.24	285.8	262.2
CT.2	65.79	64.14	130	5.6	14.24	282.7	262.2
CT.3	57.18	56.77	130	5.6	14.24	289.3	262.2

where,

L – connector length;

t_w – width of the T web;

$A_{connector}$ – area of the T cross section (half IPE 200).

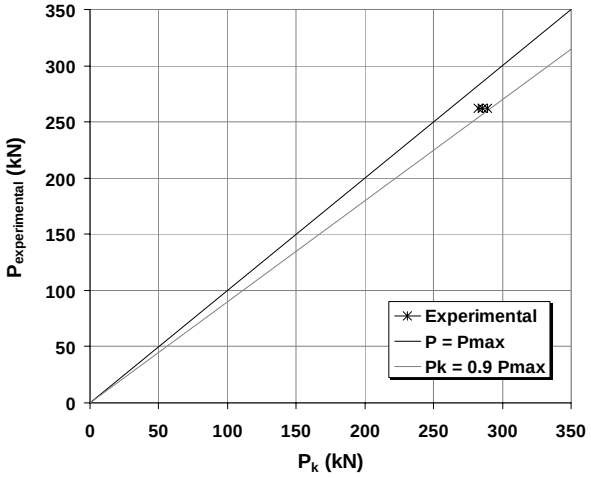

Figure 3.132 – Comparison between predicted and experimental values for maximum load

3.8.6 Stiffness measured for POST tests with T connectors

In order to evaluate the connection stiffness, *k*, for T connectors, the relation between load and slip deformation defined with equation (3.4) is also used.

The first observation to put in evidence is that there is almost a linear relation between the stiffness and the load values, which results from the form of the load-slip curve that has an approximately parabolic development, within the range in analysis.

The second aspect is that higher values of stiffness are attained for the load range in analysis (from 40 to 70% of the maximum load P_{max}), when compared to the values obtained in the tests with headed studs. However, the stiffness value, *k*, tends to have a steeper decrease for T connectors than it does for headed stud connectors. The service load level for a common structural element is usually between 40 to 60% of the ultimate

strength capacity. For 0.6 P_{max}, the T connection stiffness is around 3 to 3.5 times the headed stud connection stiffness.

If we consider that, in average, one T connector replaces around 2 headed studs with 19 mm diameter (both in LWC), it is concluded that the connection with the T connector is still stiffer and therefore a higher interaction between the concrete slab and the steel beam is guaranteed.

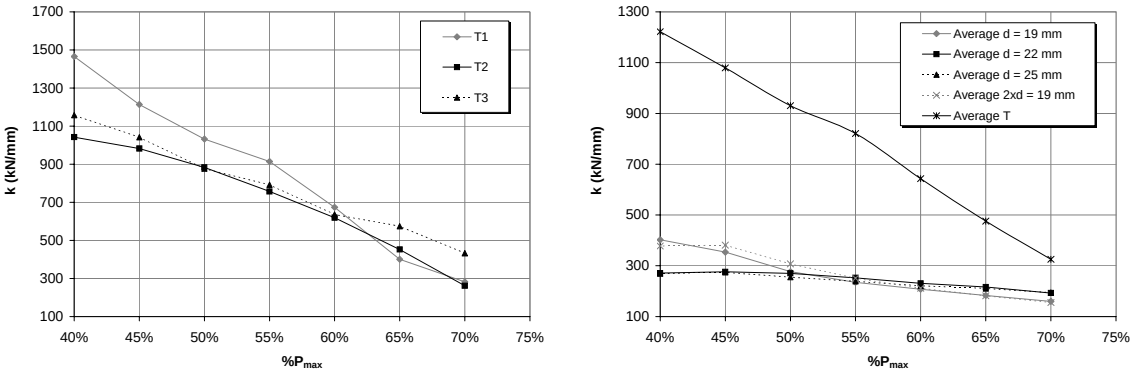

Figure 3.133 - Stiffness measured in T connectors specimens

3.8.7 Comparison of T connectors results with results from other authors

Table 3.26 shows a comparison between the results on HSLWC specimens determined within this work and the results obtained by Hegger et al (2000), in quite similar specimens with HSC slabs. The slabs crack pattern, the connector type of deformation and the overall failures are very similar in both works.

Table 3.28 – Comparison between experimental results for T connector and the results obtained by Hegger et al (2000)

Specimen Reference	$f_{lcm,Slab1}$ (MPa)	$f_{lcm,Slab2}$ (MPa)	P_{max} (kN)	$P_{average}$ (kN)	P_k (kN)	$s_{elast,90\%}$ (mm)	$s_{plast,90\%}$ (mm)	$s_{total,90\%}$ (mm)	s_k (mm)
CT.1	62.57	64.19	285.8			3.40	11.53	14.94	
CT.2	65.79	64.14	282.7	285.9	254.4	3.49	12.99	16.49	10.38
CT.3	57.18	56.77	289.3			(**)	(**)	(**)	
POST IPE 180-1 (*)	98.2	96.5	270.2			(***)	(***)	16.50	
POST IPE 180-2 (*)	98.2	96.5	252.7	262.2	227.4	(***)	(***)	18.68	14.85
POST IPE 180-3 (*)	98.2	96.5	263.6			(***)	(***)	27.28	
POST IPE 200EL-1 (*)	98.2	96.5	267.6			(***)	(***)	13.88	
POST IPE 200EL-2 (*)	98.2	96.5	302.7	282.7	240.8	(***)	(***)	13.86	12.29
POST IPE 200EL-3 (*)	98.2	96.5	277.9			(***)	(***)	13.65	

(*) – specimens tested by (Hegger et al 2001)

(**) – deformation control on CT.3 was not properly accomplished; therefore, this result is not considered.

(***) – data not available in the bibliography

In terms of maximum load, the results obtained are very close, which means that the substitution of HSC by HSLWC does not reduce the T connection load carrying capacity. The deformation capacity, defined by the slip measured at load P_k, is also very similar for all the specimens, although the initial phase of the load-slip curve is stiffer for HSC than for HSLWC.

3.8.8 Comparison of T connectors results with headed studs results

In terms of total applied load during the push-out test, the values attained for specimens with headed studs of 19 mm diameter (single disposition) and specimens with T connectors are very similar. In average, the maximum load measured in push-out tests with T connectors is equal to 1143.7 kN and the maximum load measured in push-out tests with headed studs of single 19 mm diameter is equal to 1122.0 kN.

As each of the used T connector has higher load capacity than the 19 mm diameter headed stud, fewer connectors are needed to reach the same total load value. This means that the load is transmitted to the slab in less points, but more concentrated, leading to higher stresses on the concrete slab. This observation is agreement with the observations made during the tests, as the number of visible concrete cracks on the slabs is much higher for specimens with T connectors.

If the level of cracking on the concrete slab is the term for comparison, then the specimens with headed studs of 25 mm diameter show a more similar crack pattern to the one observed for T connectors' specimens. In this case, the average total maximum load measured in the respective push-out tests is equal to 1537.6 kN, which corresponds to 1.34 times the average total maximum load measured in T connectors' specimens.

It is interesting to notice that the total load per connector attained is higher for T connectors than for headed studs with 25 mm diameter, but the result was a concrete failure on studs and connector failure on T. It seems that the T connector geometry enhances less stress concentration on the concrete slab and therefore failure is attained first on the connector. Because of this, it is observed that headed studs are less efficient than T connectors in transmitting the force between the steel section and the concrete slab.

There should be a limit to the size and length of the T connector in order to guarantee that failure happens in the T web. This was also observed for headed stud connectors, as the use of 25 mm diameter resulted in concrete failure, instead of connector failure, while the opposite happened for studs with smaller diameters. In the present case, the results obtained show that in order to enlarge the connector load capacity, a longer T connector could be used, to a point where the two types of failure would almost occur in simultaneous.

It is however, important to keep in mind that a longer T connector would difficult the disposition of transversal reinforcement, as the spacing between consecutive bars would be higher.

Figure 3.134 compares the load capacity of headed stud connectors and T connectors. The first observation is that the load capacity for each T connector is higher than the load capacity for each stud connector of the chosen diameters. As the 25 mm diameter is usually the highest dimension commonly used, the conclusion is that T connectors are capable of attaining higher loads than headed studs. For this type of concrete, it would not be possible to achieve such load values with studs, because it would be necessary to have studs with much larger diameters and therefore, failure would occur in concrete. This aspect became clear with the testing of headed studs of 25 mm diameter.

There is an almost linear relation between shear area and load capacity (Figure 3.134a). In this way, T connectors allow a better stress distribution on the concrete slab when compared to studs, avoiding concrete crushing for higher loads. A reason for this is probably the localization of the larger concrete compression area on the T flange. However, it is clear from Table 3.26 and Table 3.3 that higher slip needs to be developed to attain the connection maximum load capacity in specimens with T connectors than in specimens with headed studs.

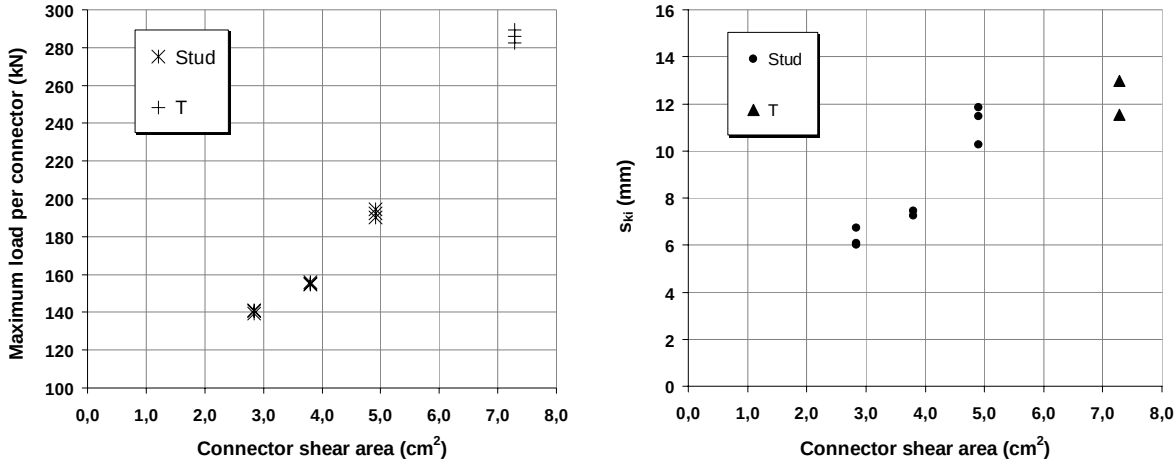

a) Maximum load

b) Characteristic slip

Figure 3.134 - Slip vs. connector shear area

As presented in Figure 3.134b, the values of plastic slip are a bit higher for T connector than for studs, which was expected. After the maximum load is reached, the load tends to decrease in a faster rate than it did while increasing but more slowly than it did for stud connectors, leading to a more ductile failure then the one observed for the tests with studs (with exception to the 25 mm diameter studs). It is interesting to notice that there is also an approximately linear relation between the plastic slip value for the two types of

connectors. This means that the differences between the behaviour of the two types of connectors depend more on the connectors shear area than on any other parameter.

In terms of shear stress, the values determined for T connectors and 25 mm diameter studs are similar and again the values obtained for 19 mm diameter studs are higher.

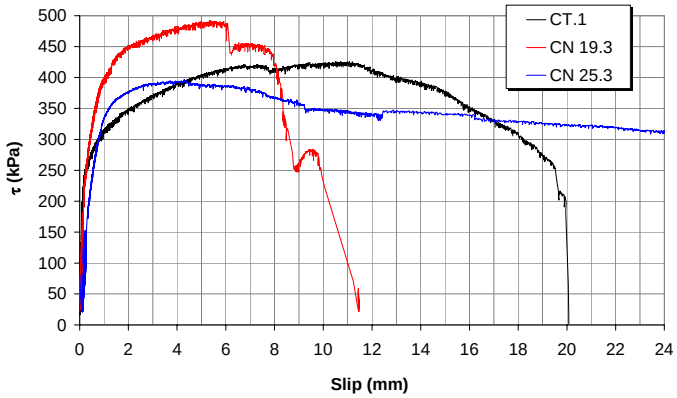

Figure 3.135 – Shear stress vs. connector shear area – comparison between stud connector and T connector

3.9 Comparison between the three types of shear connector tested

In order to establish a comparison, Table 3.29 resumes some of the results obtained for the three different types of tested shear connectors.

Table 3.29 – Comparison between the load capacity measured for the three types of shear connectors tested: headed studs, Perfobond and T

Specimen Reference	Connector weight	P_{max}	P_k	$s(P_{max})$	$s_{total,90\%}$	s_k
	(gr)	(kN)	(kN)	(mm)	(mm)	(mm)
CN19 *	269.5	140.2	125.4	6.30	7.79	5.42
CN22 *	358.9	155.2	139.1	5.75	8.65	6.53
CN25 *	466.3	192.2	171.0	5.18	11.79	9.23
CP1.2	3226	375.1	337.6	0.53	18.40	16.32
CP2.2	3226	416.8	375.1	0.61	23.93	21.26
CP4.2	3226	533.6	480.3	1.36	6.67	5.51
CT *	1454	285.9	254.4	11.34	14.94	10.38

* - Average between three identical specimens

It is interesting to observe that there is an approximately linear relation between the total quantity of steel used to fabricate one shear connector and maximum load attained in the connection. Although the Perfobond results can be fitted in this linear relation, it is observed that the quantity of transversal reinforcement disposed in the slab alter the connection load capacity independently of the Perfobond connector size. In general, this

comparison shows the cost of using any of the analysed connectors is similar, in terms of material costs. Other costs, like production and assembling costs should also be considered in evaluating which of the connectors tested is cheaper. One aspect is clear, for the same beam, more headed studs are needed on the steel to concrete interface than T or Perfobond connectors, and more Perfobond connectors are needed than T connectors, which can be an important factor for decision, because the welding task is an important part of the cost.

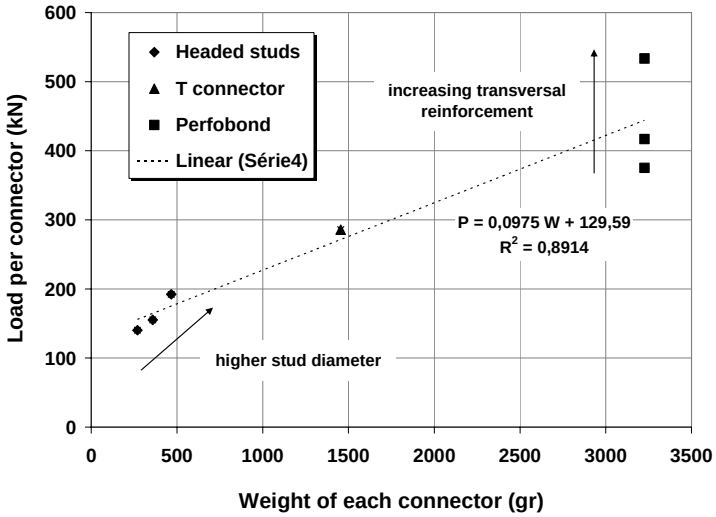

Figure 3.136 – Maximum load per connector vs. connector weight

In general, all the shear connector devices tested proved to have a ductile behaviour, which is important if the redistribution of stress along the shear connection is expected. This result shows that all the three types of shear connectors tested are adequate to be used in steel and lightweight concrete composite elements.

3.10 Conclusions

As observed and measured during the series of push-out tests performed, HSLWC is adequate to be used in composite structures. The results obtained show some loss of load capacity, compared to NWC specimens, but a good general behaviour is noticeable, with a tendency to a higher deformation capacity. The single push-out test performed at the Institute of Structural Concrete, in RWTH, Aachen, proved to be a good alternative to the standard push-out test when LWC is used, and the resulting differences matched the ones already observed for NWC.

In general, stud shear failure was identified, with exception to the 25 mm diameter studs in the POST tests. In this case, the type of failure observed shows that a HSLWC with a compressive strength that is at least higher than 55 MPa should be used in order to insure the stud shear failure. The headed studs showed a ductile behaviour, as the plastic slip exceeded the value of 6 mm demanded in EN 1994-1-1. The double stud association

resulted in a decrease on the connection load capacity, but allowed an increase on the slip deformation for the same shear load applied. This disposition guarantees a more ductile behaviour of the shear connection.

The push-out tests performed with the Perfobond connector, showed that the specimens' failure was always verified with large cracking and crushing in some zones of the concrete slab. The rib connector itself never suffered failure. This connector device presents very high load capacity associated with a ductile behaviour, as the connection load capacity is maintained after very high values of slip are attained. The connection components could be identified. The tests performed, showed that the maximum load attained depends on the area of transversal reinforcement disposed and on the concrete strength. The effects of using lightweight concrete were also analyzed. It was verified that the connection load capacity tends to diminish when NWC is substituted by LWC. It was also verified that the Perfobond connector presents a very stiff behaviour during the initial phase of loading, with small slip values developed for high shear loads. The stiffness measured for Perfobond connector is higher than the stiffness measured for headed studs. In a second phase, the load is kept more or less constant for values of slip that present a constant growth.

The push-out tests performed with T connector showed that this connector device also presents high load capacity associated with a ductile behaviour. The maximum loads attained are smaller than the ones verified for Perfobond connectors but higher than the ones verified for headed studs. The connector itself tends to behave similarly to a stud connector because it suffers shear failure at its basis, right above the welded fillet and its deformed shape shows that the deformation is concentrated on the T half web basis. The stiffness value measured for a T connector is smaller than the stiffness measured for Perfobond, but higher than the stiffness measured for headed studs.

Chapter 4

EXPERIMENTAL STUDY ON SHEAR CONNECTION BETWEEN STEEL AND HIGH STRENGTH LIGHTWEIGHT CONCRETE SUBJECTED TO CYCLIC LOADING

4.1 Introduction

Fatigue testing on shear studs have been evaluated through either push-out tests or beam tests. Some of these studies were conducted by Slutter and Fisher (1966), Mainstone and Menzies (1967), Oehlers and Foley (1985), Oehlers (1990), Oehlers (1995), Yen et al (1997), Bursi and Gramola (1999), Civjan and Singh (2003). The unidirectional fatigue conditions studied in the majority of these tests are specifically applicable to highway bridge loading. Such loading consists of a high number of cycles imposed on a bridge beam subjected to sagging bending moment. It was therefore of concern to determine the number of cycles to failure (fatigue life) for shear studs subjected to a percentage of their static capacity (generally in the range of 40 to 60%) or to determine the reserve monotonic capacity of the studs after a certain number of fatigue cycles has occurred. Load ranges varied from the peak load considered to a percentage of the peak load. (Hanswille et al. 2007) tested a total of 71 push-out specimens to determine the reduced static strength after high-cycle preloading and to examine the effects of the loading sequence on the fatigue life. The test results indicate an early crack initiation in approximately 10%–20% of the fatigue life which causes the reduction of the static strength. Constant amplitude tests have shown that the magnitude of the peak load P_{max} of the cyclic loading has a significant effect on the crack form occurring at the stud foot.

Reversal of load was rarely considered and full load reversal was considered in specimens tested by Oehlers (1995) and tests made by Erlicher et al. (2001). Values of load reversal were always well below the stud capacity. Fatigue life was generally in the thousands to millions of cycles and it was determined that shear studs subjected to fatigue loading can have significantly reduced load capacity. From these tests, fatigue-strength relationships were developed. Data was extrapolated into the low-cycle range, inferring that only a slight loss of strength would be expected for a low number of inelastic cycles.

Low-cycle fatigue generally concerns loading approaching or exceeding the yield capacity of a section, with failures occurring prior to 1000 load cycles. Unidirectional

testing of shear studs considering low-cycle fatigue was performed by Gattesco and Giuriani (1996) and Gattesco et al. (1997). Fatigue life was shown to be greatly reduced when large slip was present. Testing was performed using a direct shear test method to model low slab compressive stresses at the end of a typical beam section. These researchers as well as Taplin and Grundy (1997) noted the accumulation of slip and damage under reversed cyclic loading. Shake down (stabilization of residual deformations in a structure during a series of repeated loading beyond the elastic limit) did not occur, but instead incremental collapse (increasing residual deformations until failure) was verified. Gattesco and Giuriani (2001) proposed a new type of shear connection test to better analyze experimental fatigue.

4.2 Tests conducted to investigate the slip characteristics of stud shear connectors under repeated loading

Hallam (1976/1978) reported thirteen push-out tests conducted under constant amplitude unidirectional repeated loading. Although the tests were performed for the primary purpose of determining fatigue strengths, they are important because quantitative expressions for the slip growth per cycle, as a function of the load range, were developed. The push-out specimens had two 19 mm diameter studs in each slab, and the slabs were tied to prevent spreading at the base. The interface between the slab and the steel beam was oiled to reduce friction. This author found that under constant amplitude loading, the slip increased almost linearly with cycles. The maximum load varied from 21% to 43% of the static strength. The available data (ten tests) is summarized in Table 2.1. He calculated the static strength P_u from CP117 - Composite Construction in Structural Steel and Concrete (BSI 1967).

Table 4.1 - Load-slip data from Hallam (1976)

Test	f'_c	Static strength	Maximum load	Minimum load	Load range / static strength	Slip / cycle
	(MPa)	(kN)	(kN)	(kN)		(mm)
PS4	35.2	116	49.8	2.27	0.410	203×10^{-7}
PS5	35.2	116	49.8	2.27	0.410	191×10^{-7}
PS6	33.2	112	29.2	2.27	0.240	178×10^{-9}
PS7	33.2	112	29.2	2.27	0.240	117×10^{-9}
PS8	32.8	111	23.1	1.29	0.196	35.6×10^{-9}
PS9	32.8	111	23.1	1.29	0.196	48.3×10^{-9}
PS10	30.3	107	44.3	2.27	0.393	164×10^{-7}
PS11	30.3	107	44.3	2.27	0.393	51.8×10^{-7}
PS12	22.8	96	33.7	2.27	0.327	51.5×10^{-7}
PS13	22.8	96	33.7	2.27	0.327	70.0×10^{-7}

Hallam found that the slip per cycle could be related to the load range by equation (4.1), where, the slip value is expressed in millimetres. The correlation coefficient is equal to $r^2 = 0.94$.

$$\log(\text{slip}/\text{cycle}) = -10.00 + 12.99 \times \left(\frac{\text{load range}}{\text{static strength}} \right) \tag{4.1}$$

Lo (1978) conducted unidirectional fatigue tests on 16 mm diameter stud shear connectors using push-out specimens which comprised a 210 mm × 210 mm concrete block cast between a pair of 9.5 mm plates. Each plate had one stud welded centrally. Lo, like Hallam, found that the slip increased approximately linearly with cycles of loading. He did not develop a relationship between the rate of slip growth and the magnitude of the repeated load, but the necessary data was reported. From his data, a relationship similar in form to equation (4.1) can be obtained, corresponding to equation (4.2), where the correlation coefficient is equal to $r^2 = 0.86$. In Lo's tests the maximum load varied from 27% to 81% of the static strength.

$$\log(\text{slip}/\text{cycle}) = -8.36 + 5.28 \times \left(\frac{\text{load range}}{\text{static strength}} \right) \tag{4.2}$$

Oehlers and Foley (1985) conducted eleven push-out tests under unidirectional cyclic loading, and analyzed the data from 129 existing tests to review the methods for the estimation of the fatigue strength of stud shear connectors. Maximum loads in the eleven tests varied from 18% to 75% of the static strength. The authors found that slip increased with cyclic loading and that slip increased approximately linearly with the number of load cycles. By assuming that the stiffness reduction is attributable to the propagation of a fatigue crack, they proposed that the equation for the rate of slip growth as a function of the load range should be similar in form to Paris's equation, that is,

$$\left(\frac{\text{slip}/\text{cycle}}{\text{stud diameter}} \right) \alpha \left(\frac{\text{load range}}{\text{static strength}} \right)^{\text{m}} \tag{4.3}$$

By reviewing the data from Hallam and Lo, as well as their own eleven tests, the authors determined the values for the coefficient *m* as given in Table 4.2.

Table 4.2 - Coefficients in equation (4.3) for the rate of slip growth as determined by Oehlers and Foley (1985)

Data source	Value of coefficient *m* in equation (4.3)
(Hallam 1976)	6.7
(Lo 1978)	5.0
(Oehlers & Foley 1985)	4.0
All authors above	5.3

In the following, Oehlers and Coughlan (1986) tested eight push-out specimens with 13 and 19 mm studs under uni-directional and reversed cyclic loading. The maximum load ranged up to 80% of the static strength. Combining the results from Hallam (1976), Lo (1978) and Oehlers and Foley (1985), the authors proposed equation (4.4) for the rate of slip growth,

$$\left(\frac{\text{slip/cycle}}{\text{stud diameter}}\right) = 1.70 \times 10^{-5} \times \left(\frac{\text{load range}}{\text{static strength}}\right) \tag{4.4}$$

Later, Taplin (1999), conducted push-out tests with studs of 12.5 mm diameter in solid slabs of 500 mm wide, 450 mm long and 90 mm thick. Two rows of 12.5 mm studs with 50 mm height were used per flange, at a lateral spacing of 65 mm and a longitudinal spacing of 50 mm. The stud height to diameter ratio was equal to 4.0. Petroleum jelly was applied to the steel flange prior to casting the concrete and the slabs were cast horizontally, with the studs in the vertical position. Transverse reinforcement, comprising two layers of 8 mm diameter wires, with a yield strength of 450 MPa, was cast into the slab to prevent longitudinal shear failure.

A total of fifteen push-out tests were conducted, comprising four monotonic tests to determine the static strength of the stud shear connectors, seven tests with symmetric cyclic loading of the specimens, and four tests with unidirectional cyclic loading of the specimens. All the cyclic tests were performed with predefined load ranges. The load was applied for 30 cycles at each load range. The results for the rate of slip growth measured for all unidirectional cyclic tests is presented in Table 4.3.

Two of the four specimens monotonically loaded, were tested in tension and two were tested in compression. In every case, failure was attained by fracture of the stud, and not by cracking, splitting, or pull-out of the slab. The results obtained on ultimate load per stud were very similar. An average value of 49 kN was determined for the static failure load. Concrete compressive strength at the date of each push-out test, measured in 100 mm diameter and 200 mm high cylindrical specimens, varied between 39.7 MPa and 55.6 MPa.

Taplin (1999) proposed equation (4.5), that corresponds to the line of best fit on the data presented in Table 4.3. The value of slip per cycle is expressed in mm/cycle.

$$\text{slip/cycle} = 10^{\left(3.71\frac{P_{\max}}{P_u} - 4.91\right)} \tag{4.5}$$

Table 4.3 – Rate of slip growth for unidirectional cyclic tests, (Taplin 1999)

Test	P_{max} (per load range) (kN)	$\Delta P/P_u$	rate of slip growth (mm/cycle)		Test	P_{max} (per load range) (kN)	$\Delta P/P_u$	rate of slip growth (mm/cycle)	
			Lvdt 1	Lvdt 2				Lvdt 1	Lvdt 2
9	110	0.250	0.000372	0.000557	14	110	0.250	0.000410	0.000741
	160	0.375	0.000931	0.00105		160	0.375	0.00130	0.00155
	190	0.450	0.00133	0.00160		190	0.450	0.00160	0.00202
	210	0.500	0.00237	0.00252		210	0.500	0.00211	0.00254
	230	0.550	0.00349	0.00355		230	0.550	0.00312	0.00444
	260	0.625	0.00884	0.00752		260	0.625	0.00981	0.0206
	280	0.675	0.0234	0.0145		280	0.675	0.0234	0.0527
	310	0.750	0.211	0.184		310	0.750	0.145	0.333
13	110	0.250	0.000095		17	110	0.250	0.000056	0.000030
	160	0.375	0.000776			160	0.375	0.000497	0.000079
	190	0.450	0.00142			190	0.450	0.00124	0.000559
	210	0.500	0.00172			210	0.500	0.00141	0.000236
	230	0.550	0.00229	0.00253		230	0.550	0.00291	0.000431
	260	0.625	0.00917	0.00803		260	0.625	0.00320	0.000918
	280	0.675	0.0141	0.0186		280	0.675	0.00282	0.00112
	310	0.750	0.0483	0.0540		310	0.750	0.00395	0.00150
	330	0.800	0.0599	0.0560		330	0.800	0.00524	0.00200
	360	0.875	0.233	0.300		360	0.875	0.0114	0.00423
						380	0.925	0.0176	0.00576

4.3 Objectives

Standard push-out tests under cyclic loadings have already been performed with normal weight concrete and stud connectors. The experimental campaign here presented is the result of performing push-out tests with headed studs in high strength lightweight concrete solid slabs, following the description and procedure presented in Chapter 3. In order to establish a proper comparison, both monotonic and cyclic tests are defined. The objectives of this research are:

- to analyse the adequacy of using lightweight concrete in composite elements or structures that will be subjected to cyclic loadings, focusing on the shear connection behaviour with headed stud connectors;
- to determine the stud connector load capacity after a large number of cycles has been imposed to the test specimen and compare it with the stud connector load capacity under monotonic loading;
- to evaluate the evolution of slip during the load cycles;

- to establish a relation between the slip evolution and the number of load cycles for a specific load range;
- to establish a relation between the slip evolution and the cycle load range;
- to evaluate the connection deformation capacity after the load cycles;
- to evaluate the evolution of slip after the load cycles process, until failure;
- to analyse the connection stiffness for service loads;
- to compare all the mentioned parameters with the ones obtained for normal weight concrete in experimental tests performed by other authors.

The tests here presented were done to study two main parameters: the rate of slip growth during the load cycles, and the connection load capacity after a given number of load cycles has been imposed to the specimens. The evaluation on the connection fatigue strength, done for some specimens, is not a main issue.

4.4 The push-out test for static and cyclic loadings

The experimental study of the steel to concrete shear connection cyclic behaviour is done with the push-out test. This test allows for a rigorous analysis on the shear connection behaviour, by assessing the load-slip relation until failure and the failure mechanisms. As explained in Chapter 3, this test can adequately simulate the forces flow through the concrete slab of a composite beam and is specially adequate to analyse the shear connectors load capacity.

The test set up follows the EN 1994-1-1 dispositions for the study of shear connection between steel and concrete, (CEN 2004b), with some adjustments on the solid slabs dimensions that will be explained. EN 1994-1-1 states that the push-out specimen is also adequate for fatigue tests on shear connectors. In this case, the push-out test is associated with cyclic loadings in order to study fatigue effects on shear studs.

4.4.1 Test program and procedures

This work aims to characterize the connection between steel and lightweight concrete subjected to cyclic loadings and for that, the experimental approach is chosen.

Six push-out specimens are prepared. Of these six specimens, two are intended for monotonic loading, in order to evaluate the connection load-bearing capacity and the load-slip curve, and four specimens are used for cyclic loading, with the characteristics presented in Table 4.4. In general, all the tests are conducted in the following steps:

1. The system applies *N* cycles of load/unload between the extreme values of the load range.
2. Following the load cycles, the system applies a monotonic loading controlled by a slip rate of 0.002 mm/s until a total slip of 6 mm is completed (the control is done with one of the transducers used for measuring slip); this step is only completed for specimens CN13.3 and CN13.4.
3. The system applies a monotonic loading controlled by the displacement of the actuator, with a rate of 0.01 mm/s, until failure of the specimen is attained.

Table 4.4 – Experimental program for cyclic push-out tests

Test specimen	Test type	Load range	Nominal load range	Number of cycles (*N*)	Load/unload speed	Monotonic loading until failure, after the load cycles
CN13.1	monotonic	5-40% $P_{expected}$	1.5 – 26.25	25	Loading = 5 kN/s Unloading = 5 kN/s	Yes
CN13.2	monotonic	5-40% $P_{expected}$	1.5 – 26.25	25	Loading = 5 kN/s Unloading = 5 kN/s	Yes
CN13.3	cyclic	10-50% P_{min}	5.0 – 25.0	10000	Sinusoidal: f=0.125 Hz	Yes
CN13.4	cyclic	10-60% P_{min}	5.0 – 30.0	16000	Sinusoidal: f=0.125 Hz	Yes
CN13.5	cyclic	8-24% P_{min}	4.0 – 12.0	1000	Sinusoidal: f=0.25 Hz	Yes
		8-48% P_{min}	4.0 – 24.0	1000	Sinusoidal: f=0.20 Hz	
		8-60% P_{min}	4.0 – 30.0	1000	Sinusoidal: f=0.125 Hz	
		8-72% P_{min}	4.0 – 36.0	1000	Sinusoidal: f=0.125 Hz	
		8-80% P_{min}	4.0 – 40.0	1000	Sinusoidal: f=0.10 Hz	
CN13.6	cyclic	10-31.2% P_{min}	5.0 – 15.625	1000	Sinusoidal: f=0.25 Hz	No
		10-62.5% P_{min}	5.0 – 31.25	1000	Sinusoidal: f=0.20 Hz	
		10-78.8% P_{min}	5.0 – 39.375	1000	Sinusoidal: f=0.125 Hz	
		10-95% P_{min}	5.0 – 47.5	1000	Sinusoidal: f=0.10 Hz	

In Table 4.4, P_{expected} refers to the value predicted for the connection load-bearing capacity, before any test is performed. This value is needed to establish the 25 cycles procedure, which is defined between 5 and 40% of P_{expected}. In the same table, P_{min} is the minimum value of the two maximum load values determined in CN13.1 and CN13.2 tests, respectively. This value is considered equal to 50.0 kN, although a slightly higher value was determined in CN13.1 and CN13.2 push-out tests.

The values for frequency defined for the sinusoidal load law, are small and vary with the load range. These values are a result of the machine limitations on performing the load cycles with higher frequency. If this was possible, a larger number of cycles could have been imposed within a smaller period of time.

For CN13.3 and CN13.4 tests, a constant load range is applied through all the cycles, while for CN13.5 and CN13.6, the load cycles range is increased each 1000 cycles (see Figure 4.1).

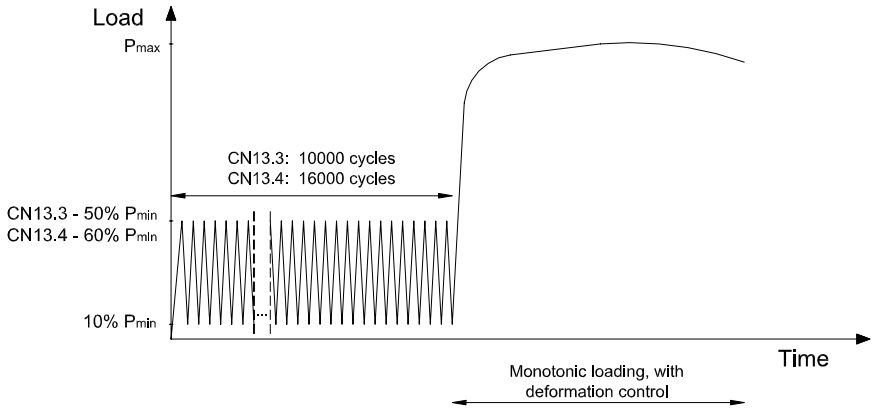

a) Constant load range

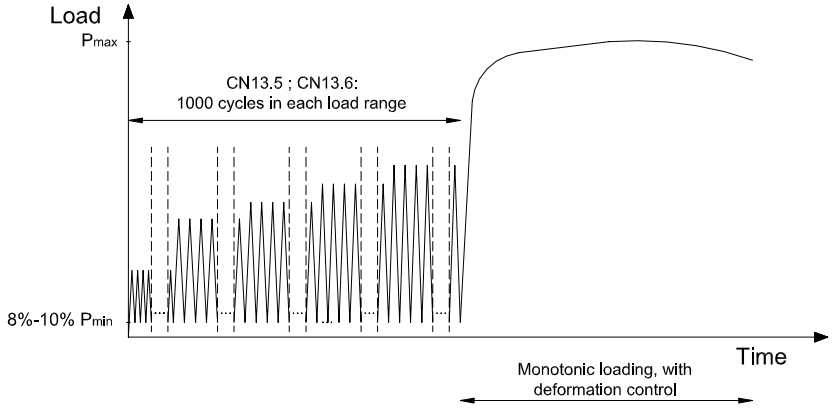

b) Variable load range

Figure 4.1 – Loading procedure for cyclic push-out tests

Table 4.5 shows the effective load values applied during the push-out cyclic tests.

Table 4.5 – Push-out cyclic tests: shear load range and shear stress range

Test specimen	Test type	Effective load range	ΔP (per connector)	$\Delta\tau$ (per connector)	$\Delta P/P_u$ (%)	Monotonic loading until failure, after the load cycles
CN13.1	Static	1.635 – 26.200	24.57	185.07	45.5	Yes
CN13.2	Static	1.710 – 26.300	24.59	185.26	45.5	Yes
CN13.3	Cyclic	5.138 – 26.691	21.55	162.38	37.8	Yes
CN13.4	Cyclic	4.885 – 31.931	27.05	203.76	47.4	Yes
CN13.5	Cyclic	3.748 – 12.354	8.61	64.83	15.1	Yes
		3.357 – 24.639	21.28	160.34	37.3	
		3.549 – 30.603	27.05	203.82	47.5	
		3.232 – 36.466	33.23	250.38	58.3	
		3.160 – 40.311	37.15	279.90	65.2	
CN13.6	Cyclic	4.786 – 16.057	11.27	84.92	20.9	No
		4.533 – 31.872	27.34	205.97	50.6	
		4.571 – 39.889	35.32	266.08	65.4	
		4.477 – 48.158	43.68	329.10	80.9	

The effective load range applied by testing machine the differs from the nominal values presented in Table 4.4, because there were some difficulties in assuring the predefined load ranges. This happened, although the values of load and load rate were defined in order to minimize the discrepancies.

4.4.2 Fabrication of the push-out test specimens

EN 1994-1-1, (CEN 2004b), presents some considerations on the fabrication of push-out test specimens, already referred in Chapter 3. This time, in order to concrete the slabs in the horizontal position, the first slab was concreted and after three days, the specimen was turned up and the second slab was cast (see Figure 4.2). The decision on doing each slab concreting in different days was based on the analysis of the evolution of compressive strength and modulus of elasticity done in Chapter 2 and on the analysis of the values of these concrete properties, done for the series of push-out tests presented in Chapter 3. It was verified that concrete compressive strength values are very high at early ages and then tend to stabilize in time after 7 days, with a very slow increase from this moment on. Therefore, a difference of three days in the concrete age after a period of 30 days was considered irrelevant.

a) First slab

b) Second slab, after turning over

Figure 4.2 – Casting conditions for cyclic POST specimens

During preparation for the specimens concreting, it was necessary to define the formwork geometry and assembly. It was important that the formwork could be reutilised, guarantying the identical shape for both specimens' slabs and an easy way of preparing the work (see Figure 4.3). To avoid water absorption, the entire formwork surface in contact with concrete was protected with isolating strips. A mould release agent was spread over the isolating strips to facilitate the separation between the formwork and the concrete slab (see Figure 4.4).

Figure 4.3 – Formwork

Figure 4.4 – Isolating the mould

Again, the discontinuity between the steel profile flange and the concrete slab was assured by greasing the steel flange before concreting with a mould release agent. After concreting, all the specimens were cured in the laboratory environmental conditions. Some concrete amount was reserved for cylindrical specimens, in order to test the concrete for compressive strength and modulus of elasticity.

Longitudinal and transversal reinforcement was disposed for the slab (see Figure 4.4). The reinforcement consists on a welded wire mesh.

All the considerations regarding the testing frame, the load actuator, the Diwidag® bars that restraint the concrete slabs lateral displacement, the plates and sheeting under the slabs and the spherical seat remain as were described in Chapter 3.

4.4.3 Measuring devices

The measuring devices used during the static tests are exactly the same as were defined in Chapter 3. Regarding the cyclic tests, the only difference is that four displacement transducers are positioned to measure slip between the steel profile and the concrete slabs instead of the two used in the previous tests. The disposition for these transducers is the same as described for the monotonic tests, but this time they are positioned in each of the slabs' corner (see Figure 4.5). These four LVDT's have short stroke (5 mm) and high precision, in order to measure small deformation values as the ones expected during the load cycles. No strains gauges are used in this test series.

In the following, all the results of slip presented correspond to an average value, calculated from the measurements performed by these four transducers.

One LVDT was also positioned horizontally, to measure the lateral displacement between the two concrete slabs.

a) Side 1-2 b) Side 3-4 Horizontal LVDT

Figure 4.5 – Displacement transducers in each corner of the cyclic push-out specimen

4.4.4 Materials properties

The HSLWC mixture was defined with the available materials. The tests used a lightweight concrete studied and presented in Chapter 2. Concrete properties are not exactly the same for all castings, although the same mixture was always used. The variations found are not considered relevant.

The values for compressive strength and modulus of elasticity presented in Table 4.6 are determined for all castings at the same day of the respective test. Concrete specimens were concreted simultaneously with the push-out specimens. Cylinders of 150mm diameter and 300mm high are always used.

Table 4.6 – Concrete properties for cyclic push-out specimens with headed stud connectors

Concrete Ref.	Specimens	Test	Connectors disposition	Concrete density (kg/m^3)	f_{lcm} (MPa)	E_{lcm} (MPa)
BL44	CN13.1 (Slab1) CN13.2 (Slab1) CN13.6 (Slab1)	POST	Single	1937	56.65	23.73
BL45	CN13.1 (Slab2) CN13.2 (Slab2) CN13.6 (Slab2)	POST	Single	1860	54.04	22.38
BL46	CN13.3 (Slab1) CN13.4 (Slab1) CN13.5 (Slab1)	POST	Single	1920	63.79	25.78
BL47	CN13.3 (Slab2) CN13.4 (Slab2) CN13.5 (Slab2)	POST	Single	1912	63.34	25.33

4.4.5 Test specimens

The specimens prepared for the standard push-out test were produced according to Figure 4.7. The geometry of the test specimens is always the same, with no variation on the stud diameter and disposition. The 13 mm stud diameter is chosen to match the headed studs used in the beams' monotonic and cyclic loadings (see Figure 4.6).

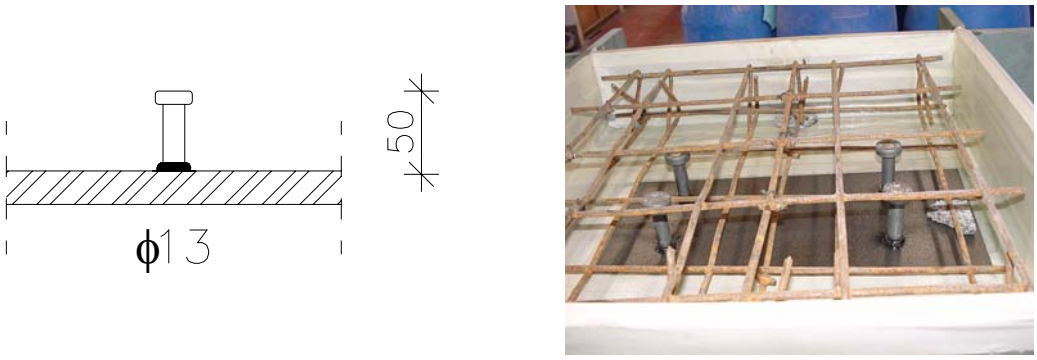

Figure 4.6 – Headed studs: configuration and dimensions

The specimens consist of two lightweight concrete slabs held in the vertical position, and a steel HEB200 profile positioned between them, with automatically welded studs cast inside the slabs. The slab dimensions are 450 mm × 450 mm × 100 mm. All the slab reinforcement, represented in Figure 4.7, corresponds to two layers of 5 mm diameter bars, with spacing as represented.

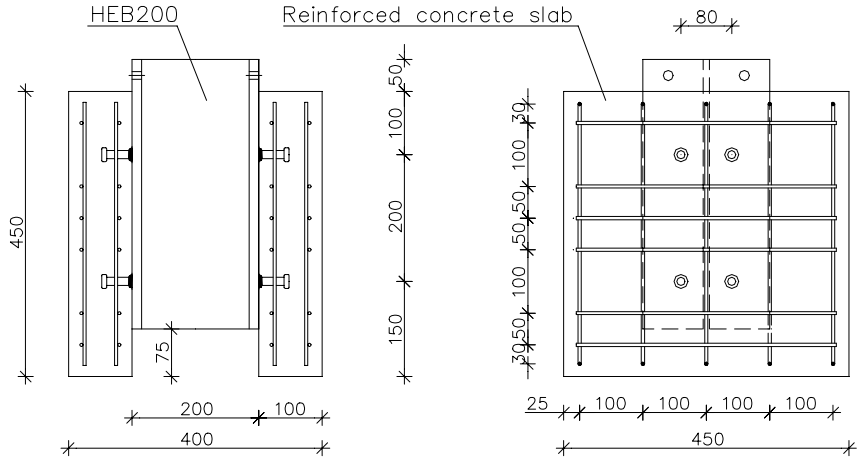

Figure 4.7 – Specimens geometry for cyclic POST tests

The decision of not using the EN 1994-1-1 standard dimensions is justified by the small dimensions of the headed stud. As presented in Chapter 3, the slabs that used 19 mm diameter studs only suffered small cracking, and therefore it was thought that a smaller slab would be appropriate for a smaller stud. The advantages of using smaller slabs have to do with the smaller quantity of concrete to be used, in this case allowing for the

simultaneous concreting of three slabs and the easier transportation of the specimens, because they are lighter.

Some checks were done in order to insure that the chosen geometry is appropriate. Considering the headed studs shear failure, equation (3.6) from Chapter 3 was used to predict the maximum load applied during the tests.

$$P = \left(0.8 \times \frac{\pi \times 0.013^2}{4} \times 500 \times 10^3 \right) \times 8 = 424.7 \text{ kN}$$

The total shear force in each slab is

$$F_s = \frac{424.7}{2} = 212.4 \text{ kN}$$

(Johnson 1970) defined Equation (4.6) to evaluate the transverse reinforcement that is necessary to prevent longitudinal shear failure. The failure can either occur through failure plane 1 or failure plane 2 as represented in Figure 4.8,

$$p\, f_y = 1.26\, v_u - 0.28\, (f_c)^{0.5} \geq 0.552 \qquad (4.6)$$

where f_y is the yield strength of the transverse reinforcement (MPa), p is the transverse reinforcement in relation to the concrete shear area, f_c is the concrete compressive strength determined in cubes (MPa) and v_u is the shear stress in any proposed failure plane (MPa).

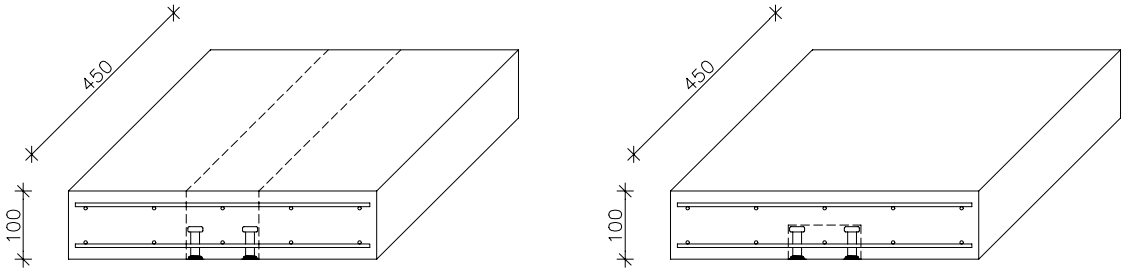

Figure 4.8 – Longitudinal shear failure plane 1 (left) and longitudinal shear failure plane 2 (right)

For the following analysis, the minimum compressive strength measured (see Table 4.6) is considered: f_c = 54 MPa.

Longitudinal failure through plane 1:

$$\text{Shear force} = \frac{212.4}{2} = 106.2 \text{ kN}$$

$$\text{Shear area} = 0.10 \times 0.45 = 0.045 \text{ m}^2$$

$$\text{Shear stress} = v_u = \frac{106.2}{0.045} = 2.36 \text{ MPa}$$

$$p = 0.00183 \quad \Rightarrow \quad A_{st} = 0.00183 \times 0.10 \times 0.45 = 0.82 \text{ cm}^2$$

In this plane, the total reinforcement is 2 layers of six bars with 5 mm diameter, which gives a total of 2.36 cm^2.

Longitudinal failure through plane 2:

Shear force = 212.4 kN

Shear area = $(0.102 + 0.05 \times 2) \times 0.45 = 0.0909$ m^2

Shear stress = $v_u = \dfrac{212.4}{0.0909} = 2.34$ MPa

$p = 0.00178 \quad \Rightarrow \quad A_{st} = 0.00178 \times (0.102 + 0.05 \times 2) \times 0.45 = 1.62$ cm^2

In this plane, the total reinforcement is one layer of six bars with 5 mm diameter but the shear plane crosses this layer twice, which gives a total of 2.36 cm^2.

The previous calculations show that the total amount of reinforcement is sufficient for each failure case considered.

4.5 Push-out test under static loading

4.5.1 Static push-out test results

Shear failure is identified on studs for the two specimens with 13 mm diameter studs that are static loaded: CN13.1 and CN13.2. Figure 4.9 and Figure 4.10 present the load-slip curves for these specimens. The two specimens are identical and the correspondent load-slip curves show very similar evolution.

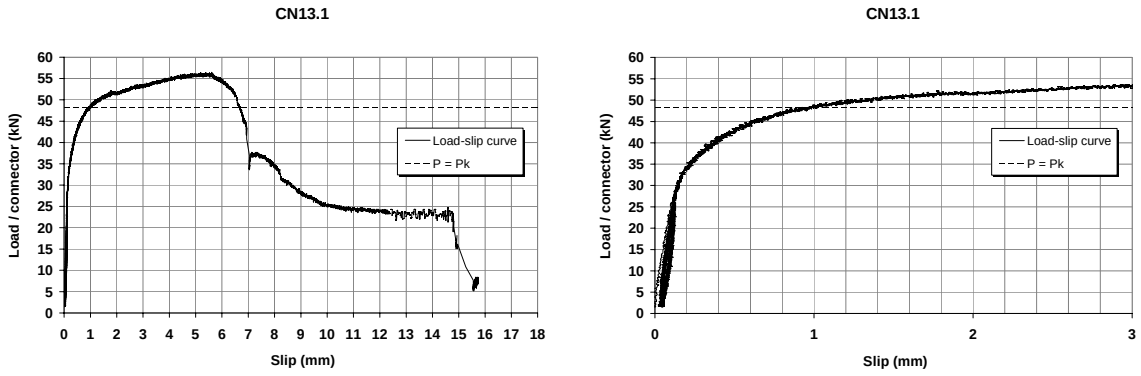

a) Complete load-slip curve b) Initial part of the load-slip curve

Figure 4.9 – Load-slip curves for specimen CN13.1

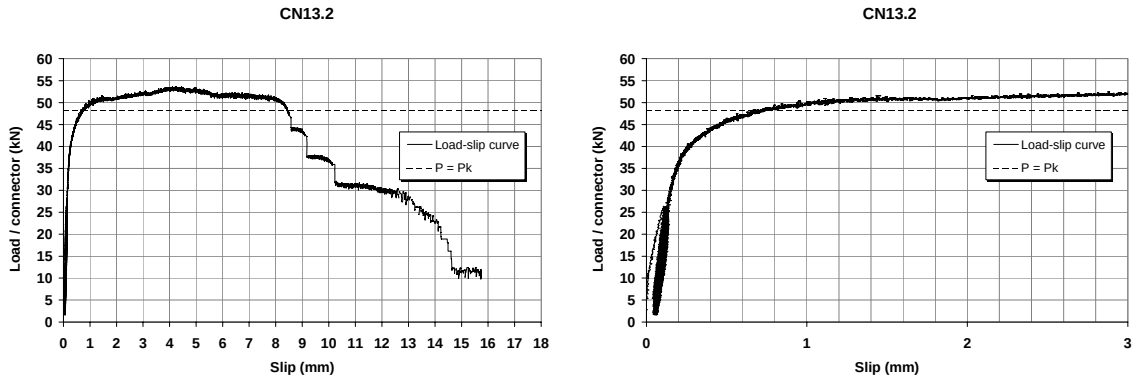

a) Complete load-slip curve b) Initial part of the load-slip curve

Figure 4.10 – Load-slip curves for specimen CN13.2

The load-slip curves for 13 mm diameter studs show an initial almost linear progression, until about 60 to 65% of the maximum load value is attained. The initial phase of loading is very similar for both specimens. Then, both curve develop a new branch with a softer slope, while the load is still increasing.

For specimen CN13.1, the second branch slope is higher than for specimen CN13.2, and therefore the specimen attains higher load capacity. However, the total slip before load capacity loss is higher for CN13.2 (see Figure 4.11).

The values for the maximum load obtained in the two tested specimens are very similar. A standard deviation of 2.0 kN and a variation coefficient of 3.7% are verified.

As visible in the load-slip curves presented, headed studs are characterized by an initially stiffer behaviour that is followed by a plastic behaviour, with a constant or slow increasing load capacity in the plastic range. After the maximum load is attained, the specimen still holds important load capacity, that decreases slowly. This observation corroborates the behaviour already observed for larger stud diameters.

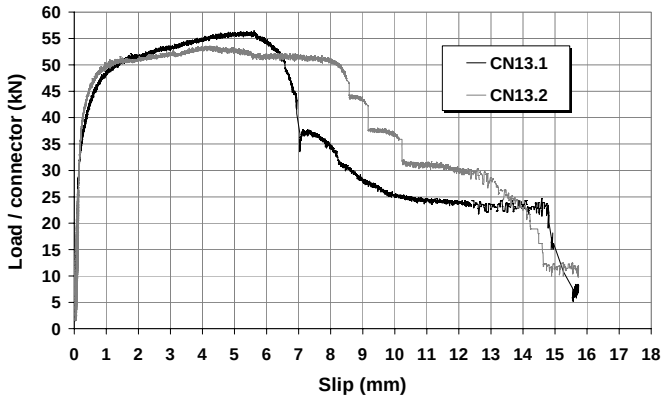

Figure 4.11 – Load-slip curves for static tests on 13 mm diameter studs

The stud failure usually happens right above the welded collar. In some of the tested specimens, part of the stud failure is within the welded collar zone, (Figure 4.12.a). There

is always some crushed concrete under the stud welded collar (Figure 4.12.b). This zone is very localized (Figure 4.12.c).

a) b) c)

Figure 4.12 – Monotonic loading: failure pattern on the stud shank (CN 13.1)

The lightweight concrete slabs are observed for identification of the crack pattern. There is some spread cracking around the stud position towards every direction of the slab (Figure 4.13.a). There is also some horizontal cracking between the two studs positioned at the same horizontal level (Figure 4.13.b). The studs achieve important deformation before failure, as can be observed in Figure 4.13.c. No cracking is observed on the exterior face of the concrete slabs.

The slab dimensions chosen for these tests are considered appropriate, as the cracking observed in both specimens, CN13.1 and CN13.2, is mostly localized in the proximity of the studs positions and never gets to the exterior face of the concrete slab.

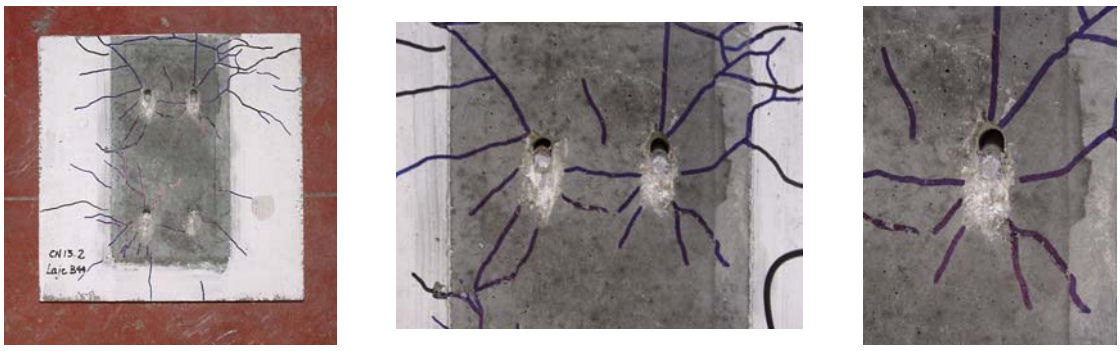

a) b) c)

Figure 4.13 – Monotonic loading: failure pattern on the concrete slabs (CN 13.2)

After the tests were performed, some slabs were destructed in order to observe the deformed connectors. An exemplar of these is shown in Figure 4.14. The stud deformation, that is directly related to the connection load-slip relation, is particularly localized on the stud basis. This is a common failure mode for studs in high strength concrete. In this perspective, the use of high strength lightweight concrete introduces no changes on the connection behaviour when compared to high strength normal weight concrete. When comparing the stud deformed shape with the generalized failure types presented in Figure 3.6 from Chapter 3, a combination of failure types a) and b) is identified, with a

predominance of type a) failure. A more deformed stud should be expected if normal strength lightweight concrete is used. redraw

Figure 4.14 – Stud redrawn from the lightweight concrete slabs of cyclic push-out test specimens

The maximum load applied in the push-out test, divided by the number of similar connectors, corresponds to the connection maximum load capacity. The maximum load value is measured for each specimen and the connection characteristic load capacity value, P_k, is calculated considering 90% of the minimum value taken from the two specimens results.

Table 4.7 presents the maximum load value determined for each tested specimen, $P_{u,i}$, and the corresponding characteristic load value determined for the two identical specimens.

In each of the diagrams presented (Figure 4.9 and Figure 4.10), the characteristic load value is also defined with the curve $P = P_k$. This load limit is used to define the elastic slip value and the plastic slip value. The elastic slip corresponds to the parcel of slip when $P < P_k$. and the plastic slip corresponds to the parcel of slip when $P > P_k$. The characteristic value of slip corresponds to the plastic slip value. Graphically, it can be defined as the slip portion measured between the two intersections of the curve $P = P_k$ with the load-slip curve.

Table 4.7 - Experimental results for push-out tests with 13 mm diameter

Specimen Ref[a]	$P_{u,i}$ (kN)	$s_{Pu,i}$ (mm)	$P_{average}$ (kN)	P_k (kN)	$s_{elast,i}$ (mm)	s_{ki} (mm)	s_k (mm)	$s_{max,i}$ (mm)
CN 13.1	56.4	5.62	55.0	48.19	0.93	5.76	5.18	6.94
CN 13.2	53.5	4.46			0.67	7.78		8.51

$P_{u,i}$ maximum load, for each specimen

$P_k = 0.9\ P_u$ (where P_u is the minimum value for a group of identical specimens)

$s_{elast,i}$ elastic slip for load P_k

s_{ki} plastic slip for load P_k

s_k 0.9 * minimum plastic slip for a group of three similar specimens

s_{max} maximum slip measured right before failure of the first stud

Figure 4.15 presents the relation between characteristic slip and ultimate load, measured in all static push-out tests.

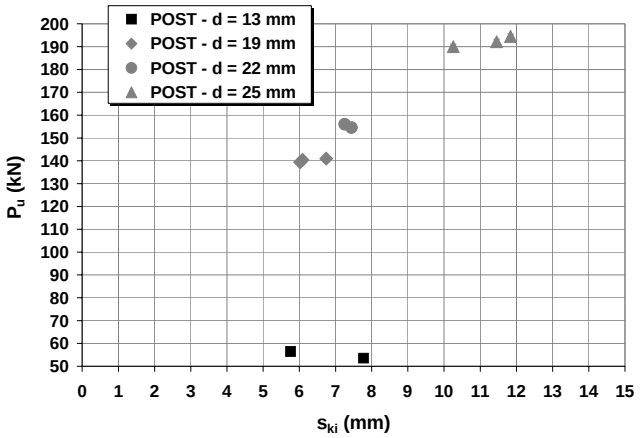

Figure 4.15 - Maximum load and corresponding characteristic slip (static tests)

There is a close relation between maximum load value and corresponding characteristic slip value for larger stud diameters. For studs with 13 mm diameter, the decrease in characteristic slip is very small, attaining more or less the same slip value as was verified for 19 mm diameter studs.

Figure 4.16 plots the relation between the stud shank area and the ultimate load attained in each push-out test. The results show that there is a strong linear relation between these two parameters, which means that the equation to predict the connection ultimate load capacity should depend on the stud shear area. In the present case, considering the values of the steel ultimate tensile strength presented in Table 3.2 (see Chapter 3), the relation proposed in Figure 4.16 takes the form of equation (4.7).

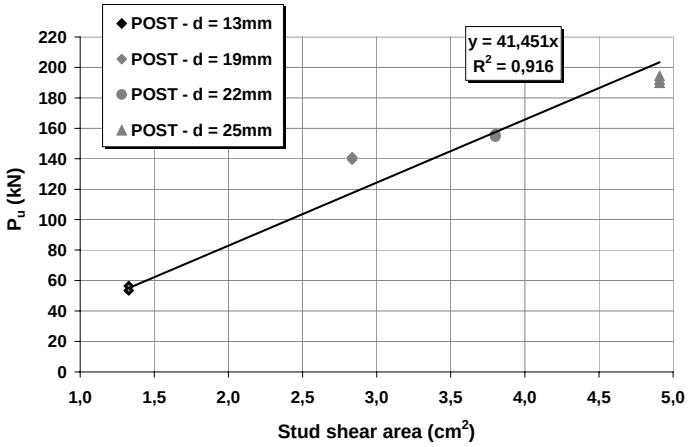

Figure 4.16 - Maximum load value and corresponding connector shear area

Due to the small size of the 13 mm diameter studs, no experimental testing was done on these connectors' steel properties. The smallest value of tensile strength, equal to 557 MPa, was found for the 25 mm diameter studs. As a result, equation proposed in Figure 4.16 takes the form of equation (4.7).

$$P_u = 0.744 \cdot f_u \cdot A_{shank} \tag{4.7}$$

If we now consider the characteristic load value, determined for each stud diameter, a new relation is obtained, as presented in Figure 4.17.

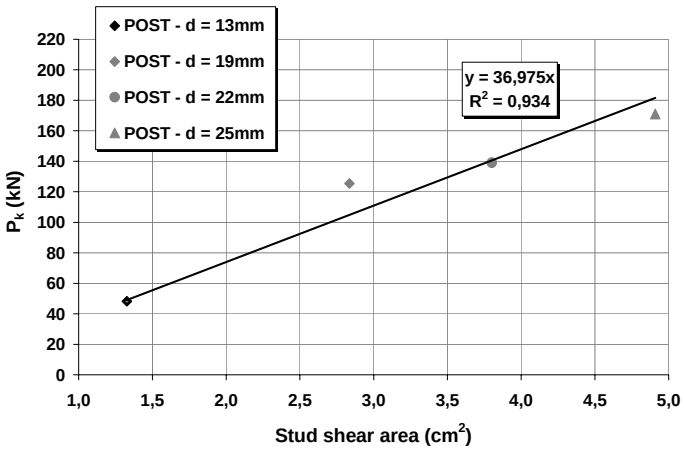

Figure 4.17 - Characteristic load value and corresponding connector shear area

Considering equation (4.7) form, a new equation can be derived, corresponding to equation (4.8). Comparing this equation with equation (3.6) proposed by EN 1994-1-1 to calculate the characteristic load value, and considering the limitation of $f_u \leq 500$ MPa imposed by this code, it is verified that the use of lightweight concrete results in a diminution on the connection load capacity.

$$P_k = 0.74 \cdot f_u \cdot A_{shank} \tag{4.8}$$

Considering this, the important conclusion obtained from equation (4.8) is that the equation defined in EN 1994-1-1 to calculate the characteristic shear strength of a headed stud automatically welded should be revised, if lightweight concrete is considered.

4.5.2 Stiffness measured for static push-out tests with headed stud connectors

As defined in Chapter 3, the connection stiffness, k, is defined as the ratio between a given percentage of the maximum applied load and the correspondent value of slip.

The interest of the ratio k-%P_u concerns the evaluation of k values for service loadings. The idea is to define a region of the load-slip curve where the slip deformation is mainly elastic and recoverable after unloading. This information is valuable to the analysis of beams behaviour, because the connection flexibility will enhance slip between steel and concrete sections. Table 4.8 establishes a direct relation between applied load (per connector) and corresponding slip value, for both specimens, CN13.1 and CN13.2.

Table 4.8 - Connection stiffness values (for 40%, 45%, 50%, 55%, 60% and 65% of P_u)

		CN13.1	CN13.2
P_u (per connector)	(kN)	56.41	53.54
0.40 *P*	(kN)	22.55	21.40
s (0.40*P*)	(mm)	0.110	0.115
k	(kN/mm)	205.00	186.90
0.45 *P*	(kN)	25.37	24.08
s (0.45*P*)	(mm)	0.110	0.135
k	(kN/mm)	230.83	178.33
0.50 *P*	(kN)	28.19	26.75
s (0.50*P*)	(mm)	0.125	0.130
k	(kN/mm)	225.50	205.77
0.55 *P*	(kN)	31.01	29.43
s (0.55*P*)	(mm)	0.140	0.150
k	(kN/mm)	221.47	196.17
0.60 *P*	(kN)	33.83	32.10
s (0.60*P*)	(mm)	0.190	0.165
k	(kN/mm)	178.03	194.55
0.65 *P*	(kN)	36.64	34.78
s (0.65*P*)	(mm)	0.250	0.190
k	(kN/mm)	146.58	183.03

These values of stiffness, *k*, are determined assuming an elastic behaviour of the connection, until a particular percentage of the test maximum load per connector is reached, as was defined in equation (3.4) from Chapter 3. The limit of 0.65 P_u was defined considering the approximately elastic behaviour of the connection, observed until this load level is attained.

As presented in Table 4.8 and Figure 4.18, the stiffness value, *k*, tends to decrease when higher percentages of the maximum load value are considered. In the case of these studs with 13 mm diameter, the stiffness value, *k*, is almost constant until the load reaches 55% of the maximum load, and then decreases as the load increases. The evolution of the average curves *k*-%P_u is similar to the evolution of the same curves established for specimens with 22 and 25 mm diameter studs (see Figure 4.18b), although the values obtained for diameter 13 mm are a bit lower. For load values over 0.50 P_u, the values for stiffness *k* tend to be similar for all stud diameters.

If the value of stiffness is established for values between 0.50P_u and 0.55P_u, then the value of stiffness varies between 196 and 226 kN/mm, for 13 mm diameter specimens, which are close to the values determined in Chapter 3 for larger diameter studs.

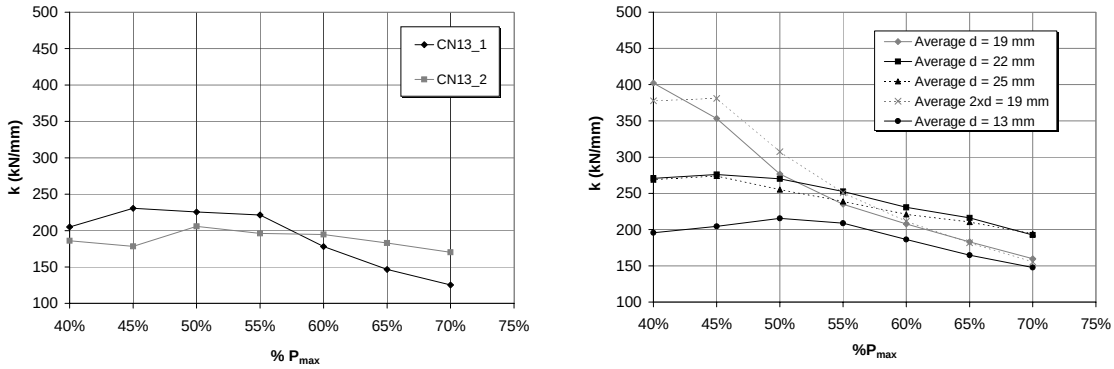

a) Diameter d = 13 mm

b) Average d = 13, 19, 22 and 25 mm

Figure 4.18 - k-%P_u for isolated stud disposition

4.5.3 Comparison between results obtained in static tests and the use of standard equations to predict the ultimate load capacity

Based on the results of standard push-out tests, EN 1994-1-1, (CEN 2004b), proposes equations (3.6) and (3.7) to calculate the design resistant shear load for one single stud (see Chapter 3). These equations predict two possible failure modes, equation (3.6) has to do with the stud shear failure and equation (3.7) has to do with the concrete crush failure.

In AASHTO (2004), the shear strength of one headed stud shear connector embedded in a concrete slab is defined by equation (3.8).

Another expression was proposed by Oehlers and Johnson (1987), to calculate the shear load capacity of headed studs. Equation (3.9) includes the main essential parameters that influence the shear connector load capacity.

Table 4.9 presents an evaluation on the characteristic load capacity of specimens CN13.1 and CN13.2, considering the referred equations. For all the equations, f_u is considered equal to 500 MPa,

Table 4.9 – Concrete properties for push-out test specimens with stud connectors

Specimens	Concrete Ref.	Test	$f_{lc\,(1)}$ (MPa)	$f_{lc\,(2)}$ (MPa)	$E_{lc\,(1)}$ (GPa)	$E_{lc\,(2)}$ (GPa)	$P_{k,exp}$ (kN)	P (3.6) (kN)	P (3.7) (kN)	P (3.8) (kN)	P (3.9) (kN)
CN 13.1	BL44/ BL45	POST	56.65	54.04	23.73	22.38	48.19	53.09	52.24	51.00	56.41
CN 13.2		POST									

where $P_{k,exp}$ corresponds to the experimental result.

The results presented in Table 4.9 show that the standard equations used to predict the connection load capacity for headed studs in high strength lightweight concrete solid slabs give results that are higher than the experimental ones. Therefore, a proper revision of these equations should be considered, for this particular type of concrete.

4.6 Push-out test under cyclic loading

4.6.1 Load and slip capacity

Table 4.10 resumes the effective average load range and number of load cycles effectively applied in the experimental tests with headed studs of 13 mm diameter and presents the ultimate load values obtained in each test.

As defined in Table 4.6, specimens CN13.3, CN13.4 and CN13.5 result from the same casting. The ultimate load value is similar for these three specimens, although the number of cycles and the load range imposed vary significantly. The ultimate load values obtained for these specimens are also similar to the ultimate load values obtained for the statically loaded specimens (CN13.1 and CN13.2). This aspect is very important as it means that, for these specimens, the load levels and number of cycles applied were not in the magnitude to diminish the connection load capacity. On the opposite, specimen CN13.6 was affected by the load cycles applied, as failure occurred during this phase.

Table 4.10 – Ultimate load values experimentally determined during the cyclic push-out tests

Test specimen	Concrete ref.	Test type	Effective average load range	Number of cycles	ΔP (per connector)	$P_{u,i}$	Monotonic loading until failure, after the load cycles
					(kN)	(kN)	
CN13.1	BL44/BL45	static	1.635 – 26.200	25	24.57	56.4	Yes
CN13.2	BL44/BL45	static	1.710 – 26.300	25	24.59	53.5	Yes
CN13.3	BL46/BL47	cyclic	5.138 – 26.691	10000	21.55	58.0	Yes
CN13.4	BL46/BL47	cyclic	4.885 – 31.931	16000	27.05	57.7	Yes
CN13.5	BL46/BL47	cyclic	3.748 – 12.354	1000	8.61	58.1	Yes
			3.357 – 24.639	1000	21.28		
			3.549 – 30.603	1000	27.05		
			3.232 – 36.466	1000	33.23		
			3.160 – 40.311	1000	37.15		
CN13.6	BL44/BL45	cyclic	4.786 – 16.057	1000	11.27	48.2	No
			4.533 – 31.872	1000	27.34		
			4.571 – 39.889	1000	35.32		
			4.477 – 48.158	1000	43.68		

The average ultimate load determined for specimens CN13.1 and CN13.2 is equal to 55.0 kN. The average ultimate load determined for specimens CN13.3, CN13.4 and CN13.5 is equal to 57.9 kN. As a result, the static strength for specimens cast with BL44/BL45 is considered equal to 54 kN and the static strength for specimens cast with BL46/BL47 is considered equal to 57 kN, in the following analysis.

Table 4.11 resumes the tests results on important parameters, like ultimate load value ($P_{u,i}$), corresponding slip ($s_{Pu,i}$), average ultimate load for specimens of the same casting ($P_{u,medium}$) and slip correspondent to 90% of the ultimate load ($s_{0.9Pu,i}$).

Table 4.11 – Ultimate load and correspondent slip

Specimen Ref.	$P_{u,i}$ (kN)	$s_{Pu,i}$ (mm)	$P_{u,medium}$ (kN)	s_{max} (mm)	$s_{(0.9Pu,I)}$ (mm)
CN 13.1	56.4	5.62	55.0	6.94	6.54
CN 13.2	53.5	4.46		8.51	8.44
CN 13.3	58.0	4.37	57.9	4.93	4.93
CN 13.4	57.7	1.26*		1.74*	1.74*
CN 13.5	58.1	3.99		5.73	5.62
CN 13.6	48.2	4.56	-	5.33	-

* - problems with the test machine when CN13.4 test was initiated caused some permanent deformation on the specimen, and therefore, the specimen did not develop the same level of slip as other specimens did

s_{max} maximum slip measured right before failure of the first stud.

The values of slip correspondent to the maximum load value are of similar magnitude, even for specimen CN13.6 whose failure occurred during the load cycles.

The results obtained induce three important conclusions:

- the connection ultimate load capacity is only affected by the cyclic loading when the relation $\Delta P/P_u$ is high (as occurs with CN13.6);
- the value of slip, correspondent to the maximum load, is not affected by the relation $\Delta P/P_u$ or the number of load cycles applied, as far as the obtained results can tell, which means that the slip obtained during the static loading gives a good measure of the connection deformation capacity;
- the value of slip measured right before failure of the first stud, s_{max}, tends to be higher for the specimens loaded statically, although the difference between these and the specimens subjected to cyclic loadings is small; this means that failure under static loading can be considered more ductile than failure under cyclic loading.

The previous conclusions show that it may be important to develop equations that can predict the evolution of slip with the number of load cycles, in order to evaluate the total number of load cycles that can presumably be applied.

It was observed that the relation $\Delta P/P_u$ can influence the ultimate load. It is important to evaluate if this parameter influences also the evolution of slip.

4.6.2 Maximum slip per load cycle

Figure 4.19 presents the maximum slip values, measured at each load cycle, for specimens CN13.3, CN13.4, CN13.5 and CN13.6.

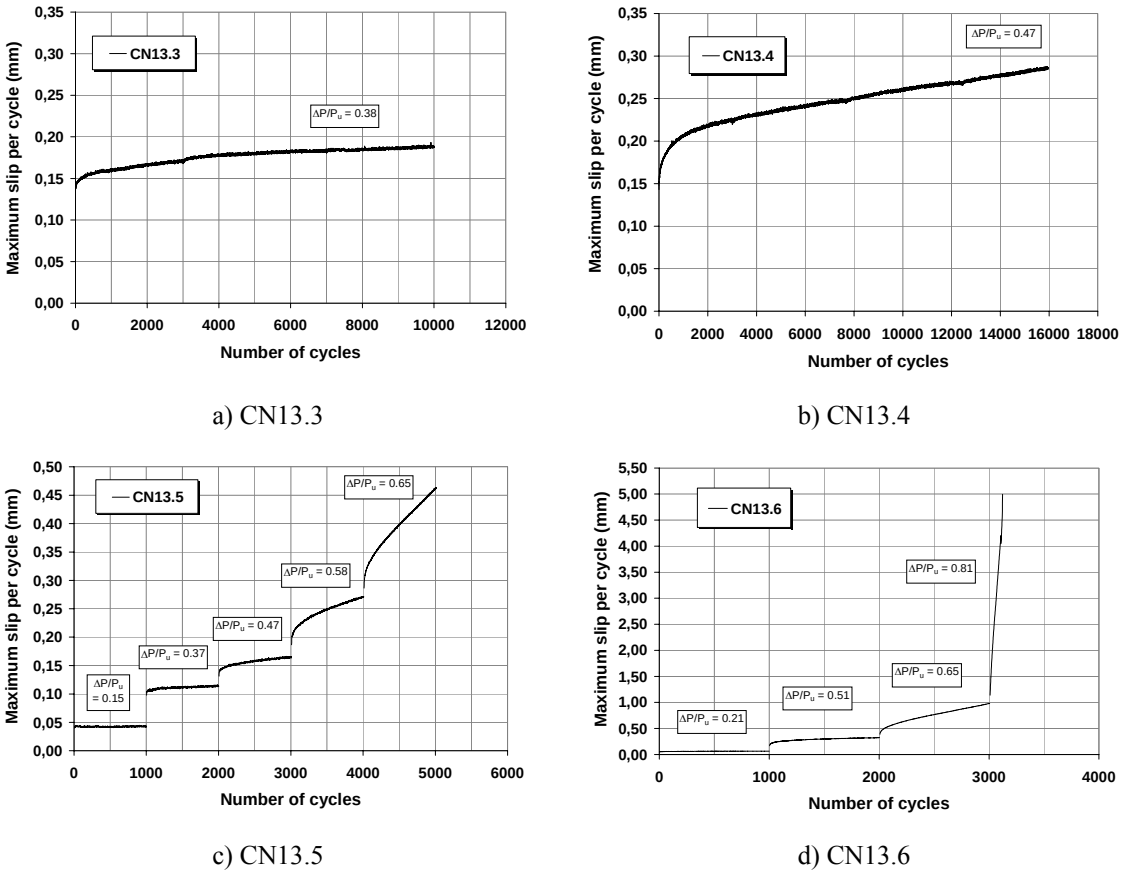

a) CN13.3 b) CN13.4

c) CN13.5 d) CN13.6

Figure 4.19 – Maximum slip at each load cycle for: a) CN13.3; b) CN13.4; c) CN13.5; d) CN13.6

Figure 4.19 shows that the relation $\Delta P/P_u$ influences the rate of slip growth. As the relation $\Delta P/P_u$ gets higher, the total slip, measured for the same number of load cycles, tends to grow faster, showing that the slip value evolution depends on the $\Delta P/P_u$ relation. Therefore, an equation to predict the rate of slip growth should include not only the number of load cycles applied, but also the influence of $\Delta P/P_u$.

4.6.3 Influence of the number of load cycles applied on the evaluation of the rate of slip growth

In the following equations, the rate of slip growth is directly dependent on the number of load cycles applied. Equations (4.9) and (4.10) are used to establish a linear trend,

$$s' = a + b(n) \tag{4.9}$$

$$\Delta s' = b \cdot \Delta n \tag{4.10}$$

where,

s' – slip value;

n – number of load cycles;

a – value of slip at the first load cycle;

b – rate of slip growth – linear;

Δs – variation of slip;

Δn – number of load cycles considered;

and equations (4.11) to (4.13) are used to set the logarithmic trend,

$$s'' = c + d \cdot ln(n) \tag{4.11}$$

$$\Delta s'' = d \cdot ln\left(\frac{n_2}{n_1}\right) \tag{4.12}$$

$$\Delta s'' = d \cdot ln(\Delta n) \quad \text{if} \quad n_1 = 1 \tag{4.13}$$

where,

s'' – slip value;

c – value of slip at the first load cycle;

d – rate of slip growth – logarithmic.

In order to check the influence of the number of load cycles applied on the evaluation of slip growth, some comparisons are established. Specimens CN13.3 and CN13.4 results are analysed considering the following situations: 1) only the first 1000 cycles applied are accounted for; 2) 10000 load cycles applied are evaluated; 3) all the load cycles applied are considered. Figure 4.20 to Figure 4.24 present the evolution of maximum slip measured in each load cycle, considering the situations described. A linear trend and a logarithmic trend are approximated to each curve, in order to check the rate of slip growth.

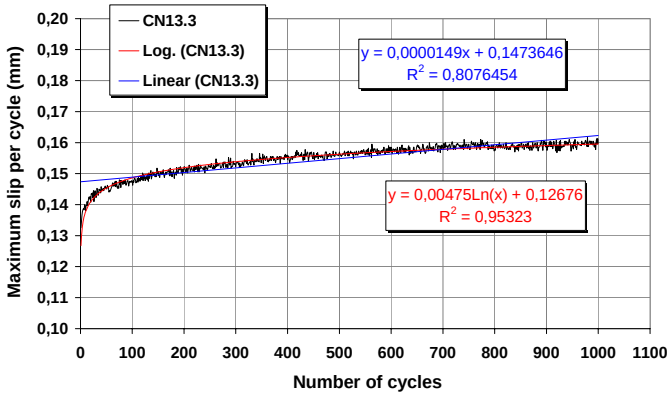

Figure 4.20 - Evolution of slip during the load cycles for CN13.3 (ΔP = 21.55 kN): N_{cycles} = 1000

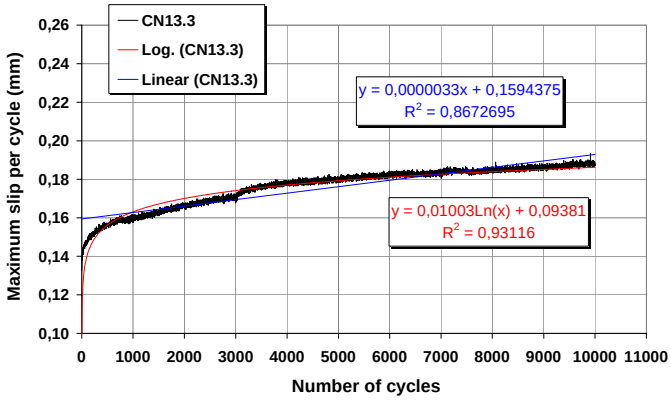

Figure 4.21 - Evolution of slip during the load cycles for CN13.3 (ΔP = 21.55 kN): N_{cycles} = 10000

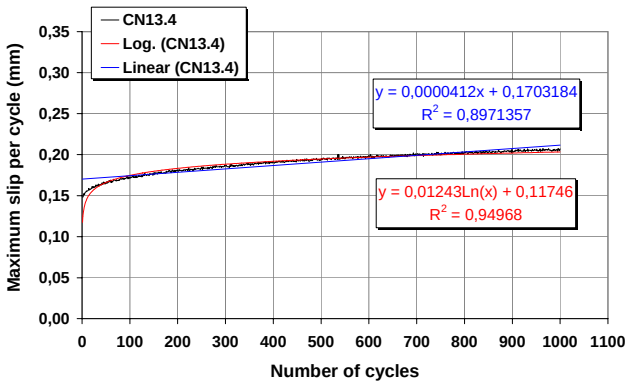

Figure 4.22 - Evolution of slip during the load cycles for CN13.4 (ΔP = 27.05 kN): N_{cycles} = 1000

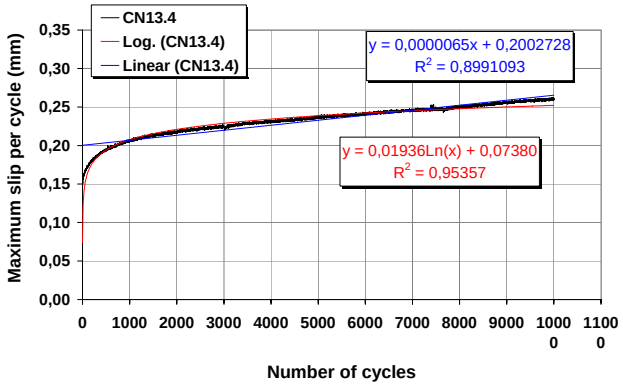

Figure 4.23 - Evolution of slip during the load cycles for CN13.4 (ΔP = 27.05 kN): N_{cycles} = 10000

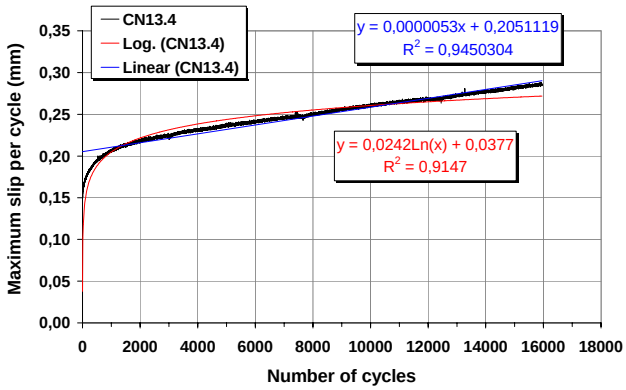

Figure 4.24 - Evolution of slip during the load cycles for CN13.4 (ΔP = 27.05 kN): N_{cycles} = 16000

The analysis of Figure 4.20 to Figure 4.24 leads to the following observations:

- the number of load cycles considered influences the evaluation on the rate of slip growth;
- the slip growth rate is higher for the initial phase of load cycles;
- slip tends to maintain a linear growth rate only after a significant number of load cycles is applied;
- for specimen CN13.3, the logarithmic law is always a better approach to the experimental results on slip growth;
- however, for the same specimen (CN13.3), when a higher number of cycles is considered (N_{cycles}=10000), the correlation between maximum slip per load cycle and number of load cycles applied increases for a linear law approach and decreases for a logarithmic law approach;

- for specimen CN13.4, the logarithmic law is a better approach to the experimental results on slip growth when N_{cycles}=1000 and the linear law is a better approach to the experimental results on slip growth when N_{cycles}=16000;
- when a higher number of cycles is considered (N_{cycles}=16000) for specimen CN13.4, the correlation between maximum slip per load cycle and number of load cycles applied increases for a linear law approach, but decreases for the logarithmic law approach (similar to what happened to specimen CN13.3);
- the linear growth rate tends to be lower when a higher number of load cycles is considered;
- the logarithmic growth rate tends to be higher when a higher number of load cycles is considered;
- as ΔP increases (comparison between CN13.3 and CN13.4), the rate of slip growth tends to be better approximated by a linear law.

4.6.4 Rate of slip growth under cyclic loading

Figure 4.25 presents the evolution of slip during the initial phase of CN13.1 and CN13.2 experimental tests. Although the load was monotonically applied to these specimens, the initial phase of the test is done with the application of 25 cycles of load and unload, varying between 5 and 40% of the ultimate load value expected.

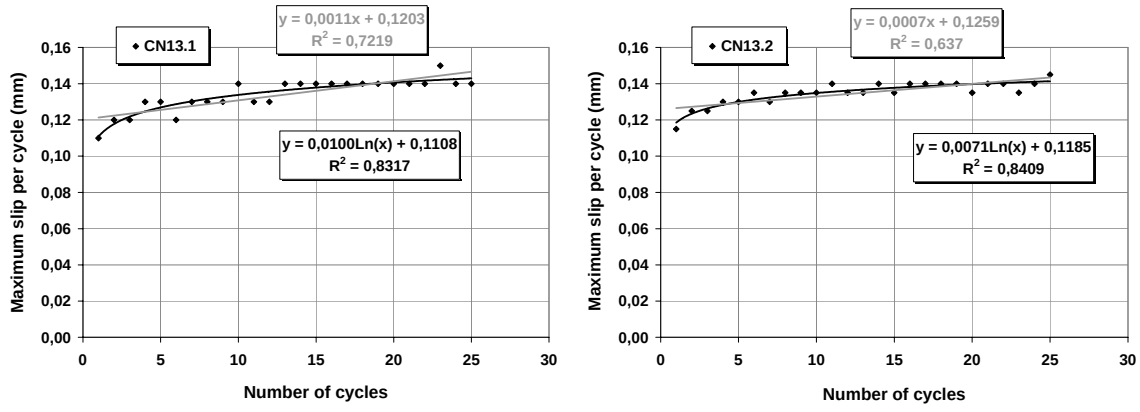

a) CN13.1 : ΔP = 24.57 kN ; N_{cycles} = 25 b) CN13.2 : ΔP = 24.59 kN ; N_{cycles} = 25

Figure 4.25 - Evolution of slip during the load cycles, comparison between CN13.1 and CN13.2

The similarity between CN13.3 and the previous tests (CN13.1 and CN13.2) is that the load cycle range is almost the same. The main difference is that 10000 load cycles were applied to specimen CN13.3, while only 25 cycles were considered for CN13.1 and

CN13.2. The relation between maximum slip per cycle and the number of load cycles applied, presented in Figure 4.25 for CN13.1 and CN13.2, is again better approximated with a logarithmic law. The logarithmic relation obtained for CN13.3 (N = 10000 cycles) is close to the equations obtained for specimens CN13.1 and CN13.2 (N = 25 cycles) (see also Figure 4.21). However, when a linear trend is used, the correspondent equations are quite different.

The linear and the logarithmic trend determined for specimen CN13.3 were already presented in Figure 4.20 (N = 1000 cycles) and the same was done for specimen CN13.4 in Figure 4.22. Figure 4.26 presents the linear and the logarithmic trends calculated for each load range imposed on specimen CN13.5. The same is done for specimen CN13.6 in Figure 4.27.

The first load range applied to specimen CN13.5 has a close amplitude to the load range applied to specimen CN13.3 (see Figure 4.26). The curves obtained show that the rate of slip growth for specimen CN13.3 is higher than the rate of slip growth for specimen CN13.5.

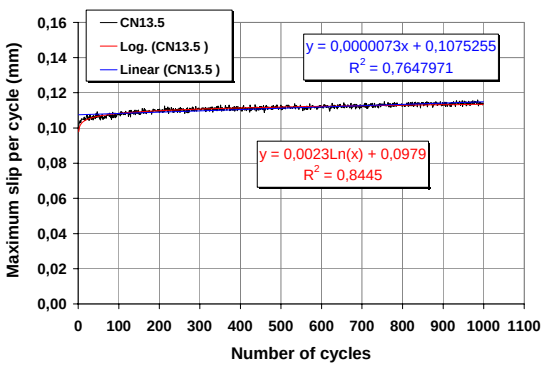

a) ΔP = 21.28 kN ; N_{cycles} = 1000

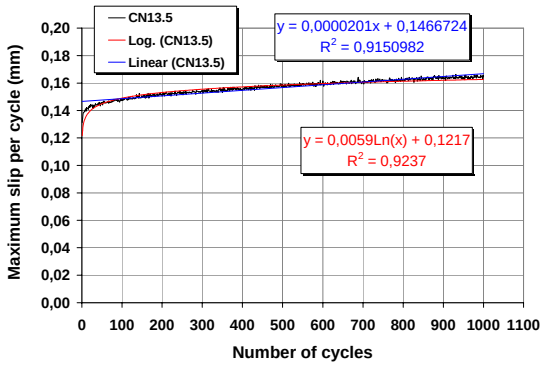

b) ΔP = 27.05 kN ; N_{cycles} = 1000

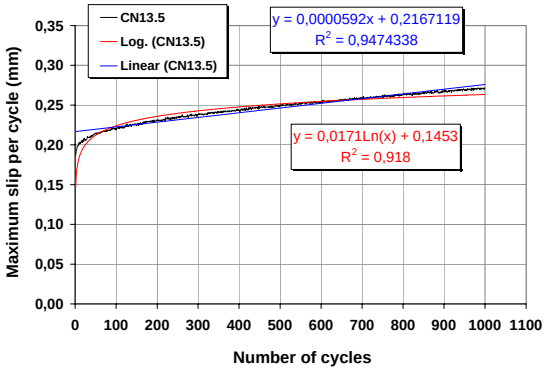

c) ΔP = 33.23 kN ; N_{cycles} = 1000

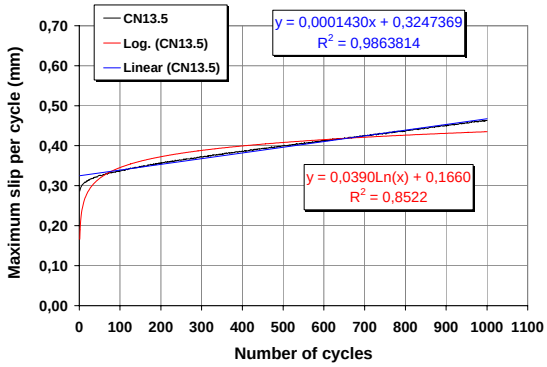

d) ΔP = 37.15 kN ; N_{cycles} = 1000

Figure 4.26 – Evolution of slip during the load cycles for specimen CN13.5

In the same way, the second load range applied to specimen CN13.5 and the second load range applied to specimen CN13.6 are of similar amplitude to the load range applied to specimen CN13.4 (see Figure 4.27) and the fourth load range applied to specimen CN13.5 is of similar amplitude to the third load range applied to specimen CN13.6. Again, there is some variability on the results obtained, as can be confirmed in Table 4.12.

The results variability verified when the same load range of different tests is compared can result from the number of load cycles applied that, as was shown, influences the rate of slip growth. It is also clear that a large number of experimental tests is needed to get sufficient data to better resolve the problems associated with the results variability.

The results obtained on CN13.5 and CN13.6 tests confirm the observations made for CN13.3 and CN13.4. As far as the results obtained can tell, the logarithmic trend is a better approach when the load range value is lower: $\Delta P/P_u < 0.5$, while the linear trend is best fitting when the load range is higher: $\Delta P/P_u > 0.5$.

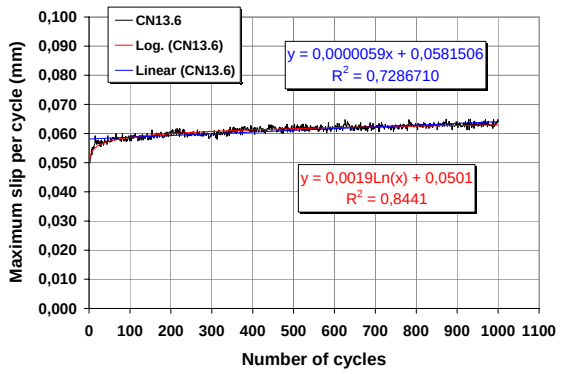

a) ΔP = 11.27 kN ; N_{cycles} = 1000

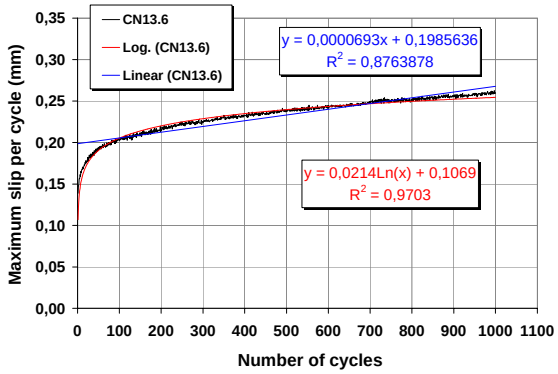

b) ΔP = 27.34 kN ; N_{cycles} = 1000

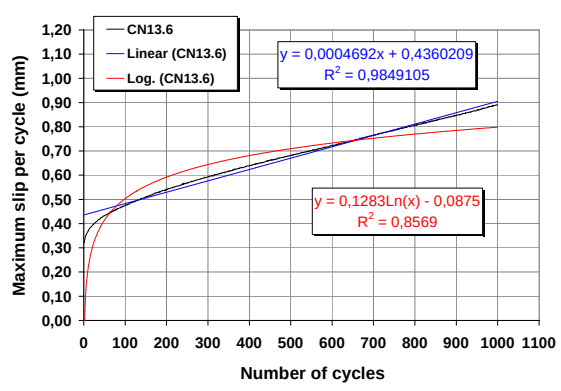

c) ΔP = 35.32 kN ; N_{cycles} = 1000

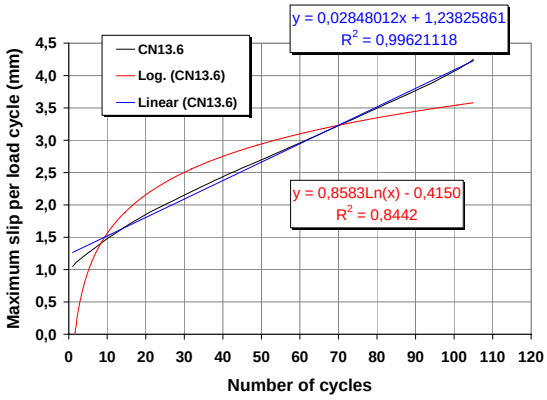

d) ΔP = 43.68 kN ; N_{cycles} = 1000

Figure 4.27 – Evolution of slip during the load cycles for specimen CN13.6

Table 4.12 collects the values obtained for the rate of slip growth for each specimen and load range, considering the linear approach and the logarithmic approach to the experimental results. With the results presented, it is possible to calculate the variation on the rate of slip growth as a function of the load range correspondent to each load cycle applied. An alternative would be to express the variation on the rate of slip growth as a function of the maximum load applied in each load cycle.

Table 4.12 – Rate of slip growth per cycle – linear trend and logarithmic trend

Test	P_{max} (kN)	Number of load cycles	ΔP (per stud) (kN)	$\Delta P/P_u$	Rate of slip growth (Linear) (mm/cycle)	r^2 (Linear)	Rate of slip growth (Logarithmic) (mm/ln(cycle))	r^2 (Logarithmic)
CN13.1	26.20	25	24.57	0.43	1054×10^{-6}	0.7219	0.00998	0.8317
CN13.2	26.30	25	24.59	0.43	700×10^{-6}	0.6370	0.00710	0.8409
CN13.3	26.69	10000	21.55	0.38	3.34×10^{-6}	0.8673	0.01003	0.9312
CN13.4	31.93	16000	27.05	0.48	5.33×10^{-6}	0.9450	0.02420	0.9147
CN13.5	12.35	1000	8.61	0.15	0.49×10^{-6}	0.0389	0.000076	0.0109
	24.64	1000	21.28	0.38	7.38×10^{-6}	0.7560	0.002295	0.8523
	30.60	1000	27.05	0.48	20.12×10^{-6}	0.9151	0.005924	0.9237
	36.47	1000	33.23	0.59	59.24×10^{-6}	0.9474	0.017091	0.9180
	40.31	1000	37.15	0.65	143.0×10^{-6}	0.9864	0.038955	0.8522
CN13.6	16.06	1000	11.27	0.20	5.92×10^{-6}	0.7287	0.001867	0.8441
	31.87	1000	27.34	0.48	69.27×10^{-6}	0.8764	0.021360	0.9703
	39.89	1000	35.32	0.62	469.23×10^{-6}	0.9849	0.128272	0.8569
	48.16	1000	43.68	0.77	28483×10^{-6}	0.9956	0.837822	0.8501

P_{max} – maximum load per load range and per stud

4.6.4.1 Linear rate of slip growth vs. load range

The values of linear rate of linear slip growth determined during the cyclic push-out tests of specimens CN13.3, CN13.4, CN13.5 and CN13.6, presented in Table 4.12, are now considered to establish a relation between the slip growth per cycle and the quotient of load range and ultimate load value determined during the static test.

Figure 4.28.a) presents the described relation for specimen CN13.5 results and Figure 4.28.b) does the same for specimen CN13.6. The *y-axis* is represented on a logarithmic scale. The best fitting curves are also represented in the figures.

For specimen CN13.5, the correlation coefficient determined is equal to $r^2 = 0.998$ and for specimen CN13.6, the correlation coefficient determined is equal to $r^2 = 0.915$.

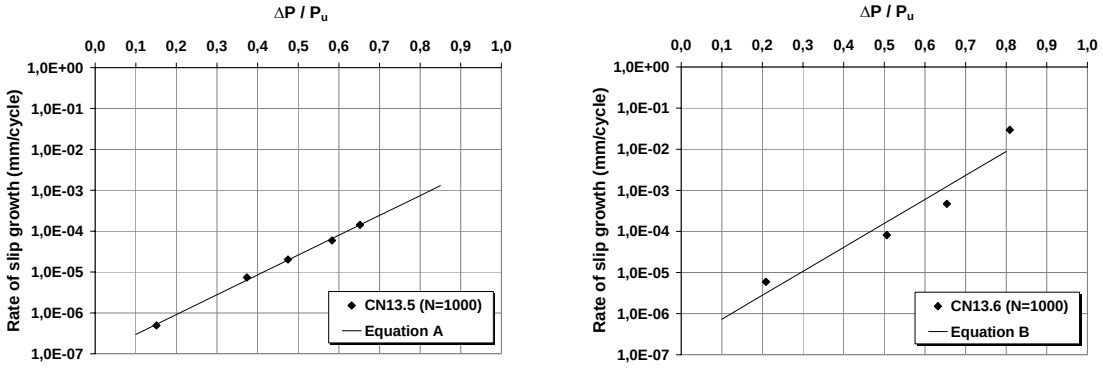

a) Eq. A: $log\ (s'/\ cycle) = -7.01 + 4.85 \left(\frac{\Delta P}{P_u} \right)$ b) Eq. B: $log\ (s'/\ cycle) = -6.74 + 5.82 \left(\frac{\Delta P}{P_u} \right)$

Figure 4.28 – Evolution of slip depending on the cycles load range (N_{cycles} = 1000), for a) CN13.5 and b) CN13.6

Figure 4.29 presents the relation between the linear slip growth per cycle and the load range in relation to the ultimate load value determined during the static test, for all the load cycles performed during the push-out tests. Again, the best fitting law is logarithmic and the correspondent correlation coefficient is equal to $r^2 = 0.872$.

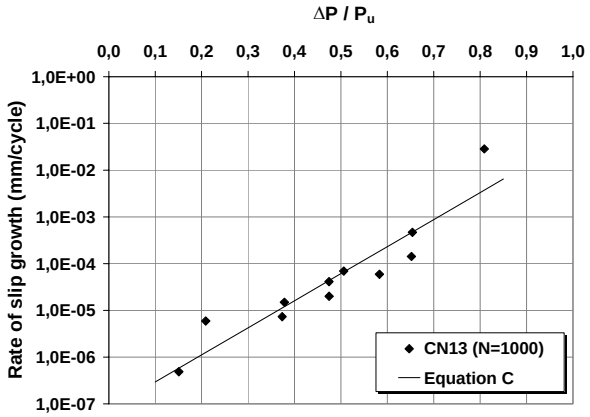

Figure 4.29 – Evolution of slip depending on the cycles load range (considering N_{cycles} = 1000), for all cyclic push-out tests CN13: $log\ (s'/\ cycle) = -7.11 + 5.79 \left(\frac{\Delta P}{P_u} \right)$

The relation obtained with Equation C of Figure 4.29 is now compared to the results obtained by other authors (see 4.2), as represented in Figure 4.30.

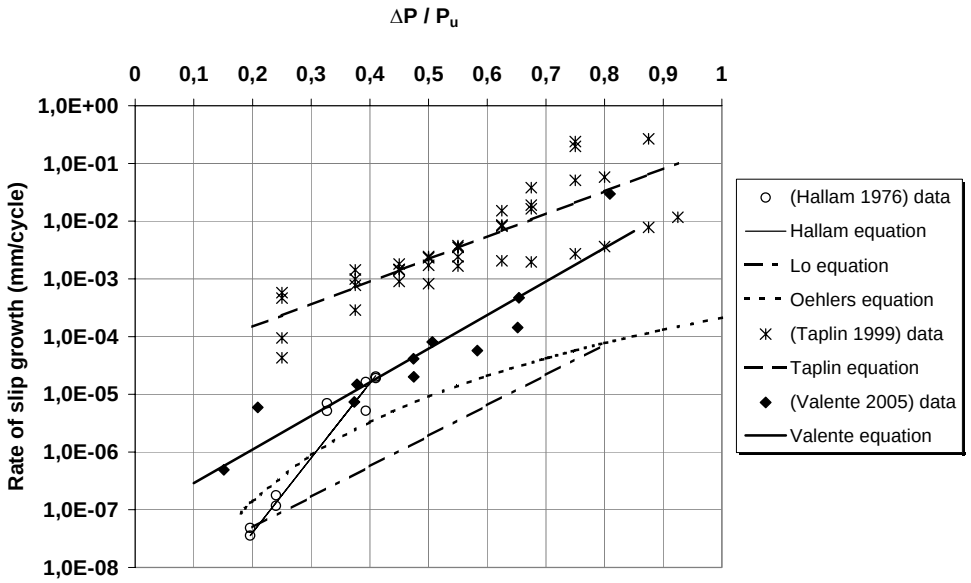

Figure 4.30 – Evolution of slip depending on the cycles load range (N_{cycles} = 1000), for all cyclic push-out tests CN13: $log\ (s'/\ cycle) = -7.11 + 5.79 \left(\frac{\Delta P}{P_u} \right)$

The equation obtained follows depends on the value of $\Delta P/P_u$ in similar manner as the equation obtained by (Lo 1978) does, but the values obtained for the rate of slip growth are always higher than the values obtained by Lo. With exception on the results obtained by (Taplin 1999), it seems that the rate of slip growth is higher for lightweight concrete than for normal density concrete.

4.6.4.2 Logarithmic rate of slip growth vs. load range

The values of logarithmic rate of slip growth determined during the cyclic push-out tests of specimens CN13.3, CN13.4, CN13.5 and CN13.6 were presented in Table 4.12.

The procedure presented in 4.6.4.1 is followed, in order to evaluate the relation between the slip growth per cycle and the quotient of load range and ultimate load value determined during the static test. Figure 4.31.a) presents the described relation for specimen CN13.5 results and Figure 4.31.b) does the same for specimen CN13.6.

For specimen CN13.5, the correlation coefficient determined is equal to r^2 = 0.987 and for specimen CN13.6, the correlation coefficient determined is equal to r^2 = 0.988.

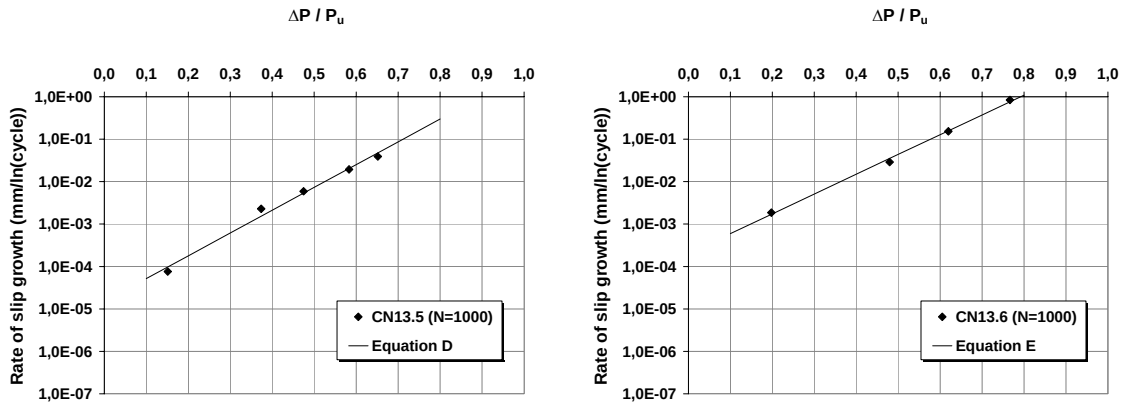

a) Eq. D:

$$log\,(s''/\,ln(cycle)) = -4.81 + 5.32\left(\frac{\Delta P}{P_u}\right)$$

b) Eq. E:

$$log\,(s''/\,ln(cycle)) = -3.74 + 4.40\left(\frac{\Delta P}{P_u}\right)$$

Figure 4.31 – Evolution of slip depending on the cycles load range (N_{cycles} = 1000), for a) CN13.5 and b) CN13.6

Figure 4.35 presents the relation between the slip growth per logarithmic number of cycles and the load range in relation to the ultimate load value determined during the static test, for all the load cycles performed during the push-out tests. Again, the best fitting law is logarithmic, where the correlation coefficient is equal to $r^2 = 0.907$.

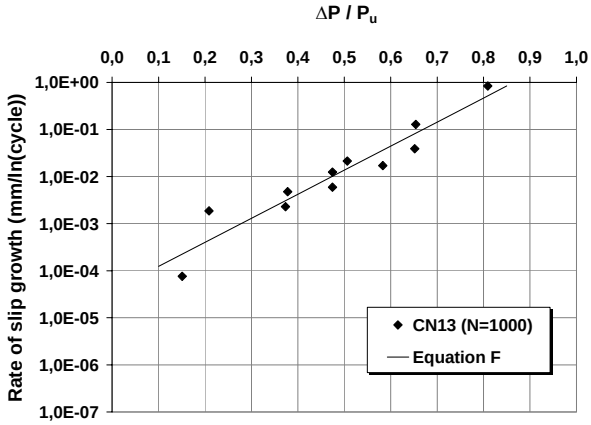

Figure 4.32 – Evolution of slip depending on the cycles load range (N_{cycles} = 1000), for all cyclic push-out tests CN13: $log\,(s'/\,ln(cycle)) = -4.42 + 5.11\left(\frac{\Delta P}{P_u}\right)$

4.6.5 Complete load-slip curve

Table 4.13 presents the total increase of maximum slip verified during the cyclic push-out tests, for each load range imposed. This information is then included in the load-slip curves of each tested specimen, in order to evaluate the influence of this slip growth on the connection load capacity and deformation capacity.

Table 4.13 – Total increase of maximum slip verified during the cyclic push-out tests, for each load range imposed

Test specimen	Concrete ref.	Test type	Number of cycles	ΔP (per connector)	$\Delta P/P_u$	Average Δs_{max}	Static loading until failure, after the load cycles
				(kN)	(kN)	(mm)	(mm)
CN13.3	BL46/BL47	Cyclic	10000	21.55	0.38	0.060	Yes
CN13.4	BL46/BL47	Cyclic	16000	27.05	0.47	0.143	Yes
CN13.5	BL46/ Bl47	Cyclic	1000	8.61	0.15	0.005	Yes
			1000	21.28	0.37	0.016	
			1000	27.05	0.47	0.033	
			1000	33.23	0.58	0.085	
			1000	37.15	0.65	0.177	
CN13.6	BL44/BL45	Cyclic	1000	11.27	0.21	0.013	No
			1000	27.34	0.51	0.155	
			1000	35.32	0.65	0.579	
			115	43.68	0.81	4.170	

* - problems with the test machine when CN13.4 test was initiated caused some permanent deformation on the specimen, and therefore, the specimen did not develop the same level of total slip as other specimens did.

Δs_{max} variation of maximum slip (from each load cycle), measured between the first and the last load cycle applied

As described in 4.4.1, the specimens that did not suffer failure during the load cycles were statically loaded after completing the load cycles. Figure 4.33 presents the complete load-slip curves for specimens CN13.3, CN13.4, CN13.5 and CN13.6.

There were some problems with the test machine when the test on CN13.4 was initiated, causing some permanent deformation on the specimen. That is probably why this specimen did not develop the same level of slip for maximum load as other specimens did.

Some important aspects result from the diagrams of Figure 4.33 and Table 4.13:

- when the relation $\Delta P/P_u$ is small, the values for total slip obtained during the load cycles have little importance on the total load-slip curve development;
- as the relation $\Delta P/P_u$ gets higher, the maximum slip increase grows, at each load range;
- the values of total slip measured during the static tests and total slip measured during the cyclic tests are close (see Table 4.7 and Table 4.13);
- the relation $\Delta P/P_u$ is critical and can lead the specimen to failure if the number of load cycles applied is enough to impose a total deformation that is close to the connection deformation capacity.

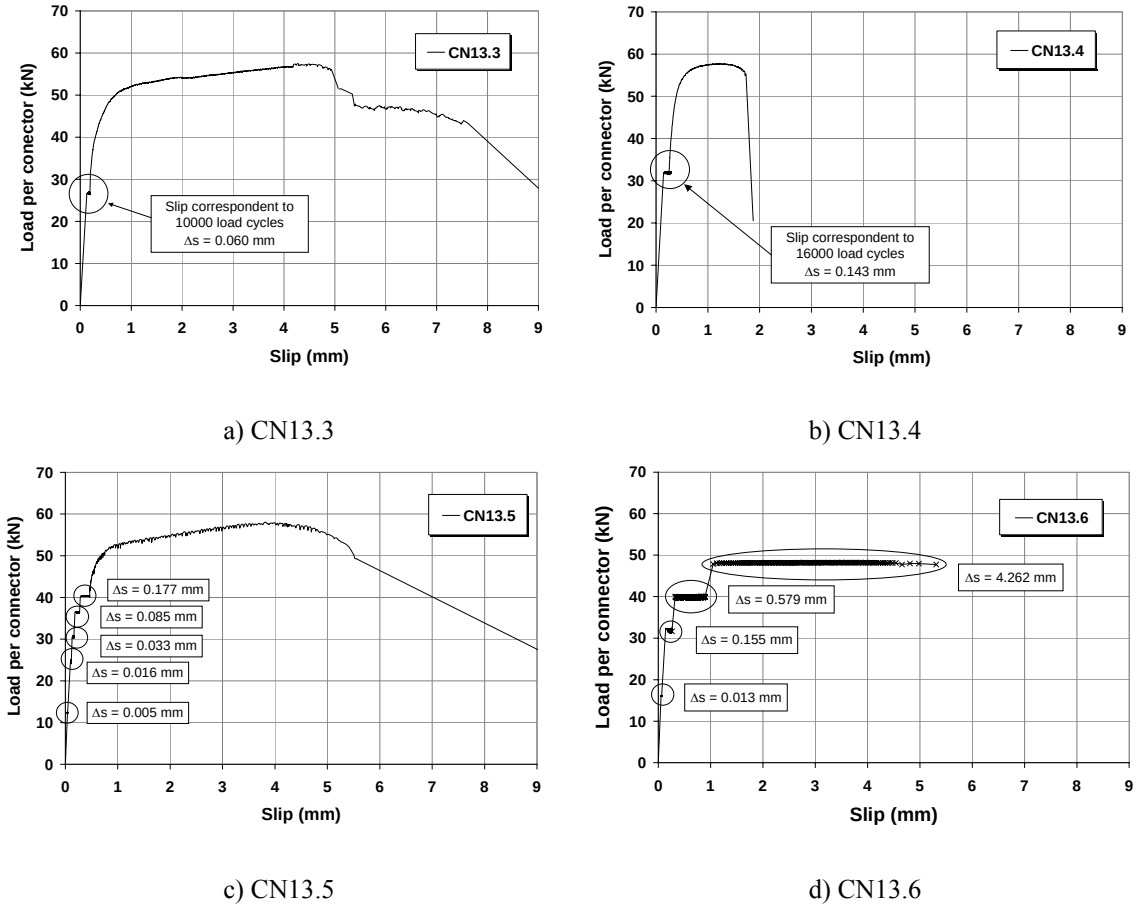

Figure 4.33 – Complete load-slip curve for: a) CN13.3; b) CN13.4; c) CN13.5; d) CN13.6

Applying equation C, defined in 4.6.4, to specimens CN13.3 and CN13.4, and considering the number of load cycles applied and the load cycles range, a total slip of 0.120 mm for specimen CN13.3 and 0.690 mm for specimen CN13.4 would be achieved. These values are higher than the slip values measured during the experimental tests (0.060 mm for CN13.3 and 0.143 mm for CN13.4) but are rather smaller than the connection total deformation capacity verified for these specimens. Using now equation F, also referred in 4.6.4, applied to specimens CN13.3 and CN13.4, and considering the number of load cycles applied and the load cycles range, a total slip of 0.030 mm for specimen CN13.3 and 0.098 mm for specimen CN13.4 would be achieved.

4.7 Fatigue strength of automatically welded headed studs

EN 1994-1-1, (CEN 2004b), defines the fatigue strength curve of an automatically welded headed stud with shank diameter $d \geq 16$mm, using equation (4.14).

$$(\Delta\tau_R)^m N_R = (\Delta\tau_c)^m N_c \tag{4.14}$$

Considering that N_R is the number of stress-range cycles, $\Delta\tau_R$ is the stress range, $\Delta\tau_c$ is the reference stress value at 2 million cycles, with $\Delta\tau_c$ = 90 MPa and m is the slope of the fatigue strength curve (m = 8), then equation (4.14) is transformed into equation (4.15).

$$\log N_R + 8 \log (\Delta\tau_R) = 21.935 \tag{4.15}$$

For studs placed in lightweight concrete slabs, the fatigue strength should also be determined in accordance with equation (4.14), but replacing $\Delta\tau_R$ by $\eta_E\Delta\tau_R$ and $\Delta\tau_c$ by $\eta_E\Delta\tau_c$, where the conversion factor for calculating the modulus of elasticity, η_E, is defined with equation (2.13) from Chapter 2 and ρ denotes the lightweight concrete oven-dry density (if ρ>1400 kg/m^3).

Figure 4.34 represents equation (4.15) graphically and is included EN 1994-1-1.

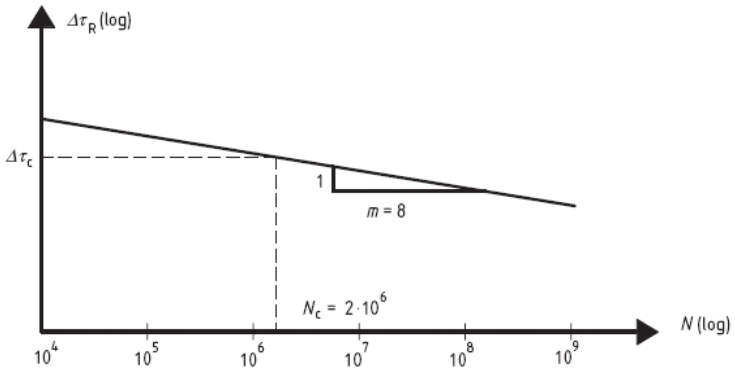

Figure 4.34 - Fatigue strength curve for headed studs in solid slabs (CEN 1994)

According to AASHTO (2004), the fatigue strength of an individual headed stud connector should be taken as defined by equation (4.16).

$$\Delta\tau_R = \frac{4}{\pi}\alpha = 303 - 37.6 \log N_R \tag{4.16}$$

The british standard BS 5400: Part 10, (BS 5400 1980) uses equation (4.17) to evaluate headed studs fatigue strength, where P_R is defined with equation (3.9).

$$\log N_R + 8 \log (\Delta P_k/P_R) = 1.29 \tag{4.17}$$

The fatigue strength of the specimens subjected to cyclic loadings within only one stress range is evaluated by considering equations (4.15), (4.16) and (4.17), and the corresponding results are presented in Table 4.14, in terms of the expected number of load cycles to failure. The value of lightweight concrete oven-dry density is considered equal to 1820 kg/m^3.

Table 4.14 – Fatigue strength evaluation for specimens CN13.3 and CN13.4

Specimen Ref.		CN13.3	CN13.4
Stud diameter d	(mm)	13	13
Applied stress range $\Delta\tau_R$	(MPa)	162.4	203.8
Applied load range ΔP	(kN)	21.55	27.05
Ultimate static load P_u	(kN)	57.0	57.0
Number of load cycles applied	(cycles)	10000	16000
N_R (EN 1994-1-1)	(cycles)	17796	2893
N_R (AASHTO)	(cycles)	5502	435
P_R (BS5400)	(kN)	54.93	54.93
N_R (BS5400)	(cycles)	34746	5638

The values presented in Table 4.14 show that for the stress ranges imposed, the number of load cycles defined for CN13.3 and CN13.4 should be insufficient to achieve fatigue failure, according to EN 1994-1-1.

If we now consider the number of load cycles predicted by EN 1994-1-1 to achieve fatigue failure (see Table 4.14), a total of 1.490 mm for CN13.3 and 0.872 mm for CN13.4 correspond to the predicted increase of slip during the load cycles, by using equation C, values that are also reduced and should not lead to the specimens failure. In the case of using equation F, the predicted increase of slip during the load cycles would be equal to 0.038 mm for CN13.3 and equal to 0.100 mm for CN13.4, leading to the same conclusions.

According to AASHTO equation, failure should occur for both of the specimens within the load cycles applied, which is not coherent with the experimental results obtained. According to BS5400 equation, failure should not occur for specimens CN13.3 and CN13.4. The application of EN 1994-1-1 equation shows that failure should not occur for specimens CN13.3, but should happen for specimen CN13.4, within the number of load cycles applied.

Globally, the BS5400 model seems more appropriate to evaluate the fatigue strength of headed stud connectors than the other models referred in this text.

4.8 Conclusions

This chapter discussed the fabrication, set up, testing and analysis of cyclic push-out tests on headed stud connectors of 13 mm diameter inside high strength lightweight concrete slabs.

The static tests gave results on the connection static strength, deformation capacity and stiffness. Joining the results obtained on 13 mm diameter studs with the results presented in Chapter 3 for 19, 22 and 25 mm diameter studs, it is verified that the use of

lightweight concrete results in a diminution on the connection load capacity. In terms of stiffness, the values obtained for 13 mm diameter studs are close to the values presented in Chapter 3 for 19, 22 and 25 mm diameter studs.

The measurements done during the cyclic tests allowed an evaluation on the slip growth, per load cycle. First, it was verified that the evaluation on the rate of slip growth is influenced by the number of load cycles performed or considered in the analysis. The linear and the logarithmic trends were analysed, because they gave the best correlations between rate of slip growth and number of load cycles applied. In global terms, the logarithmic trend is a better approach when the load range value is lower: $\Delta P/P_u < 0.5$, while the linear trend is best fitting when the load range is higher: $\Delta P/P_u > 0.5$.

The variation on the load range cycles imposed during the testing confirmed that the rate of slip growth is highly dependent on the $\Delta P/P_u$ relation, and therefore, equations to evaluate the rate of slip growth were defined considering this parameter. In general, a comparison between this work and the results obtained by other authors with normal density concrete, shows that the rate of slip growth is higher for lightweight concrete.

Fatigue strength was not achieved in any of the specimens tested with a constant load range. The results obtained are not consistent with the number of load cycles needed to attain fatigue failure, predicted by the various codes. Even so, EN 1994-1-1 is the code that gives results closer to the experimental ones.

Chapter 5

SHORT TERM STATIC LOADINGS IN STEEL AND HIGH STRENGTH LIGHTWEIGHT CONCRETE COMPOSITE BEAMS

5.1. Introduction

Composite construction is gathering increasing interest in many European countries. Steel and concrete are materials with different nature and properties. When properly associated, it is possible, in a mechanical point of view, to take the best advantage of each one's properties and of its association, respecting the purpose of a composite structure.

The most traditional structural element in this type of construction is the composite beam, used mainly in buildings and bridges. For this structural element, the steel profile is associated with a concrete slab by using steel connectors. Presently, there are several different typologies of connectors that can be used in a composite structure and some of them were discussed in the previous chapters. The most commonly used are the headed stud connectors, massively produced by well-known firms such as Nelson, Köco, Hilti etc.

Composite beams can appear in different configurations, as presented in Figure 5.1. The most common, and the one that is the subject of this study, consists on a laminated steel profile and the respective concrete slab (type S4 of Figure 5.1).

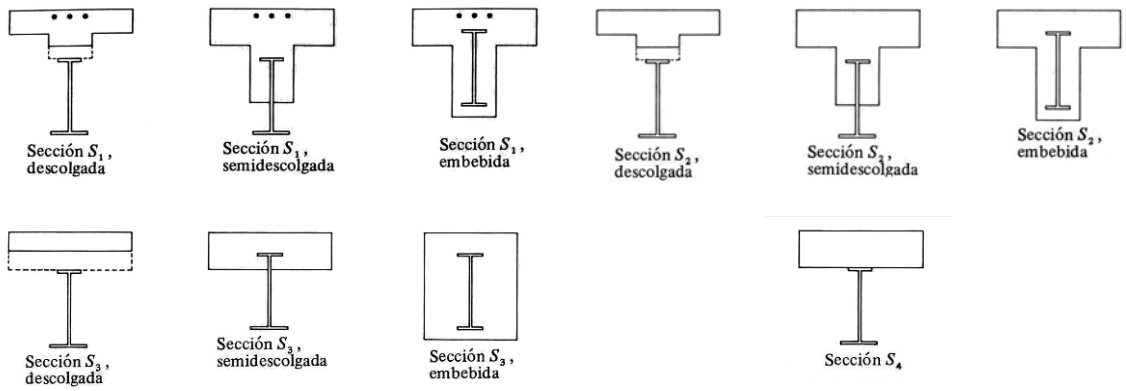

Figure 5.1 – Composite steel and concrete cross section types: S1, S2, S3 and S4, (Calzon and Ortiz 1978)

The existence of a concrete slab has the fundamental benefit of constituting the horizontal surface of the building or bridge pavement. Structurally, it plays the important role of resisting the compressive stresses developed at the composite cross section when

the beam is submitted to sagging bending moments. The concrete slab presence enhances not only the cross section strength but also increases its stiffness.

The use of lightweight concrete in a composite beam is in study within this work. This option has a particular interest, considering the reduction on the concrete slab weight, which usually constitutes an important parcel of the dead load. As a result, a reduction in the steel section can be considered, resulting in a globally lighter solution.

It is possible to produce lightweight concrete that is comparable to normal weight concrete in terms of compressive strength. However, other mechanical properties, like tensile strength, modulus of elasticity, or long-term properties show some differences that should be taken into account, when the same grade of compressive strength for normal density concrete and lightweight concrete is in comparison (see Chapter 2).

The present chapter describes the design, production, testing and test results analysis of six composite beams, composed by a laminated steel profile and a slab made of high strength lightweight concrete. The tests on this group of beams try to put in evidence the beam's behaviour, in terms of failure mechanisms, which can either occur by bending at a particular cross section or at the connection level, for the beam total or partial length.

The beam design accounts for each cross section characteristics and also for the global structural behaviour. The beams initial design takes into consideration dispositions from EN 1992-1-1, (CEN 2004a), EN 1993-1-1, (CEN 2005), and EN 1994-1-1, (CEN 2004b), as well as other aspects mentioned in the presented bibliography.

Cross section, beam span and supporting conditions are common characteristics for every tested composite beam. The disposition of steel to concrete connection elements and the loading distribution are variable.

The steel to concrete connection is accomplished with common headed studs. Particular emphasis is put on the connection behaviour and its effect on the beam global behaviour. It is to be noticed that the type of connection and its stiffness play an important role on the stress distribution along the composite cross section. All the elements that constitute the composite beam are also analysed in terms of their contribution to the beam load carrying capacity and deformation capacity.

The steel connectors are welded to the steel beam and afterwards concreted inside the lightweight concrete slab, in order to guarantee their functioning as a unique element. This is achieved if the slip at the interface of these two elements is prevented or at least reduced. As a result, important shear stresses appear in this zone, which must be resisted by the shear connectors.

A beam is designed for total connection when the cross section ultimate strength does not depend on the connection resistance. This means that failure occurs on one of the

composite section elements before the connection failure happens. In this case, adding one or more connectors does not increase the beam load capacity. However, if the beam is designed for partial shear connection, it means that the beam failure is conditioned by the shear connection failure, which will decrease the composite beam strength.

The main parameter in analysis in the experimental tests is the steel connectors' distribution. These elements are disposed in three different ways: one guarantying the total connection design, other that guarantees total connection but disposes the studs in pairs on the beams' longitudinal direction and a last one that allows for a partial connection.

The design of a composite beam should also take into account the beam behaviour in service conditions, which is sometimes decisive. A total interaction is obtained if there is no slip between the steel and the concrete elements. In this case, the Navier-Bernoulli hypothesis is applicable: plane sections are still plane after deformation. A partial interaction exists when slip between steel and concrete is admitted. As can be concluded from Chapter 4, slip always occurs for a real structure, but its magnitude depends on the number of shear connectors disposed, the material, type and geometry of the shear connector and the type and class of concrete. The major consequence on the existence of slip between the steel profile and the concrete slab is the loss of composite action and therefore an increase on the beam vertical deflection. According to Oehlers et al. (1997), the effect of partial interaction on the full-shear-connection strength of a composite beam in buildings, where the axial strength of the concrete section is usually much larger than that of the steel section, has virtually no effect on strength. Conversely, partial interaction can reduce the strength of composite beams with very strong steel sections, that is where the axial strength of the steel section is much greater than that of the concrete section.

The composite beams are submitted to short-term static loadings. Two load configurations are considered. The first corresponds to four concentrated loads, equally spaced along the beam, approximating a uniformly distributed loading. The second case corresponds to two concentrated loads closely spaced, near the beam mid span, approximating a concentrated loading.

5.2. Objectives of the experimental static tests on composite beams

The main objective of the experimental tests on composite beams is to check the behaviour of the shear connection between steel and concrete. This intention was already fulfilled with the work presented in Chapter 3 and Chapter 4, but it is now important to check if the push-out tests performed reflect the connection behaviour in the composite beam, as there are some differences in the stress distribution between the two tests. The tests on composite beams are also appropriate to observe and measure other important parameters

that could not be checked with the previous experimental work, like bending strength, cracking or vertical deformation and to identify the beam failure modes.

The layout of the shear connectors and the load distribution are the most important parameters of the composite beams' tests. By varying them, it is possible to investigate the variation of force in the shear connection and to analyse how the less loaded connectors influence the more loaded ones, for static loading. Those results are then compared with the results obtained in the push-out tests.

The measurements on slip are important to check if the load-slip relation measured during the push-out tests is repeated in beams. The existence of slip at the steel to concrete interface changes the stress distribution within the composite cross section. It is interesting to investigate the variation of the neutral axis position, the cracks initiation, the initial steel yielding and the concrete crushing.

A numerical analysis will try to reproduce or at least approximate the results obtained in the experimental tests, in order to calibrate simple models to evaluate the phenomena in analysis.

5.3. Beams in study

5.3.1 Test specimens

The design of the composite beam specimens required the definition of the following aspects: cross section type, dimensions of the concrete slab; cross section size for the steel beam; concrete strength; shear stud connector layout; beam span; reinforcement in the concrete slab; influence of the interface friction.

Cross section type - The beam cross section is composed by a standard steel profile and a solid concrete slab, of the same type as section S4 represented in Figure 5.1.

Dimensions of the concrete slab - For convenience of the formwork system and limits of the concreting machine, a slab of 350 mm × 60 mm cross section is chosen. This slab, combined with the steel beam chosen provides a composite cross section where the plastic neutral axis is positioned on the concrete slab.

Section size for the steel beam - The steel section size is chosen considering two aspects: the composite cross section classification as class 1, according to EN1994-1-1 (CEN 2004b) and the neutral axis position at the concrete slab for plastic analysis.

Concrete strength - The concrete selected for the beam tests is the same mixture of high strength lightweight concrete characterized in Chapter 2 and also used for the push-out tests presented in Chapter 3 and Chapter 4. The LWC compressive strength is around 60 MPa.

Layout of shear stud connectors - The shear stud connectors are uniformly disposed along the beam span. The total number of studs used guarantees total shear connection between the concrete slab and the steel beam in some cases and partial shear connection in other cases.

Beam span - The evolution of the composite beams' deflection is an important parameter to measure. The longer is the span of the composite beam, the greater is the deflection for a given applied load and the force in the shear connection. Therefore, the beam span is made long, keeping in mind the span to depth ratios that can be met in practice and the limits of the laboratory facilities. In reality, the chosen span is of 4.5 m and the span to depth ratio is equal to 25, a relation that is around 30% higher than the commonly chosen solutions.

Reinforcement in the concrete slab - Reinforcement in the slabs is needed to prevent longitudinal shear failure. Two layers of 5 mm diameter wires, spaced of 10 cm and yield strength of 500 MPa are used, as happened for the push-out tests.

Influence of the interface friction - The force in the shear connectors is reduced, if any of the interface shear forces are carried out by friction between the steel beam and the concrete slab. To eliminate friction in the beam tests, the top surface of the steel beam is greased with a concrete mould releasing agent, with exception of the stud locations.

5.3.2 Stud distribution

The beams in study are composed by an IPE120 steel profile and a $350\ \text{mm} \times 60\ \text{mm}$ lightweight concrete slab (Figure 5.2a). Shear connection is provided with equally spaced stud connectors of 13 mm diameter and 50 mm high. These connectors are commercially available and were in this case supplied by Köco®. The shear connectors' distribution is of three types (Table 5.1 and Figure 5.2b).

Table 5.1 – Shear connectors' distribution

Connection type	Connection	Distribution
Type A	Total	8 studs of 13 mm diameter and 50 mm high, in half span the beam
Type B	Partial	4 studs of 13 mm diameter and 50 mm high, in half span the beam
Type C	Total	8 studs of 13 mm diameter and 50 mm high, grouped in pairs, in half span the beam

The connectors' distribution of Type A aims for a total connection between the concrete slab and the steel profile, with a uniformly distributed disposition of steel connectors. The connectors' distribution of type B aims for a partial connection between the concrete slab and the steel profile and therefore failure at the connection should be

expected. The connectors' distribution of type C aims for a total connection between the concrete slab and the steel profile, but associating connectors in pairs. The aim is to achieve a more ductile behaviour of the beam connection, (Döinghaus 2001), (Hegger et al. 2001). This effect was verified during the push-out tests presented in Chapter 3 and is now under evaluation for beams.

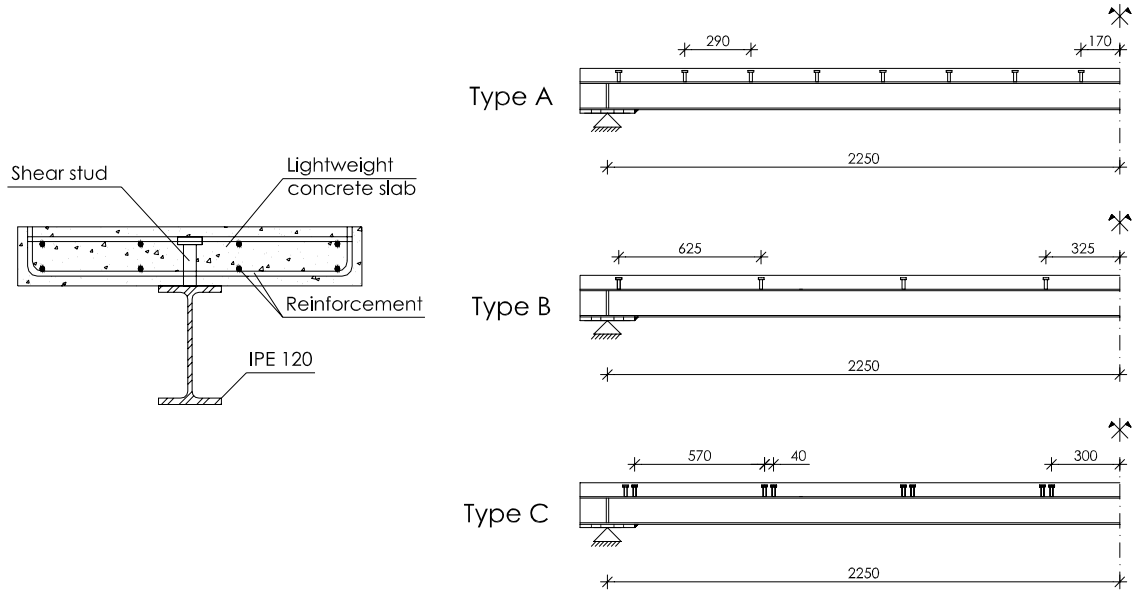

a) Cross section b) Stud distribution types

Figure 5.2 – Cross section and stud distribution types

The number of shear connectors disposed in beams designed for total connection is the minimum that guarantees the maximum axial force that is possible to mobilize either at the steel or the concrete section (depending on the position of the plastic neutral axis).

5.3.3 Load distribution

Two load configurations were considered for the tests. The first corresponds to four concentrated loads, equally spaced of 900 mm along the beam, approximating a uniformly distributed loading. The second case corresponds to two concentrated loads closely spaced, near the beam mid span, approximating a concentrated loading. The beams structural schemes for Loading 1 and Loading 2 cases are presented in Figure 5.3 and Figure 5.4, respectively.

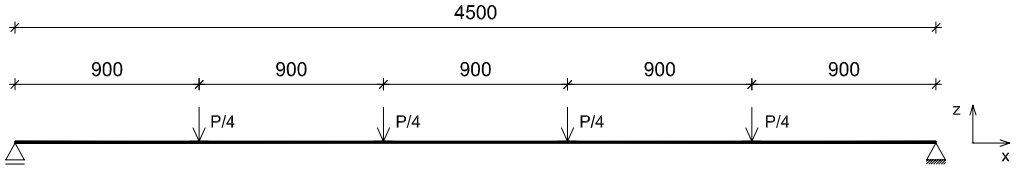

Figure 5.3 – Loading 1 structural scheme

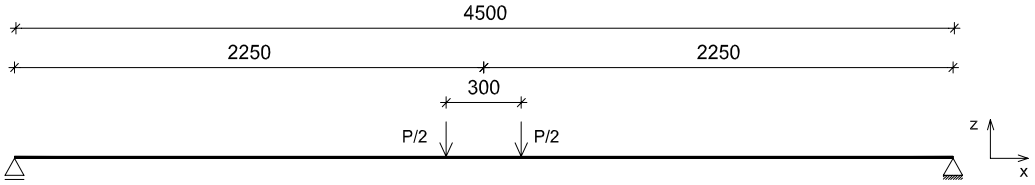

Figure 5.4 – Loading 2 structural scheme

These load configurations result in different forms of the bending moment and the shear force diagram, as presented in Figure 5.5. The longitudinal shear force diagram, at the connection interface level, is similar to the vertical shear force diagram with a difference of scale. The difference between the diagrams that result from the two loading cases is an important issue for the beams' analysis and is established as one of the parameters in study.

a) Loading distribution 1

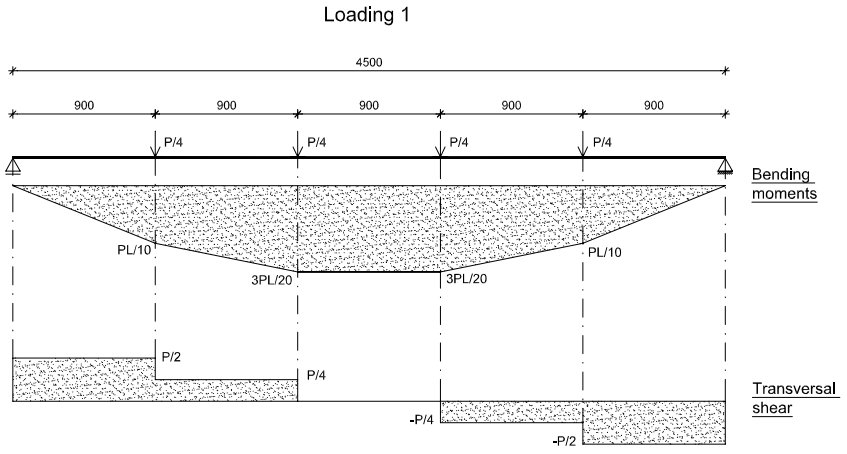

b) Loading distribution 2

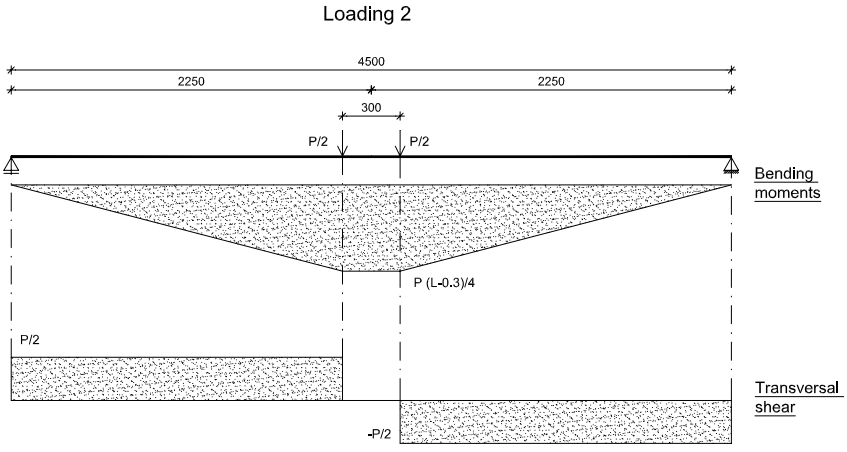

Figure 5.5 – Loading and corresponding bending moment and shear force diagrams

Table 5.2 resumes each beam's loading and stud distribution, according to the dispositions of Table 5.1.

Table 5.2 – Stud connectors' distribution

Beam	Test date	Stud distribution	Loading
VM4	06-02-04	Type A	Loading 1
VM5	18-02-04	Type C	Loading 1
VM6	10-02-04	Type B	Loading 1
VM7	05-04-04	Type A	Loading 2
VM3	13-04-04	Type C	Loading 2
VM8	16-04-04	Type B	Loading 2

5.4. Materials characterization

Experimental testing was done to analyse the properties of the materials in use. Some properties were identified as more influent and representative of the beams' behaviour and then subjected to testing (see Figure 5.6).

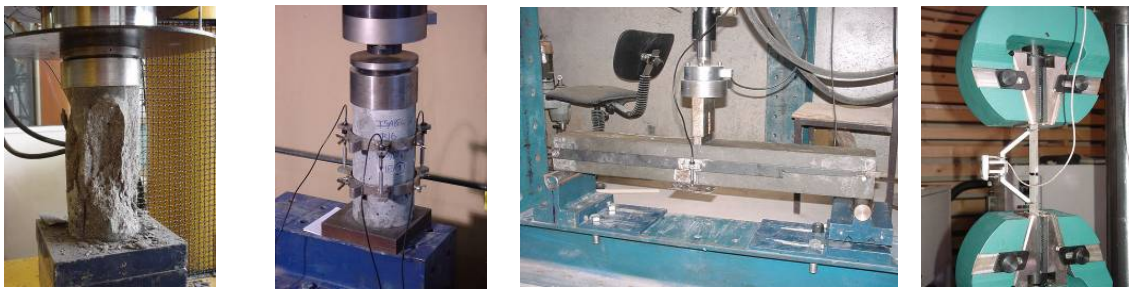

a) Concrete compressive strength test

b) Concrete modulus of elasticity test

c) Concrete tensile strength test

d) Steel tensile strength test

Figure 5.6 – Materials testing

The values for the tested materials properties are presented in Table 5.3.

Table 5.3 – Compressive strength and modulus of elasticity for the HSLWC used in beams

Concrete Ref.	Casting date	Test date	Beam	Concrete density (kg/m^3)	Compressive strength f_{lcm} (MPa)	Modulus of elasticity E_{lcm} (GPa)
BL33	16-12-03	05-02-04	VM4	1791	55.60	22.08
BL32	12-12-03	16-02-04	VM5	1855	64.40	25.00
BL34	19-12-03	12-02-04	VM6	1804	54.72	23.82
BL38	05-03-04	06-04-04	VM7	1801	58.36	22.00
BL37	27-02-04	14-04-04	VM3	1797	60.49	22.02
BL39	12-03-04	14-04-04	VM8	1800	58.16	22.23

The concrete specimens were produced at the same time as the corresponding beam and later tested at the same date of the beam test. The medium values presented for each property corresponds to the average result of three specimens' tests.

The same concrete mixture was used for every beam, but as they were cast in different dates, one at a time, slight variations on the concrete properties were expected and later verified during testing. However, this differences are very small and therefore, a direct comparison of results is accepted.

The specimens used to determine the concrete tensile strength were cast at a different time of the beams, as there was not sufficient concrete quantity to cast the corresponding specimens for every beam. The compressive strength and modulus of elasticity values measured for BL42 and BL43 are similar to the ones obtained for the beams concrete and therefore, the tensile strength and fracture energy values are considered valid for the beams analysis (Table 5.4).

Table 5.4 – Flexural tensile strength and fracture energy for the HSLWC used in beams

Concrete Ref.	Casting date	Test date	Age	Compressive strength f_{lcm}	Modulus of elasticity E_{lcm}	Tensile strength f_{lt}	Fracture energy G_{Fm}
			(days)	(MPa)	(GPa)	(MPa)	
BL42	24-03-2004	31-03-2004	7	56.43	21.63	4.26	68.02
BL42	24-03-2004	21-04-2004	28	59.54	23.17	4.16	-
BL43	05-05-2004	03-06-2004	28	59.07	22.34	3.84	78.42

Specimens were cut from the reinforcement bars and from the tested steel beams, in order to characterize the steel tensile properties. These last specimens were cut from the steel profile web, near the supports region. The specimens' size and the tensile test procedure follow the disposition defined in EN 10002-1 (2001). Table 5.5 shows the obtained results on tests performed on steel profile and reinforcement specimens.

Table 5.5 – Mechanical properties of the steel profile and reinforcement

Type of specimen	Cross section (mm^2)	f_y (MPa)	f_u (MPa)
Steel (cut from the steel section)	19.6×5	335.7	491.1
Reinforcement	ϕ5	583.4	606.1

Due to the small size of the headed studs used (13 mm diameter and 50 mm height), no experimental testing was done on the steel properties of these connecting devices. Considering the values of steel tensile properties determined in specimens cut from studs of 19, 22 and 25 mm, presented in Table 3.2, of Chapter 3, an average value of yielding strength, f_y = 450 MPa, and ultimate strength, f_u = 550 MPa, is considered in the following analysis.

5.5. Composite beams design

5.5.1 Ultimate strength

The flexural strength of steel and concrete composite beams in buildings is normally derived from standard rigid-plastic equilibrium analysis is of the forces across a section. This analysis assumes that the three materials components of the composite beam (steel, concrete and shear connectors) have unlimited ductility, and hence that each can reach and maintain their plastic or yield strengths. Concrete is assumed to have zero tensile strength and equivalent compressive yield strength of about 85% of the cylinder strength and steel is assumed to be fully yielded, (Oehlers and Sved 1995). The resisting bending moment value depends on the neutral axis position.

It is generally assumed that the steel section resists the shear stress. Bending moment and vertical shear interaction is considered on cross sections over the supports of continuous beams or on cross sections under concentrated loads, when acting shear stress is higher than 50% of the steel resisting shear stress.

Horizontal shear results from the longitudinal force that exists at the steel to concrete slab interface. It is resisted by steel shear connecting devices.

Other important verification to consider is the number, flexibility and disposition of the shear connection devices. If the total number of connectors used is not sufficient to transmit all the calculated shear stress, the beam failure occurs by shear and therefore, bending moment at failure is smaller than the predicted maximum plastic bending moment. On the other hand, the connectors' deformability alters the internal distribution of stress between steel and concrete. As a consequence, the beams' stiffness is diminished, resulting in larger vertical deformation.

When the structure is continuous, there is the possibility of stress redistribution. This redistribution results in a stress transfer from the critical section to other cross sections. In this case, certain characteristics are needed, such as enough rotation capacity that results from the cross section typology and dimensions, and the materials behaviour. In a composite cross section, there is also the possibility of stress transfer between the steel and concrete section, provided that the connection has the capacity to suffer deformation.

5.5.2 Cross section classification

The beam behaviour at failure depends on its capacity to develop plastic strains. In order to decide if the cross section has the ability to develop the plastic behaviour, EN 1994-1-1, (CEN 2004b), classifies steel sections into four classes, depending on the local buckling behaviour of the flange and/or web in compression and on the material properties. In the

case of a simply supported single span beam, plastic design methods may be used for Class 1 and 2 sections. Sections of Class 2 are only allowed when no rotation capacity is required. Class 1 classification considers plastic cross-sections that can form a plastic hinge with sufficient rotation capacity for plastic analysis and Class 2 classification considers compact cross-sections, which can develop the plastic moment but have limited rotation capacity. The steel compression flange, if properly attached to the concrete flange, may be assumed to be of Class 1. If the section is classified as Class 3, elastic design should be considered. Composite cross sections of Class 3 have always a slender web, because if the compressed flange is properly connected to the concrete slab, it is always classified as Class 1 or 2.

Table 5.6 resumes the necessary conditions to classify the cross section.

Table 5.6 – Composite cross section classification (EN 1994-1-1)

	Profile flange classification	Profile web classification
Class 1	$c / t_f \leq 9\varepsilon$	$d / t_w \leq 72\varepsilon$
Class 2	$c / t_f \leq 10\varepsilon$	$d / t_w \leq 83\varepsilon$
Class 3	$c / t_f \leq 14\varepsilon$	$d / t_w \leq 124\varepsilon$

The parameters used in Table 5.6 are defined with equations (5.1), (5.2) and (5.3), considering the dimensions presented in Figure 5.7.

$$c = \frac{b - t_w - 2r}{2} \tag{5.1}$$

$$d = h - 2t_f - 2r \tag{5.2}$$

$$\varepsilon = \sqrt{\frac{235}{f_y}} \tag{5.3}$$

For the steel section, a laminated profile of type IPE was chosen, with the geometrical and mechanical characteristics presented in Figure 5.7.

b = 64 mm
h = 120 mm
t_w = 4.4 mm
t_f = 6.3 mm
d = 93.4 mm
r = 7 mm
A_a = 13.21 cm^2 (cross section area)
I_y = 317.8 cm^4 (second moment of area)
W_{pl} = 60.73 cm^3 (plastic bending modulus)
W_{el} = 52.96 cm^3 (elastic bending modulus)

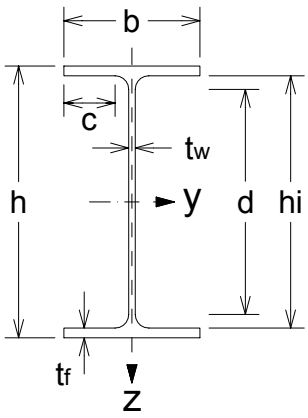

Figure 5.7 – Steel profile: geometrical and mechanical characteristics

As referred before, the cross section classification is important in order to establish the type of analysis to be considered for the cross section design (consider $\varepsilon = \sqrt{235/335.7}$ = 0.837). This section is classified as Class 1.

Flange classification: c = 22.8 mm; c/t_f = 22.8 / 6.3 = 3.62 < 9 × 0.837 $\Rightarrow$ Class 1

Web classification: d = 93.4 mm; d/t_w = 93.4 / 4.4 = 21.23 < 72 × 0.837 $\Rightarrow$ Class 1

5.5.3 Bending

There are three possible situations in terms of the neutral axis position, for bending failure of a composite beam submitted to sagging bending moments, when plastic behaviour is considered. The neutral axis can be positioned on the concrete slab, on the steel profile upper flange or on the steel profile web. Table 5.7 defines the necessary conditions to establish the cross section neutral axis position and the corresponding resisting bending moment.

Table 5.7 – Composite section under sagging moment: neutral axis position and resisting moment

	1)	2)	3)
Description	Neutral axis positioned on the concrete slab	Neutral axis positioned on the steel profile upper flange	Neutral axis positioned on the steel profile web
Condition	$N_c > N_{pla}$	$N_{pla} - N_c < 2\ b_f\ t_f\ f_y$	$N_{pla} - N_c > 2\ b_f\ t_f\ f_y$
Axial forces	$F_c = b_{eff}\ z\ \alpha\ f_{lcm}$ $F_a = N_{pla}$	$N_1 = b_f\ (z - h_c - h_p)\ f_y$ $F_c = N_c + N_1$ $F_a = N_{pla} - N_1$	$N_2 = z_w\ t_w\ f_y$ $F_c = N_c + N_{pla} / 2 - N_2$ $F_a = N_{pla} / 2 + N_2$
Neutral axis position	$z = F_a / (b^+_{eff}\ \alpha\ f_{lcm})$ $(x < h_c)$	$N_c + 2\ N_1 - N_{pla} = 0$ $(z > h_c)$	$z_w = N_2 / (t_w\ f_y)$ $z = h_a / 2 + h_p + h_c - z_w$
Resisting moment	$M^+_{pl.R}$ = $= N_{pla}\ (0.5h_a + h_c + h_p - 0.5z)$	$M^+_{pl.R}$ = $= N_{pla}\ (0.5h_a + h_p + 0.5h_c)$ $- 0.5\ (N_{pla} - N_c)\ (z + h_p)$	$M^+_{pl.R}$ = $= M_{apl.R} + N_c\ (0.5h_a + h_p + 0.5h_c) -$ $0.5\ N_c\ z_w$
Stress diagram	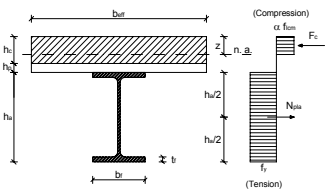	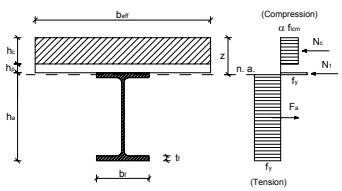	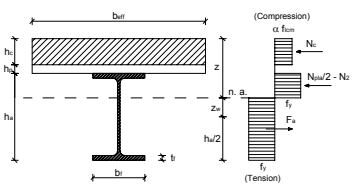

N_c, N_{pla}, and $M_{apl,R}$ are defined with equations (5.4), (5.5), and (5.6) respectively.

$$N_c = b_{eff} \cdot h_c \cdot \alpha \cdot f_{lcm} \tag{5.4}$$

$$N_{pla} = A_a \cdot f_y \tag{5.5}$$

$$M_{apl,R} = W_{a,pl} \cdot f_y \tag{5.6}$$

The three situations described in Table 5.7 are valid when the beams are designed for total connection, which means that the total number of connectors disposed is enough to prevent failure at the interface between the steel profile and the concrete section. In this case, failure occurs either on the steel section or on the concrete section.

For a total connection design, the number of connectors used should be at least equal to the number of calculated connectors. If the number of used connectors is smaller than the number of calculated connectors, then a partial connection is obtained. EN 1994-1-1, (CEN 2004b), defines a minimum number of shear studs if a partial shear connection is intended, depending on the beam length and on the cross section properties.

The partial connection design admits that only part of the total shear stress is resisted with shear connectors. The resisting bending moment, M_R, is inferior to the composite section resisting bending moment, $M_{pl,R}$, considering a total connection. The degree of shear connection is defined by the ratio N/N_f, where N_f corresponds to the number of shear connectors disposed between two critical sections and calculated for a total connection design and N corresponds to the number of shear connectors in fact disposed.

The reduction on the resisting bending moment can be calculated according to equation (5.7), which is a simplified way to calculate M_R,

$$M_R = M_{apl,R} + (M_{pl,R} - M_{apl,R}) \times \frac{N}{N_f} \tag{5.7}$$

where,

$M_{apl,R}$ – steel section resisting bending moment

$M_{pl,R}$ – total section resisting bending moment, considering total connection

M_R, can be more exactly calculated with equation (5.8),

$$M_R = F_a \times (h_a/2 + h_c + h_p - z''/2) - (F_c - V_f) \times (h_c + h_p - z''/2 + z'/2) \tag{5.8}$$

where,

V_f – shear force transferred with N shear connectors disposed at the steel to concrete interface

$z'' = V_f / (0.85\, f_{cm}\, b_{eff})$ – neutral axis position on the concrete slab, measured from the top fibbers of the concrete slab;

$z' = (F_c - V_f) / (2\, f_y\, b_f)$ – neutral axis position, on the steel beam flange, measured from the top fibbers of the steel beam;

At failure, the total plastic behaviour of the composite cross section is accepted, as it is classified of class 1. Beams VM4, VM5, VM7 and VM3 are designed for total connection and fit situation 1) described in Table 5.7. The material properties needed for that calculation are presented in Table 5.3.

In the case of partial connection design, shear connection failure is admitted, resulting in an inferior value for the maximum bending moment. Beams VM6 and VM8 correspond to this last situation. The predicted values for maximum sagging resisting bending moment ($M^{+}_{pl,R}$) are presented in Table 5.8.

The total slab width is considered as effective for the calculation of the compressive force N_c on the concrete slab: b_{eff} = 350mm.

V_{f} is calculated considering the average maximum force measured in the push-out tests presented in Chapter 4 (see Table 4.7). Therefore, for partial connection it is considered that,

$V_{\text{f}} = 55.0 \times 4 = 220$ kN

Table 5.8 – Predicted maximum bending moments

Concrete Ref. / Beam	Connection	N_c (equation (5.4))	N_{pla} (equation (5.5))	V_f	Neutral axis position	z	z'	$M^{+}_{pl.R}$	ε_y
		(kN)	(kN)	(kN)		(m)	(m)	(kN.m)	(mm/m)
BL33/VM4	Total	992.46	443.46	min (N_c, N_{pla})	Concrete slab	0.0268	-	47.27	20.00
BL32/VM5	Total	1149.54		min (N_c, N_{pla})	Concrete slab	0.0231	-	48.08	23.72
BL34/VM6	Partial	976.75		220	Concrete slab and steel flange	-	0.0052	37.74	29.73
BL38/VM7	Total	1041.73	443.46	min (N_c, N_{pla})	Concrete slab	0.0255	-	47.55	21.17
BL37/VM3	Total	1079.75		min (N_c, N_{pla})	Concrete slab	0.0246	-	47.75	22.07
BL39/VM8	Partial	1038.16		220	Concrete slab and steel flange	-	0.0058	37.83	31.60

where,

N_c – maximum compressive force that can be mobilized at the concrete section;

N_{pla} – maximum tensile force that can be mobilized at the steel section;

z – neutral axis position, as represented in Table 5.7;

z' – distance between the steel upper fibber and the steel section neutral axis position (for partial connection).

5.5.4 Shear connection

Shear connecting devices and transversal reinforcement on the concrete slab are designed to transfer the longitudinal shear forces mobilized at the composite beam between the concrete slab and the steel profile. The number of shear connectors is calculated between

two near maximum bending moment cross sections. If a plastic design is possible, the shear force value that is considered for the shear connectors' design is the minimum value chosen between N_c and N_{pla}.

Each connector average load capacity was experimentally determined and is presented in Chapter 4. An average load capacity of 55 kN was obtained. This value is now used for the analysis of the beam connection. For a total connection, the number of shear connectors to be disposed in half span of the beam corresponds to the minimum value chosen between N_c and N_{pla}, divided by the shear connector load capacity. Therefore, the total number of shear connectors to be disposed in half span of the composite beam is 8.

According to EN 1994-1-1 (CEN 2004b), headed studs with an overall length after welding not less than 4 times the diameter, and with a shank of nominal diameter not less than 16 mm and not greater than 25 mm, may be considered as ductile, within some limits for the degree of shear connection. The degree of shear connection is defined by the ratio N/N_f. If the cross section is composed by a steel profile with equal flanges, the following conditions are defined by equation (5.9), if the beam length is less or equal to 25m,

$$N / N_f = 1 - (355 / f_y)\,(0.75 - 0.03\,L_e) \quad \wedge \quad N / N_f \geq 0.4 \tag{5.9}$$

and equation (5.10), if the beam length is superior to 25m;

$$N / N_f = 1.0 \tag{5.10}$$

where,

N – number of shear connectors disposed between two critical sections;

N_f – number of shear connectors between two critical sections calculated for a total connection design;

L_e – distance (in meters) in sagging bending between points of zero bending moment; for typical continuous beams, L_e may be assumed as defined in (CEN 2004b).

The headed studs used in the beams have 13 mm diameter and therefore, do not fulfil the conditions defined by EN 1994-1-1 to guarantee a ductile connection. However, during the static tests presented in Chapter 4, the 13 mm diameter studs presented a ductile behaviour. Therefore, the conditions referred will be considered to define the minimum degree of partial connection for some of the composite beams:

$N / N_f = 1 - (355 / 335.7) \times (0.75 - 0.03 \times 4.5) = 0.35 \ \wedge \ N / N_f \geq 0.4.$

The minimum degree of partial connection is equal to 0.4. The degree of partial connection considered in the beams' analysis is 0.5, as the number of studs to be disposed is half of the number of studs needed for total connection.

5.5.5 Maximum acting bending moment

Two loading cases and the corresponding stress diagrams were defined in 5.3. The test is controlled with deformation, which is imposed with a constant rate. As a result, the applied loads are variable on time. The diagrams values presented in Figure 5.5 are dependent on the applied load value. Beside the load applied with the hydraulic system, other loads should be taken into account, like the beam self-weight and the weight of the test set up loading elements. The considered values are:

Concrete slab weight = $0.350 \times 0.06 \times 18.2 = 0.382$ kN/m

Steel section weight = 10.4 kg/m = $(10.4 \times 9.81)/1000 = 0.102$ kN/m

Total weight: $p = 0.102 + 0.382 = 0.484$ kN/m

For Loading 1 case, the maximum applied bending moment is given by (5.11),

$$M_{\max} = \frac{pL^2}{8} + \frac{3PL}{20} = 1.225 + 0.675\,P \tag{5.11}$$

and for Loading 2 case, the maximum applied bending moment is expressed by (5.12),

$$M_{\max} = \frac{pL^2}{8} + \frac{P(L-0.3)}{4} = 1.225 + 1.05\,P \tag{5.12}$$

where, P is the load applied by the hydraulic machine, added to the weight of steel elements that distribute the loadings.

5.5.6 Neutral axis position for elastic analysis

The initial increments of loading are done while the beam maintains its elastic properties. An important aspect is the neutral axis position considering an elastic behaviour and total interaction, presented for every beam in Table 5.9. The values presented show that it is positioned at the profile flange and that the concrete slab is totally compressed during the first steps of loading.

Table 5.9 – Neutral axis positions for elastic analysis – connection with total interaction

Concrete Ref.	Beam	E_{cm} (GPa)	E_s (GPa)	$n = E_s / E_{cm}$	y_G (m)
BL33	VM4	22.08	210	9.511	0.1163
BL32	VM5	25.00	210	8.400	0.1189
BL34	VM6	23.82	210	8.816	0.1179
BL38	VM7	22.00	210	9.545	0.1162
BL37	VM3	22.02	210	9.537	0.1163
BL39	VM8	22.23	210	9.447	0.1165

y_G – distance between the cross section lower fibber and the neutral axis position

5.6. Casting conditions

Figure 5.8a presents a scheme of the beam formwork, disposition of reinforcement and supporting elements. Figure 5.8b to Figure 5.8e present the various steps of preparation before casting.

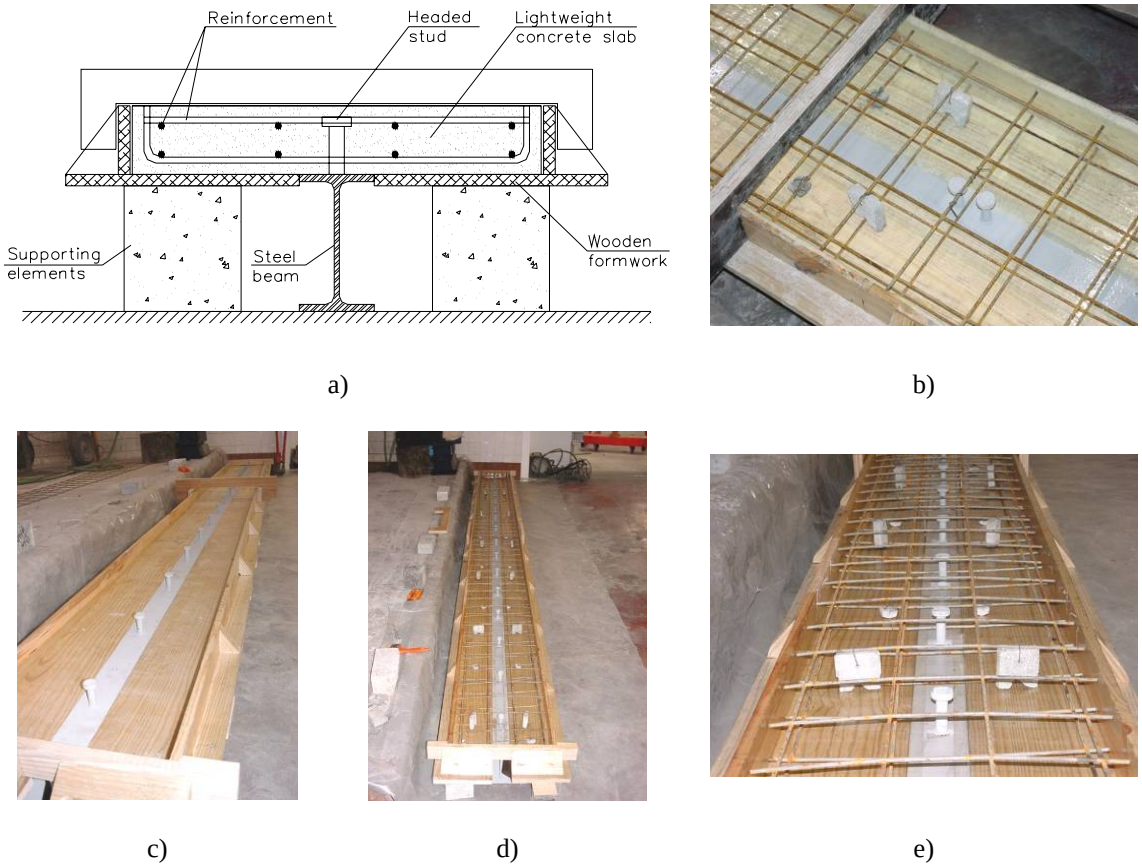

Figure 5.8 – Beams' formwork

The steel beam is laid on the floor and then the wooden formwork is positioned next to it. The wooden formwork is supported with some concrete cubes. The formwork inner surface is protected and then greased with a mould-releasing agent. The reinforcement is carefully positioned over the formwork. Some special holders are fabricated, so that the reinforcement is positioned in two layers with the proper distances between them and the slab surface. Lateral fixing elements are also added to prevent the transversal separation of the elements that constitute the formwork.

Then the beam is ready for casting. A total quantity of 120 litres is prepared for each beam and respective concrete cylinders (used for specimens to test compressive strength and modulus of elasticity).

5.7. Test dispositions

5.7.1 Test setup

Two loading configurations were chosen to study the composite beams' behaviour, as referred in 5.3. The actuator load is divided into several smaller loads to accomplish the two loading configurations, presented in Figure 5.3 and Figure 5.4. The set up is represented in Figure 5.10, as well as the final test configuration, immediately before the test begins.

The steel sections chosen to distribute the load along the beam have sufficient load capacity to avoid early failure in these secondary elements and sufficient stiffness to avoid excessive deformation that could influence the beams' behaviour. For Loading 1 case, the secondary elements are two simply supported HEA120 steel beams with 0.9m span distributing the load applied through one simply supported HEA200 steel beam with 1.8m span. This disposition, as represented in Figure 5.9, guarantees an equal division of the load applied by the load cell, if geometrical symmetry is verified. This loading disposition aims to simulate a uniformly distributed load on the beam in an approximate way.

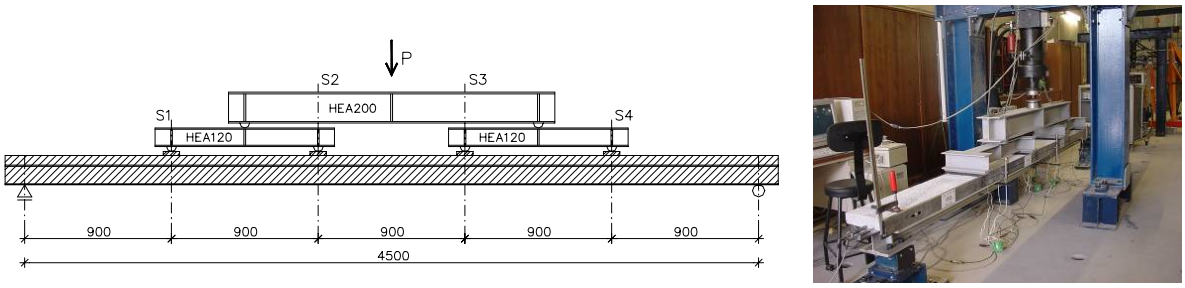

Figure 5.9 – Setup for Loading 1 distribution

For Loading 2 case, the secondary element is a steel plate that divides the load cell in two equal loads. These two loads are now closely spaced and the intention is to simulate a concentrated loading at the beam mid span (Figure 5.10).

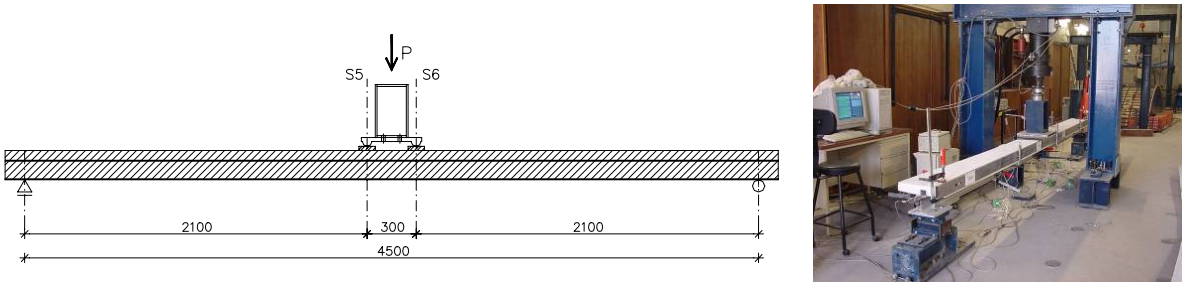

Figure 5.10 – Setup for Loading 2 distribution

The division of the load into two loads is just to avoid the concentration of stresses on the beams' mid span and the possibility of premature concrete crushing on the concrete upper fibber, avoiding complete measurements until total failure. With the chosen disposition, it is believed that better measurements will be obtained in the sensors.

All tests are carried out with measurements of applied load value, vertical deformation along the beam, slip between steel profile and concrete slab and vertical separation between these two elements. Displacement transducers V1 to V3 measure the beam vertical deformation (see Figure 5.11, a) and b)) and displacement transducers H1 and H2 measure slip between the steel beam and the LWC slab (see Figure 5.11, b) and c)).

a) Vertical deformation at the beam mid span and vertical separation between the steel and the concrete sections

b) Vertical deformation along the beam

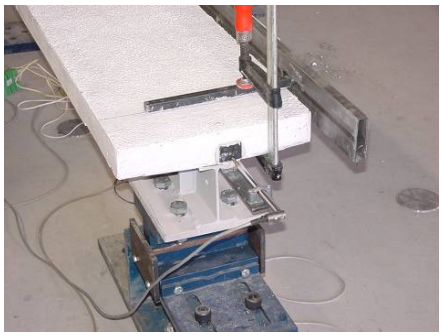

c) End-slip between the steel and the concrete sections

d) Slip between the steel and the concrete section, measured near the supports

Figure 5.11 – Displacement transducers

The tests are performed with deformation control. The deformation is controlled in the beam mid span with V2, but other points of deformation are also measured during loading, like V1 and V3.

Strain gauges are positioned in representative transversal sections in order to measure strain and curvature variation during the tests. They are positioned in three different cross sections, defined from left to right as Cross section A-A' in the first quarter of the beam (1.065m), Cross section B-B' in the beam mid span (2.250m) and Cross section C-C' in the third quarter of the beam (3.435m), as presented in Figure 5.12.

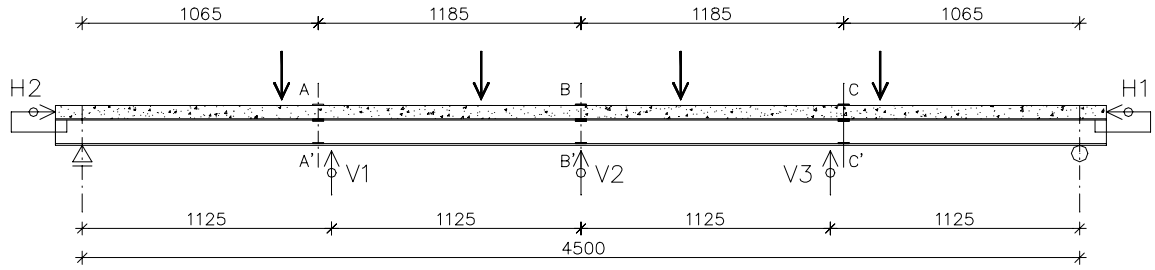

Figure 5.12 – Monitoring and control of testing

In the cross section, the strain gauges are located both on the upper and bottom fibber of the concrete slab and on the inner extreme fibbers of the steel section (see Figure 5.13).

As represented in Figure 5.13, two strain gauges are positioned in the same fibber level. The mean value of these two devices is considered for the measured strain at that fibber, unless one of the gauges suffers failure or damage during testing.

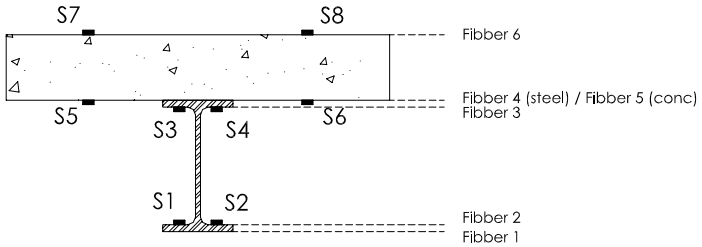

S_i – strain gauge numbering

S_1 to S_4 – strain gauges on steel: TML FLA-5-11

S_5 to S_8 – strain gauges on concrete: TML PFL-30-11

Figure 5.13 – Strain gauges disposition at the cross section

All the devices are connected to an acquisition system that insures the periodic reading and saving of all measured values, including the applied loading. In this way, the recorded data can be analysed in any time.

Figure 5.14 shows the load actuator and the spherical seat that is positioned between this device and the steel beams used to distribute the load along the composite beam. This element acts as a hinge because it allows the rotation in all directions and ensures that the actuator is not fixing the steel beam, giving it freedom to adapt to the composite beam.

Figure 5.14 – Spherical seat acting as a hinge

Figure 5.15 shows the metallic bar used to support the LVDT's that measure the beams' vertical deformation. This bar is as long as the composite beam and is fixed exactly over the beams' supports so that the measurements do not account the supports adjustments (see Figure 5.11.a/b). The bar is rigidly fixed to the supports. Rotation in both sides and horizontal sliding in one side are permitted. The displacement transducers are positioned as presented in Figure 5.12.

Figure 5.15 – Metallic bar to support the vertical transducers

Some other aspects of the tests' setup can be referred. The beams supports are materialized with two hinges that allow the support rotation around the *y-y* axis (see Figure 5.7). Teflon sheeting is positioned on one support to allow its sliding along *x-x*. This material is also used to guarantee the free rotation over the supports (see Figure 5.16.b).

a) b)

Figure 5.16 – Beams supports

The lateral steel plates, that are visible in Figure 5.16, were disposed to avoid an eventual lateral displacement of the beams, over the supports.

5.7.2 Test procedure

The beams' tests are divided in four steps. The first step consists on a cyclic loading, varying 25 times the applied load between 2 and 15 kN. These cycles are done with a rate of 0.5 kN/s, resulting in a total of 20 minutes for this stage. The next step consists on applying a constantly increasing load from 2 to 20 kN. At the end of this, the test control changes to deformation, setting a linear increase of 0.02 mm/s in the beams mid span deformation. This step ends when a total increase of 70 mm is attained. The last step consists on taking the beams to failure, at a constant mid span deformation rate of 0.05 mm/s.

Table 5.10 – Test procedure

Step	V_1	V_2	V_3	V_4
Control	force	force	deformation	deformation
Type of loading	cyclic	linear	linear	linear
Number of cycles	25	-	-	-
Velocity	0.5 kN/s (increasing and decreasing)	0.2 kN/s	0.02 mm/s	0.05 mm/s
Lower limit	2 kN (absolute)	2 kN (absolute)	-	-
Upper limit	15 kN (absolute)	20 kN (absolute)	70 mm (relative)	Until failure
Duration	21 m 40 s	90 seconds	58 m 20 s	Until failure

5.8. Observed behaviour during tests and failure modes

The beam tests lead all the specimens to failure, and different types of collapse are observed. Two types of failure were found: bending failure with concrete crushing on the slab top fibbers and connection failure with shear failure of part of the connectors. A brief description on the beams' failure modes is given, with particular emphasis on the identification of these two failure types: bending failure and shear failure.

5.8.1 VM4

Beam VM4 shows a bending failure. Concrete crushes near the load application point at section S3. At the same time, concrete crushing initiates in the upper fibre near position S2. This occurs while a longitudinal crack at the concrete section mid height grows towards the beam mid span (Figure 5.17).

Figure 5.17 – VM4 at failure

5.8.2 VM5

Beam VM5 also shows a bending failure. Concrete crushes near the load point application at section S2. At the same time, concrete crushing initiates in the upper fibre, near position S3. VM5 failure is very similar to VM4 failure (Figure 5.18).

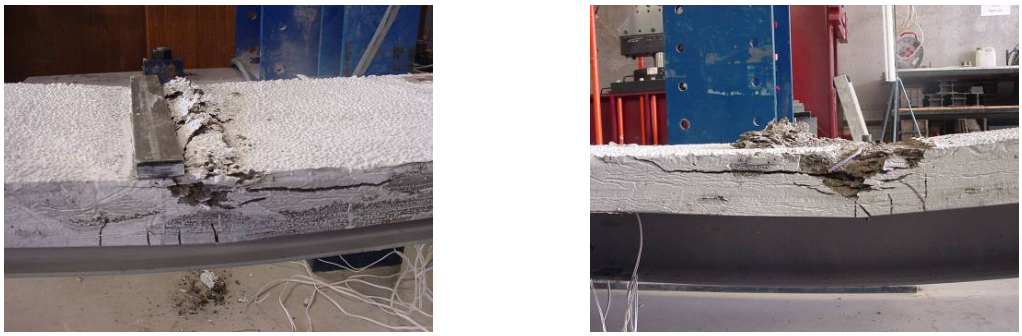

Figure 5.18 – VM5 at failure

5.8.3 VM6

Different from the previous beams, VM6 has a shear connection failure between the concrete slab and the steel beam.

Figure 5.19 – VM6 at failure

Connector failures are phased, with load capacity losses associated. Important slip between the steel section and the concrete slab is verified during testing, finally provoking the beam failure. This failure happens essentially in one side of the beam and vertical separation between steel and the concrete sections is visible near the support (Figure 5.19).

5.8.4 VM7

Beam VM7 suffers a bending failure. Concrete crushes near the load point application at section S5, with a longitudinal crack at the concrete section mid height, growing towards the beam mid span (Figure 5.20). The slab reinforcement near the crushing zone shows some local buckling (Figure 5.20).

Figure 5.20 – VM7 at failure

5.8.5 VM3

Beam VM3 shows a bending failure. Concrete crushes near the load point application at section S5 (Figure 5.21a), with a longitudinal crack at the concrete section mid height, growing towards the nearest support (Figure 5.21b). Some longitudinal cracks are observed on the concrete slab upper face. These cracks are coincident with the double studs' positions and they are 15 to 20 cm long (Figure 5.21c).

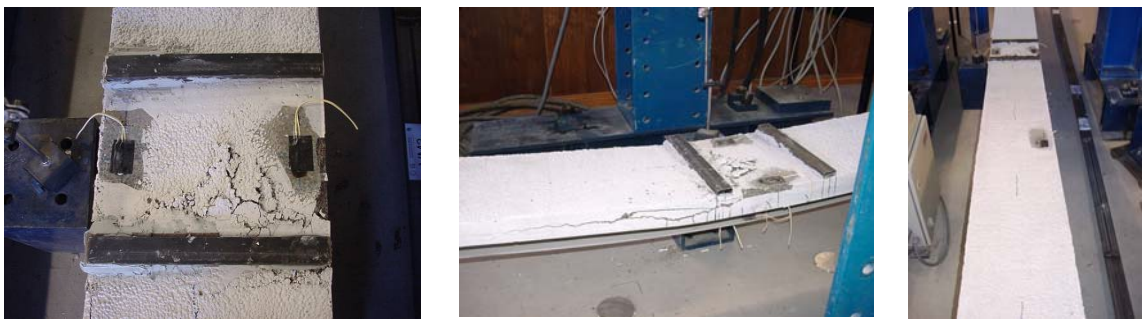

a) b) c)

Figure 5.21 – VM3 at failure

5.8.6 VM8

VM8 suffers bending failure associated with shear connection failure (Figure 5.22). Concrete crushing takes place at the upper fibre of both sections S5 and S6. The first to occur is in the proximity of section S5. At the final stages of loading, stud failure takes place in association with load capacity loss.

Figure 5.22 – VM8 at failure

In all tested beams tensile cracks appear closely and similarly spaced at the bottom face of the concrete slab, along the failure zone (Figure 17). Horizontal slip between steel profile and concrete slab is always visible (Figure 17).

Figure 5.23 – Distributed cracking and slip

5.9. Test results

5.9.1 Bending moment and vertical deflection

Table 5.11 presents the values of maximum bending moment and correspondent vertical deflection, measured experimentally.

All beams designed for total connection (VM4, VM5, VM7 and VM3) present similar results for maximum applied bending moment, varying from a minimum of 47.52 kNm to a maximum of 52.60 kNm. The maximum bending moment value for beams designed for partial connection (VM6 and VM8) is always lower.

The difference of maximum bending moment between VM4 and VM5 (Loading distribution 1) probably reflects a worse connection efficiency of VM5 that results from a less efficient capacity to redistribute the stress between the steel and the concrete sections, when one of them reaches its limit capacity.

For Loading distribution 2, the maximum bending moment is very similar for the beams of Type A and Type C (VM7 and VM3). In this case, the connectors' distribution does not affect the stress redistribution, as probably happened for the beams submitted to Loading distribution 1.

Table 5.11 – Maximum bending moment and corresponding vertical deformation (at mid span)

Concrete Ref.	Beam	Connectors distribution	Failure type	M_{max} (kNm)	$d_{z,mid\ span}$ (M_{max}) (mm)
BL33	VM4	Type A	Bending	52.60	161.5 to 170.1
BL32	VM5	Type C	Bending	47.52	172.9 to 195.4
BL34	VM6	Type B	Shear connection	41.96	146.6 to 154.3
BL38	VM7	Type A	Bending	50.10	124.2 to 130.9
BL37	VM3	Type C	Bending	49.76	157.1 to 180.4
BL39	VM8	Type B	Bending & shear connection	44.51	236.1 to 244.9

The comparison between Table 5.8 and Table 5.11 puts in evidence some differences between measured and predicted bending moment values. Measured values are always higher than the predicted values (with the exception of VM5). The same was observed by Nie et al. (2004) in experimental tests performed on composite beams with high strength concrete slab. The difference can result from steel tensile strength, as higher values than the yield tensile strength can be attained in the steel section. Another possibility is a small deviation in the concrete slab dimensions, despite the efforts to make every slab similar, as was in general confirmed.

For partial connection design beams, the difference between measured and predicted maximum bending moments can result from underestimating the studs deformability, as it results in a decrease of shear stress flow through steel and concrete interface, retarding failure because the value of the shear force acting in each connector is smaller than predicted.

Figure 5.24 presents the diagrams of bending moment vs. vertical deflection, both experimentally measured at the beams mid span. Elastic behaviour is observable for both types of loading (Loading case 1 and Loading case 2), at the initial phase of the test, as there is an approximately linear relation between the bending moment value and the deflection value. This was of course expected, because all the materials used in the beams

– lightweight concrete, steel, reinforcement steel and connectors steel – proved to have an initial elastic behaviour in all tests carried out to characterize them.

In Chapter 3, a comparison was made on the evolution of the connection stiffness for the various diameters of studs that were tested. The values of stiffness measured show that the stiffness value is not much influenced by the change of the stud diameter. In Chapter 4, this analysis was repeated for the 13 mm diameter studs and the tendency was confirmed, as the result values obtained were only slightly inferior (see Table 4.8 and Figure 4.18 from Chapter 4).

The diagrams plotted in Chapter 3 show that the initial phase of the load-slip curve is similar for specimens with studs of 19 mm diameter, both for single and double stud disposition. It was also observed for the same specimens, that the average value of stiffness, measured at different load values, is very similar, although some higher variability was associated with the stiffness values measured for the tests performed with the double stud disposition. Considering this aspect on the analysis of composite beams, it could be expected that both beams of Type A and Type C would have very close deformation diagrams for the initial phase of loading because the connectors' disposition is the only parameter varied between them.

During the tests, the Type A beams (total connection – beams VM4 and VM7) show higher stiffness than the Type C beams (total connection and studs grouped in pairs - beamsVM5 and VM3). As the same number of identical shear connectors was disposed in these two types of beams, the stiffness measured for both beams at the initial phase of loading should be the same. However, this is not the case and the higher stiffness measured for the beams with equally spaced studs can only result from some loss of efficacy on the transmission of shear forces when the studs are very closely spaced. This means that one of the two studs grouped is receiving a higher load than the other. This result may indicate that the connectors' distribution along the beam affects not only its behaviour at failure, but also influences its response for service loadings.

All beams present a very ductile behaviour, both for total and for partial connection design, because there is significant vertical deformation developed, while the maximum bending moment is kept almost constant (see Figure 5.24). Therefore, the values of vertical deformation for maximum bending moment are expressed in terms of an interval (see Table 5.11).

A second important aspect when comparing Type A and Type C beams is the higher deformation capacity, at failure, for the second group of beams. For the beams designed for total connection and submitted to the Loading distribution 1, the vertical deformation correspondent to the maximum measured bending moment is slightly higher for the double stud disposition. However, the maximum load applied is higher for the single stud

disposition. The same beams, now submitted to the Loading 2 group, present a maximum bending moment that is very similar for both total connection beams, but the corresponding maximum vertical deformation is higher for VM3 (double stud disposition).

In resume, for beams of Type C, failure is attained at a lower load level than for beams of Type A, but in both load cases the corresponding maximum vertical deformation is higher.

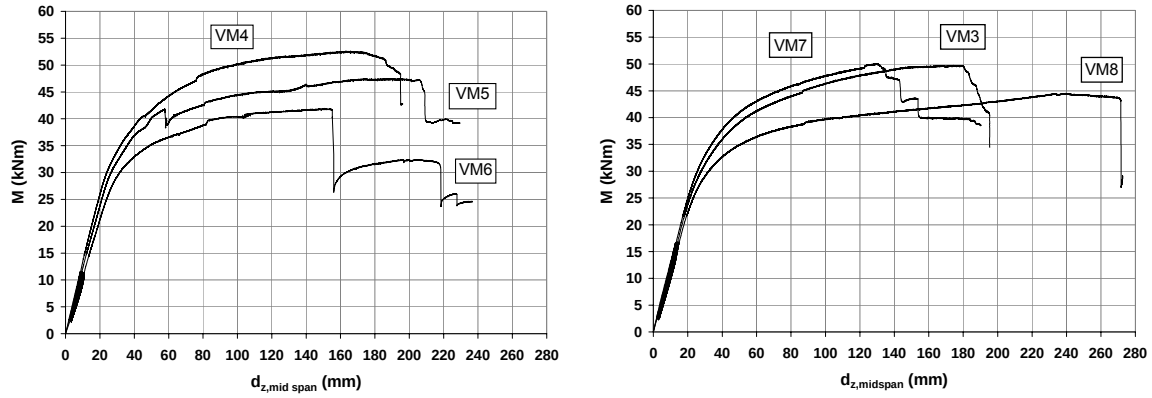

a) Loading case 1 b) Loading case 2

Figure 5.24 – Maximum bending moment vs. vertical deformation (at mid span)

The push-out tests presented in Chapter 3 for 19 mm diameter double stud disposition showed a loss of the shear connection load capacity when compared to the single stud disposition. This loss of load capacity would only be recognized in the Type C beams ultimate load if they were designed for partial connection. As beams of Type A and Type C were designed for total connection and therefore suffered bending failure, the difference of load capacity between the two different stud dispositions should be small. The same push-out tests showed that the single and the double stud disposition result in a similarly stiff connection for the initial phase of loading, when the load-slip relation is linear. The double stud disposition results in a less stiff connection for high loads, as higher slip values occur for the same load level. This loss of stiffness can influence the beams' behaviour, by inducing higher vertical deformability of Type C beams, as there is loss of composite action. The two pair of curves, VM4 and VM5 presented in Figure 5.24a and VM7 and VM3 presented in Figure 5.24b, show that the two curves are similar at the initial phase of loading, although the Type A disposition is always a bit stiffer. At the final phase of loading, the curves drift apart and the Type C beams are less stiff. It can be concluded that these results are in agreement with the ones observed for the push-out tests.

A loss of stiffness is verified at each tested specimen for values over 0.45 M_{max}. A change in the beams behaviour is noticeable for higher stresses than 0.45 M_{max}, as the

increase in load values is now smaller while deformation keeps the same growing rate (the tests are controlled by deformation at the beam mid span, as referred in 5.7.2).

The Type B beams (designed for partial connection - VM6 and VM8) show lower stiffness, when compared to all other beams, as they present larger vertical deformation for the same load level. This aspect is more or less observable since the beginning of loading and was expected because less shear studs result in more load applied to each connector, which results in higher deformation at the steel to concrete interface, for the same total load applied to the beam. The connection is more flexible, which results in a less stiff beam.

The beams load capacity is conditioned by the connection, as the studs suffer shear failure. The studs' failure is identified, in Figure 5.24, for beam VM6, with localized load losses. For beam VM8, the shear connectors' failure is coincident with the crushing of the concrete slab.

Figure 5.25 presents the comparison between bending moment and vertical deformation measured at the beams' mid span, established for two identical beams, one subjected to Loading case 1 and the other to Loading case 2. The bending moment diagrams of Loading cases 1 and 2 are generically presented in Figure 5.5. These bending moment diagrams are not equal if the same value of maximum bending moment is considered in the two beams. In this case, the deformation measured at the beam mid span should be higher for Loading case1 than for Loading case 2, because the corresponding bending moment diagram has more area. This hypothesis is valid when the beams are behaving elastically. In fact, there is almost no difference between diagrams at elastic phase of behaviour, as all pairs of beams show the same relation between bending moment and deflection at mid span.

When the bending moment value is higher than 40 kNm, for the pair of Type A beams, the vertical deformation is higher for beam VM7. However, beam VM4 achieves both higher vertical deformation and higher maximum bending moment (Figure 5.25.a).

Again, for the pair of Type C beams, the two curves stop being coincident when the bending moment value is approximately equal to 40 kNm. The maximum bending moment value is higher for beam VM3, but the maximum deformation is higher for beam VM5 (see Figure 5.25.b).

Some of the differences observed can result from minor characteristics of the composite beams, which can influence their total behaviour. However, a common characteristic can be appointed, which is the higher vertical deformation for maximum load suffered by the beams submitted to Loading case 1.

The diagrams for the pair of Type B beams, VM6 and VM8, show a very similar evolution, (Figure 5.25c). When a beam of class 1 is designed for partial connection, the number of shear connectors to be disposed is defined in function of the maximum bending moment and the internal forces at the steel and the concrete sections. However, as the loading in VM6 is more distributed, the shear stress value is higher than in beam VM8, when the same total load is applied to both beams. Therefore, beam VM6 suffers an earlier failure that is caused by the shear connectors' failure. This aspect is important, because it shows that the failure mode of beams designed for partial connection can depend on the loading distribution.

Before failure, VM6 and VM8 always present higher vertical deformation than the other beams, when comparing the same level of loading. Beam VM8 develops a very high vertical deflection.

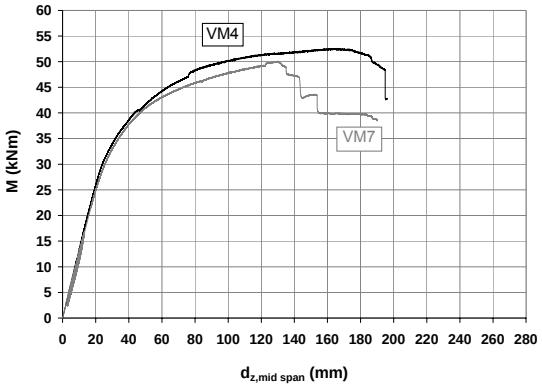

a) Type A beams

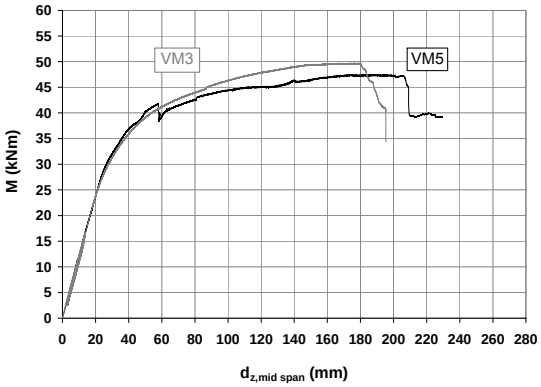

b) Type C beams

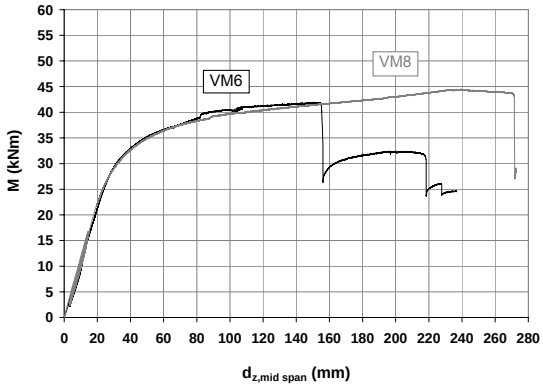

c) Type B beams

Figure 5.25 – Maximum bending moment vs. vertical deformation at mid span, for each beam type

5.9.2 Strain diagrams

Figure 5.26 to Figure 5.30 illustrate the strain diagrams at the beam mid span cross section for all composite beams tested. The strain diagrams represented correspond to the maximum measured bending moment and 40% and 90% of this value.

For $0.4M_{max}$, the strain distribution is uniform, with nearly total compatibility between both materials, in all tested beams. The steel to concrete connection guarantees the shear force transmission at this moment, and the effect of the studs' deformation does not alter the beams behaviour. At this load level, the strain diagrams are very similar for all tested beams.

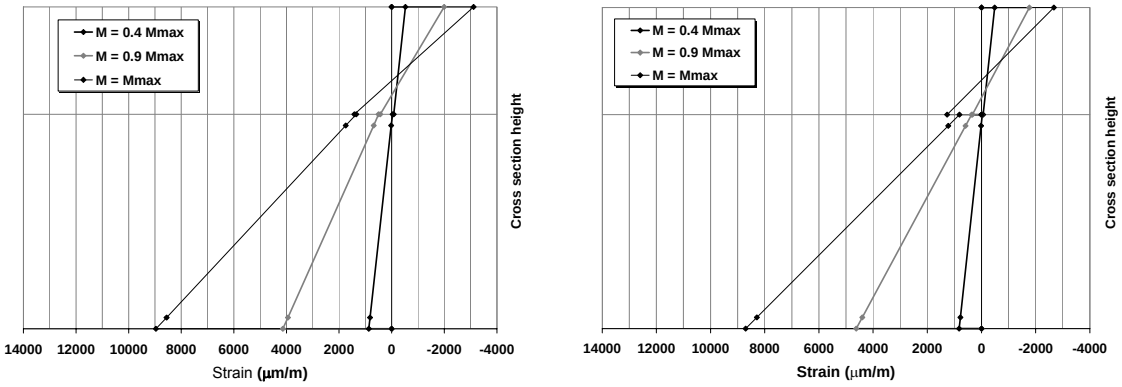

Figure 5.26 – Strain diagram for VM4 (left) and VM5 (right)

The total interaction is valid for beam VM4, even for maximum bending moment, as there is little variation of strain at the steel to concrete interface. An influence of the stud flexibility is observable for the other beams with total connection design, like VM5, VM3 and VM7. In the case of VM5, the total interaction is valid for most of the loading process, and the influence of the connection flexibility is only observable near the beam's failure. In both cases of VM4 and VM5, the strain diagrams are very similar for maximum bending moment. A similar strain diagram for these two beams means that the vertical deformation (for maximum bending moment) is also approximate, as confirmed in Table 5.11.

For VM6, the partial connection design results in a different strain diagram. The connection's deformation is influent when the bending moment value is higher than $0.5M_{max}$ (Figure 5.27 and Figure 5.28). There is significant strain variation at the steel to concrete interface for $0.9M_{max}$ and M_{max}, much higher than verified for beam VM5 when $M = M_{max}$.

As presented in Figure 5.26 and Figure 5.27, the concrete slab is completely compressed, in every tested beam of Loading distribution 1, at the initial phase of loading. As the loading increases, the connection deformation makes the neutral axis go up and tensile stress begins at the concrete slab lower fibbers. This change comes for values of 37.1 kNm and 36.2 kNm for VM4 and VM5, respectively. The values correspond to

around 70-75% of the maximum bending moment value. For beam VM6, tensile stresses at the concrete slab begin earlier, for 32.5 kNm, with significant values of slip registered for this level of loading. The steel upper fibbers are always compressed during loading, which did not happen with VM4 and VM5.

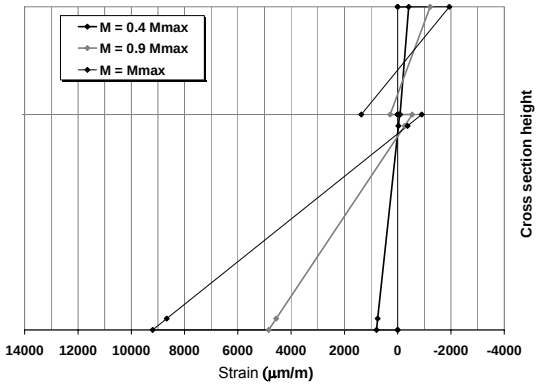

Figure 5.27 – Strain diagram for VM6

Figure 5.28 presents the variation of strain at the interface between steel and concrete sections for beams VM4, VM5 and VM6 (Loading distribution 1). The beams designed for total connection (VM4 and VM5) show little variation of slip strain until values of the bending moment that are very close to the maximum bending moment, which means that the slip at the steel to concrete interface hardly influences these beams behaviour. Beam VM6, that is designed for partial connection begins to suffer the influence of slip at the steel to concrete interface sooner, when the bending moment is approximately 60% of the maximum bending moment.

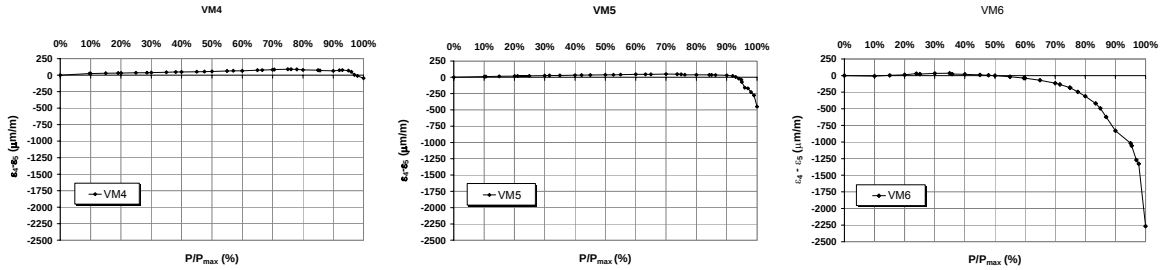

Figure 5.28 – Variation of slip strain at the interface between steel and concrete sections ($\varepsilon_4 - \varepsilon_5$), for VM4, VM5 and VM6 (Loading distribution 1)

As occurred before, the strain distribution is uniform for $0.4M_{max}$, with nearly total compatibility between both materials, in all tested beams submitted to Loading distribution 2.

In general, the strain diagrams for these beams – VM7, VM3 and VM8 – reflect more loss of composite action than those of beams of Loading distribution 1, as higher values of slip strain are measured at the steel to concrete interface. These are visible when the bending moment value is higher than $0.4M_{max}$.

The maximum bending moment values for beams VM7 and VM3 are very close. However, the vertical deformation of beam VM7 for maximum bending moment is lower than the vertical deformation of beam VM3, which means that some differences should be expected in the strain diagrams. In fact, higher maximum strains at steel and concrete sections are measured for beam VM3 (Figure 5.29).

For $M = 0.9M_{max}$ or $M = M_{max}$, the total interaction hypothesis is not valid for beams submitted to Loading distribution 2. Again, the slip strain value is higher for the beam with double stud distribution (VM3) than for the beam with single stud distribution (VM7).

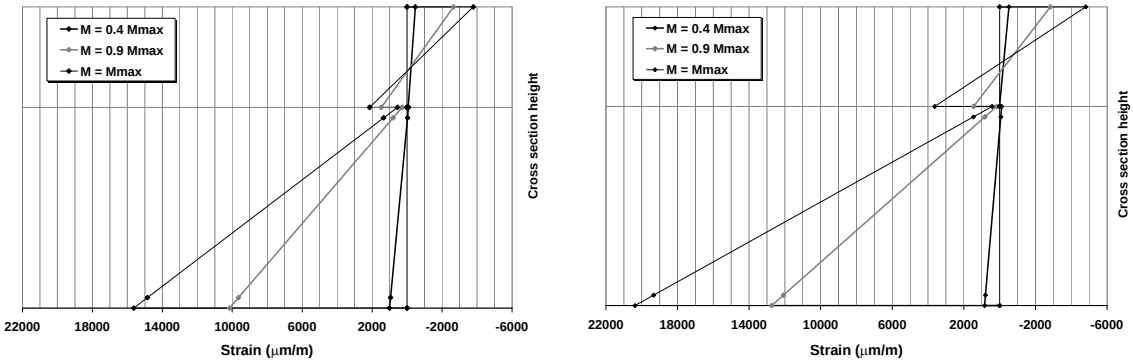

Figure 5.29 – Strain diagrams for VM7 (left) and VM3 (right)

The strain diagram of beam VM8, for $M = M_{max}$, was not possible to obtain due to strain gauge failure. At $M = 0.9M_{max}$, the strain values are much higher than verified for VM7 or VM3.

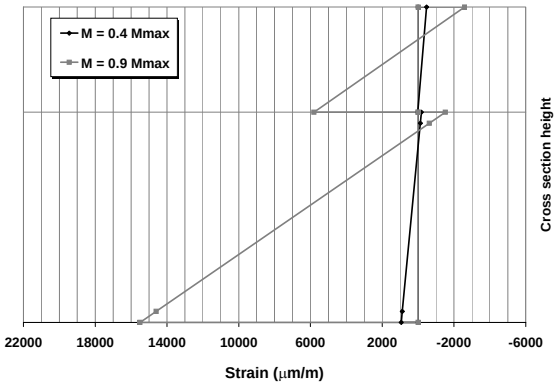

Figure 5.30 – Strain diagram for VM8

Figure 5.31 presents the variation of strain at the interface between steel and concrete sections for beams submitted to Loading distribution 2 - VM7, VM3 and VM8. All these beams show higher variation of strain at the steel to concrete interface than the beams from loading distribution 1. The beams designed for total connection (VM7 and VM3) are earlier affected by the increase of slip strain than beams VM4 and VM5. Beams VM3 and VM8 show increase in slip strain since the first load steps. For beam VM7, this only occurs when the bending moment is approximately 45% of the maximum bending moment.

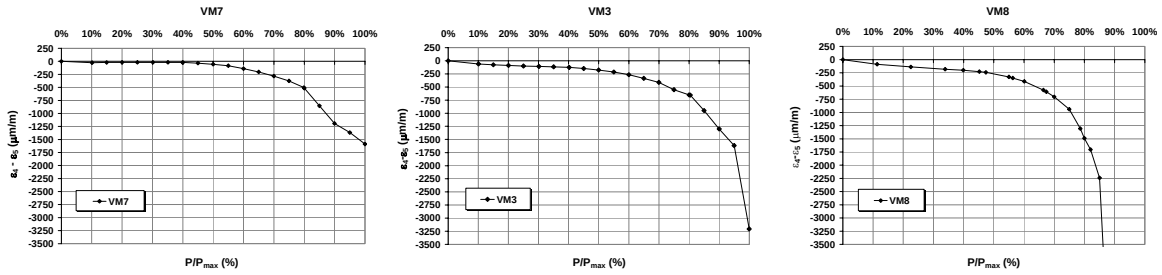

Figure 5.31 – Variation of slip strain at the interface between steel and concrete sections ($\varepsilon_4 - \varepsilon_5$), for VM7, VM3 and VM8 (Loading distribution 2)

The comparison between Figure 5.28 and Figure 5.31 shows that the Loading distribution 2 enhances higher slip strain at the steel to concrete interface. At the same time, this variation of strain takes place earlier, both for total and partial connection design beams. The beams with double stud distribution show higher values of strain variation at the steel to concrete interface than beams with single stud disposition, for the highest values of load applied. The beams with partial connection design are earlier and more sensibly affected by the slip at the steel to concrete interface, showing higher values of slip strain than all other beams.

Table A5.3 form Appendix 5.3 presents all the values of strain needed to build the diagrams presented from Figure 5.26 to Figure 5.31. Figure 5.32 presents the strain diagram for beams submitted to Loading case 1 and beams submitted to Loading case 2.

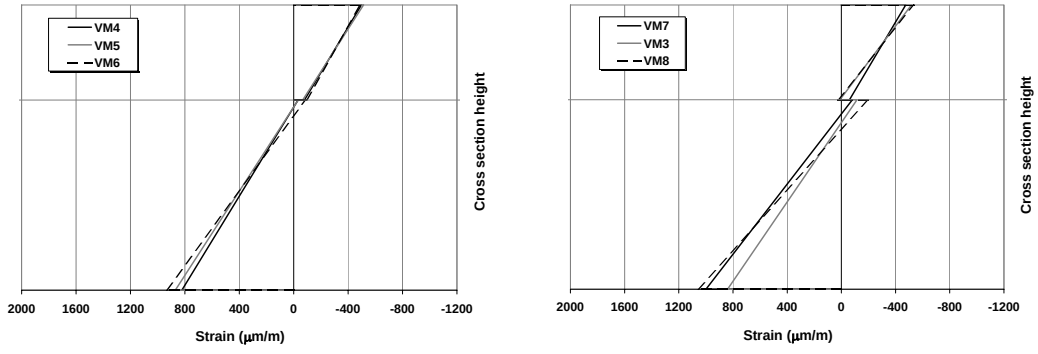

a) Loading case 1 ; M = 20 kNm b) Loading case 2 ; M = 20 kNm

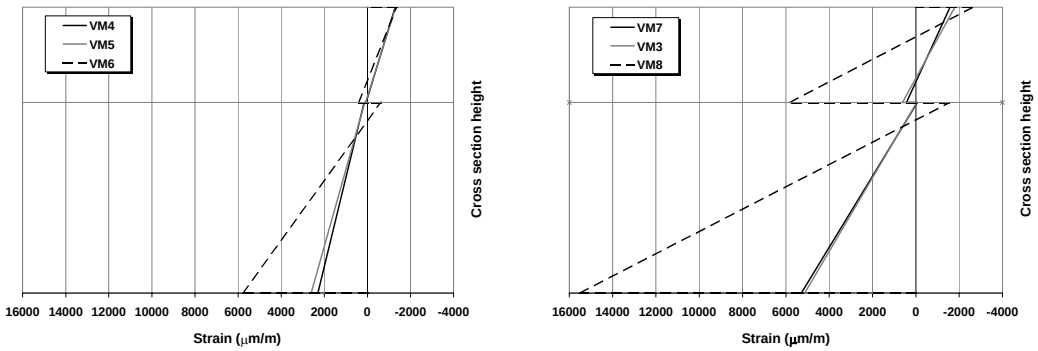

a) Loading case 1 ; M = 40 kNm b) Loading case 2 ; M = 40 kNm

Figure 5.32 – Strain diagram for fixed bending moment values

When M = 40 kNm, steel strain and slip strain values are much higher for beams submitted to Loading distribution 2. The concrete slab lower fibbers of this loading group should be cracked. Higher values of strain at the steel lower fibre are attained for this group of beams, but not higher values of maximum bending moment. This is caused by the loss of composite action that is higher on this group of beams, enhancing a higher curvature of the steel and concrete sections. For M = 40 kNm, strain values on the lower concrete fibbers of VM6, VM7, VM3 and VM8 indicate possible cracks.

5.9.3 Neutral axis position

According to the elastic strain diagram, the yielding of the steel section lower fibber occurs before the concrete cracking on the slab lower fibber. Both phenomena cause the change of the neutral axis position during loading. The connection deformability is also an important factor, as the loss of composite action induces a redistribution of stress within the cross section, altering the neutral axis position.

The yielding of the steel section results in a higher neutral axis. As the neutral axis position is initially close to the concrete slab, it is probable that if it changes its position, tensile stresses will appear on the lower fibbers of the concrete slab, leading to its cracking.

Table 5.12 presents, for each tested beam, the experimental value of bending moment that cause the yielding of the lower steel fibbers ($M_{a,y}$) and the experimental value of bending moment that cause cracking of the lower fibbers of the concrete section (M_{cr}). The first column of Table 5.12 also presents the value of the bending moment that causes the initial yielding of the steel section lower fibber, but now calculated elastically and considering a rigid connection between the steel beam and the concrete slab.

The initial yielding of the steel section occurs when the value of strain at the steel section lower fibber is equal to 1598.6 μm/m (= 335.7 / 210 × 10^3).

A medium value of concrete tensile strength, f_t = 3.8 MPa, is considered, taking into account the values determined in Chapter 3. During the experimental tests, it was very difficult to detect visually the exact moment when the cracks appear, because they are located at the concrete slab lower fibbers and these are not directly visible. However, it was possible to register approximate loads for the first moments when cracks were identified, which pretty much correspond to the values presented in Table 5.12, that were obtained by analysis of the recorded measurements.

As predicted, it is experimentally confirmed that the yielding of the steel section lower fibber always occurs before the concrete cracking on the slab lower fibber. The experimental values of $M_{a,y}$ are always a bit higher than the corresponding values determined with the elastic analysis for the beams submitted to Loading distribution 1. On

the contrary, the values of $M_{a,y}$ for the beams submitted to Loading distribution 2 are lower than the corresponding values determined with the elastic analysis

Table 5.12 – Initial yielding of the lower steel fibbers and cracking of the lower concrete fibbers

Concrete Ref.	Beam	$M_{a,y}$ (total interaction, elastic) (kNm)	$M_{a,y}$ (experimental) (kNm)	M_{cr} (experimental) (kNm)	M_{max} (experimental) (kNm)
BL33	VM4	30.41	33.47	42.62	52.60
BL32	VM5	30.80	33.09	41.75	47.52
BL34	VM6	30.62	31.40	36.47	41.96
BL38	VM7	30.33	27.70	35.61	50.10
BL37	VM3	30.33	29.59	31.83	49.76
BL39	VM8	30.37	26.74	29.56	44.51

where,

$M_{a,y}$ – bending moment that causes the yielding of the lower steel fibbers;

M_{cr} – bending moment that causes the cracking of the lower concrete fibbers;

Figure 5.33 presents the evolution of the neutral axis position in all tested beams. The first parameter to calculate is the position of the neutral axis for total interaction hypothesis and elastic behaviour of all materials. For this hypothesis, the neutral axis position is always at the steel section, although very close to the concrete section, as presented in Table A5.1 from Appendix 5.1 and also represented in Figure 5.33.

At beginning of experimental loading, the neutral axis position is always at the steel section, which is in agreement with the theoretical calculations. The neutral axis position is slightly lower than predicted, which is not a surprise, as small variations are to be expected when dealing with experimental specimens. However, due to slip at the steel to concrete interface, it would be expectable to have a lower neutral axis at the steel section, which is also verified. For beams VM4 and VM5 (total connection design and loading distribution 1), the position of the neutral axis at the steel section is more or less constant until the acting bending moment is around 60 to 70% of the maximum bending moment. This limit corresponds precisely to the initiation of yielding at the steel section lower fibbers. At the final phase of loading, the steel section is all tensioned and the neutral axis is positioned at the concrete section due to cracking of its lower fibbers.

For beams VM7 and VM3 (total connection design and loading distribution 2), the position of the neutral axis at the steel section is initially lower and suffer some variation as the load rises. The neutral axis position at the concrete section occurs earlier than what was verified for the beams submitted to loading distribution 1. A reason for this is the higher slip strain verified for these beams at the steel to concrete interface (see Figure 5.31).

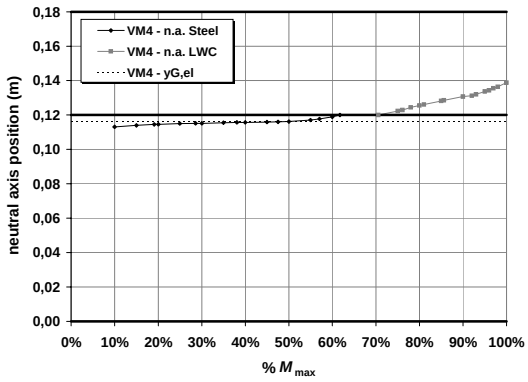

a) VM4 - Type A, Loading distribution 1

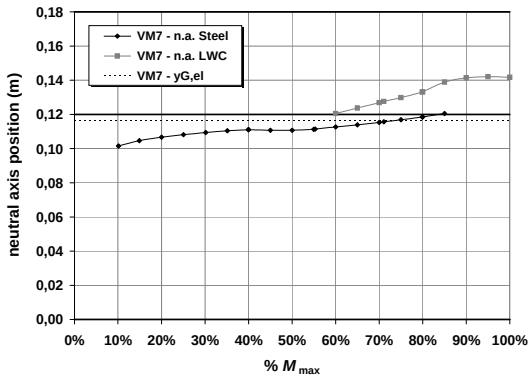

b) VM7 - Type A, Loading distribution 2

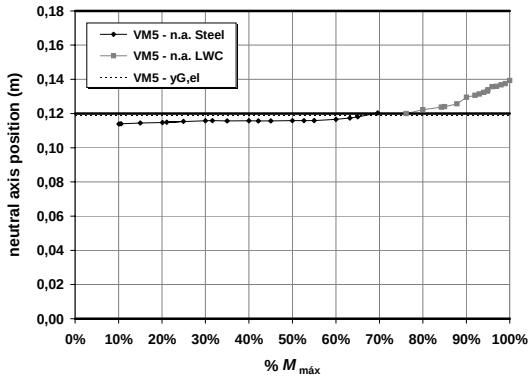

c) VM5 - Type C, Loading distribution 1

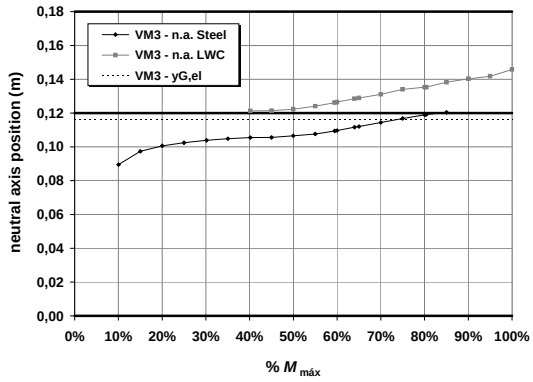

d) VM3 - Type C, Loading distribution 2

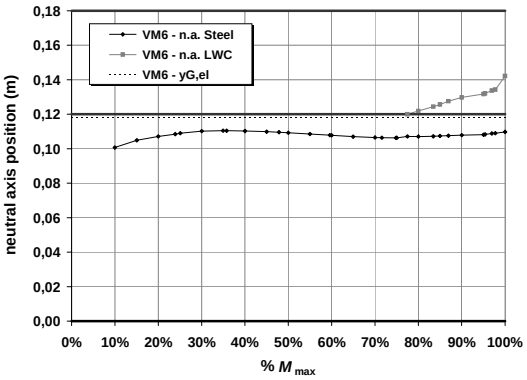

e) VM6 - Type B, Loading distribution 1

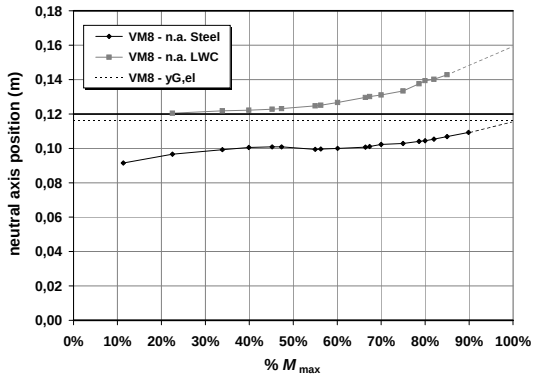

f) VM8 - Type B, Loading distribution 2

Figure 5.33 – Evolution of the neutral axis position evolution for beams VM4, VM5, VM6, VM7, VM3 and VM8

At maximum bending moment, the neutral axis position at the concrete section is similar for all total connection beams (VM4, VM5, VM7 and VM3), which is coherent with similar results obtained for maximum bending moment.

The evolution of the neutral axis for the beams designed for partial interaction (VM6 and VM8) shows some differences when compared to the beams designed for total

connection. The position of the neutral axis measured with steel strain gauges is almost constant in all tests, which means that the upper fibbers of the steel section are always compressed. The position of the neutral axis measured with concrete strain gauges shows an evolution similar to observed for the beams with total connection design.

An important observation is that the neutral axis evolution measured reproduces the observations made during the experimental tests, where cracking at the concrete slab lower fibbers takes place only for significantly high load values.

In every tested beam, the strain values in the steel section are lower than predicted (see Table 5.8). For beams with total connection design, failure is conditioned by concrete, which means that the neutral axis position is lower than what was predicted, an aspect confirmed during the experimental testing and showed in Figure 5.33. It also means that in order to guarantee internal equilibrium, higher forces need to be mobilized in the steel section, overcoming the steel yield strength.

5.9.4 Slip between the concrete slab and the steel beam

Figure 5.34 presents the end-slip values measured for beams VM4, VM5 and VM6 along time. Initially, both transducers measure similar values of slip for beam VM4. On the final phase of the test, H1 measures values that are a bit higher than H2, although failure never occurs at the steel to concrete connection. The failure of beam VM4 initiates by concrete crushing at section S3, which is positioned on the same half side of the beam as displacement transducer H1.

Beam VM5 lost one of the transducers that were measuring slip when the shear force was around 32 kN. Until this moment, both transducers were measuring very similar values of slip. The values of slip measured for beam VM5 are of the same magnitude of the ones measured for beam VM4.

The slip values measured for VM6 are much higher than the ones measured for VM4 or VM5, and grow particularly on one side of the beam (measured by H2). In the initial phase of the test, the slip evolution measured by both transducers is very similar. Following the failure of the first connector, the slip growth concentrates on one side of the beam ending with the progressive failure of all the studs localized at this half.

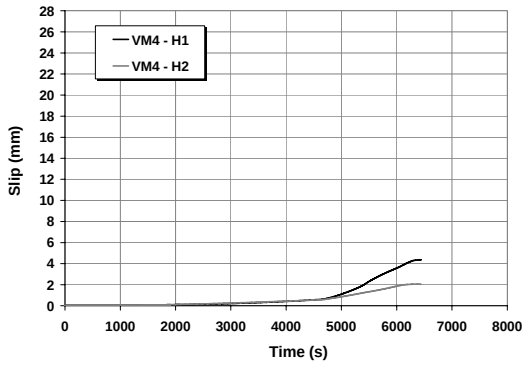

a) VM4 – Slip along time

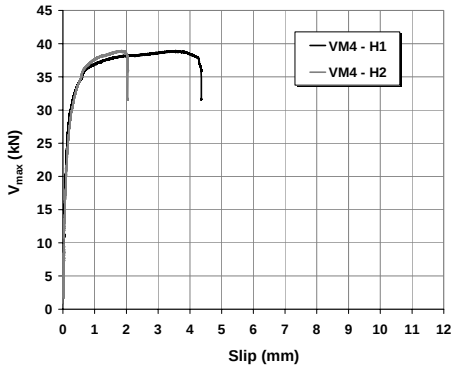

b) VM4 – Shear load vs. slip

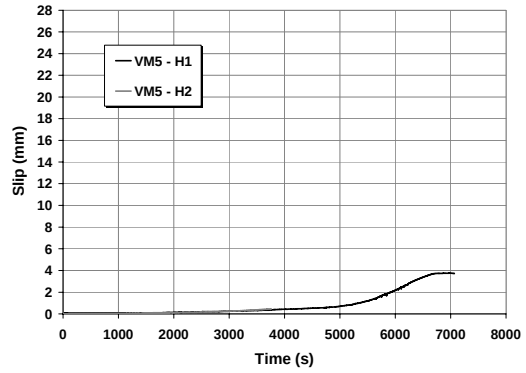

c) VM5 – Slip along time

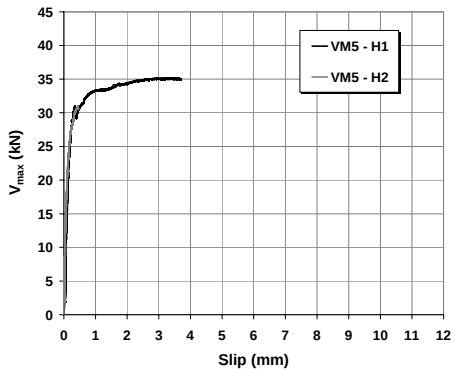

d) VM5 – Shear load vs. slip

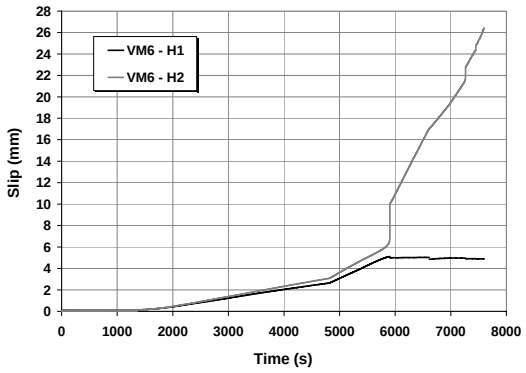

e) VM6 – Slip along time

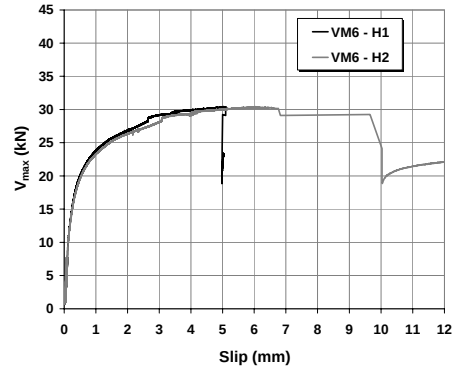

f) VM6 – Shear load vs. slip

Figure 5.34 – End-slip for beams subjected to Loading type 1 - VM4, VM5 and VM6

On beams VM7 and VM3, initially both transducers measure similar values of slip (see Figure 5.35). On the final phase of the tests, H2 measures values that are a bit higher than H1 and failure initiates in both beams at section S5, positioned on the same half side of the beam.

In beam VM8, the horizontal slip tends to be much higher than the values measured for the other beams of the same loading group. The connectors' failures occur in H2 half side of the beam, coincidently with the bending failure localized at section S5 and S6.

Both VM7 and VM3 were designed for total shear connection. VM7 had stud distribution of Type A, which proved to be more efficient for Loading 2 type, as the values of measured slip were a bit smaller than the ones measured for VM3.

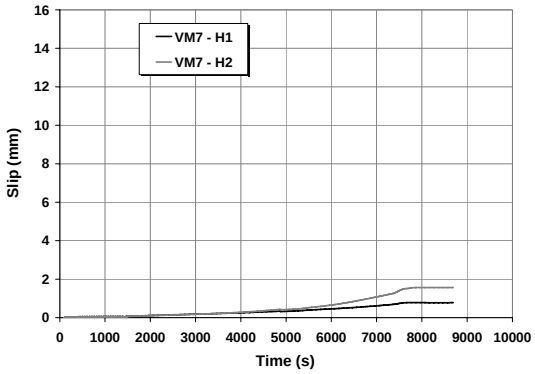

a) VM7 – Slip along time

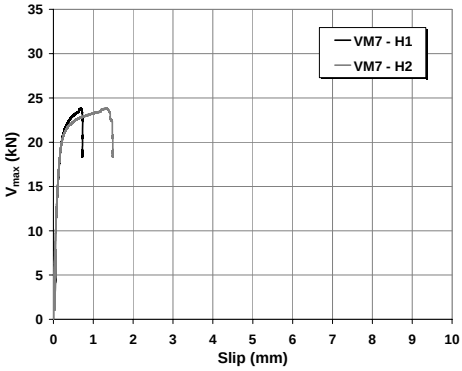

b) VM7 – Shear load vs. slip

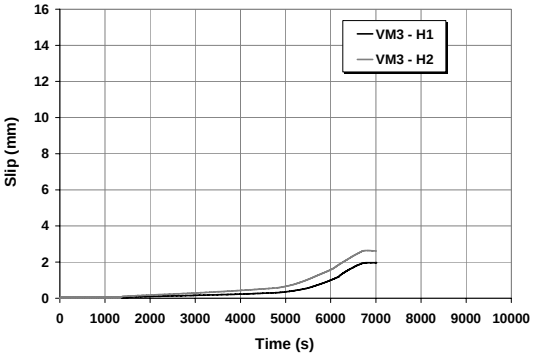

c) VM3 – Slip along time

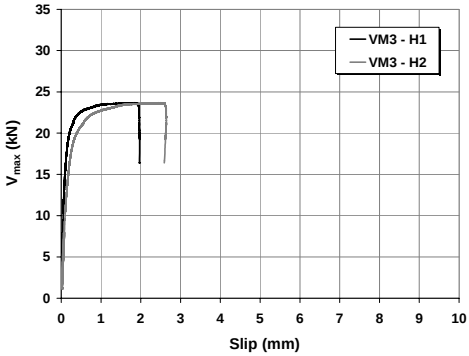

d) VM3 – Shear load vs. slip

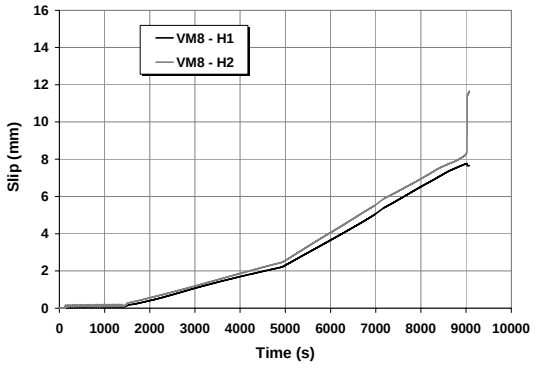

e) VM8 – Slip along time

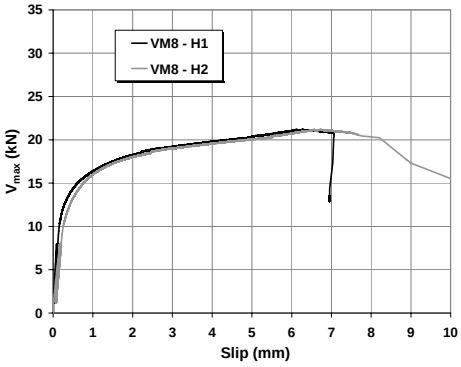

f) VM8 – Shear load vs. slip

Figure 5.35 – End-slip for beams subjected to Loading type 2 - VM7, VM3 and VM8

Experimental research done by Oehlers and Coughlan (1986), has shown that the characteristic load-slip relation of stud shear connectors in solid slabs of normal density concrete, has a ductile branch until a slip value of s_f. A statistical analysis of experimental test results gave equation (5.13) for slip prediction,

$$s_f / d = 0.45 - 0.0021 f_{cm} \quad (5.13)$$

where,

s_f – maximum slip, right before the stud failure;

f_{cm} – concrete compressive strength measured in cylinders;

d – shank diameter of the shear stud.

The value of slip for maximum load capacity is defined with equation (5.14),

$$s_u / d = 0.41 - 0.0030 f_{cm} \quad (5.14)$$

where,

s_u – value of slip for maximum load capacity.

Table 5.13 compares the values of maximum slip and slip before failure obtained experimentally in beams designed for partial connection (where failure occurred at the steel and concrete interface), with the results of using equations (5.13) and (5.14). The values of slip obtained with the referred equations are always smaller than the values of slip measured experimentally. This comparison shows that the values of slip measured in studs inside solid slabs of lightweight concrete are usually higher than values of slip measured in studs inside solid slabs of normal density concrete.

Table 5.13 – Comparison of slip values determined experimentally and equations (5.13) and (5.14)

	f_{cm}	s_u (experimental)	s_f (experimental)	s_u (equation (5.14))	s_f (equation (5.13))
	(MPa)	(mm)	(mm)	(mm)	(mm)
VM6	54.72	5.53	5.93	3.20	4.36
VM8	58.16	6.51	7.37	3.06	4.26

Figure 5.36 compares the values of end-slip (average of the values measured at both supports) in terms of the stud distribution defined in 5.3.2. Due to early fall of transducers H1 and H2 from beam VM5, it was not possible to measure all slip deformation in this test.

The behaviour of the pairs of beams VM4/VM5, and VM7/VM3 are analogous regarding the evolution of slip: similar magnitude of values for the initial phase of loading and similar curve evolution. However, for the same value of transversal shear stress, the end-slip measured for beams VM5 and VM3 is always higher than the end-slip measured for beams VM4 and VM7, respectively. This is coherent with the results of vertical deformation previously analysed for these beams. It is verified that the double stud disposition (beams VM5 and VM3) enhances higher connection deformability, which is the cause for higher vertical deformation.

For beam VM3, the total slip developed until the beam failure is higher than the total slip developed for beam VM7, which is again in accordance with the results obtained in push-out tests with double stud disposition.

The values of slip measured for beams VM6 and VM8 (partial connection) are significantly higher than the values of slip measured for all other beams. The partial connection design keeps bending failure from occurring previously to shear failure. Therefore, high values of slip develop before failure, like it happens in push-out tests. The connection behaviour is ductile, as high slip values develop while the beam load capacity is maintained. This result is in accordance with the results obtained in push-out tests, where high slip is developed while the applied load is more or less constant.

In this case, the beams' vertical deflection is influenced by the connection behaviour, as very high vertical deformation is attained. The measurements made on end-slip show that the ductile behaviour of composite beams result not only from the ductile behaviour of steel and the ductile behaviour of steel acting together with lightweight concrete, but also from the ductile behaviour of the shear connection.

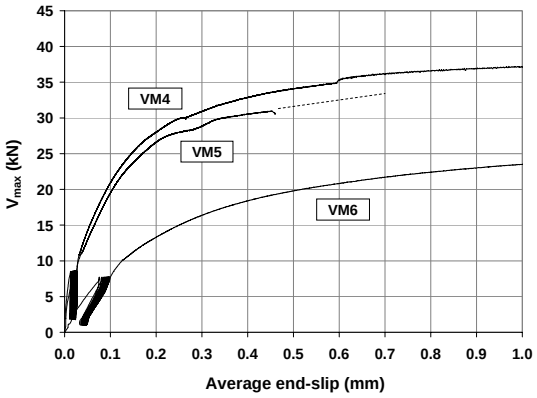

a) Loading distribution 1: initial phase of loading

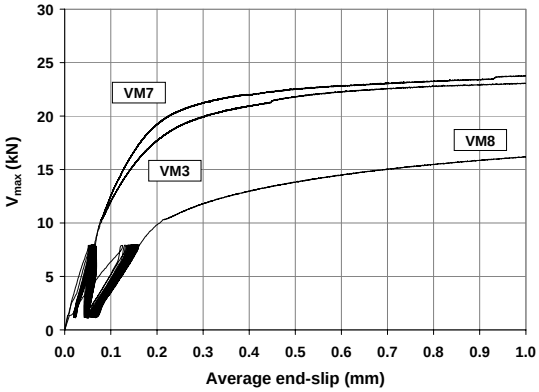

b) Loading distribution 2: initial phase of loading

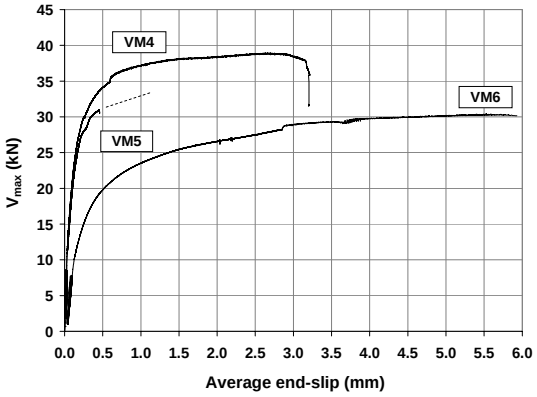

c) Loading distribution 1: total curve

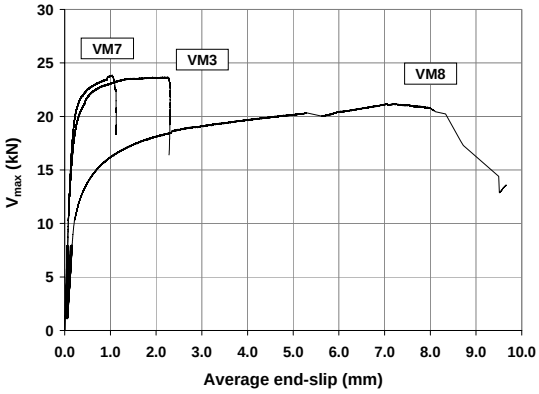

d) Loading distribution 2: total curve

Figure 5.36 – Comparison of end-slip values for beams subjected to: a) Loading distribution 1 and b) Loading distribution 2

A second comparison is established between beams that belong to each of the loading types defined in 5.3.3. Figure 5.37 shows that the value of slip is always higher for beams submitted to Loading distribution 2. The difference is small and expected when all the beams components behave elastically. In this case, the total shear force at the steel to concrete interface is higher for the beams submitted to Loading distribution 2 and therefore, the values of slip measured are higher.

However, this difference becomes much higher when the transversal shear stress is over 15 kN. This is only possible, for the same transversal shear load, if higher longitudinal shear loads are acting on each shear connector of beams submitted to Loading distribution 2. In this load case, the shear stress diagram is constant between the support and the beam mid span zone. All the shear connectors are submitted to the same shear loads, so there is no need for load redistribution. For Loading distribution 1, the shear stress diagram is not constant along the beam and it is possible that shear loads are transferred from the more loaded connectors to the less loaded ones.

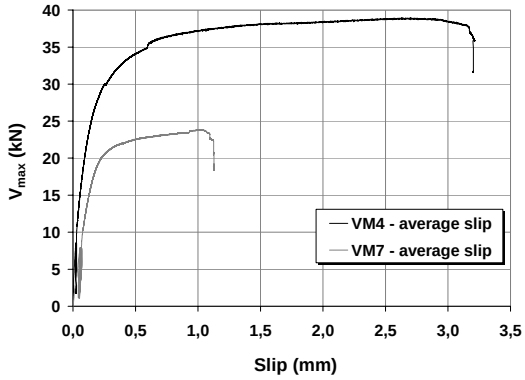

a) Type A beams

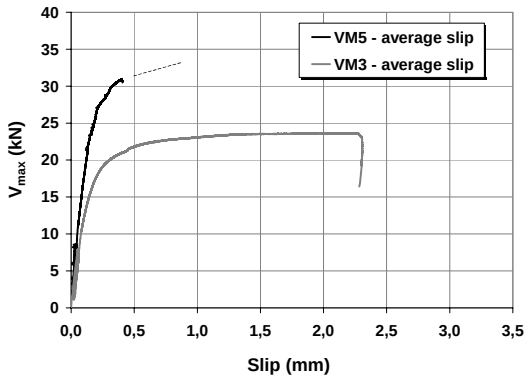

b) Type C beams

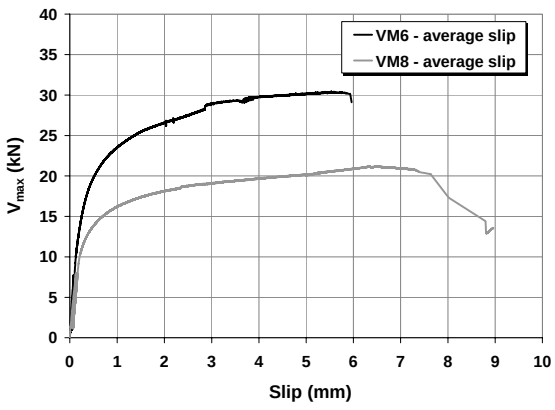

c) Type B beams

Figure 5.37 – Comparison of end-slip values for beams with stud distribution of Type A, B and C

5.9.5 Shear force per connector and slip between the concrete slab and the steel beam

Beams VM7, VM3 and VM8 are subjected to a concentrated loading, which results in a constant shear force diagram, as is represented in Figure 5.5b. This type of diagram allows an easier analysis on the distribution of the shear force between the various studs distributed along the beam. Equation (5.15) can be used to calculate the elastic longitudinal shear force, supposing that the shear force is equally distributed between all the studs disposed at the steel to concrete interface. Equation (5.15) is based on the assumption that there is total interaction between the concrete slab and the steel beam.

$$R = \frac{V \cdot S}{I} \cdot L / N \tag{5.15}$$

L – length of the constant shear stress diagram (L = 2.1 m for beams VM7, VM3 and VM8);

N – number of shear connectors disposed in half span of the composite beam (N = 7 for VM7 and VM3 and N = 4 for VM8).

In reality this is not completely true, because the connection deformability changes the longitudinal shear flow. The connectors positioned near the supports become more loaded than the connectors positioned near the beam mid span. Even so, at this phase, equation (5.15) will be used for analysis.

Due to the connection deformation, the shear flow diagram is not exactly constant and tends to zero near the cross section where the load is applied. For VM7 and VM3, the studs positioned nearer the beam mid span are right next to the points of load application. Therefore, only 7 studs (in each half span) are considered to distribute the total shear load.

It is considered that no friction forces are developed between the concrete slab and the steel beam and therefore all the shear forces are transmitted through the shear studs.

Figure 5.38 presents the evolution of the shear force applied during loading to each stud connector of the beams designed for total connection (VM7 and VM3), and establishes its relation with the end-slip measured for each beam. The same figure also presents the load-slip curve obtained on the push-out test of specimen CN13.1.

It is verified that the load–slip relation for the initial phase of the tests is very similar for both test types. This means that the connection elastic behaviour is well represented in the push-out test and corresponds directly to what occurs in a composite beam. When the connection behaviour starts to be non-linear, the situation is altered: the beam test gives a more rigid behaviour, where higher shear forces need to be mobilized to impose the same slip values that are measured in the push-out tests. The maximum slip values measured in

beams VM7 and VM3 are much smaller than the slip values measured in the push-out tests because the beams' failure occurs by bending. Therefore, not all the slip can be developed.

The maximum shear load applied to each stud is approximately equal to 44.21 kN for beam VM7 and 43.91 kN for beam VM3, which is always less than the maximum load value applied to each connector during the static push-out tests presented in Chapter 4.

The values of slip measured in the push-out test, correspondent to the maximum load imposed during the beam test are much smaller than the values of slip measured at the composite beam.

These observations result in some important conclusions for beams designed for total connection:

- the behaviour of the steel to concrete connection of a composite beam during the non-linear phase is more rigid than expected;
- if the beam is designed for total connection, bending failure occurs before shear connection failure; when bending failure happens, the values of slip are much smaller than those the connection can develop;
- the minimum slip of 6 mm, defined in EN 1994-1-1, to consider the connection as ductile, is in this case far from reality because the connection shows ductility for much smaller values of slip and ability to develop higher slip deformation when failure happens;

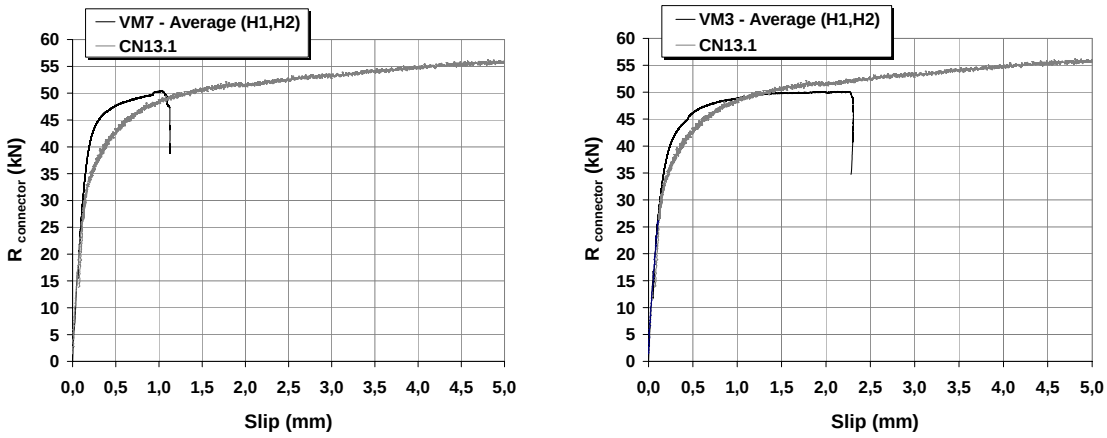

Figure 5.38 – Evolution of the shear force applied during loading to each stud connector of beams VM7 and VM3

In the case of beam VM8, equation (5.15) is not appropriate to calculate the shear force installed on each connector, because the connection deformability has an important influence on reducing the shear flow value. As a consequence, the values of the shear force calculated with equation (5.15) would much higher than the results obtained in the push-out tests.

If a numerical method is used to calculate the shear flow, by taking into account the connection elastic deformation, the shear flow is only slightly reduced for the cases in analysis.

Therefore, the diagram presented shows that when the connection behaviour is no longer linear, the shear flow is greatly reduced and an important loss of composite action takes place.

The diagram of Figure 5.39 also shows that the maximum slip developed in composite beams and in push-out tests is similar, which means that the test type does not condition the slip growth.

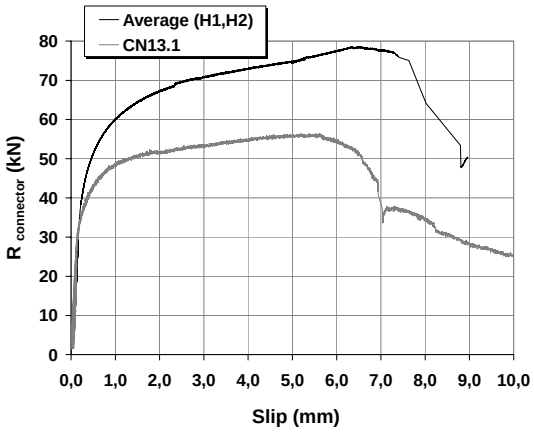

Figure 5.39 – Evolution of the shear force applied during loading to each stud connector of beam VM8

5.10. Comparison with push-out tests results

Beams VM6 and VM8, designed for partial connection, suffered shear connection failure during testing, as expected. It is verified that the values of maximum bending moment predicted in Table 5.8 for these beams, considering the shear connectors ultimate load determined experimentally in Chapter 4, are lower than the values obtained in the respective experimental tests. One possible conclusion to take is that the results on shear ultimate load obtained with push-out tests are conservative for the design of composite beams, for the scope of materials and tested performed within this work. According to (Lee et al. 2005), similar conclusions were achieved when comparing push-out tests and composite beam tests performed with large diameter studs in solid slabs of normal density concrete.

Therefore, a more adjusted failure criterion could be looked for, by considering the slip deformation capacity instead of the ultimate load capacity.

In Table 5.14, the slip results for the two beam tests designed for partial connection (VM6 and VM8) are compared to the results obtained during the static push-out tests performed on studs of 13 mm diameter.

The values of slip measured in beam tests, when the maximum load is applied, are similar to the corresponding values measured in push-out tests. Average slip values of 5.62 mm and 4.46 mm are obtained in push-out specimens. The values measured in beams are only slightly superior.

Table 5.14 – Comparison of slip results for push-out tests and beam tests

					Values for M_{max} (or P_{max})			Values for s_{max}		
Concrete Ref.	Specimen	Failure type	M_{max} (kNm)	V_{max} (kN)	s_{H1} (mm)	s_{H2} (mm)	$s_{average}$ (mm)	$s_{H1,max}$ (mm)	$s_{H2,max}$ (mm)	$s_{aver.,max}$ (mm)
BL34	VM6	Shear connection	41.96	30.22	5.03	5.95		5.10	6.66	
BL39	VM8	Bending & Shear con.	44.51	21.20	6.29	6.74		7.07	7.72	
BL43/44	CN13.1	Shear connection	-	-	-	-	5.62	-	-	6.94
BL43/44	CN13.2	Shear connection	-	-	-	-	4.46	-	-	8.51

s_{max} – maximum slip measured right before failure of the first stud

grey color – results from push-out tests

For beam VM6, the localized load capacity loss presented in Figure 5.24 occurs simultaneously with the failure of one or more shear studs in one half span of the beams. A noise correspondent to the failure of the studs could be identified during the tests. Right before this load loss happens, the slip values measured at the beams' supports correspond to 5.10 mm and 6.66 mm, as presented in Table 5.14. The value of 6.66 mm was measured on the half side of the beam where failure took place. This value is close to the maximum slip values measured in the push-out tests performed with 13 mm diameter studs (see item 4.5.1 from Chapter 4 and Table 5.14), which means that failure was conditioned by slip (the maximum load had already been reached one minute before).

Beam VM8 also suffered shear connection failure together with bending failure. Studs failure is identified in one half span of the beam. The slip values measured at the beams' supports right before failure correspond to 7.07 mm and 7.72 mm, as presented in Table 5.14. These values are higher than the ones measured for beam VM6, but still within the range of the slip values measured in the static push-out tests of specimens CN13.1 and CN13.2.

Three important conclusions can be taken from these results. The first is that the push-out tests performed could assess not only the connection load capacity but also its deformation capacity and therefore confirm that this type of test is very adequate to study

the phenomena in analysis. The second is that failure only occurs a while after the maximum load is reached, showing that the connection is ductile, as it develops deformation maintaining the load capacity. This observation confirms again what was previously found during the push-out tests. The third is that as the connection behaviour is ductile, the maximum load is maintained for high slip values, allowing high vertical deformation of the beam.

5.11. Numerical analysis

It is considered that a 2D finite element model is appropriate to reproduce the composite beams loading and behaviour, at least during the initial phase of loading, when the behaviour of the connection and of the materials that constitute the beam are approximately elastic, (Virtuoso and Vieira 1999).

This numerical model here used is built and calculated with the finite element program ATENA® (2003). The FEM geometry, mesh, supports and loadings are represented in Figure 5.40. Only half of the beam is considered, because the beam and the loadings are symmetrical. To define the beam mesh, both quadrilateral and triangular elements were considered. The mesh is automatically generated with elements' size of 0.01m. Interface elements are considered for the zones between steel and concrete sections.

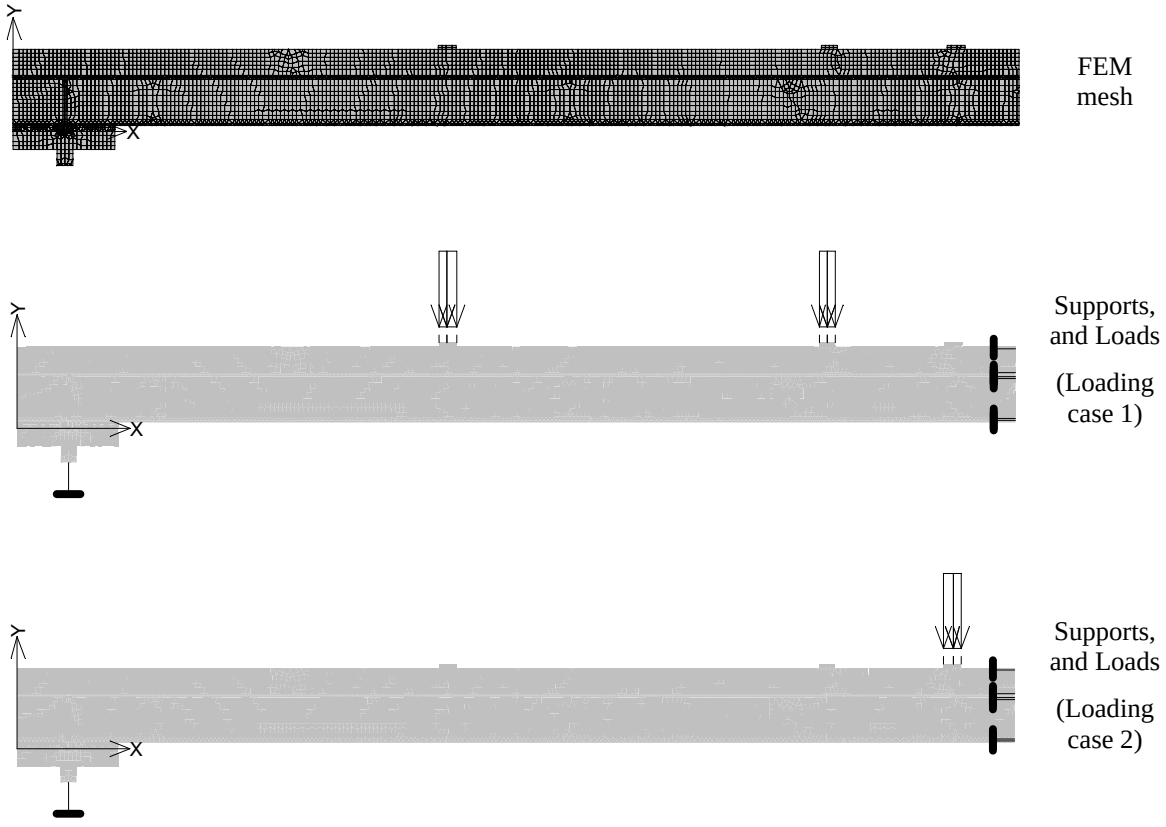

Figure 5.40 – FEM mesh, supports and loads

5.11.1 Linear analysis to evaluate the flexural stiffness

The composite beams flexural stiffness is affected by the loss of composite action between the steel profile and the concrete slab. The loss of composite action results from the connection deformability. The connection deformability is usually elastic for the initial part of the load-slip curve, as there is a linear relation between the shear load applied and the correspondent slip. This means that there is always loss of composite action, even for small loads. For higher shear loads, the relation between shear load and slip is not linear, as the load capacity grows slower and high slip values develop. At this phase, the increase of slip is faster and the loss of composite action is therefore higher.

The consequence of the loss of composite action is a loss of flexural stiffness, which means that the beam will develop higher vertical deformation for the same load level. Therefore, the objectives of the following analysis are: to check if the value of stiffness determined for the push-out tests is reliable for the analysis of the composite beams and to measure the level of load for which the elastic behaviour is no longer valid.

The non-linear behaviour of the materials that constitute the beams is not considered at this stage of analysis. With the numerical model, it is considered that there is a linear relation between shear stress and slip at the steel to concrete interface, during the initial phase of loading, as was verified during the push-out tests. The concept of connection stiffness was presented in Chapter 3. This parameter value was then evaluated as k=220 kN/mm/stud and is now used to analyse the beams results.

The steel to concrete connection is modelled with interface elements. The value of the connectors' stiffness is defined from the value obtained with the push-out tests presented in Chapter 4. Generically:

K_N = stud stiffness × number of studs in half span / (width of the steel beam × half span length)

Beams of Type A: $K_N = 220 \times 8 / (0.064 \times 2.25) = 12222$ kN/m^2/mm

Beams of Type B: $K_N = 220 \times 4 / (0.064 \times 2.25) = 6111$ kN/m^2/mm

All the beams' tests are analysed in Figure 5.41. Their vertical deflection, measured at the beams' mid span is compared to the total load applied to the beam. The beams of the Loading distribution 1 – VM4, VM5 and VM6 – show a more or less good agreement with the numerical results. The experimental behaviour is always less stiff than the numerical one. Beam VM4 corresponds to the case of worse agreement between experimental and numerical results.

The beams of the Loading distribution 2 – VM7, VM3 and VM8 – show a very good agreement with the numerical results. The value of the connection stiffness taken from the push-out tests clearly corresponds to the experimental results obtained.

The diagrams presented in Figure 5.41 show that a loss of stiffness is verified at each tested specimen for values over $0.5P_{max}$. A change in the beams behaviour is noticeable for higher loads than $0.5P_{max}$, as the increase in load values is now smaller, while deformation keeps the same growing rate (the tests are controlled by deformation at the beam mid span, as referred in 5.7.2). This change of behaviour seems to take place a little later ($0.6P_{max}$) for beams VM5 and VM6, submitted to Loading distribution 1.

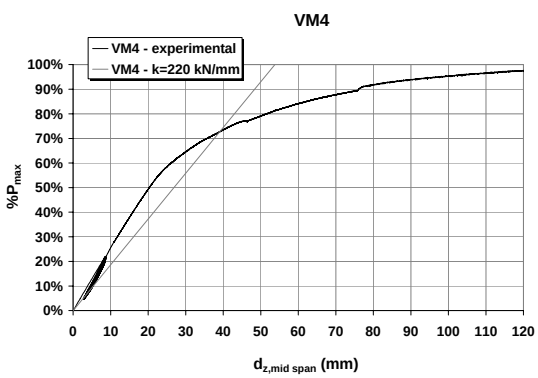

a) VM4 - Type A, Loading distribution 1

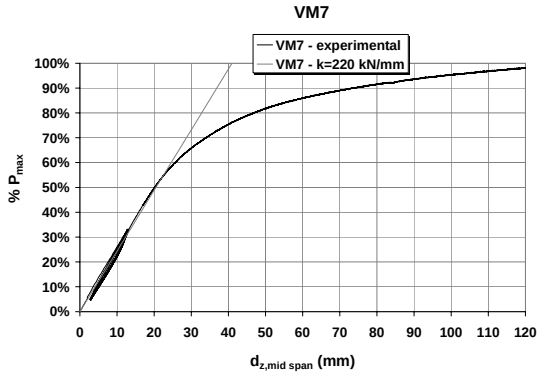

b) VM7 - Type A, Loading distribution 2

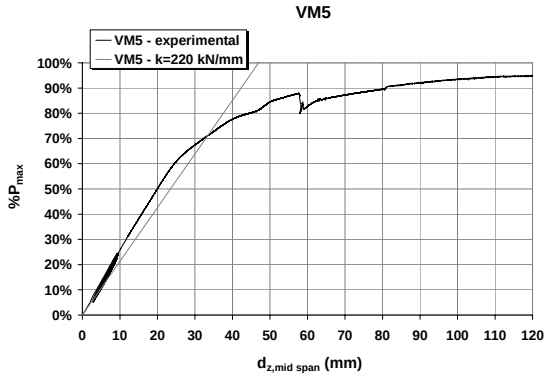

c) VM5 - Type C, Loading distribution 1

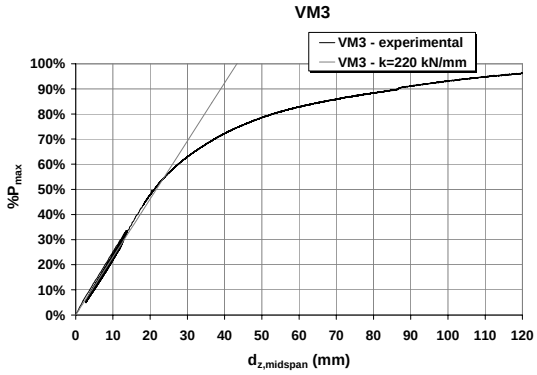

d) VM3 - Type C, Loading distribution 2

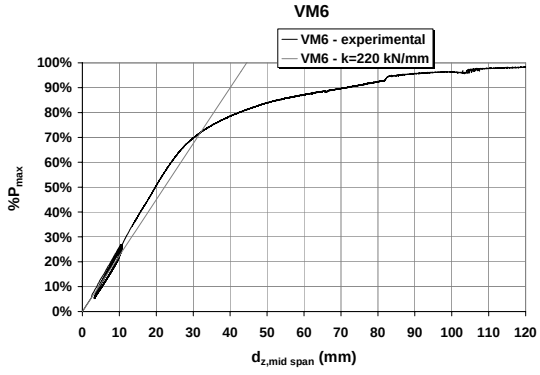

e) VM6 - Type B, Loading distribution 1

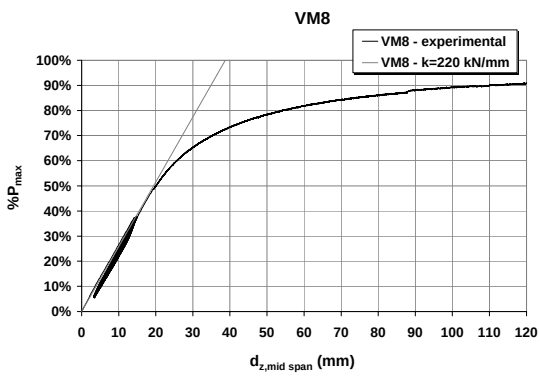

f) VM8 - Type B, Loading distribution 2

Figure 5.41 – Relation between applied load and maximum vertical deflection at beam mid span

A similar comparison is now established between the beams end-slip and the total vertical load applied to the beams. The corresponding diagrams are presented in Figure 5.42.

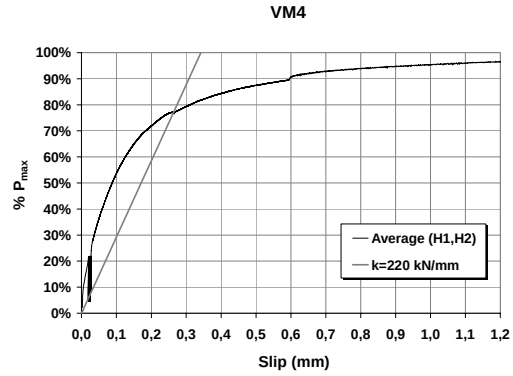

a) VM4 - Type A, Loading distribution 1

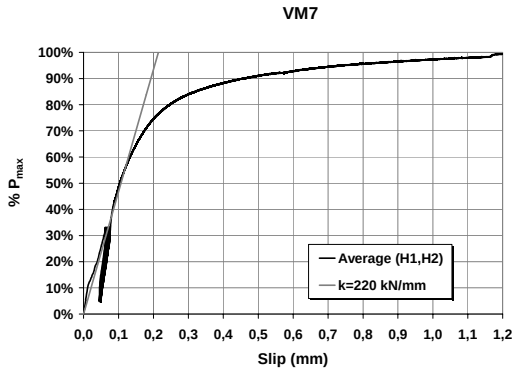

b) VM7 - Type A, Loading distribution 2

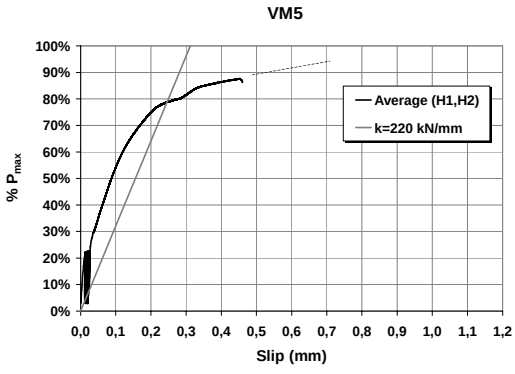

c) VM5 - Type C, Loading distribution 1

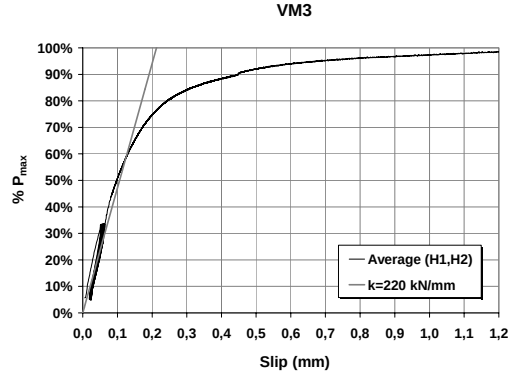

d) VM3 - Type C, Loading distribution 2

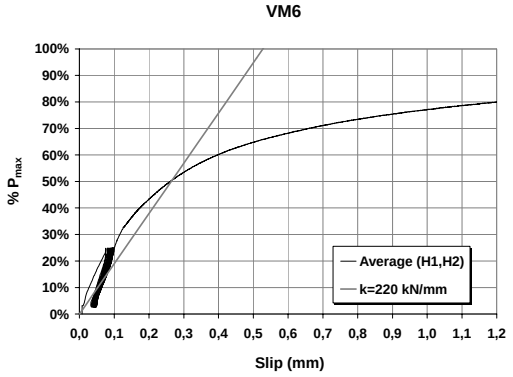

e) VM6 - Type B, Loading distribution 1

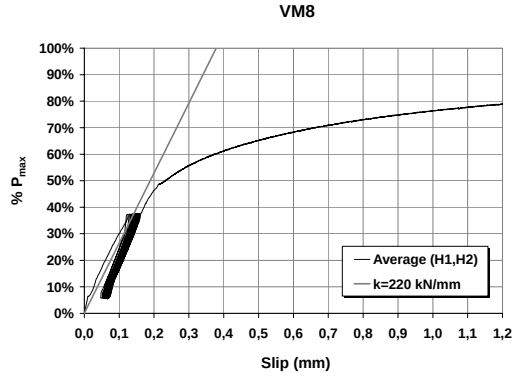

f) VM8 - Type B, Loading distribution 2

Figure 5.42 – Relation between applied load and end-slip

The beams of the Loading distribution 1 – VM4, VM5 and VM6 – show a more or less good agreement with the numerical results. Again the experimental values of slip are smaller than the numerical ones. In this case, the difference is higher than it was for vertical deflection. Beam VM4 corresponds to the case of worse agreement between

experimental and numerical results. A very good agreement is obtained for the beams of Loading distribution 2 – VM7, VM3 and VM8, where the elastic phase of the load slip curve is almost identical for the experimental and the numerical models.

In the diagrams presented in Figure 5.42, it is more difficult to identify the limits for which the non-linear behaviour occurs than it was in the diagrams presented in Figure 5.41. The linear relation between applied load and slip is not so clear in beams submitted to Loading distribution 1 and the variation of stiffness takes place for different ratios of P/P_{max}, in beams submitted to Loading distribution 2. However, it can be pointed out that a loss of stiffness is verified for lower ratios of P/P_{max} for beams VM6 and VM8, designed for partial connection.

5.11.2 Non-linear behaviour

The main objective of the following analysis is to identify if the non-linear behaviour of the composite beams is more affected by the non-linear behaviour of the shear connection or the non-linear behaviour of the materials that constitute the beam.

In this second stage of analysis, the complete material behaviour is considered, until failure. The model used for concrete considers the non-linear behaviour in compression including hardening and softening, the fracture of concrete in tension, the reduction of compressive strength after cracking, the tension stiffening effect, the reduction of shear stiffness after cracking and a fixed crack direction. Perfect bond between concrete and reinforcement is assumed. Reinforcement is in the uniaxial stress state and is modelled with a bilinear stress-strain diagram.

The stress-strain model considers the values of density, concrete compressive strength and modulus of elasticity presented in Table 5.3, together with the values of concrete tensile strength and fracture energy that are collected from Chapter 2 and again presented in Table 5.4. This happens because no specific specimens were tested to evaluate these properties, for the mixes of lightweight concrete used to fabricate the composite beams. The values of concrete tensile strength and fracture energy considered in the numerical models are f_{lt} = 3.9 MPa and G_{Fm}= 78 N/m^2.

Steel is defined with a bi-linear stress-strain model, where the modulus of elasticity is considered equal to 210 GPa for the initial phase of loading. The second branch is defined with a hardening modulus of 1.5 GPa. This parameter is calculated from the experimental results obtained on the steel specimens tested. The steel yielding strength is defined in Table 5.5.

Interface elements are used to model the connection between steel and concrete sections. The connection elastic behaviour is modelled as presented in 5.11.1. Only the

beams with single stud disposition are analysed, because the 2D model here used is not adequate to analyse the problem of the studs' proximity for the double stud disposition. The interface elements considered simulate well the uniformly distributed connection.

The maximum stress at the interface element is defined with the value of cohesion, *c*. The value obtained in Chapter 4 for the stud maximum load capacity is equal to 55.0 kN (corresponds to the average value obtained from specimens CN13.1 and CN13.2).

Beams of Type A: $c = 55.0 \times 8 / (0.064 \times 2.25) = 3.06$ MPa $\cong$ 3 MPa

Beams of Type B: $c = 55.0 \times 4 / (0.064 \times 2.25) = 1.53$ MPa $\cong$ 1.5 MPa

The presence of reinforcement in the concrete slab is also considered. The steel reinforcement is modelled in the same manner as the steel profile. The value of yielding strength is also taken from Table 5.5.

The intersection between the numerical and the experimental load-vertical deformation curve is verified when P/P_{max} is around 0.55 (see Figure 5.41), for the beams with best correspondence between experimental and numerical results - beams VM7 and VM3 (designed for total connection). As presented in Figure 5.42, the intersection between the numerical and the experimental load-slip curve is verified for approximately the same value of P/P_{max}. For the same level of loading, the strain diagrams at the beam mid span show that both steel and concrete sections are working at the elastic range (see Figure 5.43). The lower fibbers of the steel section are very close to the yielding strain (ε_y = 1599 μm/m), which means that the non-linear behaviour observed for $P/P_{max} > 0.55$ is initially conditioned by the steel section. According to the strain values measured, the first cracks on the concrete slab of beams VM7 and VM3 will appear when $P/P_{max} > 0.70$.

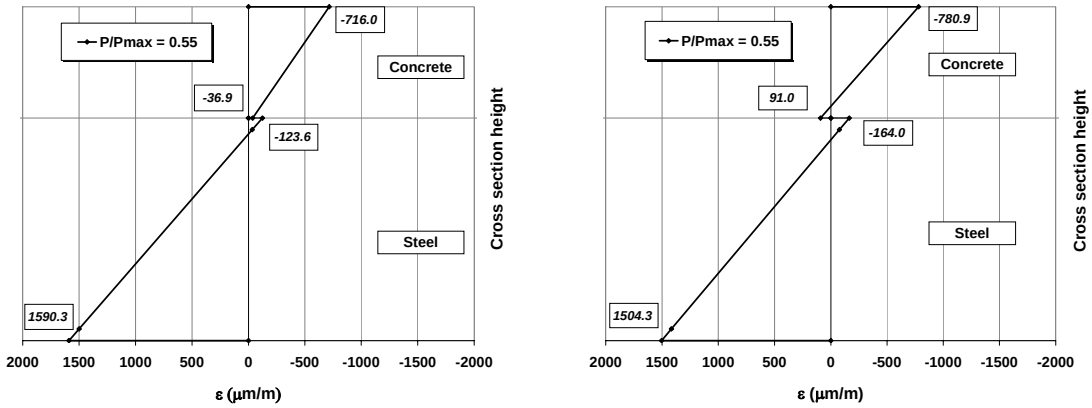

VM7 VM3

Figure 5.43 – Strain diagrams for beams VM7 and VM3 when $P/P_{max} = 0.55$

For beam VM8 (designed for partial connection), the intersection between the numerical and the experimental curves of bending moment vs. vertical deflection curve is

verified when P/P_{max} is around 45% (see Figure 5.41). The shear–slip curve, presented in Figure 5.42 for beam VM8, also shows some change in its development when P/P_{max} is between 45% and 50%. The diagram presented in Figure 5.44 shows that either the steel beam yielding or the concrete cracking are not conditioning the non-linear behaviour of the composite beam, as the values of strain for both materials are far from those limits. Therefore, the non-linear behaviour can only result from the steel to concrete connection.

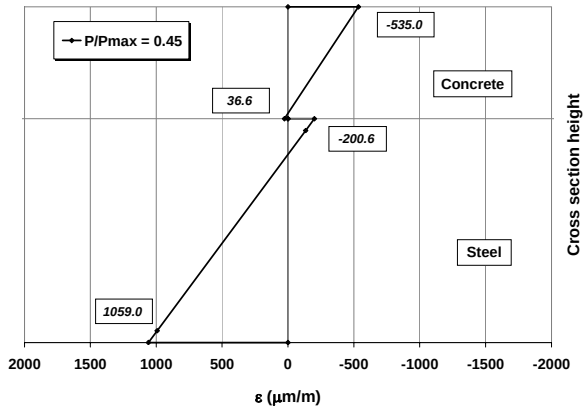

Figure 5.44 – Strain diagrams for beam VM8 when P/P_{max} = 0.45

The same approach can be established for the beams subjected to Loading distribution 1: VM4, VM5 and VM6. It is possible to identify approximately, in Figure 5.41, the load for which the load-deflection relation becomes not linear. For every beam of this group, the interval of P/P_{max} between 60% and 65% can be identified.

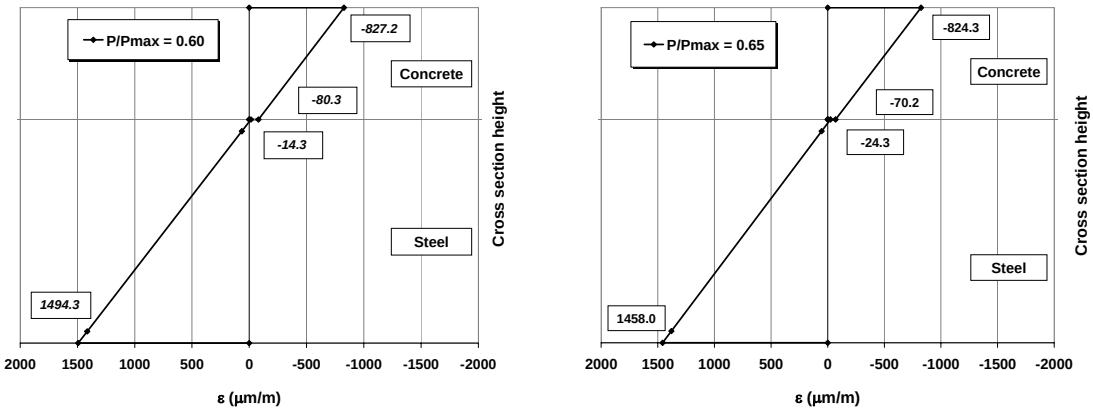

VM4 VM5

Figure 5.45 – Strain diagrams for beams VM4 and VM5 when P/P_{max} = 0.65

As the maximum load applied to beam VM4 is higher than the maximum load applied to beam VM5 (see Table 5.11), the relation of P/P_{max} = 0.6 for VM4 and P/P_{max} = 0.65 for VM5 correspond to similar loads applied.

The strain diagrams presented in Figure 5.45 show that, for the load level in analysis, the steel beams lower fibber are again close to yielding. Therefore, the observations made for beams VM7 and VM3 are also valid for beams VM4 and VM5.

For beam VM6 (designed for partial connection), the intersection between the numerical and the experimental load-vertical deflection curve is verified when P/P_{max} is also around 65% (see Figure 5.41). The diagram presented in Figure 5.46 shows that either the steel beam yielding or the concrete cracking is not conditioning the non-linear behaviour of the composite beam. In fact, this level of loading corresponds precisely with the moment when the slip strain at the steel to concrete interface begins to grow significantly, as can be identified in Figure 5.28. Again, it is confirmed that the non-linear behaviour results from the steel to concrete connection for the beams designed for partial connection.

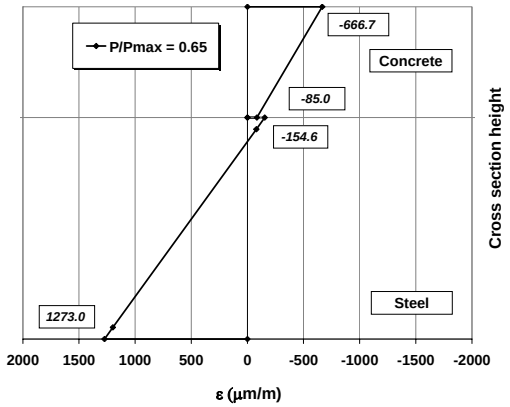

Figure 5.46 – Strain diagrams for beam VM6 when $P/P_{max} = 0.65$

The complete load-deformation curves are obtained with the finite element program ATENA®, for the four beams with single stud distribution, VM4, VM6, VM7 and VM8.

The numerical models confirm that due to the existence of slip at the steel and concrete interface, there is stress redistribution within the cross section and between the shear connectors disposed along the beam. The redistribution of stress within the composite cross section results in a transfer of stress from the concrete section to the steel section, while the redistribution between the shear connectors results in the transfer of shear force from the more loaded connectors to the less loaded ones.

Table 5.15 presents the comparison between experimental and numerical curves of bending moment versus maximum vertical deflection. In general, the numerical models are never capable of attaining neither the maximum bending moments that are measured during the experimental tests nor the total vertical deformation that is imposed. As presented in Table 5.15, the maximum bending moments obtained with ATENA® vary between 76% and 95% of the bending moments obtained experimentally.

Table 5.15 – Maximum bending moment and correspondent vertical deflection at mid span

Conc. Ref.	Beam	$M_{max,\ exp}$	$d_{z,mid\ span}$ (M_{max})	$M_{max,\ Atena}$	$d_{z,mid\ span}$ (M_{max})	$M_{max,Atena}$ / $M_{max,exp}$
		(kNm)	(mm)	(kNm)	(mm)	(%)
BL33	VM4	52.60	161.5 to 170.1	44.16	147.9	84.0
BL34	VM6	41.96	146.6 to 154.3	31.82	163.2	75.8
BL38	VM7	50.10	124.2 to 130.9	47.48	93.7	94.8
BL39	VM8	44.51	236.1 to 244.9	37.25	134.6	83.8

Figure 5.47 presents the comparison between experimental and numerical curves of bending moment versus maximum vertical deflection. Despite the identified differences, the numerical and the experimental curves show similar growing tendencies. The failure modes identified with ATENA® are also in agreement with the experimental ones:

- for beam VM4, crushing of the concrete upper fibbers in two cross sections where the load is applied, closer to the mid span (S2 and S3 from Figure 5.9), and lack of capacity to redistribute more shear stress along the steel and concrete interface;
- beam VM6 attains its maximum load capacity and keeps deforming for a more or less constant load value; the beam vertical deformation is accompanied by the increase of slip; after a while, the shear studs have no deformation capacity to admit higher values of slip that are still being imposed; at this moment, the shear studs begin to fail;
- crushing of the concrete upper fibbers, in the cross section where the load is applied (S5 and S6 from Figure 5.10), for beam VM7;
- crushing of the concrete upper fibbers, between the cross sections where the load is applied (S5 and S6 from Figure 5.10), for beam VM8 and lack of capacity to redistribute more shear stress along the steel and concrete interface.

The numerical models obtained with ATENA® show that a total redistribution of shear stress at the steel to concrete interface was necessary for the beams to attain the maximum load. Even though, the experimental maximum loads applied were always higher than the numerical values obtained with ATENA®. In view of the values of slip experimentally measured at the steel to concrete interface, it is considered that this redistribution of stress also took place on the experimental models. In the tests performed, it is verified that the shear studs distributed inside the HSLWC slab are always capable of attaining high slip values, allowing the stress redistribution to take place.

It is important to remember that the redistribution of shear stress along the beam is possible, because the connectors are able to suffer significant deformation before failure. This is the reason why it is important to establish a criterion for the connectors' ductility,

expressed in terms of slip: it insures the possibility of shear stress redistribution along the total span of the composite beam. If this deformation capacity of the connection is not possible, the connectors positioned closer to the supports suffer failure short after the maximum stress is installed, which corresponds to lower load level applied and to lower vertical deflection.

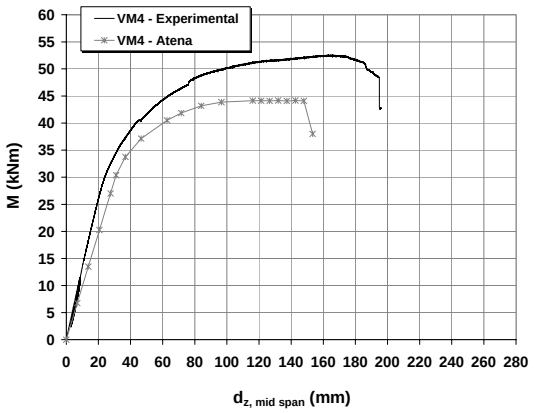

a)VM4

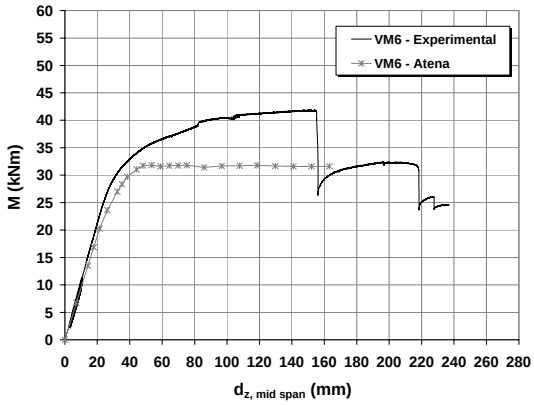

b) VM6

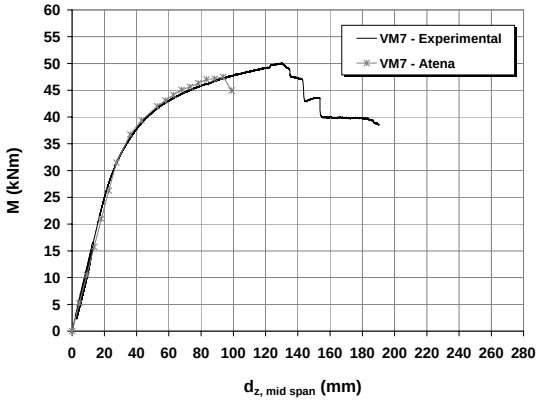

c) VM7

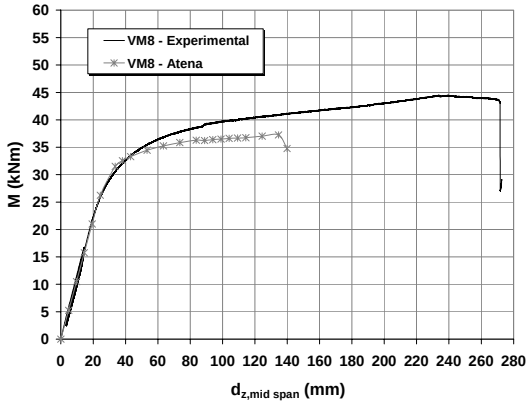

d) VM8

Figure 5.47 – Maximum bending moment vs. vertical deformation at beam mid span: comparison between experimental results and ATENA® results

Figure 5.48 presents the comparison between experimental and numerical curves of maximum transversal shear force and average end-slip. In general, the numerical curves are in accordance with the experimental ones for the initial phase of loading. With ATENA®, the maximum slip is obtained for lower shear loads than the numerical ones. The numerical maximum slip values are always smaller than the experimental ones. For beam VM7, the shear connection is notable to develop any non-elastic slip.

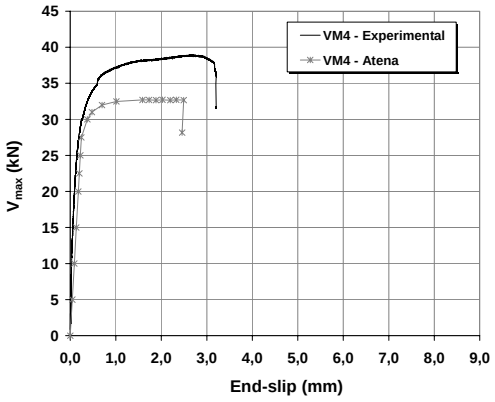

a) VM4

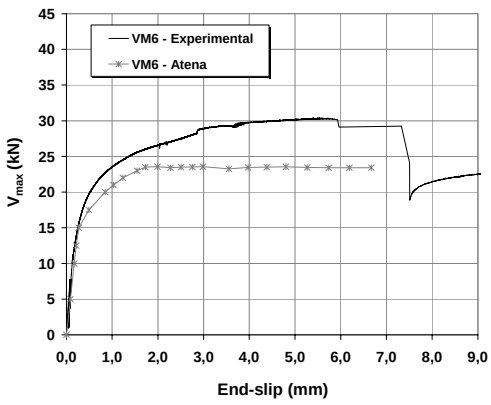

b) VM6

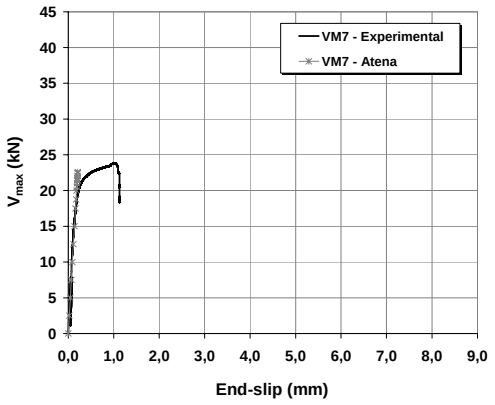

c) VM7

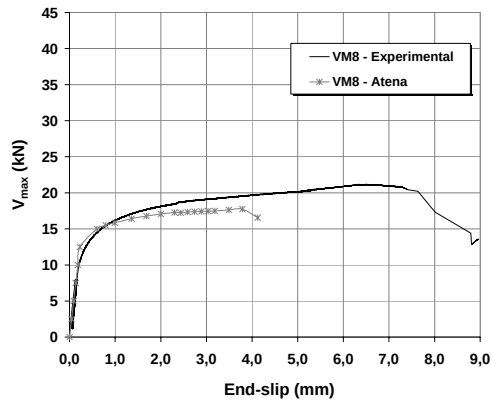

d) VM8

Figure 5.48 – Maximum shear force vs. end-slip: comparison between experimental results and results obtained with ATENA®

5.12. Conclusions

The work done in this chapter made it possible to analyse the behaviour of steel and lightweight concrete composite beams with headed studs connectors. In global terms, the behaviour observed is similar to what could be expected for normal density concrete, although not equal. The steel to concrete connection behaviour is similar to the behaviour previously observed during the push-out tests performed in Chapter 3 and Chapter 4, as failure occurs in the shear stud, instead of concrete smashing near the stud position. The concrete slab cracking on the upper side of the concrete slab, was only identified near the studs positions in beams with double stud disposition.

The uniform and equally spaced stud distribution proved to be the most efficient type of connection, allowing the higher load capacity. Grouping studs in pairs allowed larger vertical deformation but resulted in a reduction on load capacity.

The connection deformability is an important issue, as it influences directly the beams' behaviour. The beams with uniform and equally spaced stud distribution had smaller slip deformation than the beams with studs grouped in pairs, even if both were designed for total connection. All the beams designed for total connection suffered failure with concrete crushing in the cross sections submitted to higher stresses. The beams designed for partial connection suffered higher slip deformation. In these cases, failure was conditioned by shear, which was always localized in one particular side of the beam.

The results on maximum load and bending moment applied show that a good redistribution of shear load, along the composite beam, was achieved. All the beams suffered ductile failure because high deformation was measured while their load capacity was maintained.

The numerical models could not predict with exactitude the ultimate load value and the corresponding vertical deflection. The numerical values for ultimate load and vertical deflection were always smaller than the experimental ones. Even though, the failure modes could be identified.

Chapter 6

CYCLIC LOADINGS IN STEEL AND HIGH STRENGTH LIGHTWEIGHT CONCRETE COMPOSITE BEAMS

6.1. Introduction

Composite beams consisting of steel beams and reinforced concrete slabs connected with shear studs are frequently used in steel-frame building structures and bridges. Current building design codes are primarily based on static load conditions. Bridge design codes recognize and give explicit considerations to the stud fatigue problems, but usually do not consider explicitly the decay of the structural behaviour (including strength and stiffness) and the interaction between steel, concrete and reinforcement, (Yen et al. 1997).

Stud shear connectors are a mechanical form of shear connection that requires slip to occur between the concrete slab and the steel beam in order to resist shear. Hence, composite beams that rely on stud shear connectors to resist the longitudinal shear always behave as if they have partial interaction, that is, there must always be some slip at the concrete slab / steel beam interface, (Oehlers et al. 2000). So, even for service loads, the stud shear connection at a composite bridge deck is submitted to cycles of shear stress of various ranges and various peak loads that cause slip at the steel to concrete interface.

Experimental research shows that the strength of stud shear connectors in composite bridge beams immediately reduces when fatigue loads are applied to them, (Oehlers 1995). They also show that repeated loading of composite beams causes slip damage to accumulate in the shear connection with a consequent loss of stiffness and an increase in the deflection of a composite beam, (Taplin 1999).

Fatigue design is often based on full interaction analyses. The partial interaction behaviour of the stud shear connectors reduces the shear flow forces and therefore, the endurance of the shear connectors will be longer than originally anticipated. However, partial interaction increases the flexural stresses, (Oehlers et al. 2000). A full interaction analysis overestimates the shear flow forces on the stud shear connectors and therefore is conservative, as it will underestimate the endurance and strength. However, a full interaction analysis underestimates the flexural stresses.

The unloading path of a stud shear connector always occurs at a permanent set. Each cycle of load on a stud shear connector induces an increase in the permanent set. This

incremental set is a benefit, as it allows stud shear connectors to fail as a group, so that the remaining endurance and strength is much closer to the mean materials properties than the characteristic property of an individual connector on which the present design practice is usually based, (Oehlers et al. 2000).

Excluding cases where the design ranges of longitudinal shear were clearly incorrect, no fatigue failures have been reported in composite bridges, (Johnson 2000). This is because the real shear ranges acting on connectors are lower than calculated, for the following reasons:

- shear resisted by bond, at least in the early part of the fatigue life;
- the effects of flexural cracking of concrete, if ignored in design;
- the effects of incremental slip during the fatigue life;
- the effects of shear lag, especially in closed-top box girders;
- neglect of effects of slip in calculations of shear flow and in analyses of cross-sections.

These effects slightly increase the stress ranges in the structural steel, but these changes are much less significant ($m \leq 4$) than they are for the connectors ($m \geq 5$ or 8). Another potential explanation is that the live loading is less adverse than the design loading model. Although clearly correct for many young bridges, there is much evidence that loads on highway bridges have exceeded the design values of 30 to 40 years ago, leading to failures of other types of weld; and one would expect the design fatigue loading for some railway bridges to be quite accurate.

Although the previous research results provide some preliminary information on the fatigue behaviour of composite structures, most of them were gathered and analysed from push-out tests. The push-out test specimens are short, contain only some shear studs and the tests are essentially pure shear tests. In reality, a composite beam contains numerous shear connectors and is subjected to bending moments and transverse shear forces. The stress field in the concrete slab and the interaction between the shear studs and the concrete slab are quite different. Direct application of the push-out test results to the behaviour of flexural members needs to be validated.

Taplin (1999) performed tests on simply supported composite beams submitted to cyclic loadings where the shear connectors were only placed at the beam mid span and over the supports. In this case, the connectors positioned over the supports resist all the shear flow and there is no shear force redistribution along the composite beam. The shear stress distribution is well known and the results should be similar to the results obtained in cyclic push-out tests. However, this connectors' distribution is not coherent with the design of common composite beams.

6.2. Objectives

This chapter, focused on the analysis of experimental tests performed on composite steel and lightweight concrete beams subjected to cyclic loadings, intends to establish some general comparisons:

- between the behaviour of composite beams subjected to static and cyclic loadings;
- between the results obtained in push-out tests and the results obtained on composite beams tests, both under cyclic loadings;
- between the results obtained on composite beams with lightweight concrete and the expected results for composite beams with normal density concrete.

The stud shear connection guarantees the composite action between steel and concrete elements. As presented in Chapter 4, the application of load cycles to the stud shear connection causes an increase of slip at the steel to concrete interface. In a composite beam, the increase of slip results in loss of composite action, causing changes on the beam behaviour. Therefore, it is important to analyze how the repetition of load cycles influences:

- the beam failure modes;
- the evolution of slip;
- the increase in vertical deflection;
- cracking at the concrete section;
- the strain distribution at the cross section.

6.3. Beams in study

The beams in study consist of an IPE120 steel profile and a 350 mm × 60 mm, solid lightweight concrete slab (Figure 6.1). An important aspect of the composite beam tests is the layout of the stud shear connectors. Shear connection is provided with equally spaced stud connectors of 13 mm diameter and 50 mm high. The beams' cross section, span and stud distribution, used for cyclic loadings, are identical to the ones considered for beams under monotonic loading, already presented and discussed in Chapter 5.

The shear connectors' distribution is of two types, following the designation already used during Chapter 5:

- Type A: 8 studs of 13mm diameter and 50mm high in half span of the beam;
- Type B: 4 studs of 13mm diameter and 50mm high, in half span of the beam.

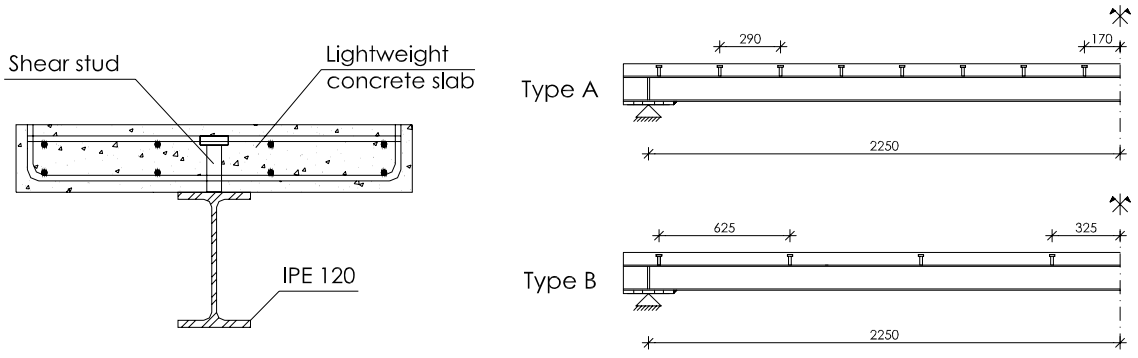

Cross section Stud distribution types

Figure 6.1 – Cross section and stud distribution

The connectors' distribution of type A is designed for a full connection between the concrete slab and the steel profile, with a uniformly distributed disposition of steel connectors. The connectors' distribution type B is designed for a partial connection between the concrete slab and the steel profile and therefore a failure at the connection should be expected. These connectors are commercially available and in this case are provided by Köco®.

The number of shear connectors disposed in beams designed for full connection is the minimum that guarantees the maximum axial force that is possible to mobilize either at the steel or the concrete section (depending on the position of the plastic neutral axis).

The load configuration chosen is the same as the one used for the monotonic testes presented in Chapter 5. This load configuration was already presented in Figure 5.3 and corresponds to four concentrated loads, equally spaced of 900 mm along the beam, approximating a uniformly distributed loading. The corresponding bending moment and shear force diagrams were also presented in Figure 5.5a.

Table 6.1 resumes the loading and stud distribution applied to each tested beam, according to the defined dispositions. Beams VM4 and VM6 were already analysed in Chapter 5, but are again included in this chapter for comparison purposes.

Table 6.1 – Stud connectors' distribution and loading type

Beam	Stud distribution	Loading type
VM4*	Type A	Monotonic
VM6*	Type B	Monotonic
VM1	Type A	Cyclic
VM2	Type B	Cyclic
VM9	Type A	Cyclic
VM10	Type B	Cyclic

* - beams VM4 and VM6 were already discussed in Chapter 5. They are again presented for comparison reasons.

It is important to know the shear force that is carried by individual studs. If any of the interface shear force is carried by friction between the steel beam and the concrete slab, this should reduce the value of the shear force in any of the studs. Research has shown that friction has an influence in composite beams, (Seracino et al. 1997). It is though important to eliminate the effect of friction in these tests, so that reliable data can be obtained on the shear force at each connector. For this reason, the top surface of the steel beam is coated with the mould releasing agent used for concrete formwork, with exception for the studs' locations.

6.4. Materials characterization

Experimental testing was done to analyse the properties of the materials in use. Concrete compressive strength, concrete modulus of elasticity, concrete tensile strength, steel yielding strength and steel ultimate strength are the properties identified as more influent and representative of the beams' behaviour.

The values for the tested materials properties are presented in Table 6.2. The concrete specimens were produced at the same time as the corresponding beam and also tested at the same date of the beam test. The medium values presented for each property are the average result of three specimen tests.

Table 6.2 – Compressive strength and modulus of elasticity for the high strength lightweight concrete used

Concrete Ref.	Concreting date	Test date	Beam	Concrete density	Compressive strength f_{lcm}	Modulus of elasticity E_{lcm}
				(kg/m^3)	(MPa)	(GPa)
BL33	16-12-03	05-02-04	VM4	1791	55.60	22.08
BL34	19-12-03	12-02-04	VM6	1804	54.72	23.82
BL35	05-01-04	31-03-05	VM1	1806	64.71	25.53
BL36	07-01-04	10-04-05	VM2	1811	65.79	25.34
BL30	02-12-03	25-05-05	VM9	1814	65.81	25.71
BL31	09-12-03	15-06-05	VM10	1812	65.51	25.03

The values for concrete tensile strength were determined for a concrete cast at a different date of the beams concreting, as there was not sufficient concrete quantity to cast the corresponding specimens for every beam. The values considered for concrete tensile strength are identical to the ones considered for the monotonic beams' tests, presented in Table 5.4, of Chapter 5.

Steel specimens were cut from the reinforcement bars and from the tested steel beams. These last specimens were cut from the steel profile web, near the supports region.

The values considered for the steel beam tensile properties and for the reinforcement steel tensile properties were already presented in Table 5.5 of Chapter 5. The specimens' size and the tensile test procedure follow the dispositions defined in EN 10002-1 (2001).

Due to the small size of the headed studs used (13 mm diameter and 50 mm height), no experimental testing was done on the steel of these connecting devices. Considering the values of steel tensile properties determined in specimens cut from studs of 19, 22 and 25 mm, presented in Table 3.2, of Chapter 3, an average value of $f_y = 450$ MPa and $f_u = 550$ MPa is considered.

6.5. Test dispositions

6.5.1 Test setup

The test setup used for the cyclic tests on composite beams repeats the setup used with the monotonic tests of composite beams, submitted to the Loading distribution 1 (see Figure 5.9 from Chapter 5). Again, the actuator load is divided into several smaller loads to accomplish the intended load distribution.

The steel sections chosen to distribute the load along the beam have sufficient load capacity to avoid early failure in these secondary elements and sufficient stiffness to avoid excessive deformation that could influence the beams' behaviour.

The secondary elements are two simply supported HEA120 steel beams with 0.9 m span distributing the load applied through one simply supported HEA200 steel beam with 1.8m span. This disposition guarantees an equal division of the load applied by the load cell, if geometrical symmetry is verified. This loading disposition aims to simulate a uniformly distributed load on the beam in an approximate way.

All tests are carried out with measurements of applied load value, vertical deformation along the beam, slip between steel profile and concrete slab and vertical separation between these two elements. Displacement transducers V1 to V3 measure the beam vertical deformation and displacement transducers T2 and T4 measure slip between the steel beam and the lightweight concrete slab, at the beams' extremes. Displacement transducers T1 and T3 also measure slip between the steel beam and the lightweight concrete slab, but they are positioned at a variable position (between 0.40 m and 0.80 m measured from the beams' supports).

The tests are performed with deformation control. The deformation is controlled in the beam mid span with V2, but other points of deformation are also measured during loading, like V1 and V3.

Strain gauges are positioned in representative transversal sections in order to measure strain and curvature variation during the tests. They are positioned in three different cross sections, defined from left to right as Section A-A' in the first quarter of the beam (1.065m), Section B-B' in the beam mid span (2.250m) and Section C-C' in the third quarter of the beam (3.435m), as presented in Figure 6.2.

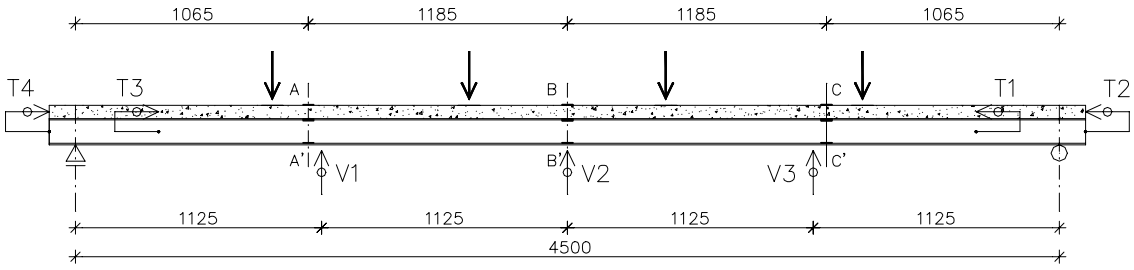

Figure 6.2– Positions for measuring devices

In the cross section, the strain gauges are located both on the upper and bottom fibber of the concrete slab and on the inner extreme fibbers of the steel section. The strain gauge disposition is identical to the disposition previously defined for the monotonic tests on beams and therefore follows the configuration presented in Figure 5.12 and Figure 5.13, from Chapter 5.

6.5.2 Test program and procedure

Four composite beam specimens were prepared in order to evaluate the composite beams cyclic behaviour. The characteristics of the test program are presented in Table 6.3.

In general, all the tests are conducted in the following steps:

1. The system applies *N* cycles of load/unload between the extreme values of the load range;
2. Direct load increase is applied between different load ranges, to fulfil the necessary load increase for VM1 and VM2 tests;
3. If failure is not attained during the load cycles, the system applies a monotonic loading controlled by a slip rate of 0.02 mm/s until a total vertical deformation of 60 mm, measured at the beam mid span, is completed (the control is done with transducer V2); this step is only completed for VM9 and VM10;
4. Following this, the system applies a monotonic loading controlled by the displacement of the actuator, with a rate of 0.05 mm/s, until failure of the specimen is attained (given the same conditions as referred in the previous item).

Table 6.3 - Experimental program for composite beams tests

Beam	Connection	Test type	Nominal load range	Number of cycles
VM1	Total	Cyclic	5 – 20	1000
			5 – 40	1000
			5 – 50	1000
			5 – 60	1000
			5 – 65	235
VM2	Partial	Cyclic	5 – 10	1000
			5 – 20	1000
			5 – 25	1000
			5 – 30	1000
			5 – 35	1000
			5 – 40	842
VM9	Total	Cyclic	5 – 35	5000
VM10	Partial	Cyclic	5 – 30	11000

The nominal load range presented in Table 6.3 refers to the loading options defined for the test procedures. In reality, the system applies load values that are proximate to the defined ones, but not necessarily the same.

The load ranges defined for beams VM1 and VM2 are defined considering the maximum load values applied to beams VM4 and VM6, respectively. The load range values are progressively increased in order to check levels of load for which the growth of vertical deformation and slip is identified and measured.

The load range values defined for beams VM9 and VM10 are meant to be approximately 40% of the maximum load value applied to beams VM4 and VM6, respectively. The maximum loads applied to beams VM9 and VM10 are intended to be approximately 50% of the maximum load value applied to beams VM4 and VM6, respectively. In fact, these percentages will be a bit higher because of some limitations of the testing machine, as will be presented in the following.

6.5.3 Loads effectively applied

The loading distribution and the corresponding stress diagram are defined in 6.3. During the cyclic phase, the test is load controlled. For some of the beams, the load cycles are imposed with increasing load range. As a result, the applied loads are variable on time and therefore, the diagram values presented in Figure 5.5a depend on the applied load value. All the loads and corresponding maximum bending moments are calculated according to item 5.5.5 from Chapter 5.

Table 6.4 presents the effective load range values applied to the composite beams during the cyclic tests. Due to some limitations of the hydraulic machine and control system, the load values effectively applied differ from the values established in the software procedure. The minimum load value effectively applied tends to be smaller than the minimum predefined load value and the maximum load value applied tends to be higher than the maximum predefined load value. Therefore, all load ranges are larger than previously thought.

The average effective load range, ΔP, presented in Table 6.4, corresponds to the interval between the average minimum load value and the average maximum load value, applied in the respective load cycle range. The average effective bending moment range, ΔM, follows the same definition.

Table 6.4 – Experimental range of applied load and applied bending moment

Beam	Load range ref.	Nominal load range	Average effective load range (*)	ΔP	ΔP / $P_{max,VM4}$	ΔP / $P_{max,VM6}$	ΔM (at beam mid pan)	Number of cycles
VM1	Range 1	5 – 20	8.186 – 22.205	14.02	18.0%		9.46	1000
	Range 2	5 – 40	4.371 – 44.052	39.68	50.9%		26.78	1000
	Range 3	5 – 50	4.018 – 54.556	50.54	64.9%		34.11	1000
	Range 4	5 – 60	3.445 – 64.395	60.95	78.2%		41.14	1000
	Range 5	5 – 65	3.394 – 69.260	65.87	84.5%		44.41	235
VM2	Range 1	5 – 10	6.505 – 11.958	5.45		8.8%	3.68	1000
	Range 2	5 – 20	4.429 – 24.275	19.85		31.9%	13.40	1000
	Range 3	5 – 25	4.711 – 28.162	23.45		37.7%	15.83	1000
	Range 4	5 – 30	2.667 – 33.379	30.71		49.4%	20.73	1000
	Range 5	5 – 35	2.372 – 38.567	36.19		58.2%	24.43	1000
	Range 6	5 – 40	2.056 – 43.854	41.80		67.3%	28.21	842
VM9	-	5 – 35	3.520 – 39.455	35.93	46.1%		24.26	5000
VM10	-	5 – 30	3.814 – 32.776	28.96		46.6%	19.55	11000

(*) – the load values presented include the weight of the steel profiles used to distribute the load

6.6. Analysis on the composite beams strength

6.6.1 Neutral axis position

The initial increments of loading are done while the beam maintains its elastic properties. The neutral axis position is presented for every beam in Table 6.5, considering an elastic behaviour and the full interaction between the steel and the concrete sections. The values presented show that the neutral axis is positioned at the profile flange and that the concrete slab total height is initially compressed.

Table 6.5 – Neutral axis positions for elastic analysis – full interaction

Concrete Ref.	Loading type	Beam	E_{cm} (GPa)	E_s (GPa)	$n = \frac{E_s}{E_{cm}}$	y_G (m)
BL33	Monotonic	VM4	22.08	210	9.511	0.1163
BL34	Monotonic	VM6	23.82	210	8.816	0.1179
BL35	Cyclic	VM1	25.53	210	8.226	0.1193
BL36	Cyclic	VM2	25.34	210	8.287	0.1192
BL30	Cyclic	VM9	25.71	210	8.168	0.1195
BL31	Cyclic	VM10	25.03	210	8.390	0.1189

These neutral axis positions indicate that strain values should be positive for Fibber 1, (see Figure 5.13 from Chapter 5), corresponding to tensile stresses, and negative for Fibber 4, Fibber 5 and Fibber 6, corresponding to compressive stresses.

If repeated loading causes slip in the shear stud connectors, there is a loss of composite action between the concrete slab and the steel beam, changing the strain distribution along each cross section. As the position of the neutral axis is close to the interface between steel and concrete, it is probable that the occurrence of slip may induce tensile stresses on the lower fibber of the concrete section (Fibber 5).

6.6.2 Predicted maximum bending moments

The resistant bending moments for the composite beams studied in this chapter are initially calculated without considering fatigue effects, as was done in item 5.5 of Chapter 5. The objective is to analyze composite beams submitted to cyclic loadings and compare them with identical beams tested for static loadings. Beams VM4 and VM6, submitted to static loadings, where analyzed in Chapter 5 and serve now as comparison to the cyclic tests. Beam VM4 (designed for full connection) is identical to beams VM1 and VM9 and beam VM6 (designed for partial connection) is identical to beams VM2 and VM10. Table 6.6 presents the values predicted for maximum bending moment of all the beams in analysis.

The steel used in the beams is always the same and the concrete compressive strength and elasticity modulus only shows some small variations, as referred in 6.4. Therefore, the resisting bending moment values calculated for the beams designed for full connection (VM4, VM1 and VM9) are very similar. The same happens for the beams designed for partial connection (VM6, VM2 and VM10).

Table 6.6 – Predicted maximum bending moments (without fatigue effect)

Concrete Ref. / Beam	Connection	N_c (equation (5.4)) (kN)	N_{pla} (equation (5.5)) (kN)	V_f (kN)	Neutral axis position	z (m)	z' (m)	$M^+_{pl.R}$ (kN.m)	ε_y (μm/m)
BL33/VM4	Full	992.46	443.46	min (N_c, N_{pla})	Concrete slab	0.0268	-	47.27	20.00
BL34/VM6	Partial	976.75		220	Concrete slab and steel flange		0.0052	37.74	29.73
BL35/VM1	Full	1155.07		min (N_c, N_{pla})	Concrete slab	0.0230	-	48.11	23.85
BL36/VM2	Partial	1174.35		220	Concrete slab and steel flange		0.0052	37.99	31.97
BL30/VM9	Full	1174.71		min (N_c, N_{pla})	Concrete slab	0.0227	-	48.19	24.31
BL31/VM10	Partial	1169.35		220	Concrete slab and steel flange		0.0052	37.98	31.97

6.6.3 Shear forces on stud connectors

If small loads are applied to the composite beam, the shear stress distribution is done according to the elastic diagram presented in Figure 5.5a. However, the connectors' deformability alters the shear flow diagram.

The use of deformable connectors results in the development of slip at the steel to concrete interface, which results in some loss of composite action. This effect leads to the diminution of shear stress at the steel to concrete interface

The numerical models created in Chapter 5 are here used to exemplify how the shear stress diagram changes when the connection deformability is considered. The example presented in Figure 6.3 consists of a composite beam, identical to VM4 (geometry, connection and materials), and also submitted to four concentrated loads.

If the connection is rigid, the shear stress diagram is constant between concentrated loads (see Figure 5.5a). However, if the same loading is applied to the beam and the connection is deformable, the maximum shear stress (over the support) is smaller and the shear stress value is no longer constant between concentrated loads (Figure 6.3b).

The stud connector presents a ductile behaviour, developing high deformation while maintaining the load capacity. This high deformation enhances the shear stress redistribution when the maximum shear stress is attained. If the connectors have no deformation capacity, failure occur at the most loaded connector, immediately after maximum shear stress is reached. The shear stress diagram is now limited by the shear strength value and develops a new configuration (Figure 6.3c).

a) Rigid connection	The shear stress diagram is constant between concentrated loads; diagram shape according to Figure 5.5a r_{max} = 141.2 kN/m
b) Flexible connection, shear connection with elastic behaviour	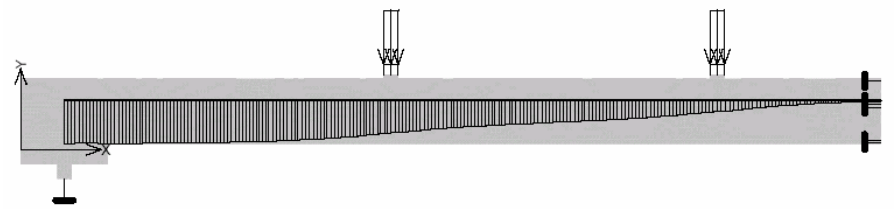 r_{max} = 138.2 kN/m
c) Flexible connection, shear connection with plastic behaviour	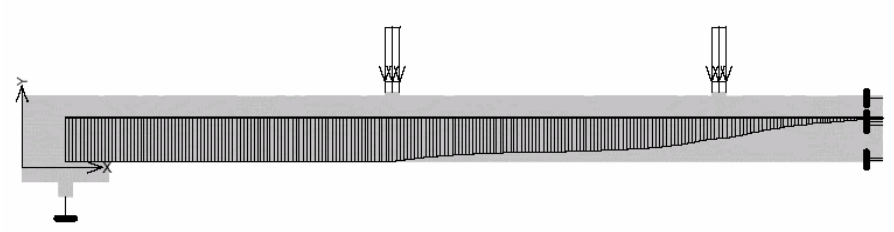 $r_{max} = r_R$ = 192 kN/m

Figure 6.3 - Comparison between shear flow diagrams, considering:

a) Four concentrated loads of 10 kN each - Rigid connection

b) Four concentrated loads of 10 kN each - Flexible connection, k = 220 kN/mm/stud

c) Four concentrated loads of 15.1 kN each - Flexible connection, k = 220 kN/mm/stud

The load ranges applied to beams VM1 and VM2 are increasingly higher. Therefore, the analysis on the shear stress distribution considers two situations: the first is the elastic shear stress diagram and the second is the redistribution of shear stress between connectors (see Table 6.7). Situation 1 is valid when the maximum shear load per connector is less than 60% of its ultimate load capacity. In this case, the shear stress distribution is close to the elastic distribution. When this limit is over passed, the connection stiffness is altered and a total redistribution of shear stress between studs is considered, corresponding to Situation 2.

Table 6.7 – Situations considered for the analysis of shear stress distribution

	Situation 1	Situation 2
Description	consider the elastic shear stress diagram	consider the complete shear stress redistribution between studs
Position of the more loaded studs	studs closer to the beam supports	all studs are equally loaded
Full connection	$\Delta R_1 = \Delta r_{max} \times 0.29$	$\Delta R_2 = \Delta r_R \times 0.29$
Partial connection	$\Delta R_1 = \Delta r_{max} \times 0.58$	$\Delta R_2 = \Delta r_R \times 0.58$

Δr_R – maximum shear stress that is possible to mobilize at the steel to concrete interface (equal to the cohesion value, *c*, defined in item 5.11.2)

Table 6.8 resumes the maximum shear stress applied to the beams shear studs, considering:

- an elastic analysis with deformable connectors at the steel to concrete interface; the connection stiffness is considered k = 220 kN/mm/stud, according to the calculations presented in Chapter 4;
- the load values applied, presented in Table 6.4;
- the transverse shear diagram presented in Figure 5.5 from Chapter 5;
- the equations proposed in Table 6.7, that calculate the longitudinal shear force range acting in each connector disposed at the steel to concrete interface.

Table 6.8 – Beam cyclic tests: shear load range and shear stress range
(connection stiffness, k = 220 kN/mm/stud)

Beam	P_{max}	ΔP	ΔV_{max}	Δr_{max}	ΔR_1 (per stud)	$\Delta\tau_1$ (per stud)	$\Delta R_1 / P_u$	ΔR_2 (per stud)	$\Delta\tau_2$ (per stud)	$\Delta R_2 / P_u$
	(kN)	(kN)	(kN)	(kN/m)	(kN)	(MPa)	(%)	(kN)	(MPa)	(%)
VM1	22.21	14.02	7.01	49.04	14.24	107.3	25.8	-	-	-
	44.05	39.68	19.84	138.68	40.22	303.0	73.1	-	-	-
	54.56	50.54	25.27	177.19	51.59	388.7	93.8	-	-	-
	64.40	60.95	30.48	182.10	-	-	-	51.52	388.2	93.7
	69.26	65.87	32.93	182.21	-	-	-	51.58	388.6	93.8
VM2	11.96	5.45	2.73	18.19	10.55	79.5	19.2	-	-	-
	24.28	19.85	9.92	66.29	38.45	289.7	69.9	-	-	-
	28.16	23.45	11.73	78.35	45.44	342.4	82.6	-	-	-
	33.38	30.71	15.36	85.31	-	-	-	49.48	372.8	90.0
	38.57	36.19	18.10	86.36	-	-	-	50.09	377.4	91.1
	43.85	41.80	20.90	87.49	-	-	-	50.74	382.3	92.3
VM9	39.46	35.93	17.97	125.77	36.47	274.8	66.3	-	-	-
VM10	32.78	28.96	14.48	83.30	-	-	-	48.31	364.0	87.8

ΔP – average load range applied to the composite beam

P_{max} – average maximum load applied to the composite beam, in each load cycle range

ΔV_{max} – average transverse shear load range, determined at the beam's supports

Δr_{max} – average longitudinal shear flow range, determined at the beam's supports

ΔR_1 – average shear load, calculated per connector according to situation 1

ΔR_2 – average shear load, calculated per connector according to situation 2

$\Delta\tau_1$ – average shear stress, calculated per connector according to situation 1

$\Delta\tau_2$ – average shear stress, calculated per connector according to situation 2

P_u = 55 kN

The cyclic loadings applied induce variation of shear stress at the interface between steel and concrete sections. It is important to evaluate the range of shear force that is applied to each stud and establish the relation between the variation of shear force per load

cycle in each stud and the stud ultimate shear force. The final objective is to evaluate how the variation of slip depends on the shear load range and how the possibility of shear stress redistribution alters the slip growth.

The values of ultimate shear load, applied to headed studs in lightweight concrete solid slabs were experimentally determined and presented in Chapter 4, for studs with diameter equal to 13 mm. An average value of P_u = 55.0 kN was obtained in the monotonic push-out tests presented there (see Table 4.7).

6.7. Observed behaviour during tests and failure modes

The beam tests lead all the specimens to failure, and different types of collapse are observed. Two types of failure were found: bending failure with concrete crushing on the slab top fibbers and connection failure with shear failure of part of the connectors. A brief description on the beams' failure modes is given, with particular emphasis on the identification of these two failure types: bending failure and shear failure.

The shear connectors' failures occur always with the stud shear failure and never with concrete crushing around it (see Figure 6.8d). This result is in accordance with the failure modes identified in the cyclic push-out tests performed (see Chapter 4).

6.7.1 VM1

Beam VM1 suffered shear connection failure. Failure occurred during the load cycles range, between 5 and 65 kN (see Table 6.3). Significant vertical deformation and slip could be observed previous to the beam failure. It was mainly visible on one half span of beam VM1, where all stud connectors positioned between the support and a distance of 1.20m failled (Figure 6.4a). This corresponds to the failure of four studs.

Important transversal cracking is visible next to the shear studs positioned near the beam mid span (Figure 6.4b). The cracks are oriented to the studs' positions and are visible in all the studs that did not suffer failure (Figure 6.4c). Next to the supports, there are almost no transversal cracks. There is important residual end-slip of the composite beam (Figure 6.4d).

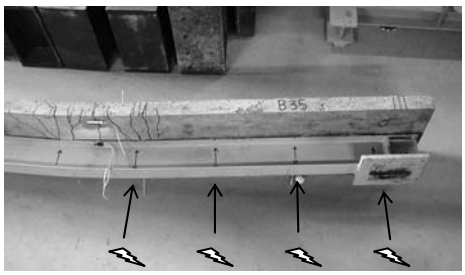

a) Stud failure positions (identified with ↯)

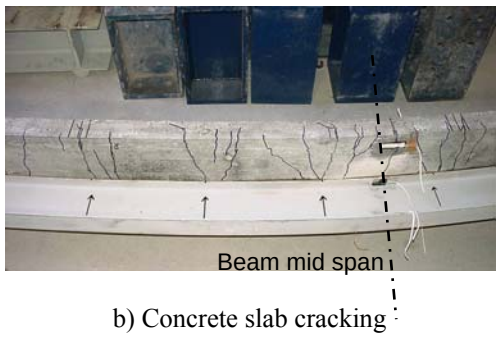

b) Concrete slab cracking

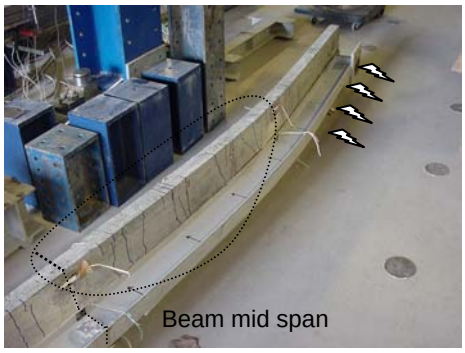

c) Complete half span

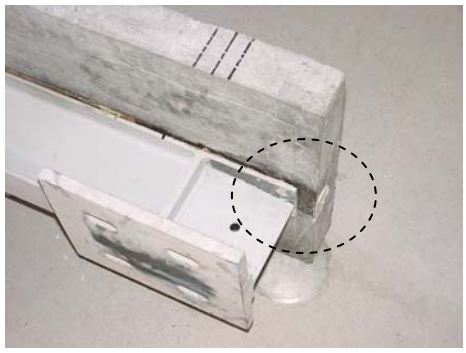

d) Residual end-slip

Figure 6.4 - VM1 failure

6.7.2 VM2

Beam VM2 suffered shear connection failure. Failure occurred during the load cycles range, between 5 and 40 kN (see Table 6.3). As for beam VM1, it was mainly visible on one half span of beam VM2. All stud connectors positioned between the support and a distance of 1.80m suffered failure, which corresponds to three studs. The positions of stud connectors that suffered failure are represented in Figure 6.5a. Transversal cracks developed in the positions where the studs that did not suffer failure. These cracks are mainly concentrated near the position of the central loads applied (Figure 6.6a).

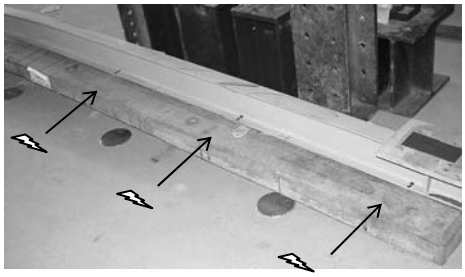

a) Stud failure positions

b) Concrete slab cracking

Figure 6.5 – VM2 failure

As for beam VM1, there is important residual end-slip of the composite beam (Figure 6.6b).

a) Cracks at the positions of loading

b) Residual end-slip

Figure 6.6 – VM2 failure: cracks and residual end-slip

6.7.3 VM9

The load range cycle applied to beam VM9 is of smaller magnitude than the maximum load applied to beam VM4. As Beam VM9 did not suffer failure during the 5000 load cycles applied, a monotonic loading was applied, until failure was attained. The result is that beam VM9 suffers bending failure (Figure 6.7). Concrete crushes near the load application point at section S2 (identified in Figure 5.9).

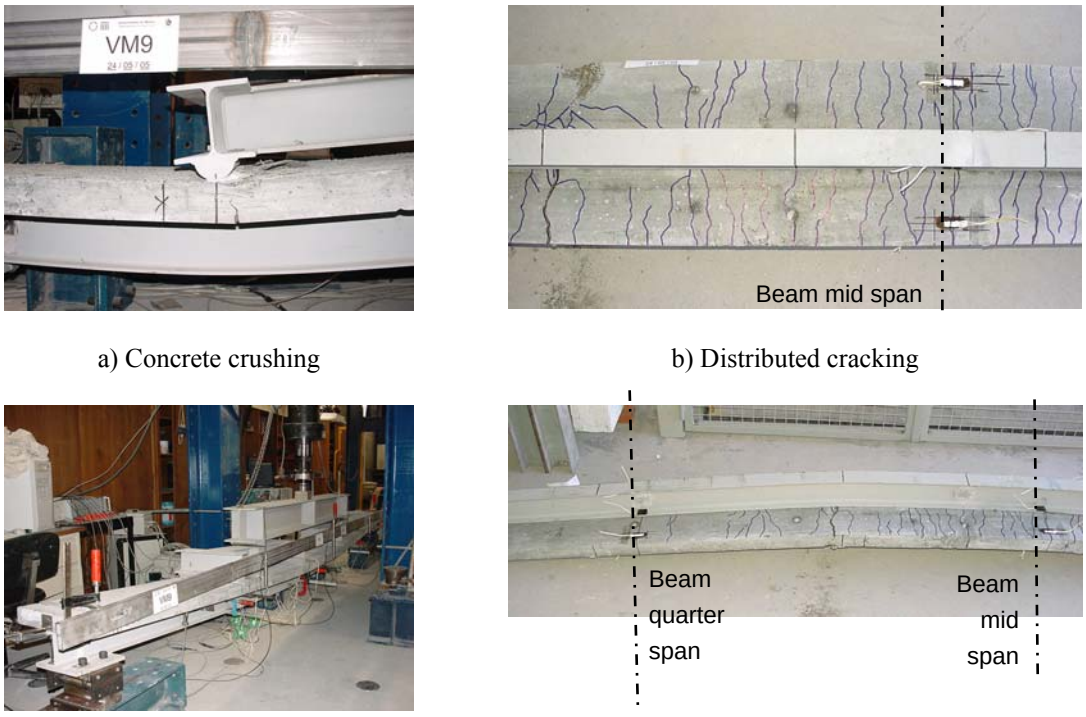

a) Concrete crushing

b) Distributed cracking

c) High vertical deformation before failure

d) Cracks near the studs' positions

Figure 6.7 – VM9 failure

As shown in Figure 6.7b, at the beam mid span, the cracks on the concrete slab lower fibbers are uniformly distributed and perpendicular to the beam span. As we move from the beam mid span to the beam quarter span, the transversal cracks tend to show higher spacing and their orientation heads for the studs' positions (Figure 6.7d).

6.7.4 VM10

The load range cycle applied to beam VM10 was of smaller magnitude than the maximum load applied to beam VM6. The 11000 load cycles applied to beam VM10 were not enough to provoke failure and therefore a monotonic loading was also applied to this beam after the load cycles. Beam VM10 suffered shear connection failure during this last phase.

Beam VM10 suffers high vertical deformation before failure, with distributed cracking on the slab lower fibbers. These cracks are perpendicular to the beam span, are evenly distributed and have more expression near the zones of load application (Figure 6.8a).

The connetion failure is located in one half span of the beam. Stud failure takes place in three of the four studs disposed in this half of the beam (Figure 6.8b and c).

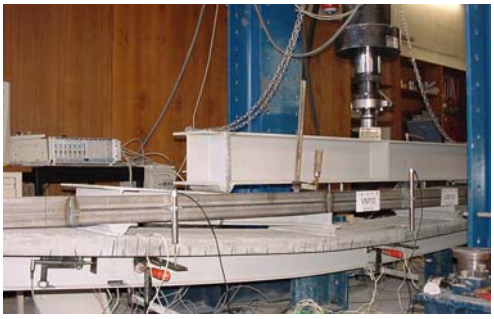

a) High vertical deformation before failure and distributed cracking

b) Stud failure, vertical separation between the steel and the concrete sections

c) Distribution of stud failure

d) Stud failure

Figure 6.8 – VM10 failure

6.8. Test results

6.8.1 Bending moment and vertical deflection

The experimental values of maximum sagging bending moment and maximum applied load, measured during the experimental tests, are presented in Table 6.9.

Beams VM4, VM1 and VM9 are all identical and designed for full connection – Type A beams. Beam VM1 is submitted to load cycles of increasing load range, while beam VM4 is just monotonically loaded. The effect of these load ranges is that the beam failure mode is altered and as a consequence connection failure occurs instead of the bending failure verified for beam VM4.

The test made on beam VM1 proves that even beams designed for full connection are affected by cyclic loadings. Although it was necessary to impose high load range cycles to provoke the shear failure, it is verified that this type of loading alters the beam ultimate behaviour. As a consequence of shear failure, the beam load capacity is diminished. Beam VM1 maximum bending moment is equal to 89% of the correspondent value obtained for beam VM4.

Beam VM9 is submitted to a constant load cycle range. The load cycle value applied to beam VM9 is smaller than the load cycle values that induce failure on beam VM1. Beam VM9 is submitted to 5000 load cycles of constant load range and afterwards is incrementally loaded until failure.

Both beams VM4 and VM9 suffer bending failure. The maximum bending moments applied to beams VM4 and VM9 are very similar and exceed the maximum bending moments predicted in Table 6.6. The failure modes identified for beams VM4 and VM9 are also very similar. The average load range value effectively applied to beam VM9 by the hydraulic system is equal to 35.93 kN and the average maximum load applied is equal to 39.46 kN (see Table 6.4). This maximum load corresponds to 50.6% of the maximum load applied to beam VM4. In terms of load capacity, beam VM9 is not affected by the load cycles imposed (Table 6.9).

Table 6.9 - Maximum bending moment and corresponding applied load

Concrete Ref. / Beam	Connection	Failure type	P_{max} (kN)	M_{max} (kNm)	V_{max} (kN)
BL33/VM4	Total	Bending	77.92	52.60	38.96
BL34/VM6	Partial	Shear connection	62.16	41.96	31.08
BL35/VM1	Total	Shear connection	69.44	46.87	34.72
BL36/VM2	Partial	Shear connection	44.28	29.89	22.14
BL30/VM9	Total	Bending	78.32	52.86	39.16
BL31/VM10	Partial	Shear connection	38.08	25.70	19.04

Beams VM6, VM2 and VM10 are all identical and designed for partial connection – Type B beams. Beam VM6 is just monotonically loaded, while beams VM2 and VM10 are submitted to cyclic loading. Beam VM2 is submitted to an increasing load cycle range, while beam VM10 is submitted to a constant load cycle range.

Like beam VM6, VM2 suffers shear connection failure. Beam VM2 is affected by the load cycles, because the maximum bending moment applied to it is smaller than the maximum bending moment applied to beam VM6. Beam VM2 maximum bending moment is equal to 71% of the correspondent value obtained for beam VM6.

The same type of failure and loss of load capacity is verified for beam VM10. The average load range value effectively applied to beam VM10 by the hydraulic system is equal to 28.96 kN and the average maximum load applied is equal to 32.78 kN (see Table 6.4). This maximum load corresponds to 52.7% of the maximum load applied to beam VM6. Beam VM10 maximum bending moment is equal to 61% of the correspondent value obtained for beam VM6. The loss of load capacity is more severe for beam VM10 than for beam VM2.

In addition, the maximum bending moments applied to both beams VM2 and VM10 are inferior to the maximum bending moments predicted in Table 6.6, which did not happen with VM6, for which the maximum bending moment measured during testing is higher than the maximum bending moment predicted.

The test made on beam VM10 shows that moderate load cycle ranges can affect the behaviour of a composite beam designed for partial connection by reducing its load capacity. This load capacity reduction is not observed for beam VM9 (designed for full connection and submitted to a similar $\Delta P/P_{max,VMi}$ – see Table 6.3).

In general, the comparison established between the composite beams that were tested puts in evidence that, in terms of load capacity, a composite beam designed for partial connection is more affected by cyclic loading than a composite beam designed for full connection.

Figure 6.9 presents the experimental bending moment vs. vertical deformation diagram, measured at the beams' mid span, for VM1, VM2, VM9 and VM10. Each diagram is compared with the reference beam statically loaded – VM4 for full connection design and VM6 for partial connection design. All beams show an initial elastic behaviour, approximate to the estimated by an elastic approach. It was concluded in Chapter 5 that beam VM4 behaved stiffer than expected during the elastic loading phase, which is now reconfirmed, with the comparison between VM4 and VM1 and VM4 and VM9.

The diagram correspondent to beam VM1 shows that the last load cycles applied impose an increase of vertical deflection that ends with the beam failure. The diagram

evolution also shows that failure would probably take place for lower loads if more load cycles were applied during load range 3 or load range 4.

The diagram for beam VM2 is almost identical to the diagram of beam VM6, during five load cycle ranges. During load range 6, the beam vertical deflection suffers a constant and significant increase that ends up with the beam failure.

The diagram correspondent to beam VM9 is very similar to the diagram presented for beam VM4 and the 5000 load cycles could not induce a deformation increase that could alter the diagram shape. On the opposite, a significant increase on the vertical deformation is observable for beam VM10 during the 11000 load cycles applied, leading to an early failure of the beam.

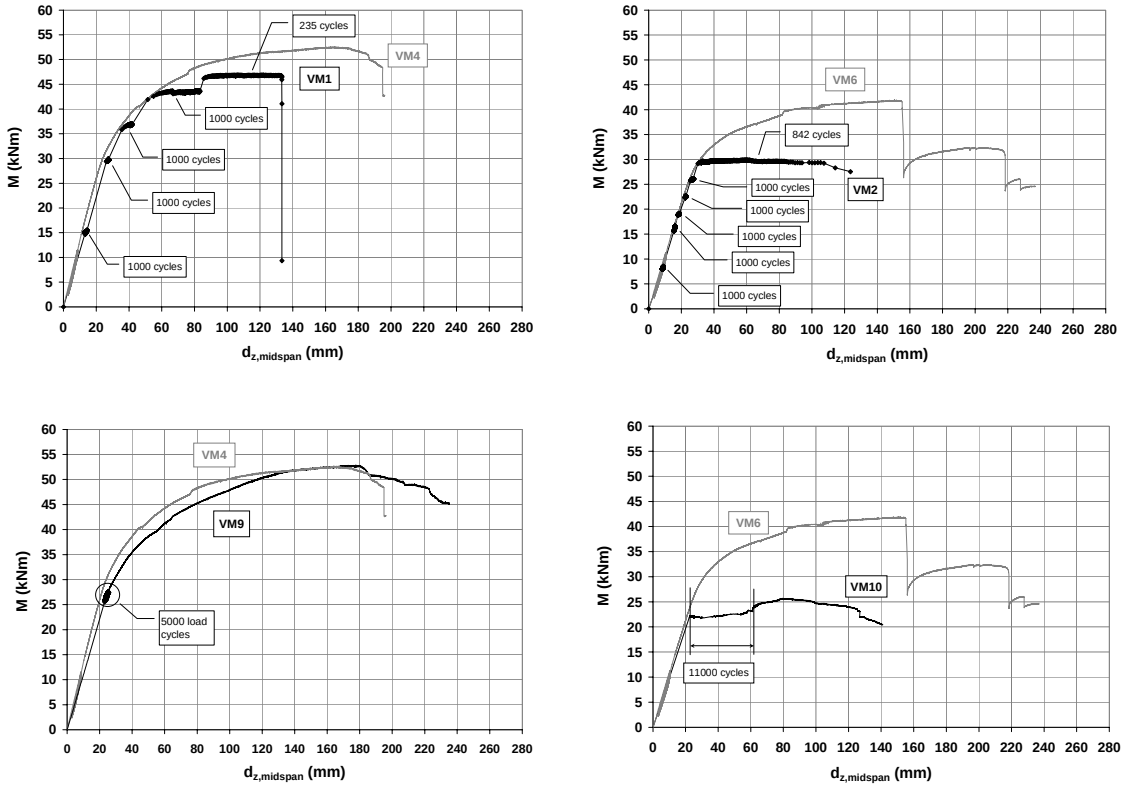

Figure 6.9 - Maximum bending moment vs. vertical deformation (at beam mid span) – all beams

6.8.2 Comparison on the evolution of vertical deformation and slip during the load cycles

Figure 6.10 compares the evolution of vertical deflection measured at the beam mid span and slip measured between steel and concrete sections, at the beams' extremes, for beams VM1 and VM2. These beams are loaded with increasing load ranges, and therefore it is important to check if there is any relation between these two parameters.

Figure 6.10 shows that the load ranges where the slip growth is visible are also the ones where the vertical deflection grows faster. Also, different rates of slip growth correspond to different rates of vertical deflection increase. Good examples of this are the two last load ranges applied on beam VM1.

When the slip attains high values, the vertical deflection grows rapidly. Finally, there is shear connection failure always associated with very high vertical deflection. In the last load ranges applied to beam VM1 and VM2, the vertical deflection increases 51.4% and 286%, respectively.

In view of this these diagrams, it is concluded that the increase of slip due to repeated loading alters the composite beam behaviour, causing shear connection failure to happen (even in beam VM1 that was designed for full connection) and enhancing the beams' vertical deflection. Therefore, slip is one of the parameters that have higher influence on vertical deflection of composite beams subjected to cyclic loadings.

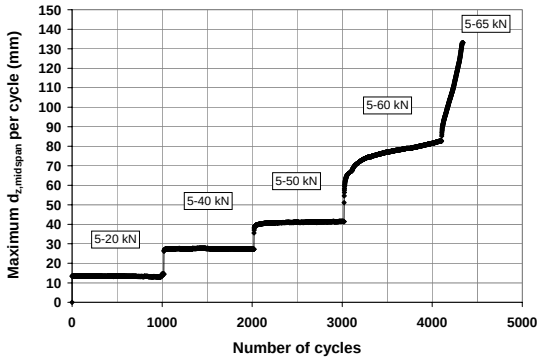

a) Vertical deflection at mid span - VM1

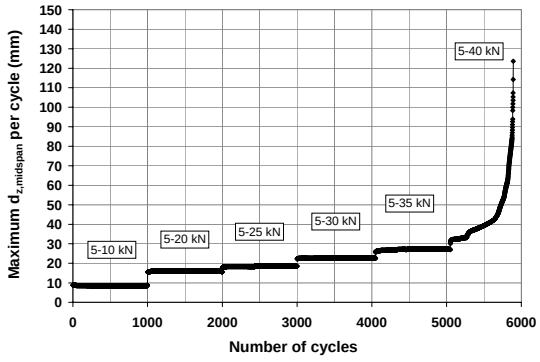

b) Vertical deflection at mid span - VM2

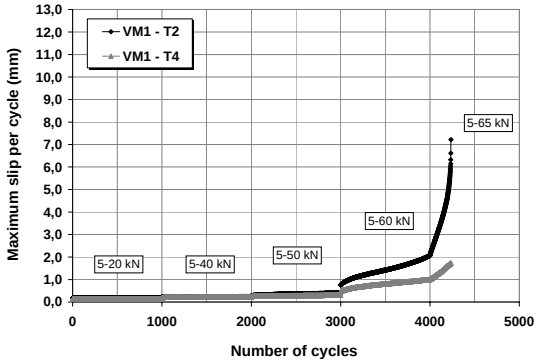

c) End-slip – VM1

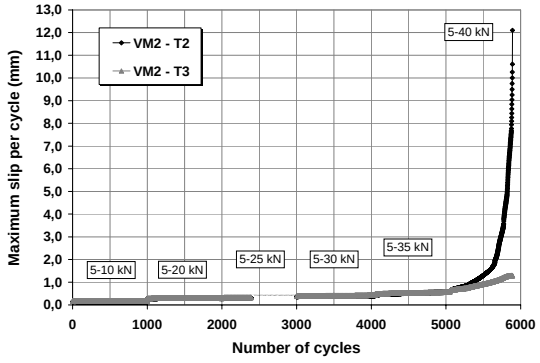

d) End-slip – VM2

Figure 6.10 – Comparison of vertical deflection and end-slip evolution for beams VM1 and VM2

6.8.3 Evolution of vertical deflection during the load cycles

Figure 6.11 presents the values of maximum vertical deformation measured in each load cycle applied to beam VM1. In all the load cycle ranges (see Figure 6.11a to Figure 6.11e), there is an initial higher increase of vertical deformation, during the first load cycles applied. For the two first load ranges (ΔP = 14.02 kN and ΔP = 39.68 kN), the vertical deflection tends to stabilize and becomes approximately constant after the first load cycles.

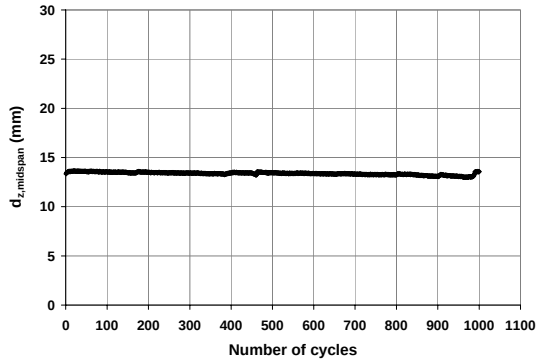

a) Range 1: ΔP = 14.02 kN ; N_{cycles} = 1000

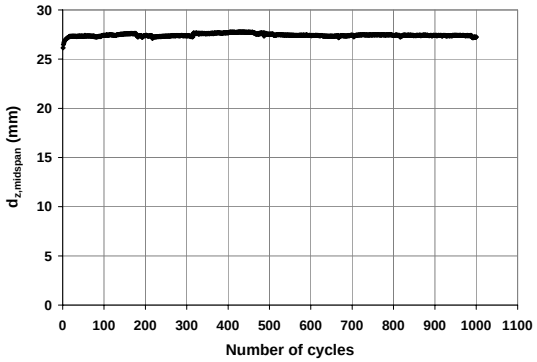

b) Range 2: ΔP = 39.68 kN ; N_{cycles} = 1000

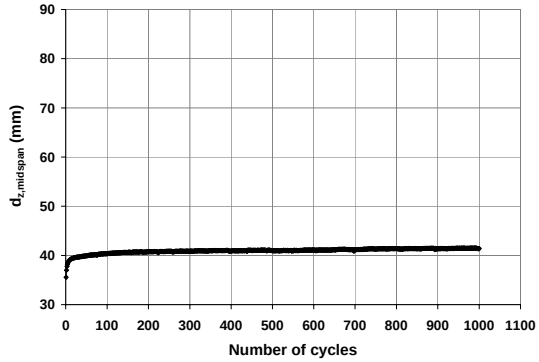

c) Range 3: ΔP = 50.54 kN ; N_{cycles} = 1000

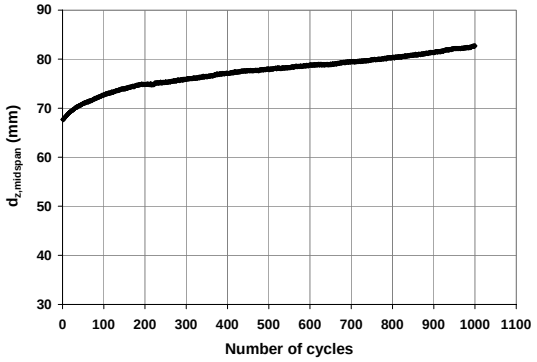

d) Range 4: ΔP = 60.95 kN ; N_{cycles} = 1000

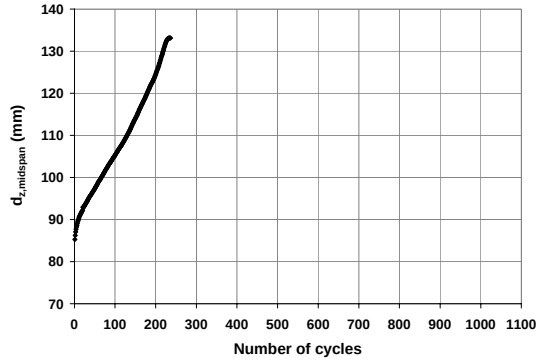

e) Range 5: ΔP = 65.79 kN ; N_{cycles} = 235

Figure 6.11 – Evolution of maximum vertical deformation measured during the load cycles applied to VM1

During the third load cycle range (ΔP = 50.54 kN), there is a small increase of vertical deflection with the number of load cycles imposed. According to Table 6.8, the level of shear force imposed on the more loaded stud is now at its maximum, but the shear stress distribution is still elastic. Therefore, only one stud is submitted to the maximum shear force. At this load range, the maximum applied load is already equal to 64.9% of the maximum load applied to beam VM4.

The last load cycle ranges (ΔP = 60.95 kN and ΔP = 65.79 kN) show a different trend: the vertical deformation tends to increase linearly with the number of load cycles applied. The linear trend reflects very well the deflection growth, if the first load cycles of each load range are not considered. VM1 vertical deflection only presents a significant growth when ΔP = 60.95 kN, corresponding to the first load cycle range for which the shear stress distribution is no longer elastic.

Figure 6.12 presents the values of maximum vertical deflection measured in each load cycle applied to beam VM2. As occurred with beam VM1, the vertical deflection increases during the first load cycles applied in each load range and afterwards tends to maintain its value. The vertical deformation of beam VM2 is kept approximately constant in all the load range cycles applied, with exception to the last load range (ΔP = 41.80 kN), where it increases exponentially after the first 200 cycles.

The maximum applied load at load range 6 is equal to 67.3% of the maximum load applied on beam VM6 (see Table 6.4). This percentage is similar to the one calculated for the first load cycle applied on beam VM1, for which the vertical deflection grows with the number of load cycles. However, the vertical deformation growth is here much faster than it was for beam VM1 and follows an exponential trend.

The longitudinal shear stress distribution is elastic for the three first load ranges and is plastic for the following ones. Unlike it occurred with beam VM1, the maximum vertical deflection of beam VM2, measured in each load cycle, is more or less constant for the first load range where the shear stress distribution is plastic (range 4: ΔP = 30.71 kN). For the range 5: ΔP = 36.19 kN, only a very small deflection growth is observed and for load range 6: ΔP = 41.80 kN, the vertical deflection rapidly grows until shear failure is verified.

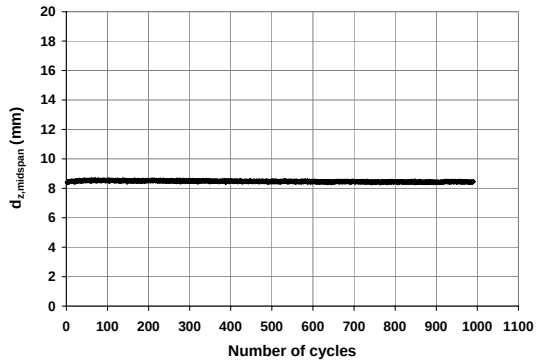

a) Range 1: ΔP = 5.45 kN ; N_{cycles} = 1000

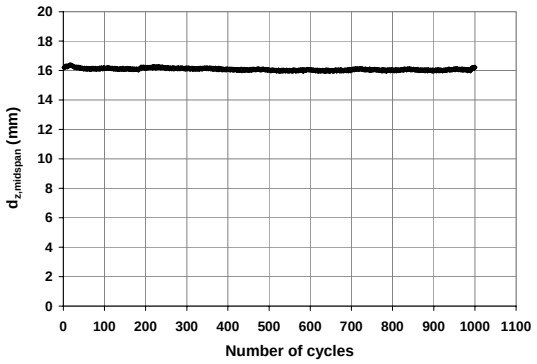

b) Range 2: ΔP = 19.85kN ; N_{cycles} = 1000

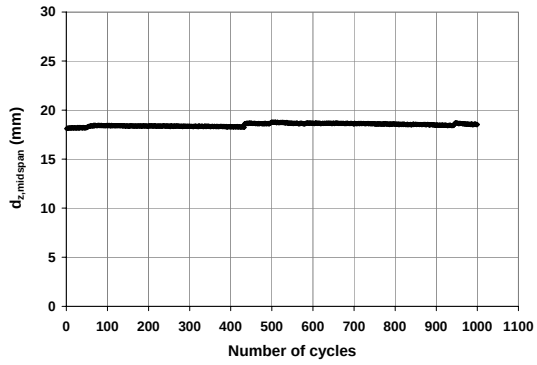

c) Range 3: ΔP = 23.45 kN ; N_{cycles} = 1000

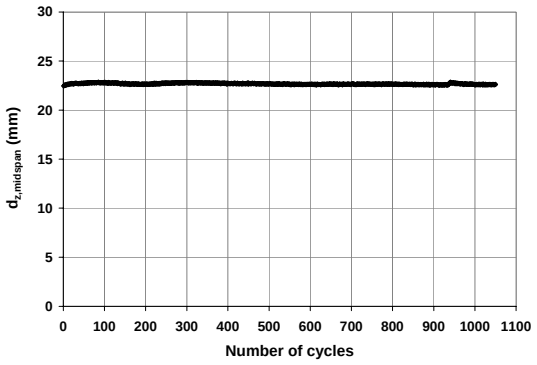

d) Range 4: ΔP = 30.71 kN ; N_{cycles} = 1000

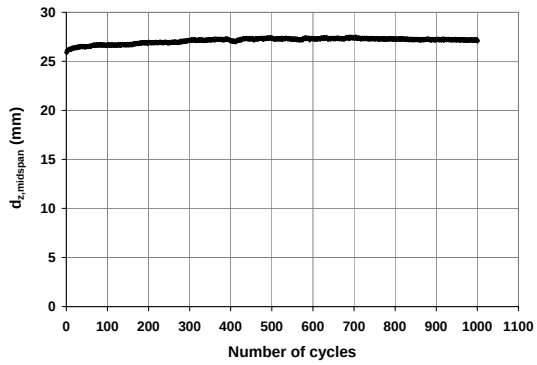

e) Range 5: ΔP = 36.19 kN ; N_{cycles} = 1000

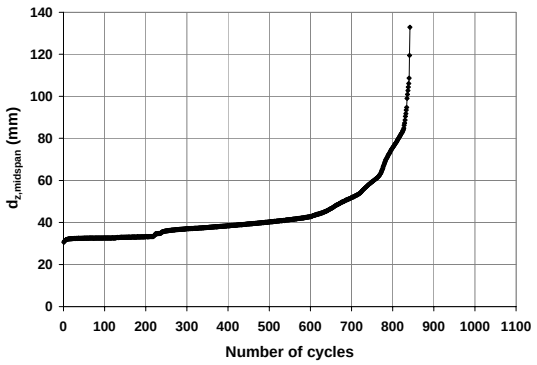

f) Range 6: ΔP = 41.80 kN ; N_{cycles} = 842

Figure 6.12 – Evolution of maximum vertical deformation measured during the load cycles applied to VM2

Figure 6.13a presents the values of maximum vertical deflection measured in each load cycle applied to beam VM9. The diagram shows that the maximum vertical deflection increases with the number of load cycles applied. A linear trend approximates well the relation between maximum vertical deflection and the number of load cycles applied, when the first 1000 load cycles are not considered.

Figure 6.13b is a copy of Figure 6.13a but now only the first 1000 load cycles are represented. During these first 1000 cycles, it is not possible to clearly identify the evolution of vertical deformation with the number of load cycles applied. In the same manner, Figure 6.11b represents the evolution of vertical deformation with the number of load cycles applied for the second load range applied to beam VM1 that is similar to beam VM9. The load range applied to beam VM1 is slightly superior to the load range imposed on beam VM9 and even so, it is not possible to identify a clear trend of deformation growth. At this point, an important conclusion is that for low load cycle ranges it is necessary to impose a high number of load cycles in order to identify the trend of deformation growth.

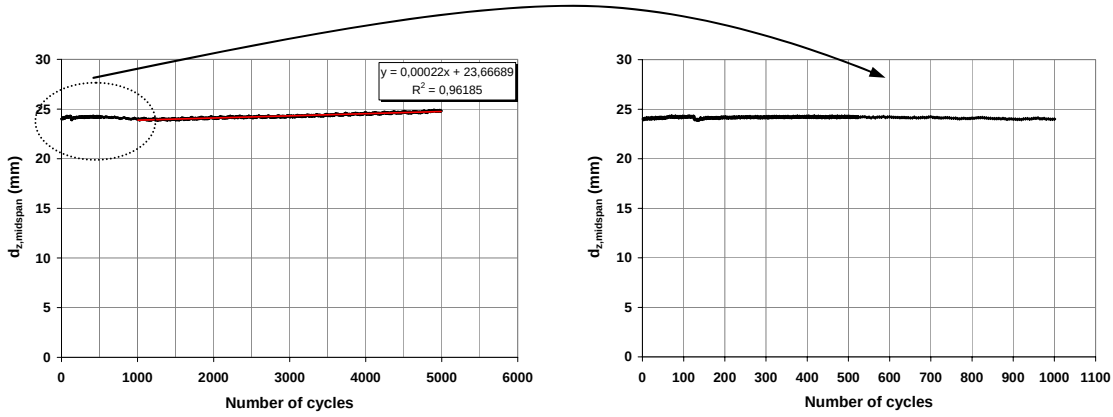

a) N_{cycles} = 5000 b) N_{cycles} = initial 1000 cycles

Figure 6.13 – Evolution of maximum vertical deformation measured during the load cycles applied to VM9 (ΔP = 35.93 kN ; N_{cycles} = 5000)

Figure 6.14 presents the values of maximum vertical deflection measured in each load cycle applied to beam VM10. The values of maximum vertical deflection measured during the initial 2225 cycles applied on beam VM10 were lost due to an electrical failure that stopped the test. After this problem was solved, the test was reinitiated and all the parameters in analysis were properly measured.

During the first 7000 load cycles applied to this beam, the vertical deflection presents a constant growth. Afterwards, it is not possible to establish a direct relation between this parameter and the number of load cycles applied.

This result was not identified in any of the previously presented beams, where it was always possible to identify some trend on the vertical deflection evolution that could be related to the number of load cycles applied.

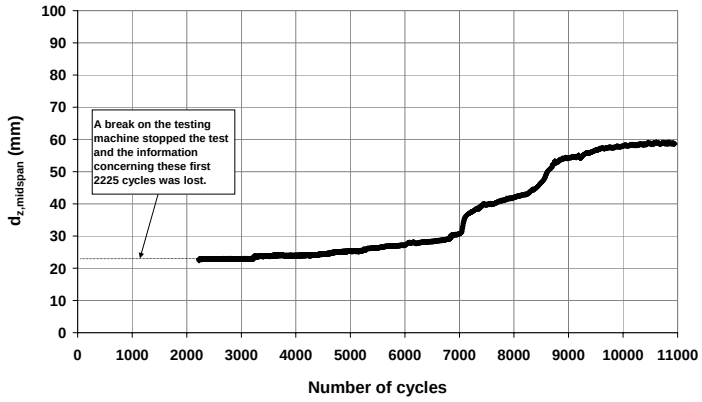

Figure 6.14 – Evolution of maximum vertical deformation measured during the load cycles applied to VM10 (ΔP = 28.96 kN ; N_{cycles} = 11000)

6.8.4 Evolution of slip during the load cycles

Figure 6.15 presents the values of maximum slip measured in each load cycle applied to beam VM1. As referred before, the longitudinal shear stress diagram follows an elastic distribution for the three first load ranges.

During the two first load ranges (range 1: ΔP = 14.02 kN and range 2: ΔP = 39.68 kN) applied to beam VM1, the maximum slip values tend to stabilize after few load cycles.

In the following load ranges, the longitudinal slip tends to grow with the number of load cycles applied and the rate of slip growth gets higher as the value of ΔP is increased. The third load range cycle, ΔP = 50.54 kN, is the first where the slip growth is significant. The increase of slip has an impact on the vertical deformation, as it is also the load range cycle where the vertical deformation shows some increase, although still small (see Figure 6.11c). During load range 4: ΔP = 60.95 kN, the slip develops higher values on one side of the composite beams (Figure 6.15d). This growth gets faster with the number of load cycles applied.

Slip develops higher values in one side of the beam. For this side and before failure, the slip values tend to increase exponentially during the last load range applied to the beam - range 5: ΔP = 65.79 kN (Figure 6.15e). This exponential growing trend was not identified in the push-out tests presented in Chapter 4. Considering the curves presented there, this is an unexpected result.

Table 6.8 shows that for the applied load ΔP = 50.54 kN, the shear force range acting on the more loaded stud is approximately equal to the shear force range applied to the more loaded stud when ΔP = 60.95 kN and ΔP = 65.79 kN. For these last load ranges, more than one stud is loaded to its maximum. Figure 6.15 shows that the beam end-slip growth gets

higher when the load range is increased, which means that the studs that are not loaded to their maximum should have an effect on the slip evolution, causing the differences observed between diagrams c), d) and e) from Figure 6.15. In this case, the less loaded studs are limiting the slip developed by the more loaded studs and therefore are reducing the effects of repeated loading on the more loaded studs.

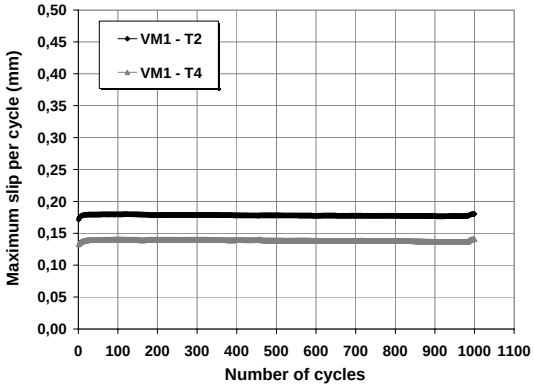

a) Range 1: ΔP = 14.02 kN ; N_{cycles} = 1000

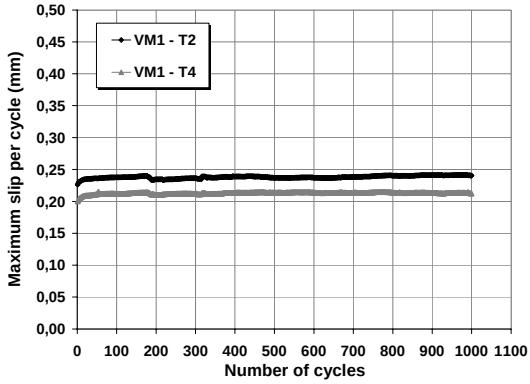

b) Range 2: ΔP = 39.68 kN ; N_{cycles} = 1000

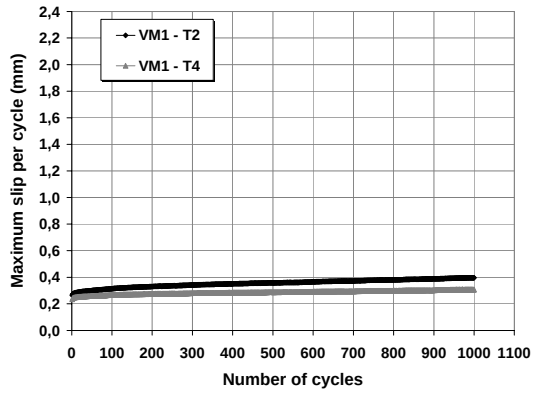

c) Range 3: ΔP = 50.54 kN ; N_{cycles} = 1000

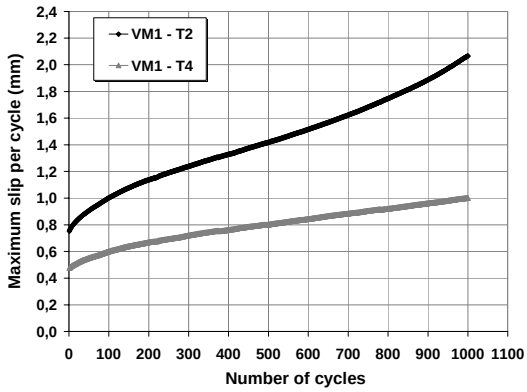

d) Range 4: ΔP = 60.95 kN ; N_{cycles} = 1000

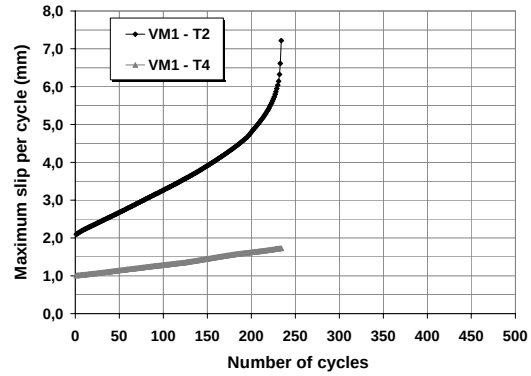

e) Range 5: ΔP = 65.79 kN ; N_{cycles} = 235

Figure 6.15 – Evolution of slip during the load cycles applied to VM1

Figure 6.16 presents the values of maximum slip measured in each load cycle applied to beam VM2.

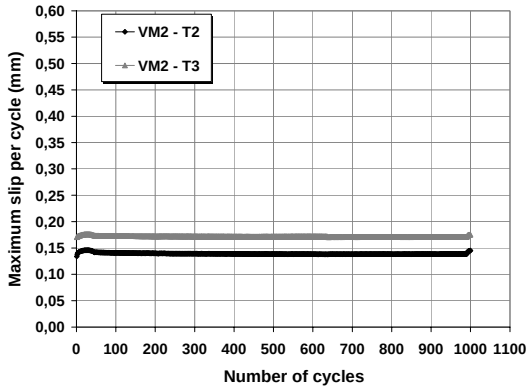

a) Range 1: ΔP = 5.45 kN ; N_{cycles} = 1000

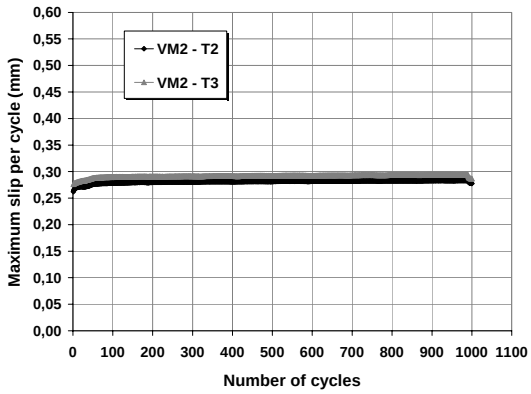

b) Range 2: ΔP = 19.85kN ; N_{cycles} = 1000

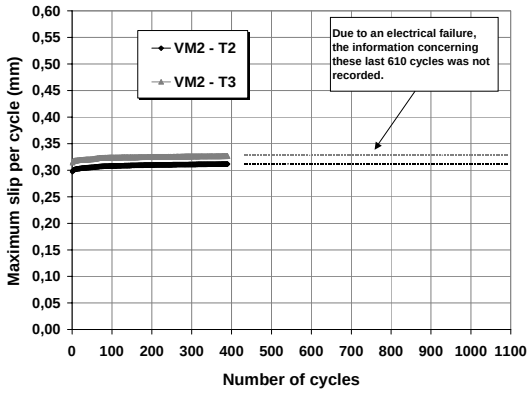

c) Range 3: ΔP = 23.45 kN ; N_{cycles} = 1000

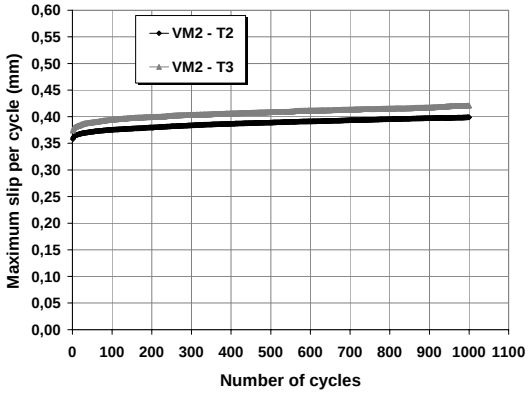

d) Range 4: ΔP = 30.71 kN ; N_{cycles} = 1000

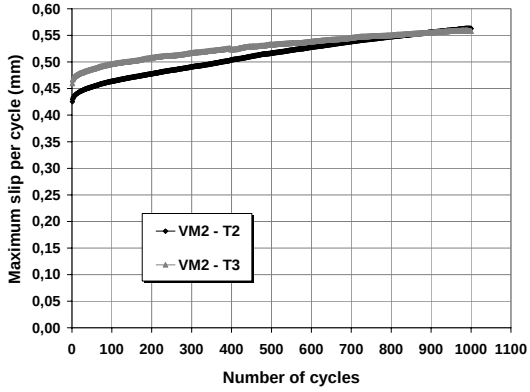

e) Range 5: ΔP = 36.19 kN ; N_{cycles} = 1000

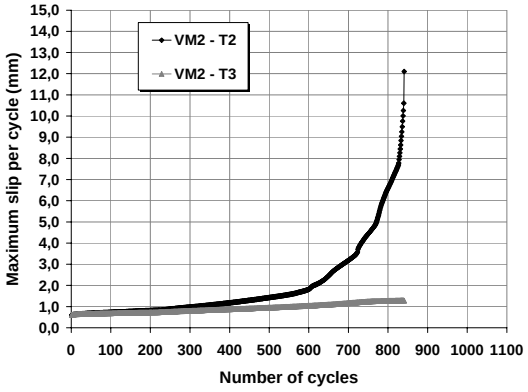

f) Range 6: ΔP = 41.80 kN ; N_{cycles} = 842

Figure 6.16 – Evolution of slip during the load cycles applied to VM2

The same type of behaviour is identified for beam VM2. During the three first load ranges (ΔP = 5.45 kN, ΔP = 19.85kN and ΔP = 23.45 kN) applied to beam VM2, the maximum slip values tends to stabilize after few load cycles.

As the number of shear connectors in beam VM2 is smaller than in beam VM1, larger slip values are attained when similar load ranges of VM1 and VM2 are compared.

As occurred with VM1, the slip values tend to increase exponentially before failure. Larger total slip is attained for beam VM2 at this moment.

A common result obtained on breams VM1 and VM2 is that the rate of slip growth is different for each load range, even when there is plastic distribution of shear stress and one or more studs are loaded to their maximum shear strength. An important conclusion to take is that the studs that are not loaded to their maximum should have an important influence on the connection behaviour. In fact, it seems that the shear studs that are not submitted to their maximum load capacity are limiting the value of slip along the composite beam, because different rates of slip growth are verified when at least one connector is loaded to its maximum.

It is therefore more difficult to establish relations that can predict the slip growth just based on the number of load cycles applied, because they depend on the connectors' distribution.

Figure 6.17 shows the evolution of maximum slip during the load cycles applied to VM9. The level of load applied is in a range that fits the elastic behaviour of the shear connection, as shown in Table 6.8. Even so, during the 5000 cycles of a constant load range applied to beam VM9, it is possible to identify that slip grows with the number of load cycles applied and that this growth is approximately linear. The linear growth rate is equal to 4.33×10^{-6} mm / cycle.

If the rate of slip growth measured for beam VM9 is compared to the values of slip growth measured during the cyclic push-out tests presented in Chapter 4, it is possible to state two important observations:

- the configuration of the maximum slip vs. number of load cycles is better approximated by a linear law, than a logarithmic law;
- the value here obtained is smaller than any of the growth rates measured during the cyclic push-out tests, presented in Chapter 4 (see Table 4.12), although it is close to the value obtained for specimen CN13.4, when $\Delta P/P_u$ = 0.48 (for VM9, $\Delta R/P_u$ = 0.66, see Table 6.8)

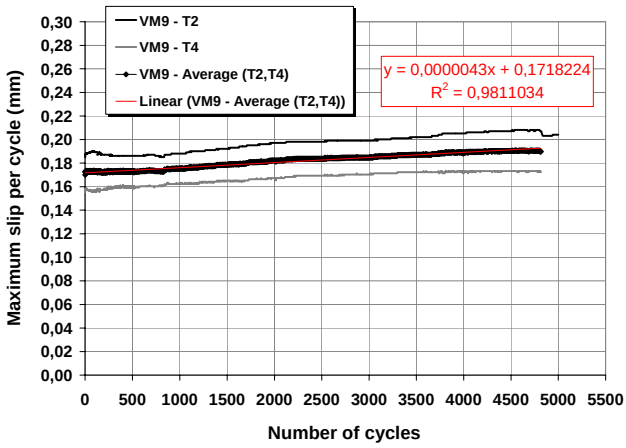

Figure 6.17 – Evolution of slip during the load cycles applied to VM9

Figure 6.18 shows the evolution of maximum slip during the load cycles applied to VM10. The rate of slip growth is approximately the same for the first 4500 load cycles. After these cycles, it suffers a small increase until around 7000 cycles are completed. From this moment on, large slip values develop on one side of the beam, while the other side tends to maintain the slip previously achieved. The rate of slip growth until $N = 7000$ cycles is well approximated by a linear law (Figure 6.18b). This linear growth rate is equal to 105.0×10^{-6} mm / cycle.

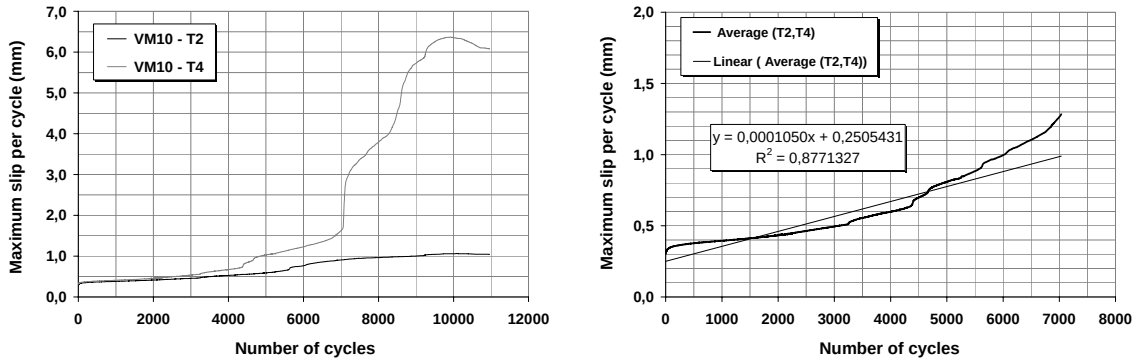

a) Complete curve ($N_{cycles} = 11000$) b) Initial part of the curve ($N_{cycles} = 7000$)

Figure 6.18 – Evolution of slip during the load cycles applied to VM10

The 4th load range applied to beam VM2 is comparable to the load range applied to beam VM10, as both are of similar load range and similar maximum load value. The increase in slip measured during the 1000 load cycles of the 4th load range applied to beam VM2 is equal to 0.044 mm, while the increase in slip measured during the first 1000 load cycles of the applied to beam VM10 is equal to 0.093 mm. Although the value of slip measured for VM10 is higher, it is considered that these values are close. This aspect shows again the importance of the number of load cycles applied, because the evolution of slip on VM10 changes a lot when $N > 7000$ cycles. So, the story of loading and the number of load cycles applied have also an important influence on the evolution of slip.

The level of load applied to beam VM10 causes a shear stress distribution that is no longer elastic, as shown in Table 6.8. The shear load range applied to the more loaded studs is equal to $\Delta R/P_u = 0.88$. The results obtained in the cyclic push-out tests presented on Chapter 4 show that the rate of slip growth measured there is higher than the one measured for beam VM10. For example, specimen CN13.5, when submitted to a load range of $\Delta P/P_u = 0.65$, presents a rate of slip growth that is equal to 143.0×10^{-6} mm / cycle.

In the push-out tests presented in Chapter 4, the slip growth is always directly dependent on the number of load cycles applied. A linear or logarithmical relation between these two parameters is usually found. The results on beam VM10 show another aspect that was not possible to identify during the push-out tests: after a large number of load cycles is applied, the slip growth may no longer have a direct relation with the number of load cycles applied. As presented in Figure 6.18a, after 7000 load cycles are applied, the slip growth is focused on one half of the beam and does not always present the same trend, it is sometimes faster and other times slower.

As was observed for beams VM1 and VM2, the rates of slip growth measured in the tests of beams VM9 and VM10 are always smaller than any of the values measured in the cyclic push-out tests presented in Chapter 4, for load ranges that are close to the ones imposed on beams. In beams, not all the shear studs are loaded with the same shear load range. It is important to remember that the values of shear load presented in Table 6.8 only regard the more loaded stud(s). Therefore, it can be concluded that the rate of slip growth measured in composite beams tends to be smaller than the rate of slip growth measured in push-out tests. This last type of test can be considered as conservative regarding the evaluation of this parameter.

6.8.5 Evolution of strain during the load cycles

Figure 6.19 presents the values of strain measured in each load cycle applied to beam VM1. The curves presented are the average of two strain gauges positioned at the same level of the cross section (see Figure 5.13, from Chapter 5).

The values of strain grow with increasing load range value. Concrete lower fibbers are initially under compression and later in tension. The steel section upper fibbers never get compressed and therefore the steel section is always in tension. There is initial strain growth in every load range. Afterwards, the strain values tend to stabilize. Strain growth is visible for load ranges 4 and 5, the ones where vertical deflection and slip present significant increase.

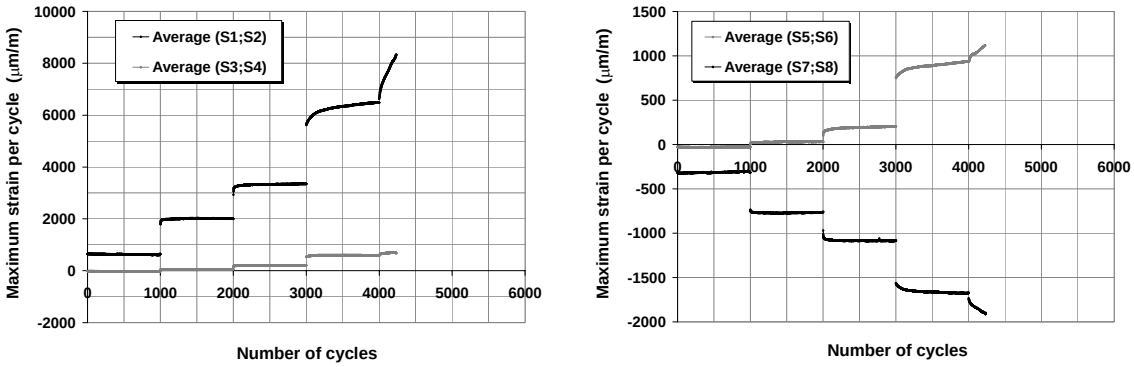

Figure 6.19 – Evolution of strain at the beam mid span during the load cycles applied to VM1

Figure 6.20 presents the variation of strain along cross section B-B' (at beam mid span) and Figure 6.21 presents the variation of strain along cross sections A-A' and C-C', both positioned at opposite quarter spans of the composite beam. The strain diagrams represented correspond to load cycle number 5 and load cycle number 1000, for each load range applied to beam VM1 (see Table 6.4).

The values of strain, measured at the initial and final cycles of each load range applied to cyclic loaded beams are also presented in Table A6.1, from Appendix 6.1.

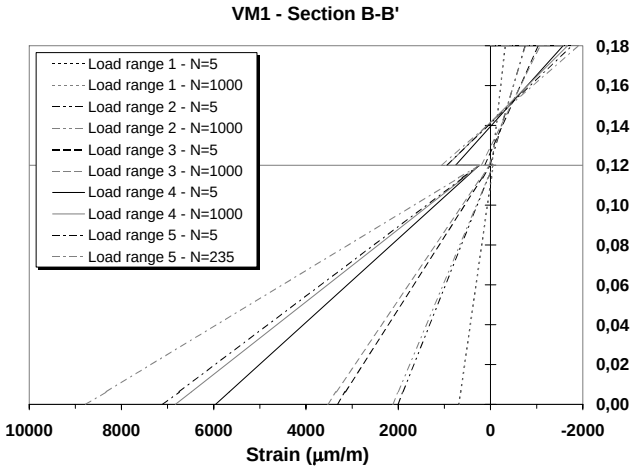

Figure 6.20 – Evolution of strain during the load cycles applied to VM1 at cross section B-B'

These figures shows that, with exception to load range 1, there is always strain variation due to cyclic loading. An increase of tensile strain on the steel section and a smaller increase of compressive strain on the concrete upper fibbers characterize this variation. There is also an increase of slip strain during the repetition of cycles. The increase in slip strain should exist in order to enhance slip, which is in accordance with the results presented in 6.8.4.

Until load range 3, the strain distribution in opposite quarter spans is almost identical. For load ranges 4 and 5, the strain values and especially the slip strain are higher at cross section C-C', confirming the half side of the beam where slip growth is higher and finally shear failure occurs.

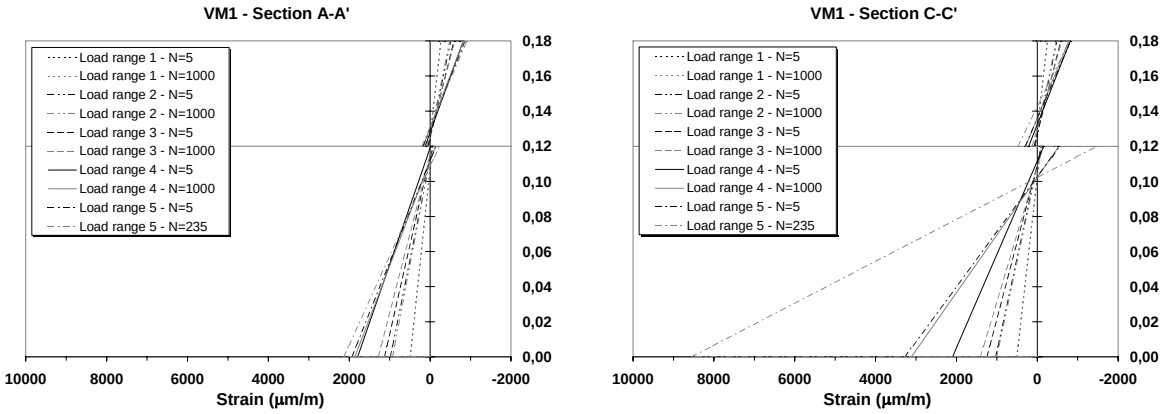

Figure 6.21 – Evolution of strain during the load cycles applied to VM1 at cross section A-A' and C-C'

The strain diagrams presented for beam VM1 show that the loss of composite action begins with load range 3 and ends up with failure during load range 5. For these load ranges, the ratio $\Delta P/P_{max,VM4}$ is equal to 64.9%, 78.2% and 84.5%, respectively (see Table 6.4).

Beam VM1 is mostly affected by cyclic loading when the load range applied to it is over 60% of the beam strength. However, it is important to remember that 1000 cycles may not be enough to identify the alterations on the strain diagrams for load range 1 and 2, as was previously observed for low load ranges.

There is curvature increase during each load range applied on beam VM1, with exception to load range 1, where curvature remains more or less constant. The curvature increase is similar for load ranges 2, 3 and 4, varying from 7.5 to 15% in each load range. In the last load range, curvature increases 27.3%.

Figure 6.22 presents the values of strain measured in each load cycle applied to beam VM2. As for beam VM1, the values of strain grow with increasing load range value. In this case, concrete lower fibbers are always in tension. The steel section is always in tension, except during the final load cycles applied in range 6. The diagrams presented show that at these final load cycles, there is large tensile strain increase on the steel lower fibbers and the steel upper fibbers become compressed. At the same time, tensile strains at concrete lower fibbers increase very rapidly and compression strains at the concrete upper fibbers tend to decrease. This final behaviour can only be explained with the loss of composite action between steel and concrete, where each section tends to work separately. When the

loss of composite action takes place, there is stress transfer from the concrete section to the steel section, as proved by the decrease of compression strains at the concrete upper fibbers. The tensile strains at the concrete lower fibbers show a more rapid increase due to concrete cracking.

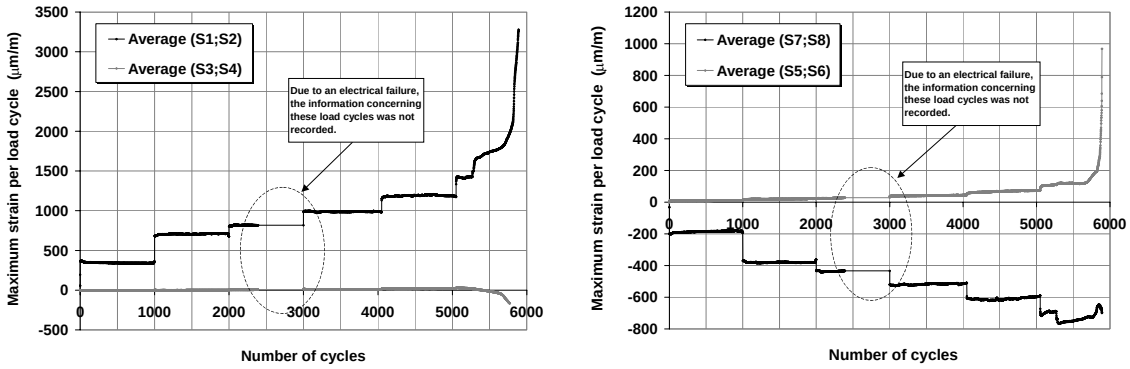

Figure 6.22 – Evolution of strain during the load cycles applied to VM2

Figure 6.23 presents the variation of strain along cross sections B-B' (at beam mid span) and A-A' (at beam quarter span). The strain diagrams represented correspond to load cycle number 5 and number 1000, for each load range applied to beam VM2 (see Table 6.4). For the last load range (range 6), the strain diagram is represented only until $N = 700$, because of strain gauge failure.

For the first four load ranges applied, almost no strain variation is verified due to cyclic loading and for load range 5, only a very small strain variation is measured. A significant strain variation due to cyclic loading is verified for load range 6, ending with the beam failure.

There is a very small increase of slip strain (ds/dx) during the repetition of the first load cycle ranges (range 1 to range 5). Again, the increase of slip strain is only significant for load range 6. According to Figure 6.16, the increase in slip is mainly verified during load range 6, which means that the values of strain measured are in accordance with the results obtained on slip.

All the strain diagrams presented for beam VM2 show that the loss of composite action is mainly produced during load range 6 and takes place much faster than it did for VM1 in any load range. For this load range, the ratio $\Delta P/P_{max,VM6}$ is equal to 67.3%, while for the previous load cycles, this ratio is always lower than 60% (see Table 6.4). It is possible that a beam designed for partial connection is rapidly affected by cyclic loading if the load range applied to it is over 60% of the beam strength. This issue should be object of further analysis, in order to have more results that can confirm this hypothesis.

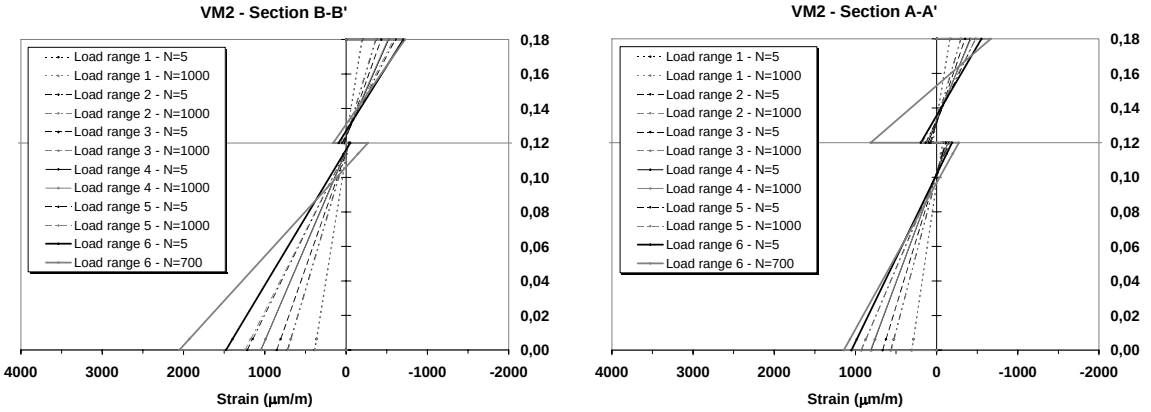

Figure 6.23 – Evolution of strain during the load cycles applied to VM2 at cross sections B-B' (mid span) and A-A' (quarter span)

Curvature remains approximately constant during the load ranges 1 and 2, applied to VM2 (see Table 6.1). The curvature suffers small increases in the load ranges applied, always less than 4%, with exception to the last load cycle, where the curvature increase is higher than 2.5.

Beam VM9 is designed to have full connection. The level of load applied on beam VM9 imposes an elastic distribution of shear stress at the steel to concrete interface (see Table 6.8), and also an elastic distribution of strains at all composite cross sections, as all the strain values are kept within the elastic range its material behaviour. The concrete slab lower fibbers are always in tension, but the values of strain that were measured show that there is no cracking during the 5000 load cycles applied (see Figure 6.24).

As presented in Figure 6.24, the values of strain grow approximately linearly with the number of load cycles applied. At the beam mid span, there is an increase of tensile strain on the lower steel fibbers while the compressive strains on the upper concrete fibbers remain more or less constant. At the beam quarter spans, the tensile strain on the lower steel fibbers is more or less constant during the load cycles and the compression strains on the upper concrete fibbers also tend to decrease.

As the load cycles value is constant and the strain values are within the materials elastic range, it can be concluded that the variation of strain can only be caused by the evolution of slip that is also growing linearly with the number of load cycles applied, as presented in Figure 6.17.

During the 5000 load cycles applied, the loss of composite action is very small, because the slip strain varies very little.

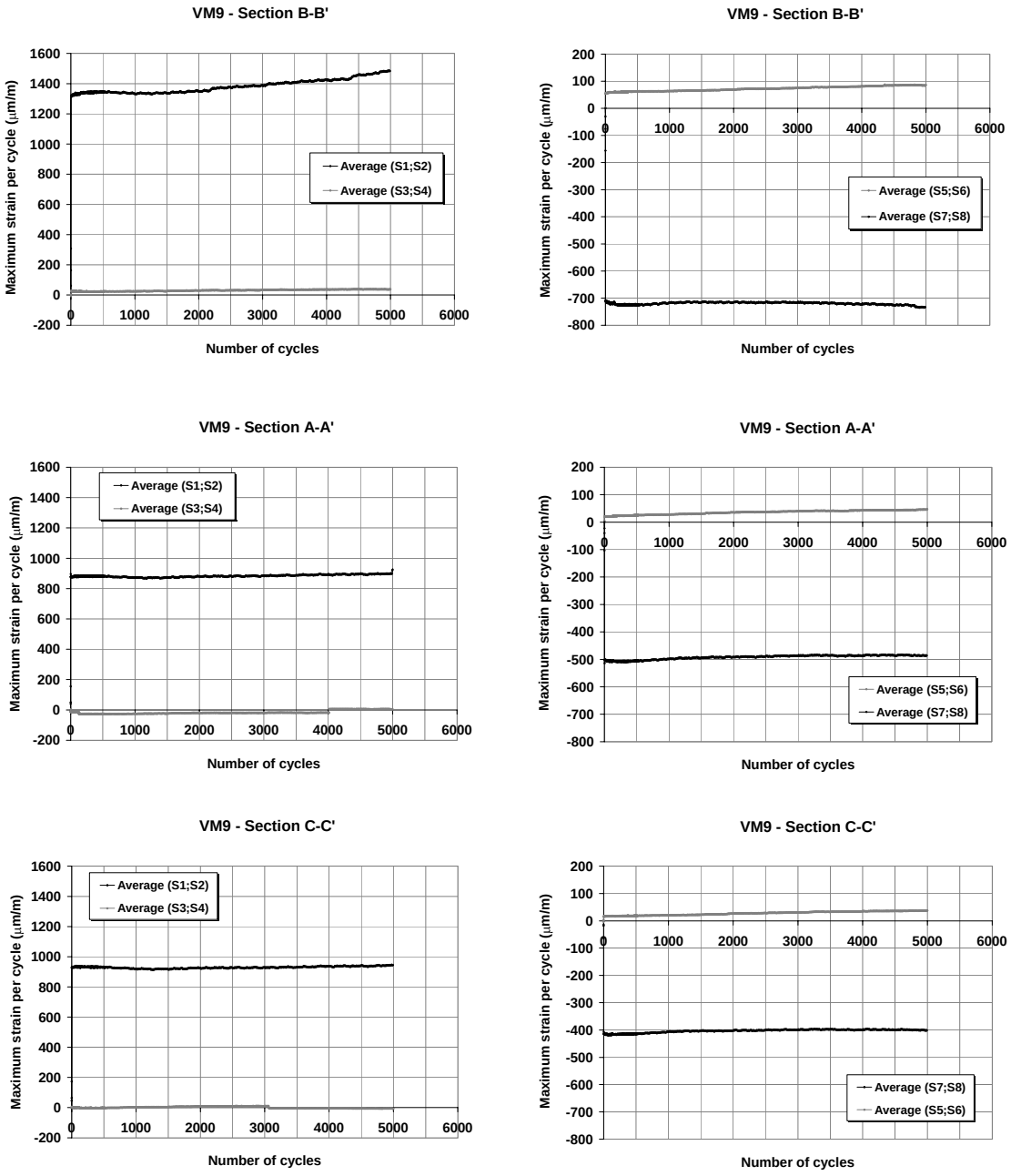

Figure 6.24 – Evolution of strain during the load cycles applied to VM9

Figure 6.25 presents the strain diagrams of cross section B-B' of beam VM9 (beam midspan). Figure 6.26 presents the strain diagrams of cross sections A-A' and C-C' of beam VM9, both positioned in opposite quarter spans of the composite beam (see Figure 5.12, from Chapter 5).

There is little variation on the strain diagram during the load cycles. In the three cross sections, the slip strain, *ds/dx*, suffers a small increase during the 5000 load cycles, which means that there is increase of slip during the load cycles applied but that the evolution of slip, as presented in Figure 6.17, is small. The loss of composite action is

small, which means that the increase of vertical deformation should not be very high, as was verified in 6.8.3.

During the 5000 load cycles applied, a curvature increase at mid span of approximately 9% is verified, according to the strain measurements done. The increase in vertical deformation, presented in Figure 6.13, is equal to 0.97 mm, which corresponds to 4.1% of the beam maximum vertical deformation measured in the initial load cycles. The increase of curvature and vertical deflection at the beam mid span should be identical, in percentage of the initial value. These values are considered to be close.

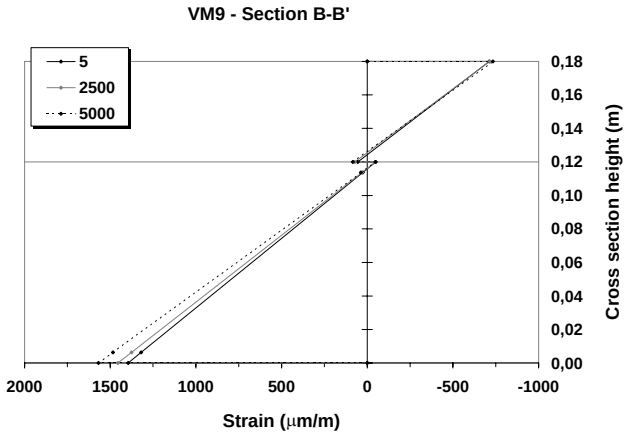

Figure 6.25 – Evolution of strain during the load cycles applied to VM9 at cross section B-B' (mid span)

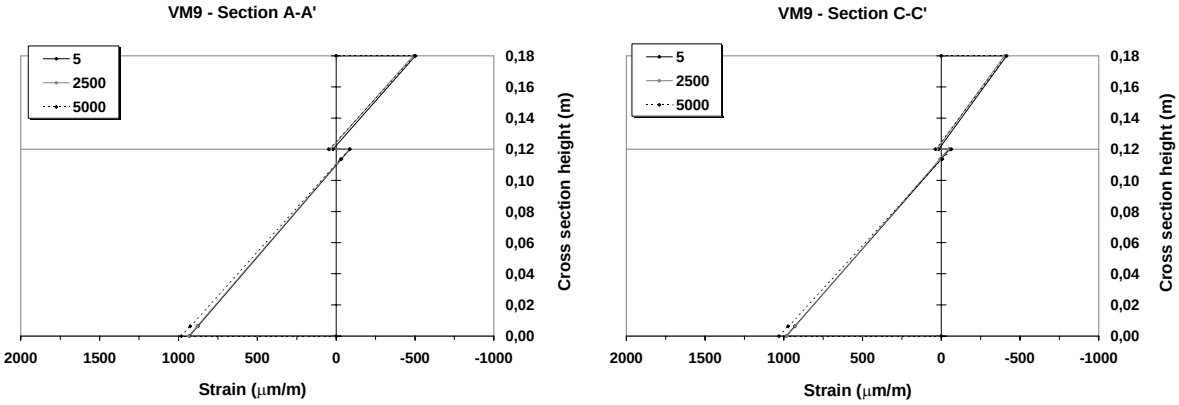

Figure 6.26 – Evolution of strain during the load cycles applied to VM9 at cross sections A-A' and C-C' (positioned in opposite quarter spans)

The strain diagram for maximum bending moment at cross section B-B' of beam VM9 is compared with the same diagram of beam VM4, in order to check on the alterations imposed by the 5000 load cycles applied. The two strain diagrams are similar. The principal differences consist on the slip strain and the higher strains measured on the

steel section verified for beam VM9. Both aspects may reflect the result of 5000 load cycles applied.

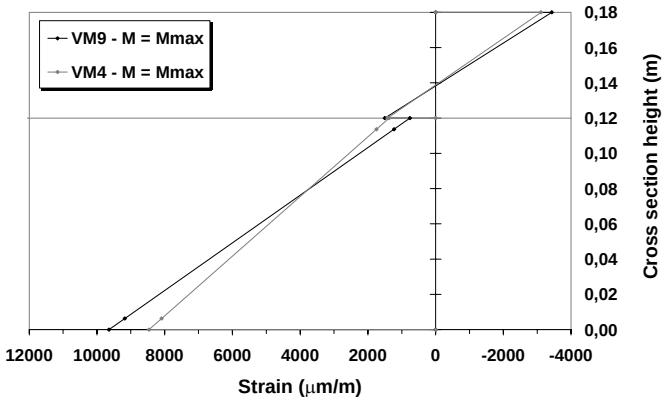

Figure 6.27 – Strain diagram for maximum bending moment at cross section B-B' of beams VM9 and VM4

Figure 6.28 presents the values of strain measured in each load cycle applied to beam VM10. During the first 7000 load cycles applied to beam VM10, strain grows very slowly and approximately linearly with the number of load cycles applied, as occurred with beam VM9. The strain values at the upper fibbers of the concrete section tend to decrease, which means that there should be stress transfer from the concrete section to the steel section. Again, there is small slip strain at the interface between the two materials, until 7000 load cycles are applied.

The loading is evenly distributed along the composite beam. As presented in Figure 6.28, the strain evolution in cross sections positioned in opposite quarter spans (cross sections A-A' and C-C') is very similar.

After around 7000 load cycles are applied to beam VM10, the increase of vertical deformation, slip and strain becomes faster and the relation between all the referred parameters and the number of load cycles applied is altered. All the graphs (vertical deformation, slip and strain) show this similar tendency. At the beam quarter span (cross sections A-A' and C-C'), there is a sudden strain increase in the steel section while in the concrete section there is a sudden strain decrease, which means that there is a stress transfer from the concrete section to the steel section. From this moment on, this stress transfer happens in every load cycle applied on VM10: steel strains keep increasing and concrete strains keep decreasing until $N = 11000$ cycles.

The strain values measured in the upper fibbers of the concrete slab, at cross section B-B', decrease slowly, with approximately the same rate through all the load cycles applied. On the opposite, the strains measured in the steel section, at cross section B-B' also increase slowly until $N = 7000$ cycles and then start increasing much faster. The difference in the variation of curvature measure between the steel and the concrete section

is only possible if there is uplift at the steel and concrete interface, which is confirmed with the transducer positioned near the beam mid span, to measure this effect.

During the 11000 load cycles applied, a curvature increase at mid span of approximately 16% is verified for the concrete section and 369% is verified for the steel section, according to the strain measurements done. The increase in vertical deformation, presented in Figure 6.13, is equal to 35.9 mm (measured since $N = 2225$ cycles), which corresponds to 158% of the beam maximum vertical deformation measured in the initial load cycles.

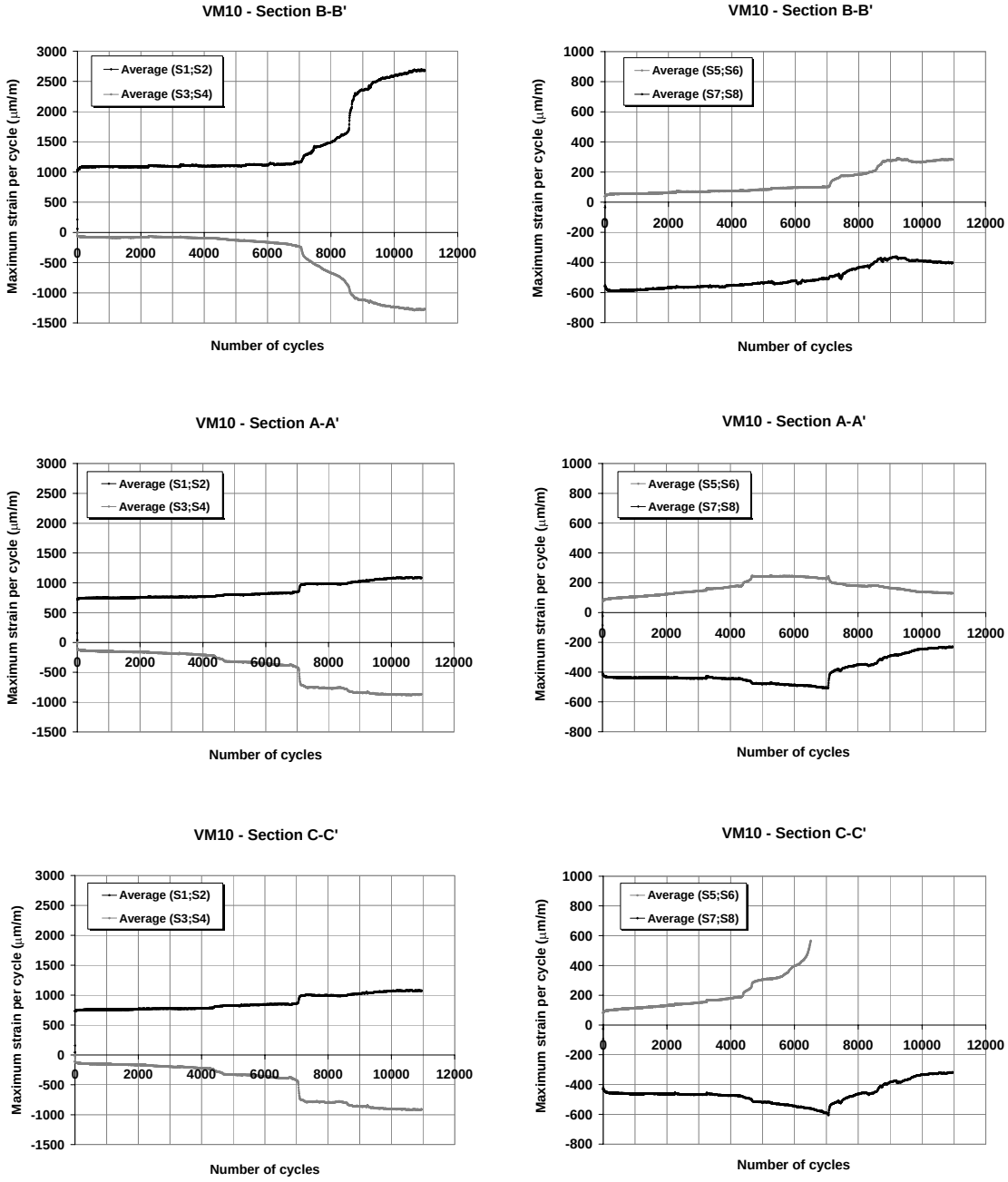

Figure 6.28 – Evolution of strain during the load cycles applied to VM10

Figure 6.29 presents the strain diagrams in two cross sections of beam VM10: B-B' (mid span) and A-A' (quarter span). Beam VM10 was designed to have only partial connection at the interface between steel and concrete sections. In this case, the strain diagrams presented show high variation during the load cycle application. There is an important increase on the variation of slip, *ds/dx*, during the 11000 load cycles applied, resulting in an important transfer of stress between the concrete and the steel sections. At section B-B', maximum strain at the steel section grows to more than twice its initial value, while maximum strain at the top fibber of the lightweight concrete section tends do decrease as there is loss on the steel to concrete connection.

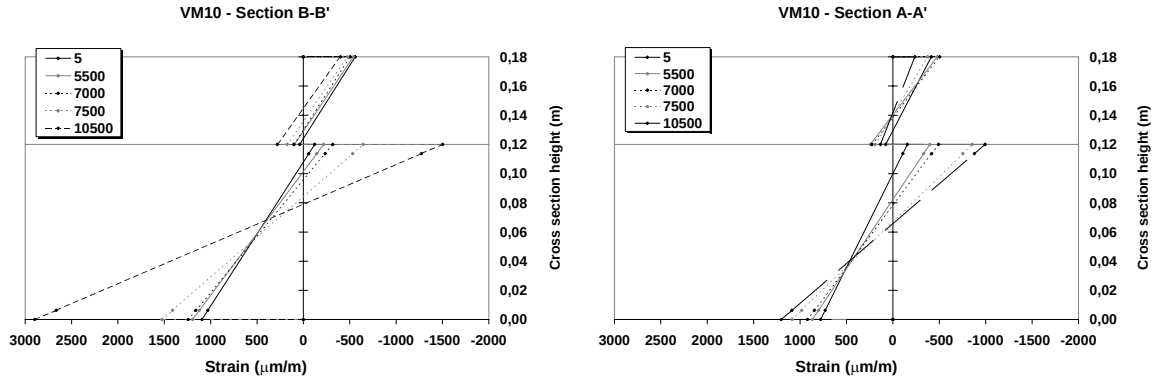

a) Beam VM10 – Mid span

b) Beam VM10 – Quarter span

Figure 6.29 – Evolution of strain during the load cycles applied to VM10 at cross sections B-B' (mid span) and A-A' (quarter span)

6.9. Comparison between beam test results and push-out test results

There is a relevant relation between the results obtained in beam tests and push-out tests for static loadings, as presented in Chapter 5. In the same manner, it is important now to establish some comparisons between the results obtained with the two types of tests, concerning cyclic loadings. The comparison presented in the following concerns push-out tests and beam tests where the shear load range, applied on each connector is similar.

Figure 6.30 establishes a comparison between the values of slip measured in the tests of CN13.5, CN13.6 and VM2. The measurements presented for specimens CN13.5 and CN13.6 correspond to the first load range applied to each specimen (see Table 4.5). The values measured for beam VM2 correspond to the first load range applied to the beam (see Table 6.8). According to the analysis made for Table 6.8, the loads applied to beam VM2 during the first load cycle range induce shear stresses that are still in the elastic range.

Specimens CN13.5 and VM2 show hardly no increase of slip – the maximum slip value per load cycle is almost constant during the 1000 load cycles applied. On the other

hand, the values of slip measured for specimen CN13.6 show that there is a small increase of the slip value during the load cycles.

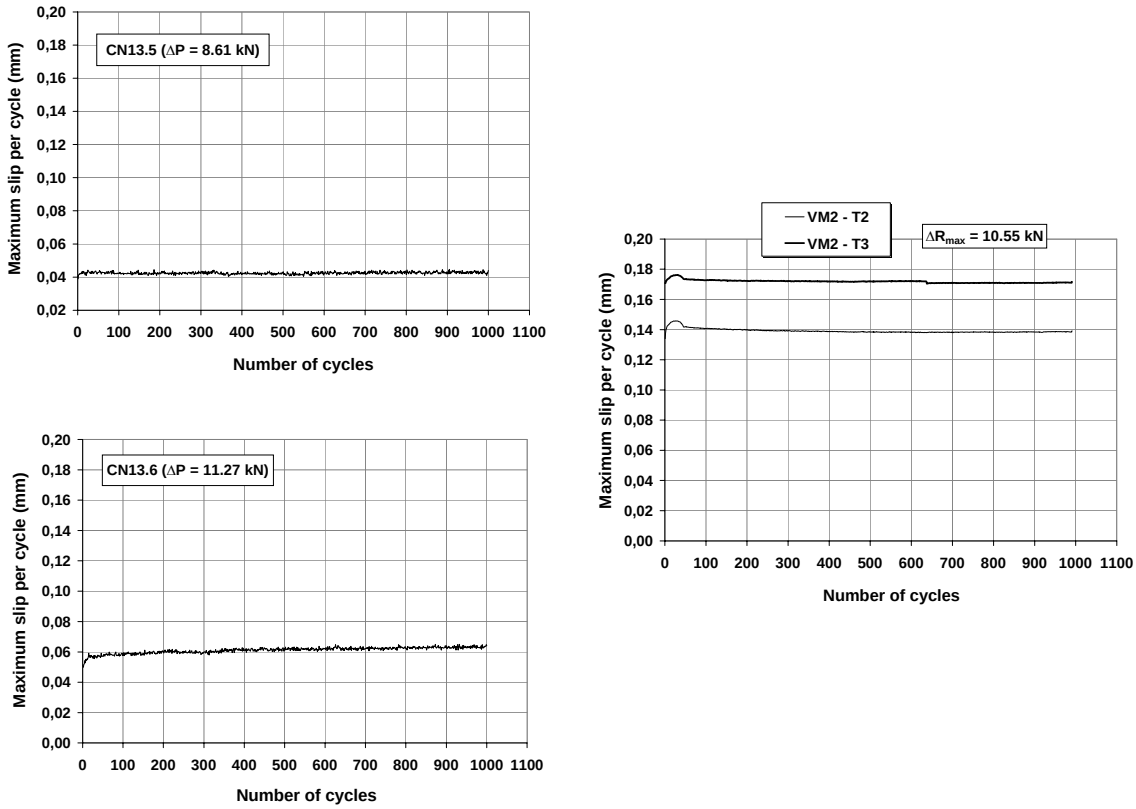

Figure 6.30 – Evolution of slip – comparison between CN13.5, CN13.6 and VM2

Figure 6.31 establishes a comparison between the values of slip measured in the tests of CN13.5 and VM9. The measurements presented for specimen CN13.5 correspond to the fourth load range applied to the specimen (see Table 4.5). The values measured at beam VM9 correspond to the unique load range applied to the beam (see Table 6.8). According to the analysis made in Table 6.8, the loads applied to beam VM9 during the first load cycle range induce shear stresses that are still in the elastic range.

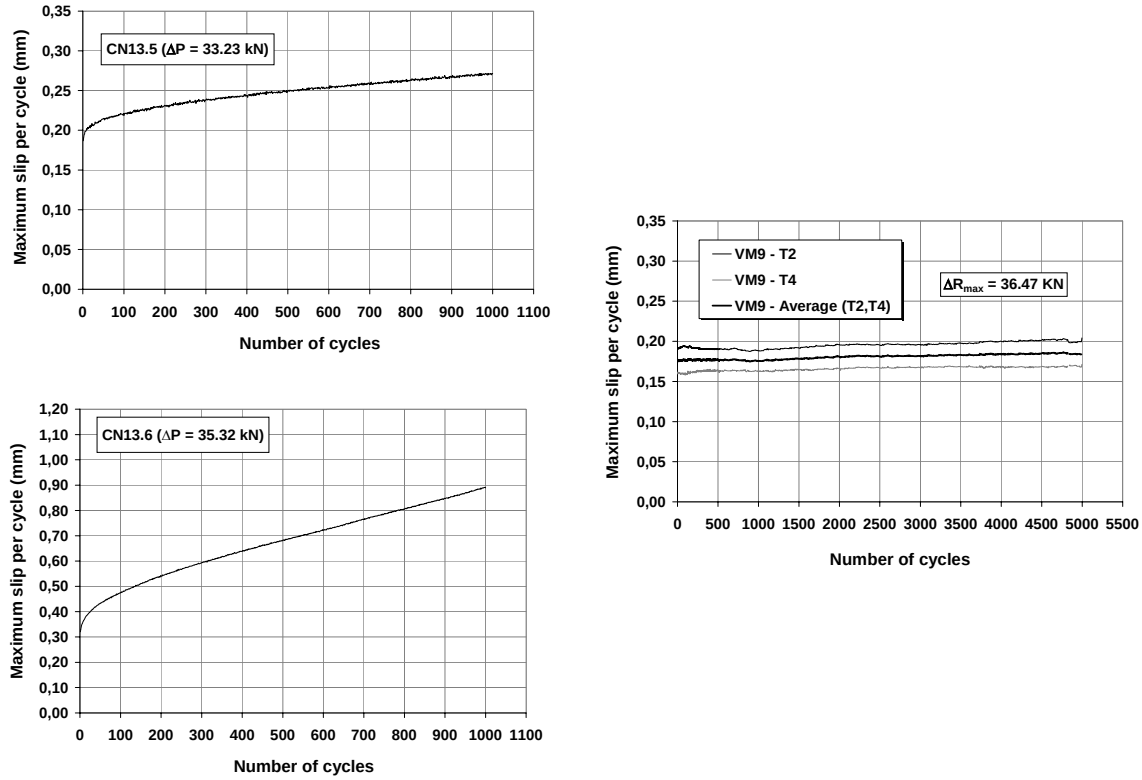

Figure 6.31 – Evolution of slip – comparison between CN13.5, CN13.6 and VM9

Figure 6.32 establishes a comparison between the values of slip measured in the tests of CN13.5 and VM2. The measurements presented for specimen CN13.5 correspond to the fifth load range applied to the specimen (see Table 4.5). The values measured for beam VM2 correspond to the second load range applied to the beam (see Table 6.8). According to the analysis made for Table 6.8, the loads applied to beam VM2 during the first load cycle range induce shear stresses that are still in the elastic range.

The initial maximum slip value is similar for both tests. In the push-out test, the slip value tends to grow significantly with the number of load cycles applied. However, in the beam test, the maximum slip tends to grow initially with the number of load cycles applied and after 60 or 70 load cycles, the values of slip tend to stabilize. The maximum slip value suffers only very small increases now.

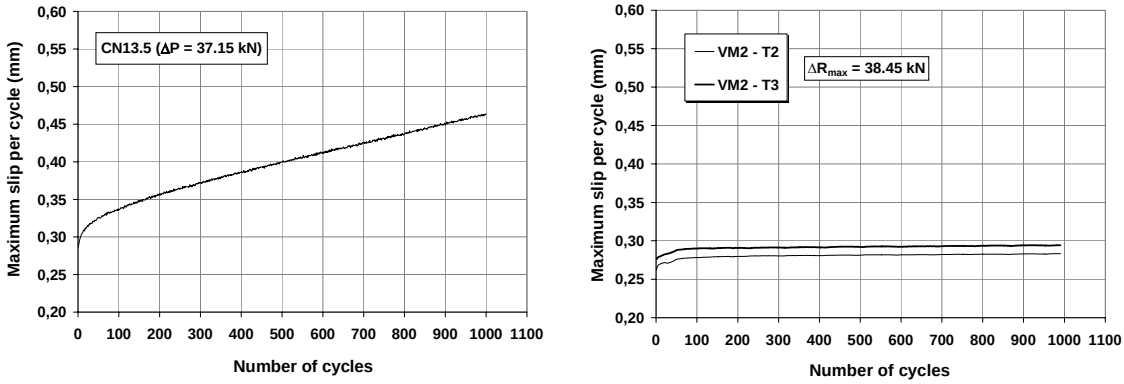

Figure 6.32 – Evolution of slip – comparison between CN13.5 and VM2

Figure 6.33 establishes a comparison between the values of slip measured in the tests of CN13.6 and VM10. The measurements presented for specimen CN13.6 correspond to the fourth load range applied to this specimen (see Table 4.5). The values measured for beam VM10 correspond to the unique load range applied to the beam (see Table 6.8). According to the analysis made for Table 6.8, the loads applied to beam VM10 during the respective load cycle range induce shear stresses that are not in the elastic range.

Initially, the rate of slip growth is much higher for CN13.6 than for VM10. While the rate of slip growth is constant for CN13.6, the slip growth is more or less constant until N=7000 cycles for VM10. After N=7000 cycles, the slip growth is inconstant for VM10 and for N>10000 cycles, the maximum slip attains a higher value than it did for CN13.6, although the difference towards CN13.6 is relatively small.

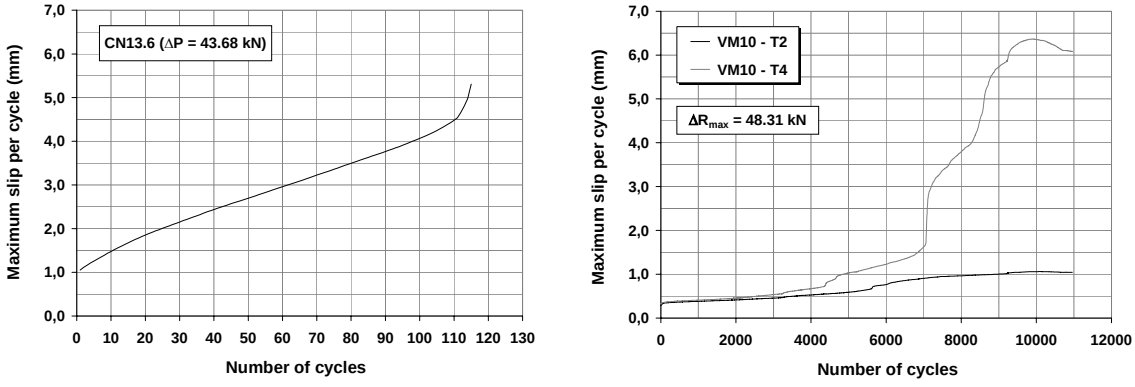

Figure 6.33 – Evolution of slip – comparison between CN13.6 and VM10

In item 4.6.1 of Chapter 4, a comparison is made between the push-out specimens tested for monotonic loading and the push-out specimens tested for cyclic loading, regarding the slip correspondent to maximum load (s_u) and the maximum slip measured right before failure of the first stud (s_{max}). In item 5.10 from Chapter 5, a similar comparison is established, now between the maximum slip measured right before failure of the first stud, for the push-out specimens tested with monotonic loading and the beams

tested with static loading. In Chapter 4, it is verified that both slip parameters (s_u and s_{max}) present values of the same magnitude for specimens tested with static and cyclic loading. In Chapter 5, a similar conclusion is taken: the values of total slip (s_{max}), measured in push-out tests and beams are similar.

A common failure criterion could be devised from these observations by considering a limit slip instead of a maximum shear load. If the evolution of slip in a composite beam can be expressed as a function of the number of load cycles applied and the shear load range defined, failure is obtained when the number of load cycles applied is enough to impose a total slip that is close or equal to the slip limit.

If a linear trend is adjusted to the average slip growth of the first load ranges applied to beams VM1 and VM2, where the slip growth is well defined, and also to VM9, the result is expressed by equation (6.1) for range 3 applied to beam VM1, equation (6.2) for range 4 applied to beam VM2 and equation (6.3) for VM9. All these equations present correlation coefficients with the experimental values that are higher than 0.93.

$$s_{VM1,range3} = 0.00007N + 0.2852 \quad (6.1)$$

$$s_{VM2,range4} = 0.00003N + 0.3828 \quad (6.2)$$

$$s_{VM9} = 0.0000043N + 0.1718 \quad (6.3)$$

Considering a limit slip of 6 mm at failure (see Table 4.11, from Chapter4) combined with equations (6.1), (6.2) and (6.3), it is possible to calculate the number of load cycles that would be needed, at the load range applied to each beam, to provoke shear failure, considering that the slip evolution will remain similar until failure. The results obtained are N (VM1, range3) = 81640 cycles, N (VM2, range4) = 187240 cycles and N (VM9) = 1355395 cycles.

The equation taken from Figure 4.30 of Chapter 4, calculates the evolution of slip based on the ratio between the shear load range and the ultimate load applied on the stud connector: $log\ (s'/\ cycle) = -7.11 + 5.79\left(\frac{\Delta P}{P_u}\right)$. This equation can now be used to determine how many cycles would be needed to attain failure in each beam. The ratio between the shear load range and the ultimate load applied to the stud connector is presented in Table 6.8. The results obtained are N (VM1, range3) = 273 cycles, N (VM2, range4) = 445 cycles and N (VM9) = 10883 cycles. The number of load cycles needed to attain failure, obtained with the equation derived from the push-out tests is much lower than the values that would be obtained by considering the slip growth rate derived from the beam test results. Again, the presence of distributed connectors along the beam, where some of them are less shear loaded than others, retards the evolution of slip.

6.10. Conclusions

Beams VM4 and VM9, designed for full connection, suffered bending failure and beams VM6, VM2 and VM10, designed for partial connection, suffered shear connection failure as predicted. However, beam VM1, designed for full connection, suffered shear connection failure due to the application of repeated loading. The load cycles of increasing load range applied on beams VM1 and VM2 induced early failures, by reducing the beams load capacity. Beams VM9 and VM10 were submitted to cyclic loadings of constant load range. The load levels and number of cycles applied induced a reduced loss of shear connection on beam VM9 that did not result in a decrease on the beam strength. The maximum load applied to beam VM9 was similar to the maximum load applied to VM4 (identical to VM9 and statically loaded). For beam VM10, however, the loss of shear connection was significant and resulted in a reduced maximum resistant bending moment.

In general, repeated loading induces loss of shear connection in all the tested beams. The loss of shear connection is reflected in an increasing slip strain, increasing slip values and finally in increasing vertical deflection. Due to slip strain, the strain diagram at the composite cross section is altered, with higher strains at the steel section and lower strains at the concrete cross section when the loss of composite action is significant.

For all the tested beams it was possible to establish defined relations between slip or vertical deflection and the number of load cycles applied. However, after the first 7000 load cycles applied to beam VM10, slip and vertical deflection stop presenting a constant growth. From this moment on, it was not possible to establish a direct relation between these parameters and the number of load cycles applied.

The rate of slip growth is always higher in push-out tests than in composite beams. In push-out tests, all the shear connectors are loaded with similar shear load, while in composite beams the shear force applied on each connector depends on the connectors' distribution. In the same way, the rate of slip growth is different for each load range applied to each beam, even when there is plastic distribution of shear stress and one or more studs are loaded to their maximum shear strength.

In the case of simply supported beams, the studs positioned near the supports are submitted to higher shear loads, while the studs positioned near the beam mid span are submitted to lower shear loads. Studs that are not loaded to their maximum should have an important influence on the connection behaviour. It seems that the shear studs that are not submitted to their maximum load capacity are limiting the value of slip along the composite beam, because different rates of slip growth are verified when one or more connectors are loaded to their maximum capacity. It is therefore more difficult to establish relations that can predict the slip growth just based on the number of load cycles applied, because they depend on the connectors' distribution.

Chapter 7

LONG TERM LOADINGS IN STEEL AND HIGH STRENGTH LIGHTWEIGHT CONCRETE COMPOSITE BEAMS

7.1 Introduction

The adequate behaviour of a composite beam in service conditions means that it should remain fit for use and that its appearance and durability remain satisfactory. For that reason, consideration has to be given, during design, to "serviceability limit states". These limit states relate to aspects of a structure's behaviour such as cracking, deformation and vibration, when checked under normal service conditions.

The economic consequences, for the client, of failure to satisfy serviceability criteria can prove as severe as structural failure. Failure to meet serviceability criteria is likely to result in increased maintenance and repair costs. In some cases it will result in a loss of utility, of durability, and ultimately, of the integrity of the structure.

For a composite beam, serviceability is guaranteed if vertical deformation, concrete cracking width and natural frequency are kept within some pre-defined limits. Beside the applied loading, the beam deflection depends on other phenomena that may alter the beam behaviour along time, which can be temperature variation, concrete shrinkage and concrete creep.

Composite steel-concrete beams, in which a steel I-section supports a concrete deck or slab, find wide spread application in buildings and bridges. In buildings particularly, composite action is achieved by the use of a large number of shear connectors, so that there is nearly full interaction between the steel and the slab. Thus, under service loads the effect of slip between steel and concrete is very small and the longitudinal strain in the top fibber of the steel is very close to that which exists in the soffit of the concrete slab, (Bradford 1991).

In a composite beam, a slab that is suffering shrinkage is restrained by the steel member, which exerts a tensile force on it, through the shear connectors near the free ends of the beam, so that its apparent shrinkage is less than the “free” shrinkage. The loads on the shear connectors act in the opposite direction to those due to the dead and imposed load, and so can be neglected in the connection design (Johnson 1994).

As a result of the concrete slab creep and shrinkage, a transfer of stresses from concrete to the steel girder occurs, which is more meaningful as the connection system flexibility decreases, (Vieira and Virtuoso 2002). According to Bradford (1997), shrinkage of the reinforced concrete slab in an unloaded steel and concrete composite beam may lead to substantial curvatures and deflections of the beam, as well as cracking of the slab, even in positive bending moment regions. The prediction on the behaviour under sustained service loads is complicated by time-dependent deformations in the concrete due to creep and shrinkage and the additional non-linearity caused by cracking of concrete over each interior support, (Gilbert and Bradford 1995).

The present text reports the study of two composite beams subjected to a long term constant loading, with the duration of one year. The applied loading results from the use of some old and heavy test specimens that were weighted and then positioned over the beams (Figure 7.1). The beams were initially loaded in January of 2004 and were left with that same disposition for a period of 1 year. Measuring devices were disposed at some chosen locations and a large number of measurements were done for representative sections of the beams, at regular intervals of time. These measurements allowed the identification of changes in vertical deformation, longitudinal slip between the steel profile and the concrete slab, strain and curvature.

Figure 7.1 – a) Loading sequence ; b) Loading disposition

7.2 Objectives

The aim of this work is to study the behaviour of steel and lightweight concrete composite beams under long term loadings. Two beams were tested, with similar geometry, span, support and loading conditions. The loads are constant in value and distribution, along time. The beams differentiate from each other at the connection degree: one guarantees full connection and the other only allows for partial connection.

The principal objective of this work is to study the influence of the lightweight concrete long term behaviour on the composite beam. Because of it, creep and shrinkage tests are performed with the same thermo-hygrometric conditions as defined for the beams

while loaded. Therefore, specimens for the experimental determination of shrinkage and creep are cast along with the composite beams.

The initial phase of loading is analysed to check if the beam characteristics are in accordance with predicted and if elastic behaviour is to be expected. Then the long term analysis is done regarding parameters calibrated at this phase.

The effects of temperature variation, shrinkage and creep are analysed through the period of testing, considering partial interaction between the steel section and the concrete section.

7.3 Serviceability limit states

7.3.1 Criteria

Serviceability limit state criteria may be categorised for composite structures as follows:

- slip at the steel-concrete interface, when it becomes large enough to invalidate design checks;
- excessive compressive stress in the concrete, leading to micro cracking and affecting durability;
- excessive cracking in concrete tension zones;
- unacceptable deformations or deflections, which affect the appearance or efficient use of a structure or cause damage to finishes or other non-structural elements. These deformations are affected by cracking, creep and shrinkage; and by slip, where significant;
- vibrations producing discomfort or affecting non-structural elements or equipment;

Within these categories, a variety of limit states may be defined, corresponding to different structural types and conditions. Some of the serviceability requirements are satisfied implicitly, by virtue of assumptions made or restrictions introduced whilst designing the section for strength.

7.3.2 Elastic analysis

The mechanical and geometrical properties of the composite section are required for the calculation of service stresses and deformations. At service stress levels, the concrete in compression and the steel are assumed to behave in a linearly elastic way. Within some limits, concrete in tension may be considered uncracked. Where the flexural stiffness of the cracked section must be used, the strength of concrete in tension is ignored. Even after

cracking has occurred, the section derives stiffness from the concrete. This "tension stiffening" is due to the uncracked concrete between cracks.

In calculating the composite section properties for serviceability checks, use is made of the concept of the transformed section. Using this concept, the steel-concrete composite section is replaced by an equivalent homogeneous section in steel. For a section subjected to positive bending, the concrete flange of area A_c is replaced with a fictitious steel flange of area A_c/n, where n is the modular ratio, (7.1). The fictitious steel flange is of similar depth to the concrete flange, (Figure 7.2).

$$n = \frac{E_s}{E_c} \tag{7.1}$$

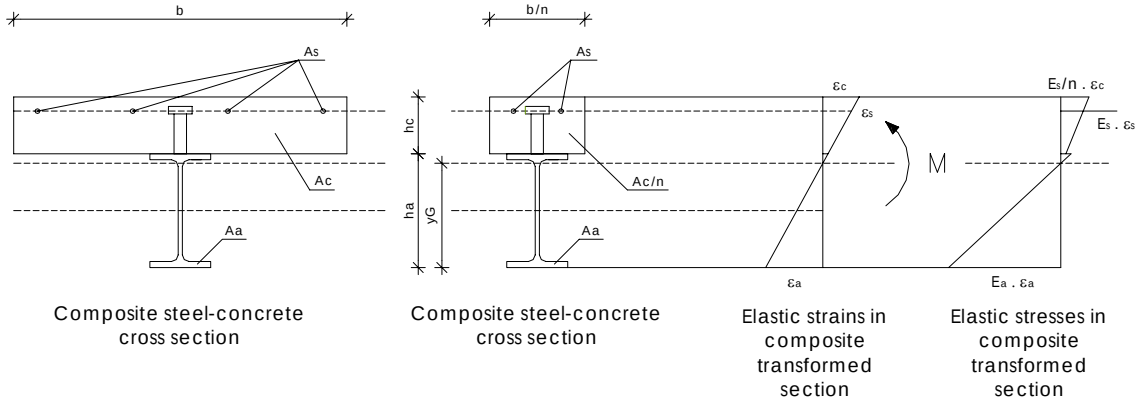

Figure 7.2 – Design for serviceability- the transformed section

Geometrical properties are calculated for the transformed section and strains may be obtained using the modulus of elasticity for steel. Use is made of the modular ratio in calculating elastic stresses in the concrete flange of the original composite section as shown in Figure 7.2. The values for deformation or stiffness, calculated as described before are valid only if the stresses resultant from the applied loadings do not induce plastic strains on any cross section fibber. This plastic strains can either occur at the concrete slab or at the steel profile, when the value of strain overcomes the value for yielding of the corresponding material. The yielding value depends on the material characteristics.

7.3.3 Connection elastic properties

There is a relation between the applied shear load on a stud connector and the corresponding deformation. The results presented in Chapter 4 put in evidence that this connection load-slip relation is not linear in its total development. It was experimentally determined that this behaviour is elastic in the initial loading phase, until around 50 to 55% of the maximum load level is attained and therefore a linear relation between load and slip

can be considered, until that limit is reached. Large deformations occur for higher loads, when the load is near its maximum value.

Equation (7.2) defines the shear load installed in each stud connector, related to slip between steel and concrete, where *R* is the longitudinal shear force, mobilized on each stud connector.

$$R = k \cdot s \tag{7.2}$$

An uniform spacing of studs was defined and the shear force at the interface between steel and lightweight concrete is therefore proportional to slip between steel and concrete, (7.3),

$$r(x) = \frac{k}{p} \cdot s(x) \tag{7.3}$$

where *r* is the shear flow at the interface between steel and lightweight concrete and *p* is the longitudinal spacing between studs.

The connection stiffness, *k*, is usually established considering a load value that is a percentage of the maximum load value and the corresponding slip deformation, (7.4). The chosen value of *k* is estimated considering the results taken from the weights application, as presented in the following, and the results presented in Chapter 4, taken from the results of push-out tests. The push-out tests were performed with studs of 13 mm diameter and the results in the elastic region were considered for the analysis. In terms of concrete, the mixture used in the beams is exactly the same as was used for the push-out tests specimens.

$$k = \frac{50\%\, P_u}{s_{50\% P_u}} \tag{7.4}$$

where,

P_u – maximum shear force resisted by one shear stud

$s_{50\%Pu}$ – value of slip correspondent to 50% of the maximum shear force resisted by one shear stud

7.4 Beams geometry and test set up

7.4.1 Description

The two beams in study are identical to the beams studied in Chapter 5 and Chapter 6, under the designation of Type A and Type B beams. Figure 6.1, from Chapter 6, defines properly the cross section, span, supports and stud distribution for the beams types here analysed.

In the present case, the beams tested can be classified as presented in Table 7.1. The materials properties are also presented.

Table 7.1 – Concrete properties for composite beams tested for long term loading

	Concrete Ref.	Type	No. of shear studs in half span	f_{cm} (MPa)	$E_{cm,28d}$ (GPa)
Beam VM1	BL35	A	8	64.71	22.9
Beam VM2	BL36	B	4	65.79	22.2

All tests are carried out with measurements of applied load value, vertical deformation, slip between steel profile and concrete slab and strain at the steel profile and at the concrete slab, in particular cross sections along the beams' span. The devices chosen are connected to a data acquisition system. Measurements are done periodically and corresponding data is recorded for later analysis.

7.4.2 Strain gauges

Strain gauges are positioned in representative transversal sections in order to measure strain and curvature variation during the tests. They are positioned in two different cross sections, defined from left to right as Section A-A' in the first quarter of the beam (1.065m from nearest support) and Section B-B' in the beam mid span (2.250m from both supports), as presented in Figure 7.3.

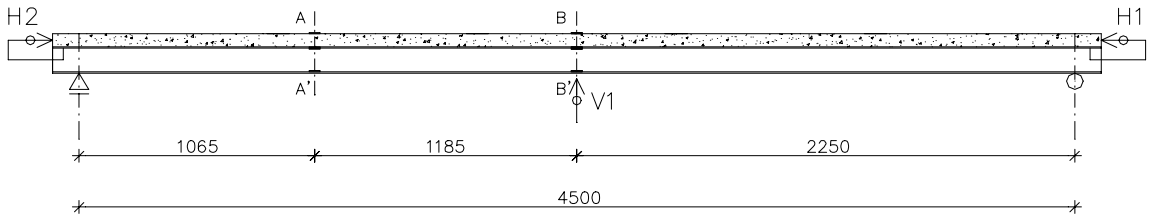

Figure 7.3 – Longitudinal view – Cross section positions for transducers and strain gauges

In the cross section, the strain gauges are located both on the upper and bottom fibber of the concrete slab and on the inner extreme fibbers of the steel section. The strain gauge disposition along the cross section repeats the distribution already presented in Figure 5.13 from Chapter 5.

7.4.3 Displacement transducers

For each tested beam, three mechanical displacement transducers were disposed as shown in Figure 7.3, with the objective of measuring the deformation suffered by the structural element. Figure 7.4 shows the transducers, positioned in the beams and ready to perform measurements.

a) Transducer to measure horizontal slip (H1 e H2) b) Transducer to measure vertical deformation (V1)

Figure 7.4 – Displacement transducers

Transducer V1 measures the vertical displacement at the beams' mid span, identifying the maximum deformation suffered by the beam for the applied loading. Transducers H1 and H2 measure slip between the steel beam and the lightweight concrete slab, at the beams extremes, right next to the supports.

7.5 Applied loadings

The loadings applied to the beams are represented in Figure 7.5. They consist on some heavy old test specimens, weighted before being put in place. The weights distribution tries to repeat, with the possible approximation, an uniformly distributed load along the beam span. The weights are represented in Figure 7.5 and the appointed numbering (Weight 1, …, Weight 7) results from the order adopted to set them in place.

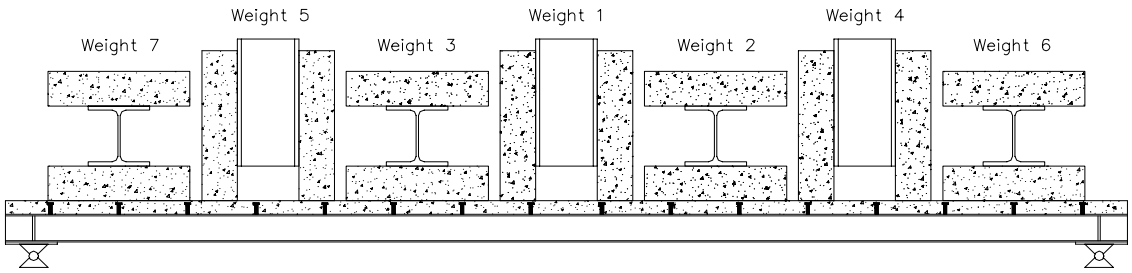

Figure 7.5 – Individual loads put over the composite beam

The individual weights of the elements that constitute the beam loading are presented in Table 7.2. Each of them was weighted right before being positioned over the beam.

Table 7.2 – Individual weights positioned over the beams

	Weight 1 (kgf)	Weight 2 (kgf)	Weight 3 (kgf)	Weight 4 (kgf)	Weight 5 (kgf)	Weight 6 (kgf)	Weight 7 (kgf)
Beam VM1	294.7	288.2	291.2	302.4	296.7	284.5	292.1
Beam VM2	298.2	310.0	302.3	293.3	281.9	292.8	295.3

Each element is put in place according to the order described in Figure 7.5. The corresponding imposed loading is schematically represented in Figure 7.6, allowing to determine the corresponding stress and deformation increase.

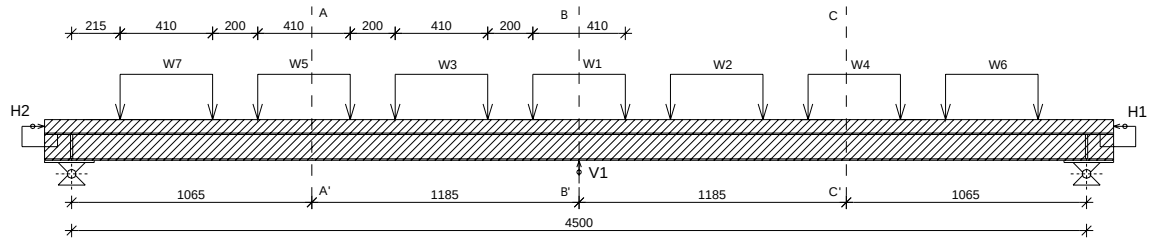

Figure 7.6 – Load distribution resultant from each weight

7.6 Loading phase

The analysis of the loading phase allows for a good assessment of all the parameters that are needed for the long term analysis. The results of experimentally measured vertical deformation, slip and strains are compared to the ones obtained with numerical models that intend to describe the beams real behaviour as closely as possible.

The numerical models are defined to predict vertical deformation, slip and strain evolution. Software ATENA 2D® is used, (ATENA 2003). It is based on the finite element method and allows for a non-linear material and geometrical analysis. These particular models are defined considering the beams symmetry and therefore only half span of the beams is modelled. The FEM geometry, mesh and supports are identical to the ones considered in the models analysed in Chapter 5. Loading is represented in Figure 7.7. Because of the symmetry conditions considered, the mean value of the opposite individual loads positioned over the composite beams is considered.

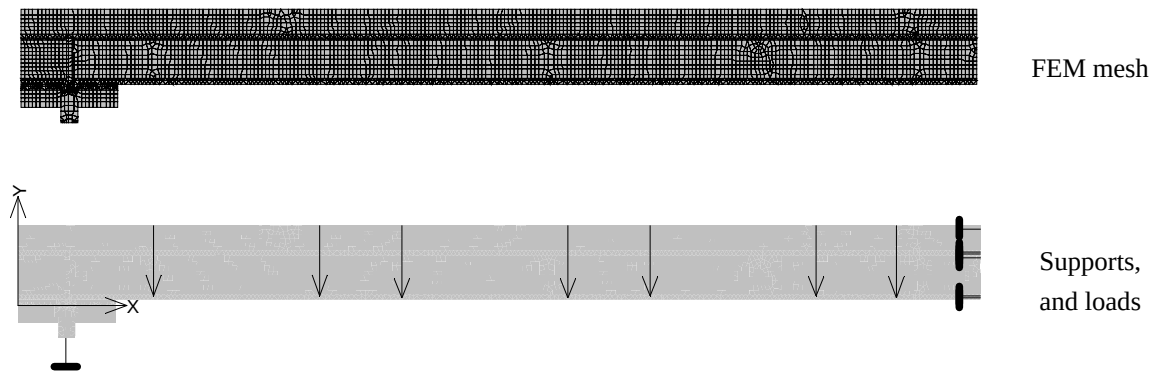

Figure 7.7 – FEM model for the loading phase analysis

Bending moment, transversal shear and longitudinal shear diagrams are presented for the loadings applied to the composite beams. The diagrams are established for the moment

when all the weights are positioned over the beams. They represent the total stresses that will be imposed to the beams for the time that they are under study.

7.6.1 Diagrams for bending moment, transversal shear and longitudinal shear

The partial bending moment values that result from each weight that is positioned over the beams are presented in Table A7.3 of Appendix 7.2. After all the weights are positioned over the composite beams, the total bending moment diagrams correspond to the ones represented in Figure 7.8a. Shear stress diagrams for the total loading in beams VM1 and VM2 are presented in Figure 7.8b. These are the stresses installed on the composite beam for the period of the analysis, as the loads will remain in that position.

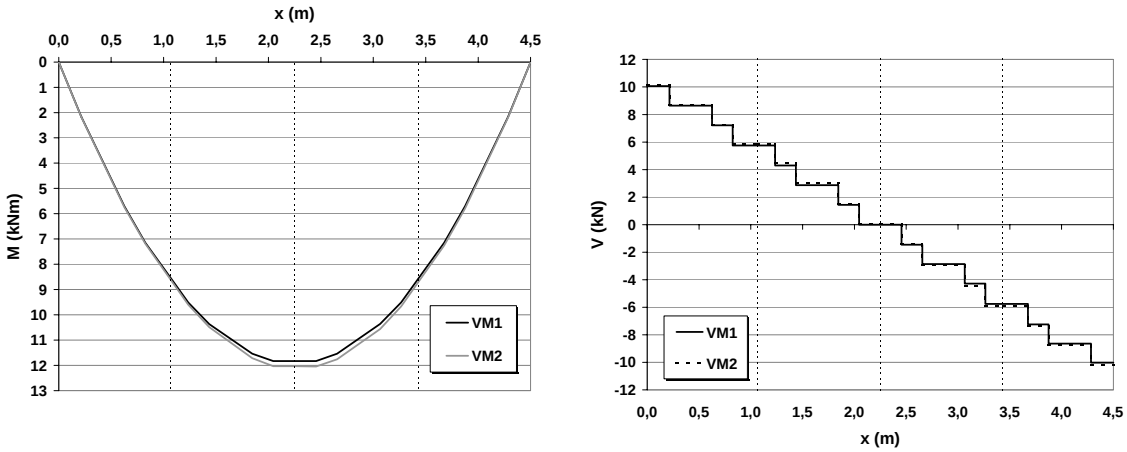

a) Total bending moment

b) Total transversal shear stresses

Figure 7.8 – Stress diagrams for beams VM1 and VM2

Sections A-A' and B-B' are analyzed and the values of cumulative bending moments presented in Table 7.3 are considered for the calculation of stresses and strains. The values presented in Table 7.3 result directly from the sum of partial bending moment values presented in Table A7.3 from Appendix 7.2. This procedure allows to determine the evolution of stress and deformation state, which can be compared to the one measured during loading.

Predicted stresses for total interaction analysis at the studied cross sections are determined with equation (7.5) applied on the values of Table A7.5 and Table A7.6, reported in Appendix 7.2,

$$\sigma = \frac{M}{I} \cdot z \tag{7.5}$$

where,

M – bending moment acting on the cross section;

I – moment of inertia at the homogenised composite cross section;

z – distance between the fibber in study and the neutral axis.

Table 7.3 – Cumulative bending moments at VM1 and VM2 (kNm)

		W 1	W 2	W 3	W 4	W 5	W 6	W 7	**Final state**
VM1	Weights in VM1 (kgf)	294.7	288.2	291.2	302.4	296.7	284.5	292.1	
	Loads in VM1 (kN)	2.89	2.83	2.86	2.97	2.91	2.79	2.87	
	Supports	0	0	0	0	0	0	0	**0**
	Cross section A-A' x = 1.065m	1.54	2.64	4.57	5.29	7.33	7.61	8.53	**8.53**
	Cross section B-B' x = 2.250m	2.96	5.28	7.62	9.15	10.65	11.23	11.83	**11.83**
	Cross section C-C' x = 3.435m	1.54	3.45	4.56	6.64	7.35	8.24	8.53	**8.53**
VM2	Weights in VM2(kgf)	298.2	310.0	302.3	293.3	281.9	292.8	295.3	
	Loads in VM2 (kN)	2.93	3.04	2.97	2.88	2.77	2.87	2.90	
	Supports	0	0	0	0	0	0	0	**0**
	Cross section A-A' x = 1.065m	1.56	2.74	4.75	5.45	7.39	7.67	8.60	**8.60**
	Cross section B-B' x = 2.250m	2.99	5.49	7.92	9.40	10.83	11.43	12.04	**12.04**
	Cross section C-C' x = 3.435m	1.56	3.62	4.77	6.79	7.46	8.38	8.67	**8.67**

The total values for bending moment, shown in Figure 7.8, are also presented in Table 7.2, specified for the cross sections where strain gauges are positioned.

For an elastic and full interaction analysis, the longitudinal shear stress is calculated with equation (5.15) from Chapter 5. Figure 7.9 presents the longitudinal shear stress flow at the steel to concrete interface for beams VM1 and VM2, in accordance with Table A7.4 of Appendix A7.2.

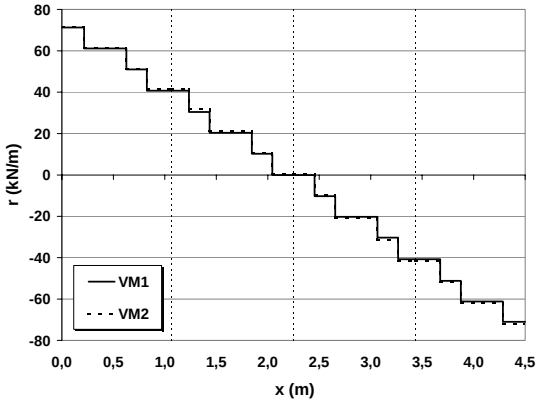

Figure 7.9 - Total longitudinal shear stresses on beams VM1 and VM2 (full interaction)

7.6.2 Effects of the steel to lightweight concrete connection deformability

As the beams are loaded for serviceability analysis, it is considered that the shear force values are considerably smaller than the connection load capacity. In this case, the linear relation between load and slip can still be used. A check on the connection acting shear load is presented in Table 7.4. According to the diagrams presented in Figure 7.9, the total shear force in one half span of the beam, R_s, is 83.8 kN for VM1 and 85.0 kN for VM2.

The shear connector load capacity was experimentally determined in Chapter 4. This result is used in the following analysis.

As for the stud distribution considered for beam VM1 and beam VM2, the total shear force to be mobilized at the beam half span, R_r, is presented in Table 7.4, considering an elastic behaviour for the distribution of stresses on the beam and the full interaction between steel and concrete elements.

Table 7.4 – Longitudinal shear forces

		VM 1	VM 2
Number of shear connectors in half span of the beam (N)		8	4
P_u / stud (see Chapter 4)	(kN)	55.0	55.0
R_r (= P_u x N)	(kN)	440	220
$r_{s,max}$	(kN/m)	71.3	72.0
R_s	(kN)	83.8	85.0
R_s / R_r		0.20	0.40
k	(kN/mm/stud)	220	220

The ratio between applied and resistant total shear load is always equal or smaller than 40%, which confirms that the linear load-slip relation can be considered for the present analysis. However, as the longitudinal shear diagram is not constant, the studs positioned near the beams supports will undertake higher loads and the single stud located in the extreme position takes a load that is more approximate to the connectors load capacity. In this case, redistribution of stress among connectors is allowable, as recommended in EN1994-1-1, (CEN 2004b).

For two composite beam with the same configuration, cross section, supporting conditions, and shear connection devices disposition as were used for Beams VM1 and VM2 (defined as Type A and Type B), a sensitivity analysis is done on the influence of the connection stiffness. For these two beams a uniformly distributed load, where the total load is equal to the sum of the loads presented in Table 7.2, was considered.

Figure 7.10a and Figure 7.10b show the variation of slip for the two beams. Figure 7.10c and Figure 7.10d show the corresponding variation of vertical deformation.

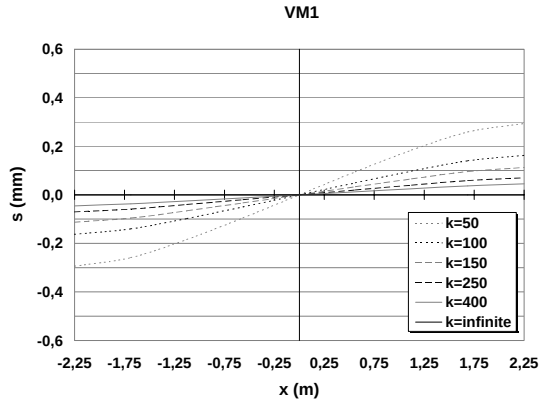

a) Type A: variation of slip resultant from varying *k*

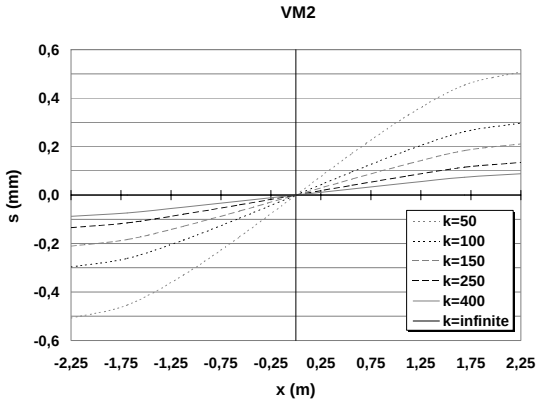

b) Type B: variation of slip resultant from varying *k*

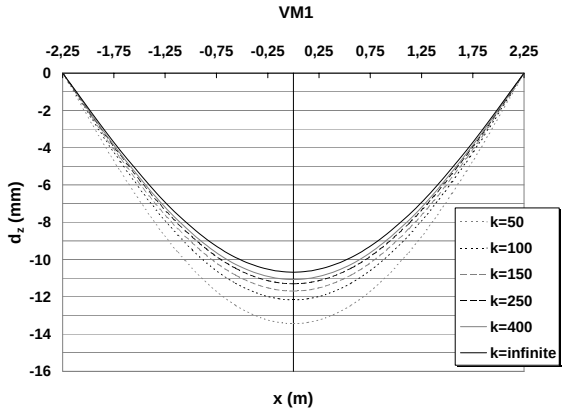

c) Type A: Variation of vertical deflection resultant from varying *k*

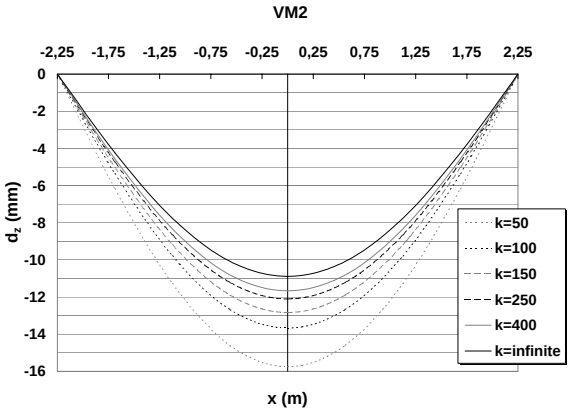

d) Type B: Variation of vertical deflection resultant from varying *k*

Figure 7.10 – Variation of slip and vertical deflection resultant from varying *k*

Figure 7.11 presents the percentage evolution of vertical deflection caused by the defined distributed loading for beams VM1 and VM2.

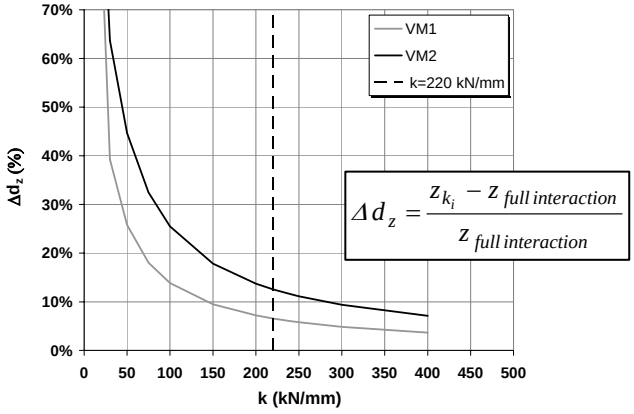

Figure 7.11 – Variation on vertical deflection measured for different *k* values applied to beam VM1 and VM2

For a stiffness value of k=220 kN/mm, the maximum vertical deflection suffers an increase of 6.6% for the beam with total connection and 12.6% for the beam with partial shear connection, when compared to the total interaction hypothesis.

7.6.3 Vertical deflection

Vertical deflection values are measured after each weight is put in place. Table 7.5 shows the values of vertical deflection, measured at the mid span of beam VM1 and beam VM2, respectively.

Table 7.5 – Vertical deflection for VM1 and VM2, measured at section B-B'

		W 1	W 2	W 3	W 4	W 5	W 6	W 7
Weights	(kgf)	294.7	288.2	291.2	302.4	296.7	284.5	292.1
Loads in VM1	(kN)	2.89	2.83	2.86	2.97	2.91	2.79	2.87
Measured (accumulated)	(mm)	-2.55	-4.17	-6.70	-8.62	-10.13	-10.77	-11.40
Weights	(kgf)	298.2	310.0	302.3	293.3	281.9	292.8	295.3
Loads in VM2	(kN)	2.93	3.04	2.97	2.88	2.77	2.87	2.90
Measured (accumulated)	(mm)	-3.14	-5.59	-7.89	-9.79	-11.16	-12.02	-12.53

The predicted values of vertical deformation are calculated assuming the linear elastic behaviour of the materials that are part of the composite beams, for the applied loads. Regarding the steel and concrete interaction, two situations are considered: one is the full interaction between the steel and concrete sections and the other is the partial interaction. In both cases, the value of k is considered constant for the applied loads.

The value of the connection stiffness considered for the partial interaction analysis was taken from push-out tests performed for the same type of concrete and for the same connector as the ones used in the composite beams. These results were already presented and discussed in Chapter 4. The average value of k=220 kN/mm was taken from these tests and is now considered in the analysis. Considering the possibility of some friction between the concrete slab and the steel beam, a second value of k=250 kN/mm was also considered for comparison. The values calculated for the beams' mid span are then compared to the ones measured with the displacement transducer. Table A7.1, from Appendix 7.1 presents the corresponding results.

All the calculations account for the materials and cross section characteristics. Modulus of elasticity, E_s = 210GPa, was considered for construction steel. This value was taken from EN1994-1-1, (CEN 2004b), as no experimental testing was done on this property. For lightweight concrete, experimental testing of elasticity modulus was done on

specimens concreted at the same time as the beams. The values $E_{cm,VM1}$ = 22.9 GPa for beam VM1 and $E_{cm,VM2}$ = 22.2 GPa for beam VM2 were determined.

Table 7.6 and Figure 7.12 summarize the total values of vertical deflection, measured at the beams' mid span, after all the weights are in their respective position.

For beam VM1, the measured values and the values calculated for total interaction are close, showing that considering a total interaction behaviour for this beam is a good approach. Changing the connection stiffness value from k=220 kN/mm to k=250 kN/mm, introduces a very small change on vertical deflection. The experimentally measured values are still closer to the total interaction hypothesis, but the second hypothesis is a bit stiffer, as expected.

For beam VM2, the measured values are closer to the values determined with the partial interaction analysis. In this case, the values determined for full interaction are clearly smaller than the experimentally measured ones and the connection stiffness value that better approximates the experimental values is k=250 kN/mm.

Table 7.6 – Comparison between final values of vertical deformation for cross section B-B', right after total loading

	VM 1	**VM 2**
Measured	-11.40	-12.53
Predicted – full interaction hypothesis	-11.19	-11.48
Predicted – partial interaction hypothesis (k = 220 kN/mm)	-12.06	-13.05
Predicted – partial interaction hypothesis (k = 250 kN/mm)	-11.97	-12.89

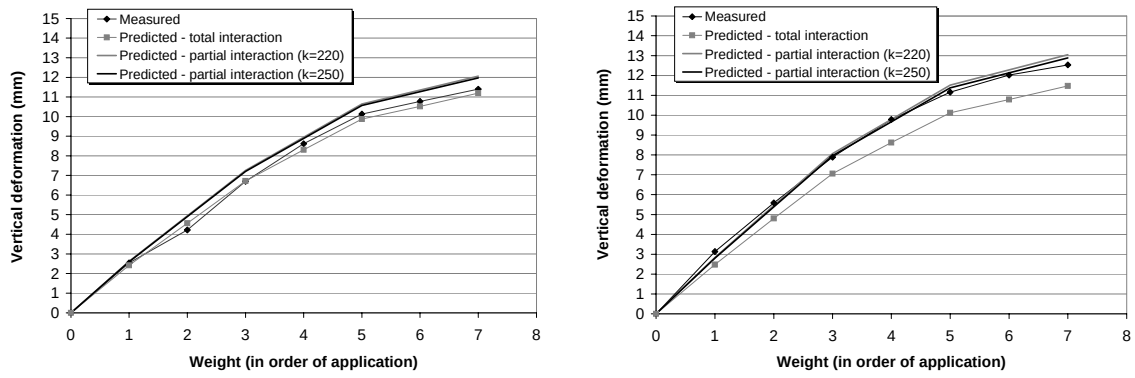

a) VM1 b) VM2

Figure 7.12 – Comparison between measured and predicted vertical deflection

Despite some small differences, a good agreement is verified between experimental and numerical results, for both beams. As described in 7.4.1, VM1 and VM2 have the same geometrical configuration, are built with similar materials and loaded in a similar manner

but differ in the connectors distribution. The effect of the connection degree is clearly observable, resulting in higher values of vertical deformation when its value diminishes.

For beam VM1, the difference between experimental and numerical results is always inferior to 5%. This good agreement shows that the connection flexibility is not important for the chosen level of loading, meaning that the total interaction hypothesis would be appropriate for the analysis of beam VM1.

For beam VM2, the differences between measured and predicted deflection values are higher, always around 10%. In this case, the beam stiffness is reduced by the connection flexibility and the total interaction hypothesis is less appropriate for the beam analysis.

7.6.4 End-slip

As is done regarding the vertical deflection, the slip values between the concrete slab and the steel beam are measured after each weight is put in place. The measurements are done at each beam's extreme, right over the supports. Table 7.7 shows the values of end-slip, measured at beam VM1 and beam VM2, respectively.

Table 7.7 – Measured end-slip for beams VM1 and VM2, at the beam's supports

		W 1	W 2	W 3	W 4	W 5	W 6	W 7
Weights (kgf)	(kgf)	294.7	288.2	291.2	302.4	296.7	284.5	292.1
Loads in VM1 (kN)	(kN)	2.89	2.83	2.86	2.97	2.91	2.79	2.87
Predicted (k=220kN/mm) Accumulated (left=right)		0.013	-	0.039	-	0.063	-	0.076
Measured (accumulated) – H1	(mm)	0.004	0.005	0.021	0.048	0.056	0.069	0.075
Measured (accumulated) – H2	(mm)	0.003	0.014	0.024	0.037	0.055	0.059	0.073
Weights	(kgf)	298.2	310.0	302.3	293.3	281.9	292.8	295.3
Loads in VM2	(kN)	2.93	3.04	2.97	2.88	2.77	2.87	2.90
Predicted (k=220kN/mm) Accumulated (left=right)		0.026	-	0.076	-	0.120	-	0.139
Measured (accumulated) – H1	(mm)	0.011	0.042	0.056	0.096	0.117	0.134	0.145
Measured (accumulated) – H2	(mm)	0.010	0.027	0.050	0.059	0.105	0.113	0.130

The predicted values of slip are calculated assuming the linear elastic behaviour of the materials that constitute the composite beams, for the applied loads. Therefore, all the considerations made remain valid. It is important to remember that the slip value is null for the total interaction hypothesis. Table A7.2 from Appendix 7.1 presents the corresponding results.

Table 7.6 and Figure 7.13 summarize the total measured and predicted values of slip, at the beams' extremes, after all the weights are in their respective position. In both cases,

the average slip value experimentally measured is very close to the predicted slip value considering the stiffness value k=250 kN/mm.

Table 7.8 – Comparison between final values of maximum slip, right after total loading

	VM 1	**VM 2**
Measured – H1	0.075	0.145
Measured – H2	0.073	0.130
Predicted – partial interaction hypothesis (k = 220 kN/mm)	0.083	0.157
Predicted – partial interaction hypothesis (k = 250 kN/mm)	0.073	0.140

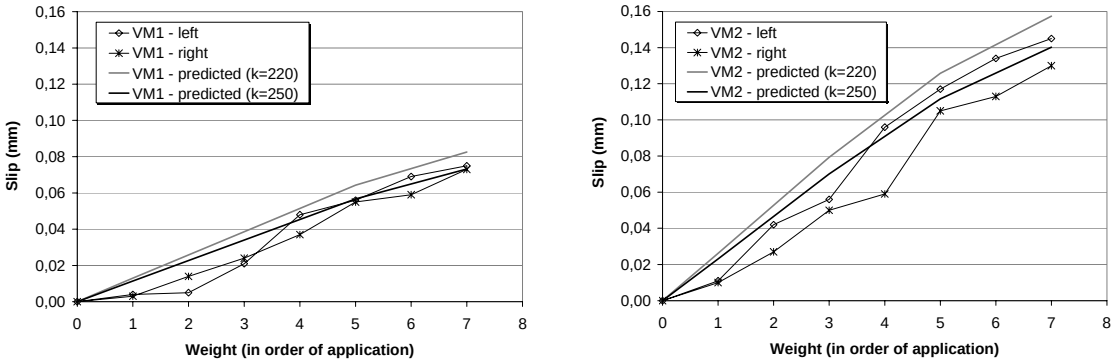

a) VM1 b) VM2

Figure 7.13 – Comparison between measured and predicted maximum slip

7.6.5 Strains

The fibbers in study are numbered according to Figure 5.13 from Chapter 5 and correspond to strain gauge positions: fibbers 2 and 3 are located in the steel section and fibbers 5 and 6 are located in the lightweight concrete slab.

Strain values are measured in four different cross section fibbers and predicted in six different cross section fibbers, allowing for comparison between measured and calculated values at strain gauges positions (see Figure 5.13 from Chapter 5). Each fibber level corresponds to the position of two strain gauges. The results presented for each fibber are the average value of the measurements done by two strain gauges.

The presented values correspond to strains measured during load application. Therefore, these are cumulative values that result from Weight 1, Weight 2, Weight 3, Weight 4, Weight 5, Weight 6 and Weight 7. Strain values for beam VM1 are presented in Table 7.9.

Table 7.9 – Measured values of strain at VM1

		zero	W 1	W 2	W 3	W 4	W 5	W 6	W 7
Section A-A' x = 1.065 m	Fibber 2	0	72.96	160.14	212.54	318.08	361.52	383.53	403.93
	Fibber 3	0	1.22	1.02	3.22	-7.27	-12.42	-12.81	-15.61
	Fibber 5	0	-5.24	-7.04	-8.06	-0.35	-0.67	-0.78	0.39
	Fibber 6	0	-42.29	-90.26	-118.08	-173.63	-197.77	-213.62	-225.74
Section B-B' x = 2.250 m	Fibber 2	0	140.21	244.50	353.34	425.24	504.91	515.17	551.14
	Fibber 3	0	3.93	1.34	5.97	6.60	7.23	7.55	6.37
	Fibber 5	0	-5.05	-12.40	-19.87	-24.61	-32.36	-35.13	-35.95
	Fibber 6	0	-76.64	-135.68	-191.28	-231.77	-274.45	-281.89	-299.84

And strain values for beam VM2 are presented in Table 7.10.

Table 7.10 – Measured values of strain at VM2

		zero	W 1	W 2	W 3	W 4	W 5	W 6	W 7
Section A-A' x = 1.065 m	Fibber 2	0	77.24	133.65	232.31	268.47	367.22	374.45	414.43
	Fibber 3	0	-11.12	-4.76	-18.91	-23.11	-45.40	-51.73	-60.42
	Fibber 5	0	0.20	-6.92	-3.09	-3.48	12.60	13.69	14.98
	Fibber 6	0	-40.69	-71.01	-129.50	-151.53	-212.32	-219.68	-247.93
Section B-B' x = 2.250 m	Fibber 2	0	137.11	261.64	375.67	447.99	512.11	532.35	556.60
	Fibber 3	0	4.40	-9.87	-12.30	-18.04	-15.25	-16.51	-20.95
	Fibber 5	0	-1.72	4.11	2.86	3.09	2.11	0.04	-2.07
	Fibber 6	0	-77.35	-146.48	-216.12	-259.90	-295.85	-310.13	-330.67

The linear elastic behaviour of the composite beams was assumed at the beginning of this text, for the level of loading applied to the beams. Taking Hooke's Law into account, it is possible to calculate the value of strain at any cross section fibber, considering (7.6). Total interaction between steel and concrete sections was also considered at this moment.

$$\sigma = E * \varepsilon \tag{7.6}$$

where E is the modulus of elasticity of the material used at the fibber in study.

The values of strain for the full interaction hypothesis are calculated from the values of stresses presented in Table A7.5 and Table A7.6 from Appendix 7.2. The resulting strains are presented in Table A7.7, Table A7.8, Table A7.9 and Table A7.10 from Appendix 7.3.

The comparison between measured and predicted strains is done for two extreme fibbers: fibber 2 at the steel section and fibber 6 at the concrete section. Sections A-A' and B-B' are analysed for each load increment.

As a result, the following diagrams, presented in Figure 7.14 resume the values presented in Table A7.7, Table A7.8, Table A7.9 and Table A7.10.

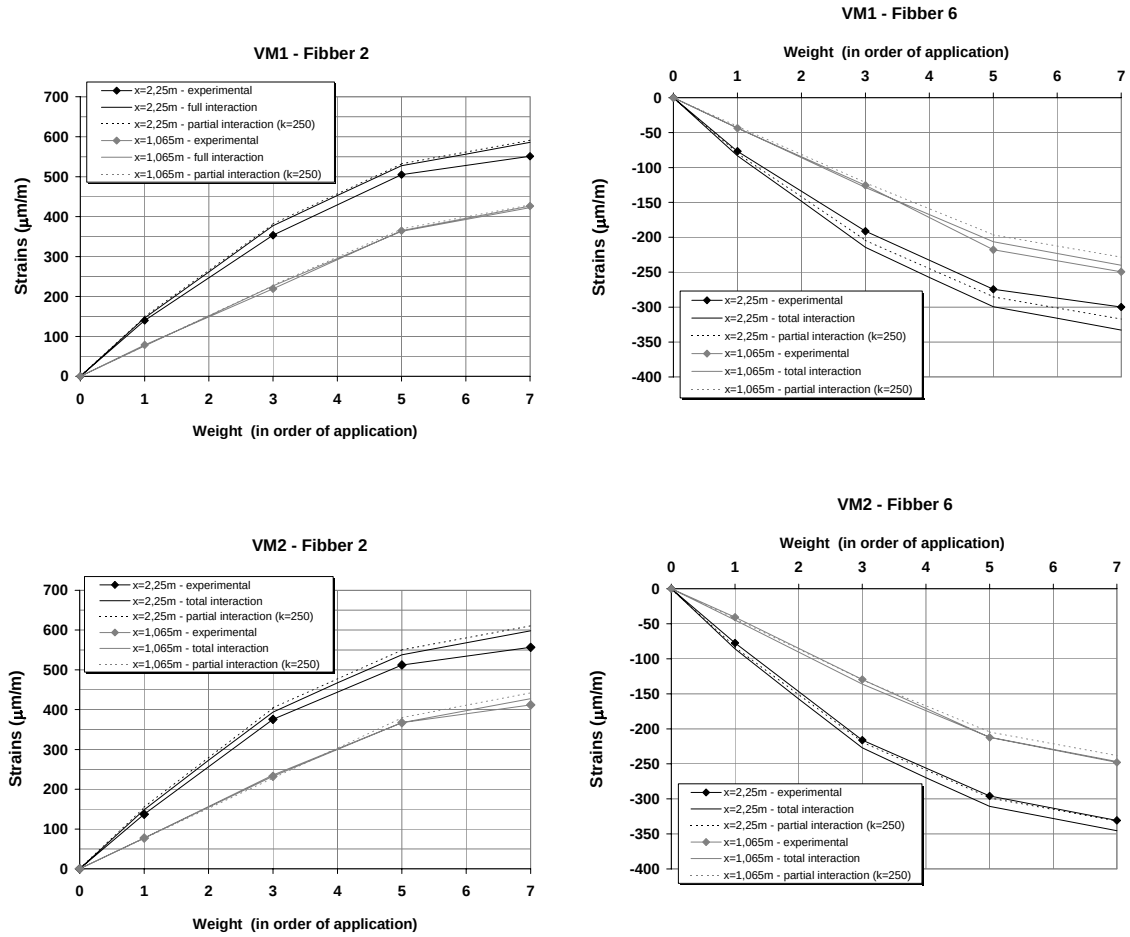

Figure 7.14 – Evolution of strain at the extremes fibbers of beams VM1 and VM2

As expected, strain values are higher for the cross section positioned at the beam mid span, both for concrete and for steel sections.

The difference between predicted and measured strain values is presented in Table 7.11, for the final loaded state. The differences between predicted and measured strain values are small. Predicted strain values are usually higher than measured strain values and their difference varies between 0 and 11%, according to Table 7.11. On one hand, the difference can be justified by the difficulty of guarantying the exact pre-defined position of the Weights, as small adjusts are expected in their position. On the other hand, with the values of vertical deflection, we can check if these differences are attributable to some increased stiffness on the real models. Comparing the values of vertical deflection and the values of strain, this is a possibility for both beams, as the values obtained considering the total interaction between the steel and the concrete section are higher than the values experimentally measured. However, the differences are small and become mostly evident in the beam mid span (section B-B'). For section A-A', measured and predicted values are almost coincident, which contradicts the hypothesis of a higher stiffness.

Table 7.11 – Predicted strain / Measured strain – final state at cross section B-B'

		Measured strain (1)	Predicted strain (2) – total interaction	Predicted strain (3) – partial interaction (k=250)	(2) / (1)	(3) / (1)
VM1	Fibber 2	551.14	585.94	591.81	1.063	1.074
	Fibber 6	-299.84	-332.83	-317.40	1.110	1.058
VM2	Fibber 2	556.60	598.12	610.78	1.075	1.097
	Fibber 6	-330.67	-345.29	-331.70	1.044	1.003

7.7 Effects of concrete shrinkage

Even in the absence of applied loading, concrete is subjected to volume changes arising from changes in water content, from long-term chemical processes occurring within the cement paste, and from thermal dilation. The most significant of these changes is shrinkage, which is the reduction in concrete volume due to loss of water by evaporation, hydration of the cement, or by carbonation. The opposite effect is the swell in concrete during hydration. Swelling of concrete is normally in order of magnitude less than shrinkage, and is not usually of concern in design. However, as was shown in Chapter 2, swelling occurred at early ages of lightweight concrete and was considered in the long term analysis of the beams.

The significance of such volume changes is due to the fact that they are usually wholly or partially restrained, and thus give rise to tensile stresses and cracking in concrete. The resulting change in stiffness will in turn influence deformations. In the case of composite beams, as the ones in study, the effect of concrete shrinkage is that stresses will appear in both materials resulting from internal equilibrium. The choice to analyse an isostatic structure was done to simplify the analysis, as some parameters, like bending moment or transversal shear, will not change in time due to changes of stiffness.

In considering the effects of shrinkage on a beam with full interaction between steel and concrete sections, equilibrium can be obtained by introducing forces that don't change the element global equilibrium and can re-establish the compatibility of deformation between steel and concrete.

This compatibility stops existing when the connection between steel and concrete is destroyed and free shrinkage of concrete is allowed. It is again re-established by introducing a group of internal forces that guarantee compatibility between the two materials.

Free shrinkage deformation, ε_{cs}, can be annulled by applying an axial force to the concrete section,, N_t, that is proportional to this deformation value and variable in time. This implies the introduction of a pair of forces N_t and $M = -(x_{G,c} - x_{GR}) \times N_t$, applied to the

cross section. In order that equilibrium is again established, the same pair of forces is now applied to the complete section, with the opposite direction. The final state of stress is the result of overlapping the two partial states.

Figure 7.15 presents the internal forces and calculation sequence to perform this analysis.

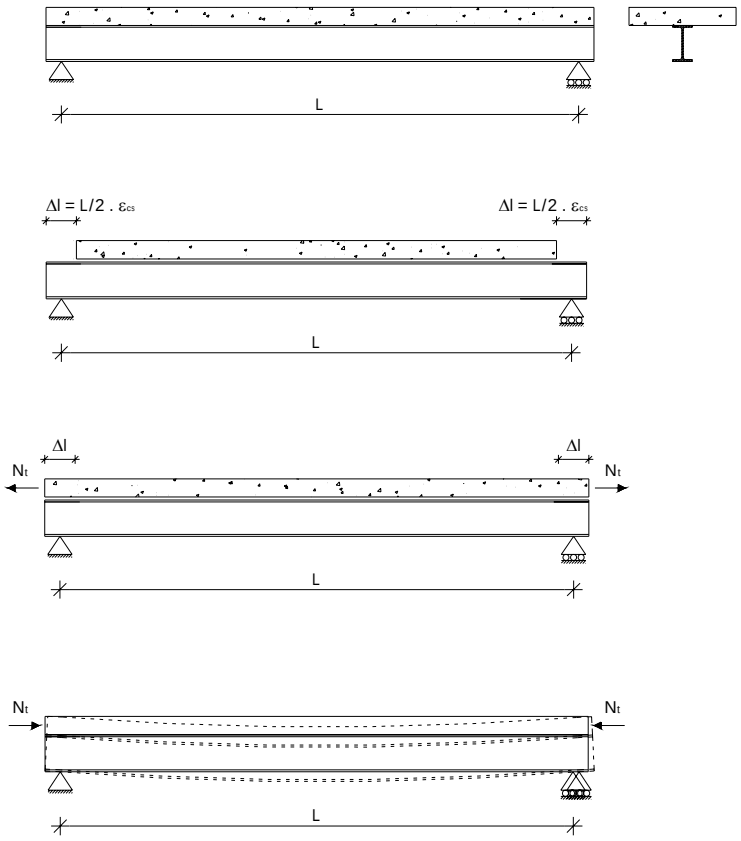

Composite element is internally hyperstatic.

Break of link between steel and concrete. Free shrinkage of concrete.

Compatibility is recovered, introducing an axial force, N_t.

The same axial force, N_t, is applied to the complete composite element, with opposite direction, in order to reestablish equilibrium.

Figure 7.15 – State of stress induced by concrete shrinkage

The account for shrinkage should consider long term effects like creep, because shrinkage happens along the structure's life. It should also consider each material's axial deformation. Equations (7.7) are considered to calculate the force that re-establishes compatibility between the two materials,

$$N(t) = E_c A_c \, \varepsilon_{cs}(t)/\varphi(t)$$
$$N_\infty = E_c A_c \, \varepsilon_{cs\infty}/\varphi_\infty \tag{7.7}$$

where,

$\varphi(t)$ – creep coefficient for instant t

φ_∞ – creep coefficient for $t = \infty$

In order to determine the axial force in each material, equation (7.8) is considered.

$$N'(t)\cdot\left(\frac{1}{\frac{E_c}{\varphi(t)}A_c}+\frac{1}{E_s A_S}\right)=\varepsilon_{cs}(t)$$
$$N'_{\infty}\cdot\left(\frac{1}{\frac{E_c}{\varphi_{\infty}}A_c}+\frac{1}{E_s A_S}\right)=\varepsilon_{cs\infty} \qquad (7.8)$$

One second approach, is to consider the partial interaction effects. An analytical model can be established to consider this effect. This approach is chosen, because the resulting equations are easy to establish and use. The equations are developed according to (Johnson 1994) and are presented in Appendix 7.4.

7.7.1 Shrinkage – sensitivity analysis

A sensitivity analysis is performed, in order to have a previous idea on the behaviour of the tested beams when shrinkage is considered. The beams' properties, defined in 7.4.1, and the connection stiffness of k=250 kN/mm are considered. Table 7.12 shows the values of total shrinkage considered for the analysis and the corresponding calculated values for maximum vertical deflection and slip.

On a simply supported beam, the effect of shrinkage on slip deformation is opposite to the effect of the permanent loads. However, the effect of shrinkage on vertical deflection is additional to the effect of the permanent loads.

Table 7.12 – Shrinkage – sensitivity analysis on deflection and slip

	ε_{lcs} (μm/m)	-100	-200	-300	-400	-500
VM1	d_{zmax} (mm)	-1.741	-3.482	-5.223	-6.964	-8.705
	s_{max} (mm)	-0.0268	-0.0536	-0.0804	-0.1072	-0.1340
VM2	d_{zmax} (mm)	-1.688	-3.376	-5.063	-6.751	-8.439
	s_{max} (mm)	-0.0378	-0.0755	-0.1133	-0.1510	-0.1888

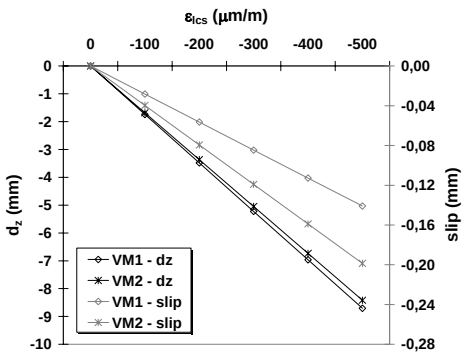

The values and the graphic presented in Table 7.12 show that, for the same value of concrete shrinkage strain, ε_{lcs}, the diminution on the composite interaction makes the beam

less sensible to the effects of shrinkage by diminishing the internal stresses and allowing smaller values of vertical deflection. At the same time, the diminution on the connection degree results in higher values of slip along the composite beams. The results presented in Table 7.12 show that the duplication on the connection stiffness value (VM1 has twice the number of shear studs of VM2) results in an increase of 3.15% on the vertical deformation value and a decrease of 29% on the slip value.

As was observed, the connection deformability has a favourable effect on the composite beam when shrinkage is in cause, as it leads to smaller values of vertical deformation. When comparing to a beam with total interaction and the material and geometry characteristics of VM1, the connection deformability leads to a decrease in the maximum vertical deformation due to shrinkage of 2.8%. In the case of a beam with total interaction and the characteristics of VM2, the corresponding decrease of maximum vertical deflection due to shrinkage is 5.6%.

The loss of composite action reduces the internal stresses due to shrinkage, at the composite beams. As presented in Table 7.13, it has a favourable effect on the beam steel fibbers, as it tends to diminish those strain values due to concrete shrinkage and approximates the concrete strains to the free shrinkage strain. This becomes even more evident along the beam span, as the values of strain tend to be smaller when approaching the supports. For the concrete fibbers, the values of strain suffer only very small changes, when partial interaction is considered.

Table 7.13 – Shrinkage – sensitivity analysis on strains

	ε_{lcs} (μm/m)	-500	
		Mid span	Quarter span
VM2 (k=50 kN/mm)	$\varepsilon_{c,max}$ (mm)	-532.741	-526.646
	$\varepsilon_{s,max}$ (mm)	84.181	68.510
VM2 (k=250 kN/mm)	$\varepsilon_{c,max}$ (mm)	-537.808	-535.737
	$\varepsilon_{s,max}$ (mm)	97.211	91.885
VM2 (total interaction)	$\varepsilon_{c,max}$ (mm)	-538.005	-538.005
	$\varepsilon_{s,max}$ (mm)	97.716	97.716

7.7.2 Shrinkage tests - Measured values

The evolution of shrinkage strains for both concretes BL35 and BL36 is measured since the specimens are 24 hours old. For each mixture, measurements are done in two specimens: one sealed and the other with no protection. This allows to measure total shrinkage, basic shrinkage and drying shrinkage. These tests description and results were already presented and discussed in Chapter 2.

All the specimens were put in the same room, so that the concrete curing conditions were similar for beams and cylinders. The most important parameter for the beams' analysis is total shrinkage, as the beams were tested with the concrete section exposed to the ambient conditions of the testing room.

Figure 7.16 presents the shrinkage strain values measured during the shrinkage test and the corrected strain values, considering that loading only began when t = 9 days of concrete age. As the loading application and measurements on the beams are only initiated when they are 9 days old, the values of shrinkage considered for analysis are accounted from this moment on. This means that the values of total shrinkage have to be corrected in order to consider only the parcel of shrinkage that occurs after the first 9 days. The shrinkage curves corrected for t = 9 days are simplified by choosing only a limited number of points from the total shrinkage curve. This is done to simplify the numerical analysis.

The shrinkage values measured in specimens of concrete BL35 show an evolution that is a bit different from the one measured in specimens of concrete BL36. Both concretes suffer swelling in the early ages. If the measurements are considered from t = 9 days, it is verified that BL35 inverts this tendency at the concrete age of 120 days and BL36 at the concrete age of 40 days. This behaviour affects both concretes: at 400 days, the total shrinkage measured for BL35 is around –300 μm/m, while total shrinkage measured for BL36 is around -500 μm/m.

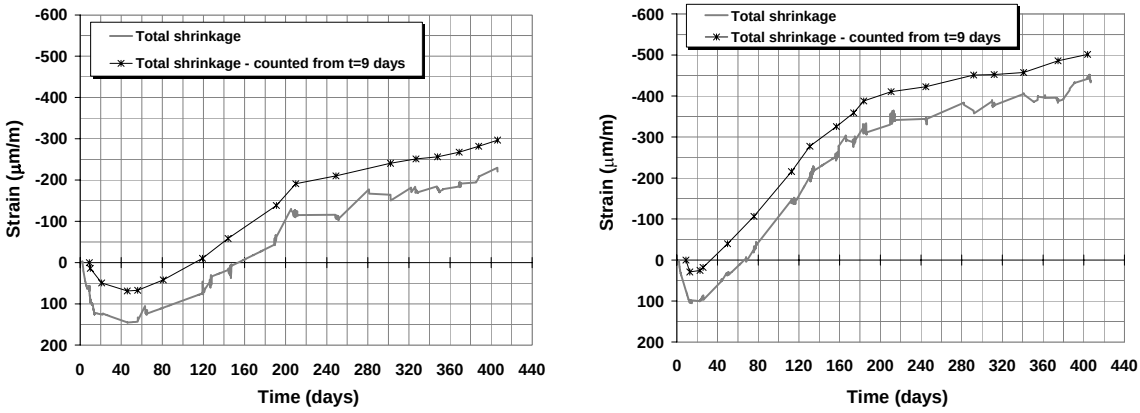

a) BL35 b) BL36

Figure 7.16 – Evolution of total shrinkage strain in time – measured from t = 1 day and t = 9 days

7.8 Effects of concrete creep

In concrete made with normal weight aggregates, creep occurs in the hardened cement paste, and is resisted by the aggregate. Material and environmental factors influencing creep are the composition of the concrete, the concrete rate of hardening, the dimensions of

the element, ambient humidity and ambient temperature. In addition, the magnitude of creep deformations is affected by age at loading, duration of loading, and applied stress level.

The theories of creep, normally applied to concrete structures, assume creep strain to vary linearly with stress. It is a reasonable simplifying assumption for normal levels of serviceability stress.

Creep is conventionally described by reference to a creep function and to a creep coefficient. The creep function, $\varphi(t,t_0)$, refers to the total strain - instantaneous elastic and creep strain - at a given time, under the action of constant unit stress. The creep coefficient, $\varphi(t,t_0)$, is the ratio of the creep component of this strain to the instantaneous elastic component.

According to specification E399 from LNEC (1993), that describes the procedures for creep tests, the creep coefficient may be calculated according to (7.9),

$$\varphi(t,t_0) = \frac{\varepsilon_c(t) \cdot E'_{c,28}}{\sigma_c} \tag{7.9}$$

where the creep strain, $\varepsilon_c(t)$, is calculated according to (7.10),

$$\varepsilon_c(t) = \varepsilon_t(t) - \varepsilon_s(t) - \varepsilon_i \tag{7.10}$$

being,

$\varepsilon_t(t)$ - total strain, for a constant stress value, counted since the first measurement

$\varepsilon_s(t)$ - medium shrinkage strain, counted since the first measurement

ε_i - instant strain measured when the maximum load is applied to the creep specimen

If the stresses N and M are applied to the cross section within a sufficiently large time interval $t_0 < t < t_1$, the stress distribution along the cross section is affected by creep, resulting in a transfer of stress between the two materials. In this case, concrete tends to unload, while steel tends to be overloaded. This phenomena can be analyzed, in a simplified way, by considering the equivalence factor n, as presented in (7.1), altered accordingly to creep results and type of loading as presented in (7.11). Again, if the structure is isostatic, the stresses distribution along the beam span will remain the same in time.

$$n(t) = [1 + j_t \cdot \varphi(t)] \cdot n(0) \tag{7.11}$$

The acting stresses are constant and won't be changed by variation on the cross section mechanical characteristics. If the structure is hyperstatic, the stresses are altered by these changes.

According the EN1994-1-1 (CEN 2004b), the equivalence factor, *n*, is determined with equation (7.12) for the effect of permanent loads,

$$n(t) = [1 + 1.1 \times \varphi(t, t_0)] \cdot n(0) \tag{7.12}$$

and with equation (7.13) for the primary and secondary effect of shrinkage.

$$n(t) = [1 + 0.55 \times \varphi(t, t_0)] \cdot n(0) \tag{7.13}$$

In general, creep has the effects on the composite beam that were identified for shrinkage: the effect of creep on vertical deflection is additional to the effect of the permanent loads, while the effect of creep on slip deformation is opposite to the effect of the permanent loads.

7.8.1 Creep tests - Measured values

Creep coefficient was experimentally determined for the analyzed composite beams. More detailed results on creep tests were presented in Chapter 2. Figure 2.37 from Chapter 2 shows the evolution of creep coefficient in time, measured in lightweight concrete specimens that were cast at the same time as the composite beams.

Some particular points of these curves are plotted in Figure 7.17, in order to define a simpler curve that will be used in the numerical analysis.

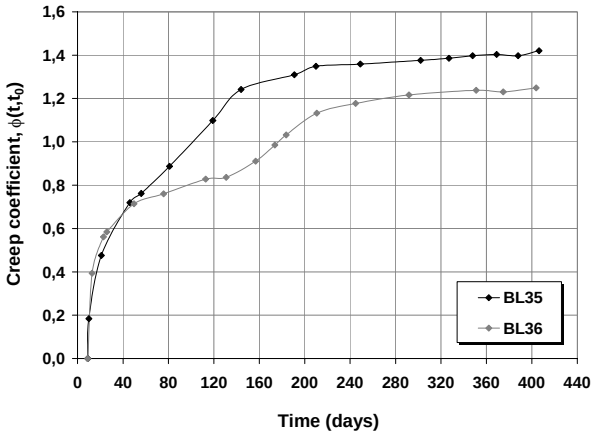

Figure 7.17 – Creep coefficient, in time

7.9 Effects of temperature variation

The tests are done in a laboratory environment. Because the room is not acclimatized, regular measurements of temperature and relative humidity are taken. Temperature varies in time, but is considered constant on the beams cross section and along the beams span, as they are not exposed to outside climate changes.

The variation of temperature in time can result in two effects on the beams behaviour: the uniform temperature variation induces axial stresses and bending stresses, that result from the different thermal expansion coefficients of steel and lightweight concrete, and differences in materials elasticity modulus of elasticity will enhance the redistribution of stresses between the two materials.

At the cross section, the strain that results, in each material, from the temperature variation is calculated with (7.14). The procedure to calculate stresses and strains due to temperature variation is similar to the one presented for shrinkage. In this case, the difference of strain between the two materials must be considered.

$$\varepsilon_T = \alpha \,.\, \Delta T \tag{7.14}$$

The axial force that results from this temperature variation is given by (7.15), taking into account the materials axial deformability.

$$N\left(\frac{1}{E_c A_c} + \frac{1}{E_s A_S}\right) = \left(\alpha_s - \alpha_c\right) \cdot \Delta T \tag{7.15}$$

$$N_T = E_c \,.\, A_c \,.\, (\alpha_s - \alpha_c) \,.\, \Delta T$$

The bending moment that results from the internal forces at the cross section is calculated according to (7.16).

$$M_T = N_T \,.\, (z_{c,G} - z_{s,G}) \tag{7.16}$$

The variation of temperature is considered an instantaneous effect and therefore, no long term effects are associated with it.

7.9.1 Measured values of temperature

Figure 7.18 shows the evolution of room temperature measured along the period of time in which the beams where tested. The temperature measurements were done at the same time as the beams strain measurements, for a period of around 400 days.

Although the tests were performed in a closed environment, in this case, a laboratory room, there is significant daily variation of temperature. Daily gradients of 8ºC could be measured, during the tests period.

The effect of temperature is analysed considering the variation of temperature verified since the initial moment of loading. Therefore, the curves of measured temperature presented in Figure 7.18 are transformed into curves of variation of temperature since the initial loading, that took place at 9 days of concrete age. The points considered to build this second curve correspond to the moments chosen for the shrinkage and the creep analysis.

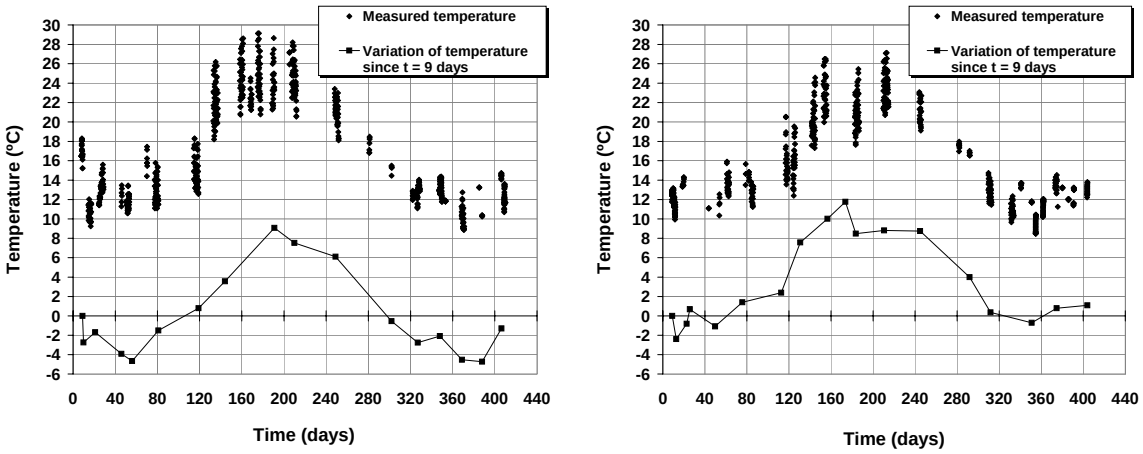

a) VM1 b) VM2

Figure 7.18 – Temperature evolution in the laboratory room where the tests where performed

The values considered for the coefficient of thermal expansion are presented in Table 7.14. These values were collected from EN1992-1-1, (CEN 2004b). The values for concrete modulus of elasticity are experimentally determined, at the age of 28 days.

Table 7.14 – Coefficients of thermal expansion and modulus of elasticity

	α (/ºC)	E_s (GPa)	$E_{c,28d}$ (GPa)
Steel	0.000012	210	-
Concrete – VM1	0.000006	-	22.9
Concrete – VM2	0.000006	-	22.2

7.10 Shrinkage and creep – size effect

The time dependent properties of the lightweight concrete used in the present beams were analysed in Chapter 2. As described then, the specimens tested for shrinkage and creep are cylinders with 150 mm diameter and 300 mm high. On the other side, the beams' concrete slab has a cross section of 350 mm × 60 mm and 4.5 m length and therefore the size effect can be of importance when considering the values of creep and shrinkage obtained in experimental tests applied to the beam model. EN1992-1-1, (CEN 2004a) and CEB-FIP Model Code 1990 (CEB 1990) take into consideration the relation between the total volume of the concrete element and the concrete surface that is in contact with the atmosphere to evaluate the values of creep coefficient and shrinkage strain. The prediction of creep and shrinkage presented in EN1992-1-1 is valid for ordinary structural concrete, with compressive strength varying between 12 and 80 MPa, subjected to compressive stress inferior to 40% of $f_{cm}(t_0)$ at an age of loading t_0 , exposed to mean relative humidity in the range of 40 to 100% and mean temperatures from 5ºC to 30ºC.

Without further detailing on the formulae used for calculating both the creep coefficient and the shrinkage strain (they are detailed in (CEN 2004a)), Table 7.15 presents the lightweight concrete data considered for calculating the curves presented in Figure 7.19, that correspond to the prediction of creep coefficient and shrinkage strains, made for the cylinders and the slab characteristics,

Table 7.15 – Lightweight concrete data

Element	f_{cm} (MPa)	E_{cm} (GPa)	RH (%)	t_s (hours)	t_0 (days)	A_c (m^2)	u (m)	h (m)
Cylinder	60.0	22.2	65	24	9	0.018	0.471	0.075
Slab	60.0	22.2	65	24	9	0.021	0.756	0.056

where,

RH – relative humidity;

t_s – age of concrete when measurements on shrinkage initiate;

t_0 – age of concrete when load is applied and measurements on creep initiate;

u – perimeter of the part exposed to drying;

h – notional size (= $2A_c$ /u), where A_c is the concrete cross-sectional area.

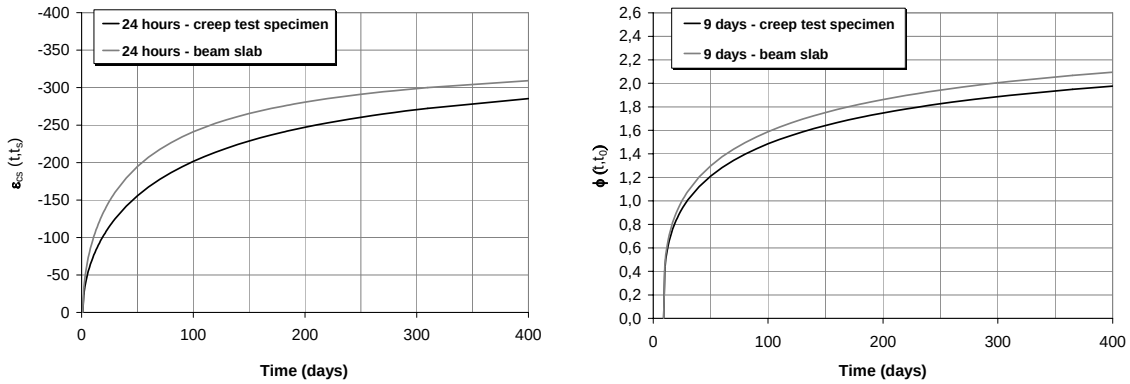

a) Shrinkage b) Creep

Figure 7.19 – Shrinkage and creep curves according to EN 1992-1-1, (CEN 2004a)

Figure 7.20 presents the relation between slab and cylinder values for shrinkage strain and creep coefficient, along time. The relation between shrinkage strain values varies between 1.35 and 1.08. The relation between creep coefficient values varies between 1.08 and 1.06, it is therefore almost constant in time.

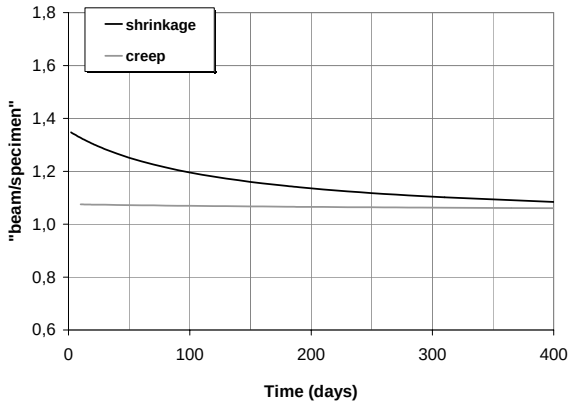

Figure 7.20 – Relation between slab and cylinder values for shrinkage strain and creep coefficient, in time

In order to account for the tested specimens size effect regarding creep and shrinkage, the values obtained for shrinkage, presented in Figure 7.16, will be corrected by a shrinkage factor according to the curve presented in Figure 7.20 and the values obtained for creep coefficient, presented in Figure 7.17, will be corrected by a creep factor with a medium value of 1.07.

7.11 Effect of stress distribution on the concrete slab

Two FEM models are designed in order to evaluate the effect of the compressive stress distribution over the concrete slabs (Figure 7.21). In a composite beam, the transmission of shear forces between the steel profile and the concrete slab is done through the steel connectors.

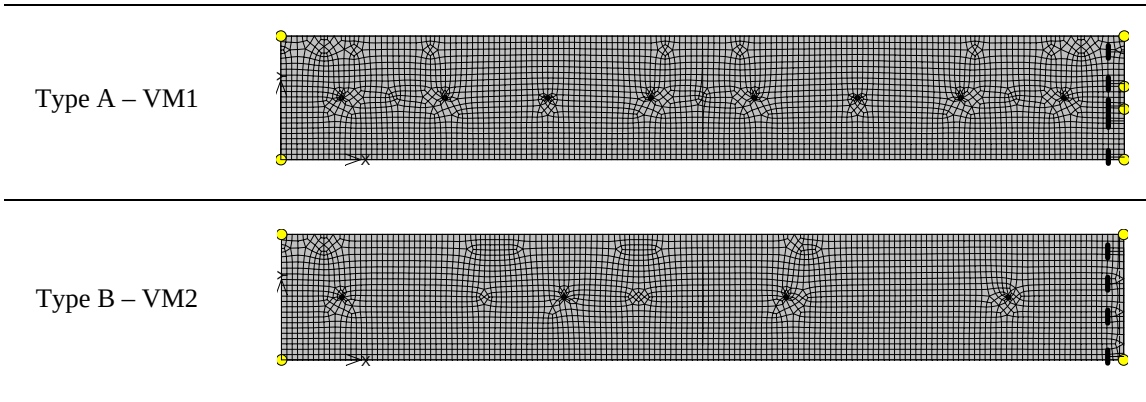

Figure 7.21 – FEM model to evaluate compressive stresses distribution

As described in 7.4.1, the connectors are spaced along the beam and positioned at the cross section symmetry axis. The darker zones of the models represented in Figure 7.21 correspond to the studs positions. The transmission of forces is done in specific points along the beam, where the connectors are positioned. The FEM model is two dimensional

and consists on half concrete slab and connectors. An unitary force is applied to each connector.

A comparison is established between the strain values measured at sections with identical positions as the ones instrumented with strain gauges. Table 7.16 establishes the percentage of medium stress verified on the chosen cross section, at the precise strain gauge position. The principal conclusion is that the variation of stress along the slab cross section is very small. In consequence, it is considered that the strain values, measured with strain gauges, can be directly used for comparison with calculated average strains.

Table 7.16 – Percentage of medium stress correspondent to the strain gauges positions

$\sigma(x) / \sigma_{uniform}$	Beam Type A	Beam Type B
Section A-A'	99.7%	100%
Section B-B'	96.8%	99.5%

7.12 Experimental and numerical results

7.12.1 Total measured deflection and slip

The total vertical deformation measured at the beam mid span of beams VM1 and VM2 is represented in Figure 7.22. The vertical deflection that is verified immediately after the weights are in place, is discounted from these diagrams. Therefore, the diagrams only consider the period when all the loads are positioned over the beams. The intention is to evaluate only the effect of concrete shrinkage, creep and temperature variation. These are the parameters that can alter the beams behaviour along time.

The diagrams presented in Figure 7.22 show two different growing rates for the vertical deflection. Until around 200 days of concrete age, the vertical deflection grows faster, and afterwards this growing rate becomes softer for both beams VM1 and VM2. This growing tendencies were also identified in the shrinkage curves presented in Figure 7.16.

The final value of vertical deflection measured for beam VM1 is smaller than the final value of vertical deflection measured for beam VM2. If the concrete conditions were identical (similar shrinkage and creep values), than the values of vertical deflection measured for beam VM1 should be higher, as the composite interaction for this beam is higher. The fact that vertical deflection is smaller for beam VM1 can only result from lower shrinkage values occurring in BL35, confirmed in Figure 7.16, where in fact the values of total shrinkage measured in specimens of BL35 are smaller than the values of shrinkage measured in specimens of BL36.

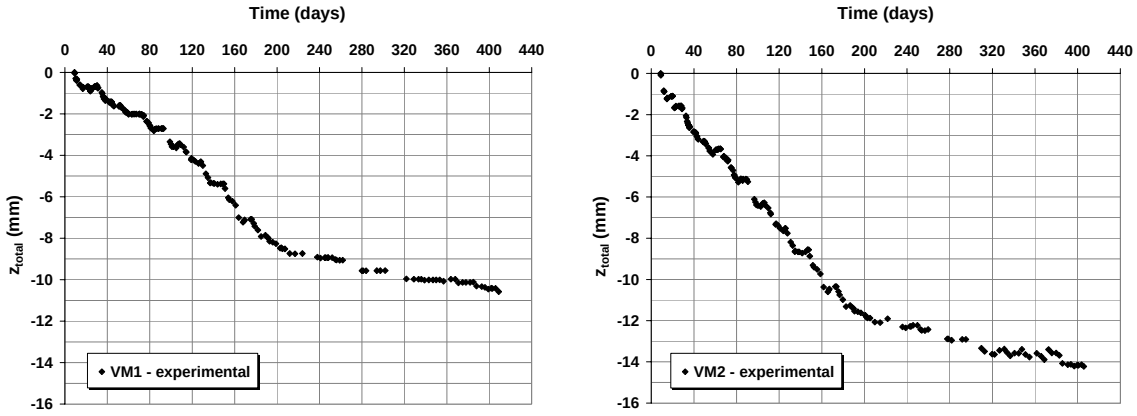

a) VM1 b) VM2

Figure 7.22 – Evolution of maximum vertical deflection after loading, measured for beams VM1 and VM2, after all the weights are positioned on the beams

In terms of total vertical deformation measured at the beam mid span, an average deflection increase of around 100% is verified, from the moment when the loads are applied until the final day of loading (Table 7.17),

Table 7.17 – Increase of vertical deflection and slip during long-term loading

Beam	t_i	t_f	$d_{z,i}$	$d_{z,f}$	Δd_z	$s_{i,H1}$	$s_{i,H2}$	$s_{i,aver}$ (H1,H2)	$s_{f,H1}$	$s_{f,H2}$	$s_{f,aver}$ (H1,H2)	Δs_{aver}
	(days)	(days)	(mm)	(mm)		(mm)	(mm)	(mm)	(mm)	(mm)	(mm)	
VM1	9	409	-11.40	-21.97	0.93	0.075	0.073	0.074	0.011	-0.028	-0.009	-1.11
VM2	9	406	-12.53	-26.76	1.14	0.145	0.130	0.138	0.018	-0.018	0.000	-1.00

where,

t_i – age of concrete when the loading is applied on the beams;

t_f – age of concrete in the final day of loading;

$d_{z,i}$ – initial vertical deflection, measured right after the weights are put in place;

$d_{z,f}$ – final vertical deflection, measured in the final day of loading;

$\Delta d_z = (d_{z,f} - d_{z,i}) / d_{z,i}$

s_i – initial slip, measured right after the weights are put in place;

s_f – final slip, measured in the final day of loading;

$\Delta s = (s_f - s_i) / s_i$

The increase in vertical deflection is around 100% for both beams, which shows clearly the importance of the long term effects for serviceability analysis. It also shows that the results of long term effects on composite beams are not very different from the result of long term effects on reinforced concrete beams in terms of vertical deflection increase.

The total slip deformation measured at the beams' extremes is represented in Figure 7.23 for beams VM1 and VM2. The slip values measured for beam VM2 are much higher than the slip values measured for beam VM2, which was expected since less composite action results in higher slip deformation.

At around 200 days of concrete age, there is a change on the slip growing rate, confirming the tendency previously observed for vertical deflection.

According to the results presented in Table 7.17, the slip value that results from the loading application is more or less annulled by the slip that results from concrete creep and shrinkage. In global terms, the variation of slip corresponds to 100% of the total slip verified after direct loading. However, while the vertical deflection caused by long term effects adds to the vertical deflection caused by direct loading, the slip caused by long term effects is contrary to the slip caused by direct loading.

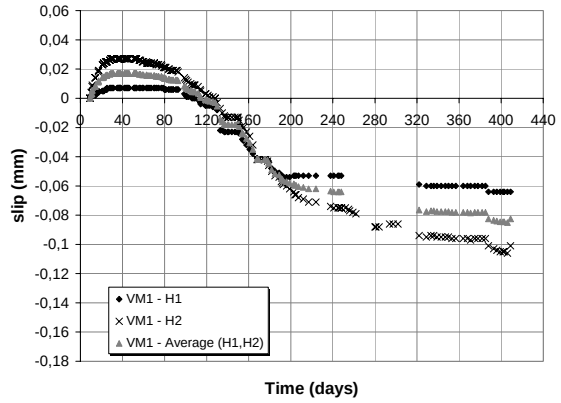

a) VM1

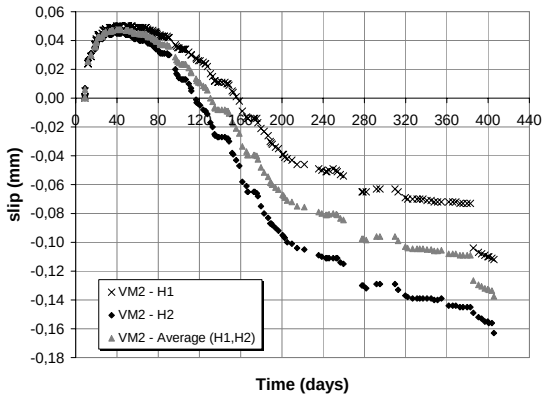

b) VM2

Figure 7.23 – Slip measured between the concrete slab and the steel section for beams VM1 and VM2

7.12.2 Total measured strains

As described in 7.4.2, strains gauges were positioned in the cross sections A-A' (quarter span) and B-B' (mid span) represented in Figure 7.3. In each cross section, they were disposed according Figure 5.13 From Chapter 5. Figure 7.24 and Figure 7.25 present the evolution of strain measured after the load application, for the extreme fibbers of the respective cross sections. Figure 7.24 refers to Fibber 2, which is the lower fibber measured of the steel section and Figure 7.25 refers to Fibber 6, which is the upper fibber of the concrete section.

Due to a lack of equipment, the measurements on the strains gauges positioned at the beams quarter span (section A-A') were only done initially and after 120 days.

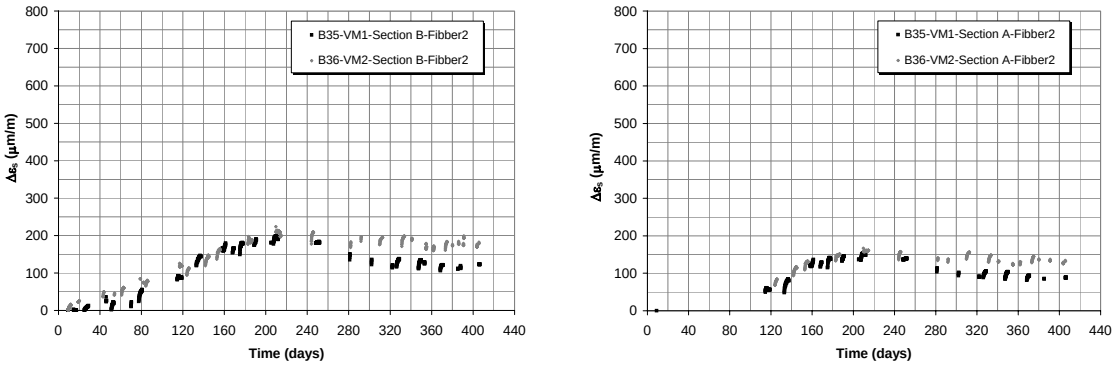

a) Cross section B-B’ b) Cross section A-A’

Figure 7.24 – Strains measured in the steel section, on fibber 2, for VM1 and VM2

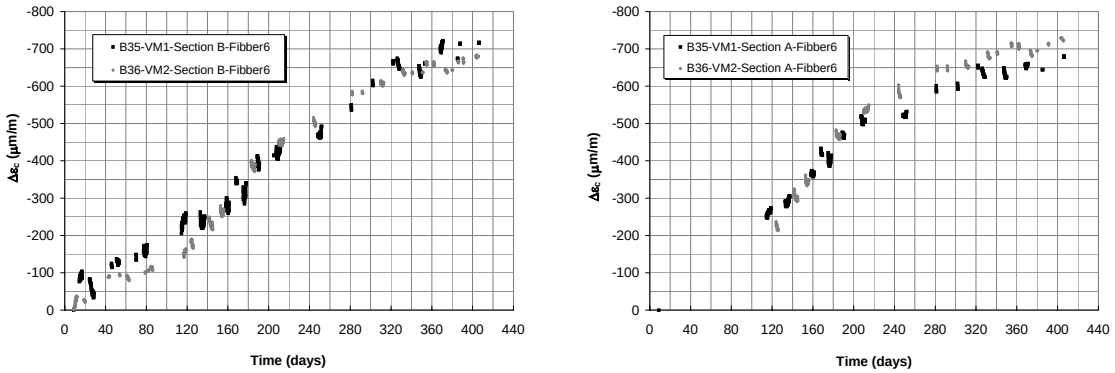

a) Cross section B-B’ b) Cross section A-A’

Figure 7.25 – Strains measured in the concrete section, on fibber 6, for VM1 and VM2

The evolution of strain on the concrete fibbers is similar for the two beams, which means that the global behaviour of both concrete mixes used for the beams fabrication should also be similar, although some differences were found in the shrinkage tests, as was referred in 7.7.2 and 7.8.1. No proper justification is found for this difference in the results.

The evolution of strain on the concrete fibbers reflects the free strain increase due to creep and shrinkage and the strain increase due to the steel beam restrain. The maximum strain increase measured on the concrete fibbers is around -700 μm/m.

The maximum increase of strain at the steel fibbers, during the long term loading, is around 200 μm/m, which means that the stress increase corresponds to around 42 MPa. This value corresponds to 33% of the stress applied on the fibber 2 of the steel section, immediately after all the weights are applied to the beams (see Table A7.5 and Table A7.6 from Appendix 7.2). It is therefore important to quantify the effect of creep and shrinkage on the steel section because it can alter substantially the stresses installed after direct loading.

In the last phase of loading, the strains on fibber 2 of the steel section tend to decrease in both beams. This decrease is higher on beam VM1. This decrease can only be explained by the temperature variation, because the values of creep and shrinkage should be increasing according to the diagrams presented in Figure 7.16 and Figure 7.17.

7.12.3 Temperature variation

Partial interaction has a favourable effect on the composite beam when temperature variation is in cause, as it leads to smaller values of vertical deformation. When comparing a beam with the characteristics of VM1 to a beam with the same cross section and materials but with full interaction, a decrease in the maximum vertical deformation of 3.2% is verified. In the case of a beam with the characteristics of VM2, the corresponding decrease of maximum vertical deformation due to temperature variation is 6.4%.

If the gradients of temperature measured during the period of the tests are small, its influence results in a small variation on the value of axial force and bending moment. In this case, the variation of temperature should not have much influence on the beam behaviour. Using the analytical model presented in Appendix 7.4, adapted to the variation of temperature, a prediction of the maximum vertical deflection and maximum slip is done, based on the values of temperature recorded in the room's tests. The diagrams of temperature variation presented in Figure 7.18 are used for this analysis.

In the analytical model, the effect of temperature can be modelled by considering the free differential strain between steel and concrete sections as the ε_c parcel. In result, the evolution of vertical deflection caused by the temperature is plotted in Figure 7.26.

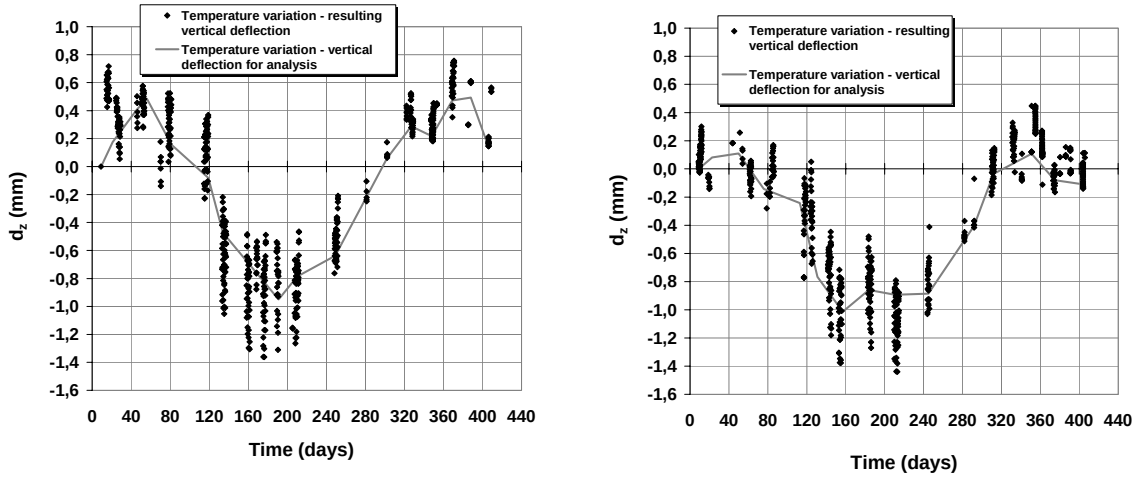

a) VM1 b) VM2

Figure 7.26 - Vertical deflection caused by temperature variation, considering partial interaction (k=250 kN/mm/stud)

The maximum value of vertical deformation resultant from temperature variation is around -1.5 mm (descendant) and 0.8 mm (ascendant), for both beams.

A second curve is drawn in both graphs of Figure 7.26 and Figure 7.27, in order to have values that correspond to the moments of measurement considered for creep and shrinkage analysis.

Figure 7.27 presents the evolution of slip that results from temperature variation.

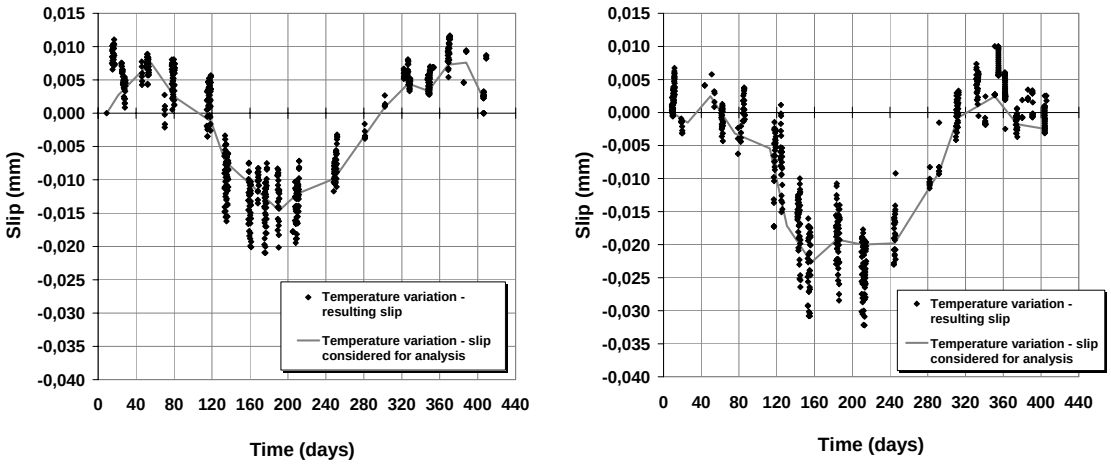

a) VM1 b) VM2

Figure 7.27 - Evaluation of maximum slip deformation caused by temperature variation, considering partial interaction (k=250 kN/mm/stud)

7.12.4 Effect of shrinkage

The stresses installed as effect of shrinkage induce vertical deflection on the composite beams. The evolution of this deformation, along time, is presented in Figure 7.28. These diagrams are obtained with the analytical model presented in Appendix 7.4, based on the curves of total shrinkage presented in Figure 7.16. As the shrinkage values are higher for BL36 than for BL35, the deflection caused by shrinkage is higher for beam VM2, although this beam works with partial interaction, which is an advantage regarding shrinkage effects.

In the same manner, the stresses installed as effect of shrinkage induce slip between the steel and the concrete sections. The evolution of shrinkage slip, along time, is presented in Figure 7.29. The values of shrinkage slip are higher for beam VM2 because of higher shrinkage strains and because of partial interaction.

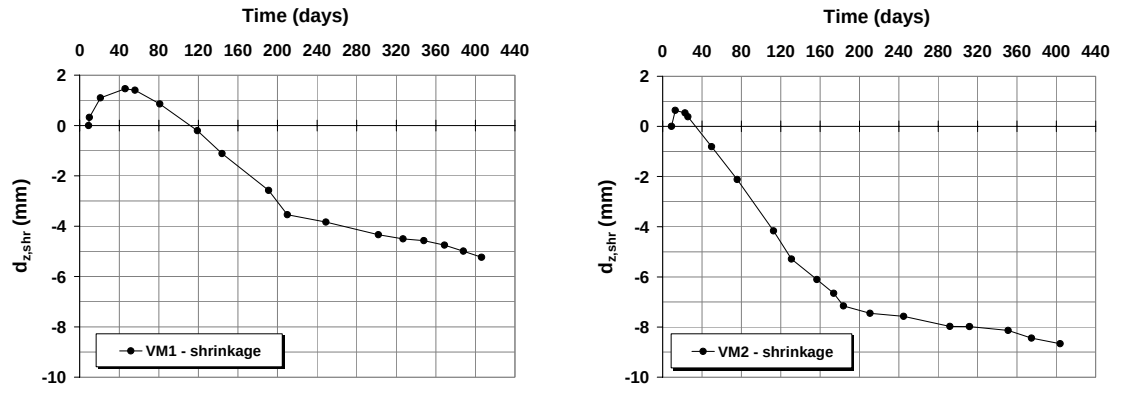

a) VM1 b) VM2

Figure 7.28 – Beams' vertical deflection, resultant from shrinkage (measured at mid span)

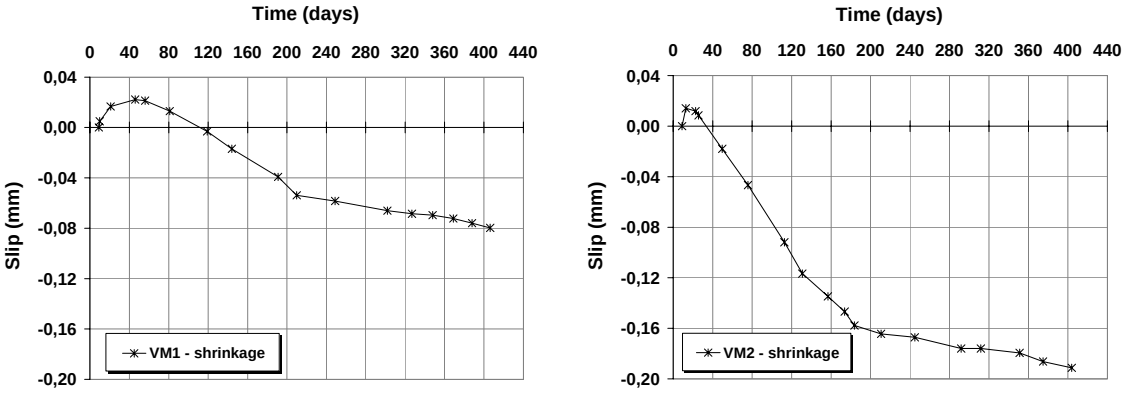

a) VM1 b) VM2

Figure 7.29 – Beams' maximum slip, resultant from shrinkage (end supports)

7.12.5 Effect of creep

The stresses installed as effect of creep induce some vertical deflection on the composite beams. The evolution of this deflection, along time, is presented in Figure 7.30. The diagrams are based on the curves of creep coefficient presented in Figure 7.17.

In global terms, the final vertical deflection caused by creep on VM1 is only a bit higher than the final vertical deflection caused by creep on VM2. The reasons for this difference are the values of the creep coefficient that are a bit higher for concrete BL35 (VM1) and the higher composite action given by the connection between steel and concrete sections.

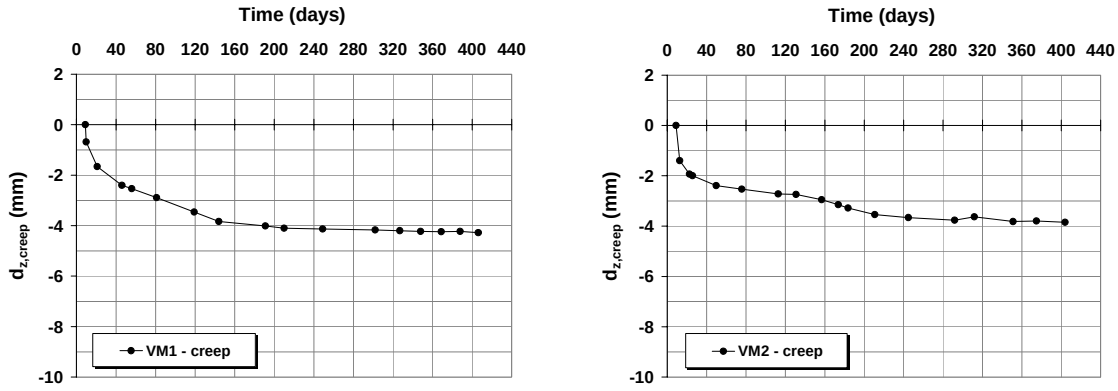

a) VM1 b) VM2

Figure 7.30 – Beams' vertical deflection, resultant from creep (measured at mid span)

In the same manner, the stresses installed as effect of creep induce some slip between the steel and the concrete sections. The evolution of slip, along time, is presented in Figure 7.31. Slip is higher for beam VM2, because of partial interaction effect.

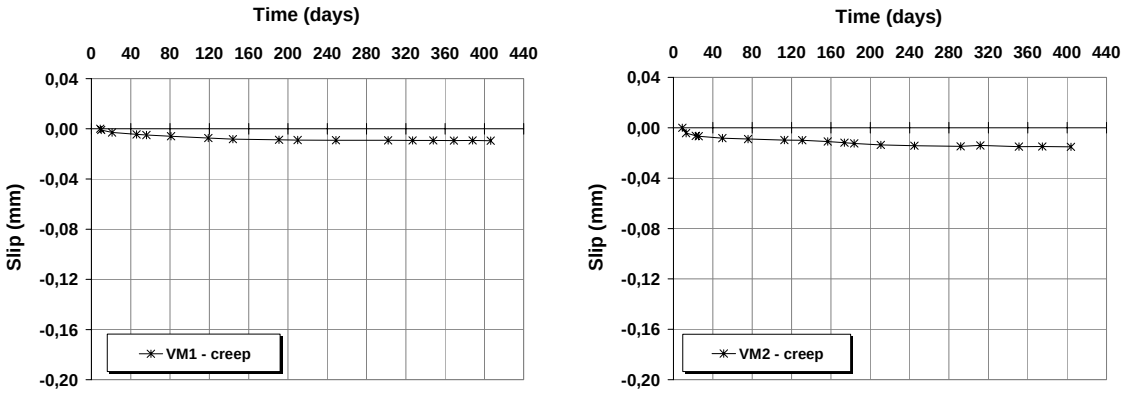

a) VM1 b) VM2

Figure 7.31 – Beams' maximum slip, resultant from creep (end supports)

The strain diagrams that result from shrinkage, creep and temperature variation are presented in Figure 7.32 for the extreme fibbers of the concrete and the steel sections of beam VM1. Final strains due to shrinkage are higher than final strains due to creep, for fibber 6 of beam VM1, while final strains due to creep are higher than final strains due to shrinkage, for fibber 2. Strains that result from temperature variation only have some relative importance at the steel section. At the concrete section, the significance of temperature variation is almost null.

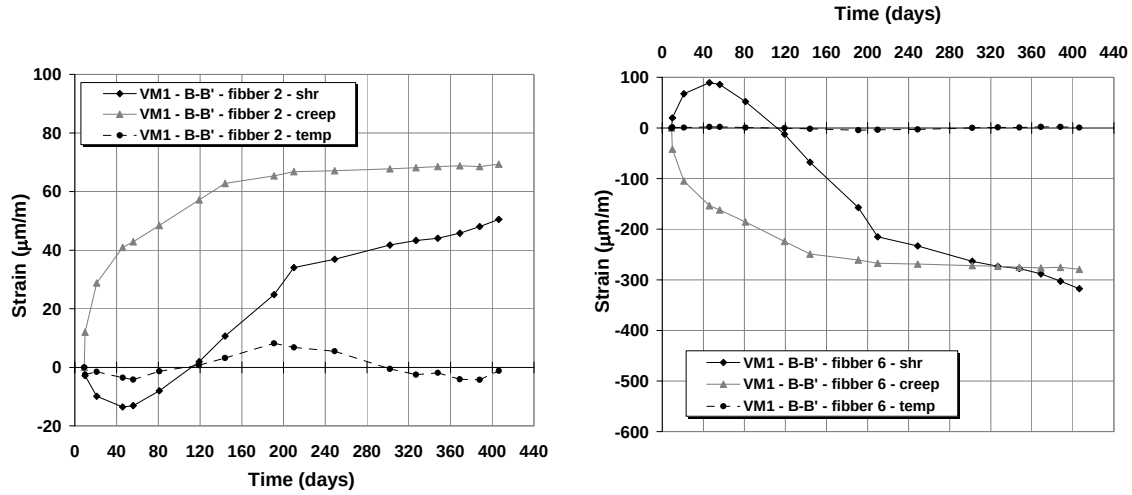

a) VM1 - Fibber 2 (cross section B-B') b) VM1 - Fibber 6 (cross section B-B')

Figure 7.32 – Beams' maximum strains at the steel section and at the concrete section, resultant from shrinkage, creep and temperature for VM1

The strain diagrams that result from shrinkage, creep and temperature variation are presented in Figure 7.33 for the extreme fibbers of concrete and steel sections of VM2.

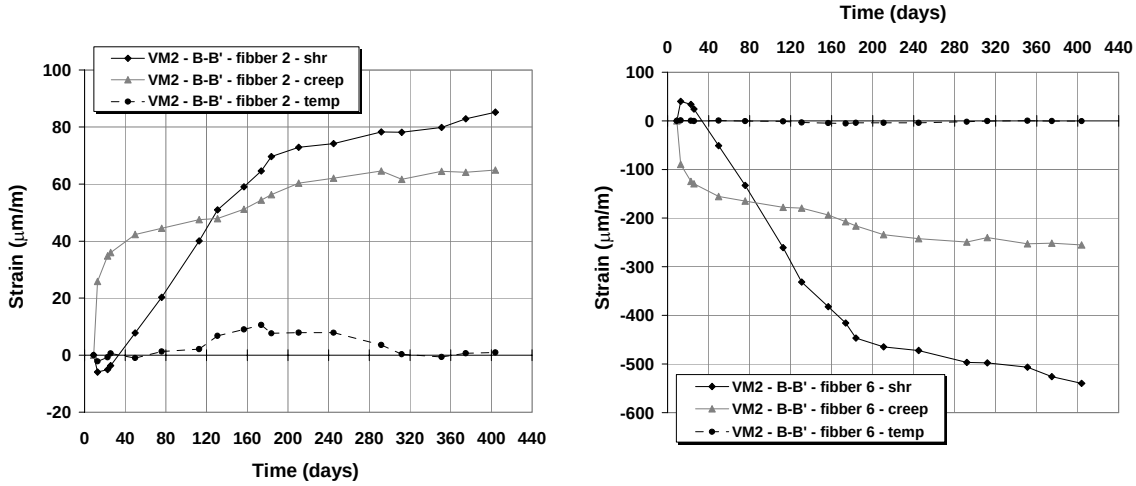

a) VM2 - Fibber 2 (cross section B-B') b) VM2 - Fibber 6 (cross section B-B')

Figure 7.33 – Beams' maximum strains at the steel section and at the concrete section, resultant from shrinkage, creep and temperature for VM2

At the initial phase of loading, the strains that result from concrete creep are higher than the strains that result from concrete shrinkage. However, the final strains due to shrinkage are higher than the final strains due to creep for beam VM2, both in concrete and in steel sections. The observations pointed out for VM1 remain valid regarding temperature variation.

7.12.6 Comparison between experimental measurements and the numerical results on creep, shrinkage and variation of temperature

The sum of shrinkage, creep and variation of temperature effects are now compared to the values of deflection and slip measured during the tests. Figure 7.34 presents all the curves of vertical deflection for each of the described effects and for each of the studied beams. In this way, it is possible to compare the relative importance of each effect on the composite beam.

According to the diagrams presented in Figure 7.34, shrinkage leads to higher vertical deflection than creep or variation of temperature. The importance of shrinkage depends on the value of free shrinkage strain considered and therefore it is more significant for beam VM2 than for beam VM1 because the shrinkage strains measured for BL35 (VM1) are smaller than the shrinkage strains measured for BL36 (VM2).

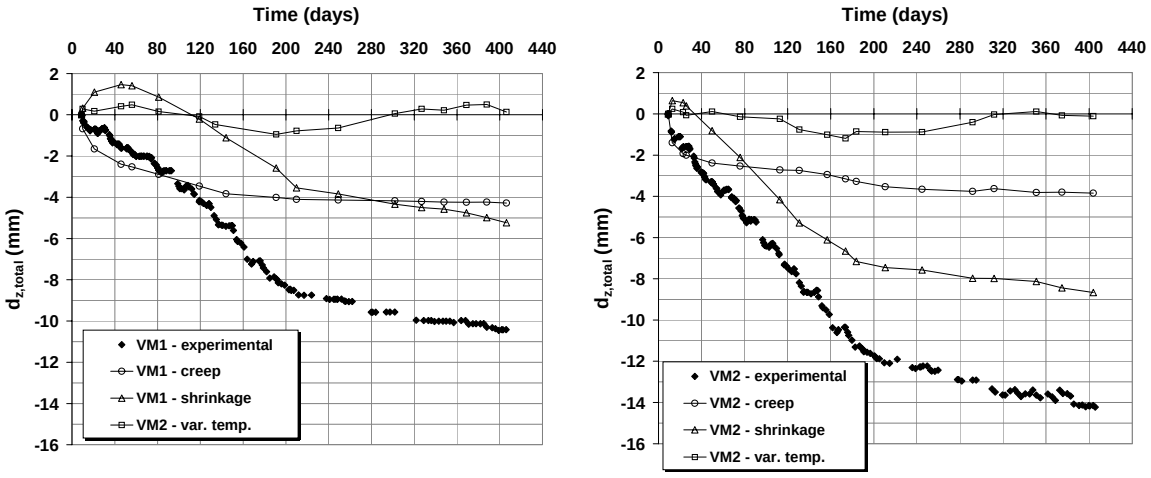

a) VM1 b) VM2

Figure 7.34 – Beams' vertical deflection: experimental results vs. numerical results of creep and shrinkage (measured at mid span)

The effects of creep are similar for both beams, although a bit smaller for beam VM2, because of less composite action. In global terms, the final vertical deflection caused by creep is only a bit smaller than the final vertical deflection caused by shrinkage, for beam VM1. The same does not occur with VM2, where the vertical deflection caused by creep is more or less half the vertical deflection caused by shrinkage.

The variation of temperature is the long term effect that causes smaller changes to vertical deflection and it depends mainly on the time of the year. Its total values are similar for both beams, as the tests were carried out in the same environment.

Figure 7.35 presents three curves: one corresponds to the superposition of creep and shrinkage deflection obtained numerically, other corresponds to the superposition of creep, shrinkage and variation of temperature deflection obtained numerically, and the third corresponds to the experimental deflection measured.

During the initial phase of loading, the development of the experimental curves and the total numerical curves (shrinkage + creep + variation of temperature) curves is very similar for both beams, until around 240 days of loading. From this moment on, the values of vertical deflection measured in the tests tend to be higher than the values predicted.

In this case, the superposition with the effect of temperature variation is not coherent with the values of deflection measured. If the variation of temperature is not considered during this period, than it is observed that the deflection growing rate is common to experimental and numerical curves. These observations are valid for both tested beams. The results seem to indicate that the deflection due to variation of temperature is not recovered after 240 days, as the value of temperature is now going back to the value measured when the loads were applied.

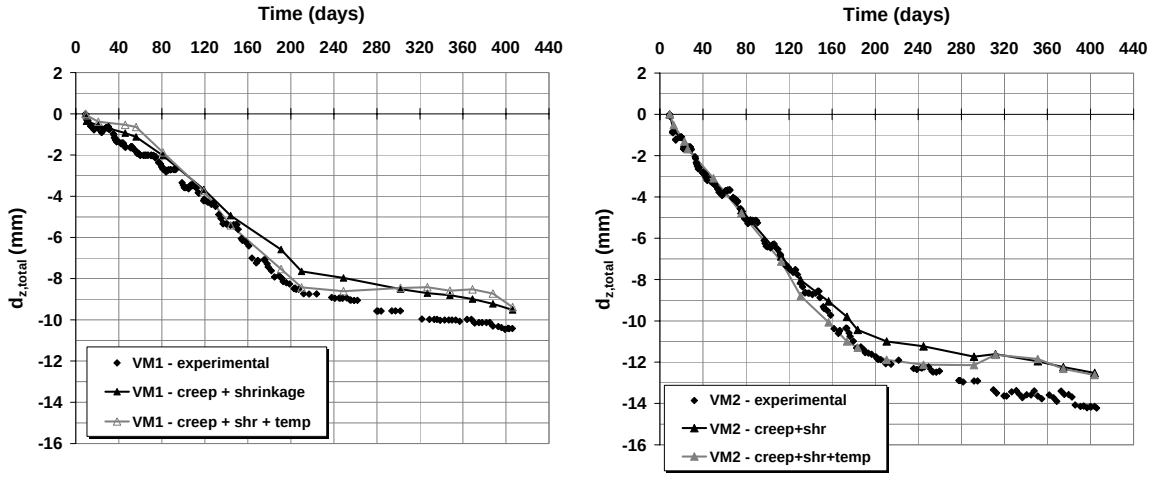

a) VM1 b) VM2

Figure 7.35 – Beams' vertical deflection: experimental results vs. numerical results of creep and shrinkage (measured at mid span)

In the same manner, creep, shrinkage and temperature slip are added and compared to the total slip values measured during the experimental tests. The evolution of slip, along time, is presented in Figure 7.36 for both VM1 and VM2. The curves for H1 and H2 correspond to the end-slip experimentally measured in both extremes of each composite beam.

The values of slip predicted with the numerical method are very close to the values measured during the experimental testing for beam VM1. However, this good agreement

between experimental and numerical results is not verified for beam VM2, in terms of slip. In this case, the values of slip predicted with the numerical model are higher than the values of slip measured during the tests. Despite this difference, it is important to observe that the slip growth and the variation on the rate of slip growth is similar for experimental and numerical analysis and that the difference between the numerical and the experimental curves is more or less maintained during the long term loading. The curves trends show that this is probably caused by a less good assessment on concrete swelling, during the initial phase of loading. Possibly, the specimens used for the shrinkage tests of BL36 did not accurately measure the strains due to concrete swelling that took place in the early days of concrete age.

Temperature variation is not considered in the diagrams presented in Figure 7.36, because the results obtained (see Figure 7.27) are not coherent with the trends measured experimentally. Therefore, the numerical curves presented in Figure 7.36 only consider the effects of creep and shrinkage.

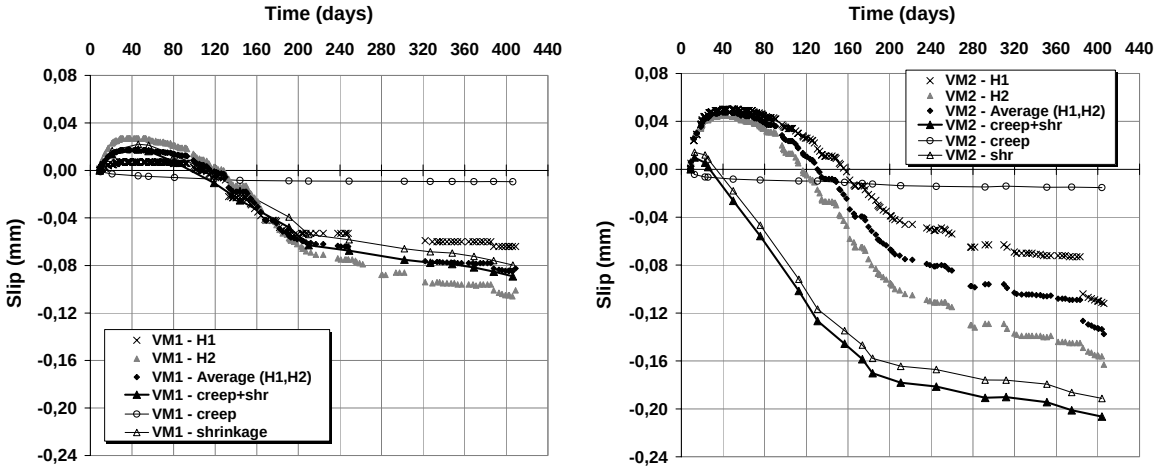

a) VM1 b) VM2

Figure 7.36 – Beams' end slip: experimental results vs. numerical results of creep and shrinkage

Figure 7.37 and Figure 7.38 compare the values of strain that result from the numerical analysis with the values of strain measured during the long term loading. Fibber 2 and fibber 3 correspond to the steel section, fibber 5 and fibber 6 correspond to the concrete section.

There is a good agreement between the numerical and the experimental results for the steel section of beam VM1. The same is observed for the concrete section until t=200 days. From this moment on, the experimental strains on the most compressed fibber (fibber 6) are higher than the strains obtained with the numerical model. The differences observed on the curves of Figure 7.37a) and Figure 7.37b) indicate that the final strains measured result in a lower curvature of the mid span cross section for the numerical

results, which is in agreement with previous results obtained, where the final values of experimental vertical deflection are a bit smaller than the final values of deflection calculated.

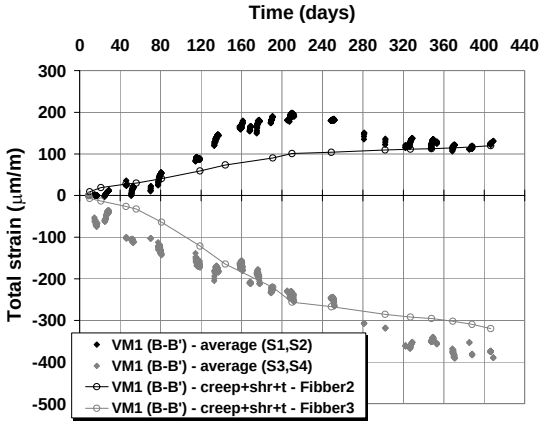

a) VM1 – steel strains

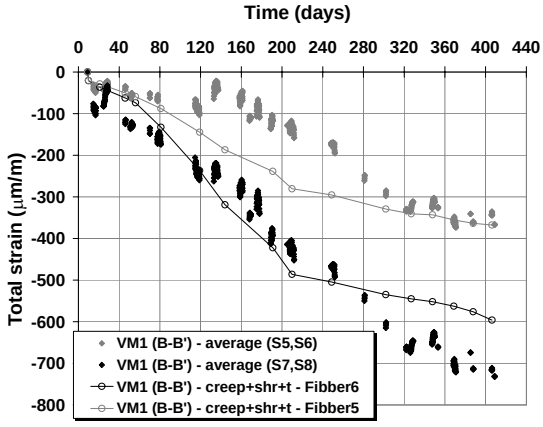

b) VM1 – concrete strains

Figure 7.37 – Comparison between numerical and experimental strains, for fibber 2 and fibber 6 of beam VM1

As for beam VM1, there is also a good agreement between the numerical and the experimental results for the steel section of beam VM2. On the other side, the strains calculated on the concrete section are always higher than the strains experimentally measured, as presented in Figure 7.38.

The differences observed on the curves of Figure 7.38a) and Figure 7.38b) indicate that the final strains measured result in a lower curvature of the mid span cross section for the numerical results, which is in agreement with previous results obtained.

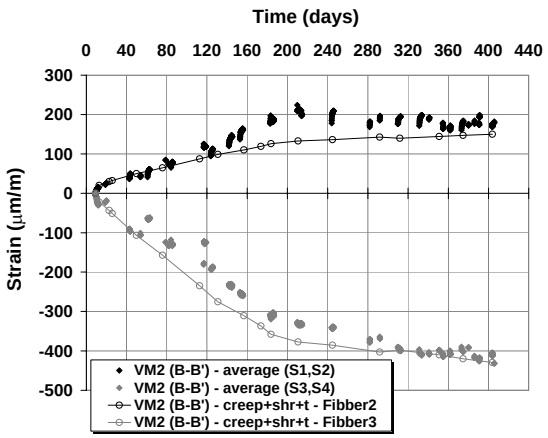

a) VM2 – steel strains

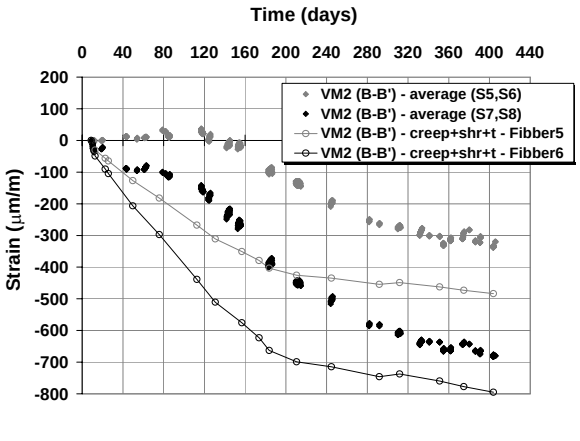

b) VM2 – concrete strains

Figure 7.38 – Comparison between numerical and experimental strains, for fibber 2 and fibber 6 of beam VM2

7.13 Conclusions

Performing experimental tests with one year of duration implied good planning and preparation regarding the fabrication of the beams, their transportation, the collocation of sensors and the application of loading. This text describes the experimental setup, the materials used and the specimens configuration.

The first analysis concerns the evaluation of load, deformation and stress level for the phase of load application, in order to check the measuring devices and some parameters. The first conclusion was that the predicted values for this phase were very approximate to the measured values and therefore, the test could proceed as planed. An evaluation on the probable value of the connection stiffness was done for both beams. The value found is consistent with the values experimentally determined during push-out tests previously performed.

At the same time as the beams' test were developing, shrinkage and creep tests were performed, together with temperature and relative humidity measuring. The measurements collected allowed the evaluation on the effects of creep, shrinkage and temperature variation for the situation of partial interaction between the concrete and the steel section, with a determined value for the connection stiffness.

In terms of shrinkage and temperature variation, it was verified that the connection deformability has a favourable effect, as it reduces the transfer of stress from the concrete section to the steel section in the case of creep and shrinkage and reduces the effect of different values for the temperature coefficient.

The variation of temperature measured during the period of the beams' tests is not very significant as it should lead to a maximum variation of the beam maximum vertical deflection of 1.5 mm.

On the opposite, the effect of concrete shrinkage has a major influence on the composite beams behaviour, as it should lead to a maximum variation of the beam maximum vertical deflection of around 5 to 8 mm, which constitutes an important parcel of the beams total deflection. It was verified that the total deflection increase due to long term effects is around the same value as the elastic deflection due to load application.

For beam VM1, the vertical deflection due to shrinkage is close to the vertical deflection due to creep, while for beam VM2, the vertical deflection due to shrinkage is higher than the vertical deflection due to creep. A good agreement is found between the experimental and the numerical results obtained on vertical deflection.

Chapter 8

CONCLUSIONS

8.1 Concluding remarks

High strength lightweight concrete was experimentally tested and characterized within Chapter 2. In general, this concrete presents similar characteristics in terms of mechanical behaviour to the ones expected for a normal density concrete with the same compressive strength. However, there are some important differences: density, modulus of elasticity and fracture energy are all lower than could be expected for a normal density concrete with the same compressive strength. The value of density determined for the HSLWC analysed is around 75% of the density of a NDC. The modulus of elasticity value is around 65 to 70% of the corresponding value of a NDC and tensile strength value is similar to the corresponding value of a NDC. Fracture energy is around half the corresponding value of a NDC.

The relation between some of these parameters was also analysed. The strongest correlation verified in the experimental tests performed is between modulus of elasticity and density, followed by the correlation between modulus of elasticity and compressive strength.

The long-term behaviour of HSLWC was analysed by means of creep and shrinkage tests. Two mixes were used to perform this analysis and each one of them presented some differences in the results. Both concretes suffered swelling, particularly during the initial phase of loading. The total shrinkage suffered by the specimens of BL36 is higher than the total shrinkage suffered by the specimens of BL35, while the creep coefficient for BL35 is higher than the creep coefficient for BL36. The evolution of creep and shrinkage strains showed different growing rates before and after the 200 days of age, for both concretes. During an initial phase, these values grow faster and in the last phase, they tend to grow slower. In general, the experimental values obtained on creep and shrinkage are not close to the corresponding values obtained with EN1992-1-1.

As observed and measured during the series of push-out tests performed within the tasks of Chapter 3, HSLWC is adequate to be used in composite structures. The results obtained show some loss of load capacity, compared to NWC specimens, but a good general behaviour is noticeable, with a tendency to a higher deformation capacity. The single push-out test performed at the Institute of Structural Concrete, in RWTH, Aachen,

proved to be a good alternative to the standard push-out test when LWC is used, and the resulting differences matched the ones already observed for NWC.

In general, stud shear failure was identified, with exception to the 25 mm diameter studs in the POST tests. In this case, the type of failure observed shows that a HSLWC with a compressive strength that is at least higher than 55 MPa should be used in order to insure the stud shear failure. The headed studs showed a ductile behaviour, as the plastic slip exceeded the value of 6 mm demanded in EN 1994-1-1. The double stud association resulted in a decrease on the connection load capacity, but allowed an increase on the slip deformation for the same shear load applied. This disposition guarantees a more ductile behaviour of the shear connection.

The push-out tests performed with the Perfobond connector, showed that the specimens' failure was always verified with large cracking and crushing in some zones of the concrete slab. The rib connector itself never suffered failure. This connector device presents very high load capacity associated with a ductile behaviour, as the connection load capacity is maintained after very high values of slip are attained. The connection components could be identified. The tests performed, showed that the maximum load attained depends on the area of transversal reinforcement disposed and on the concrete strength. The effects of using lightweight concrete were also analyzed. It was verified that the connection load capacity tends to diminish when NWC is substituted by LWC. It was also verified that the Perfobond connector presents a very stiff behaviour during the initial phase of loading, with small slip values developed for high shear loads. The stiffness measured for Perfobond connector is higher than the stiffness measured for headed studs. In a second phase, the load is kept more or less constant for values of slip that present a constant growth.

The push-out tests performed with T connector showed that this connector device also presents high load capacity associated with a ductile behaviour. The maximum loads attained are smaller than the ones verified for Perfobond connectors but higher than the ones verified for headed studs. The connector itself tends to behave similarly to a stud connector because it suffers shear failure at its basis, right above the welded fillet and its deformed shape shows that the deformation is concentrated on the T half web basis. The stiffness value measured for a T connector is smaller than the stiffness measured for Perfobond, but higher than the stiffness measured for headed studs.

Chapter 4 discussed the fabrication, set up, testing and analysis of cyclic push-out tests on headed stud connectors of 13 mm diameter inside high strength lightweight concrete solid slabs.

The static tests gave results on the connection static strength, deformation capacity and stiffness. Joining the results obtained on 13 mm diameter studs with the results presented in Chapter 3 for 19, 22 and 25 mm diameter studs, it is verified that the use of

lightweight concrete results in a diminution on the connection load capacity. In terms of stiffness, the values obtained for 13 mm diameter studs are close to the values presented in Chapter 3 for 19, 22 and 25 mm diameter studs.

The measurements done during the cyclic tests allowed an evaluation on the slip growth, per load cycle. First, it was verified that the evaluation on the rate of slip growth is influenced by the number of load cycles performed or considered in the analysis. The linear and the logarithmic trends were analysed, because they gave the best correlations between rate of slip growth and number of load cycles applied. In global terms, the logarithmic trend is a better approach when the load range value is lower: $\Delta P/P_u < 0.5$, while the linear trend is best fitting when the load range is higher: $\Delta P/P_u > 0.5$.

The variation on the load range cycles imposed during the testing confirmed that the rate of slip growth is highly dependent on the $\Delta P/P_u$ relation, and therefore, equations to evaluate the rate of slip growth were defined considering this parameter. In general, a comparison between this work and the results obtained by other authors with normal density concrete, shows that the rate of slip growth is higher for lightweight concrete.

Fatigue strength was not achieved in any of the specimens tested with a constant load range. The results obtained are not consistent with the number of load cycles needed to attain fatigue failure, predicted by the various codes. Even so, EN 1994-1-1 gives results that are closer to the experimental ones than any of the other codes analysed.

The work done on Chapter 5 made it possible to analyse the behaviour of steel and lightweight concrete composite beams with headed studs connectors. In global terms, the behaviour observed is similar to what could be expected for normal density concrete, although not equal. The steel to concrete connection behaviour is similar to the behaviour previously observed during the push-out tests performed in Chapter 3 and Chapter 4, as failure occurs in the shear stud, instead of concrete crushing near the stud position. The concrete slab cracking near the studs positions was only identified in beams with double stud disposition.

The uniform and equally spaced stud distribution proved to be the most efficient type of connection, allowing the higher load capacity. Grouping studs in pairs allowed larger vertical deformation but resulted in a reduction on load capacity, which is in agreement with the results previously obtained in Chapter 3.

The connection deformability is an important issue, as it influences directly the beams behaviour. The beams with uniform and equally spaced studs had smaller slip deformation than the beams with studs grouped in pairs, even if both were designed for total connection. All the beams designed for total connection suffered failure with concrete crushing in the cross sections submitted to higher stresses. The beams designed for partial connection suffered higher slip deformation. In these cases, failure was conditioned by shear, which was always localized in one particular side of the beam.

The results on maximum load and bending moment applied show that a good redistribution of shear load, along the composite beam, was achieved. All the beams suffered ductile failure because high deformation was measured while their load capacity was maintained.

The numerical models could not predict with exactitude the ultimate load value and the corresponding vertical deflection. The numerical values for ultimate load and vertical deflection were always smaller than the experimental ones. Even though, the failure modes could be identified.

Chapter 6 addressed the experimental study on cyclic loadings applied to composite beams. The specimens tested were identical to the ones tested monotonically for Chapter 5. In general, the beams designed for full connection suffered bending failure while the beams designed for partial connection suffered shear connection failure. However, beam VM1, designed for full connection, suffered shear connection failure due to the application of repeated loading.

The load cycles of increasing load range applied on two beams induced early failures, by reducing these beams load capacity.

Other two beams were submitted to cyclic loadings of constant load range. The load levels and number of cycles applied induced a reduced loss of shear connection on one of these beams and did not result in a decrease on its load capacity. The maximum load applied to this particular beam was similar to the maximum load applied to an identical beam that was statically loaded. For the other beam, however, the loss of shear connection was significant and resulted in a reduced maximum resisting bending moment.

In general, repeated loading induced loss of shear connection in all the tested beams, with the referred exception. The loss of shear connection is reflected in an increasing slip strain, increasing slip value and finally in higher vertical deflection. Due to slip strain, the strain diagram at the composite cross section is altered, with higher strains at the steel section and lower strains at the concrete cross section when the loss of composite action is significant.

For all the tested beams it was possible to establish defined relations between slip or vertical deflection and the number of load cycles applied. However, after the first 7000 load cycles applied to one beam, slip and vertical deflection stopped presenting a constant growth. From this moment on, it was not possible to establish a direct relation between these parameters and the number of load cycles applied. This result had not been identified in the cyclic push-out tests presented in Chapter 4.

The rate of slip growth was always higher in push-out tests than in composite beams. In push-out tests, all the shear connectors were loaded with similar shear loads, while in composite beams the shear force applied on each connector depended on the connectors' distribution. In the same way, the rate of slip growth is different for each load range

applied to the beams, even when there is plastic distribution of shear stress and one or more studs are loaded to their maximum shear strength.

In the case of simply supported beams, the studs positioned near the supports are submitted to higher shear loads, while the shear connectors positioned near the beams mid span are submitted to low shear loads. Studs that are not loaded to their maximum should have an important influence on the connection behaviour. In the tests performed, it seemed that the shear studs that were not submitted to their maximum load capacity limited the value of slip along the composite beam, because different rates of slip growth were verified when one or more connectors were loaded to their maximum capacity. It is therefore more difficult to establish relations that can predict the slip growth, just based on the number of load cycles applied, as they depended on the connectors' distribution.

Performing the experimental tests with one year of duration, that were presented in Chapter 7, implied a good preparation and the analysis of the several intervenient variables.

The first analysis concerned the evaluation of load, deformation and stress level for the phase of load application, in order to check the measuring devices and some important parameters. The first conclusion was that the predicted values for this phase were very close to the measured values and therefore, the test could proceed as planed. An evaluation on the probable value of the connection stiffness was done for both beams. The value of stiffness was consistent with the values experimentally determined during push-out tests previously performed and presented in Chapter 4.

At the same time, as the beams' tests were developing, shrinkage and creep tests were performed, together with measurements on temperature and relative humidity. The data collected allowed the evaluation on the effects of shrinkage and temperature variation for two beams with different levels of interaction between the concrete and the steel sections.

It was verified that the connection deformability has a favourable effect when shrinkage and temperature variation are considered, because it reduces the transfer of stress from the concrete section to the steel section in the case of shrinkage and reduces the effect of different values for the temperature coefficient.

The variation of temperature measured during the period of the beams' tests was not considered very significant as it should lead to a maximum variation of 1.5 mm on the beam vertical deflection.

On the opposite, the effect of concrete shrinkage had a major influence on the composite beams behaviour, as it should lead to a maximum variation of the beam vertical deflection at mid span of around 11 mm, which constitutes an important parcel of the beams total deflection.

8.2 Suggestions for future work

The work developed in Chapter 2 concerned the analysis of a high strength lightweight concrete. The experimental analysis performed is primarily focused on the characterization of mechanical properties, in order to have the necessary information to perform some of the analysis presented in the following chapters.

All the properties analysed presented clear and consistent results, with exception to creep and shrinkage, where the analysis of two different mixes based on the same composition gave some differences in the final results. More experimental testing should be done on these properties, in order to check which are the parameters that influence those differences. In this case, the number of specimens tested was not sufficient to clarify the reasons that can justify the observed differences.

The results obtained on shear strength presented higher variability than verified for other properties. It is thought that the specimens size and the test configuration may have condition the results obtained. More tests, performed on specimens with different dimensions should be performed, if proper equipment is available.

The application of this lightweight concrete in real structures and particularly in bridges also needs further work on durability aspects. Several authors refer the favourable behaviour of lightweight concrete regarding durability. However, this needs to be confirmed for mixtures with characteristics as the one used in this work.

Another important issue has to do with costs. Costs of material, production, transportation and application should be competitive when compared to the costs associated with a similar normal density concrete, after discounting the beneficial effect of weight reduction. This subject was not addressed but is considered important for possible uses of lightweight concrete.

All the tests performed with different types of shear connectors that were presented in Chapter 3 considered the same class of lightweight concrete, because the option was to study the application of high strength lightweight concrete in composite elements. Lightweight concrete with smaller compressive strength should also be analysed in order to identify the importance of the concrete strength on the connection load and deformation capacity and also on the failure modes. Even so, the experience gained with the experimental work performed on the type of concrete chosen gave very useful knowledge on the phenomena in analysis.

In the case of the Perfobond tests, some work is still to be done, regarding the testing of a higher number of specimens and the variation of more parameters that can be significant to the connection load capacity. The specimens tested varied significantly on the quantity of transversal reinforcement and less on other parameters and therefore further

analysis is recommended. These new results will allow a statistical analysis with more quality.

In the field of rib connectors defined with perforated plates, there are also other geometries that were not analysed, like for example the indented shapes, which have recently proved to be an excellent alternative to the perforated plates with closed openings, in terms of structural behaviour and in terms of constructive performance.

In the case of headed studs, it would be interesting to study the behaviour of very large stud diameters because they are able to replace a high number of studs with smaller diameters.

In the same way, it would be important to test other sizes for the T connector. In one hand, to consider connectors with smaller and with higher transversal section in order to evaluate the contribution of the frontal contact between the connector and the concrete slab and on the other hand, with a different balance between the web and the flange in order to check the relative importance of each component.

Pre-fabrication of concrete slabs is a very up-to-date and interesting issue. The possibility of constructing pre-fabricated slabs that possess the proper openings for the connectors positioning should be possible if the shear connection characteristics and the interaction between the connector, the old concrete and the new concrete are well known. This is thought to be an important field for more research.

Regarding the work presented in Chapter 4, some questions were raised that need more analysis. Further experimental testing should be considered in order to confirm the validity of the obtained results and conclusions and to assess the influence of other parameters. In special, further testing should be done, considering:

- the variation of the stud diameter;
- the variation of the lightweight concrete strength;
- cyclic tests with higher number of load cycles within the same load range;
- and, more levels of load range.

A new experimental campaign that considers the variation of these parameters would give a wider spectrum on the applicability of lightweight concrete in composite elements submitted to cyclic loadings.

The work developed within Chapter 5 helps to clarify the behaviour of a steel and lightweight concrete composite beam. Different failure modes are identified and it is possible to characterize the beams deflection, slip at the steel to concrete interface and strain distribution.

In this study, only beams with stud connectors were tested. Other types of connectors should also be tested in composite beams. Although the work done within Chapter 3 shows their particularities, issues like the shear load redistribution, concrete cracking, influence of

materials non-linear behaviour and influence of span to height ratio can only be properly analysed with tests on beams.

In the same manner, different cross section typologies and different span to height ratios should be analysed in order to identify possible differences on the beams failure modes and possible differences on the shear load distribution.

The work done with numerical models should also be improved with 3D FEM models that can more accurately approximate the numerical results with the experimental ones.

The results obtained in Chapter 6 show that it is very difficult to establish relations that can predict the evolution of slip at the interface between steel and lightweight concrete sections caused by repeated loading. It was observed that the rate of slip growth is highly dependent on the value of maximum load, on the load range and on the shear connectors distribution. Therefore, experimental testing that concerns the variation of these parameters should be in analysis.

The use of numerical models that can account the evolution of slip and therefore consider the loss of composite action could avoid large experimental testing. However, experimental work is always needed to calibrate these models. Both lines of investigation are subsequent to the work here presented.

Chapter 7 deals with long term loadings applied on composite beams. As was observed and measured, the long-term behaviour of lightweight concrete alters the composite beams deflection and internal stress distribution. The effects of creep, shrinkage and temperature variation were considered in the analysis.

Partial interaction was also considered, although the value of the connection stiffness was considered constant through the complete period of loading. This is an aspect that should be further analysed: it is to expect that the long-term loading introduces changes on the connection stiffness because the concrete slab is submitted to sustained loading.

The shrinkage of lightweight concrete was the long-term effect that presented more differences with the expected behaviour for normal density concrete. Beside shrinkage tests on lightweight concrete specimens, more long-term tests on steel and lightweight concrete composite beams should be useful to analyse this phenomenon with more depth.

Regarding the work done on Chapter 5, 6 and 7, it would also be important to study continuous steel and lightweight concrete composite beams, in order to check the influence of negative bending moment. Continuous composite beams are closer to a real structure, like for example composite bridge decks, than the examples here studied but more difficult to analyse in terms of the shear stress redistribution. That is the reason for the choice made on simply supported beams.

References

(AASHTO 2004) AASHTO LRFD. Bridge design specifications. 3rd edition. American Association of State Highway and Transportation Officials, 2004.

(ACI 2003) ACI 213R-03: Guide for Structural Lightweight Aggregate Concrete, September 2003.

(Aïtcin 1998) Aïtcin, Pierre-Claude: High-Performance Concrete. Modern Technology 5, E & FN SPON, London and New York.

(Almeida 2005) Almeida, I. Ramalho de: Concreto: ensino, pesquisa e realizações. Ed. Geraldo C. Isaia, IBRACON, São Paulo, Brasil.

(An and Cederwall 1996) An, L.; Cederwall, K.: Push-out tests on studs in high strength and normal strength concrete, Journal of Constructional Steel Research, January 1996, Vol. 36, N. 1, pp. 15-29.

(Asgeirsson 1994) Asgeirsson, H.: Henka pumice in Lightweight concrete. The Icelandic Building Research Institute - IBRI, 45 pp.

(ATENA 2003) Atena – Computer Program for Nonlinear Finite Element Analysis of Reinforced Concrete Structures. Cervenka Consulting. Program documentation. Rev. 2003.

(Bardhan-Roy 1995) Bardhan-Roy, B. K.: Lightweight aggregate concrete in the UK. CEB/FIP International Symposium on Structural Lightweight Aggregate Concrete, Sandefjord, Norway, pp 52-69.Editors: I. Holand, et al.

(Barros 1995) Barros, J. A. O.: Comportamento do betão reforçado com fibras – análise experimental e simulação numérica. PHd Thesis, Faculdade de Engenharia da Universidade do Porto, December 1995, 484 p. (in portuguese).

(Bettor-MBT 2000) Technical sheet 1.1.26: Glenium 52. October 2000, 2 p.

(BE96-3942/R1 1998) EurolightCon – Economic Design And construction with Light Weight Aggregate Concrete, Project BE96-3942, Report BE96-3942/R1: Definitions and International consensus report, 69 p.

(BE96-3942/R2 1998) EurolightCon – Economic Design And construction with Light Weight Aggregate Concrete, Project BE96-3942, Report BE96-3942/R2: LWAC Material Properties – State-of-the-Art, December 1998, 109 p.

(BE96-3942/R14 2000) EurolightCon – Economic Design And construction with Light Weight Aggregate Concrete, Project BE96-3942, Report BE96-3942/R14: Structural LWAC – Specification and guideline for materials and production, May 2000, 69 p.

(BE96-3942/R22 2000) EurolightCon – Economic Design And construction with Light Weight Aggregate Concrete, Project BE96-3942, Report BE96-3942/R22: The economic potential of lightweight aggregate concrete in c.i.p. concrete bridges. June 2000, 25 p.

(BE96-3942/R23 2000) EurolightCon – Economic Design And construction with Light Weight Aggregate Concrete, Project BE96-3942, Report BE96-3942/R23: Mechanical properties of lightweight aggregate concrete, June 2000, 50 p.

(BE96-3942/R30 2000) EurolightCon – Economic Design And construction with Light Weight Aggregate Concrete, Project BE96-3942, Report BE96-3942/R30: Creep properties of LWAC, May 2000, 61 p.

(BE96-3942/R31 2000) EurolightCon – Economic Design And construction with Light Weight Aggregate Concrete, Project BE96-3942, Report BE96-3942/R31: Long term effects in LWAC: Strength under sustained loading and Shrinkage of High Strength LWAC, June 2000, 31 p.

(Bradford 1991) Bradford, M. A.: Deflections of composite steel-concrete beams subject to creep and shrinkage. ACI Structural Journal, September-October 1991, Vol. 88, No. 5, pp. 610-614.

(Bradford 1997) Bradford, M. A.: Shrinkage behaviour of steel-concrete composite beams. ACI Structural Journal, November-December 1997, Vol. 94, No. 6, pp. 625-632.

(BS 5400 1980) BS 5400 1980. Steel, concrete and composite bridges. Part 10: Fatigue. British Standards Institution, 1980.

(BSI 1967) CP 117 - Composite Construction in Structural Steel and Concrete. Part 2: Beams for Bridges. British Standards Institution, 1967.

(Bursi and Gramola 1999) Bursi, O. S., Gramola, G.: Behaviour of headed stud shear connectors under low-cycle high amplitude displacements. Materials and Structures, May 1999, Vol. 32, pp. 290-297.

(Calzon and Ortiz 1978) Martinez Calzon, J.; Ortiz Herrera, J.: Construction Mixta Hormigon-Acero. Editorial Rueda, 1978.

(Camões 2002) Camões de Azevedo, Aires F. F. L.: Betões de elevado desempenho com incorporação de cinzas volantes. Phd Doctoral Thesis, University of Minho, July 2002. (in portuguese).

(CEB-FIP 1977) CEB-FIP Manual, “Lightweight Aggregate Concrete. CEB-FIP Manual of Design and Technology”, The Construction Press, London, pp. 169.

(Cembureau 1974) Cembureau, The European cement association: Lightweight aggregate concrete - technology and world applications. Editor G. Bologna

(CEB 1990) CEB-FIP Model Code for Concrete Structures, Comité Euro-Internatinal du Béton, 1990.

(CEN 2004a) EN 1992-1-1: Design of concrete structures. Part 1-1: General rules and rules for buildings. European Committee for standardization (CEN).

(CEN 2005) EN 1993-1-1: Design of steel structures. Part 1-1: General rules and rules for buildings. European Committee for standardization (CEN).

(CEN 2004b) EN 1994-1-1: Design of composite steel and concrete structures. Part 1-1: General rules and rules for buildings. European Committee for standardization (CEN).

(Civjan and Singh 2003) Civjan, S. A., Singh, P.: Behaviour of shear studs subjected to fully reversed cyclic loading. Journal of Structural Engineering ASCE, Vol. 129, No. 11, November 2003, pp. 1466-1474.

(Cruz et al. 2005) Cruz, P. J. S.; Valente, I.; Hegger, J.; Rauscher, S.; Goralski, C.: Experimental studies on shear connection between steel and lightweight concrete using studs. Eurosteel 2005 - European Conference on Steel Structures, Maastricht, The Netherlands, June 2005, Volume B, pp. 4.3-75-4.3-82.

(Curcio et al 1998) Curcio, F., Galeota, D., Gallo, A., Giammatteo, M.: High-performance Lightweight Concrete for the Precast Prestressed Concrete Industry. Proc. 4th Int. CANMET/ACI/JCI Symposium, Tokushima, Japan, pp. 389-406.

(Daly 2000) Daly, A. F. G.: Use of LWAC in Bridges. Second International Symposium on Structural Lightweight Aggregate Concrete, Kristiansand. Norway, June 2000, pp. 345-354.

(Döinghaus 2001) Döinghaus, P.: Zum Zusammenwirken hochfester Baustoffe in Verbundkonstruktionen. PHd Thesis, Institute of Structural Concrete, RWTH Aachen, October 2001.

(EN 1008 2002) EN 1008 2002 – Mixing water for concrete. Specification for sampling, testing and assessing the suitability of water, including water recovered from processes in the concrete industry, as mixing water for concrete. June 2002. European Committee for standardization (CEN).

(EN 10002-1 2001) EN 10002-1: Metallic materials. Tensile testing. Part 1: Method of test at ambient temperature. European Committee for Standardisation (CEN).

(EN 10025 2004) EN 10025: Hot rolled products of structural steels. Part 1: General technical delivery conditions. European Committee for Standardisation (CEN).

(EN 12390-3 2001) EN 12390-3 – Testing hardened concrete – Part 3: Compressive strength of test specimens. December 2001. European Committee for standardization (CEN).

(EN 12390-6 2000) EN 12390-6 – Testing hardened concrete – Part 6: Tensile splitting strength of test specimens. December 2001. European Committee for standardization (CEN).

(EN ISO 13918 2000) EN ISO 13918:2000. Welding. Studs and ceramic ferrules for arc stud welding. European Committee for Standardisation (CEN).

(EN ISO 14555 2000) EN ISO 14555:2000. Welding. Arc stud welding of metallic materials. European Committee for Standardisation (CEN).

(ENV 10080 1995) ENV 10080: Steel for the reinforcement of concrete. Weldable reinforcing steel. General. European Committee for Standardisation (CEN).

(Erlicher et al. 2001) Erlicher, S.; Bursi, O. S.; Zandonini, R.: Low-cycle fatigue behaviour of pull-push specimens with headed stud shear connectors. International Symposium on Connections Between Steel and Concrete, University of Stuttgart, September 2001, Vol.2, pp. 1303-1312.

(ESDEP 1995) ESDEP Society - The European Steel Design Education Programme. CD-Rom.

(Faust et al. 2000) Faust, T.; Leffer, A.; Mensinger, M.: LWAC in Composite Structures, Second International Symposium on Structural Lightweight Aggregate Concrete, Kristiansand, Norway, June 2000, pp. 365-374.

(Ferreira 2000) Ferreira, L. T. S.: “Semi-rigid systems for composite building construction“, PhD Thesis, Pontifícia Universidade Católica do Rio de Janeiro, Brazil, April 2000 (in portuguese).

(Galjaard and Walraven 1999) Galjaard, J. C.; Walraven, J. C.: New and existing shear connector devices for steel-concrete composite structures. Static tests, results and observations. First International Conference on Structural Engineering, Kunming, China, October 1999, ISSN 1000-4750.

(Galjaard and Walraven 2000) Galjaard, J. C.; Walraven, J. C.: Behavior of shear connector devices for lightweight steel-concrete composite structures – results, observations and comparisons of static tests. Second Int. Symposium on Structural Lightweight Aggregate Concrete, Kristiansand, Norway, June 2000, pp 221-230.

(Galjaard and Walraven 2001) Galjaard, J. C.; Walraven, J. C.: Static tests on various types of shear connectors for composite structures. International Symposium on Connections between Steel and Concrete, University of Stuttgart, September 2001, Vol.2, pp 1313-1322.

(Gattesco and Giuriani 1996) Gattesco, N.; Giuriani, E.: Experimental study on stud shear connectors subjected to cyclic loading. Journal of Constructional Steel Research, January 1996, Vol. 38, pp. 1-21.

(Gattesco et al. 1997) Gattesco, N., Giuriani, E. & Gubana, A.: Low-cycle fatigue test on stud shear connectors, Journal of Structural Engineering ASCE, February 1997, pp. 145-150.

(Gattesco and Giuriani 2001) Gattesco, N.; Giuriani, E.: A test proposal for fatigue experimental studies on stud shear connectors. International Symposium on Connections between Steel and Concrete, University of Stuttgart, September 2001, Vol.2, pp 1162-1171.

(Gilbert and Bradford 1995) Gilbert, R. I.; Bradford, M. A.: Time-dependent behaviour of continuous composite beams at service loads. Journal of Structural Engineering, ASCE, Vol. 121, No. 2, February 1995, pp. 319-327.

(Hallam 1976) Hallam, M. W.: The behaviour of stud shear connectors under repeated loading. University of Sydney, School of Civil Eng., Research Report 281, August 1976.

(Hallam 1978) Hallam, M.W. 1978, The behaviour of shear studs under repeated loading. Civil Engineering Transactions IEAust, vol. CE 20, No. 1, pp. 28-36.

(Hammer et al 1995) Hammer, T.A., Smeplass, S. (1995). The influence of lightweight aggregate properties on material properties of the concrete. CEB/FIP International Symposium on Structural Lightweight Aggregate Concrete, Sandefjord, Norway, pp 517-532. Editors: Holand, I., et al.

(Hanswille et al. 2007) Hanswille, G.; Porsch, M.; Ustundag, C.: Resistance of headed studs subjected to fatigue loading. Journal of Const. Steel Research, April 2007, Vol. 63, N.4, Part I : Experimental study, pp. 475-484 and Part II: Analytical study, pp. 485-493.

(Hauke 2005) Hauke, B.: Shear connectors for composite members of high strength materials. Eurosteel 2005 - European Conference on Steel Structures, Maastricht, The Netherlands, June 2005, Volume B, pp. 4.2-57-4.2-64.

(HBM 2000) Amplifier system MG*Cplus* with display and control panel AB22A/AB32 - Operating Manual. HBM - Hottinger Baldwin Messtechnik GmbH, October 2000.

(Hegger et al. 2000) Abschlussbericht zum Forschungsvorhaben Untersuchungen zur Duktilität der Verbundmittel bei Anwendung vor hochfestem Stahl und hochfestem Beton; AIF-Nº12124; RWTH Aachen, November 2000.

(Hegger et al. 2001) Hegger, J.; Sedlacek, G.; Döinghaus, P.; Trumpf, H.: Studies on the ductility of shear connectors when using high-strength concrete. International Symposium on Connections between Steel and Concrete, University of Stuttgart, September 2001, Vol.2, pp 1025-1045.

(Hegger et al. 2004) Hegger, J.; Goralski, C.; Rauscher, S. and Kerkeni, N.: Finite Elemente Berechnungen zum Trag- und Verformungsverhalten von Kopfbolzendübeln. Stahlbau 73, January 2004, Vol.1, pp. 20-25,.

(Hegger et al. 2005) Hegger, J., Rauscher, S., Goralski, C.: Push-out tests on headed studs covered with UHPC. Eurosteel 2005 - European Conference on Steel Structures, Maastricht, The Netherlands, June 2005, Volume B, pp. 4.2-49 to 4.2-56.

(Hiragi et al. 1981) Hiragi, H.; Miyoshi, E.; Kurita, A.; Ugai, M.; Akao, S.: Static Strength of Stud Shear Connectors in SRC Structures. Transactions of the Japan Concrete Institute, Vol.3, pp. 453-460, 1981.

(Hoff et al. 1995) Hoff, G. C., Walum, R., Weng, J. K., Nunez, E.: The use of Structural Lightweight Aggregate in Offshore Concrete Platforms. CEB/FIP International Symposium on Structural Lightweight Aggregate Concrete, Sandefjord, Norway, pp 349-362. Editors: I. Holand, et al.

(Hofmann et al. 1983) Versuche zum Kriechen und Schwinden von hochfestem Leichtbeton. Deutscher Ausschuss für Stahlbeton, H. 343, pp. 1-20.

(Johnson 1970) Johnson, R. P.: Longitudinal shear strength of composite beams, ACI Journal, Vol. 67, June 1970, pp. 464-466.

(Johnson 1994) Johnson, R. P.: Composite Structures of Steel and Concrete – Beams, Slabs, Columns, and Frames for Buildings. 2nd edition, Oxford (UK): Blackwell Science Ltd., 1994. Vol.1.

(Johnson 2000) Johnson, R. P.: Resistance of stud shear connections to fatigue. Journal of Constructional Steel Research, Elsevier, February 2000, Vol.56, No. 2, pp. 101-116.

(Kraus and Wurzer 1997a) Kraus, D.; Wurzer, O.: Bearing capacity of concrete dowels. Composite Construction - Conventional and Innovative, IABSE International Conference, Innsbruck, pp. 133-138, 1997.

(Kraus and Wurzer 1997b) Kraus, D.; Wurzer, O.: Nonlinear Finite Element Analysis of Concrete Dowels, Computer and Structures, May-June 1997, Vol. 64, No. 5/6, pp. 1271-1279.

(Lam and Ellobody 2005) Lam, D., Ellobody, E.: Behavior of headed stud shear connectors in composite beams. ASCE Journal of Structural Engineering, 2005;Vol. 131, Nº1: pp. 96–107.

(Lee et al. 2005) Lee, Pil-Goo ; Shim, Chang-Su ; Chang, Sung-Pil : Static and fatigue behavior of large stud shear connectors for steel-concrete composite bridges. Journal of Constructional Steel Research, Elsevier, May-June 2005, Vol.61, pp. 1270-1285.

(Leonhardt et al. 1987) Leonhardt, F.; Andrä, W.; Andrä, H.P.; Harre, W.: Neues vorteilhaftes verbundmittel für stahlverbundtragwerke mit höher dauerfestigkeit (New advantageous shear connection for composite structures with high fatigue strength). Beton und Stahlbetonbau 62, Nº 12, pp. 325-331, 1987.

(LNEC 1993) Especificação E-397 do LNEC: Betão – Ensaio de módulo de elasticidade. 1993.

(Lo 1978) Lo, K.K.: Fatigue behaviour of stud connectors in composite plate and slab systems. MSc Thesis, University of Melbourne, 1978.

(Lopez et al. 2004) Lopez, M.; Kahn, L. F.; Kurtis, K. E.: Creep and shrinkage of high-performance lightweight concrete. ACI Structural Journal, September-October 2004, Vol. 101, Nº 5, pp. 391-399.

(Lourenço et al 2004) Lourenço, J.; Júlio, E.; Maranha, P.: Betões de agregados leves de argila expandida – Guia para a sua utilização. ISBN 972-9071-30-6, Associação Portuguesa das Empresas de Betão Pronto, 196 p.

(Lungershausen 1988) Lungershausen, H.: Zur Schubtragfähigkeit von Kopfbolzendübeln, Technisch-wissenschaftliche Mitteilung Nr. 88-7, Institut für konstruktiven Ingenieurbau, Ruhr-Universität Bochum, 1988.

(Machacek and Studnicka 2002) Machacek, J.; Studnicka, J.: Perforated shear connectors, Steel and Composite Structures, an International Journal, February 2002, Vol. 2, Nº1, pp 51-66.

(Mainstone Menzies 1967) Mainstone, R. J.; Menzies, J. B.: Shear connectors in steel-concrete composite beams for bridges. Part I: Static and Fatigue Tests on Push-out Specimens. Concrete, Vol. 1, No.9, 1967, pp. 271-302.

(Magalhães et al 2002) Magalhães. A. F.; Jalali. S. e Cruz. P.J.S.. Durability of High Performance Lightweight Aggregate Concrete. XXX IAHS World Congress on Housing, Coimbra, Portugal, September 2002, Vol. 3, pp 1753-1760.

(Magalhães 2002) Magalhães, Ana Raquel F. O.: Estudo de Betão Estrutural de Agregados Leves, MSc Master Thesis, University of Minho, July 2002. (in portuguese)

(Marecek et al. 2005) Marecek, J., Samec, J., Studnicka, J.: Perfobond shear connector behaviour. Eurosteel 2005 - European Conference on Steel Structures, Maastricht, The Netherlands, June 2005, Volume B, pp. 4.3-1-4.3-8.

(Maxit 2004) 0099-CPD-A60/114: ARLITA F-7 granel; ARLITA F-7 Big Bag 1.5 m^3.

(Medberry and Shahrooz 2002) Medberry, S. B.; Shahrooz, B. M.: Perfobond shear connector for composite construction, AISC Journal, Chicago, 2002-1, pp. 2-12.

(Neville et al. 1987) Neville, A. M., Brooks, J. J.: Concrete Technology. University Press, Belfast, 1987, 438 p.

(Newman 1993) Newman, J. B.: Properties of structural Lightweight Aggregates in Structural Lightweight Concrete, Ed. J.L. Clarke, Blackie, Chapman & Hall, pp. 19-44.

(Nie et al. 2004) Nie, Jianguo; Xiao, Yan; Tan, Ying; Wang, Hongquan: Experimental studies on behaviour of composite steel high-strength concrete beams, ACI Structural Journal, March-April 2004, Vol. 101, Nº 2, pp. 245-251.

(Nishido et al. 2000) Nishido, T.; Fujii, K.; Ariyoshi, T.: Slip behaviour of Perfobond rib shear connectors and its treatment in FEM. Conference on Composite Construction in Steel and Concrete IV. May-June 2000. Banff, Alberta, pp. 379-390.

(NP EN 197-1 2001) NP EN 197-1 – Cement. Part 1: Composition, specifications and conformity criteria for common cements. Portuguese Quality Institute (IPQ).

(NP EN 206-1 2005) NP EN 206-1 – Concrete. Part 1: Specification, performance, production and conformity. June 2005. Portuguese Quality Institute (IPQ).

(NS 1992) NS 3473 E. Design of concrete structures. Norwegian standard, English version, 1992.

(NS 1998) NS 3473 E. Design of concrete structures. Norwegian standard, English version, 1998.

(Oehlers 1981) Oehlers, D. G.: Results in 101 Push-Specimens and 4 Composite T Beams. University of Warwick, Dept. of Civil Eng., Research Report CE 8, Jan. 1981.

(Oehlers 1995) Oehlers, D. J.:Design and assessment of shear connectors in composite bridge beams. Journal of Structural Engineering ASCE, Vol. 121, No. 2, February 1995, pp. 214-224.

(Oehlers and Coughlan 1986) Oehlers, D.J. & Coughlan, C.G.: The shear stiffness of stud shear connections in composite beams. Journal of Constructional Steel Research, Vol. 6, January 1986, pp. 273-284.

(Oehlers and Foley 1985) Oehlers, D.J. and Foley, L.: Fatigue strength of stud shear connections in composite beams', Proceedings of the Institute of Civil Engineers, June 1985, Pt. 79(Part 2), pp. 349-364.

(Oehlers and Jonhson 1987) Oehlers D. G., Jonhson, R. P.: The strength of stud shear connections in composite beams. The Structural Engineer, June 1987, Vol. 65B, No. 2, pp. 44-48.

(Oehlers and Sved 1995) Oehlers, Deric John; Sved, George: Composite beams with limited-slip-capacity shear connectors. Journal of Structural Engineering, ASCE, June 1995, Vol. 121, Nº6, pp. 932-938.

(Oehlers et al. 1997) Oehlers, D. J.; Nguyen, N. T.; Ahmed, M.; Bradford, M. A.: Partial Interaction in Composite Steel and Concrete Beams with Full Shear Connection. Journal of Constructional Steel Research, Elsevier, February-March 1997, Volume 41, Number 2-3, pp. 235-248.

(Oehlers et al. 2000) Oehlers, Deric J. ; Seracino, Rudolf; Yeo, Michael F.: Fatigue behaviour of composite steel and concrete beams with stud shear connectors. Progress in Structural Engineering Materials, John Wiley & Sons, Nº2, pp. 187-195.

(Oguejiofor and Hosain 1994) Oguejiofor, E. C.; Hosain, M. U.: A parametric study of perfobond rib shear connectors, Canadian Journal of Civil Engineering, Vol. 21, pp. 614-625, 1994.

(Oguejiofor and Hosain 1996) Oguejiofor, E. C.; Hosain, M. U.: Numerical analysis of Push-Out specimens with Perfobond rib connectors, Computers & Structures, Vol. 62, Nº4, 1996, pp. 617-624.

(Ollgard et al 1971) Ollgard, J. G.; Slutter, R. G.; Fisher, J. W.: Shear Strength of Stud Connectors in Light-Weight and Normal-Weight Concrete. AISC Engineering Journal, April 1971, Vol. 8, No. 2, pp. 55-64.

(Poot 2001) Poot, S.: Perfobond connection and tests. International Symposium on Connections Between Steel and Concrete, University of Stuttgart, September 2001, Vol.2, pp. 1095-1104.

(Reichard 1964) Reichard, T. W.: Creep and drying shrinkage of lightweight and normal weight concretes. Monograph No.84, Nat. Bur. of Standards, Washington DC., 1964, 30 p.

(RILEM 1985) RILEM TC50-FMC: Determination of fracture energy of mortar and concrete by means of three point bend tests on notched beams, Materials and Structures, Vol. 18, Nº 106, Jul-Aug 1985, pp 285-290.

(Roik and Hanswille 1983) Roik, K.; Hanswille, G.: Beitrag zur Bestimmung der Tragfähigkeit von Kopfbolzendübeln. Stahlbau, 1983, Vol. 10, pp. 301-308.

(Roik et al. 1988) Roik, K.; Hansville, G.; Cunze-O.Lanna, A.: Hintergrungbericht zu EC4: 6.3.2-Bolzendübel; University of Bochum, December 1988, 10, 96 pp.

(Seracino et al. 1997) Seracino, R.; Oehlers, D. J.; Yeo, M. F.: The influence of friction on the fatigue life of stud shear connectors in composite bridge beams. University of Adelaide, Department of Civil and Environmental Engineering, Research Report No. R 154, July 1997.

(Smeplass 1992) Smeplass, S.: Mechanical Properties - Lightweight Concrete. Report 4.5, High Strength Concrete. SP4 - Materials Design, SINTEF.

(Slutter and Fisher 1966) Slutter, R. G., Fisher, J. W.: Fatigue strength of shear connectors. Highway research record 1966, 147, pp. 65-88.

(Taplin and Grundy 1997) Taplin, G.; Grundy, P.: Incremental slip of stud shear connectors under repeated loading. Proceedings of the IABSE Int. Conference Composite Construction – Conventional and Innovative, Innsbruck, pp. 145-150.

(Taplin 1999) Taplin, Geoff: The behaviour of composite beams under repeated loading. PHd Thesis, Monash University, Australia, August 1999.

(Thorenfeldt 1995) Thorenfeldt, E.: Design Criteria of Lightweight Aggregate Concrete. CEB/FIPInternational Symposium on Structural Lightweight Aggregate Concrete, Sandefjord, Norway, pp. 720-732.

(TML 2001) TML, Tokyo Sokki Kenkyujo, Ltd.. Catalogue on Strain Gauges. TML Pam E-101, 66 pp.

(Ushijima et al 2001) Ushijima, Y.; Hosaka, T.; Mitsuki, K.; et al.: An experimental study on shear characteristics of Perfobond strip and its rational strength equations. International Symposium on Connections Between Steel and Concrete, University of Stuttgart, September 2001, Vol.2, pp. 1066-1075.

(Valente and Cruz 2003) Valente, I., Cruz, P. J. S.: Caracterização da ductilidade de ligações aço-betão leve com conectores tipo perno. 4º Congresso de Construção Metálica e Mista, December 2003, Lisbon, Portugal, pp. 535-545. (in portuguese)

(Valente and Cruz 2004a) Valente, I.; Cruz, P. J. S.: Experimental Analysis on Perfobond Shear Connection between Steel and Lightweight Concrete. Journal of Constructional Steel

Research, Elsevier, January-March 2004, Volume 60, Number 3-5, pp. 465-479.

(Valente and Cruz 2004b) Valente, I.; Cruz, P. J. S.: Experimental Studies on Shear Connection between Steel and Lightweight Concrete. Second International Conference on Bridge Maintenance, Safety and Management, Kyoto, Japan, October 2004. (CD-Rom)

(Veríssimo et al 2006a) Veríssimo, G. S.; Paes, J. L. R.; Valente, I.; Cruz, P. J. S.; Fakury, R. H.: Experimental tests on a new shear connector for steel-concrete composite structures. Third International Conference on Bridge Maintenance, Safety and Management, Porto, Portugal, July 2006 (CD-Rom).

(Veríssimo et al 2006b) Veríssimo, G. S.; Valente, I., Paes, J. L. R.; Cruz, P. J. S.; Fakury, R. H.: Análise experimental de um conector de cisalhamento em chapa de aço endentada para estruturas mistas de aço e concreto. XXXII Jornadas Sulamericanas de Engenharia Estrutural, Campinas, Brasil, May 2006, pp. 410-419. (in portuguese)

(Veríssimo et al 2007) Veríssimo, G., Oliveira, A., Fakury, R., Rodrigues, F., Paes, J. L., Valente, I., Cruz, P. J.: Avaliação do desempenho de um conector de cisalhamento em chapa dentada para estruturas mistas de aço e concreto. Congress CMNE – CILAMCE, June 2007. (in portuguese)

(Verissimo 2007) Veríssimo, G. S.: Desenvolvimento de um conector de cisalhamento em chapa dentada para estruturas mistas de aço e concreto e estudo do seu comportamento. PhD Thesis. Universidade Federal de Minas Gerais, Brasil. Conclusion predicted for June 2007. (in portuguese)

(Vieira 1999) Vieira, Manuel: Betões de elevado desempenho com agregados leves. Durabilidade e microestrutura. Master in Science Thesis, IST e LNEC, May 2000. (in portuguese)

(Vieira and Virtuoso 2002) Vieira, R., Virtuoso, F.: Time dependent behaviour of continuous composite beams with flexible connection. Journal of Constructional Steel Research, Elsevier, January-March 2004, Volume 60, Number 3-5, pp. 451-463.

(Virtuoso and Vieira 1999) Virtuoso, F., Vieira, R.: Análise dos efeitos da deformabilidade da conexão em vigas mistas. Coimbra, Portugal, November 1999, pp. 413-422. (in portuguese)

(Weigler et al 1972) Weigler, H., Karl, S., Lieser, P.: The bending load capacity of reinforced lightweight concrete. Betonwerk und Fertigteil-Technik 38, No. 5, pp. 324-334 and No. 6, pp. 445-449.

(Yamamoto and Nakamura 1962) Yamamoto, M.; Nakamura, G.: The Study on Shear Connectors, The Public Works Research Institute, Construction Ministry Japan, Vol.5, Research Paper 9, 1962.

(Yen et al. 1997) Yen, J.Y. Richard; Lin, Yiching; Lai, M. T.: Composite beams subjected to static and fatigue loads, ASCE Journal of Structural Engineering, June 1997, Vol 115, Nº 2, pp. 765-771.

(Zellner 1987) Zellner, W.: Recent designs of composite bridges and a new type of shear connectors. Proceedings of the IABSE/ASCE Engineering Foundation Conference on Composite Construction, Henniker, N.H., pp.240-252.

(Zhang et al 1990) Zang et al.: Mechanical properties of HSLWC. ACI Materials Journal, vol. 88. nº3, 1990, pp.240-247.

(Zhang 1992) Zhang, M.H. “Characteristics of Lightweight Aggregates for High Strength LWA Concrete“. SINTEF Report STF65 A92022, Trondheim, Norway.

Appendix 5.1

Neutral axis position for elastic analysis

Table A5.1 – Neutral axis position, defined from strain gauge measurements: VM4, VM5, VM6, VM7, VM3 and VM8

Conc. Ref.	BL33		BL32		BL34		BL38		BL37		BL39	
Beam	VM4		VM5		VM6		VM7		VM3		VM7	
$y_{G,el}$ (m)	0.1163		0.1189		0.1179		0.1162		0.1163		0.1165	
% M_{max}	Steel section	Conc. section	Steel section	Conc. section	Steel section	Conc. section	Steel section	Conc. section	Steel section	Conc. section	Steel section	Conc. section
10%	0.113	-	0.114	-	0.101	-	0.101	-	0.089	-	0.091	-
15%	0.114	-	0.114	-	0.105	-	0.105	-	0.097	-	0.094	-
20%	0.115	-	0.115	-	0.107	-	0.107	-	0.101	-	0.096	0.120
25%	0.115	-	0.115	-	0.109	-	0.108	-	0.102	-	0.097	0.121
30%	0.115	-	0.116	-	0.110	-	0.109	-	0.104	-	0.098	0.122
35%	0.115	-	0.116	-	0.111	-	0.110	-	0.105	-	0.100	0.122
40%	0.116	-	0.116	-	0.110	-	0.111	-	0.106	0.121	0.101	0.122
45%	0.116	-	0.116	-	0.110	-	0.111	-	0.106	0.121	0.101	0.123
50%	0.116	-	0.116	-	0.109	-	0.111	-	0.107	0.122	0.100	0.124
55%	0.117	-	0.116	-	0.109	-	0.111	-	0.108	0.124	0.099	0.125
60%	0.119	-	0.117	-	0.108	-	0.113	0.120	0.110	0.126	0.100	0.127
65%	0.120	0.120	0.118	-	0.107	-	0.114	0.124	0.112	0.129	0.101	0.129
70%	0.120	0.120	0.120	0.120	0.107	-	0.115	0.127	0.114	0.131	0.102	0.131
75%	-	0.122	0.120	0.120	0.106	-	0.117	0.130	0.117	0.134	0.103	0.133
80%	-	0.126	-	0.122	0.107	0.122	0.119	0.133	0.119	0.135	0.104	0.139
85%	-	0.128	-	0.124	0.107	0.126	-	0.139	0.120	0.138	0.107	0.143
90%	-	0.131	-	0.123	0.108	0.130	-	0.141	-	0.140	0.109	*
95%	-	0.134	-	0.134	0.108	0.132	-	0.142	-	0.142	0.111	*
100%	-	0.139	-	0.139	0.110	0.142	-	0.142	-	0.146	*	*

* - these values could not be calculated due to strain gauge ruin

Appendix 5.2

Strain diagrams at cross sections A-A’ and C-C’

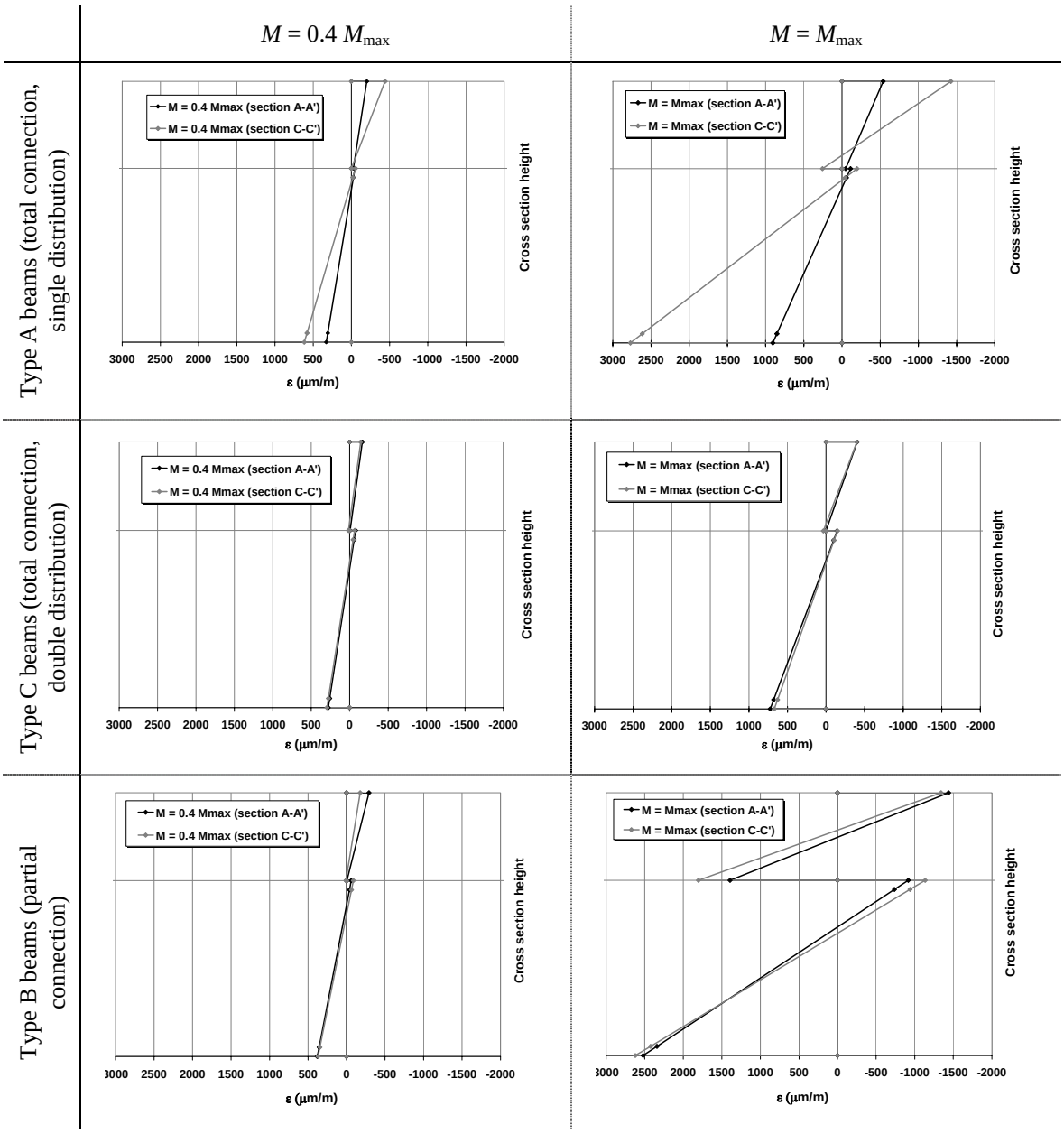

Figure A5.1 – Strain diagrams for the composite beams VM4, VM5 and VM6 correspondent to $0.4M_{max}$ and M_{max}, at cross sections A-A’ and C-C’

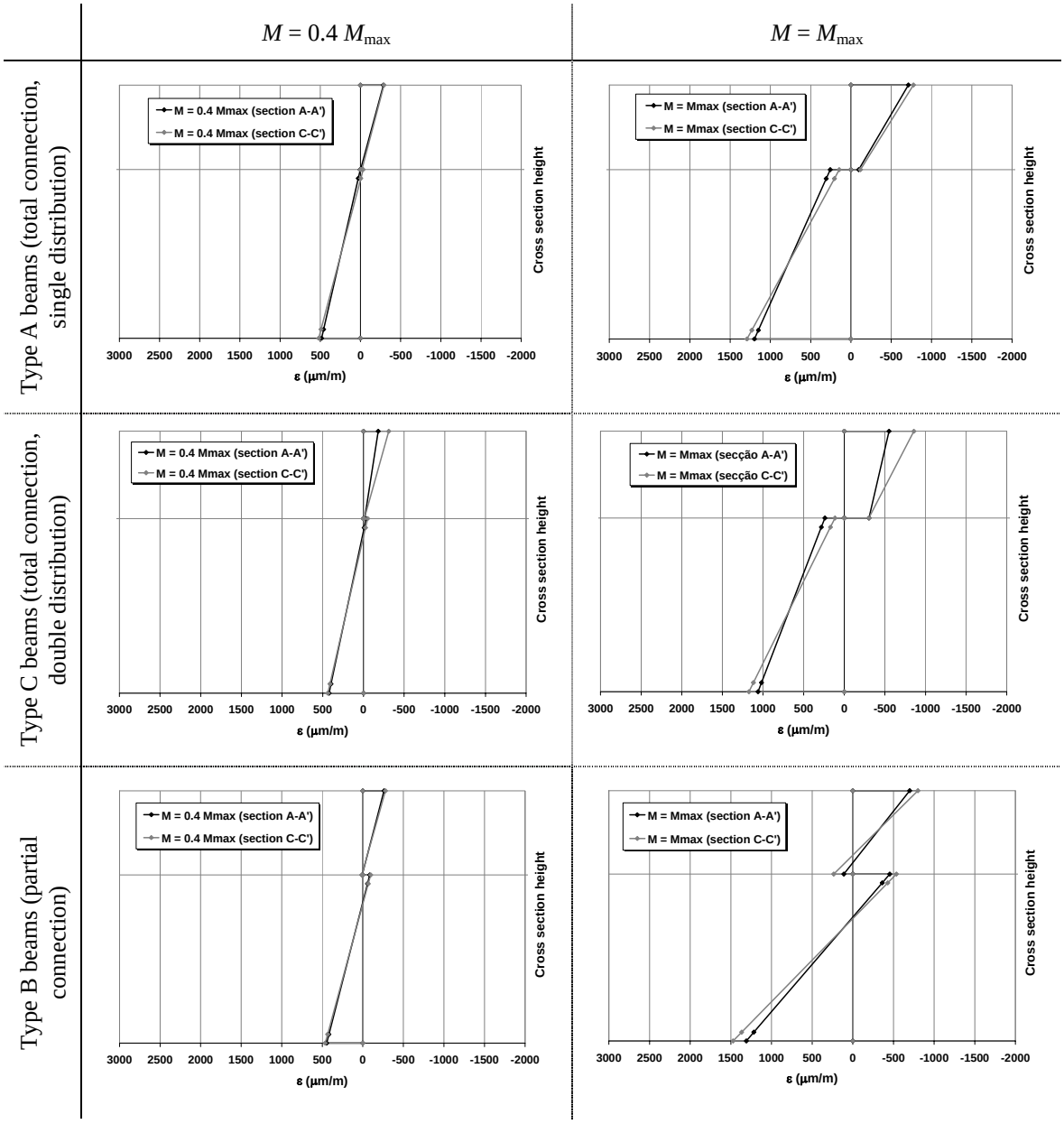

Figure A5.2 – Strain diagrams for the composite beams VM7, VM3 and VM8 correspondent to $0.4M_{max}$ and M_{max}, at cross sections A-A' and C-C'

Appendix 5.3

Strain values at cross section B-B' for fixed values of applied bending moment

Table A5.3 – Strain values at cross section B-B' for 0.4 M_{max} , 0.9 M_{max} and M_{max}

Beam		VM4	VM5	VM6	VM7	VM3	VM8
0.4 M_{max}	(kNm)	21.03	19.01	16.79	20.05	19.98	17.76
ε_1	(μm/m)	866.5	824.4	798.3	1004.4	839.80	941.56
ε_4	(μm/m)	-32.2	-30.2	-70.1	-81.1	-115.28	-182.29
ε_5	(μm/m)	-81.0	-62.4	-88.1	-59.6	11.31	28.65
ε_6	(μm/m)	-523.4	-488.3	-412.6	-476.8	-517.06	-475.90
ε_4 - ε_5	(μm/m)	48.9	32.2	18.49	-21.5	-126.59	-210.94
ϕ_a		7489	7122	7237	9046	7959	9365
ϕ_c		7372	7098	5407	6953	8806	8409
0.9 M_{max}	(kNm)	47.34	42.78	37.77	45.09	44.80	39.91
ε_1	(μm/m)	4135.4	4621.2	4843.9	10156.3	12738.5	15498.0
ε_4	(μm/m)	495.2	364.0	-547.8	282.3	154.8	-1521.8
ε_5	(μm/m)	430.9	333.7	283.8	1474.7	1453.9	5804.7
ε_6	(μm/m)	-1994.4	-1772.5	-1213.3	-2663.0	-2834.4	-2596.0
ε_4 - ε_5	(μm/m)	64.3	30.3	-787.19	-1192.3	-1299.0	-7326.5
ϕ_a		30335	35477	44931	82282	104864	141831.5
ϕ_c		40421	35104	24951	69961	71471	140010.7
M_{max}	(kNm)	52.60	47.52	41.96	50.01	49.76	44.51
ε_1	(μm/m)	8958.4	8706.3	9199.7	15639.7	20379.1	*
ε_4	(μm/m)	1346.1	814.5	-902.4	553.3	416.4	*
ε_5	(μm/m)	1419.56	1264.1	1365.0	2140.9	3623.1	*
ε_6	(μm/m)	-3115.3	-2669.2	-1935.6	-3785.5	-4816.3	*
ε_4 - ε_5	(μm/m)	-46.0	-449.6	-2267.4	-1587.6	-1616.31	*
ϕ_a		63435	65765	84185	125719	166356	*
ϕ_c		75581	65556	55009	98773	140657	*

* – due to strain gauge ruin, these values were not measured

ε_1 to ε_6 – strain according to **Erro! A origem da referência não foi encontrada.**

Table A5.4 – Strain values at cross section B-B' for fixed values of applied bending moment

Beam		VM4	VM5	VM6	VM7	VM3	VM8
M	(kNm)	20.0	20.0	20.0	20.0	20.0	20.0
ε_1	(μm/m)	822.61	870.14	935.16	1013.22	855.25	1058.99
ε_4	(μm/m)	-30.96	-32.30	-88.65	-81.69	-116.13	-200.59
ε_5	(μm/m)	-78.21	-65.31	-93.30	-59.53	37.68	36.16
ε_6	(μm/m)	-497.66	-513.08	-490.42	-474.18	-517.06	-535.04
$\varepsilon_4 - \varepsilon_5$	(μm/m)	47.25	30.00	4.65	-22.16	-126.59	-226.78
ϕ_a		7113	7520	8532	9124	8095	10497
ϕ_c		6991	7463	6619	6911	9246	9354
M	(kNm)	40.0	40.0	40.0	40.0	40.0	40.0
ε_1	(μm/m)	2298.60	2614.84	6138.33	5907.99	5136.72	15563.65
ε_4	(μm/m)	154.14	124.19	-661.94	-104.26	-38.73	-1525.08
ε_5	(μm/m)	63.81	86.95	334.10	435.21	615.87	
ε_6	(μm/m)	-1292.12	-1314.72	-1362.88	-1572.26	-1798.21	-2607.08
$\varepsilon_4 - \varepsilon_5$	(μm/m)	90.33	37.24	-1006.05	-539.48	-654.60	-2590.52
ϕ_a		17870	20755	56669	50102	43129	142406
ϕ_c		22599	23361	28450	33458	40235	-

Appendix 6.1

Initial and final strain values, measured at each load range of beams VM1, VM2, VM9 and VM10

Table A6.1 – Evolution of strain during the load cycles applied to beams VM1 and VM2, at cross section B-B'

Beam	P_{max}	ΔP	N^*_{final}	ε_1 (N = 5)	ε_1 (N_{final})	ε_4 (N = 5)	ε_4 (N_{final})	ε_5 (N = 5)	ε_5 (N_{final})	ε_6 (N = 5)	ε_6 (N_{final})
	(kN)	(kN)		(μm/m)	(μm/m)	(μm/m)	(μm/m)	(μm/m)	(μm/m)	(μm/m)	(μm/m)
VM1	22.21	14.02	1000	682.4	672.0	-56.7	-62.2	-28.4	-27.5	-322.2	-315.6
	44.05	39.68	1000	1932.7	2001.6	-55.3	-54.0	14.9	30.3	-756.6	-761.7
	54.56	50.54	1000	3346.2	3542.0	0.2	20.4	130.8	204.5	-1045.8	-1086.2
	64.40	60.95	1000	5990.9	6822.7	244.6	235.4	761.1	937.1	-1581.2	-1670.2
	69.26	65.87	235	7133.9	8934.1	252.3	238.0	943.3	1070.8	-1760.3	-1930.0
VM2	11.96	5.45	1000	371.6	362.0	-23.2	-22.3	8.3	10.0	-191.7	-182.5
	24.28	19.85	1000	758.1	748.7	-38.6	-42.8	17.8	22.8	-388.5	-378.5
	28.16	23.45	1000	856.8	**	-41.9	**	22.8	**	-434.4	**
	33.38	30.71	1000	1054.6	1037.9	-42.7	-46.9	37.7	44.5	-524.6	-510.3
	38.57	36.19	1000	1221.9	1244.8	-47.8	-49.8	53.2	74.5	-608.8	-589.4
	43.85	41.80	700*	1489.8	2038.3	-49.2	-265.0	93.1	159.0	-711.1	-721.5

N^*_{final} – does not correspond to the final load cycle, because of strain gauge failure

** – due to an electrical failure, this information was not recorded

Table A6.2 – Evolution of strain during the load cycles applied to beams VM9 and VM10, at cross section B-B'

Beam	P_{max}	ΔP	N^*_{final}	ε_1	ε_4	ε_5	ε_6
	(kN)	(kN)		(μm/m)	(μm/m)	(μm/m)	(μm/m)
VM9	39.46	35.93	1	1385.3	-48.9	54.1	-710.0
			2500	1454.9	-47.9	72.6	-715.1
			5000	1569.0	-47.6	83.7	-733.5
VM10	32.78	28.96	1	1077.0	-116.5	35.7	-550.3
			5500	1196.0	-219.5	94.0	-538.4
			7000	1241.7	-316.9	101.6	-506.3
			7500	1524.6	-645.0	174.4	-477.2
			10500*	2896.9	-1503.5	280.4	-398.9

Table A6.3 – Evolution of strain during the load cycles applied to beams VM1 and VM2, at cross section A-A'

Beam	P_{max} (kN)	ΔP (kN)	N^*_{final}	ε_1 (N = 5) (μm/m)	ε_1 (N_{final}) (μm/m)	ε_4 (N = 5) (μm/m)	ε_4 (N_{final}) (μm/m)	ε_5 (N = 5) (μm/m)	ε_5 (N_{final}) (μm/m)	ε_6 (N = 5) (μm/m)	ε_6 (N_{final}) (μm/m)
VM1	22.21	14.02	1000	496.7	489.1	-62.4	-56.4	30.0	32.3	-274.0	-266.5
	44.05	39.68	1000	983.7	931.2	-66.9	-59.9	43.8	49.2	-518.5	-486.7
	54.56	50.54	1000	1154.0	1282.9	-50.6	-58.2	58.0	85.2	-614.9	-614.6
	64.40	60.95	1000	1804.5	1859.6	-30.2	-137.2	123.1	172.5	-824.1	-825.7
	69.26	65.87	235	1923.3	2135.5	-138.3	-230.9	176.6	208.8	-866.5	-912.7
VM2	11.96	5.45	1000	306.0	303.4	-77.2	-69.7	47.5	51.2	-166.3	-161.7
	24.28	19.85	1000	564.3	557.9	-112.8	-101.9	70.7	77.6	-299.8	-297.0
	28.16	23.45	1000	664.6	**	-114.8	**	81.6	**	-350.8	**
	33.38	30.71	1000	807.2	813.3	-139.0	-140.7	105.4	121.9	-414.5	-422.6
	38.57	36.19	1000	928.9	930.1	-158.5	-169.1	134.7	178.8	-482.8	-485.5
	43.85	41.80	700*	1049.6	1143.3	-189.6	-274.2	196.2	811.7	-551.8	-665.9

N^*_{final} – does not correspond to the final load cycle, because of strain gauge failure

** – due to an electrical failure, this information was not recorded

Table A6.4 – Evolution of strain during the load cycles applied to beams VM9 and VM10, at cross section A-A'

Beam	P_{max} (kN)	ΔP (kN)	N^*_{final}	ε_1 (μm/m)	ε_4 (μm/m)	ε_5 (μm/m)	ε_6 (μm/m)
VM9	39.46	35.93	1	950.6	-87.6	20.0	-514.6
			2500	935.1	-82.8	37.3	-488.9
			5000	953.6	-84.3	45.6	-486.1
VM10	32.78	28.96	1	769.7	-146.3	71.0	-405.8
			5500	868.3	-398.3	241.9	-478.7
			7000	920.3	-491.6	226.1	-503.7
			7500	1084.4	-855.7	191.7	-377.0
			10500*	1203.1	-994.0	134.6	-237.2

Table A6.5 – Evolution of strain during the load cycles applied to beams VM1 and VM2, at cross section C-C'

Beam	P_{max} (kN)	ΔP (kN)	N^*_{final}	ε_1 (N = 5) (μm/m)	ε_1 (N_{final}) (μm/m)	ε_4 (N = 5) (μm/m)	ε_4 (N_{final}) (μm/m)	ε_5 (N = 5) (μm/m)	ε_5 (N_{final}) (μm/m)	ε_6 (N = 5) (μm/m)	ε_6 (N_{final}) (μm/m)
VM1	22.21	14.02	1000	508.7	511.3	-86.2	-86.7	48.3	58.9	-254.9	-260.6
	44.05	39.68	1000	1030.8	1001.9	-96.3	-111.5	55.1	72.1	-487.9	-470.9
	54.56	50.54	1000	1290.2	1216.8	-108.6	-152.4	87.6	127.4	-598.3	-610.3
	64.40	60.95	1000	2109.5	3115.1	-169.7	-535.8	216.7	287.0	-817.8	-781.2
	69.26	65.87	235	3430.1	8551.7	-560.9	-1477.5	312.3	484.0	-832.7	-800.3
VM2	11.96	5.45	1000	298.8	297.6	-55.5	-41.6	**	**	-177.3	-174.6
	24.28	19.85	1000	547.0	543.7	-69.4	-51.0	**	**	-324.2	-317.1
	28.16	23.45	1000	646.6	**	-60.2	**	**	**	-376.4	**
	33.38	30.71	1000	819.6	833-2	-86.3	-70.2	**	**	-460.2	-465.6
	38.57	36.19	1000	948.1	963.6	-80.5	-55.0	**	**	-530.4	-529.0
	43.85	41.80	700*	1080.3	1357.3	-65.8	-92.6	**	**	-598.1	-557.9

N^*_{final} – does not correspond exactly to the final load cycle, because of strain gauge failure

** – due to an electrical failure, this information was not recorded

Table A6.6 – Evolution of strain during the load cycles applied to beams VM9 and VM10, at cross section C-C'

Beam	P_{max} (kN)	ΔP (kN)	N^*_{final}	ε_1 (μm/m)	ε_4 (μm/m)	ε_5 (μm/m)	ε_6 (μm/m)
VM9	39.46	35.93	1	982.4	-53.4	16.3	-406.4
			2500	980.9	-44.9	28.5	-400.4
			5000	1000.6	-62.3	36.6	-401.4
VM10	32.78	28.96	1	777.7	-153.0	77.1	-420.3
			5500	898.7	-404.1	318.0	-529.9
			7000	934.1	-499.9	1084.4	-590.3
			7500	1103.0	-889.9	**	-505.9
			10500*	1195.2	-1032.8	**	-325.9

Appendix 7.1

Predicted vertical deflection and end-slip for loading phase

Table A7.1 – Predicted vertical deformation for VM1 and VM2, at section B-B'

		W 1	W 2	W 3	W 4	W 5	W 6	W 7
Weights (kgf)	(kgf)	294.7	288.2	291.2	302.4	296.7	284.5	292.1
Loads in VM1 (kN)	(kN)	2.89	2.83	2.86	2.97	2.91	2.79	2.87
Total interaction – accumulated	(mm)	-2.42	-4.56	-6.72	-8.31	-9.87	-10.52	-11.19
Partial interaction (k=220) – accumulated	(mm)	-2.62	-	-7.26	-	-10.64	-	-12.06
Partial interaction (k=250) – accumulated	(mm)	-2.60	-	-7.21	-	-10.57	-	-11.97
Weights (kgf)	(kgf)	298.2	310.0	302.3	293.3	281.9	292.8	295.3
Loads in VM2 (kN)	(kN)	2.93	3.04	2.97	2.88	2.77	2.87	2.90
Total interaction – accumulated	(mm)	-2.48	-4.80	-7.06	-8.62	-10.12	-10.80	-11.48
Partial interaction (k=220) – accumulated	(mm)	-2.84	-	-8.06	-	-11.52	-	-13.05
Partial interaction (k=250) – accumulated	(mm)	-2.81	-	-7.96	-	-11.38	-	-12.89

Table A7.2 – Predicted end-slip for VM1 and VM2

		W 1	W 2	W 3	W 4	W 5	W 6	W 7
Weights	(kgf)	294.7	288.2	291.2	302.4	296.7	284.5	292.1
Loads in VM1	(kN)	2.89	2.83	2.86	2.97	2.91	2.79	2.87
Partial interaction (k=220) - accumulated	(mm)	0.013		0.039		0.064		0.083
Partial interaction (k=250) - accumulated	(mm)	0.011		0.034		0.057		0.073
Weights	(kgf)	298.2	310.0	302.3	293.3	281.9	292.8	295.3
Loads in VM2	(kN)	2.93	3.04	2.97	2.88	2.77	2.87	2.90
Partial interaction (k=220) - accumulated	(mm)	0.026		0.079		0.126		0.157
Partial interaction (k=250) - accumulated	(mm)	0.023		0.070		0.112		0.140

Appendix 7.2

Predicted stresses

Cross sections A-A’ and B-B’ are represented in Figure 7.3. Cross section C-C’ is position in the beam quarter span, opposite to cross section A-A’.

Table A7.3 – Partial bending moment values for VM1 and VM2 (kNm)

	zero	W 1	W 2	W 3	W 4	W 5	W 6	W 7
Weights (kgf)		294.7	288.2	291.2	302.4	296.7	284.5	292.1
Loads in VM1 (kN)		2.89	2.83	2.86	2.97	2.91	2.79	2.87
Supports	0	0	0	0	0	0	0	0
Cross section A-A’ x = 1.065m	0	1.539	1.098	1.933	0.723	2.041	0.277	0.917
Cross section B-B’ x = 2.250m	0	2.956	2.320	2.342	1.528	1.499	0.585	0.601
Cross section C-C’ x = 3.435m	0	1.539	1.914	1.109	2.080	0.709	0.893	0.284
Weights (kgf)		298.2	310.0	302.3	293.3	281.9	292.8	295.3
Loads in VM2 (kN)		2.93	3.04	2.97	2.88	2.77	2.87	2.90
Supports	0	0	0	0	0	0	0	0
Cross section A-A’ x = 1.065m	0	1.558	1.181	2.008	0.702	1.940	0.285	0.927
Cross section B-B’ x = 2.250m	0	2.991	2.495	2.432	1.483	1.424	0.603	0.608
Cross section C-C’ x = 3.435m	0	1.558	2.059	1.151	2.018	0.674	0.921	0.288

Table A7.4 – Total transversal and longitudinal shear stress values at sections A-A’, B-B’ e C-C’

		VM1		VM2	
Cross section	x (m)	V (kN)	r (kN/m)	V (kN)	r (kN/m)
Support	0.000	-10.07	-71.286	-10.14	-71.625
	0.215	-8.64	-61.163	-8.69	-61.382
	0.625	-7.21	-51.040	-7.25	-51.211
	0.825	-5.75	-40.704	-5.86	-41.392
Section A-A’	1.065	-5.75	-40.704	-5.86	-41.392
	1.235	-4.30	-30.440	-4.48	-31.645
	1.435	-2.87	-20.317	-3.00	-21.191
	1.845	-1.44	-10.194	-1.51	-10.666
	2.045	0.00	0.000	-0.05	-0.353
Section B-B’	2.250	0.00	0.000	-0.05	-0.353
	2.455	0.00	0.000	-0.05	-0.353
	2.655	1.45	10.265	1.41	9.960
	3.065	2.86	20.246	2.93	20.696
	3.265	4.28	30.298	4.45	31.433
Section C-C’	3.435	5.76	40.775	5.89	41.604
	3.675	5.76	40.775	5.89	41.604
	3.875	7.24	51.252	7.33	51.776
	4.285	8.64	61.163	8.77	61.947
Support	4.500	10.03	71.003	10.20	72.048

Table A7.5– Stresses at VM1 (MPa) – full interaction

		zero	W 1	W 2	W 3	W 4	W 5	W 6	W 7
Section A-A' x = 1.065 m	Fibber 1	0	16.92	28.99	50.24	58.19	80.62	83.67	93.75
	Fibber 2	0	16.01	27.43	47.54	55.06	76.28	79.17	88.70
	Fibber 3	0	0.49	0.09	0.16	0.18	0.25	0.26	0.29
	Fibber 4	0	-0.42	-0.72	-1.25	-1.45	-2.01	-2.09	-2.34
	Fibber 5	0	-0.05	-0.08	-0.14	-0.16	-0.22	-0.23	-0.26
	Fibber 6	0	-0.99	-1.70	-2.94	-3.41	-4.73	-4.90	-5.49
Section B-B' x = 2.250 m	Fibber 1	0	32.49	58.00	83.74	100.54	117.01	123.44	130.04
	Fibber 2	0	30.75	54.87	79.23	95.13	110.71	116.80	123.05
	Fibber 3	0	0.94	1.67	2.41	2.90	3.37	3.56	3.75
	Fibber 4	0	-0.81	-1.45	-2.09	-2.51	-2.92	-3.08	-3.25
	Fibber 5	0	-0.09	-0.16	-0.23	-0.27	-0.32	-0.34	-0.35
	Fibber 6	0	-1.90	-3.40	-4.91	-5.89	-6.86	-7.23	-7.62
Section C-C' x = 3.435 m	Fibber 1	0	16.92	37.96	50.15	73.02	80.81	90.63	93.75
	Fibber 2	0	16.01	35.92	47.45	69.09	76.46	85.75	88.70
	Fibber 3	0	0.49	1.09	1.45	2.11	2.33	2.61	2.70
	Fibber 4	0	-0.42	-0.95	-1.25	-1.82	-2.02	-2.26	-2.34
	Fibber 5	0	-0.05	-0.10	-0.14	-0.20	-0.22	-0.25	-0.26
	Fibber 6	0	-0.99	-2.22	-2.94	-4.28	-4.74	-5.31	-5.49

Table A7.6– Stresses at VM2 (MPa) – full interaction

		zero	W 1	W 2	W 3	W 4	W 5	W 6	W 7
Section A-A' x = 1.065 m	Fibber 1	0	17.19	30.22	52.37	60.12	81.52	84.67	94.89
	Fibber 2	0	16.26	28.58	49.54	56.86	77.11	80.08	89.76
	Fibber 3	0	0.40	0.71	1.23	1.41	1.91	1.98	2.22
	Fibber 4	0	-0.53	-0.93	-1.61	-1.85	-2.50	-2.60	-2.91
	Fibber 5	0	-0.06	-0.10	-0.17	-0.20	-0.26	-0.27	-0.31
	Fibber 6	0	-0.99	-1.74	-3.02	-3.47	-4.71	-4.89	-5.48
Section B-B' x = 2.250 m	Fibber 1	0	33.00	60.53	87.36	103.72	119.43	126.09	132.79
	Fibber 2	0	31.22	57.25	82.63	98.11	112.97	119.26	125.60
	Fibber 3	0	0.77	1.42	2.04	2.43	2.80	2.95	3.11
	Fibber 4	0	-1.01	-1.86	-2.68	-3.19	-3.67	-3.87	-4.08
	Fibber 5	0	-0.11	-0.20	-0.28	-0.34	-0.39	-0.41	-0.43
	Fibber 6	0	-1.91	-3.49	-5.04	-5.99	-6.89	-7.28	-7.67
Section C-C' x = 3.435 m	Fibber 1	0	17.19	39.90	52.60	74.87	82.30	92.47	95.64
	Fibber 2	0	16.26	37.74	49.76	70.82	77.85	87.46	90.47
	Fibber 3	0	0.40	0.93	1.23	1.75	1.93	2.16	2.24
	Fibber 4	0	-0.53	-1.23	-1.62	-2.30	-2.53	-2.84	-2.94
	Fibber 5	0	-0.06	-0.13	-0.17	-0.24	-0.27	-0.30	-0.31
	Fibber 6	0	-0.99	-2.30	-3.04	-4.32	-4.75	-5.34	-5.52

Appendix 7.3

Predicted strains

Table A7.7 – Predicted strains in VM1 (μm/m) – total interaction

		W 1	W 2	W 3	W 4	W 5	W 6	W 7
Section A-A' x = 1.065 m	Fibber 1	80.58	138.06	239.24	277.08	383.92	398.42	446.42
	Fibber 2	76.25	130.63	226.36	262.17	363.26	376.98	422.39
	Fibber 3	2.32	0.43	0.75	0.87	1.21	1.25	1.40
	Fibber 4	-2.01	-3.45	-5.98	-6.92	-9.59	-9.95	-11.15
	Fibber 5	-2.01	-3.45	-5.98	-6.92	-9.59	-9.95	-11.15
	Fibber 6	-43.31	-74.20	-128.58	-148.92	-206.34	-214.14	-239.93
Section B-B' x = 2.250 m	Fibber 1	154.73	276.17	398.76	478.74	557.18	587.80	619.26
	Fibber 2	146.41	261.31	377.30	452.98	527.20	556.17	585.94
	Fibber 3	4.46	7.96	11.50	13.80	16.06	16.95	17.85
	Fibber 4	-3.87	-6.90	-9.96	-11.96	-13.92	-14.68	-15.47
	Fibber 5	-3.87	-6.90	-9.96	-11.96	-13.92	-14.68	-15.47
	Fibber 6	-83.16	-148.43	-214.32	-257.31	-299.47	-315.92	-332.83
Section C-C' x = 3.435 m	Fibber 1	80.58	180.77	238.82	347.69	384.81	431.55	446.42
	Fibber 2	76.25	171.04	225.97	328.98	364.10	408.33	422.39
	Fibber 3	2.32	5.21	6.89	10.02	11.09	12.44	12.87
	Fibber 4	-2.01	-4.52	-5.97	-8.68	-9.61	-10.78	-11.15
	Fibber 5	-2.01	-4.52	-5.97	-8.68	-9.61	-10.78	-11.15
	Fibber 6	-43.31	-97.16	-128.36	-186.87	-206.82	-231.94	-239.93

Table A7.8– Predicted strains in VM2 (μm/m) – total interaction

		W 1	W 2	W 3	W 4	W 5	W 6	W 7
Section A-A' x = 1.065 m	Fibber 1	81.84	143.89	249.39	286.27	388.19	403.17	451.87
	Fibber 2	77.41	136.10	235.89	270.78	367.19	381.35	427.42
	Fibber 3	1.92	3.37	5.84	6.70	9.09	9.44	10.58
	Fibber 4	-2.51	-4.42	-7.66	-8.79	-11.92	-12.38	-13.88
	Fibber 5	-2.51	-4.42	-7.66	-8.79	-11.92	-12.38	-13.88
	Fibber 6	-44.69	-78.57	-136.18	-156.32	-211.98	-220.15	-246.75
Section B-B' x = 2.250 m	Fibber 1	157.15	288.23	416.01	493.92	568.74	600.42	632.34
	Fibber 2	148.65	272.64	393.50	467.20	537.96	567.93	598.12
	Fibber 3	3.68	6.75	9.74	11.56	13.31	14.05	14.80
	Fibber 4	-4.83	-8.85	-12.78	-15.17	-17.47	-18.44	-19.42
	Fibber 5	-4.83	-8.85	-12.78	-15.17	-17.47	-18.44	-19.42
	Fibber 6	-85.81	-157.39	-227.17	-269.71	-310.57	-327.87	-345.29
Section C-C' x = 3.435 m	Fibber 1	81.84	190.02	250.49	356.51	391.92	440.31	455.44
	Fibber 2	77.41	179.74	236.94	337.22	370.72	416.49	430.80
	Fibber 3	1.92	4.45	5.86	8.34	9.17	10.30	10.66
	Fibber 4	-2.51	-5.84	-7.69	-10.95	-12.04	-13.52	-13.99
	Fibber 5	-2.51	-5.84	-7.69	-10.95	-12.04	-13.52	-13.99
	Fibber 6	-44.69	-103.76	-136.78	-194.68	-214.01	-240.44	-248.70

Table A7.9 – Predicted strains in VM1 (μm/m) – partial interaction (*k*=250 kN/mm)

		zero	W 1	W 3	W 5	W 7
Section A-A' x = 1.065 m	Fibber 1	0	80.78	241.00	390.90	454.40
	Fibber 2	0	76.47	227.98	369.27	429.24
	Fibber 3	0	3.07	6.10	0.45	0.31
	Fibber 4	0	-1.24	-6.91	-21.18	-24.85
	Fibber 5	0	-4.13	-10.69	-12.36	-14.26
	Fibber 6	0	-40.87	-121.70	-196.50	-228.60
Section B-B' x = 2.250 m	Fibber 1	0	158.40	404.60	563.30	625.80
	Fibber 2	0	149.24	381.85	531.99	591.13
	Fibber 3	0	-6.93	-6.02	-1.75	0.16
	Fibber 4	0	-2.38	-28.77	-33.06	-34.51
	Fibber 5	0	-1.61	-12.16	-20.39	-23.74
	Fibber 6	0	-79.52	-204.40	-285.30	-317.10

Table A7.10– Predicted strains in VM2 (μm/m) – partial interaction (*k*=250 kN/mm)

		zero	W 1	W 3	W 5	W 7
Section A-A' x = 1.065 m	Fibber 1	0	82.84	255.10	403.40	470.00
	Fibber 2	0	78.46	241.62	379.88	442.49
	Fibber 3	0	3.70	11.78	-21.12	-26.45
	Fibber 4	0	-0.68	-1.70	-44.64	-53.96
	Fibber 5	0	-0.68	-1.70	-29.27	-33.25
	Fibber 6	0	-42.44	-130.10	-204.50	-238.20
Section B-B' x = 2.250 m	Fibber 1	0	164.90	430.10	584.30	648.50
	Fibber 2	0	154.68	404.45	550.09	610.78
	Fibber 3	0	-19.47	-32.86	-33.03	-32.19
	Fibber 4	0	-29.69	-58.51	-67.24	-69.91
	Fibber 5	0	-8.05	-29.66	-45.93	-53.13
	Fibber 6	0	-83.19	-218.90	-298.50	-331.70

Appendix 7.4

Analytical model to consider partial interaction in composite beams

Figure A7.1 shows the equilibrium forces at an infinitesimal element of the composite beam, of length *dx* and distant of *x* from the mid span cross section. The two components of the composite element are separated and all deformation is exaggerated.

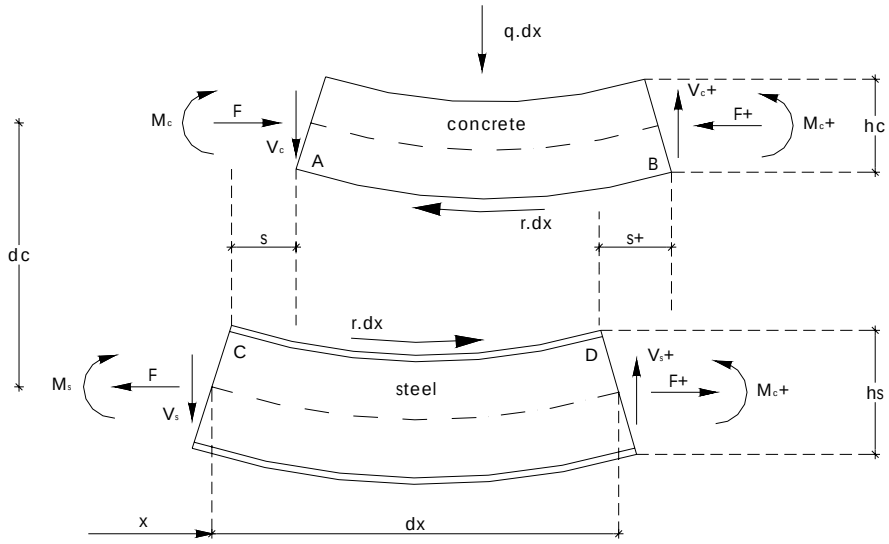

Figure A7.1 – Equilibrium forces in an infinitesimal element (Johnson 1994)

The following equations, from (7.1) to (7.21), establish the behaviour of a simply supported composite beam, consisting of a steel profile connected to a concrete slab through equally spaced headed stud connectors and subjected to the shrinkage effect. An infinitesimal element of beam, with length equal to *dx*, is considered to establish the equations.

The equations take into consideration the deformability of the headed stud connectors and define the correspondent slip between the steel profile and the concrete slab at their interface. The referred equations follow the analytical methodology proposed by (Johnson 1994).

The equilibrium of horizontal forces is established with equation (7.1).

$$\frac{dF}{dx} = -r \tag{7.1}$$

At section *x*, vertical shear is null, (7.2),

$$V_c + V_s = 0 \tag{7.2}$$

The bending moments equilibrium at section *x* is established with equations (7.3).

$$\begin{cases} \dfrac{dM_c}{dx} + V_c = r.\dfrac{h_c}{2} \\ \dfrac{dM_s}{dx} + V_s = r.\dfrac{h_s}{2} \end{cases} \tag{7.3}$$

As $\frac{1}{2}(h_c + h_s) = d_c$, the sum of the two equations (7.3), substituting with (7.2), gives equation (7.4).

$$\frac{dM_c}{dx} + \frac{dM_s}{dx} = r \cdot d_c \tag{7.4}$$

In beams with adequate shear connection, the effects of uplift are negligible in the elastic range. If there is no gap between the two components of the composite section, steel and concrete, they should have the same curvature, ϕ, because the vertical deformation is the same. The moment-curvature relations are established by equation (7.5).

$$\phi = \frac{M_s}{E_s I_s} = \frac{M_c}{E_c I_c} = \frac{n M_c}{k E_s I_c} \tag{7.5}$$

The longitudinal strains, in concrete, along AB and in steel, along CD, are respectively established by equation (7.6) and equation (7.7).

$$\varepsilon_{AB} = \frac{1}{2} h_c \phi - \frac{nF}{k_c E_s A_c} - \varepsilon_c \tag{7.6}$$

$$\varepsilon_{CD} = -\frac{1}{2} h_c \phi + \frac{F}{E_s A_s} \tag{7.7}$$

The difference between ε_{AB} and ε_{CD} is the slip strain, so from equation (7.6) and equation (7.7), results equation (7.8).

$$\frac{ds}{dx} = \phi \cdot d_c - \frac{F}{E_s}\left(\frac{n}{k_c A_c} + \frac{1}{A_s}\right) - \varepsilon_c \tag{7.8}$$

Substituting equation (7.5) on equation (7.4), the result is equation (7.9), where, $I_0 = \frac{k_c I_c}{n} + I_s$.

$$\frac{d\phi}{dx} = \frac{k d_c s / p}{E_s I_0} \tag{7.9}$$

Differentiating equation (7.8) and eliminating ϕ from equation (7.9), F from (7.1) and r from (7.3),

$$\frac{d^2 s}{dx^2} = \frac{k d_c^2 s / p - q d_c x}{E_s I_0} + \frac{ks}{E_s A_0 p} \tag{7.10}$$

where $\frac{1}{A_0} = \frac{n}{k_c A_c} + \frac{1}{A_s}$.

Introducing $\frac{1}{A'} = d_c^2 + \frac{I_0}{A_0}$; $\alpha^2 = \frac{k}{p E_s I_0 A'}$ and $\beta = \frac{A' p d_c}{k}$, equation (7.10) results in equation (7.11), which is the general differential equation that describes slip at the steel to concrete interface, for a simply supported beam, subjected to an uniformly distributed load, and with regularly spaced studs to accomplish the steel to concrete connection.

$$\frac{d^2 s}{dx^2} - \alpha^2 s = -\alpha^2 \beta q x \tag{7.11}$$

The general solution for the differential equation (7.11) is described by equation (7.12).

$$s = K_1 \, sinh(\alpha x) + K_2 \, cosh(\alpha x) \tag{7.12}$$

For a simply supported beam, the following boundary conditions are defined with equation (7.13), where from symmetry, the slip is zero at the beam mid span,

$$s = 0 \quad \Leftarrow \quad x = 0 \tag{7.13}$$

and equation (7.14), where at the beam extremes, the difference between longitudinal strains is the differential strain ε_c.

$$\frac{ds}{dx} = -\varepsilon_c \quad \Leftarrow \quad x = \pm \frac{L}{2} \tag{7.14}$$

Substituting equations (7.12) and (7.13) on equation (7.14), results in (7.15).

$$\begin{aligned} K_2 &= 0 \\ \varepsilon_c &= -K_1 \alpha \, cosh\left(\frac{\alpha L}{2}\right) \end{aligned} \tag{7.15}$$

For a simply supported beam, the slip at the steel and concrete interface can be calculated with equation (7.16),

$$s = -\frac{\varepsilon_c}{\alpha} \cdot sech\left(\frac{\alpha L}{2}\right) \cdot sinh(\alpha x) \tag{7.16}$$

which means that the value of slip between the steel profile and the concrete slab is directly proportional to the concrete strain level.

If equation (7.16) is substituted on equation (7.9), equation (7.17) is obtained,

$$\frac{d\phi}{dx} = -A_1\left(\frac{\varepsilon_c}{\alpha}\right) sec\, h\left(\frac{\alpha L}{2}\right) sinh(\alpha x) \tag{7.17}$$

where,

$$A_1 = \frac{kd_c}{pE_s I_0} \tag{7.18}$$

Integrating equation (7.17), the result is defined by equation (7.19),

$$\phi = -A_1\left(\frac{\varepsilon_c}{\alpha^2}\right) sec\, h\left(\frac{\alpha L}{2}\right) cosh(\alpha x) + C_1 \tag{7.19}$$

where C_1 is defined with (7.20).

$$C_1 = A_1\left(\frac{\varepsilon_c}{\alpha^2}\right) sec\, h\left(\frac{\alpha L}{2}\right) cosh\left(\frac{\alpha L}{2}\right) \tag{7.20}$$

And finally, integrating equation (7.19) twice, the beam vertical deformation is obtained with equation (7.21).

$$z = -A' d_c \frac{\varepsilon_c}{\alpha^2}\left(\sec h\left(\frac{\alpha L}{2}\right)\cosh(\alpha x) - \frac{x^2}{2} - \frac{1}{\alpha^2} + \frac{L^2}{8}\right) \tag{7.21}$$

Equation (7.21) shows that the value of vertical deflection is directly proportional to the value of shrinkage or creep strain or even to the variation of temperature, as it results from a differential value of strain in the steel and the concrete sections.